CONF-970126

Proceedings
for the

Nondestructive Assay and Nondestructive Examination Waste Characterization Conference

Salt Lake City, Utah
January 14 - 16, 1997

Cosponsored by

The Department of Energy
Idaho Operations Office

and

Lockheed Martin Idaho Technologies Company
Idaho National Engineering Laboratory
Transuranic Waste Department

DISTRIBUTION OF THIS DOCUMENT IS UNLIMITED

HH

MASTER

Neutron NDA Techniques/Design/Applications

DISCLAIMER

This report was prepared as an account of work sponsored by an agency of the United States Government. Neither the United States Government nor any agency thereof, nor any of their employees, makes any warranty, express or implied, or assumes any legal liability or responsibility for the accuracy, completeness, or usefulness of any information, apparatus, product, or process disclosed, or represents that its use would not infringe privately owned rights. Reference herein to any specific commercial product, process, or service by trade name, trademark, manufacturer, or otherwise does not necessarily constitute or imply its endorsement, recommendation, or favoring by the United States Government or any agency thereof. The views and opinions of authors expressed herein do not necessarily state or reflect those of the United States Government or any agency thereof.

DISCLAIMER

Portions of this document may be illegible in electronic image products. Images are produced from the best available original document.

Gamma NDA Techniques/Design/Applications

Tomographic Methods and NDE Systems

NDA Modality and Information Combination Techniques

Poster Presentations

Forward

The 5th Nondestructive Assay and Nondestructive Examination Waste Characterization conference is provided as a forum for the consideration of the current status of waste NDA/NDE technology in terms of capability and implementation readiness. For a number of waste characterization facilities, the TRU Waste Program schedule requires commencement of TRU waste shipments to the Waste Isolation Pilot Plant in the near future. This places considerable emphasis not only on waste NDA/NDE system capability but on techniques used for the demonstration of compliance with applicable Program requirements and quality assurance objectives. The papers contained in this conference proceedings document provide a reasonable sampling of the status of systems in the development phase and those nearing the implementation phase. Of interest is the utility of such systems with respect to the waste form configurations to which they will be applied as well as approaches used to demonstrate compliance.

This conference papers are broadly categorized into five sessions; (1) Compliance - Regulations/Demonstration/Experience, (2) Technical - Neutron NDA Techniques/Design/Applications, (3) Technical - Techniques/Design/Applications, (4) Tomographic Methods and NDE Systems, and (5) NDA Modality and Information Combination Techniques. These categories represent those areas where the majority of waste NDA/NDE activities are underway. The proceedings document is organized per those general activity areas to assist the reader in quickly locating topic of interest.

Greg Becker
Program Chairman

OPENING REMARKS
5th Nondestructive Assay and Examination Waste Characterization Conference

Thomas L. Clements Jr.
Lockheed Martin Idaho Technologies Company

Good morning. On behalf of the Idaho National Engineering Laboratory, I welcome you to the 5th Nondestructive Assay and Examination Waste Characterization Conference. The next three days will cover a broad range of topics concerning the characterization of waste. The structure of the conference provides a forum for exchanging information on characterization approaches, result of development activities and performance evaluations, and lessons-learned. This exchange is particularly important given the evolving requirements and technical challenges that have been encountered for measuring transuranic waste for future disposal at the Waste Isolation Pilot Plant. Although a number of papers are given by the national laboratories, I am pleased to see continued participation by commercial firms and universities.

Since we last met in October 1995, notable progress has been made in enhancing characterization methods and evaluating assay system performance.

- Implementation of the performance demonstration program for transuranic waste radioassay has been a significant step forward. While many technical challenges remain, a path has been established to systematically evaluate performance against quality assurance objectives.

- Generation data of known quality is necessary to convince regulatory agencies that the waste can be safely transported and disposed in compliance with limits set to ensure public, worker, and environmental protection.

The continued participation of the commercial sector in developing and demonstrating alternative or improved approaches to waste characterization is also important and provide a means for making informed management decisions to replace or upgrade existing systems, especially in a reduced budget environment. Additionally, the increased interest in mobile characterization capabilities can provide an alternative approach for sites to achieve waste disposal without the expense of constructing fixed facilities. Activities are currently underway to establish a project that will allow demonstration of mobile characterization capabilities.

Nondestructive examination and assay methods are a key component in the suite of capabilities needed to characterize, certify, and transport waste. This year could see the fruition of your efforts with the planned opening of WIPP in November. By the time the next conference is held, hopefully there will be many success stories.

To all the authors, I want to thank you for your time spent in preparing papers and posters, and to the vendors for their exhibits. Additionally, I appreciate the efforts of Greg Becker, Dan Menkhaus, and Sonja Slade for setting up the conference.

In summary, I hope you find the conference beneficial and thank you for your participation.

Compliance - Regulations/Demonstration/Experience

PERFORMANCE ASSESSMENT REQUIREMENTS FOR THE IDENTIFICATION AND TRACKING OF TRANSURANIC WASTE INTENDED FOR DISPOSAL AT THE WASTE ISOLATION PILOT PLANT

Craig A. Snider
Office of Regulatory Compliance
Department of Energy
Carlsbad Area Office
Carlsbad, NM 88220

William W. Weston
Long-Term Regulatory Compliance
Westinghouse Electric Corporation
Waste Isolation Division
Carlsbad, NM 88221

ABSTRACT

To demonstrate compliance with the environmental radiation protection standards for the management and disposal of transuranic (TRU) radioactive wastes, as promulgated in 40 CFR Part 191, Subparts B and C[1], a performance assessment (PA) of the Waste Isolation Pilot Plant (WIPP) was undertaken to evaluate waste-waste and waste-repository interactions and their impact on the disposal system performance. An estimate of the waste components and their accumulated quantities was derived from a roll-up of the generator/storage sites' TRU waste inventories in the TRU Waste Baseline Inventory Report[2] (TWBIR), Revision 3. Waste components considered to be of significance, in addition to others of negligible effect, were used as fixed input parameters in the PA modeling. The results of the PA have identified several components of the waste that require identification and tracking with regard to their quantities to ensure that performance-related repository limits are not exceeded. The rationale used in establishing the waste component limits based on the input estimates is discussed. The distinction between repository limits and waste container limits is explained. Controls used to ensure that no limits are exceeded are identified. For those waste components having no explicit repository based limits, other limits may be applicable as established by the WIPP Land Withdrawal Act (LWA), transportation, operational safety, and/or operational permits. These other limits are contained in the WIPP Waste Acceptance Criteria[3] (WAC). The ten radionuclides targeted by PA for identification and tracking on either a waste container or a waste stream basis include Am-241, Pu-238, Pu-239, Pu-240, Pu-242, U-233, U-234, U-238, Sr-90, and Cs-137. The accumulative activities of these radionuclides are to be inventoried at the time of emplacement in the WIPP. Changes in the inventory curie content as a function of radionuclide decay and ingrowth over time will be calculated and tracked. Due to the large margin of compliance demonstrated by PA with the 10,000 year release limits specified in Appendix A of 40 CFR Part 191, the quality assurance objective (QAOs) for the radioassay of the ten radionuclides identified above need to be no more restrictive than those QAOs already identified for addressing the requirements imposed by transportation and WIPP disposal operations as contained in Section 9 of the TRU Waste Characterization Quality Assurance Program Plan[4] (QAPP).

INTRODUCTION

With the recent completion of the WIPP's PA and the submittal of the WIPP's Compliance Certification Application[5] (CCA) by the Department of Energy (DOE) to the Environmental Protection Agency (EPA) on October 29, 1996, it is now possible to identify those waste component limits necessary for demonstrating compliance with the disposal standards established by 40 CFR Part 191, Subparts B and C. In conjunction with other limits established by the WIPP LWA, transportation in the transuranic package transporter-II (TRUPACT-II), operational safety, and/or operating permits, these performance based limits serve to ensure the long-term health and safety of the public and protection of the environment for at least 10,000 years after repository closure.

The waste component limits (WCL) are contained in Appendix WCL of the CCA. These limits are on a repository basis. For each waste component identified, the corresponding limiting value (expressed as an upper or lower limit of mass, volume, curies, concentration, etc.) is of the total inventory of such waste proposed for disposal in the WIPP repository. This is in contrast with container-based limits typically associated with transportation, disposal operations, and RCRA requirements as contained in the WAC. Compliance with these repository based limits is ensured by using the WIPP Waste Information System (WWIS) to track the waste component quantity as waste is emplaced in the repository. As an example, the curie content relating to a particular radionuclide can be accumulated as waste is emplaced throughout the operational phase. At the time of repository decommissioning, when these repository limits apply, the total curie content for that radionuclide can then be provided to demonstrate compliance with the waste component limits. The topical discussion that follows pertains exclusively to the radionuclide components of the TRU waste identified in Appendix WCL of the CCA, and includes Am-241, Pu-238, Pu-239, Pu-240, Pu-242, U-233, U-234. U-238, Sr-90, and Cs-137.

DISCUSSION

From 40 CFR Part 194, "Criteria for the Certification and Re-Certification of the WIPP's Compliance with the 40 CFR Part 191 Disposal Regulations[6]," the regulatory definitions of "waste component" and "waste characteristic" are provided. Waste component means an ingredient of the total inventory of the waste (e.g., the radionuclide inventory) that influences a waste characteristic. Waste components are synonymous with waste

material parameters used in the TWBIR. Waste characteristic means a property of the waste that has an impact on the containment of waste in the disposal system (e.g., radionuclide solubility, radionuclide redox state, colloid formation, etc.).

Components can be controlling factors for the characteristics of the waste, and limits imposed on the waste components may contribute to limiting the waste characteristics. In the case where a characteristic is unimportant to the long-term performance of the repository, no control of the corresponding component is necessary, and no limits need be imposed on that component. On the other hand, should the long-term performance of the repository be sensitive to a particular waste characteristic, control of the corresponding component may be necessary and limits should be established to restrict the maximum/minimum amounts of that component permitted for disposal.

Earlier PAs and sensitivity analysis were performed in which waste components and characteristics that may influence containment of the waste in the disposal system were assessed for their impact on the disposal system performance. In this paper, disposal system performance means the ability of WIPP to comply with 40 CFR Part 191, Subparts B and C. The rationale for including or excluding these waste components and characteristics in the final PA are contained in Appendix WCA (Waste Characterization Analysis) of the CCA.

The radionuclide release limits are given in Appendix A of 40 CFR Part 191, Subpart B. For a release to the accessible environment that involves a mixture of radionuclides, the limits in Appendix A of 40 CFR Part 191, Subpart B, are used to determine a normalized release (nR) of radionuclides for comparison with the release limits

$$nR = \Sigma (Q_i/L_i)(1 \times 10^6 \text{ Ci/C}), \qquad \text{Equation 1}$$

where

Q_i = cumulative release in curies (Ci) of radionuclide i into the accessible environment during the 10,000-year period following closure of the repository,

L_i = release limit in curies for radionuclide i given in Appendix A of 40 CFR Part 191, Subpart B, and

C = amount of curies of TRU waste (alpha-emitting TRU radionuclides with half-lives greater than 20 years) emplaced in the repository.

As indicated in Note 1(e) to the Table in Appendix A of 40 CFR Part 191, Subpart B, the "other unit of waste" for TRU waste shall be an amount of TRU wastes containing one million curies of alpha-emitting TRU radionuclides with half-lives greater than 20 years. Using the alpha-emitting TRU radionuclides with half-lives greater than 20 years listed in the TWBIR, and decaying this inventory to the time of repository decommissioning (2033), the waste unit factor for the WIPP is equal to 3.44. As a result, the release to the accessible environment over 10,000 years after disposal for Pu-238, Pu-239, Pu-240, Pu-242, U-233, U-234, U-238, or Am-241 is 344 curies. In comparison, the release limit allowed by the EPA for Sr-90 or Cs-137 is a factor of 10 greater and equals 3440 curies. Radionuclides with half-lives less than 20 years are not regulated by 40 CFR Part 191, Subparts B and C.

The number of EPA units of a radionuclide is the activity (in curies) of the radionuclide divided by its release limit. EPA units are important because the containment requirement for the repository is expressed in EPA units. For example, the Pu-239 inventory at closure is estimated to be 7.95×10^5 curies (TWBIR), and the release limit for Pu-239 is 344 curies as discussed in the preceding paragraph. The number of EPA units is calculated to be $7.95 \times 10^5/344 = 2{,}311$. In modeling a scenario where a mixture of radionuclides is released to the accessible environment, the cumulative releases over 10,000 years shall be limited so that the sum of their EPA units is less than or equal to unity:

$$Q_a/L_a + Q_b/L_b + Q_c/L_c \leq 1, \qquad \text{Equation 2}$$

where Q and L are defined in Equation 1. For each radionuclide whose inventory at decommissioning has a corresponding EPA unit less than unity, the entire inventory could be released. There are many radionuclides identified in the TWBIR whose curie content at closure is sufficiently small such that their corresponding EPA units are much less than unity. These radionuclides have a negligible impact on long-term performance.

Of the ten major constituent radionuclide components of the TRU waste inventory that have been identified as requiring assay by PA, nine have activities at decommissioning yielding EPA units greater than one. These nine are Am-241, Pu-238, Pu-239, Pu-240, Pu-242, U-233, U-234, Sr-90, and Cs-137. The combined EPA units of these nine radionuclides is in excess of 99.9 percent of the radionuclide inventory regulated by

40 CFR Part 191, Subpart B. As such they provide an adequate representation of the source term for long-term PA. Of these radionuclides, only U-238 has an EPA unit less than one. It is included in Appendix WCL because of its large mass fraction that serves to dilute the overall activity of the subsurface transported uranium species,

Because the containment requirements are normalized to the inventory, the total activity of the waste at the time of repository closure is not important for demonstrating compliance with 40 CFR Part 191. Due to radioactive decay and ingrowth, the major contributors to the overall activity of the repository change during 10,000 years — making the results of the PA analysis conditional on the initial ratios of the total activities of the assayed radionuclides at the time of repository closure. For the first several hundred years, Am-241, Pu-238, Pu-239, Pu-240, Sr-90, and Cs-137 are important contributors to the total activity of the waste. At the present and projected inventory level, Sr-90 and Cs-137 are important for about 200 years. Am-241 is important for about 3,000 years. At 10,000 years, Pu-239 and Pu-240 remain as the only significant contributors to the total activity of the waste.

The PA has determined there are no minimum or maximum emplacement limits for these ten radionuclides other than the inventory limits based on the TWBIR or imposed through the WAC. The coarse limits based on the TWBIR are the result of using the radionuclide inventory contained in the TWBIR as fixed input parameters to the PA modeling. As a control to ensure compliance with these coarse limits, the accumulative activities of the ten radionuclides will be tracked. Changes in inventory curie content as a function of radionuclide decay and ingrowth over time will be calculated and tracked.

RESULTS

Ten radionuclides have been identified from PA modeling of WIPP whose activities need to be tracked during emplacement. These ten radioisotopes include Am-241, Pu-238, Pu-239, Pu-240, Pu-242, U-233, U-234, U-238, Sr-90, and Cs-137. This requirement does not necessitate any new waste characterization requirements to the imposed on the generator/storage sites. Hence, no changes in Revision 5 of the WIPP WAC are required.

Knowledge of the TRU waste's radionuclide inventory is presently required for demonstrating compliance with radiological requirements imposed by transportation and WIPP operations. A determination of the radionuclide inventory is already a prerequisite for (1) distinguishing TRU waste from low-level waste, (2) criticality control, (3) gas generation evaluation, (4) respiratory protection, and (5) thermal loading. Since the radionuclides identified in Appendix WCL of the CCA are a subset of the radionuclides required for calculations relating to the above five areas, no additional waste characterization burden to the generator/storage sites is anticipated.

Due to the large margin of compliance demonstrated by PA with the 10,000 year release limits in Appendix A of 40 CFR Part 191, Subpart B, the QAOs for the radioassay of the ten radionuclides identified in Appendix WCL of the CCA need to be no more restrictive than those that already exist for addressing the requirements imposed by transportation and WIPP disposal operations as contained in Section 9 of the QAPP.

CONCLUSIONS

Based on the results of the PA, there are no compelling arguments for making the quality assurance objectives for radioassay either more or less restrictive than presently formulated in Section 9 of the QAPP. With the requirements for characterizing TRU waste now known and with no changes to the waste characterization requirements anticipated in the near future, the generator/storage sites can now focus without distraction on the process of characterizing and certifying their waste for disposal at WIPP. Time is of the essence, however, since the planned opening of WIPP, per the WIPP Disposal Decision Plan (DDP), is November 1997.

ACKNOWLEDGEMENT

The herculean effort demonstrated by the regulatory compliance organizations of the Carlsbad Area Office (DOE), the Sandia National Laboratories, the Waste Isolation Division (Westinghouse), and the Technical Assistance Contractors in preparing the 23 volumes of the CCA in a timely and orderly manner is to be commended for the magnitude of the accomplishment. Recognition of the dedication, diligence, and team work of these organizations in getting the job done deserves special recognition. The CCA presents the conclusions of more than 20 years of scientific and engineering work specifically dedicated to the disposal of TRU waste at the WIPP.

REFERENCES

1. U.S. Environmental Protection Agency, 40 CFR Part 191, "Environmental Radiation Protection Standards for Management and Disposal of Spent Nuclear Fuel, High-Level and Transuranic Radioactive Wastes," Final Rule (Federal Register, Vol. 58, No. 242), December 20, 1993.

2. U.S. Department of Energy, "Transuranic Waste Baseline Inventory Report," DOE/CAO-95-1121, Revision 3, Carlsbad Area Office, Carlsbad, NM, June 1996.

3. U.S. Department of Energy, "Waste Acceptance Criteria for the Waste Isolation Pilot Plant," DOE/WIPP-069, Revision 5, Carlsbad Area Office, Carlsbad, NM, April 1996.

4. U.S. Department of Energy, "Transuranic Waste Characterization Quality Assurance Program Plan," CAO-94-1010, Revision 0, Carlsbad Area Office, Carlsbad, NM, April 1995.

5. U.S. Department of Energy, "40 CFR Part 191 Compliance Certification Application," DOE/CAO-2056, October 29, 1996.

6. U.S. Environmental Protection Agency, 40 CFR Part 194, "Criteria for the Certification and Re-Certification of the Waste Isolation Pilot Plant's Compliance with 40 CFR Part 191 Disposal Regulations," Final Rule (Federal Register, Vol. 61, No. 68), February 9, 1996.

PERFORMANCE IN THE WIPP NONDESTRUCTIVE ASSAY PERFORMANCE DEMONSTRATION PROGRAM

Charles J. Marcinkiewicz
Consolidated Technical Services, Inc.
Frederick, MD

Michael J. Connolly and Gregory K. Becker
Lockheed Martin Idaho Technologies Company
Idaho National Engineering Laboratory, Idaho Falls, ID

ABSTRACT

Measurement facilities performing nondestructive assay (NDA) of wastes intended for disposal at the United States Department of Energy (DOE) Waste Isolation Pilot Plant (WIPP) are required to demonstrate their ability to meet specific Quality Assurance Objectives (QAOs). This demonstration is performed, in part, by participation in the NDA Performance Demonstration Program (PDP). The PDP is funded and managed by the Carlsbad Area Office (CAO) of DOE and is conducted by the Idaho National Engineering Laboratory. It tests the characteristics of precision, system bias and/or total uncertainty through the measurement of variable, blind combinations of simulated waste drums and certified radioactive standards. Each facility must successfully participate in the PDP using each different type of measurement system planned for use in waste characterization. The first cycle of the PDP was completed in July 1996 and the second is scheduled for completion by December 1996. Seven sites reported data in cycle 1 for 11 different measurement systems. This paper describes the design and operation of the PDP and provides the performance data from cycle 1. It also describes the preliminary results from cycle 2 and updates the status and future plans for the NDA PDP.

INTRODUCTION

As part of the transuranic (TRU) waste characterization program for the Waste Isolation Pilot Plant (WIPP), the Carlsbad Area Office (CAO) of the U.S. Department of Energy (DOE) conducts a series of Performance Demonstration Programs (PDPs). These programs are designed to help ensure compliance with the Quality Assurance Objectives (QAOs) identified in the *Transuranic Waste Characterization Quality Assurance Program Plan for the Waste Isolation Pilot Plant* (QAPP)(DOE 1995b). CAO conducts PDPs for headspace gas analysis, analysis of solidified wastes for RCRA constituents, and for nondestructive assay. The PDPs are used in the assessment and approval process for measurement facilities supplying services for the characterization of WIPP TRU waste. The other two parts of the approval process include the evaluation of method performance data submitted by the measurement facility and the performance of quality assurance audits. All sites that intend to certify wastes for shipment to the WIPP must ensure that their measurement facilities, whether owned, operated, or subcontracted, successfully participate in all of the applicable PDPs.

This paper describes the results of cycle 1 of the nondestructive assay (NDA) PDP. The PDP was conducted according to strategies described in *Performance Demonstration Program Plan for Nondestructive Assay for the TRU Waste Characterization Program* (DOE 1995a). This plan requires that acceptable performance in the NDA PDP be demonstrated by all participating measurement facilities on a semiannual basis. Single blind test drums will be prepared at 6-month (±1 month) intervals. The criteria for acceptable performance are given in the PDP Plan. The PDP samples must be analyzed using the methods the measurement facility anticipates using for the analysis of WIPP wastes. These methods must have been developed and approved within the specifications of the QAPP. Only the methods actually used in the PDP will be considered acceptable to support the analysis of WIPP wastes.

Seven facilities participated in cycle 1 and six participated in cycle 2. The participants are listed by name in Table 1.

Table 1. NDA PDP Participants

Facility
Battelle Pacific Northwest Laboratory
Hanford
Idaho National Engineering Laboratory
Lawrence Livermore National Laboratory
Los Alamos National Laboratory
Oak Ridge National Laboratory (Cycle 1 only)
Rocky Flats Environmental Technology Site

Throughout the balance of this paper the participating facilities are identified only by a two letter identification code. The cycle 1 test consisted of blind measurements of two drums, one empty and one containing a noninterfering matrix, each containing a known quantity of plutonium. The combinations of drums and standards were assembled onsite and the cycle 1 tests were scheduled to begin on April 29, 1996. The actual start dates for cycle 1 varied between April 29 and June 12, 1996. The date spread was caused when two facilities were not prepared to begin on April 29. All data were returned to the PDP Coordinator by July 3, 1996 and the final scoring report was issued by the end of July 1996. Table 2 gives the sequence of events for the conduct of cycles 1 and 2 of the NDA PDP.

Table 2. Chronology for NDA PDP

Site SPT Training	February 1996
Drum delivery	February 1996
Standards delivery	March 1996
Start Cycle 1	April 1996
Cycle 1 final report	June 1996
Start Cycle 2	November 1996
Cycle 2 final report	January 1997

Cycle 2 had been scheduled to begin on November 4, 1996 and be completed by December 23, 1996. However, again not all facilities were able to start on schedule. As a consequence the due date for final data was extended and the final report will be issued in January 1997. Results of cycle 2 of the PDP were, therefore, not available for publication in these proceedings.

ANALYTICAL PARAMETERS

The isotopes intended to be analyzed in cycles 1 and 2 of the NDA PDP are presented in Table 3. The parameter used for the overall scoring in the NDA PDP was the total alpha activity. In addition, participants were required to report the results of analyses of PDP samples in terms of activity of the individual isotopes, fissile grams equivalent (FGE), and thermal wattage. Table 4 lists the test ranges for the NDA PDP and the associated QAOs required in the QAPP as applicable to cycles 1 and 2 of the PDP.

Table 3. PDP isotopes of interest.

Isotope
1. ^{238}Pu
2. ^{239}Pu
3. ^{240}Pu
4. ^{241}Am

The isotopes measured, the limits of the activity ranges, and other parameters of the test plan may be altered in future cycles of the NDA PDP in response to changes in the QAPP for TRU waste characterization.

Table 4. PDP ranges of test activities and associated quality assurance objectives.

Activity range	Range of waste activity in α-Curies[a]	QAO for relative precision[b] ($\%RSD_Q$)	Measured relative precision[c] ($\%RSD_m$)	QAO for instrument bias[d] (%R)	QAO for total accuracy[e] (%R)
Low	> 0 to 0.04	20%	9.6%	Low: 75% High: 125%	Low: 40% High: 175%
Mid-Low	> 0.04 to 0.4	15%	7.2%	Low: 50% High: 150%	Low: 30% High: 200%
Mid-High	> 0.4 to 4.0	10%	4.8%	Low: 50% High: 150%	Low: 30% High: 200%
High	> 4.0	5%	2.4%	Low: 75% High: 125%	Low: 50% High: 150%

a. Applicable range TRU activity in a 208-L (55-gallon) drum to which the QAOs apply; units are Curies of alpha-emitting TRU isotopes with half-lives greater than 20 years.

b. Limits for one relative standard deviation (σ/μ_o), expressed as a percent.

c. Maximum measured relative standard deviations (expressed as a percent) that must be obtained based on six measurements to demonstrate at the 95% confidence level that the QAPP QAOs have been met.

d. Limits on the two-sided 95% confidence bound for the ratio of the mean of the measured values to the known (or accepted) value, expressed as a percent.

e. Calculated as limits on the two-sided 95% confidence bound for the mean of the ratio of the measured to the known (or accepted) value, expressed as a percent.

NDA PDP MATERIALS

An initial inventory consisting of nine PDP standards and two matrix drums was provided to each measurement facility prior to the start of that facility's participation in PDP measurement activities. The PDP standards are radioactive sources specifically prepared and certified for the PDP. The matrix drums are standard 208-L (55-gallon) waste drums acquired and serial numbered for the PDP. Each drum contains an insert that was designed and manufactured to simulate an expected waste matrix condition. Ultimately each of the participating sites will have an inventory of over 30 standards and on the order of eight matrix drums.

In each PDP cycle the number of standards and the amount of radioactive material inserted in each matrix drum will be selected from an inventory of available PDP standards at each site. The PDP standards distributed for cycle 1 consisted of weapons-grade plutonium dioxide (WG PuO_2) uniformly mixed in diatomaceous earth, encapsulated in a dual stainless steel cylinder configuration. The bottom end of both the outer and inner stainless steel seamless tubes have electron beam welded endcaps. The WG PuO_2/diatomaceous earth mixture is contained in the inner cylinder, packed and stabilized with a press fitted frit 0.25 inches in height. The top endcap was press fit and welded using a tungsten inert gas method. The assembled inner tube was inserted into the outer tube and the outer endcap similarly welded in place. The assembled PDP standard is illustrated in Figures 1 and 2.

The PDP standards were manufactured and individually certified by Los Alamos National Laboratory and are designated as Working Reference Materials (WRMs). A complete PDP standard specification with supporting analyses is provided in the

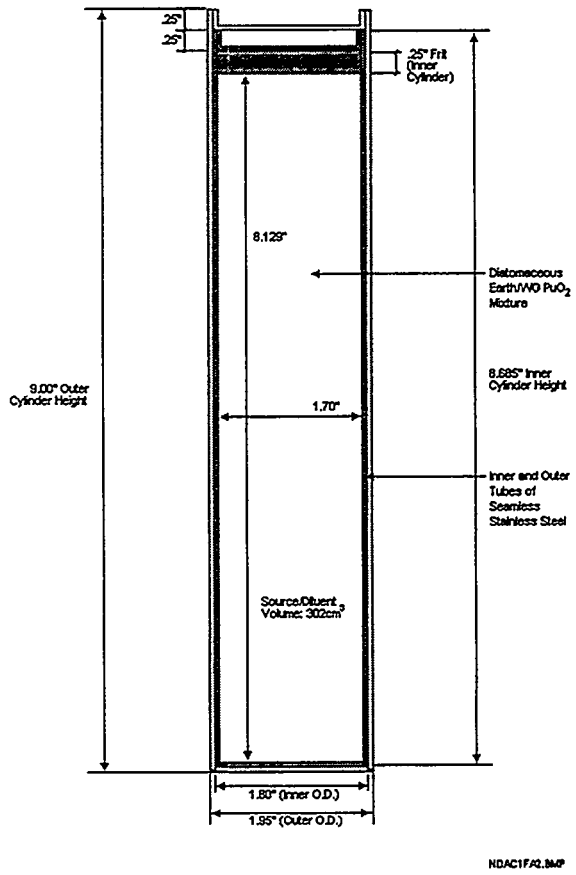

Figure 1. Design of PDP standard assemblies.

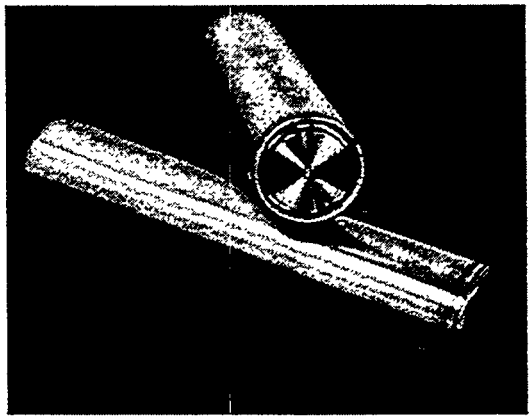

Figure 2. Photo-illustration of the NDA PDP standards.

Lockheed Idaho Technologies Company document, *Design of Phase I Radioactive Working Reference Materials for the Nondestructive Assay Performance Demonstration Program for the National TRU Program* (INEL 1996a).

Two PDP matrix drum designs, the zero matrix and low density polyethylene matrix drums were manufactured for the first performance demonstration program cycle. The matrix drum configurations were based on the cycle 1 PDP plan objectives, i.e., establish baseline nondestructive waste assay system performance characteristics and provide for a means to assess system comparability. Assessment of baseline performance required a zero matrix or empty matrix drum useful for verifying fundamental calibrations. This drum is referred to as the empty drum for convenience. A second matrix drum was provided to test nondestructive assay system performance for a nominally noninterfering matrix. The noninterfering matrix chosen was a uniform, low density polyethylene matrix (ETHAFOAM HS-900, plank polyethylene plastic foam, density 0.15 g/cm^3, manufactured by the DOW Chemical Company). This drum is referred to as the ethafoam drum for convenience.

The matrix drum configuration includes external provisions allowing the convenient introduction and precise location of PDP standards within the drum volume. Figure 3 shows the zero matrix drum configuration minus the DOT 17C drum. Figure 4 provides an overall view and dimensions of the structural components. A cutaway view of the assembled low density polyethylene ethafoam drum is illustrated in Figure 5. A photo-illustration of the interior of the ethafoam drum is shown in Figure 6. The internal support structure of the ethafoam drum is identical to that of the zero matrix drum shown in Figure 3.

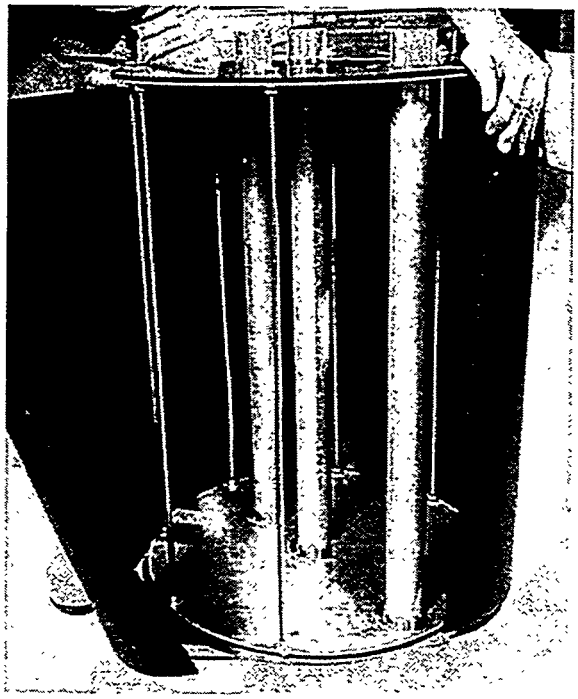

Figure 3. Interior structure of the NDA PDP "empty drum".

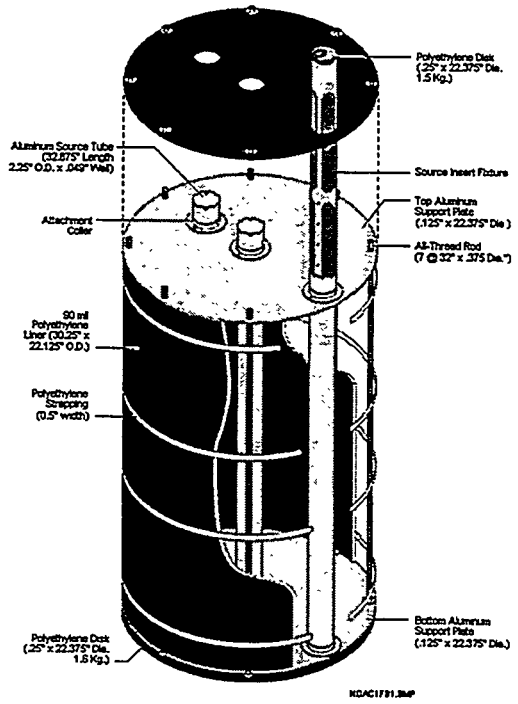

Figure 4. Assembly configuration of the zero matrix (empty) drum.

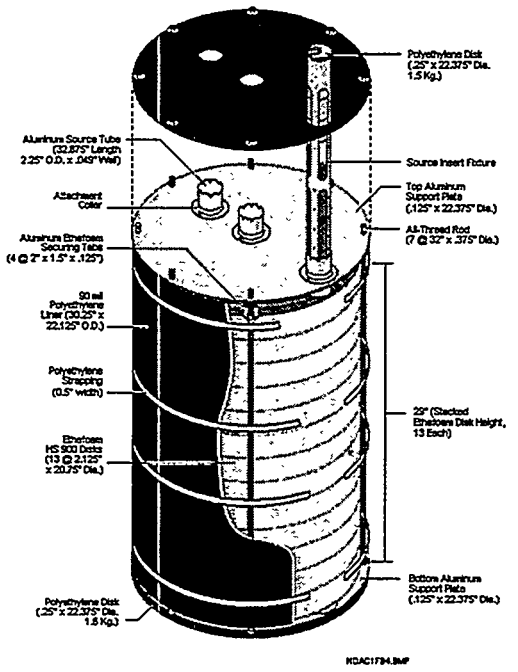

Figure 5. Assembly configuration of the noninterfering matrix (ethafoam) drum.

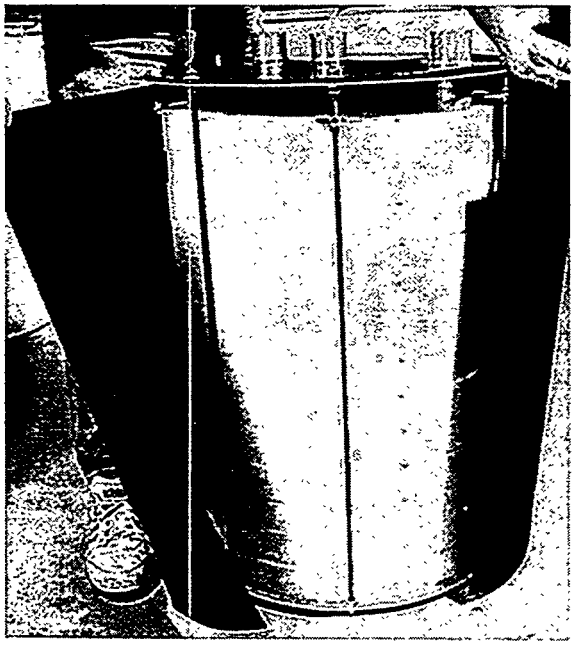

Figure 6. Internal view of the ethafoam drum.

Aluminum source insert fixtures are provided for each of the three insert tube radii. The PDP standards are positioned at the desired vertical locations in the source insert fixture using small plunger rods. The insert fixture is then positioned into the source insert tube. Figures 4 and 5 each show one partially inserted fixture. Matrix spacers were provided for use with the ethafoam matrix drum to fill any void space within the source insert fixture not occupied by PDP standard(s) thus assuring that the internal matrix was as uniform as possible. Figure 7 shows the WRM, spacers and locating pin in place in an insert tube. Assembled PDP samples were sealed with a tamper indicating device (TID) to prevent undetected inspection of the contents by the staff responsible for performing the assay measurements. An assembled PDP sample is shown in Figures 8 and 9 with the TID in place.

Complete technical details on the design of the cycle 1 PDP matrix drums are provided in the Lockheed Idaho Technologies Company document, *Design of Matrix Drums for the Nondestructive Assay Performance Demonstration Program for the National TRU Program* (INEL 1996b).

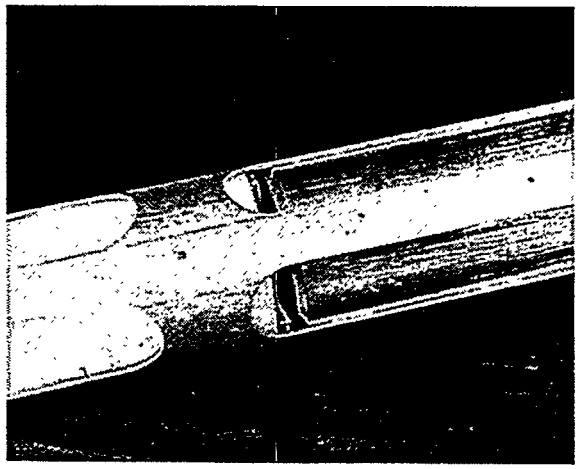

Figure 7. WRM and spacers in insert tube.

PDP SAMPLE PREPARATION

All planning and decisions about the total activity and location of that activity in each drum were made by a Program Coordinator designated by CAO. Approximately two weeks prior to the scheduled start date for the PDP cycle, a letter of instruction was forwarded to each site. This letter of instruction specified the locations, identification, and activities of each WRM to be inserted in each matrix drum to be used in that cycle. Table 5 lists the complete inventory of NDA WRMs provided to the sites for use in the NDA PDP tests. The facilities to which the standards were assigned are identified in Table 5 by their two letter identification code. The Program Coordinator selected the standards to be used in cycle 1 from this inventory.

Using the instructions provided by the Program Coordinator, PDP samples were prepared onsite by a two-person Sample Preparation Team (SPT), consisting of a PDP Standards Custodian and a PDP Standards Configuration Attestant, who were designated by the measurement facility. The SPT members were required to be full-time employees of the measurement facility but independent of the measurement group being tested. The members of the SPT and any site designated backups received specific training in their responsibilities and the documentation requirements of the program prior to cycle 1 of the NDA PDP. The PDP Standards Custodian, as the lead member of the SPT, was responsible for coordination of onsite activities and physical preparation of the PDP samples. The PDP Standard Configuration Attestant verified the placement of all standards and sealed the PDP sample with the appropriate serialized TID. Table 6 lists the individual standards and their locations in the matrix drums at each participating facility. After preparation and sealing, the PDP Standards Custodian transferred the PDP samples to the Assay Coordinator for measurement. The transfer to the Assay Coordinator and all subsequent transfers were made using Chain-of-Custody Forms required by the NDA PDP Plan.

Figure 8. Completed PDP Test drum.

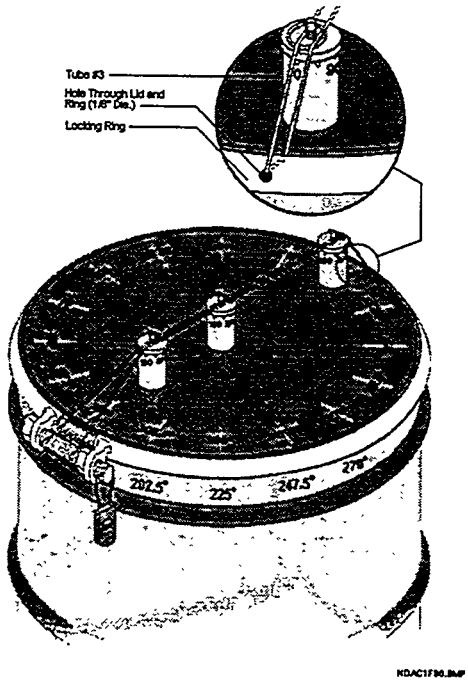

Figure 9. Assembled NDA PDP sample with TID detail.

Table 5. Inventory of Pu working reference materials for the NDA PDP.				
		Reference Date:		05/01/1996
Site Code	WRM#	Plutonium (g)	Total Alpha (mCi)	241-Am (mg)
WR	NTP-0067	0.0321	2.482	0.0307
WR	NTP-0074	0.0322	2.491	0.0308
WR	NTP-0081	0.0294	2.278	0.0282
WR	NTP-0088	0.2997	23.19	0.2869
WR	NTP-0095	0.3037	23.50	0.2908
WR	NTP-0102	0.2986	23.10	0.2858
WR	NTP-0109	2.968	229.7	2.842
WR	NTP-0116	2.933	226.9	2.807
WR	NTP-0123	3.051	236.1	2.921
AC	NTP-0068	0.0299	2.316	0.0287
AC	NTP-0075	0.0298	2.304	0.0285
AC	NTP-0082	0.0290	2.241	0.0277
AC	NTP-0089	0.3070	23.75	0.2939
AC	NTP-0096	0.3010	23.29	0.2882
AC	NTP-0103	0.2987	23.11	0.2859
AC	NTP-0110	2.950	228.3	2.824
AC	NTP-0117	2.943	227.7	2.817
AC	NTP-0124	2.950	228.3	2.824
DC	NTP-0066	0.0304	2.356	0.0291
DC	NTP-0073	0.0322	2.490	0.0308
DC	NTP-0080	0.0321	2.482	0.0307

Table 5. Inventory of Pu working reference materials for the NDA PDP (Cont.).				
		Reference Date:		05/01/1996
Site Code	WRM#	Plutonium (g)	Total Alpha (mCi)	241-Am (mg)
DC	NTP-0087	0.2990	23.14	0.2863
DC	NTP-0094	0.3001	23.22	0.2873
DC	NTP-0101	0.3070	23.76	0.2939
DC	NTP-0108	3.052	236.2	2.922
DC	NTP-0115	3.012	233.1	2.883
DC	NTP-0122	2.936	227.2	2.810
PE	NTP-0064	0.0315	2.436	0.0301
PE	NTP-0071	0.0286	2.210	0.0273
PE	NTP-0078	0.0307	2.376	0.0294
PE	NTP-0085	0.3066	23.73	0.2935
PE	NTP-0092	0.3057	23.65	0.2926
PE	NTP-0099	0.2927	22.65	0.2802
PE	NTP-0106	3.055	236.4	2.925
PE	NTP-0113	2.922	226.1	2.797
PE	NTP-0120	3.012	233.1	2.883
NG	NTP-0065	0.0301	2.327	0.0288
NG	NTP-0072	0.0290	2.244	0.0278
NG	NTP-0079	0.0294	2.276	0.0282
NG	NTP-0086	0.3088	23.90	0.2956
NG	NTP-0093	0.3006	23.26	0.2878
NG	NTP-0100	0.3054	23.63	0.2924

Table 5. Inventory of Pu working reference materials for the NDA PDP (Cont.).				
		Reference Date:		05/01/1996
Site Code	WRM#	Plutonium (g)	Total Alpha (mCi)	241-Am (mg)
NG	NTP-0107	2.942	227.6	2.816
NG	NTP-0114	2.994	231.7	2.866
NG	NTP-0121	2.918	225.8	2.794
CP	NTP-0069	0.0323	2.497	0.0309
CP	NTP-0076	0.0288	2.230	0.0276
CP	NTP-0083	0.0316	2.442	0.0302
CP	NTP-0090	0.3056	23.65	0.2925
CP	NTP-0097	0.3034	23.50	0.2908
CP	NTP-0104	0.3013	23.31	0.2884
CP	NTP-0111	3.049	235.9	2.919
CP	NTP-0118	2.982	230.8	2.855
CP	NTP-0125	2.990	231.4	2.862
BR	NTP-0070	0.0316	2.448	0.0303
BR	NTP-0077	0.0295	2.280	0.0282
BR	NTP-0084	0.0307	2.372	0.0293
BR	NTP-0091	0.2989	23.13	0.2861
BR	NTP-0098	0.2991	23.14	0.2863
BR	NTP-0105	0.3089	23.90	0.2957
BR	NTP-0112	2.950	228.3	2.824
BR	NTP-0119	3.070	237.6	2.939
BR	NTP-0126	2.992	231.5	2.864

Table 6. Utilization and placement NDA PDP WRMs in cycle 1.

Nominal Activity (mCi)	Drum	Tube	Height (in.)	Site						
				WR	AC	DC	PE	NG	CP	BR
23.2	Empty	1	1	NTP-0088	NTP-0089	NTP-0087	NTP-0085	NTP-0086	NTP-0090	NTP-0091
232	Empty	2	8	NTP-0123	NTP-0110	NTP-0122	NTP-0120	NTP-0121	NTP-0125	NTP-0126
2.32	Empty	2	17	NTP-0067	NTP-0068	NTP-0066	NTP-0064	NTP-0065	NTP-0069	NTP-0070
23.2	Empty	3	1	NTP-0095	NTP-0096	NTP-0094	NTP-0092	NTP-0093	NTP-0097	NTP-0098
Total:										
281	Empty									
23.2	Ethafoam	1	1	NTP-0102	NTP-0103	NTP-0101	NTP-0099	NTP-0100	NTP-0104	NTP-0105
2.32	Ethafoam	1	17	NTP-0074	NTP-0075	NTP-0073	NTP-0078	NTP-0072	NTP-0076	NTP-0077
232	Ethafoam	2	9	NTP-0109	NTP-0117	NTP-0108	NTP-0106	NTP-0107	NTP-0111	NTP-0112
232	Ethafoam	3	1	NTP-0116	NTP-0124	NTP-0115	NTP-0113	NTP-0114	NTP-0118	NTP-0119
Total:										
490	Ethafoam									

ANALYTICAL AND DATA REPORTING REQUIREMENTS

Each measurement facility was required to analyze the contents of each PDP sample six times using the procedures that were planned for use in the WIPP waste characterization program. These procedures must have been internally demonstrated to meet the QAOs in accordance with QAPP requirements and the procedures must have been approved within the site-specific system for control of operating procedures. The PDP samples were completely removed and replaced between successive measurements.

Analytical data in the required format was to be reported to the Program Coordinator within 21 days after transfer of the assembled PDP samples from the PDP Standards Custodian to the Assay Coordinator.

DATA EVALUATION METHODS

All data were analyzed according to the criteria set forth in the PDP Plan. This plan describes the details of the scoring system which is based on meeting various criteria for bias, accuracy, and precision. The criteria used for scoring analytical data for bias, accuracy, and precision are reproduced in this paper in Table 4. The scoring system for the PDP is a pass/fail system. In order to pass a specific test, the measurement must fall within the specified QAOs of the PDP (Table 4). In order to successfully complete the PDP cycle, the measurement facility must pass all individual tests.

In cycle 1 of the NDA PDP, performance was evaluated in the areas of precision and bias. Total accuracy was not evaluated in cycle 1 of the NDA PDP. Total accuracy will be measured in future cycles for PDP samples other than the noninterfering matrices. The definitions of precision, bias, total accuracy, and total uncertainty are as defined in the QAPP (See the Glossary). Precision is measured in this context as the relative standard deviation expressed as a percent (%RSD) from several replicate measurements of the identical PDP sample under fixed conditions. Bias is the systematic error component of the total uncertainty. Instrument bias is taken to mean the bias of a particular instrument under as ideal conditions as can be practically obtained. This bias is specific to the instrument in isolation from interfering effects such as matrix effects. Instrument bias was estimated for the noninterfering samples by determining the measurement accuracy of a series of replicate measurements. Measurement accuracy is measured as the percent recovery (%R), that is, the ratio of the mean of the measured values to the known value, expressed as a percent.

Precision and instrument bias were measured for each of the two PDP samples in cycle 1. The intent of the scoring system of the PDP was to ensure that the QAOs listed in the QAPP and in Table 4 were satisfied at the 95% confidence level using six replicate measurements. The methods of arriving at the scoring criteria are summarized below. A more detailed treatment of the derivation of the PDP test criteria may be found in the PDP Plan.

Precision

Instrument precision is equal to the standard deviation of the entire underlying measurement distribution. It is estimated by making replicate measurements on a single known PDP sample. This measured standard deviation is generally not identical to the standard deviation of the underlying distribution, but the two are related by the chi-square distribution. To determine scoring criteria, a chi-square distribution

was assumed for the evaluation of precision. The degrees of freedom were selected to be five (i.e., six replicate measurements). For the precision measurement, the 95% upper confidence bound of the one-sided chi-square distribution was set equal to the QAO requirements in Table 4.

Using these assumptions and the values for the precision QAO in Table 4, Column 3, the required measured precision for each of the PDP samples was calculated. The measured precisions must be equal to or less than the values listed in Table 4, Column 4 (measured relative precision).

Bias

In a similar manner, the measured, or sampled, mean will be related to the mean of the underlying distribution by the Student's *t* distribution, because the underlying variance is not known. To determine scoring criteria, a Student's *t* distribution was assumed to evaluate the bias in the mean. Again, the degrees of freedom were selected to be five (i.e., six replicate measurements). For the bias measurements, the upper and lower 95% confidence limits of the bias can be expressed as confidence bounds using the two-sided Student's *t* distribution. The bias limits in Table 4 are reduced by the half width of the 95% confidence bounds of the Student's *t* distribution. Assuming six replicate samples and a 95% confidence interval, the new limits can be calculated using Equation 1. Since the standard deviation of the six measurements is required to calculate the limits on the measured bias, the limits could not be calculated *a priori* and included in Table 4. The calculated bias limits for each set of measurements are included in all of the appropriate data tables.

$$(\%R_L + 1.05\ \%RSD_m) \le 100 \times \frac{\bar{x}}{\mu_o} \le (\%R_H - 1.05\ \%RSD_m) \qquad (1)$$

Where,

$\bar{x}$	=	average of the six replicate results
μ_o	=	actual known PDP sample activity
$\%R_L$	=	the low % recovery limit for bias, specified in Table 4, column 5
$\%R_H$	=	the high % recovery limit for bias, specified in Table 4, column 5
$\%RSD_m$	=	the measured percent relative standard deviation of the six replicates

This equation requires that

$$1.05\%\ RSD \le |\ 100\text{-}\%\ R_{L,H}\ | \qquad (2)$$

Otherwise, the test will fail.

Evaluation Methods

To demonstrate compliance with the QAOs for precision, NDA results for total alpha activity from replicate analyses of the PDP samples were used. The requirement was that the results reported for total alpha activity from replicate measurements of an identical sample not exhibit a measured relative standard deviation greater than that specified in Table 4, Column 4. The analytical results from the six replicate measurements of an identical sample were used to calculate the relative standard deviation. The measured standard deviation was then compared with the values listed in Table 4. The selection of the appropriate precision from Table 4 was based on the known total alpha activity range in which the prepared PDP sample falls. If the measured value was less than that specified in Table 4, Column 4, the measurement passed the test for precision. If the measured relative standard deviation exceeded the relevant value in Table 4, Column 4, the measurement facility was judged as unable to satisfactorily quantitate by NDA for that alpha activity range.

The NDA results for replicate analyses of the PDP samples were then used to determine the acceptability of the bias with which a measurement facility could measure the total alpha activity. The requirement was that the mean of the results reported for total alpha activity not deviate from the reference value, μ_o (true sample value), by more than the amount specified in Equation (1) using the values for %R specified in the instrument bias column (column 5) of Table 4. The selection of the appropriate instrument bias from Table 4 was based on the known total alpha activity range corresponding to the prepared PDP sample. The bias was computed by calculating the mean and the relative standard deviation of the six replicate measurements. The bias will pass the criterion if Equation (1) is satisfied and will fail if Equation (1) is not satisfied. The values for %R in Equation (1) will be the low and high values specified in the instrument bias column of Table 4 that corresponds to the total alpha activity range in which the prepared PDP sample falls.

If the results for the total bias are not shown at the 95% confidence level to be within the limits of Table 4 for the activity range tested, the measurement facility will be judged as unable to satisfactorily quantitate by NDA for that specific activity range.

Measurement facilities must pass all performance criteria for any activity range demonstrated by this program in order to be considered qualified to perform NDA on WIPP waste drums with activities within the tested range.

RESULTS PRESENTATION

This paper presents data for alpha-Curies, only. Although the facilities also reported FGE, individual isotopic activities, and thermal wattage, there is no provision in the PDP for separately scoring under these units. Data reported as FGE were scored for comparison and did generate inquiries of the laboratories when there were apparent differences between the alpha - Curie based scores and the FGE based scores. When all data had been confirmed, there were no significant differences in the scoring results based on the two different units. Each participating facility is identified by a two letter code. Methods are identified in the data tables only to the extent of identification as a neutron or gamma based

system. When a facility submitted data for multiple measurement systems, the facility code was retained for both systems. In most cases this also served to identify the general principle of measurement used by the respective systems.

The data contained in Tables 8 and 9 appear as they were reported by the laboratories. The terms %R and %RSD are defined in detail in the PDP Plan. The %R is calculated as a percent recovery of the known value. The %RSD is calculated using the sample standard deviation from the six replicate measurements submitted for each sample drum.

Table 7 gives the total of the activities of all standards inserted in each drum for the tests in alpha-Curies. These data constitute the "Known Values" for each drum. Table 8 presents the reported data for the assay of the empty drums as submitted by the sevenparticipating facilities. Table 9 presents the reported data for the assay of the ethafoam drums as submitted by the seven participating facilities. Table 10 compares the calculated recoveries and the relative standard deviations for each tested measurement system to the performance criteria for both the empty drum and the ethafoam drum measurements. The empty drums contained between 255 and 285 milliCuries and therefore were evaluated for the Mid-Low Range category. The ethafoam drums contained between 481 and 496 milliCuries and therefore were evaluated for the Mid-High Range category.

Table 7. Activity Summary for PDP Cycle 1 Samples (alpha - Curies).

	Empty Drum		Ethafoam	
Site Code	No. of Standards.	Total Activity (α - Curies)	No. of Standards.	Total Activity (α - Curies)
WR	4	2.853e-01	4	4.822e-01
AC	4	2.777e-01	4	4.814e-01
DC	4	2.759e-01	4	4.955e-01
PE	4	2.829e-01	4	4.875e-01
NG	4	2.753e-01	4	4.852e-01
CP	4	2.553e-01	4	4.923e-01
BR	4	2.802e-01	4	4.920e-01

Table 8. Reported Results Summary for Empty Drum (alpha - Curies).

Site Code	Method	Known Values (α - Curies)	Reported Data (α - Curies)						Avg.
			1	2	3	4	5	6	
WR	NEUTRON	0.2853	0.2739	0.2826	0.2835	0.2909	0.2829	0.2856	0.2832
AC	NEUTRON	0.2777	0.3280	0.3140	0.3410	0.3120	0.3270	0.3200	0.3237
DC	NEUTRON	0.2759	0.2860	0.2860	0.2870	0.2880	0.2870	0.2860	0.2867
PE	GAMMA	0.2829	0.2810	0.2820	0.2820	0.2860	0.2920	0.2830	0.2843
PE	NEUTRON	0.2829	0.3470	0.3390	0.3440	0.3420	0.3540	0.3450	0.3452
NG	GAMMA	0.2753	0.2522	0.2548	0.2514	0.2540	0.2566	0.2548	0.2540
NG	NEUTRON	0.2753	0.4475	0.4504	0.4495	0.4493	0.4469	0.4444	0.4480
CP	NEUTRON	0.2553	0.2600	0.2600	0.2500	0.2650	0.2560	0.2600	0.2585
CP	GAMMA	0.2553	0.2630	0.2190	0.2460	0.2240	0.2160	0.2440	0.2353
BR	GAMMA1	0.2802	0.2780	0.2630	0.2860	0.2910	0.2630	0.2700	0.2752
BR	GAMMA2	0.2802	0.2440	0.2610	0.2500	0.2800	0.2620	0.2660	0.2605

Table 9. Reported Results Summary for Ethafoam Drum (alpha - Curies)

Site Code	Method	Known Values (α -Curies)	Reported Data (α -Curies)						
			1	2	3	4	5	6	Avg.
WR	NEUTRON	0.4822	0.5208	0.5003	0.4952	0.5027	0.5169	0.5153	0.5085
AC	NEUTRON	0.4814	0.4000	0.4140	0.4410	0.4150	0.4050	0.4150	0.4150
DC	NEUTRON	0.4923	0.5440	0.5370	0.5420	0.5470	0.5470	0.5400	0.5428
PE	GAMMA	0.4875	0.4910	0.4930	0.4920	0.5030	0.5110	0.4880	0.4963
PE	NEUTRON	0.4875	0.6460	0.6390	0.6520	0.6350	0.6530	0.6440	0.6448
NG	GAMMA	0.4852	0.4932	0.4663	0.4585	0.4802	0.4724	0.4654	0.4727
NG	NEUTRON[1]	0.4852	NA	NA	NA	NA	NA	NA	NA
CP	NEUTRON	0.4814	0.5230	0.4940	0.5190	0.5330	0.5190	0.5330	0.5202
CP	GAMMA	0.4814	0.4470	0.4130	0.4010	0.4060	0.4750	0.4140	0.4260
BR	GAMMA1	0.4920	0.4780	0.4570	0.4410	0.4910	0.4850	0.4530	0.4675
BR	GAMMA2	0.4920	0.3430	0.3540	0.3390	0.3380	0.3460	0.3500	0.3450

Notes: 1. No data reported. Activity in the standard drum was outside the calibration range for this instrument.

Table 10. NDA PDP cycle 1 reported data and acceptance criteria.

Site Code	Method	Drum Type	Measured Parameters		Acceptance Criteria			Status	
					System Bias		Precision		
			%R	%RSD	Lower (%R)	Upper (%R)	(%RSD)	Precision	System Bias
WR	NEUTRON	Empty	99.28%	1.95%	52.04%	147.96%	7.20%	Passed	Passed
WR	NEUTRON	Ethafoam	105.46%	2.05%	52.16%	147.84%	4.80%	Passed	Passed
AC	NEUTRON	Empty	116.57%	3.31%	53.47%	146.53%	7.20%	Passed	Passed
AC	NEUTRON	Ethafoam	86.20%	3.41%	53.58%	146.42%	4.80%	Passed	Passed
DC	NEUTRON	Empty	103.91%	0.28%	50.30%	149.70%	7.20%	Passed	Passed
DC	NEUTRON	Ethafoam	110.27%	0.73%	50.77%	149.23%	4.80%	Passed	Passed
PE	GAMMA	Empty	100.51%	1.45%	51.53%	148.47%	7.20%	Passed	Passed
PE	NEUTRON	Empty	122.02%	1.48%	51.56%	148.44%	7.20%	Passed	Passed
PE	GAMMA	Ethafoam	101.81%	1.77%	51.86%	148.14%	4.80%	Passed	Passed
PE	NEUTRON	Ethafoam	132.27%	1.10%	51.15%	148.85%	4.80%	Passed	Passed

Table 10. NDA PDP cycle 1 reported data and acceptance criteria. (Continued)

Site Code	Method	Drum Type	Measured Parameters		Acceptance Criteria			Status	
					System Bias		Precision		
			%R	%RSD	Lower (%R)	Upper (%R)	(%RSD)	Precision	System Bias
NG	GAMMA	Empty	92.25%	0.75%	50.79%	149.21%	7.20%	Passed	Passed
NG	NEUTRON	Empty	162.73%	0.49%	50.51%	149.49%	7.20%	Passed	Failed
NG	GAMMA	Ethafoam	97.42%	2.63%	52.76%	147.24%	4.80%	Passed	Passed
NG	NEUTRON[1]	Ethafoam	NA	NA	NA	NA	NA	NA	NA
CP	NEUTRON	Empty	101.24%	1.95%	52.05%	147.95%	7.20%	Passed	Passed
CP	GAMMA	Empty	92.17%	7.89%	58.28%	141.72%	7.20%	Failed	Passed
CP	NEUTRON	Ethafoam	108.04%	2.75%	52.89%	147.11%	4.80%	Passed	Passed
CP	GAMMA	Ethafoam	88.48%	6.79%	57.13%	142.87%	4.80%	Failed	Passed
BR	GAMMA1	Empty	98.19%	4.30%	54.51%	145.49%	7.20%	Passed	Passed
BR	GAMMA2	Empty	92.96%	4.84%	55.08%	144.92%	7.20%	Passed	Passed
BR	GAMMA1	Ethafoam	95.02%	4.27%	54.48%	145.52%	4.80%	Passed	Passed
BR	GAMMA2	Ethafoam	70.12%	1.81%	51.91%	148.09%	4.80%	Passed	Passed

Notes: 1. No data reported. Activity in the standard drum was outside the calibration range for this instrument.

SUMMARY OF RESULTS

The Pass/Fail status of each cycle 1 participant is described briefly below and presented in Table 11. Results were generally excellent. All of the seven participating facilities qualified at least one measurement system. Four of the seven participating facilities submitted data for two different measurement system. Two of these four failed to qualify one of the measurement systems tested.

Facility WR

This facility submitted data for one measurement system, a passive/active neutron system. Although described as a neutron system in the data tables, the system also incorporated data from a gamma spectrometry system for quantitation of Am-241. The data in this paper corresponds to that submitted for the active mode assay. The active mode data passed all scoring criteria.

Facility AC

This facility submitted data from a single system, a passive neutron system. This facility submitted the diskette version with no hard copy followup. On initial scoring of the results, two of the data files appeared identical and an inquiry was made requesting a review by the facility. The duplication was observed and the correct data file was transferred. This system passed all scoring criteria.

Facility DC

This facility submitted data from a single system, a passive/active neutron system. The facility submitted a detailed letter report describing the system and referencing the current operating procedure. No problems were encountered with data review and this system passed all scoring criteria.

Facility PE

This facility submitted data from two different measurement systems. One was a passive/active neutron system and the second was a gamma spectrometry system. No problems were encountered in the data review and the system passed all scoring criteria.

Facility NG

This facility submitted data from two different measurement systems. One was a high sensitivity neutron system and the second was a gamma spectrometry system. No problems were encountered on initial review of the report. For the neutron instrument, data were submitted only for the empty drum. The activity in the ethafoam drum was outside the calibration range of the instrument which was stated to be 0 to 5.8 grams of plutonium. The known value for this drum was, indeed, outside of this range. However, the neutron instrument also overestimated the transuranic content of the empty drum and did not meet the bias criterion. It therefore failed to qualify under the NDA PDP criteria. Results from the gamma spectrometry were submitted for both PDP samples and this system passed all scoring criteria.

Facility CP

This facility submitted data from two different measurement systems. One was a passive/active neutron system and the second was a gamma spectrometry system. On review of the original reported results, an individual value for the neutron assay system was observed which was inconsistent with the balance of the data submittal. An inquiry was made with instructions to the facility to review the submitted data for transcription errors. The inquiry did not identify the suspect data. The facility's response indicated that the datum in

question was indeed in error. A corrected report sheet was returned the next day to document the correct data. Results from the neutron assay system were then evaluated for both PDP samples and this system passed all scoring criteria. Data for both PDP samples were also submitted for the gamma spectrometry system. This system did not meet the precision criteria for either the empty drum or the ethafoam drum. It therefore failed to qualify under the NDA PDP criteria.

Facility BR

This facility submitted data from two different measurement systems. One was a high resolution gamma spectrometry system and the second was a sodium iodide based gamma system. Data was submitted as hard copies of the report forms and as the required diskette deliverable. No problems were encountered on data review and the system passed all scoring criteria.

CYCLE 2 RESULTS

Data were not available for publication at the time the proceedings went to press. An additional drum was added to the matrix drum inventory for cycle 2. This drum simulated a combustibles waste matrix and was one of the drums used in the cycle 2 tests.

Three of the participants requested an extension of the time to submit data for cycle 2 which was granted.

FUTURE PLANS

The NDA PDP will continue on a semi-annual frequency for the foreseeable future.

Additional standards are being manufactured by Los Alamos National Laboratory. The new standards will extend the testing range of the program by introducing higher activity standards. The new standards will also permit variation of the plutonium isotopic ratios, average plutonium particle size, enhancement of the ^{241}Am content, and introduction of isotopes of uranium. Although additional enhancements will always be considered based on lessons learned and new challenges, the nominal standards inventory for the NDA PDP should be complete by the end of FY97.

Additional matrix drums will be added to the test materials inventory on a frequency of at least one per year. A final inventory of eight drums is currently planned. This is felt to be sufficient to test most classes of interference with the NDA measurement systems. The basic design of the matrix drums is very flexible and will accommodate additional matrix types or even site specific waste forms if this is found to be useful at some future time.

CONCLUSIONS

The initial cycle of the NDA PDP as conducted by CAO has shown itself to be a viable and useful tool for evaluating and comparing nondestructive assay systems used for TRU waste characterization. Despite some administrative and scheduling problems, cooperation among the participants was very good and technical results were excellent. The planned enhancements to the test materials inventory will ultimately provide better simulation of real waste assay problems and an improved understanding of the capabilities and limitations of NDA systems now in use.

The initial cycle of the NDA PDP has also demonstrated that the current generation of nondestructive assay systems are generally capable of meeting the precision and bias QAO for characterization of TRU wastes intended for disposal at WIPP for the nominally noninterfering waste matrix.

Table 11. Summary of NDA PDP cycle 1 performance

Site Code	Method	Zero Matrix		Noninterfering Matrix	
		Precision	Bias	Precision	Bias
WR	NEUTRON	Passed	Passed	Passed	Passed
AC	NEUTRON	Passed	Passed	Passed	Passed
DC	NEUTRON	Passed	Passed	Passed	Passed
PE	GAMMA	Passed	Passed	Passed	Passed
PE	NEUTRON	Passed	Passed	Passed	Passed
NG	GAMMA	Passed	Passed	Passed	Passed
NG	NEUTRON[1]	Passed	Failed	NA[1]	NA[1]
CP	NEUTRON	Passed	Passed	Passed	Passed
CP	GAMMA	Failed	Passed	Failed	Passed
BR	GAMMA1	Passed	Passed	Passed	Passed
BR	GAMMA2	Passed	Passed	Passed	Passed

Notes: 1. No data reported. Activity in the standard drum was outside the calibration range for this instrument.

GLOSSARY

ACCURACY - The closeness of measured value to the true value or to an accepted reference or standard value.

ASSAY COORDINATOR - Measurement facility point-of-contact responsible for accepting PDP samples and ensuring change of custody protocols are followed.

BIAS - The systematic error component of the total uncertainty, i.e., a constant positive or negative deviation of the method average from the correct value or an accepted reference value under specific measurement conditions.

INSTRUMENT BIAS - The bias of a particular instrument (or measurement system) under essentially ideal conditions, i.e., when all sample specific or matrix effects have been reduced to their practical minima. In this program the instrument bias will be approximated by the accuracy of the measurement for samples with the zero matrix or a benign matrix.

MATRIX DRUM - Department of Transportation, Specification 17C 208-L (55-gallon) steel drum acquired and serial numbered for the PDP, including a designed and manufactured drum insert that will simulate an expected waste matrix condition. A zero matrix drum is one containing only the supports for insertable standards.

NONDESTRUCTIVE ASSAY (NDA) - A technique that allows an item to be assayed without altering its physical or chemical form.

PDP SAMPLE - A blind sample prepared and sealed by the SPT for subsequent analysis by a measurement facility for qualification under the PDP. The PDP sample is composed of a 55-gallon matrix drum and insertable PDP standards. Matrix and source characteristics will representatively span nominal waste characteristics to include, but not be limited to, isotopics, plutonium concentration, (α,n) neutron effects, fission product contamination, interfering matrices, and source distribution.

PDP STANDARD - A radioactive source specifically prepared or acquired and certified for the PDP.

PDP STANDARDS CONFIGURATION ATTESTANT - A member of the two-man SPT responsible for verifying the proper emplacement of PDP sample standards and performing sample security-related procedures.

PDP STANDARDS CUSTODIAN - The lead member of the SPT responsible for coordination of onsite PDP sample preparations activities.

PRECISION - The sample standard deviation of several replicate measurements of the identical PDP sample under fixed conditions.

PROGRAM COORDINATOR - A CAO-designated organization that administers and coordinates PDP functions, such as PDP sample component preparation, SPT oversight, scheduling, scoring, and report summary generation.

STANDARD PREPARATION TEAM (SPT) - A two-person team, consisting of a PDP Standards Custodian and PDP Standards Configuration Attestant, that prepares and certifies measurement facility PDP samples. The SPT is responsible for ensuring that each PDP sample is prepared according to the PDP sample preparation procedure. In addition, the SPT will ensure proper disassembly and return to storage of all PDP sample components after

measurement facility analysis. The SPT will be designated by the site and approved by the Program Coordinator.

TOTAL ACCURACY - The closeness of the mean results obtained from a measurement system to the known or accepted reference or standard values. In this program Total Accuracy is estimated from the measurement results for PDP samples which include sources of variance in addition to those measured in the zero and noninterfering matrix drums, such as variable matrices, isotopic compositions, spatial distributions, contaminating radionuclides, and other interfering effects.

TOTAL UNCERTAINTY - The total measurement error from all sources of variance, including the precision, the instrument bias, and interference effects such as variable matrices, isotopic compositions, spatial distributions, contaminating radionuclides, and other interfering effects.

ZERO MATRIX - Specifies a matrix drum that contains only the supports for insertable standards.

REFERENCES

DOE. 1995a. *Performance Demonstration Program Plan for Nondestructive Assay for the TRU Waste Characterization Program.* DOE/CAO-94-1045, Revision 0, March 1995. Carlsbad, New Mexico, Carlsbad Area Office, U.S. Department of Energy.

DOE. 1995b. *Transuranic Waste Characterization Quality Assurance Program Plan.* DOE/CAO-94-1010, Revision 0, April 1995, Carlsbad, New Mexico, Carlsbad Area Office, U.S. Department of Energy.

INEL. 1996a. *Design of Phase I Radioactive Working Reference Materials for the Nondestructive Assay Performance Demonstration Program for the National TRU Program*, INEL-96/0245, Idaho Falls, Idaho, Lockheed Idaho Technologies Company.

INEL. 1996b. *Design of Matrix Drums for the Nondestructive Assay Performance Demonstration Program for the National TRU Program*, INEL-96/0129, Idaho Falls, Idaho, Lockheed Idaho Technologies Company.

PDP CYCLE 1 TESTS AT INEL

Y. D. Harker, G. W. Twedell
Idaho National Engineering Laboratory, Idaho Falls, ID 83415

ABSTRACT

The Idaho National Engineering Laboratory (INEL) is a participant in the nondestructive assay Performance Demonstration Program (PDP) as part of the U. S. TRU Waste Characterization Program. The PDP program was designed to help ensure compliance with the quality assurance objectives (QAO's) in the TRU Waste Characterization Program Plan. In June, 1996, cycle 1 of PDP program was completed at the Stored Waste Examination Pilot Plant (SWEPP) at INEL. The assay capability at INEL/SWEPP consists of a passive active neutron (PAN) radioassay system (for bulk fissile material assay) and a passive gamma spectrometry system (for isotopic mass ratio determination). The results from the two systems are combined to produce a single assay report which contains isotopic information (^{238}Pu, ^{239}Pu, ^{240}Pu, ^{241}Pu, ^{241}Am, ^{235}U) and derived quantities such as thermal power, thermal power density, total activity, alpha activity, TRU activity, TRU activity concentration, Pu equivalent Curies and fissile gram equivalent. The PDP cycle 1 tests were expected to test bias and precision of the assay systems under nearly ideal conditions; i.e., non-interfering matrices and little or no source self shielding. The test consisted of two drums in which the source loading was not known by the site. One drum was essentially empty and the other was filled with ethafoam. As per PDP's instructions, the tests were to be conducted using the same procedures and equipment that normally would be used by SWEPP to assay real waste drums. This paper will discuss the lessons learned from these tests and INEL's plans to improve the capabilities of the SWEPP assay systems.

INTRODUCTION

The waste assay system at the Stored Waste Experimental Pilot Plant (SWEPP) inside the Radioactive Waste Management Complex (RWMC) at the Idaho National Engineering Laboratory (INEL) consists of a second generation Passive Active Neutron (PAN) drum assay system[1] and a modified Canberra Q2 gamma spectrometry system. The PAN system is used to determine plutonium via spontaneous fission (passive mode) or thermal-neutron stimulated fission (active mode). Based on criteria specified in the PAN assay control file, the PAN output file lists as "the reported Pu mass" either a Pu mass derived from the passive mode; i.e, "passive Pu mass," or a Pu mass derived from the active mode; i.e., "active Pu mass." Gamma spectrometry is used to measure isotopic mass ratios. The Pu mass from the PAN system and the mass ratios from the gamma system are combined to provide an output file containing the isotopic inventory and other derived parameters for each drum measured at SWEPP.

In June, 1996, the cycle 1 tests of the Waste Isolation Pilot Plant (WIPP) Performance Demonstration Program (PDP) were completed at the Stored Waste Examination Pilot Plant (SWEPP) inside the INEL Radioactive Waste Management Complex (RWMC). Two drums were prepared by the PDP for these tests. The first drum, referred to as empty drum, contained a 90 mil polyethylene liner, approximately 3g of weapons grade plutonium and internal structural support. The second drum, referred to as the ethafoam drum, contained the 90 mil polyethylene liner, approximately 6g of weapons grade plutonium, ethafoam (trade name for pure polyethylene foam) and internal structural support.

The PDP cycle 1 measurements called for six replicate measurements on each drum using the facility's normal procedures for assaying contact handled waste drums. Unless modified by specific instructions, the SWEPP procedure called for a 200 second passive coincidence count and a 2000 neutron generator pulse differential die-away active count in the SWEPP PAN system. In addition, a passive gamma spectrum count in the SWEPP Gamma-Ray Spectrometry (SGRS) system is also required. This procedure was followed during the official cycle 1 tests at SWEPP. The PAN active Pu mass was selected as the reported mass and the results (combined with the gamma ratio data) were submitted to the PDP scoring office. Using the active mode results, INEL did pass the PDP cycle 1 test. In this particular test, the passive Pu mass was not used; however, there is a local concern because the INEL technical staff consider the passive mode as the more reliable of the two modes (active or passive) for Pu masses greater than $\approx$ 1g WGPu. It is the method of choice at INEL for many waste forms. The first concern is the inability of the PAN passive mode to meet the PDP relative precision criteria using the standard 200 second count time. The second concern is the apparent negative bias of the PAN passive mode results. This paper will discuss the findings of our review of the passive mode performance and the corrective actions implemented or planned.

QAO AND PDP PRECISION CRITERIA

Listed in Table 1 are the Quality Assurance Objectives (QAO) and PDP criteria for measured precision. The PDP criteria are much more restrictive and are designed to assure compliance with QAO criteria.

Table 1 - QAO and PDP criteria for measured precision.[a]

Activity Classification	Alpha Range	QAO (rsd)[b]	PDP (rsd)[c]
Low	0.004 - 0.04 Ci (0.05g - 0.5g)[d]	20%	9.6%
Mid-Low	0.04 - 0.4 Ci (0.5g - 5g)[d]	15%	7.2%
Mid-High	0.4 - 4.0 Ci (5g - 50g)[d]	10%	4.8%
High	> 4.0 Ci (> 50g)[d]	5%	2.4%

(a) Reference 2: *Performance Demonstration Program Plan for Nondestructive Assay for the TRU Waste Characterization Program.* DOE/CAO-94-1045, Revision 0, March 1995.
(b) Based on 15 replicate measurements using a non-interfering matrix.
(c) Based on 6 replicate measurements using a non-interfering matrix.
(d) Parentheses contain the approximate Pu mass range based on nominal WgPu decayed 15 years.

The definition of measured relative standard deviation (rsd) is given in Equation (1). For the QAO tests the number of replicate measurements is 15 whereas for the PDP tests the number of replicate measurements is 6.

$$rsd = \frac{\sqrt{\dfrac{\sum_{i=1}^{n} (x_i - x_{av})^2}{(n-1)}}}{x_{av}} \qquad (1)$$

where: i is the individual measurement index,

n is the number of replicate measurements,

x_i is the individual measurement value and

x_{av} is the mean of the n measurements as given in equation 2.

$$x_{av} = \frac{\sum_{i=1}^{n} x_i}{n} \qquad (2)$$

PASSIVE MODE RESULTS

The official PDP cycle 1 tests used 200 second passive count times. Following the PDP test, additional replicate measurements were performed using the same PDP drums and loadings with passive count times of 100 seconds, 600 seconds and 1200 seconds. For all these assay measurements, the active count remained at 2000 neutron generator pulses per active count. Listed in Tables 2 and 3 are results for the empty drum and ethafoam drum, respectively. As can seen from these tables the 100 second and 200 second count time results do not meet the PDP relative precision criteria. Also from these tables it is apparent that the results from the 600 second and 1200 second counts do meet the PDP precision criteria. The obvious solution to meeting the precision requirements is to count longer. The question is how much longer? It is also evident that the PAN generated error based on counting statistics is a good indicator of the likelihood of meeting the precision requirements.

From a chi-squared analysis of the precision data for fifty measurement cases involving Pu contaminated graphite molds in 208 liter drums[3], it was determined that count time of 1200 seconds would be able to meet the PDP precision criteria with a $>95\%$ confidence. Even with the longer count time the chi-squared analysis indicates that a conservative lower mass limit for the passive mode should be 5g WGPu. This is significant because the standard definition of detection limit for this mode would be $\approx$ 1g WGPu. In effect the PDP criteria for precision has redefined the detection limit for the passive mode. The 1200 second and 5g WGPu limits do assure compliance with the PDP precision criteria. On the other hand for compliance with the QAO precision criteria in Table 1 would only require a count time of 600 seconds and a lower mass limit would be $\approx$ 3g WGPu. The impact of the more restrictive PDP criteria is to reduce SWEPP assay productivity and limit the applicable mass range of the passive mode much more than would be required to comply with the QAO requirements directly.

Table 2 - RSD data for PDP empty drum and loading.(a)

count time (sec)	passive Pu mass (g)	meas. s. dev. (g)	meas. rsd (eq. 1) (%)	PAN count s. dev. (g)	PAN count rsd (%)
100	3.382	0.281	8.30	0.378	11.2
200	3.138	0.317	10.1	0.257	8.18
600	3.247	0.109	3.36	0.158	4.88
1200	3.300	0.123	3.72	0.130	3.94

(a) PDP criterion for measured rsd is 7.2%

Table 3 - RSD data for PDP Ethafoam drum and loading.(b)

count time (sec)	passive Pu mass (g)	meas. s. dev. (g)	meas. rsd (eq. 1) (%)	Avg.PAN count s.dev. (g)	Avg.PAN count rsd (%)
100	4.353	0.500	11.5	0.630	14.5
200	4.180	0.294	7.03	0.458	11.0
600	4.053	0.133	3.27	0.277	6.83
1200	4.358	0.229	5.25	0.222	5.11

(b) PDP criterion for measured rsd is 4.8%

As a result of the PDP Cycle 1 test, the count time for the passive mode was changed from 200 seconds to 1200 seconds. In the next version of the PAN acquisition software[4] an internal count time prescription based on counting statistics will be implemented. This will eliminate the need for specifying a fixed count time and for specifying the applicable mass range.

The data indicating bias of the passive mode are given in Table 4. In this paper, bias refers to the difference between the reported PAN Pu mass and the known Pu mass. In the PAN passive mode there are two Pu mass measurements reported; i.e., the "shielded Pu mass" which comes from the short (35μs) coincidence gate mode and the "system Pu mass" which comes from the long (250μs) coincidence gate mode. The input signals for the short-gate coincidence mode are the counts coming from the "shielded" detector banks. The input signals for the long-gate coincidence mode are the counts coming from all detectors in the

PAN assembly, which includes the shielded detectors mentioned above and the "bare" detectors. All detectors used in the PAN detection system are ^{3}He detectors surrounded by a polyethylene moderator. The shielded detector assembly has a layer of cadmium and a layer of borated rubber surrounding the detector plus polyethylene, whereas the bare detector assembly has no thermal neutron shield. The gate widths of the two coincidence modes reflect the difference in die-away time between the two detector assemblies. The current PAN analysis software[5] selects either the "shielded Pu mass" or the "system Pu mass" as the "passive Pu mass" based on which mass has the smaller relative error. In the case of the results presented in Table 4 both mass estimates are given to show the individual bias errors. In the PDP cycle 1 test, the PAN analysis software reported the "system Pu mass" as the "passive Pu mass" for all measurements.

Table 5. - PAN Passive Mode Pu Mass versus Known Mass for PDP Cycle 1 Test.

PDP Drum	Known Pu mass (g)	Shielded Pu mass[a] (g)	Shielded Pu mass rel.bias (%)	System Pu mass[a] (g)	System Pu mass rel.bias (%)
#1[b]	3.69	2.5(±46%)	- 32%	3.15(±10%)	- 15%
#2[c]	6.23	3.4(±25%)	- 46%	4.18(±7.0%)	- 33%

(a) Values in parentheses are the rsd's for six replicate measurements (equation 1).
(b) Drum (208 liter) with a 90 mil polyethylene liner, PDP sources, PDP source containment and positioning hardware.
(c) Drum (208 liter) with a 90 mil polyethylene liner, filled with ethafoam (polyethylene foam), PDP sources, PDP source containment and positioning hardware.

As can be seen from the data presented in Table 5 there is a consistent negative bias associated with the PAN passive Pu mass. This negative bias was also observed in INEL's total uncertainty evaluation task[6,7]. It is also apparent that the bias magnitudes are greater for PDP drum #2 than they are for PDP drum #1 and that they are also greater for the shielded Pu masses than they are for system Pu masses. To understand the sources of the bias, a review of the PAN analysis software was performed and a computer simulation using models developed for the total uncertainty task[7] was applied to the PDP cases.

In the PAN analysis software there are routines used generate correction factors which

are expected to compensate for matrix and source absorption to the PAN response.[1,5] These correction factors multiply the net coincidence rate such that a correction factor of unity means no correction is applied. A correction factor greater than one indicates that there are matrix/source affects which reduce the measured coincidence rate. Therefore, a correction factor greater than one must be applied to compensate for the loss in coincidence response. For the passive mode these correction factors generally range between 1 and 2. For example, predominately graphite waste forms are considered the most benign (i.e., non-interfering) waste in the SWEPP inventory. Historically, the ranges for the graphite correction factors are: 1.04 to 1.68 for the short-gate (shielded) coincidence mode and 1.05 to 1.41 for the long-gate (system) coincidence mode. For PDP drum #1 (empty) these correction factors are: 1.21 for the short-gate (shielded) coincidence mode and 1.12 for the long-gate (system) coincidence mode. As expected, the empty PDP drum is in the benign range as defined from the graphite data. On the other hand, the correction factors for PDP drum #2 (ethafoam) are: 2.17 for the short-gate coincidence mode and 1.78 for the long-gate coincidence mode. Since ethafoam was supposed to be a benign matrix, it was not expected that the correction factors would be so large. Compared with graphite, ethafoam is not as benign as originally thought by the PDP organizing committee. Strictly speaking, the requirement for a non-interfering matrix was not met in the case of ethafoam; therefore, the PDP and QAO performance criteria should not be applied to measurements involving the PDP ethafoam drum.

The Monte Carlo Neutron Photon (MCNP) code and model as used in the INEL uncertainty analysis task[7] calculates the basic detector efficiency (counts per source neutron). It also provides further detail in terms of the detector die-away response; i.e., counts per unit versus time following a fission event. The MCNP results can be applied in combination with the PAN measured coincidence rate to calculate a derived "MCNP Pu mass" using equation 3 below.

$$Pu\ Mass = \frac{(net\ coinc\ rate)\ M_{240}}{MF_{240} N_a \lambda_{sf} \epsilon^2 \sum_{\nu=1} G_\nu \nu(\nu-1) \int_0^\infty \eta(t)\,dt \int_{t+t_d}^{t+t_d+T} \eta(t')\,dt'} \qquad (3)$$

where: the net coincidence rate is that reported by the PAN analysis corrected for accidental coincidences and counting loss,
M_{240} is the atomic mass for ^{240}Pu,
MF_{240} is the mass fraction for ^{240}Pu,
N_a is Avogadro's number,

λ_{sf} is the spontaneous fission decay constant for ^{240}Pu,
ϵ is the detector assembly efficiency and is calculated from the MCNP model,
ν is the number of neutrons per fission,
G_ν is the probability of a fission producing ν neutrons,
$\eta(t)$ is the normalized time distribution of the detector response following a fission and is calculated by the MCNP model,
t_d is the fixed delay between detector pulse and the opening of the coincidence gate and T is the coincidence gate width.

The results of these calculations are given in Table 6. If one compares the results in Table 6 with those given in Table 5, one can see a definite improvement in the bias using the MCNP efficiencies and die-away responses rather than the PAN correction factor algorithms. These data support the hypothesis that there is nothing wrong with the basic passive coincidence measurement and its interpretation. As expected, the problem lies in the ability to properly correct for the matrix. For the PDP case, the major contributor to the matrix effect has to be the hydrogen content in the matrix (particularly in the ethafoam drum). Since ethafoam has a very low-density, one would not expect it would produce such a pronounced effect on the passive mode response. In analyzing the MCNP results it is apparent that the moderating effect of the hydrogen not only changes the overall detector efficiency, ϵ, but also the die-away, $\eta(t)$, to the point that the double integral in equation 3 is affected by the presence of hydrogen. For the PDP case where the matrix contents of the drums are known exactly the proper corrections can be determined by the MCNP calculation. This is not the case for real waste assays. There is still a need for "generic" correction factor analysis algorithms like those used in the PAN analysis.

At INEL, the approach for correcting for the observed bias deficiencies in the PAN results is to maintain the basic PAN analysis and apply a waste form specific bias correction to the end results. The bias corrections are being developed as part of the INEL total uncertainty task[6,7]. It is planned that waste form specific bias corrections for both passive and active modes will be developed and used in future PAN analyses.

Table 6. - MCNP Passive Mode Pu Mass[a] versus Known Mass for PDP Cycle 1 Test.

PDP Drum	Known Pu mass (g)	MCNP Shielded Pu mass[b] (g)	MCNP Shielded Pu mass rel.bias (%)	MCNP System Pu mass[b] (g)	MCNP System Pu mass rel.bias (%)
#1[c]	3.69	3.2(±45%)	- 13%	3.56(±9.1%)	- 3.5%
#2[d]	6.23	6.1(±25%)	- 2.1%	6.25(±9.3%)	+ 0.3%

(a) Calculated from equation 3 using PAN net coincidence rate and MCNP model values.
(b) Values in parentheses are the rsd's for six replicate measurements (equation 1).
(c) Drum (208 liter) with a 90 mil polyethylene liner, PDP sources, PDP source containment and positioning hardware.
(d) Drum (208 liter) with a 90 mil polyethylene liner, filled with ethafoam (polyethylene foam), PDP sources, PDP source containment and positioning hardware.

CONCLUSIONS

The PDP Cycle 1 tests have produced some changes in the SWEPP operations. To meet the precision criteria, the passive mode count time for normal waste drum assay was changed from 200 seconds to 1200 seconds in those cases where the passive mode is either the method of choice or an option. There are those cases, e.g., the solidified waste forms (sludge), for which the passive Pu mass is not an option. In those cases, the passive mode is still needed by the PAN analysis routine to determine a moderator index which is used to calculate the active mode correction factor. However, the moderator index is based on singles count rates rather than coincidence count rates; therefore, the 200 second passive mode count time is sufficient to arrive at the needed precision for the moderator index. As a result, the 200 second count time will continue to be used when the passive mode is not the method of choice.

In addition to the longer passive mode count time, the lower limit of passive mode applicable mass range has been increased from ≈ 1g WGPu to ≈ 5g WGPu. The count time and mass limit changes are interim measures. They are very conservative in terms of meeting the PDP precision criteria.

In the next generation of the PAN assay control software,[4] the interim measures will be replaced by a routine which will, in real time, calculate the count time needed to achieve the applicable precision requirement. In the assays where the passive and active modes are both options, the switch from reporting the passive mass to reporting the active mass will no longer be based on a fixed Pu mass lower limit (e.g., 5g WGPu). Rather, it will be based on whether the applicable precision requirement can be met by the passive mode within maximum allowable passive count time.

The PDP Cycle 1 tests provided more evidence that there are bias deficiencies associated with the PAN passive mode assay. As a part of the INEL total uncertainty task, waste form specific bias corrections are being determined.[6,7] These bias corrections will be applied at the end of the PAN analysis to further compensate for bias associated with a particular waste form.[4]

On a general note, it has been long been known that the analysis of data from neutron based assay systems has to account for moderation effects, particularly in matrices with high hydrogen density. The PDP ethafoam drum test underscores this premise and emphasizes that moderation can be factor even in low-density matrices containing hydrogen. Since a large fraction of the assays involve low density/hydrogen bearing waste forms, developers and operators of neutron based assay systems need to give more attention to this effect.

ACKNOWLEDGEMENTS

This work was supported by the U. S. Department of Energy Office of Environmental Restoration and Waste Management. Project management was under the direction of the INEL Transuranic Waste Department in support of the Stored Waste Examination Pilot Plant (SWEPP) Operations. Technical direction and support was provided by the INEL Nuclear and Radiation Physics Department.

REFERENCES

1. J.T. Caldwell, et. al., "The Los Alamos Second-Generation System for Passive and Active Neutron Assay of Drum-Size Containers," Los Alamos National Laboratory Report LA-10774-MS (September 1986).

2. *Performance Demonstration Program Plan for Nondestructive Assay for the TRU Waste Characterization Program.* DOE/CAO-94-1045, Revision 0, March 1995.

3. Y.D. Harker, "Modified SAS Selection Criteria," Idaho National Engineering Laboratory Engineering Design File EDF-RWMC-923, (December,1996).

4. L.V. East, "SWEPP Assay System Software - An Update," Proceedings of 5th Nondestructive Assay and Nondestructive Examination Waste Conference, Salt Lake City, UT (January 14-16, 1997).

5. E.S. Marwil, S.D. Matthews, G.K. Becker, "SWEPP Assay System Software," Proceedings of the Nondestructive Assay and Nondestructive Examination Waste Conference, Pocatello, ID (February 14-16, 1994), U.S. DOE report CONF-940216), page 137.

6. L.G. Blackwood, Y.D. Harker, T.R. Meachum, W.Y. Yoon, "Passive Active Neutron Radioassay Measurement Uncertainty for Combustible and Glass Waste Matrices," Proceedings of the 5th Nondestructive Assay and Nondestructive Examination Waste Characterization Conference, Salt Lake City, UT (January 14-16,1997).

7. Y.D. Harker, L.G. Blackwood, T.R. Meachum, "Uncertainty Analysis of the SWEPP Drum Assay System for Graphite Content Code 300," U.S. DOE Technical report INEL-95/0475, (September, 1995).

NDA PDP PROGRAM PuO_2 INCREASED PARTICLE SIZE SPECIFICATION AND DESIGN

R.S. Marshall and D.P. Taggart
Los Alamos National Laboratory, MS G740, Los Alamos, New Mexico 87544

G.K. Becker and W.Y. Yoon
Lockheed Martin Idaho Technologies, Inc., INEL, PO Box 1625, Idaho Falls, Idaho 83515-2114

ABSTRACT

Provisions in the National TRU Program Quality Assurance Program Plan require an assessment of performance for nondestructive waste assay (NDA) systems employed in the program. This requirement is in part fulfilled through the use of Performance Demonstration Programs. In order to optimize the quality and quantity of information acquired during a given Performance Demonstration Program cycle, the assessment employed is to be carefully specified and designed. The assessment must yield measurement system performance data meaningful with respect to NDA system capability to accommodate attributes of interest known to occur in actual waste forms. The design and specification of the increased particle size PuO_2 PDP working reference materials (WRMs) is directed at providing a straightforward mechanism to assess waste NDA system capability to account for biases introduced by large PuO_2 particles. The increased particle size PuO2 PDP WRM design addresses actual waste form attributes associated with PuO_2 particle size and distributions thereof, the issue of a known and stable WRM configuration and equally important appropriate certification and tractability considerations.

INTRODUCTION

Nondestructive waste assay methods are used in the National TRU Waste Characterization Program to determine the mass and associated alpha activity of waste entrained radionuclides. The capability and performance of waste NDA systems employed in the Program must comply with requirements as set forth in the TRU Waste Characterization Program Quality Assurance Program Plan (QAPP).[1] Compliance with QAPP and NDA requirements and objectives are in part assessed through the use of a Performance Demonstration Program (PDP). All waste characterization facilities that intend to ship TRU waste to the Waste Isolation Pilot Plant (WIPP) are required to participate in the NDA PDP. The NDA PDP Plan provides a means to institute a measurement routine to yield quantitative performance data for key NDA system parameters under specified conditions. The QAPP and NDA PDP, employed in conjunction, are designed to ensure that nondestructive waste assays performed to characterize the radionuclide content in containerized

TRU waste, produce data of known and defensible quality. The NDA PDP also allows a complex-wide assessment of NDA system performance relative to a common basis.

Implementation of the NDA PDP plan for the 55 gallon type container requires a carefully specified apparatus. The NDA PDP measurement apparatus consists of 55 gallon matrix drums and insertable radioactive standards. The PDP radioactive standard(s), hereafter referred to as working reference materials (WRMs), are designed to be configured with matrix drums in a particular manner to test system performance with respect to the objectives of a given test cycle. The Increased Particle Size (IPS) WRM set is specifically designed to allow NDA PDP program assessment of bias induced in waste NDA measurement systems by large PuO_2 particles, i.e. greater than 400 microns diameter, or the accumulations of numerous smaller particles known to exist in actual waste forms. The initial task in developing IPS PuO_2 WRMS is to determine a nominal increased PuO_2 particle size which yields and NDA system bias commensurate with that observed in measurement of actual waste configurations. Based on the specified particle size, fabrication and assembly techniques were developed at the Los Alamos National Laboratory to produce large particles of PuO_2 and WRMs possessing the attribute for use in the program. The specification, design and fabrication of IPS WRMs is addressed in this paper.

SPECIFICATION

The specification of a PuO_2 particle size which yields a bias representative of actual waste forms was determined through the evaluation of NDA system responses where bias resulting from increased particle sizes and/or accumulations of numerous smaller particles effectively inducing the same bias, is evident. For this purpose, the response of a commonly employed passive/active neutron NDA system to a large population of actual waste drum measurements, was evaluated. The approach for extracting the magnitude of the IPS bias representative of actual waste drum measurements, consisted of identifying a population of drums spanning several waste types and evaluating the depression in the active mode response relative to the passive mode response. This technique required several steps to filter out drums with bias and precision sources *not* due to increased PuO_2 particle size or agglomerations of numerous smaller particles.

The first step in quantifying the IPS bias source was to select several waste forms which have increased PuO_2 particle sizes by observation of real time radiography images or from information on the waste generation process. It was important that these selected waste types not have exceedingly convoluted bias and precision sources that complicate the extraction or bounding of the increased particle size bias effect. Waste types selected for assessing PuO_2 particle size effects consisted of graphite, three different combustibles classifications, and metals. Next it was

necessary to identify in this population drum assays where the passive neutron mode measurement not significantly impaired by known interferences. Drum assays exhibiting excessive moderator and absorber properties were filtered our, leaving approximately 3,000 passive/active neutron measurements from which to derive an estimate of a nominal IPS induced bias.

With this select population, the IPS bias was determined by taking the ratio of the passive mass assay to the active mass and averaging this parameter over the population. This ratio will in actuality reflect the complete range of fissile material physical configurations from diffuse distributions of Pu atoms to local accumulations of fine particles to large individual clumps of Pu —and any combination thereof—existing in the population under study. The range of the IPS bias parameter estimate, derived from the conditioned population, was 3.0 to 6.5. This range estimate was discussed with waste NDA individuals at other sites to ensure that the value was reasonable and reflected experience with waste forms at these facilities. They concurred with the range, and a value was selected from the range as the basis for determining PuO_2 particle sizes which would yield such a bias. It should be noted that it is not critical that an exact representation of the waste-form derived IPS value be determined; a range is sufficient. It is important that the PDP program include a test of NDA system capability to account for this bias source and that the magnitude of the bias represented in PDP assessment apparatus, i.e., WRMs, be reasonable.

Having determined a value of IPS bias, it is necessary to use this information to determine a particle size which would induce a bias of this magnitude for performance assessment purposes. The technique used for this purpose was Monte Carlo Neutron Photon (MCNP) modeling.[3] The approach consisted of computing the number of fission-induced neutrons produced by a thermal neutron interrogating spectrum (Maxwellian) incident on a PDP WRM model from all directions. The computations were performed for both homogeneous PuO_2/diatomaceous earth mixture and heterogeneous PuO_2 particle(s) distributed in diatomaceous earth cases. Several heterogeneous PuO_2 particle(s)/diatomaceous earth configurations were modeled to span the WRM-mass range of interest. To simplify modeling efforts, the particles were represented in a spherical geometry. The MCNP PDP WRM model consisted of the homogeneous mixtures and heterogeneous distributions for low burnup, weapons grade PuO_2 within the dual encapsulation cylinder specifications and dimensions of the standard PDP WRM.

An evaluation of the active mode, thermal-neutron, induced fission-yield depression due to increased PuO_2 particle sizes requires a baseline definition. The baseline for comparing an IPS-induced active-mode response depression is an "infinite dilute" case of PuO_2, 0.001 grams, distributed uniformly throughout the WRM diatomaceous earth diluent. To obtain baseline

response data, an MCNP model was constructed to the specifications of the actual PDP WRM encapsulation assembly containing the homogeneous mixture configuration. The number of thermal-neutron interrogation, induced-fission neutrons yielded from this model was then computed to give the baseline yield. Next, a model of the heterogeneous IPS WRM containing spherical PuO_2 particles distributed in diatomaceous earth was constructed. A number of heterogeneous cases were modeled and computed for WRMs through the mass range of 0.25—16.0 grams PuO_2 for three different spherical particle sizes.

Data generated from the set of homogeneous and heterogeneous MCNP WRM cases are plotted in Figure 1, illustrating the reduction in the number of fission-induced neutrons per PuO_2 mass as compared to the homogeneous "infinite dilute" baseline case. This ratio is referred to as the IPS induced self-shielding factor. As is evident from the plot, the ratio for the homogeneous case WRMs is nearly 1.0 at the low, 0.25 gram PuO_2 loading, and drops to approximately 0.75 at 16.0 grams. For the heterogeneous IPS cases, the same self-shielding factor was calculated over the 0.25—16.0 mass range for three different spherical PuO_2 particle sizes. For the 2,000 micron spherical particle heterogeneous case, the self-shielding factor is approximately 0.25 at 0.25 gram PuO_2 loading and remains essentially unchanged to the 16.0 gram mass loading. For the 2,500 and 3,000 micron spherical particle size case, the self-shielding factors are approximately 0.22 and 0.19 respectively, and are effectively unchanged over the 0.25—16.0 gram mass range. It is noted in the Figure 1 plot of self-shielding factors versus PuO_2 mass for the heterogeneous cases that the span over 2,000 to 3,000 micron particle sizes induces a self-shielding factor variation of approximately 6% at a given mass loading. The calculated self-shielding factors have statistical uncertainties of up to 3% arising from limited computer run time.

It is concluded from Figure 1 that (1) PuO_2 particles within the range of 2,000 to 3,000 micron diameter yield an IPS bias commensurate with the waste form bias range determined in the 3,000 drum study, and (2) the self-shielding factor resulting from 2,000—3,000 micron particles does not significantly vary over the WRM weapons grade PuO_2 mass loading range of 0.25 to 16.0 grams. Hence, the active thermal-neutron interrogation-mode bias is principally due to individual particle size dimension and not large numbers of such particles.

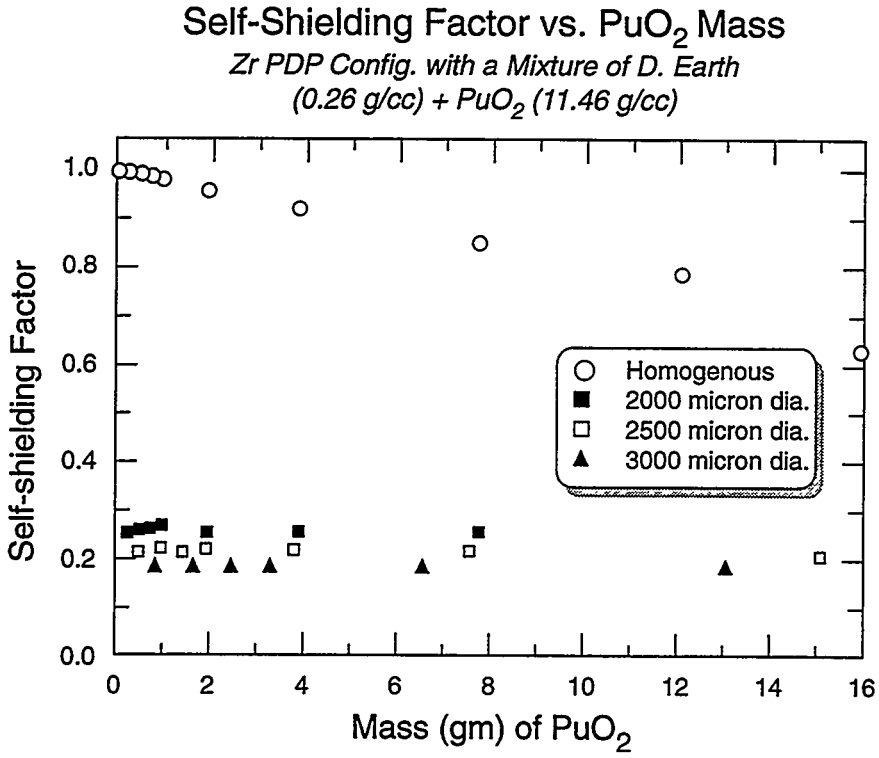

Figure 1. Plot of self-shielding factors verses PuO_2 mass.

To this point, discussion has centered on an IPS bias relative to neutron measurement modalities. It is constructive to evaluate the impact of the particle size determination with regard to gamma-based nondestructive assay techniques. To evaluate this effect, MCNP runs were performed to compute the number of gammas in a specific energy range leaving the surface of the WRM cylinder per gamma of the same energy originating within the PuO_2/diluent for both the homogeneous and heterogeneous WRM model cases. As an approximate indicator of this effect, we examine the ratio of 160 Kev gammas leaving the WRM surface per gamma originating in the homogeneous WRM model to that same parameter for the heterogeneous 2,000 micron diameter PuO_2 particle/diluent case. For a 0.24 gram PuO_2 WRM mass loading, which in the heterogeneous case is equivalent to five particles, this homogeneous/heterogeneous model ratio for 160 Kev gamma is 3.2. At a two gram WRM PuO_2 loading, approximately 40 particles for the heterogeneous configuration, this same ratio changes to approximately 3.3. For the 414 Kev gamma line at the 0.24 gram PuO_2 WRM mass loading, under these same conditions, the ratio is much less at 1.2. At two gram WRM PuO_2 loading, this same ratio is also about 1.2. In either case, increased PuO_2 particles sizes depress the yield of gammas relative to the homogeneous case, thus requiring that the gamma based NDA technique account for this effect.

DESIGN

The increased particle size (IPS) WRM specification required that large particles (granules) of PuO_2 with very accurately known mass be distributed within stainless steel cylindrical containers in a well known, uniform manner. The distribution is to be stable during normal transportation and usage. The Pu content of the IPS WRMs span a range from the sub-gram level to a few tens of grams. WRMs previously fabricated for the PDP were produced by blending finely divided PuO_2 powder in a diatomaceous earth matrix and encapsulating this mixture into cylindrical containers. This blended mixture was tested and found to be very uniform. However, IPS WRMs containing sub-grams to a few grams of Pu as millimeter-size PuO_2 granules would contain relatively few (20-50) granules, hence the established PuO_2-diatomaceous earth blending method might produce some WRMs in which the PuO_2 granules would not meet uniformity specifications. An alternate method for distributing the PuO_2 granules uniformly throughout the PDP cylinder volume was selected. This method uses a graphite felt material into which the PuO_2 granules are embedded. The graphite felt is purchased in 1/4 inch thick sheets and is readily cut into disks. The disks are drilled or punched to form holes into which PuO_2 granules are inserted. The impregnated disks are be stacked in the cylindrical container to yield a stable and uniform array of PuO_2 granules suspended in a low density matrix which does not appreciably interfere with either neutron- or gamma-based NDA measurements.

PuO_2 PARTICLE AND PROTOTYPE WRM FABRICATION

A. PuO_2 Preparation. PuO_2 is made in US facilities by either oxidizing Pu metal in air or by precipitating a Pu compound (oxalate or peroxide) from a solution and then calcining the compound in an air atmosphere. Both methods produce a fine PuO_2 powder with particles distributed through a range of typically 5 to 500 microns. The larger particles are usually quite fragile, breaking into smaller particles upon mechanical handling. We felt that large and mechanically tough PuO_2 particles could be made using methods employed to make uranium oxide or mixed Pu - U oxide (MOX) reactor fuel pellets. The fuel pellets are prepared by adding a small amount of organic binder to U oxide or MOX powder, pressing the powder in cylindrical molds at ~1,500 psi pressure, and then calcining the fuel pellets at 1600 ^{o}C for six hours. The resulting fuel pellets are extremely 'tough' and have a density above 90% of the theoretical density. The reactor fuel R&D group at the Los Alamos Plutonium Fabrication Facility (TA-55) had, as of October 1996, not made 'straight' PuO_2 fuel pellets, but agreed it would be feasible to do so and developed a successful method. After preparation, the PuO_2 fuel pellets (approximately 5 mm diameter and 10 mm long) were crushed by forcing through appropriately sized sieves, producing PuO_2 granules

meeting the size requirements determined via the MCNP modeling. Figure 2 is a photograph of the PuO_2 granules prior to final sizing. These granules have proven to be very 'tough' in that they can be stressed with tweezers or dropped with no evidence of fracturing. This toughness allows the granules to be inserted into holes in the graphite felt disks without concern of the granules breaking during fabrication or subsequent transportation or use.

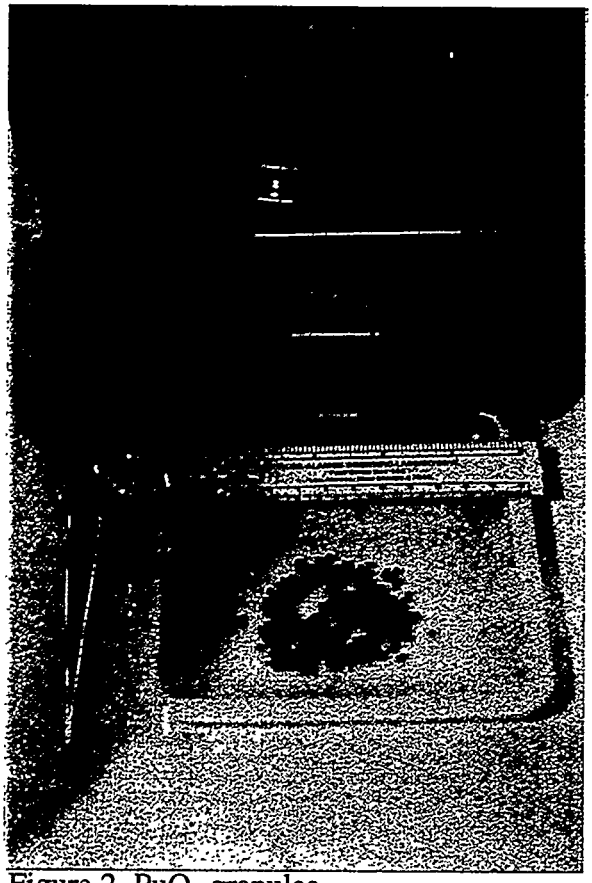

Figure 2. PuO_2 granules.

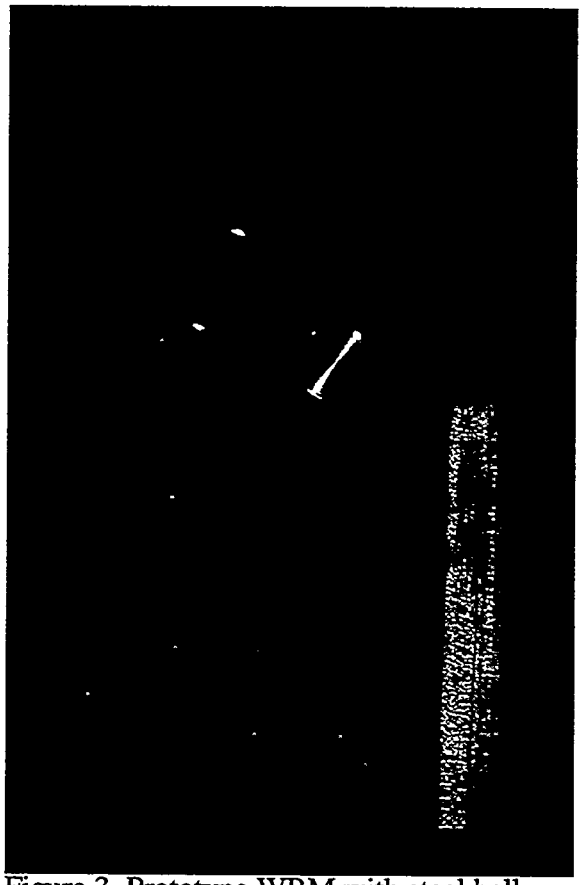

Figure 3. Prototype WRM with steel balls representing PuO_2 granules.

B. Prototype Fabrication. Of concern was whether or not the graphite disks would adequately retain the PuO_2 granules during the vibration and shock a WRM might experience during transportation and routine handling. To evaluate this stability, a prototype WRM was made using steel balls to represent PuO_2 granules. The steel balls allowed a prototype WRM to be fabricated 'on the bench' and transported and tested without the complications introduced by a WRM containing plutonium. Figure 3 is a photograph of the prototype constituents including the 1.75 inch O.D. steel cylinder plus its endcap, six graphite disks with embedded steel balls and 35

graphite disks used to space the six 'loaded' disks in a uniform vertical array. The six 'loaded' disks were prepared by drilling a ~0.17 inch hole through the disk and then pushing a 0.185 inch diameter steel ball into the hole. The graphite felt is a pliable, fibrous material that allowed the steel ball to be inserted quite gently. The felt fibers then fold in around the ball and hold it in place. The disks could be turned upside down without the steel ball falling out. To load the cylinder, five unloaded disks were introduced into the open end of the cylinder and pressed to the bottom with a large diameter rod. Then a loaded disk was introduced and pressed in place. This process was continued until the final 5 unloaded disks were introduced. Then the steel endcap was pressed in place and tack welded at four radial positions to complete the prototype assembly.

C. Prototype Testing. X-Ray imaging was used to evaluate the ability of the graphite array to withstand shock without unacceptable movement of the steel balls in the WRM configuration. An x-Ray image was photographed before subjecting the cylinder to shock. A segment of steel wire was affixed to the outside of the cylinder to provide a reference mark in the x-Ray image. Next the cylinder was dropped onto a hard floor from a height of 9 inches (the cylinders length) 15 times to simulate abusive treatment to a WRM. A second x-Ray image was photographed and then the cylinder was dropped 15 times from a 9 inch height onto it's side (same rotational orientation each drop). A third x-Ray image was photographed. Figure 4 shows the three x-Ray images. Note in the second photograph, the steel balls did move 'down' 5-10 mm in the tube after it was dropped. The third photograph shows two movements: first, the steel balls returned part way to their original axial position, and second, the steel balls moved slightly (~2 mm) towards the side of the tube receiving the impact upon dropping.

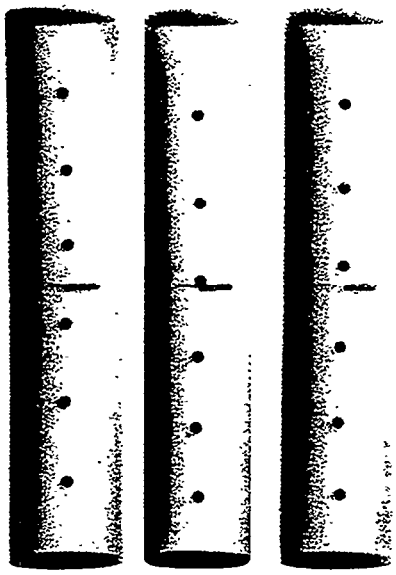

Figure 4. X-ray images of prototype WRM before and after drop testing.

It was apparent that the graphite disks were compressing upon the vertical dropping of the cylinder and that they were not decompressing after the drops were completed. Since the graphite disks were cut ~2 mm larger than the steel cylinder inside diameter, it appeared that friction provided by the somewhat oversized graphite disks prevented the disks from returning to their original position after each drop. A second prototype was prepared using graphite disks that were ~1 mm smaller in diameter than the cylinder inside diameter. This cylinder received the same testing as the first cylinder, and Figure 5 shows the results of this test. Note the second photograph shows a slight movement of the steel balls...averaging about 2 mm, and the third photograph shows a 'sideways' movement of the steel balls of 1 mm.

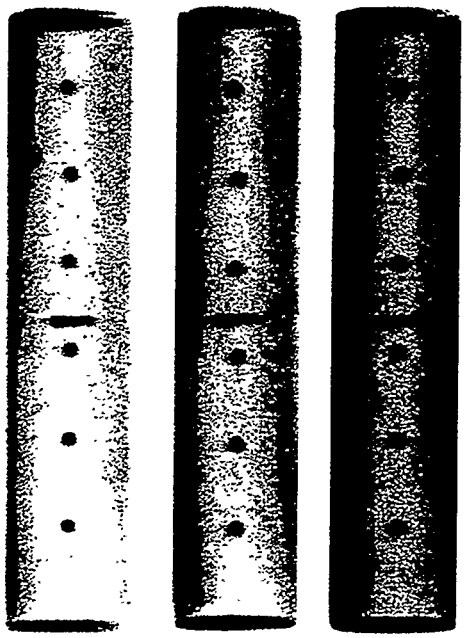

Figure 5. X-ray images of prototype WRM with loose fitting disks before and after drop testing.

The 1-2 mm movement is unlikely to introduce an observable bias to any known waste NDA measurement method used to determine the plutonium content of a WRM. Further, the steel balls had a mass approximating that of the PuO_2 granules on the most heavily loaded graphite disks, hence even less movement is expected in all but the most heavily loaded WRMs. The IPS WRMs will be fabricated using graphite disks (blanks and loaded with PuO_2) with diameter ~1 mm less than the cylinders.

Further stability tests will be conducted after the prototype WRM is subjected to vibrational stress simulating truck transportation of WRMs over a 2000 mile distance.

CONCLUSION

Through the techniques delineated, an increased PuO_2 particle size has been specified to yield and NDA system bias source reasonably approximating that of actual waste forms. Once specification of the particle size was complete, a means to produce PuO_2 particles within this range and subsequently secure them into a PDP WRM in a stable manner was devised. The completed WRM, configured in this manner, will be a valuable PDP program assessment tool for the evaluation of NDA system accounting and management of the self-shielding and self-attenuation bias source known to occur in waste forms

REFERENCES

1 Transuranic Waste Characterization Quality Assurance Program Plan, Revision 0, CAO-94-1010, April 30, 1995, U.S. Department of Energy, Carlsbad Area Office, National TRU Program Office.

2 Performance Demonstration Program Plan for Nondestructive Assay for the TRU Waste Characterization Program, Revision 0, CAO-94-1045, March 1995, U.S. Department of Energy, Carlsbad Area Office.

3 MCNP computations performed by W. Yoon of Lockheed Martin Idaho Technologies Company, Idaho National Engineering Laboratory. PO Box 1625, Idaho Falls, Idaho 83515-2114

SAMPLING AND VERIFICATION METHODS FOR THE UNCERTAINTY ANALYSIS OF NDA AND NDE WASTE CHARACTERIZATION SYSTEMS

Larry G. Blackwood
Idaho National Engineering Laboratory, Idaho Falls, ID 83415

ABSTRACT

The use of nondestructive assay (NDA) and nondestructive evaluation (NDE) systems in critical waste characterization applications requires a realistic assessment of the uncertainty in the measurements produced. The stated uncertainty must include the potential effects of a variety of complicating factors external to the system itself on the expected bias and precision of measurements. These factors include material heterogeneity (matrix effects), fluctuating background levels, and other variable operating conditions. In this context, uncertainty figures based on the application of the usual propagation of error methods to data obtained from controlled laboratory experiments using standard test materials can grossly underestimate the expected error. This paper reviews the standard propagation of errors method of uncertainty analysis, discusses some of its limitations, and presents an alternative approach based on sampling and verification. Examples of the application of sampling and verification methods to measurement systems at the Idaho National Engineering Laboratory are described.

INTRODUCTION

Evaluating the uncertainty of a complex NDA or NDE system presents a number of challenges. While, the intricate makeup of the system itself can make it difficult to adequately characterize performance, further complications occur when external factors must be considered. Such is the case, for example, with radioassay systems used to certify waste for shipment to the Department of Energy's (DOE) Waste Isolation Pilot Plant. The DOE requires that uncertainty evaluations for these systems include the effects of waste matrix parameters and other external factors having potential effects on system performance. Section 9 of the DOEs Transuranic Waste Characterization Quality Assurance Program Plan[1] requires performance goals be "achievable in the presence of backgrounds generated by alpha and gamma emitting sources and in the presence of interfering quantities of neutron and gamma

absorbing and moderating material." In other words, the uncertainty characteristics of the system in its intended "real-world" application must be established.

Standard methods of uncertainty analysis, primarily based on propagation of errors, will almost always underestimate measurement uncertainty in real-world applications. This is because the uncertainties for the component parts are generally based on laboratory experiments on standard test materials. Such assessments are useful in that they provide a best case scenario of a system's performance capability. However, to the extent that they fail to include effects of external factors, they are insufficient to establish the quality of measurements achievable in a true operational setting. Factors not commonly considered in laboratory assessments of uncertainty include highly variable background levels or interference, operator effects (e.g. fatigue, level of training), and heterogeneity of materials being tested (matrix effects). The amount of variability inherent in some of these factors makes them difficult or inappropriate to incorporate into analyses using standard methods. This paper describes the limitations of the standard propagation of errors approach and discusses an alternative approach based on sampling and verification that is better at obtaining realistic uncertainty estimates for real world applications of NDA/NDE systems. Examples of how the sampling and verification approach is being applied at the Idaho National Engineering Laboratory (INEL) are also given.

Heterogeneity of material, both within and between items being assessed, will generally have the largest effect on NDA/NDE uncertainty, particularly in waste management applications. Thus this discussion focuses primarily on methods suitable for incorporating these effects into uncertainty evaluations, referring to them generically as matrix effects. Many of the issues described regarding matrix effects apply to other external effects as well.

The two basic components of uncertainty are the expected bias and standard deviation of measurements. While these components are usually combined to form an uncertainty interval (confidence interval, prediction interval, etc.) they are dealt with directly here to avoid the distraction of the discussion that often occurs regarding the best method of combining them. Thus the concern is with methods capable of providing a realistic indication of the expected bias and standard deviation of measurements obtained using an NDA/NDE system in actual real-world use on a specific population of items.

REVIEW OF THE STANDARD PROPAGATION OF ERRORS APPROACH

In most NDA/NDE systems, measurement results are not obtained directly. Instead they are derived as the result of calculations performed on a set of input components or parameters. The system uncertainty is then a function of the uncertainties in the input parameters. A typical propagation of errors approach to deriving the final uncertainty values involves the following steps.

Identify All Input Parameters and Formulas Required to Calculate the Final Measurement Value

The first step in the uncertainty analysis is to identify all the individual components contributing to the calculation of a final measurement value for the NDA/NDE system. Examples of these inputs are detector counts, gate times, calibration coefficients, etc. The final measurement outcome is expressed as a mathematical function of these input parameters.

Assess the Uncertainty of the Individual Input Parameters

Once all the input parameters are identified, estimates of their individual uncertainties (bias and standard deviation) are obtained. Various methods are used to obtain the component uncertainties. Suitable values are sometimes available from the manufacturers specifications. Otherwise laboratory evaluations may be performed. Calibration coefficient uncertainties are usually a by-product of the analysis (e.g., least squares regression) used to derive the coefficients themselves.

Obtain the Correlation Structure of the Parameter Errors

For some components in a NDA/NDE system, measurement errors are correlated. For example, calibration intercept and slope coefficients based on least squares regression are always correlated. The correlation (or alternatively the covariance) of the errors for all pairs of interrelated input parameters must be estimated. These estimates are typically obtained through laboratory experiments.

Propagate the Results to Obtain Final Uncertainty

Once the uncertainty of the various components of a measurement system have been characterized, they are combined, i.e. propagated, to produce the uncertainty for the system output. The formula used for combining the uncertainties depends on the mathematical function or functions used to calculate the system output. In other words it depends on the form of data reduction used to process the

input parameters to obtain the final measurement result. Consider a hypothetical system in which the measurement outcome, z, is a simple linear function of two inputs x and y:

$z = ax + by.$

The precision error in z, is (expressed as a standard deviation):

$$\sigma_z = \sqrt{a^2\sigma_x^2 + b^2\sigma_y^2 + 2ab\sigma_{xy}} \tag{1}$$

where σ_x^2, σ_y^2, and σ_{xy}, are the variances and covariance of the errors in the input parameters x and y.

Often the data reduction functions are not linear. Since exact error propagation for nonlinear functions is complex, a linear approximation of the functions is employed. The linearization is achieved mathematically by the use of a Taylor series expansion, which re-expresses the function as a polynomial sum of linear and higher order terms. Under the assumption that the measurement errors in the input parameters are small, the higher order terms in the expansion are set to zero, leaving only the linear terms. Given the variances and covariances of the input parameters, uncertainty is then easily estimated. For a two input parameter system with an arbitrary (i.e. potentially nonlinear) form

$z = f(x, y),$

the Taylor series expansion produces the following expression for the variance of the final measurement

$$\sigma_z^2 = \left(\frac{\partial f}{\partial x}\right)^2 \sigma_x^2 + \left(\frac{\partial f}{\partial y}\right)^2 \sigma_y^2 + 2\left(\frac{\partial f}{\partial x}\right)\left(\frac{\partial f}{\partial y}\right)\sigma_{xy} \tag{2}$$

where $\frac{\partial f}{\partial x}$ and $\frac{\partial f}{\partial y}$ are the partial derivatives of f(x, y) with respect to x and y. Notice that this is the same formula as Equation 1 with $a = \frac{\partial f}{\partial x}$ and $b = \frac{\partial f}{\partial y}$.

LIMITATIONS OF THE STANDARD PROPAGATION OF ERRORS APPROACH WHEN MATRIX EFFECTS ARE PRESENT

Most of the limitations of the standard propagation of errors approach to uncertainty analysis derive from the circumstances in which the various component (i.e. input parameter) uncertainties are obtained. The component uncertainties are generally established through laboratory experimentation. For uncertainty results based on such data to be applicable to a particular real world setting, an implicit assumption must be made. That assumption is that the test measurement results are equivalent to those that would have been obtained on samples from the population of items to which you wish to infer the uncertainty. Even if test items for laboratory experiments are constructed to be generally similar to those in the population of interest, they can still vary considerably in terms of matrix complexity compared to the real items.

The assumption of a representative set of test items can be relaxed or ignored in applications where there is no expectation of matrix variability in characteristics that might affect measurement results. However, the assumption is crucial when matrix effects are known or suspected to be present. For example, consider the uncertainty evaluation of a micrometer to be used in a factory to perform quality assurance measures on bearings produced on an assembly line. Most likely there is little about the bearings' characteristics that can affect the micrometer's performance so matrix effects can easily be ignored. In contrast, a radioassay system for 55 gallon waste containers can be highly affected by variability in the quantity of shielding material that is often known to exist within and between drums. In fact, such matrix effects can potentially comprise the largest component of measurement error.

If matrix factors are of concern, a laboratory based uncertainty analysis can be potentially modified to include consideration of matrix effects. If the relevant matrix parameters and the extent of their variability in the population of interest are known, a factorial experimental design incorporating these effect in the study could be employed. Then the resulting data could be used to either derive uncertainty values that include the matrix effects, or possibly used to correct measurement output to account for the matrix effects.

While theoretically possible, an experiment design incorporating matrix effects is probably not practically feasible except in the simplest of cases. In most cases the number of potential matrix effects is so large that incorporating them into even a fractional factorial experimental design (which reduces the

total number of test items required when compared to a full factorial design) quickly brings the total number of test runs to an impracticably large number. Costs relating to simply constructing the required number of different test items becomes equally impractical.

An additional limitation to the standard propagation of errors methods for uncertainty analysis when matrix effects are present is due to the magnitude of the errors in measurements induced by the matrix effects. The propagation of errors formulas used for nonlinear measurement functions are based on the assumption that the measured values are close to the true values. That is the relative measurement error is small. As long as this is true, the linear approximation to the data reduction formulas obtained by setting the higher order terms in the Taylor's series expansion to zero is justifiable. However, in NDA/NDE systems measurement errors can be very large (e.g. even orders of magnitude) so the linear approximation can be invalid.

AN ALTERNATIVE APPROACH: SAMPLING AND VERIFICATION

It was mentioned above that when matrix effects are expected, a key requirement for an experiment designed to assess the uncertainty of an NDA/NDE system is that the test items must be representative of those on which the system is intended to be used. Another way to think about uncertainty that focuses on the issue of representativeness is to consider the following question. If I select an item at random from a population of items of interest and measure it, what is the expected bias and precision error for that measurement? Stated in this manner, the importance of the representativeness of sampled items in the presence of matrix effects is clear. In a waste drum radioassay system for example, results from an uncertainty evaluation using drums filled with a benign matrix cannot be legitimately used to infer the uncertainty for drums containing large quantities of shielding material such as lead.

Once uncertainty is considered from the viewpoint of the bias and precision of a randomly selected item from a population of interest, a general alternative method of uncertainty analysis emerges. This approach might be termed a sampling and verification approach. In ideal terms the method is as follows:

- draw a random sample of items from the population of interest,
- measure the items using the NDA/NDE measurement system of interest,

- establish the true quantity being measured using a "gold standard" technique,
- calculate the difference between the NDA/NDE measurement and true quantity for each of the sampled items,
- estimate bias by calculating the mean of the difference values; the standard deviation of the difference values is the precision.

(Note that the absolutely true value of a characteristic is typically unknowable. The concept of a gold standard measure of a characteristic is simply a method of assessment that produces highly accurate and precise results that are generally accepted as the appropriate reference value. What little error exists in the gold standard measurement is deemed small enough to be inconsequential.)

In the simplest case, the analysis of the difference data to get bias and standard deviation (precision) estimates for this basic sampling and verification method is based on the following basic measurement model:

$$y_i = \alpha + x_i + \varepsilon_i \qquad (3)$$

where, for item i, y_i is the value obtained by the NDA/NDE system being evaluated, x_i is the true or gold standard measurement, α is the bias error, and ε_i is a random error term. The values of ε over all measurements in the population or over repeat measures of the same item are assumed to have mean zero and some standard deviation σ. The parameters α and σ thus represent the true but unknown bias and precision of the NDA/NDE system.

To see why the mean and standard deviation of the difference values are appropriate estimates of α and σ, first rearrange Equation 3 to obtain an expression for α and σ in terms of the difference values:

$$y_i - x_i = \alpha + \varepsilon_i. \qquad (4)$$

Since the ε_i have mean zero, calculating the sample mean of the difference values provides a good estimate of the bias term α, i.e.,

$$\hat{\alpha} = \frac{1}{n}\sum_{i=1}^{n}(y_i - x_i) \tag{5}$$

(where n is the number of samples). Similarly, since α is a constant, the standard deviation of the differences is the standard deviation of the ε values, hence

$$\hat{\sigma} = \sqrt{\frac{1}{n-1}\sum_{i=1}^{n}\left[(y_i - x_i) - \bar{d}\right]^2} \tag{6}$$

(where $\bar{d}$ is the mean of the difference values over all n samples) is a good estimate of the precision parameter σ.

Bias or Precision Error Not Constant

The basic measurement model given in Equation 3 specifies a constant absolute bias and precision value. Often it will be the case that the uncertainty, particularly the precision error or standard deviation of the errors in measurement will increase with the amount of the quantity of interest that is present in an item being measured. In this case the simple mean and variance calculations described are inappropriate for estimating bias and precision. Instead, the bias and precision must be defined as a function of the quantity of interest. For bias, this most often simply means expressing it as a constant relative bias (i.e. bias is a fixed percentage of the measured value). However, it is possible for there to be both absolute and relative bias terms. In that case, a regression of the difference values on the quantity of interest will yield estimates of both components. For variable precision, an additional regression fit involving residuals from the bias regression model will give an indication of trends in standard deviation. The specific model for these regressions is described below.

A measurement model that takes variable bias and precision into account can be expressed as

$$y_i = \alpha + \beta x_i + \varepsilon_i \tag{7}$$

where as before y_i is the NDA/NDE system measurement, x_i is the gold standard measurement, and α is the absolute bias in the system. The term ε_i is the random error term as before, except that now the

standard deviation of ε_i is σ_x, signifying that it can change depending on the value of x. The new parameter β is related to the relative bias of the measurement system. For example suppose $\beta = .80$ and there is no absolute bias (i.e. $\alpha = 0$). Then the system produces measurements that are on average 80% lower than the true value. Thus the relative system bias would be (100 - 80)% = 20%.

Estimates of the bias components α and β are obtained by regression of the y_is on the x_is. A weighted least squares regression is appropriate in cases where the random error changes with values of x. (Note that, although uncommon, it is possible that a more complicated regression model for bias than that in Equation 7 is required to obtain a good fit to the data. That is the bias may be a nonlinear function of the quantity being measured.)

Precision estimates are obtained by analysis of the residuals from the regression performed to estimate the bias components. These residuals are estimates of the ε_i values and are obtained by substituting the estimated bias values $\hat{\alpha}$ and $\hat{\beta}$ into Equation 7 and rearranging the terms:

$$\hat{\varepsilon}_i = y_i - \left(\hat{\alpha} + \hat{\beta} x_i\right). \tag{8}$$

If there is no indication of varying σ_x values then precision can be estimated simply by calculating the standard deviation of the residuals. However, if the residuals themselves appear to follow a trend as a function of the x_is, then a trend in σ_x values is indicated and a function describing the trend must be estimated using regression or other appropriate techniques. Figure 1 shows examples of data for which a trend is or is not indicated. The appropriate function for a trend in precision is often nonlinear so more complicated regression models must be employed. For details see references 2-4.

TWO VARIATIONS FROM THE BASIC SAMPLING AND VERIFICATION METHOD

In specific applications, it is often not possible to strictly follow the basic sampling and verification method outlined above. Instead, a method is employed that still follows the basic sampling and verification logic, but is adapted to fit constraints placed on the evaluation. Two of these variations, described in the context of the issues which motivate their use are described below.

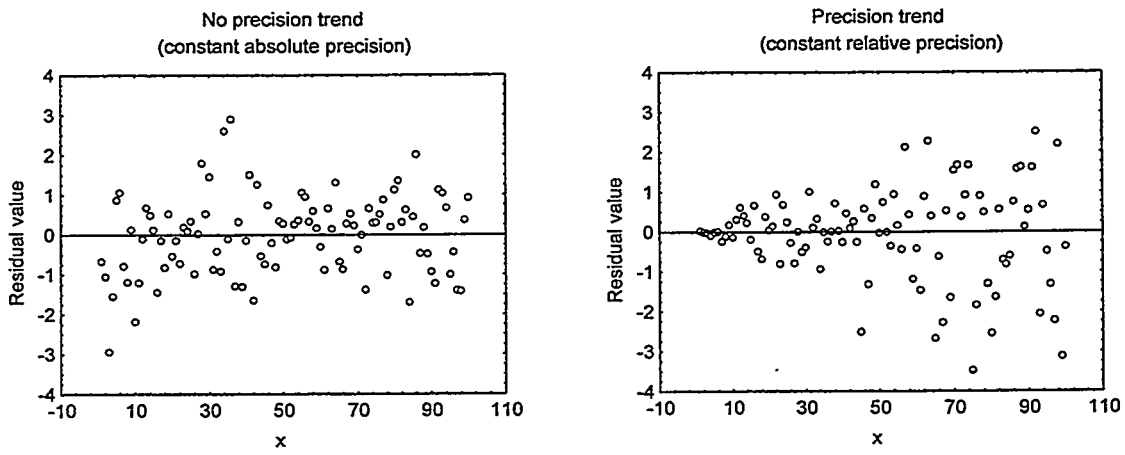

Figure 1. Examples of data showing presence or absence of trends in precision.

Analysis of Surrogate Sample Items

Sometimes it is impossible or inconvenient to perform gold standard measurements on real items from the population of interest. If random sampling and evaluation of actual test items is not feasible, it may be possible to physically construct surrogate items that mimic the matrix configurations and/or source quantities (i.e. the quantity of the component being measured by the NDA/NDE system) that would be found in a true random sample. In order to create representative surrogates, this method requires specific knowledge of both the important matrix characteristics and the distribution of these characteristics in the population of interest. In many ways, this approach is essentially the traditional laboratory experiment method of uncertainty analysis modified to consider the effects of variable matrix parameters and their distributions in the population of interest.

Advantages of this method include the ability to manipulate item configurations to simulate any type of sample desired, and the fact that gold standard values are achieved by default since the quantities of interest are accurately known ahead of time. A major disadvantage of the surrogate item method is that the results are only as good as the ability to create items that are truly representative of those in the population of interest. The credibility of the reported results will depend on adequate documentation of how representativeness was achieved. Preferably some benchmarking of the surrogate process results against measurements of actual items from the population of interest will be performed to establish the representativeness of the surrogate items.

Computer Simulation

Suppose that gold standard or other comparative measurements on real items from the population of interest are not feasible and that construction of a sufficient number of representative surrogate items is also not possible. The latter is likely to happen, for example, when matrix configurations are widely varied both within items and between items in the population. In that case, constructing the number of different items required to adequately represent the broad range of matrix configurations present in the population of interest is not feasible. Another possibility in waste management applications is that creating surrogate items would require creating additional potentially large quantities of hazardous or radioactive waste—a situation to be avoided if at all possible. In these situations an alternative approach to the uncertainty analysis is to utilize a computer simulation of the measurement process. If a realistic computer model of the measurement system can be developed, computer simulation will allow the consideration of a much wider range of matrix configurations than is possible with the actual analysis of either real or surrogate items.

As with the surrogate item method, for the simulation method to work properly requires a thorough understanding and modeling of relevant matrix parameters and their distributions in the population of interest. In addition, other variables affecting measurements (e.g., background radiation levels) must also be modeled appropriately. The ability to adequately model a representative sample of all important characteristics affecting measurements will establish the validity of the results.

With the simulation method it is necessary to establish the validity of the computer simulated measurement process as well. This is best achieved by benchmarking the modeling process against real measurements. For example, a small number of surrogate items with known contents can be constructed and their actual measurement results compared to computer simulated results. For the purpose of benchmarking a computer model, the makeup of the surrogate items is much less critical than if they are to be used to establish uncertainty for a particular population of items. Still, at least in a general sense the surrogate items should reflect typical items from the population of interest.

As with the surrogate item method, computer simulated measurements have an advantage in that they allow strict control of the source quantities being tested. This can provide better estimates of uncertainty over the entire range of interest by allowing easy manipulation of the simulated test items to create stratified samples (discussed below) or other focused investigations. Stratified sampling in

computer simulations can be achieved using Latin hypercube sampling, which provides better representations of a full range of matrix configurations for a given number of items, or by specifying strict numbers of replicates from specific categories of interest (essentially an experimental design approach).

OTHER USEFUL TECHNIQUES WHEN IMPLEMENTING THE SAMPLING AND VERIFICATION APPROACH

For either the basic sampling and verification method or the two variations on the method just described, some additional data collection and analysis techniques are described below. These techniques are not mutually exclusive; various combinations can be employed in the same uncertainty analysis, depending on the circumstances.

Variance Component Analysis: When a Gold Standard Method is Not Available

It is often the case that a gold standard method does not exist or is impractical to apply to an NDA/NDE system evaluation. If the only comparison methods available have non-negligible errors relative to the NDA/NDE methods being assessed, they can still be used in certain circumstances. In particular if the bias of the system is either zero or a known value, but the precision error is large, a statistical variance component analysis can be used to extract correct estimates of the uncertainty components for the NDA/NDE system being evaluated. Measurement models such as those in Equations 3 and 7 can be extended to include terms for the uncertainty in the comparison measurement (i.e., the variable x in the equations). Depending on the complexity of the measurement model that applies to the measurements obtained, the statistical analysis for these models can be quite simple or quite complicated. References 5 and 6 provide a starting point for researching appropriate statistical methods.

Even if a statistical variance component analysis approach is chosen, it is still preferable that the error in the comparative method relative to the NDA/NDE system of interest be as small as possible in order to produce good variance component estimates. If large errors exist in the comparative method, unstable results can occur (e.g., negative precision estimates can be obtained). Conversely, if the errors in the comparative method are small compared to that for the NDA/NDE system of interest (say an order of magnitude or more smaller), the comparative results can be treated as if they were a gold standard and analyzed as if they were the true values with little effect on the quality of the assessment.

Separate Analyses of Homogeneous Groups of Items

For some populations of items, highly variable matrix configurations may produce unacceptably large precision error results. In these cases, uncertainty can potentially be reduced by using available information to segregate data into more homogenous matrix groups. Performing a separate sampling and verification procedure for each of these more homogeneous groups (i.e. treating each as a separate population) will reduce the uncertainty. To take advantage of this technique obviously requires that the group membership be known ahead of time.

Stratified Random Sampling Plans

Sometimes a small proportion of the items in a population are of particular interest, perhaps because they contain potentially problematic quantities or matrix configurations. If it is desired to study these items in more detail than the rest of the population, a simple random sample may result in too few samples being drawn from the subpopulation of interest. In this case a stratified sample focusing on these particular items (in which the items of interest are identified and sampled at greater frequency) is appropriate. Another instance where stratified sampling might be required is when measurement uncertainty varies by the amount of the quantity of interest but only a few items contain either large or small quantities. If uncertainties are to be adequately estimated at the ends of the range of observed values, additional sampling from those items will be required. Stratified sampling will obviously only be possible if the strata membership information is available before the sample is taken.

For simulation based analysis, Latin hypercube sampling[2] can be used to improve results. Latin hypercube sampling can be viewed as a type of stratified sampling in which the strata are defined by the percentiles of the population distribution on each parameter.

EXAMPLES

The following examples describe how different forms of the sampling and verification approach to uncertainty analysis are currently being implemented at the INEL. In each case the specific sampling and verification method used was chosen based on an assessment of the unique characteristics of the measurement system and the constraints related to its evaluation.

Radioassay of Debris Waste in 55 Gallon Drums: Computer Simulation

Many types of debris waste are stored in 55 gallon drums at the INEL. Examples include combustible materials, glass, graphite molds, etc. These drums contain varying quantities of plutonium. The quantity of plutonium must be established by radioassay prior to shipment to a permanent storage facility. These measurements are obtained using a Passive-Active Neutron NDA system. The most distinguishing feature of the uncertainty analyses for these wastes is the use of computer simulations. However, the analyses also make use of the additional techniques of splitting the population into homogeneous groups for separate analysis and stratified sampling. Furthermore, surrogate drums were used to benchmark the measurement simulation process to assure adequate simulation of the PAN system's performance.

The various types of debris waste at the INEL are too heterogeneous to be considered together in a single uncertainty analysis. So the first decision that was made was to perform separate uncertainty analyses on relatively homogeneous groups of waste forms. Analyses for graphite, combustible, and glass waste forms have been completed to date.[2-4]

No gold standard method for radioassay of plutonium in 55 gallon drums was identified. For example, opening a drum and somehow verifying the plutonium quantity based on more detailed assay of the contents was not possible due to safety constraints. Furthermore, creating appropriate numbers of surrogate waste containers was impractical for a number of reasons, primarily dealing with the complexity and variability of the matrices being dealt with. These factors lead to the development of the uncertainty analysis based on computer simulation. The simulation based approach was made possible by the previous existence of both a computer program simulating the PAN system performance and extensive data necessary for deriving appropriate characteristics for simulated drums.

The computer simulation of the PAN system performance uses the Monte Carlo Neutron Photon (MCNP) code to produce a neutron transport calculation for a simulated drum. A follow-up program was written to combine the MCNP output with other parameters generated by the modeling process to yield simulated measured Pu mass values in the same manner as would be done in actual PAN system measurements. The accuracy of the combined simulation routine was verified using data from calibration (surrogate) drums with known Pu contents.

A large collection of real-time radiography (RTR) tapes for waste drums at the INEL provided the majority of the information needed for modeling the matrix configurations for the computer simulated drums. Additional information came from an extensive database of actual PAN measurements on waste drums and background drums. For each waste form of interest, a random sample of RTR tapes was reviewed. The resulting data were used to derive a representative set of simulated drum configurations. Both Latin hypercube and stratified sampling according to Pu quantity were employed in deriving the sample of simulated waste drums. Results were analyzed using regression models as described earlier. In particular the data were found to fit the model specified in Equation 7.

Radioassay of Sludge Waste in 55 Gallon Drums: Variance Component Analysis of Non-Gold Standard Comparative Measurements

Sludge waste in 55 gallon drums are also assayed for Pu content using the PAN system at the INEL. The uncertainty analysis currently under way for these wastes differs from that used for the debris waste because the RTR images of the sludge wastes are too dense to be useful for characterizing their contents for simulation purposes. Without the ability to identify the types and variability of important waste matrix parameters for the sludge wastes, there is no basis for developing a representative sample of matrix configurations. This makes a computer simulated sampling and verification uncertainty analysis problematic. Hence an alternative was developed for these waste forms based on actual comparative measurements. Since no gold standard measurement method exists for the PAN measurements, the analysis will be based on comparative measurements using a variance component analysis. As with the debris waste, separate analyses will be performed on homogeneous waste groups.

The comparative measurement results for the sludge drums are being obtained from destructive radioassay of core samples from randomly selected drums. A facility has been built at the INEL for coring and sampling of sludge waste drums. Originally motivated for sampling of Resource Conservation Recovery Act (RCRA) listed hazardous constituents, core sampling plans have been modified to include radioassay analysis as well. While the comparative drum core radioassay results will actually contain a good deal of uncertainty themselves, they are expected to be unbiased. So by comparing the mean core sample results to the mean PAN results, the bias of the PAN system can be easily established. Furthermore, applying the proper variance component analysis will allow the standard deviation of errors to be estimated as well.

Real-Time Radiography Drum Content Assessment: Basic Sampling and Verification

Evaluation of real-time radiography images by human operators is an integral part of the waste characterization efforts at the INEL. There is a quality assurance requirement that the uncertainty in operators' abilities to correctly identify and classify waste by review of RTR images be established. In this application, human factor effects (e.g. level of training, fatigue) can potentially have significant effects on uncertainty, so they need to be considered in addition to the matrix effects.

The first attempt at establishing this uncertainty was based on the construction of surrogate waste drums. Surrogates were constructed by placing different types of objects in specific configurations in 55 gallon drums according to an experimental plan. Operators were then asked to view the surrogate drums using the RTR system. The number of variables to be manipulated along with operational constraints related to the ability to build particular drum types and quantities led to a number of compromises in the design. Most notably, drum makeup often did not result in realistic or representative RTR images (i.e. they were not like those of the real waste drums), and it was necessary to have operators review the same object various times (but treated as independent observations).

The constraints placed on the experiment lead to some unanticipated results. The drum configurations did not mimic real waste drums to the extent necessary to produce a realistic overall model for uncertainty. This was evidenced by the fact that some of the uncertainty estimates produced by the model were highly inconsistent with those obtained during a previous study in which actual visual confirmation (inspection) of drum contents was performed after RTR review of over 400 real waste drums. This lack of ability to successfully benchmark the surrogate item results against those from real measurements precludes the use of the surrogate item data to address the goal of quantifying the overall uncertainty in the RTR process.

Given the failure of the surrogate drum approach, we have reverted to a true sampling and verification approach where RTR reviews of randomly selected drums are compared to results obtained from actual visual inspection of their contents (i.e. the gold standard is an intrusive, visual inspection of drum contents). This is essentially an expanded version of the methodology used to obtain the benchmark data referred to above. This does not easily allow a separate assessment of the effects of human factors on uncertainty as the surrogate item approach was designed to do, but the potential effects

of human factors are included in the assessment process since actual drum measurements by actual operators in real day-to-day operating conditions are being evaluated.

SUMMARY AND DISCUSSION

Performing an uncertainty analysis on an NDA/NDE system in applications where matrix and other external effects are expected to be significant can be extremely challenging. Standard propagation of errors techniques applied to laboratory evaluations typically do not address external effects and as such can produce overly optimistic results regarding system capabilities. Incorporating external effects in a laboratory setting could theoretically solve the problem but in practice is impractical or impossible to implement. An alternative to standard methods is to perform an uncertainty analysis by a sampling and verification process. In its purist form, this method involves random sampling of actual items from a population of items of interest, measuring those items both using the system under evaluation and a gold standard method. Analysis of the differences in these paired measurements leads to estimates of the expected bias and precision of measurements.

As soon as the presence of matrix effects is acknowledged, uncertainty analysis results become population specific. An uncertainty analysis involving random sampling from a particular population of items can not be automatically applied to other populations. This situation can require considerable effort when uncertainty for numerous populations of items is required. Even though the same measurements system is being used in each case, each population requires a separate uncertainty analysis.

An interesting feature of the basic sampling and verification approach (i.e. based on a true random sample of items from the population and verifying system performance with a gold standard method) is that it requires no knowledge of the types of matrix variability that exists in a population of items nor what kind of effects different matrix parameters can have on measurements. The simple random sample of the population of interest, coupled with an appropriate gold standard measurement assures true estimates of the system's capabilities. This is because, known or unknown, all parameters affecting measurement system performance are automatically being varied over the sampled items in the same manner in which they actually occur. Deviations from the gold standard measurement are exactly what occurs in actual practice and hence will give true representation of the system bias and precision (assuming the measurements were all taken under normal operating conditions). The same thing cannot be said for the methods based on surrogate items, computer simulations, or laboratory methods

incorporating matrix parameters. In those instances the results are only valid if all sources of potential effects have been identified and included in the construction of test items. This requires a thorough understanding of the measurement system, the matrix characteristics of the population of interest, and the distribution of those characteristics among the population of items. Failure to identify and incorporate important parameters or to properly mimic their distribution in the population will lead to invalid estimates of uncertainty.

ACKNOWLEDGMENT

This document was prepared for the U. S. Department of Energy Office of Environmental Restoration and Waste Management under DOE Idaho Operations Office Contract DE-AC07-94ID13223.

REFERENCES

1. Department of Energy, "Transuranic Waste Characterization Quality Assurance Program Plan, Revision 0," CAO-94-1010, U. S. Department of Energy, Carlsbad Area Office (1995).

2. Harker, Y. D., Blackwood, L. G., and Meachum, T. R., "Uncertainty Analysis of the SWEPP PAN Assay System for Graphite Content Code 300," INEL-95/0475, Idaho National Engineering Laboratory (September, 1995).

3. Harker, Y. D., Blackwood, L. G., Meachum, T. R., and Yoon, W. Y., "Uncertainty Analysis of the SWEPP PAN Assay System for Combustible Waste (Content Codes 330 and 336)," INEL-96/0257, Idaho National Engineering Laboratory (August, 1996).

4. Harker, Y. D., Blackwood, L. G., Meachum, T. R., and Yoon, W. Y., "Uncertainty Analysis of the SWEPP PAN Assay System for Glass Waste (Content Codes 440, 441 and 442)," INEL-96/0343, Idaho National Engineering Laboratory (October, 1996).

5. Blackwood, L. G., and Bradley, E. L., "An Omnibus Test for Comparing Two Measuring Devices," *Journal of Quality Technology*, 23, 12-16 (1991).

6. Christensen, R. L., and Blackwood, L. G., "Tests for Precision and Accuracy of Multiple Measuring Devices," *Technometrics*, 35, 411-420, (1993).

Performance Validation of Commercially Available Mobile Waste-Assay Systems: Preliminary Report

M. Schanfein, C. Bonner, R. Maez, J. Martinez, and L. Tichnor
Los Alamos National Laboratory
Los Alamos, New Mexico 87544

D.R. Davidson, G. G. Seaman, and M. F. Villani
Canberra Nuclear
Meriden, Connecticut 06450

ABSTRACT

Prior to disposal, nuclear waste must be accurately characterized to identify and quantify the radioactive content to reduce the radioactive hazard to the public. Validation of the waste-assay systems' performance is critical for establishing the credibility of the assay results for storage and disposal purposes. Canberra Nuclear has evaluated regulations worldwide and identified standard, modular, neutron- and gamma-waste-assay systems that can be used to characterize a large portion of existing and newly generated transuranic (TRU) and low-level waste. Before making claims or guaranteeing any system's performance for specific waste types, the standardized systems' performance must be evaluated.

Canberra and Los Alamos National Laboratory's (LANL) Plutonium Facility developed a three-phase validation plan. During Phase One, tests were performed using simulation sources at Canberra to determine the error bounds for measurement parameters, to determine the minimum detectable activity, and to measure precision and bias. During Phase Two, two mobile systems were installed at the Plutonium Facility. LANL is providing peer review of the systems' performance for plutonium, acting as a beta test site to evaluate the waste-assay software, and providing data for "precertification" at future Department of Energy installations. (Plutonium isotopics are determined from measurements using the Multi-Group Analysis code.) Finally, the two systems' performances are evaluated for representative waste types (salt, metal, combustibles, leaded rubber, and HEPA filters).

Phase Three of the validation, the Waste Isolation Pilot Plant Performance Demonstration Plan, will require approval by the National TRU Program Office.

This paper describes the standard mobile waste-assay systems, the test plan, and preliminary results from the peer review outlined above in Phase Two.

I. INTRODUCTION

It is necessary to evaluate regulations and waste types worldwide to identify and reconcile regulatory waste classifications and generic waste types. Regulatory waste classifications that are based on the radioactive content have resulted in categories such as transuranic or alpha waste (TRU), high-level waste (HLW), intermediate-level waste (ILW), low-level waste (LLW), and unconditional- or free-release waste. Waste types are harder to generalize because the parameters by which they are characterized vary widely: such as matrix density (low to high densities), homogeneous *vs* heterogeneous matrices, matrix composition (for example, neutron moderators and/or absorbers), uniform *vs* nonuniform source distributions, variously shaped and sized lumps of source material, and chemical composition of the source material.

Now that regulatory waste classifications and common waste types are defined, it will be possible to identify standard modular waste-assay systems that meet the characterization needs of most of the worldwide community. The process of peer review will allow potential users to determine how well the model performs for their specific waste types. Canberra Nuclear and the Los Alamos National Laboratory (LANL) Plutonium Facility developed a three-phase validation plan for this project.

Phase One: tests using simulation sources at Canberra

- determine error bounds for measurement parameters,
- determine the minimum detectable activity, and
- measure precision and bias.

Phase Two:

- Two mobile systems are installed at the LANL Plutonium Facility, which
  - provides peer review of the systems' performance for plutonium,
  - acts as a beta test site to evaluate the waste-assay software, and
  - provides data for "precertification" at future Department of Energy installations.

- The two systems' performances are evaluated for representative waste types (salt, metal, combustibles, leaded rubber, and HEPA filters).

Phase Three: Participation in the Waste Isolation Pilot Plant Performance Demonstration Plan will require approval by the National TRU Program Office.

This paper describes the standard mobile waste-assay systems that are being evaluated in Phase Two, the waste-characterization plan itself, and preliminary results from the peer review in Phase Two.

II. STANDARDIZATION OF WASTE-ASSAY SYSTEMS

Standardization provides guaranteed, repeatable performance, and modularity allows the operator to configure the system to meet site-specific measurement requirements. Because of the diverse characteristics of the waste streams to be assayed, both neutron- and gamma-counting techniques are required. Canberra identified six standard systems that can characterize a large portion of existing and newly generated radioactive, containerized waste. Canberra then installed two of these standard systems, the Segmented Gamma Scanner/Waste Assay System (SGS/WAS) passive neutron Waste Drum Assay System (WDAS), in a single trailer, where they were evaluated by LANL's Plutonium Facility.

A. The WM2200 Segmented Gamma Scanner Waste-Assay System

The SGS/WAS shown in Fig. 1 is designed to provide full quantitative analysis and isotopic ratios for containers ranging from small cans to 320-ℓ drums that contain transuranic material and fission/activation products. This scanner is efficiency-calibrated as activity-*vs*-energy and has the capability to measure many nuclides at once. The scanner does not follow the current ANSI (American National Standards Institute) guidelines for segmented gamma scanners; instead, the system is based on Canberra's new modular design and accommodates the operator's site-specific measurement requirements. The SGS/WAS includes two detectors: a coaxial detector for quantifying plutonium content on a segment-by-segment basis and a low-energy germanium (LEGe) detector for measuring both plutonium isotopic composition and uranium enrichment.

The SGS/WAS uses Canberra's gamma waste-assay software for plutonium quantification. To improve the accuracy of the assay, the instrument employs multiple techniques to correct for matrix effects, including the volume-density method and transmission correction. Multispectrum scaling (MSS) provides input for Canberra's nonuniformity correction analysis software (NUCS) to minimize errors caused by nonuniform source distributions. Data from the LEGe detector is analyzed for the plutonium isotopic composition by the Multi-Group Analysis Code (MGA), developed by Dr. R. Gunnink, and MGAU determines the uranium enrichment.

B. The WM3100 Passive Neutron Waste Drum Assay System

The WDAS, shown in Fig. 2, was jointly developed by Canberra and LANL and was authorized for use (AFU) by the International Atomic Energy Agency (IAEA). The WDAS uses a 4π detector geometry — consisting of ^{3}He detectors embedded in a high-density polyethylene moderator — to maximize efficiency and provide a uniform response. A coincidence-counting technique is employed to distinguish the neutron emission of plutonium isotopes from that of interfering (α-n) reactions. The WDAS is designed to measure 3700±3 Bq/g (100 nCi/g) in 208-ℓ drums that weigh more than 22.7 kg (50 pounds) in 1000 sec with a 2-mSv/h (20-μR/h) background.

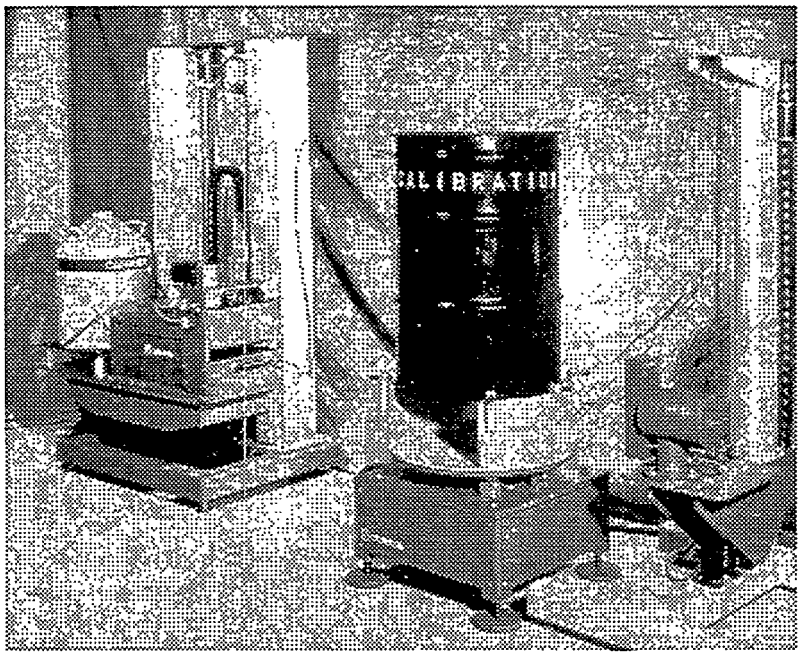

Fig. 1. Segmented Gamma Scanner Waste Assay System.

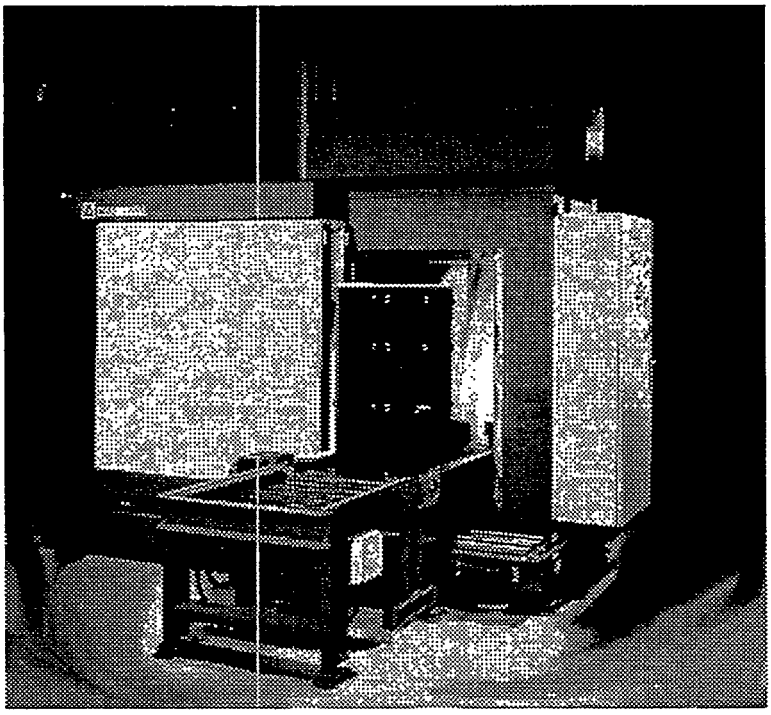

Fig. 2. WM3100 Passive Neutron Waste Drum Assay System.

The passive WDAS operates Canberra's neutron analysis software, which uses analysis algorithms developed the Safeguards Science and Technology Group of the Nonproliferation and Security Division at LANL. The Add-a-Source (AAS) correction technique, developed by LANL, uses a small ^{252}Cf source on the outside of the drum to correct for the matrix effects on the counting rate for the plutonium inside the drum. The AAS can be programmed to compute up to five measurements along the axis of the drum.

III. CHARACTERIZATION PLAN

Validation of a waste assay system's performance is critical in order to establish the credibility of the assay results for storage and disposal purposes. A three-phase validation plan was developed by Canberra and the LANL Plutonium Facility to validate performances for specific waste streams for commercially available mobile waste-assay systems. Data are currently being collected, so results reported here for some of the first tests conducted by LANL are preliminary.

A. Phase One

During Phase One, Canberra performed tests using simulation sources to baseline the performance — that is, to determine the error bounds for measurement parameters and their contribution to the total measurement uncertainty, to determine the minimum detectable activity (MDA), and to measure precision and bias. Measurement parameters include matrix effects (for example, density, composition and homogeneity), source distribution (uniform *vs* nonuniform), drum wall thickness, drum position in the counting chamber, fill height, count time, and background.

B. Phase Two

During Phase Two, the trailer-based WAS were installed and tested at the Plutonium Facility at LANL. LANL provides independent peer review of the performance of the systems for plutonium including performance demonstration program (PDP)-like tests, is acting as a beta test site to evaluate the waste-assay software, and provides data for potential "precertification" at future installations — which would minimize the measurements required to qualify the systems for use at other sites.

The Plutonium Facility benefits from this combined effort in a number of ways. The collaboration helps fulfill the DOE's Defense Programs'-designated "User Facility / Technology Development Center" mission at the LANL Plutonium Facility to test nondestructive assay instrumentation. LANL management is interested in trailer-based equipment in a wide variety of technologies, including processing capabilities to help solve difficult problems around the DOE Complex.

One of this collaboration's major nontechnical accomplishments was defining an environmental, safety, and health (ES&H) envelope that is not trailer-specific. To minimize the

effort required to bring trailers on and off site, LANL chose to avoid a trailer-specific ES&H review. This approach brings the ES&H review in-line with the normal approach for a permanent facility where a work-safety envelope is analyzed for a formal Facility Safety Analysis Report (FSAR) which, once approved, allows any work to take place that is within that envelope. This generic approach was used to examine the hazards associated with nondestructive assay (NDA) trailers and handling radioactive material for the trailers.

The first step was to review the Plutonium Facility's FSAR for similar efforts and then to compare the boundary conditions. For example, the comparison showed that the worst case condition for an accident while handling waste drums for NDA Trailers was only one fourth that stated in the FSAR for an accident while handling waste drums in the yard outside the facility. By referencing the FSAR studies, LANL avoided another review and saved considerable time.

By using the ES&H envelope, the LANL Plutonium Facility can now bring in trailers with only a review by direct group management and the local ES&H representatives who perform walkthrough audits (LANL has been averaging one day for these reviews). The LANL Plutonium Facility was originally designed to comply with 1970 requirements. As a consequence, the NDA Laboratory equipment was placed in areas of the building that exhibited high gamma and neutron background levels.

With the new emphasis on measurements of LLW waste, LANL is interested in quantifying any benefits from assay systems that can be located outside the Plutonium Facility with it's high background-radiation levels. One of the most difficult aspects of NDA measurements is the uncertainties associated with the process measurements. This is particularly true for waste streams where calibration and measurement control standards for NDA instrumentation frequently do not match the matrix of the waste being generated. By bringing in independent instruments such as the Canberra Trailer instruments to measure a wide range of actual Facility waste, LANL is able to check the consistency between measurements from Canberra and those from the Plutonium Facility's NDA Laboratory.

Finally, LANL considers the experience and knowledge of its technicians a key element in its ability to provide cost-effective, high-quality research. When Canberra requested that LANL provide beta-testing for the software interface, the Plutonium Facility chose to have Canberra train LANL technicians to operate the equipment. This removes any potential bias from a participating scientist, ensures that the technicians are intimately involved, and ultimately results in a fair and practical evaluation by those who normally operate this equipment on a routine basis. LANL benefits because the technicians increase their level of skill and develop independence.

Evaluating the Canberra Trailer Instruments required a broad spectrum of plutonium standards that are traceable to the National Institute of Standards and Technology (NIST). The Plutonium Facility has more than fifty ^{239}Pu standards, ranging from 0.2 mg to 480 g. These standards include a range of geometries: predetermined aliquots pipetted onto filter

paper and sealed, silicon sheets, food pack cans, PDP-like cylinders, and 55-gal. drums. In addition to those for ^{239}Pu, LANL also has standards for ^{235}U, ^{242}Pu, ^{238}Pu, and ^{237}Np.

To ensure that LANL maintained conditions for an independent peer review and tested not only the instruments performance but also the manufacturers capability in providing measurement support to users of these trailer systems, LANL and Canberra established the testing protocol shown in Table 1.

TABLE 1. TESTING PROTOCOL

Activity	Responsible Party
Instrument Set Up	Manufacturer
Calibration	Manufacturer
Measurement Control	Manufacturer
Measurement Time	Manufacturer
Measurement Operations	LANL
Trouble Shooting	Manufacturer
Performance Evaluation	Performed by LANL, Reviewed by Manufacturer

The instrument test plan was based on two reference documents. The first is the LANL site document *Procedure to Certify Assay Instrumentation / Techniques for Nuclear Material Accountability Measurements,* which presents LANL's testing requirements to certify an instrument for safeguards accountability measurements. The second document is the DOE/CAO (Carlsbad Area Office) NDA portion of the Performance Demonstration Program (PDP), TRU Waste Characterization Quality Assurance Program Plan (QAPP), Chapter 9, Revision 1A, which describes the method for testing NDA instruments and sets forth the required performance. All of the tests will be detailed in the following paragraphs; where available, preliminary data is also presented.

After the mobile trailer was installed, Canberra calibrated the instruments using LANL Plutonium Facility standard reference materials obtained from sources that are traceable to NIST. No PDP-like standards or PDP drums were used for the calibration; those were used only for the blind tests, which evaluated precision, bias, MDA, and sensitivity to the material forms that are representative of plutonium residues and wastes found in the DOE complex. The evaluation's goals are to demonstrate that the instruments meet or exceed the Quality Assurance Objectives (QAOs) referenced in the QAPP above, estimate total measurement uncertainty, and verify that the assay techniques are appropriate for analysis of the specific waste forms to which they are applied. The material forms include standard reference materials, salt wastes, unspecified metal waste (metal waste other than lead or cadmium), combustible waste, glass waste, leaded rubber waste, and filter waste. The plutonium content in these materials ranges from approximately 0.1 to 200 g.

With the exception of the MDA, these tests are conducted simultaneously so any cross interference between the instruments can be captured. Details for each specific test follow.

Precision — Collected over a range of standards; the drum is cycled in and out of the measurement chamber between the 15 measurements. The sequence is shown in Table 2.

TABLE 2. PLUTONIUM STANDARDS MEASUREMENT MATRIX

Plutonium Standards [approximate masses (g)]					
Instrument	0.2	7.9	100	200	ED
WDAS	15	15	15	15	15
SGS/WAS	15	15	15	15	15

WDAS = Passive Neutron Waste Drum Counter
SGS/WAS = Segmented Gamma Scanner / Waste Assay System
ED = empty drum

Preliminary Precision Results — Plutonium standards from approximately 0.2 to 200 g were run on both the SGS/WAS and WDAS instruments. Preliminary results for both instruments are shown in Table 3.

TABLE 3. PRECISION RUNS DATA MATRIX

Instrument	Standards (g) (nominal)	Ratio: Measured/ Standard	Relative Standard Deviation (%)	Machine Uncertainty (%)	Population
SGS/WAS	0.2	1.05	5.9	6.0	15
SGS/WAS	7.9	1.11	6.8	4.1	15
SGS/WAS	100	1.28	9.7	4.5	14
SGS/WAS	200		in progress		
WDAS	0.2	1.09	32.8	35.9	15
WDAS	7.9	1.00	2.1	2.1	15
WDAS	100	1.11	2.6	4.5	15
WDAS	200	1.17	2.3	2.9	15

The SGS/WAS shows an increasing positive bias and increasing random error as the mass increases. The increasing random error with increasing source strength is contrary to expected performance, as is the large positive bias at higher masses. Shortly after taking these measurements, Canberra determined that an error had occurred with the live time correction algorithm. Canberra chose ^{88}Y as the live time correction source, but because of its short half-life (106.6 days) and its current weak condition, it was necessary to reposition the source frequently to maintain a minimum count rate. This, in turn, required recalibration of the live time source algorithm. As a result of a software problem, in some calibrations, the system retained the peak intensity from the previous calibration, resulting in a positive bias. Therefore, the SGS/WAS data is suspect and will be reviewed by Canberra for possible re-analysis.

The WDAS showed a dramatic increase in random error when measuring the 0.2-g standard. Continued evaluations to determine the MDA are needed to determine whether the WDAS actually saw this standard. It is important to remember that performance, especially at an instrument's lower range, is site-specific. In addition to normal background considerations, LANL's elevation (approximately 7000 ft) produces a significant coincidence background because of cosmic rays. Table 4 shows data collected at three locations. Note that the "reals" count rates at the Canberra location in Connecticut and at the LANL Yard, where the data was collected for this paper, differed by more than a factor of 7. Also note that the "reals" rate in the LANL Plutonium Facility NDA Lab is substantially lower than the rate for the LANL Yard, attesting to the benefits of a thick concrete roof. However, there is also a high background totals rate as a result of substantial quantities of plutonium both in storage and in transit in this location. Canberra has calculated the MDA for the WDAS using the LANL formula. The 3σ MDA for background conditions in the LANL Yard is 5.8 mg ^{240}Pu (eff) or 96-mg total plutonium for weapons-grade material, indicating that the 200-mg standard is roughly twice the MDA.

TABLE 4. BACKGROUND MEASUREMENTS

	Background	
Location	**Totals (cps)**	**Reals (cps)**
N02: LANL NDA Laboratory	400-2000	0.5 - 1.
WDAS: Connecticut	6.5	0.25
WDAS: LANL Yard	35	1.8

N02 and WDAS = 18% Detection Efficiency

The WDAS neutron counter has a sensitivity of 22 cps/g* ^{240}Pu (eff). The signal from a 200-mg weapons-grade sample is 0.2*0.06*22 = 0.264 cps. With the high-background "reals" rate of 1.8 ± 0.05 cps, the measurement uncertainty contribution from background alone would be 0.05/0.264 = ~20%, accounting for nearly all of the error shown in Tables 3 and 5. In addition, when other samples are in the proximity of the WDAS (such as those on conveyors or being assayed by the SGS/WAS), there may be additional deviations between consecutive measurements of the calculated multiplication. This influence results from the R/T ratio's sensitivity to dynamic changes — specifically in the totals rate, T. If dynamic increases in the background rates caused by signal crosstalk are gross (10% or more), then a positive bias in the measured/standard ratio is expected for smaller samples with multiplication correction. This is most likely the case for the positive bias in the stability measurement of the 200-mg sample in Table 5.

TABLE 5. PRECISION *vs* STABILITY DATA MATRIX

SGS/WAS Runs

Data Type	^{239}Pu Standards (g) (nominal)	Ratio: Measured/ Standard	Relative Standard Deviation (%)	Machine Uncertainty (%)	Population
Precision	0.2	1.05	5.9	6.0	15
Stability	0.2	0.91	7.3	5.6	32
Precision	7.9	1.11	6.8	4.1	15
Stability	7.9	1.02	3.6	2.9	24
Precision	200		in progress		
Stability	200	0.91	3.5	2.3	33

WDAS Runs

Data Type	Total Plutonium Standards (g) (nominal)	Ratio: Measured/ Standard	Relative Standard Deviation (%)	Machine Uncertainty (%)	Population
Precision	0.2	1.09	32.8	35.9	15
Stability	0.2	1.20	76.1	40.3	33
Precision	7.9	1.00	2.1	2.1	15
Stability	7.9	1.00	3.2	2.2	25
Precision	200	1.18	2.3	2.9	15
Stability	200	1.19	2.8	2.9	33

The WDAS measurement of the 7.9-g standard shows no significant measurable bias; however, an increasing positive bias is shown with the two higher standards, and Canberra is reviewing the data. If possible, a multiplicity module will be used with a higher efficiency neutron counter to determine if there are higher alpha-value events than those calculated from the sample type and isotopic parameters provided by LANL. Throughout the range, the random error shows generally good correspondence to the machine-calculated uncertainty.

Measurement Stability — To study the stability of a system in its own work environment, researchers followed the measurement matrix shown in Table 6 for three work weeks. One of LANL's focuses for certification testing is to determine the control limits used in the computer-based measurement-control program; therefore, the stability data are used as the basis for provisional limits until three months of actual measurement-control data have been collected. At that point, the certification-based control limits are compared to those from three months of historical data, and adjustments are made if warranted. At LANL, the NDA control limits are compared to historical data on an annual basis.

TABLE 6. MATRIX OF MEASUREMENTS

	Plutonium Standards (approximate masses)				
	M	**T**	**W**	**T**	**F**
AM	200	0.2	7.9	200	20
AM	0.2	7.9	200	0.2	0.2
AM	7.9	200	0.2	7.9	7.9
PM	0.2	0.2	7.9	0.2	200
PM	200	7.9	0.2	200	0.2
PM	0.2	200	200	7.9	200
PM	ED	ED	ED	ED	ED
Assays	7	7	7	7	7

ED = empty drum

Comparison of precision and stability data is used to contrast instrument performance in ideal and working environments, as is shown in Table 6 and Figs. 3 and 4. Note that in the graphs the precision data are intentionally shifted to the right to avoid overlap with the stability data points. As indicated in Table 3, LANL is currently collecting precision data at the 200-g level for SGS/WAS.

The SGS/WAS data table and graph show distinct differences between the precision and stability data. In general, one would expect to see the best precision results for the precision runs and either the same or poorer performance for the stability runs. For bias, one would expect little overall differences. Although the data for the 200 g are not yet available, other data show significant bias differences and — at least in the 7.9-g case — better precision for the stability runs. These surprising results prompted Canberra to review the process. As mentioned earlier in this paper, the data are suspect, and the problem appears to lie in the live time source calibration.

Unlike the case of the SGS/WAS data, the comparison of NAS precision and stability data followed expected patterns and showed good correspondence between both tests. Pending further analysis, no conclusion can be drawn for the 0.2-g data.

Comparative Measurements of Process Materials — By remeasuring Plutonium Facility waste items, it is possible to compare current measuring capabilities to those of the new system. The measurement matrix is shown in Table 7. Data collection continues.

Minimum Detectable Activity and LLW/TRU Determination — Using the calculated MDA, the Plutonium Facility is assembling standards to check actual performance of the instrument. Table 8 shows the MDA measurement matrix for WDAS and SGS/WAS. Data collection continues.

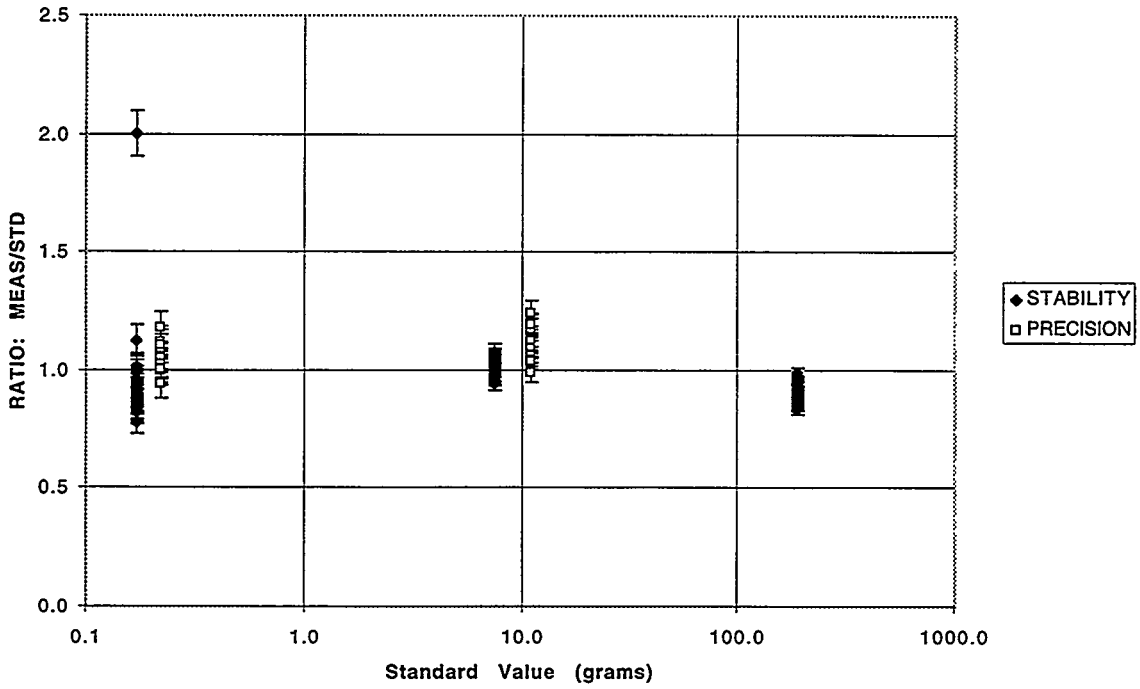

Fig. 3. SGS/WAS Precision vs Stability.

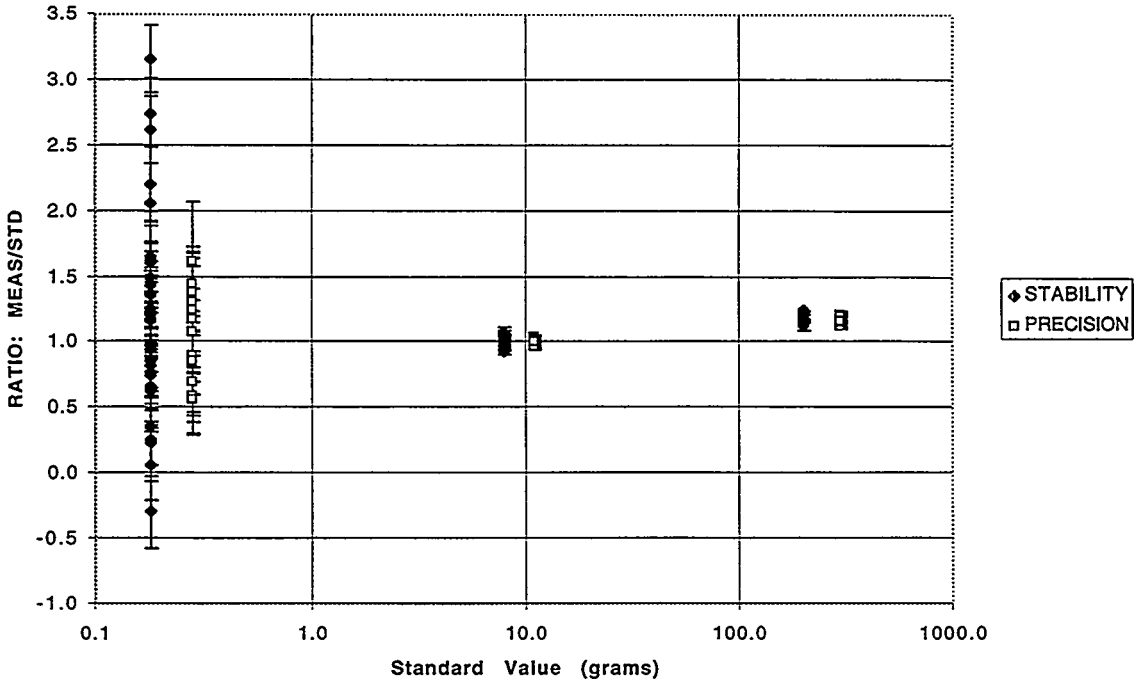

Fig. 4. WDAS Precision vs Stability.

TABLE 7. MATERIAL TYPE MEASUREMENT MATRIX

	Type of Waste Matrix					
Instrument	**1**	**2**	**3**	**4**	**5**	**6**
WDAS	10	10	10	10	10	10
SGS/WAS	10	10	10	10	10	10

5 high and 5 low plutonium loading measurements per instrument.
1 = salt
2 = metal
3 = combustable
4 = glass
5 = leaded rubber
6 = filter

TABLE 8. MDA FOR WDAS AND SGS/WAS MEASUREMENT MATRIX

Instrument	**MDA(-) (g)**	**MDA (g)**	**MDA(+) (g)**	**100 nCi/g**
WDAS	15	15	15	15
SGS/WAS	15	15	15	15

LeGe/MGA Comparison — Table 9 provides a measurement matrix for comparing MGA isotopics with analytical and FRAM isotopics (fixed energy, response function analysis with multiple effiiencies, a LANL-developed NDA gamma-ray isotopic program to determine the isotopic percentages for plutonium and uranium). Data collection continues. The CALEX (Calorimetry Exchange Standard), an identical standard located at each DOE facility, is part of a DOE complex-wide program to compare the calorimetry and isotopic measurement capabilities of the facilities.

TABLE 9. MDA FOR WDAS AND SGS/WAS MEASUREMENT MATRIX

Item	**Calorimetry Exchange Standard**	**Plutonium Standard**	**Plutonium/ Neptunium**	**Plutonium/ High Americium**
MGA	3	3	3	3
FRAM	3	3	3	3
Analytical	x	x	–	–

PDP-Like Tests — The LANL Plutonium Facility is using a suite of PDP-like standards from LANL and PDP drums from Idaho National Engineering Laboratory (INEL) in a PDP-like test of the Canberra equipment (following the Quality Assurance Objectives for Nondestructive Assay, as defined in CAO-94-1010, Section 9.0, Revision: 1A).

The initial testing modeled the cycle-1 test by using the empty and ethafoam matrices. These drums were presented as "blind" items for measurement. LANL technicians operated both instruments for all measurements, which are shown in Figs. 5 and 6. LANL chose to make 15 measurements of each PDP drum following the QAOs instead of the 6 measurements required by the PDP program. The rationale for this decision is given below.

Figure 5 shows the results from the SGS/WAS measurements. There are two sets of measurements with significant differences in both bias and precision. The first set of measurements, labeled empty-1 and ethafoam-1, was halted because of the live-time calibration problem described above. Canberra's initial review confirmed a problem with the live-time correction. The second set was run after the problem was corrected. Data from these second runs (ethafoam is incomplete, being only 8 points in this graph) show a significant negative bias. Further review by Canberra, taking into consideration the unique PDP geometry, revealed an attenuation problem that resulted from reliance on ^{239}Pu's 129-keV peak for quantitative analysis. Because of its higher activity, the 129-keV peak data are more heavily weighted than of the 414-keV peak in the SGS/WAS analysis algorithm. Normally, attenuation is addressed by using a transmission source to correct for the losses. However, in the case of the PDP standards, the 129-keV peak is significantly attenuated by the double-encapsulated stainless-steel cylinders (2-in. diam. by 9-in. length) used to encapsulate plutonium standards. At the same time, because of the slender vertical geometry of the PDP standards, the europium transmission source sees what is a noninterfering drum. The result is understated transmission correction and, therefore, a negative bias in the stated mass of plutonium.

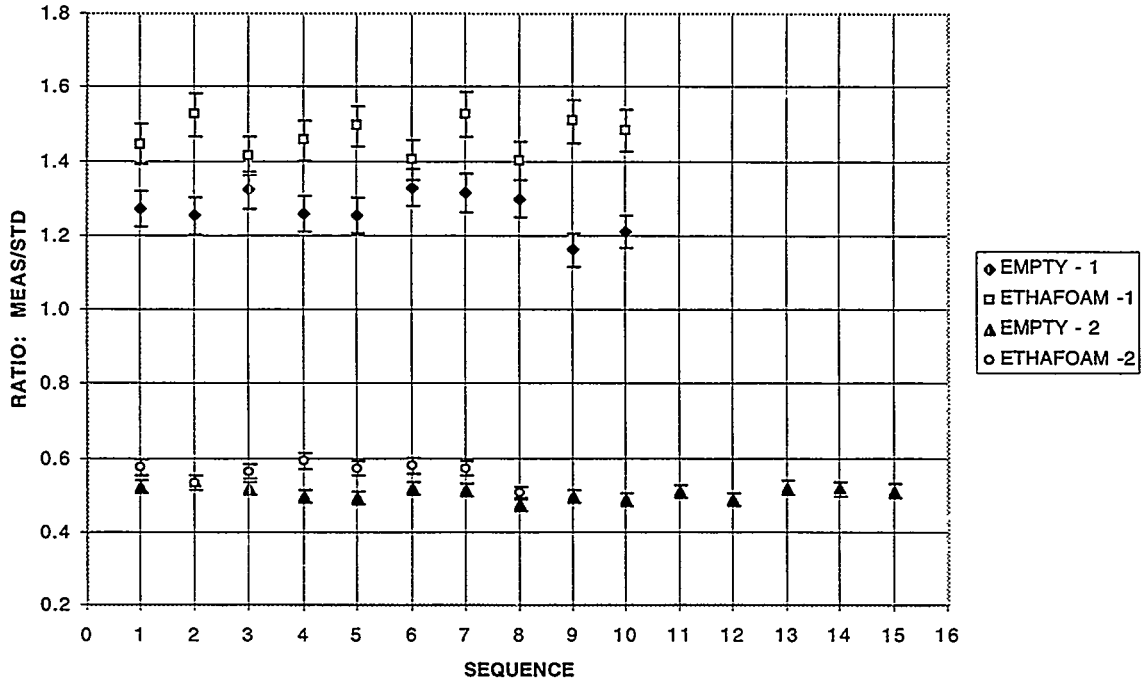

Fig. 5. SGS/WAS PDP Data.

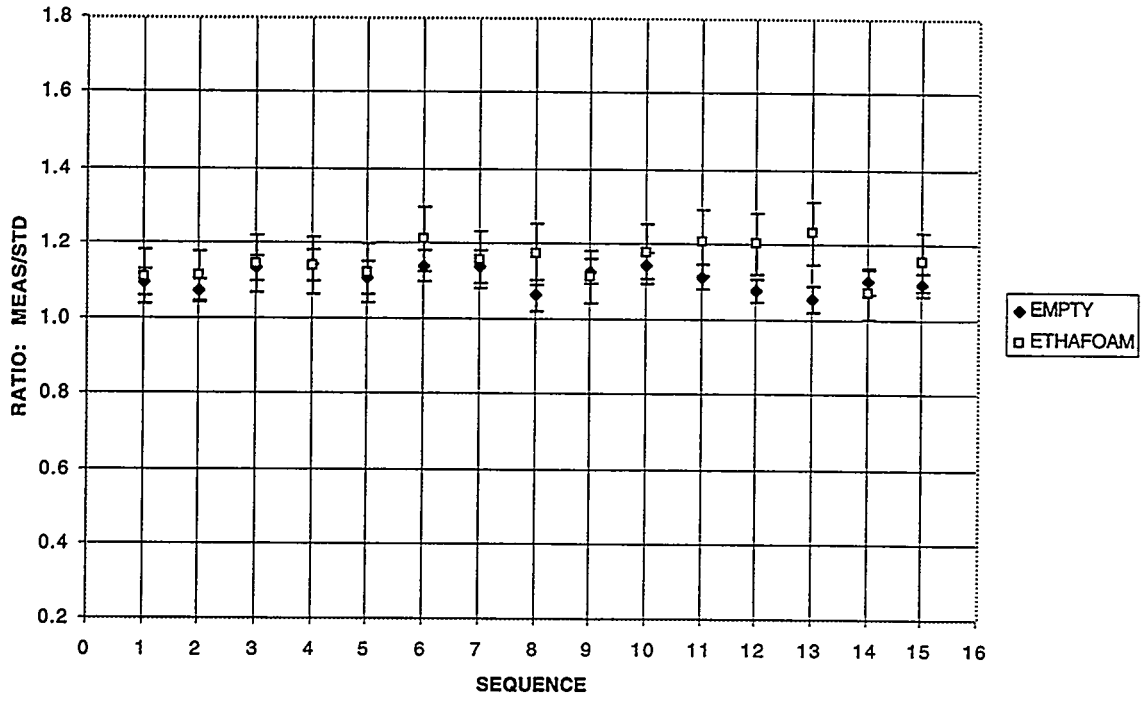

Fig. 6. WDAS PDP Drum Matrices.

The attenuation problem is further exacerbated by another problem recently discovered by Canberra. Review of the gamma spectrum for samples both with and without the ^{152}Eu transmission source revealed that the 344.3-keV europium line was being used for transmission correction that is overlapped by the 344.9-keV ^{239}Pu line. Canberra has performed a preliminary analysis of this problem using a single-center segment and a range of plutonium source strengths. Calculations of the contribution from the plutonium to the total transmission peak area ranges from ~3% in the 7.9-g standard to ~48% in the 200-g standard. This effect will also reduce the actual transmission correction, resulting in an underestimate of the mass of ^{239}Pu.

Canberra has completed a preliminary evaluation of the 129-keV attenuation problem by re-analyzing the PDP data files using only the 414-keV line. From this re-analysis, it appears the reported quantitative value for ^{239}Pu increased by 50%.

As a result of the problems described above, no final PDP analysis was done. However, the observed precision (in percent relative standard deviation - RSD) for these measurements satisfied the PDP QAO for relative precision of less than 10%. With the current reduced QAO range for instrument bias of 75 to 125% used in the PDP Cycle-2 evaluation, the current SGS/WAS bias problems would have resulted in failures. However, using the PDP Cycle-1 QAO range for instrument bias of 50 to 150%, even these biases would pass.

The WDAS graph is shown in Fig. 6. Measurement of the empty drum produced an average positive bias of ~11%. The ethafoam measurement had an average positive bias of ~16%. Evaluations of these measurements at the 95% confidence level indicated that they passed the QAOs for both bias and precision, as is indicated in Table 10.

LANL choose to run 15 measurements of the PDP drum because of a statistical review of the probability for failure using the smaller population of 6 that is required by PDP criteria. Figure 7 shows the frequency of occurrance *vs* the %RSD at the upper 95th confidence bound as well as the distribution of calculated precisions. This distribution was calculated using the existing 15 data points from the NAS data; 1000 random combinations of 6 points each were sampled and the precision at the upper 95% confidence bound was calculated. The distribution is then displayed with the 10% QAO limit. Note that approximately 13% of the NAS data points failed when only 6 points were used.

Comparison to LANL Plutonium Facility NDA Instrumentation — Only a preliminary comparison has been made at a single-gram loading of ~8 g for both SGS/WAS and WDAS and the LANL Plutonium Facility NDA Laboratory instrumentation. The closest matches in data between LANL and Canberra instruments are from the neutron drum coincidence counter, NO2, which has the same 18% detector efficiency shown by WDAS and the SGS G05. Because of the live-time correction problem in the SGS/WAS precision data, only the 7.9-g stability data was used. The comparison is shown in Table 11.

At ~8-g loading, the comparison shows a good correspondence in performance between these instruments. Analysis over the entire range is not yet complete, but some of the current data show biases that would limit the certification range at LANL.

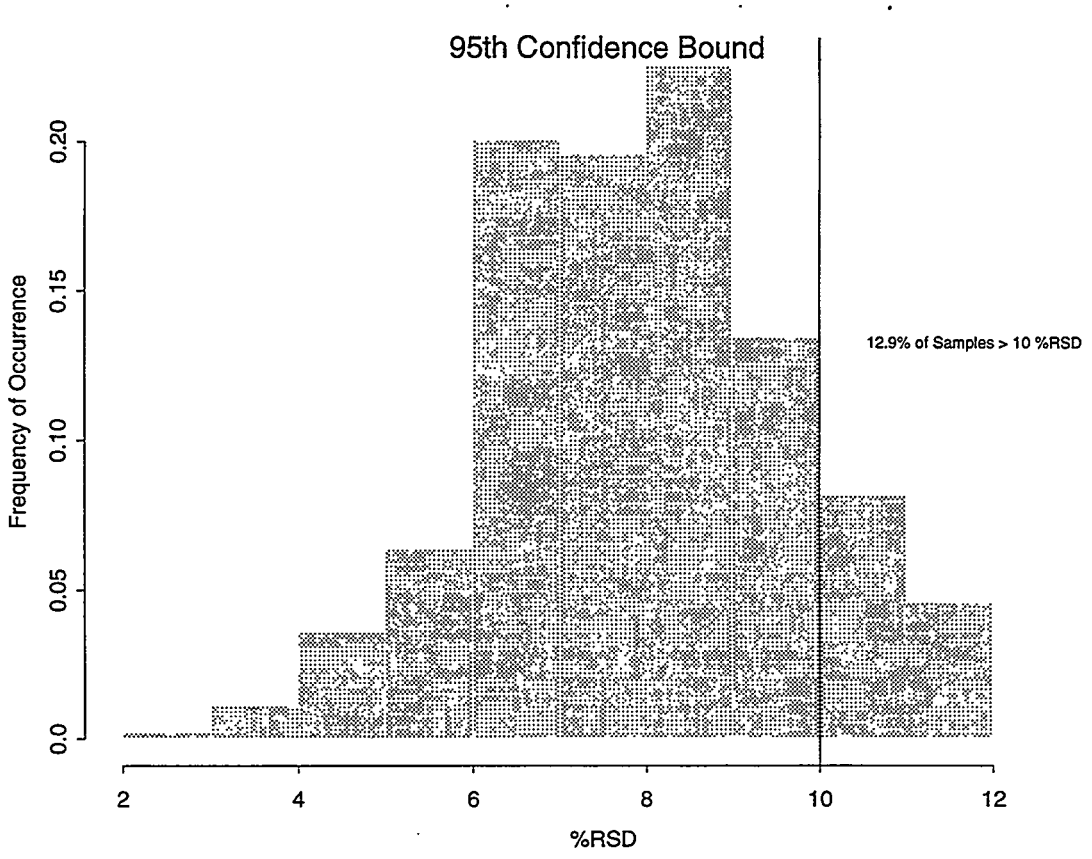

Fig. 7. WDAS PDP Data: 0.48 Ci, ethafoam matrix, 1000 random samples of size 6.

TABLE 10. WDAS PDP DATA ANALYSIS RESULTS

Method	Drum Type	N	Observed Precision (% RSD)	Upper 95% Confidence Level of Precision (% RSD)*	QAO for Relative Precision (% RSD)	Observed Bias (% RSD)	95% Confidence Bounds for Bias (% RSD)**	QAO for System Bias	Status	
									Precision	Bias
WDAS	Empty	15	2.7	3.9	10	111	109-112	75-125	pass	pass
WDAS	Ethafoam	15	3.9	5.8	10	115	113-118	75-125	pass	pass

Empty = 0.28 Ci
Ethafoam = 0.51 Ci

*Confidence Interval on variance Chi2 distribution

** Confidence interval on mean t distribution

QAO — Reference Section 9.0, Revision: 1A

TABLE 11. COMPARISON OF INSTRUMENT PERFORMANCE

Instrument	Random Error (1σ) (%)	Bias Error (%)
SGS/WAS	3.6	1.4
LANL G05	2.7	1.4
WDAS	2-3	0.2-0.4
LANL NO2	2.8	0.2

Lessons Learned — A number of important issues came to light during the testing process. Some were mentioned earlier in this paper and will be summarized here.

1. SGS/WAS Measurement Control Problem: Initial measurement control was set up by Canberra as a single-position no-container measurement of the spectra with and without the transmission source, which was performed once every morning. The assumption was that the internal diagnostics, including confirming count rate, intensity, centroid, and FWHM for the spectrum with and without the transmission source, would be a true indicator of instrument performance. However, this approach did not detect the problem with live-time correction. Both the precision runs and first PDP runs ran with this problem. As a result of this problem, Canberra now includes a known standard run as part of the measurement control program.

2. SGS/WAS Live-Time Correction Problem: The short half-life, low-intensity ^{88}Y source used for live-time correction required frequent recalibration. Because of a software problem, the program would periodically fail and use the data from the previous calibration. In the future, Canberra would use a pulser for waste assay to eliminate both the need to recalibrate and the associated difficulties in using a radioactive source.

3. SGS/WAS PDP Standard Attenuation of 129-keV Plutonium Gamma Ray: The SGS/WAS analysis algorithm relies more on the 129 keV gamma ray than the 414-keV gamma ray because of its higher activity. The PDP double stainless-steel containers significantly attenuates the 129-keV gamma ray. The PDP's geometry of long, vertical cylinders in a noninterfering matrix does not have a corresponding effect on the transmission source. Canberra is now examining the possibility of using only the 414-keV gamma ray. A preliminary re-analysis of the PDP data using only the 414-keV gamma ray shows a 50% increase in the quantitative result.

4. SGS/WAS Overlapping Transmission Source: The SGS/WAS analysis algorithm was using a ^{152}Eu gamma ray at 344.3 keV for transmission correction. Because this peak is overlapped by the 344.9-keV ^{239}Pu line, it would result in understated transmission correction. Canberra has performed a preliminary analysis of this problem using a single-center segment and a range of plutonium source strengths. When they calculated the contribution from the plutonium to the total peak area in the transmission data, it showed a contribution of ~3% in the 7.9-g standard and ~48% in the 200-g standard for this particular source. The use of this peak will be eliminated, and Canberra is considering using a stronger transmission source or eliminating this peak. If a stronger source is chosen, the appropriate flag will be added to warn users to replace the source.

C. Phase Three

Phase Three will include field demonstration of the standard waste-assay systems in the PDP at user facilities. Canberra expects that this mobile assay system will participate in the PDP following the completion and approval of QA documents required by the National TRU Program Office.

IV. SUMMARY

A brief summary of preliminary conclusions is given below.

GWAS

- Problems with software/parameters have been identified
- ^{239}Pu sensitivity comparable to WDAS ^{240}Pu sensitivity for current drums
- Self-diagnostics do not replace a known source for measurement control
- Limited LANL Plutonium Facility comparison showed good correspondence, current biases would limit working range (expected to be corrected)
- Operator interface is user-friendly

WDAS

- PDP meets current performance requirements
- Limited LANL Plutonium Facility comparison showed good correspondence, current biases would limit working range
- Operator interface is user-friendly

Every effort is being made to conduct systematic tests on these two Canberra systems to provide the highest confidence in system capabilities and performance through independent-peer testing and evaluation processes. Canberra has gained critical information during this beta-testing phase using plutonium; these tests will clearly result in a significantly improved measurement capability. After Canberra completes the suite of tests and re-analyzes specific spectra, a formal report of the test results will be issued.

Another mobile NDA trailer, manufactured by Pajarito Scientific Corporation, is just beginning to run tests at LANL. A formal report of these tests will also be issued.

An Overview of the ORNL–NFS Intercomparison

David C. Hensley

Oak Ridge National Laboratory, Oak Ridge, TN 37831

Abstract

Nuclear Fuel Services sent more than 800 drums of nuclear waste to Oak Ridge National Laboratory, with the majority of the waste packaged into five different waste matrix types. A thorough and complete assay of the waste was performed at both NFS and at ORNL. A detailed comparing of the two assay sets provides valuable insights into problems encountered in typical assay campaigns, particularly as there is, for the most part, excellent agreement between these two campaigns.

NFS and ORNL Assays

Nuclear Fuel Services (NFS) shipped more than 800 207l (55 gallon) drums of decommisioning and decontamination waste from their nuclear fuel facility in Erwin, Tennessee, to Oak Ridge National Laboratory (ORNL) beginning in 1991. They were required to assay the waste before it left their facility and ORNL was required to assay it upon its arrival. The data in this paper are a part of an intercomparison of the two sets of assay results. Figs. 1–5 show the NFS values for ^{240}Pu and ^{2390}Pu versus the corresponding *APNea* results. The five differnt waste matrices, *SOIL*, *SEG*, *CONC*, *RR*, and *IMM* refer to soil, compacted waste, concrete rubble, raschig rings, and immobablized fines, respectively. The *SEG* compacted waste was a mixture of glove box and other scrap which was (super)compacted at the Scientific Ecology Group (SEG) plant into cubes, three of which would fit in a drum. The *IMM* waste was packaged in 2l bottles and placed in drums in a bird cage arrangement with a maximum of three bottles per drum. At NFS, the assay process started with small samples, included α and γ analysis for isotopic determinations, and finished with either passive and/or active neutron assay. The ORNL analysis was passive and active neutron assay of drums only.

A very small portion of the ORNL data have not been included in the various figures because of obvious experimental errors. In addition, the data for the *SEG* drums includes over 60 repeat measurements — a fortuitous condition arising from the fact that about 60 drums were assayed and checked at ORNL and returned for remediation because they contained too much free liquid. These drums were 'fixed' without changing the essential character of the matrix and were reshipped to ORNL where they were assayed again and then accepted. These repeat drums form a valuable replicate test for the *APNea* System, and all repeat assays have been included in the following intercomparisons. The *SEG* waste stream was probably the hardest to assay because the compacted cubes filling each drum could vary in significant ways. Some of the cubes were largely metal, some contained large amounts of plexiglass and plastics. Many of the cubes resented the compacting process and started to swell. A swollen cube on top of another swollen cube left an annoying gap in the matrix which complicated the interpretation of the results. In one case, the cubes had swollen sufficiently that only two cubes could be put into a drum, leaving one third of the drum essentially empty.

^{240}Pu

Figs. 1–5a compare the NFS ^{240}Pu values and the *APNea* auto–correlation results for ^{240}Pu. Both values are expressed in milligrams. The *APNea* values are based on an absolute calibration and the calibration is linked to the various matrices through External Matrix Probe (EMP)[1] techniques. It was on the basis of these ^{240}Pu comparisons that the shipments from NFS were accepted. The straight line in the graph indicates the 'correct' answer, i.e., what would be expected if the *APNea* results agreed exactly with the NFS results. In three cases, *SOIL*, *SEG*, and *RR* the agreement in the slope of the comparison is excellent. In the two remaining cases, *CONC* and *IMM*, there is a clear disagreement.

The *RR* comparison in Fig. 4 exhibits a significant amount of scatter which will be addressed later in the discussion of the singles results. The large scatter in the *SEG* ^{240}Pu

comparison is obviously related to the large irregularities in the matrix itself. Another aspect of the *SEG* waste stream further blurs the comparison in that this waste came not from a single process line or from a single location but was the catchall for various junk that had to be shipped. Further analyses, to be discussed later, clearly indicate that there are at least two significantly different waste streams represented in the *SEG* waste. The *CONC* results, while differing significantly in slope, do show an extremely good overall relative correlation. Even this very uniform waste stream will be found to have outliers, drums whose basic characteristics are noticeably different from the rest in that stream. The *IMM* waste stream will be found to be much more consistent than is indicated in the ^{240}Pu comparison in Fig. 5a.

^{239}Pu

Figs. 1–5b compare the NFS ^{239}Pu values and the *APNea* active results, expressed in terms of ^{239}Pu. Again values are expressed in milligrams. Here the NFS ^{239}Pu values have been adjusted to include any ^{235}U present (properly scaled). This adjustment to the ^{239}Pu value is typically under 10%. The *APNea* active calibration is still relative as there is ongoing work to establish an absolute active normalization (see Refs.1 and 2). The *APNea* System performs three active measurements per assay, one with the neutron generator positioned vertically 6 inches from the bottom of the drum, a second at 18 inches, and a third at 28 inches. (The open triangles in the figures refer to the 18 inch measurements.) In two matrix cases, *SOIL*, and *CONC*, the comparison shows excellent agreement. For the *SEG* case the agreement is good but, as with the ^{240}Pu results, there is significant scatter. There are some indications that the comparison is more complicated than would be expected for a single waste stream.

As would be expected for the *RR* drums, the *APNea* active results scatter considerably, through there is a hint of agreement. The results for the *IMM* waste is actually good though these results await a more detailed treatment that considers self-shielding, since many of these drums had the most spatially concentrated waste encountered in this study.

Fortunately there is sufficient isotopic information available from the NFS assay campaign that a good comparison of the ^{239}Pu results can be made with the possibly better established ^{240}Pu results. Generally though, the relative correlation for the *IMM* ^{239}Pu results is fairly pleasing.

The Singles Rate

One of the most precise measurements made by the *APNea* system is that of the *singles* neutron rate. This is an absolute measurement whose main uncertainty has to do with the spatial distribution of the neutron emitting waste within the matrix, as the effective detection efficiency depends on this distribution. Since one of the key aspects of the *APNea* System accounts explicitly[3,1] for such effects, this is an extremely valuable measure to compare other results against. Figs. 1–5c,d, respectively, compare the *APNea* results for ^{240}Pu and ^{239}Pu with the *APNea* singles results. There are two obvious advantages for using the singles as a comparative measure. In the Fig. 1 *SOIL* comparison, there is a clear difference for the *APNea* ^{240}Pu results when they are compared to the NFS values as to when they are compared to the singles values. Some of the outliers in Fig. 1a are clearly brought into the fold in the lower figure. Part of this is to say that there is good internal consistency in the *APNea* measurements, another part is to say that the scatter observed in the upper figure is a measure of the uncertainty in the NFS values. But both of these conclusions are based on an expectation that the singles character of the waste does not vary from one drum to the next. That is, there is no significant variation in the (α, n) reactions from one drum to another— if there is twice as much plutonium, then there should be twice as much (α, n). Evidently, this is the case for the *SOIL* drums. It is largely the case for both the *CONC* and the *SEG* drums as seen in Fig. 2,3c, but there are several clear outliers in each case. It will be seen later that the *SEG* outliers, in particular, are especially anomolous.

The most important utilization of this comparison to singles can be seen in the *RR* comparisons in Fig. 4a,c. The ^{240}Pu values in Fig. 4a are poorly correlated with the NFS

values, whereas the values for the same drums in Fig. 4c show a remarkable correlation with the *APNea* singles. This is a likely result of there being problems with the NFS data. Without the singles comparison, however, there would be no way of assessing whether the scatter in Fig. 4a came from the NFS values or the *APNea* values. A very similar result is found for the *IMM* waste in Fig. 5a. In this figure neither the slope nor the overall correlation give one much insight into the quality of the various assays. But, the comparison with the singles values in Fig. 5c gives one much more confidence in the relative quality of the *APNea* results, and it clearly identifies two drums whose overall (singles) characteristics are significantly different from the rest.

APNea ^{240}Pu and ^{239}Pu Comparison

Since the *APNea* passive and active measurements are essentially independent, a comparison of the two results should be useful. For this, it is helpful (necessary) to have the NFS isotopics information, since the ^{240}Pu/^{239}Pu ratio varied over the various waste streams, in addition to which, there was occasional mixing in of ^{235}U, either from fuel diluted with uranium or from some of the special ^{235}U nuclear fuel waste streams. Given that the NFS isotopics are valid, then the ^{240}Pu and ^{239}Pu comparison should be a valuable independent comparison. Fig.6 shows this comparison for four of the waste streams. *SOIL* was not included in this since the overall intercomparison was so close that this new way of looking at things adds little to the interpretation of results. The *CONC* results are very nice. They improve upon the NFS ^{239}Pu comparison and verify that at least two of the drums have a special signature. The *SEG* comparison verifies that there is something special about the group of drums that were seen in the singles comparison to have a relatively higher singles rate. Now it is seen that they probably have a different ^{240}Pu/^{239}Pu ratio. There is some very slight improvement in the *RR* comparison, although the *APNea* active measurement is understood to be largely speculative. Of most value is the *IMM* comparison, since the NFS ^{240}Pu comparison was so poor that it left the NFS ^{239}Pu comparison in question. The comparison to the scaled *APNea* ^{240}Pu results verifies that the good correlation in the singles

comparison was not simply fortuitous. Apparently, most of the drums have a quite uniform $^{240}Pu/^{239}Pu$ ratio, in spite of the poor results noted in the ^{240}Pu comparison. Interestingly, the two drums with noticeably high singles rates are seen to have the average plutonium ratio. This improvement in the confidence level for the *IMM* measurements should allow a much better analysis of self-shielding effects for this waste.

Conclusions

The intercomparison of assay results for the NFS waste from the parallel assays by both NFS and ORNL has proven to be invaluable. Originally it provided the basis for confidence in the developing *APNea* System. As the *APNea* System matured, an extended intercomparison then revealed interesting details. For example, some of the waste in a given stream has been found to have a noticeably different character from what was thought, either by having a higher neutron output than has similar waste or by having isotopics that differ from what was expected or reported. Mistakes in individual assignments are easier to identify and understand when the results can be compared against both the campaign results and against the results of the other independent assay. For waste streams such as the *SEG* where high density and lack of spatial uniformity are major distorters of the assay results, both inter- and intra-comparisons are especially useful in finding errors and weaknesses in the method. Anomolous results then become a challenge rather than a threat, and the final result should be better assay systems with better methodologies.

Acknowledgements

In any forced collaboration between two institutions performing parallel assays, it is useful for each institution to have a *good guy* assayist and a *bad guy* assayist in order to diffuse unwanted tensions. The efforts of my colleague Jeff Chapman are gratefully acknowledged. He assumed the burden of interfacing with NFS and of collecting and collating the NFS data and information. He reported informally on much of the special aspects of the NFS waste

shipments at the previous meeting of this conference.

Oak Ridge National Laboratory is managed by Lockheed Martin Energy Research, Inc. for the U.S. Department of Energy under contract no. DE-AC05-96OR22464. The submitted manuscript has been authored by a contractor of the U.S. government. Accordingly, the U.S. Government retains a nonexclusive, royalty-free license to publish or reproduce the published form of the contribution or allow others to do so for U.S. Government purposes.

References

1. D.C. Hensley, "Autonomous Matrix Identification by the *APNea* System," *4th Nondestructive Assay and Nondestructive Examination Waste Characterization Conference*, Salt Lake City, Utah, pp. 85–108, (October 24, 1995).

2. D.C. Hensley, "The Quinby Sources, A study of Self-Shielding in the *APNea* System," submitted to the *5th Nondestructive Assay and Nondestructive Examination Waste Characterization Conference*, Salt Lake City, Utah (January 14, 1997).

3. D.C. Hensley, "Source Imaging of Drums in the *APNea* System," *4th Nondestructive Assay and Nondestructive Examination Waste Characterization Conference*, Salt Lake City, Utah, pp. 139–160, (October 24, 1995).

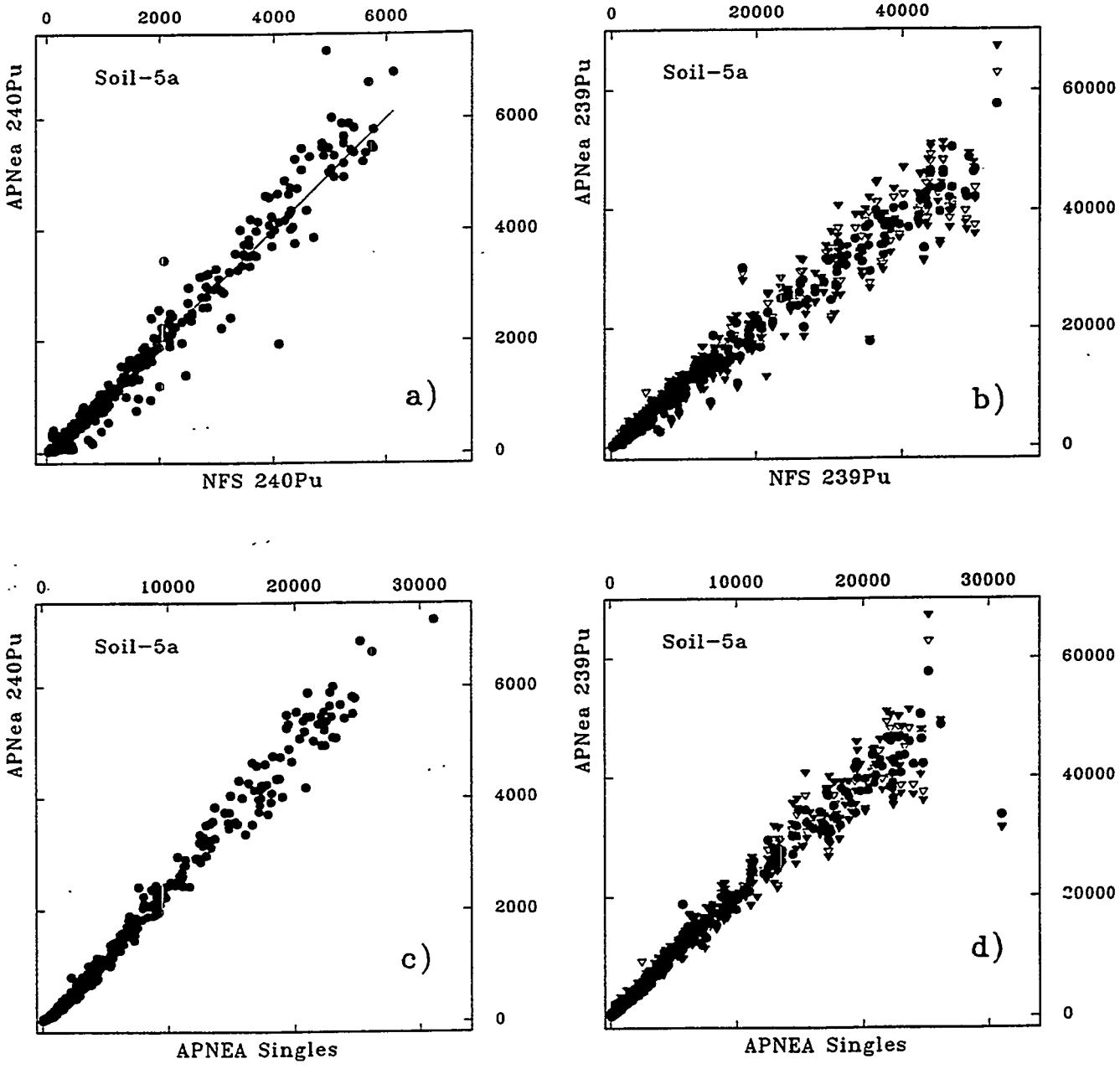

Figure 1: SOIL Intercomparison

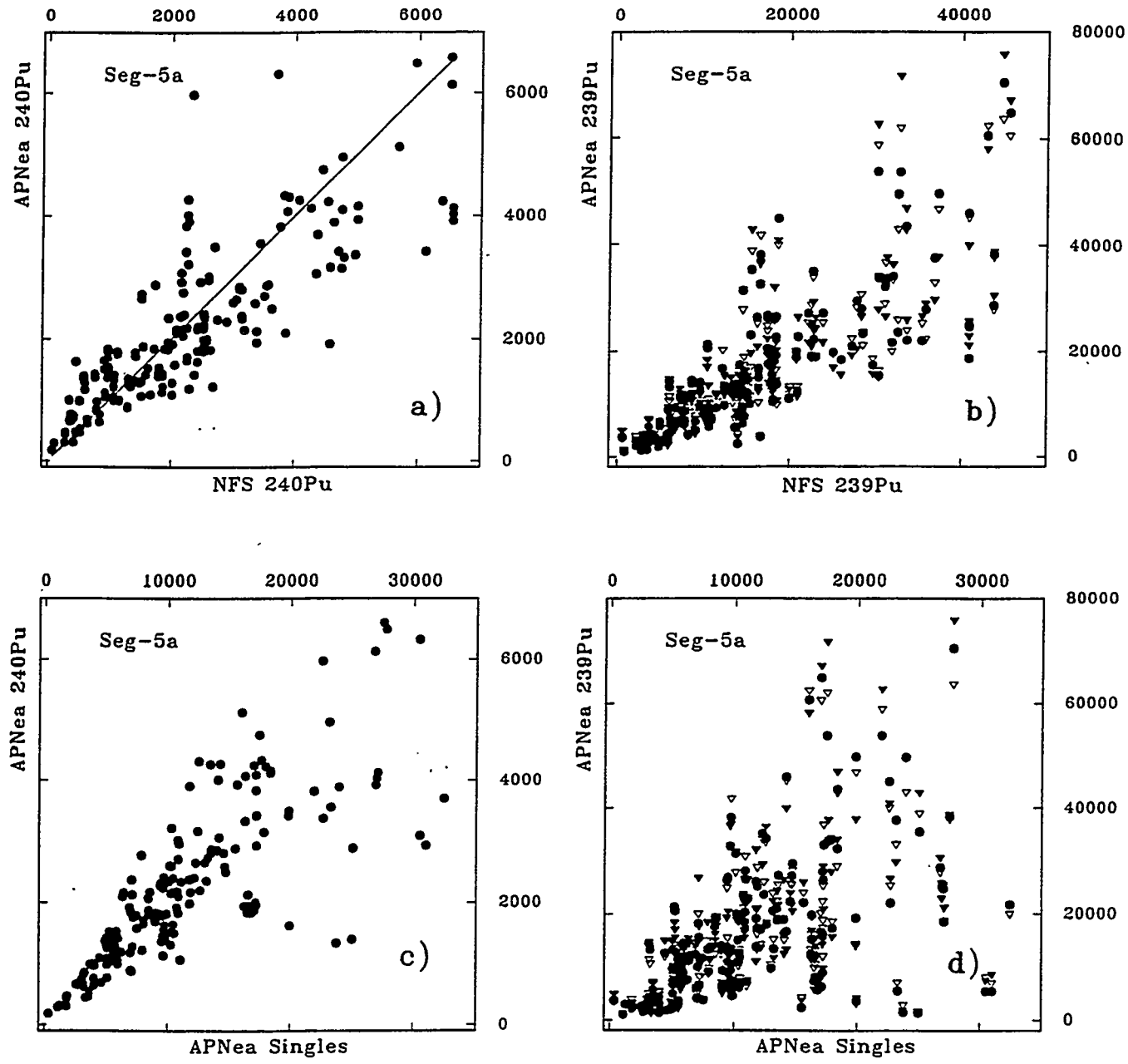

Figure 2: SEG Intercomparison

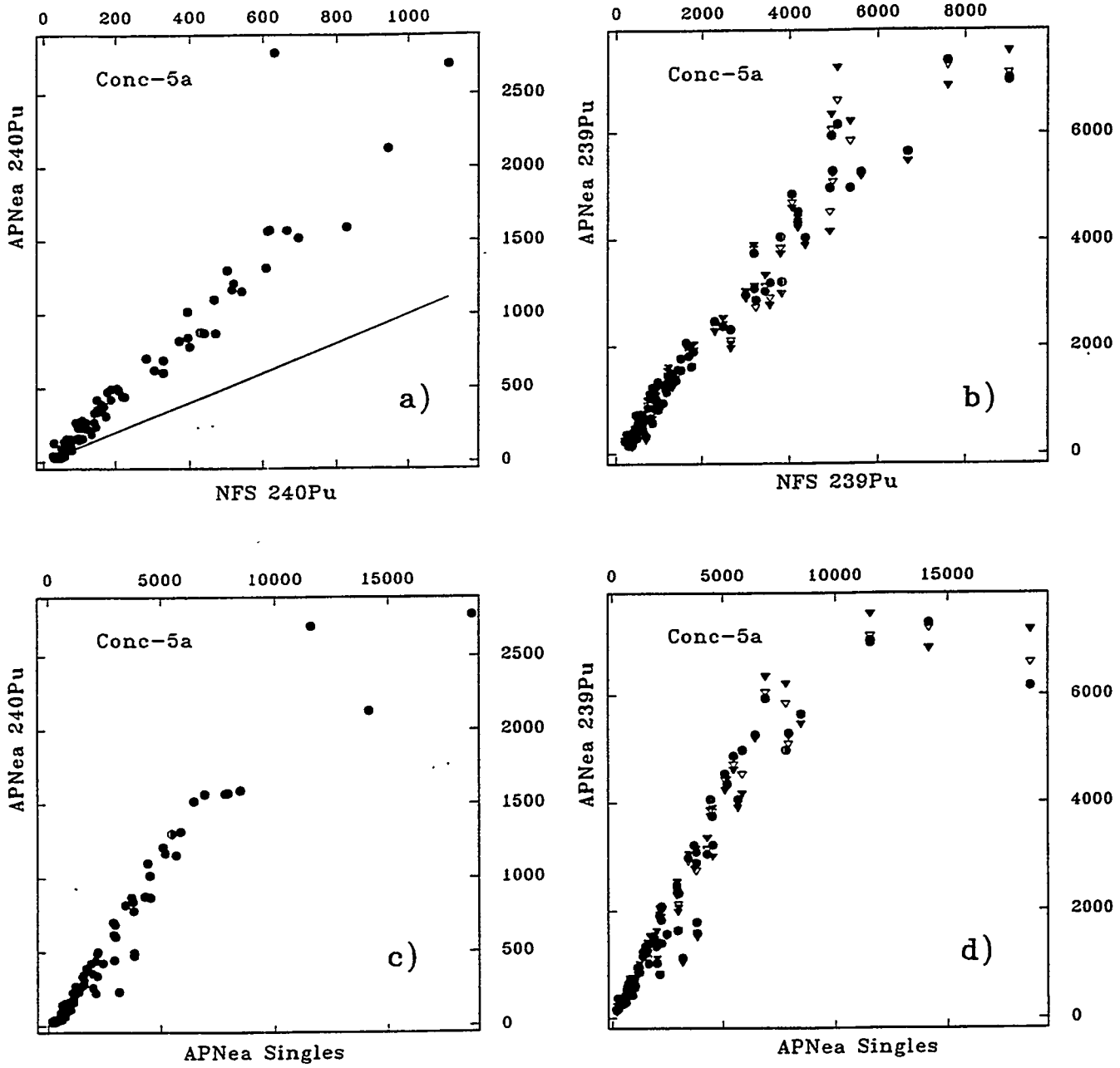

Figure 3: CONC Intercomparison

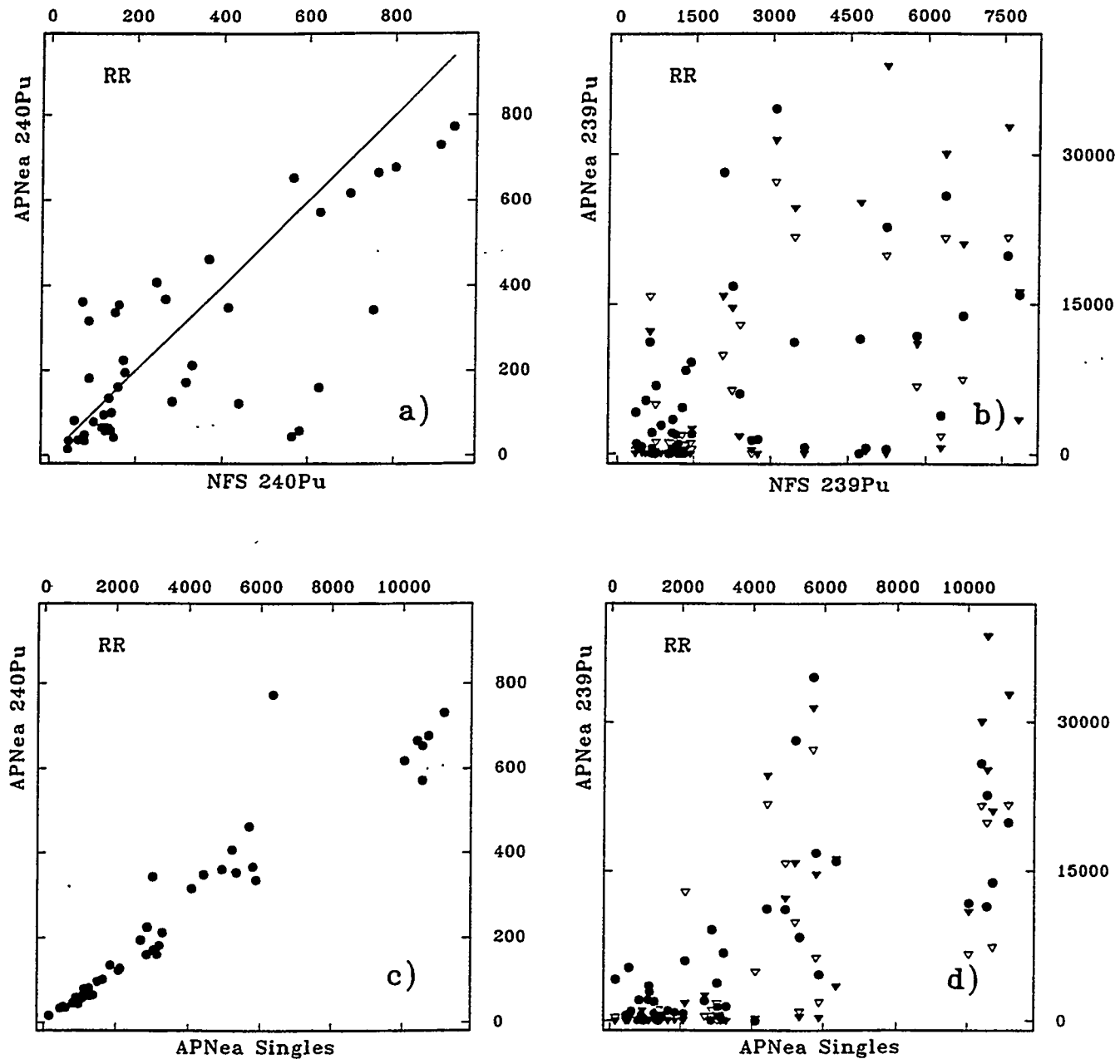

Figure 4: RR Intercomparison

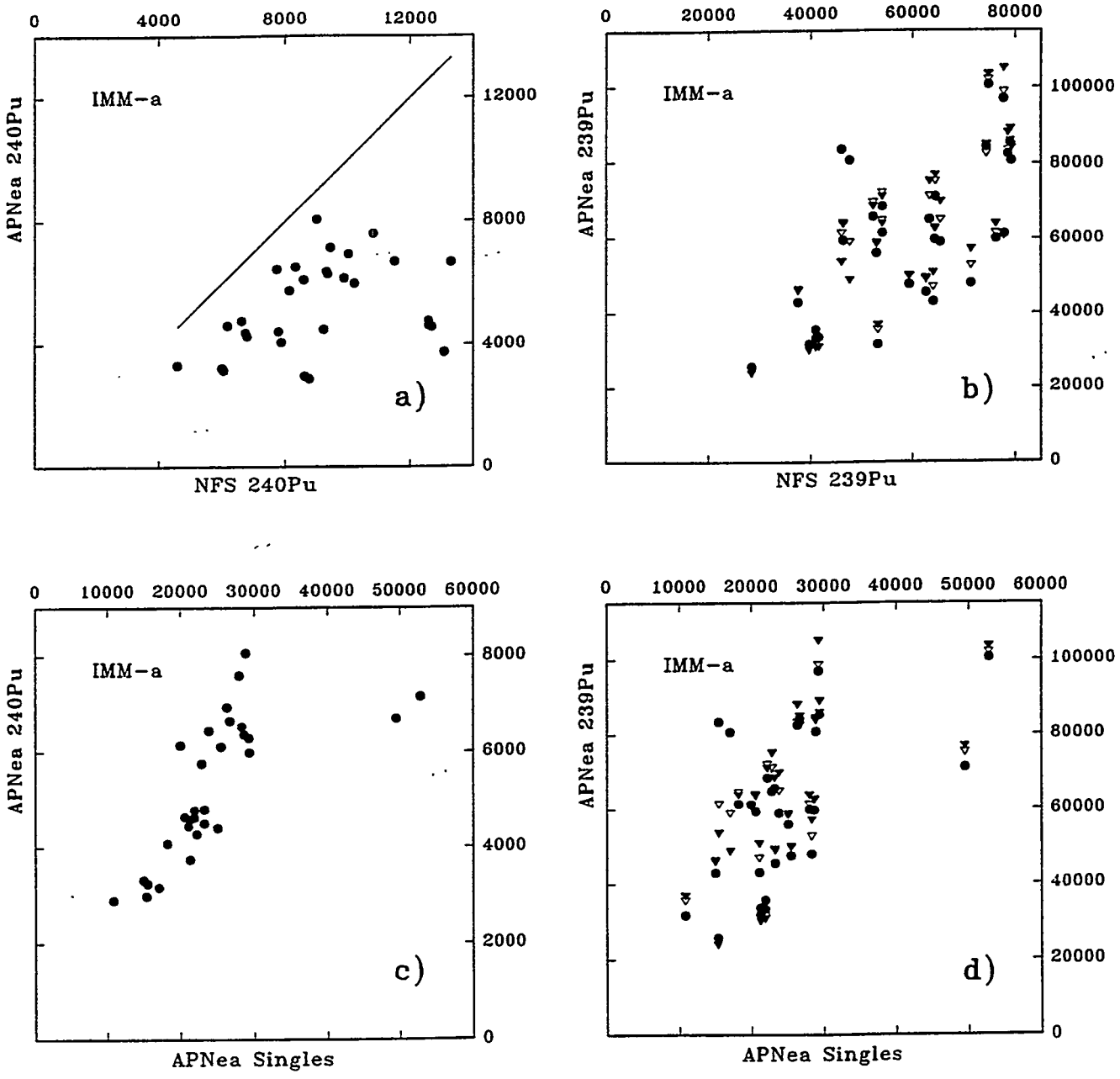

Figure 5: IMM Intercomparison

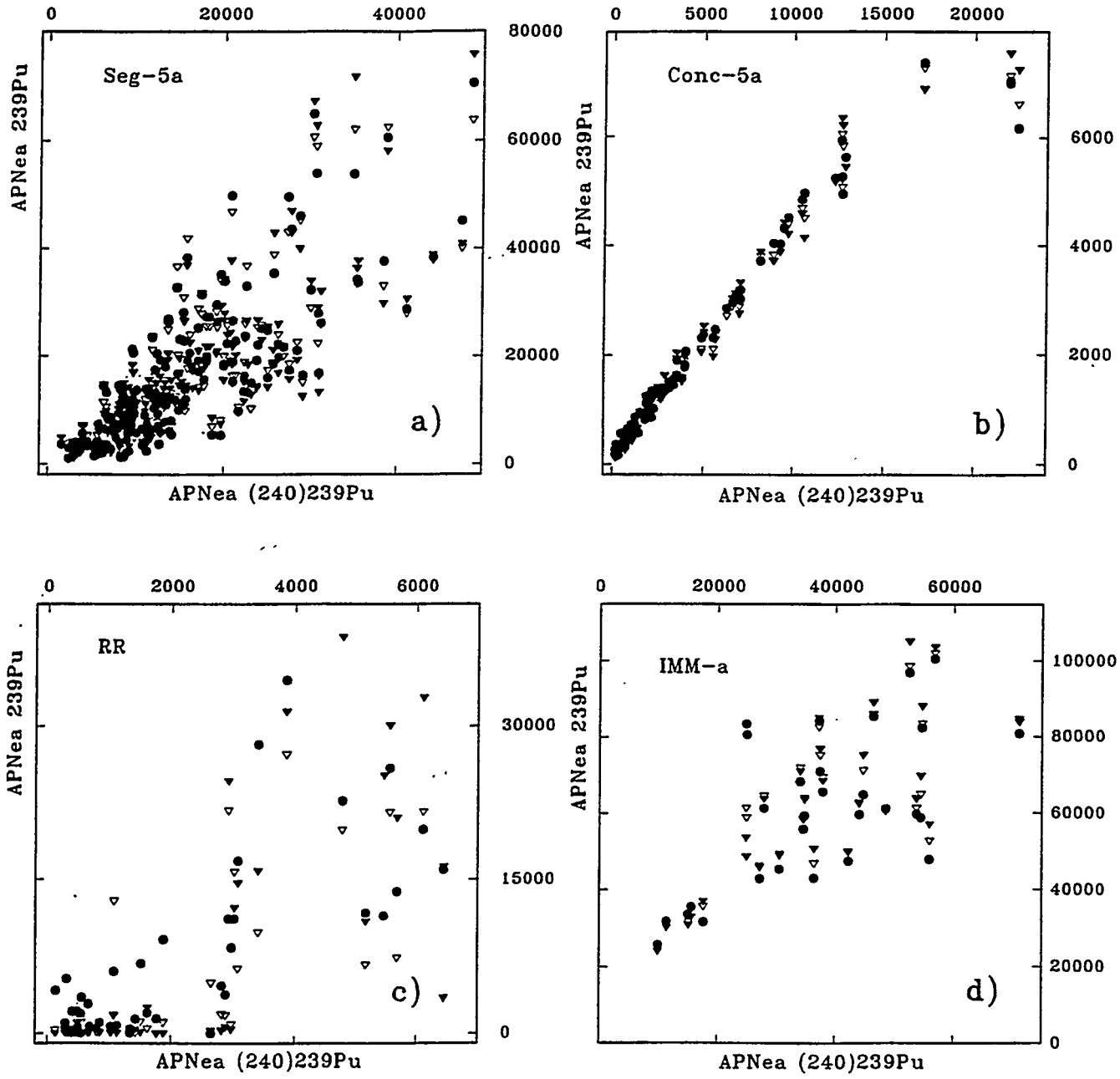

Figure 6: APNea 240Pu and 239Pu Comparison

Field Test Results for Radioactive Waste Drum Characterization with Waste Inspection Tomography (WIT)

Richard T. Bernardi
(bernardi @ interaccess.com; 847-634-6425)
Bio-Imaging Research, Inc.
425 Barclay Blvd.
Lincolnshire, IL 60069

Introduction

Waste Inspection Tomography (WIT) consists of a self-sufficient mobile semi-trailer for Non-Destructive Evaluation and Non-Destructive Assay (NDE/NDA) characterization of nuclear waste drums using X-ray and gamma-ray tomographic techniques. WIT is a Program Research and Development Announcement (PRDA) contract funded by the Environmental Management's (EM) Office of Science and Technology (OST/EM-50) for the United States Department of Energy (DOE). Bio-Imaging Research, Inc. (BIR), of Lincolnshire, Illinois has completed Phase I involving design, fabrication, factory testing, evaluation and demonstration of WIT. The recently completed 23-month WIT Phase I included the design, fabrication, and initial testing of all WIT subsystems installed on-board the trailer. Initial test results include 2 MeV Digital Radiography (DR), Computed Tomography (CT), Anger camera imaging, Single Photon Emission Computed Tomography (SPECT), Gamma-Ray Spectroscopy, Collimated Gamma Scanning (CGS), and Active and Passive Computed Tomography (A&PCT) using a 1.4 mCi source of ^{166}Ho. These techniques were initially demonstrated on a 55-gallon phantom drum with three simulated waste matrices of combustibles, heterogeneous metals, and cement using check sources of gamma active isotopes such as ^{137}Cs and ^{133}Ba with activities between 9 μCi and 250 μCi. Waste matrix identification, isotopic identification, and attenuation-corrected gamma activity determination were all demonstrated nondestructively and noninvasively in Phase I. The currently ongoing phase 2 involves DOE site field test demonstrations at LLNL, RFETS, and INEL with real nuclear waste drums. Current WIT experience includes inspecting 55 gallon drums of cement, graphite, sludge, glass, metals, and combustibles. Thus far WIT has inspected drums with 0 to 20 gms of ^{239}Pu. The minimum measured by WIT was 0.131 gm ^{239}Pu in cement. The measurement of gram loadings from 100 nCi/gm up to 200 gm ^{239}Pu is expected later in Phase 2.

The United States Department of Energy has in excess of 1,000,000 nuclear waste drums currently stored at nearly 50 sites within the United States that need to be characterized over the next few years. The contents of these drums must be characterized as either high-level waste (HLW), low-level waste (LLW) or transuranic waste (TRU), before the drums are assigned to one of three permanent storage locations. Strict permitting regulations also require information to be gathered about the condition and contents of the waste containers.

The Problem

X-ray imaging is an established method for nondestructive waste container examination. The technique generally used is real-time radiography (RTR) using a 420 kV radiation source, in which a TV camera is coupled to a two-dimensional, light-producing X-ray detector, such as an image intensifier or a scintillation screen. The camera output provides a TV image that is viewed on a monitor during X-ray exposure which, as an example, can see the motion of a moving liquid surface.

RTR systems have several disadvantages however. Area X-ray detectors typically suffer from blooming artifacts. Blooming is caused when a saturated signal spills over into neighboring sensor elements resulting in excessive brightness and limited spatial resolution. RTR systems have limited contrast discrimination with a true dynamic range of usually less than 14-bits (16,384 gray levels in the image), meaning that contrast in a single exposure is limited. An image intensifier is also limited to a small area of the drum.

RTR limits geometric depth perception because of super-positioning, and it lacks quantitative information such as two and three dimensional spatial and density measurements because the data is not in digital form. The combination of 420 kV source and a restricted detector dynamic range limits RTR penetrating and discriminating capability for inspecting the denser waste containers including cement-solidified drums, glass, sludge, and soils, which make up over half of DOE's inventory of nuclear waste drums.

Currently installed baseline gamma and neutron assay systems are limited to assumption of waste matrix homogeneity which yield assay errors with increased assay uncertainty for heterogeneous matrices, which is the majority of the waste.

The Solution

The emerging technologies in WIT are designed for nondestructive evaluation (NDE) of low level, transuranic, and mixed nuclear waste, include high-energy 2 MeV X-ray computed tomography (CT) and digital radiography (DR), with 18-bit dynamic range. Figure 1 shows a 2 MeV transmission with a DR projection image of a 55-gallon drum of TRU waste in cement, assayed by WIT with nearly 20 gms ^{239}Pu.

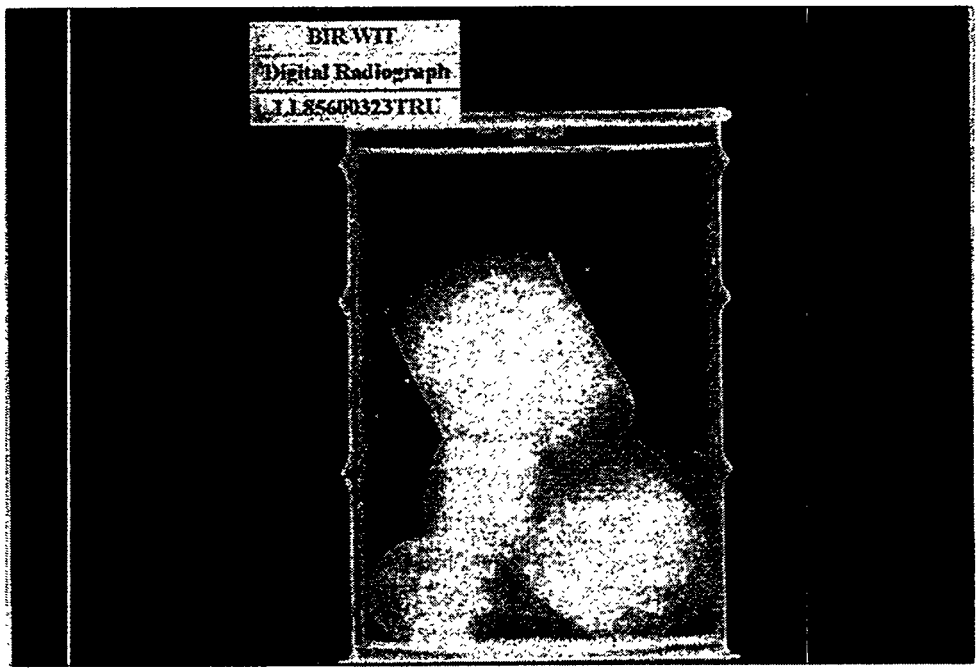

Figure 1 - 2MeV transmission DR image of 55-gallon TRU waste drum from LLNL, with nearly 20 gms ^{239}Pu.

In its conventional approach, WIT CT/DR imaging uses a curved linear array of solid-state X-ray detectors. The array is composed of individual, closely aligned detection channels. The channels are separated by thin septa that minimize crosstalk and blooming, while offering superior spatial and contrast resolution with high image quality, compared to real-time approaches. These detectors have enough dynamic range to provide contrast sensitivity of 18-bits (up to 262,144 gray levels). The greater the dynamic range and penetrating radiation, the greater the advantage in examining denser waste forms mentioned above. Thus, the WIT approach images most dense DOE waste streams with faster throughput for the lighter waste forms. This cannot be said for RTR baseline X-ray imaging systems currently used within the DOE complex. In WIT DR, the drum is moved vertically in front of the linear detector array while projection data is collected one line at a time. WIT DR requires 60 seconds per image as is shown in Figure 1. To image free liquids, a DR is acquired with a tilted drum to image the liquid surface on WIT. These techniques measure the X-ray attenuation of the waste matrix and drum. The lines are then displayed as a two-dimensional, freeze-frame projection image (like a baggage inspection X-ray) for DR.

For WIT CT, X-ray projection data is collected from a thin plane of the object, using a linear detector array on the arc of a curve while the object rotates within a thin X-ray fan beam with spiral-like motion capability. This technique is called third-generation CT. The data are mathematically combined to

form a cross-sectional CT image of a thin, irradiated plane or slice. The image in Figure 2 is a 512 x 512 10 mm thick slice through a LLNL TRU waste drum showing two different densities of cemented waste. Each 10 mm thick CT image slice is scanned and reconstructed between 8 and 30 seconds per slice.

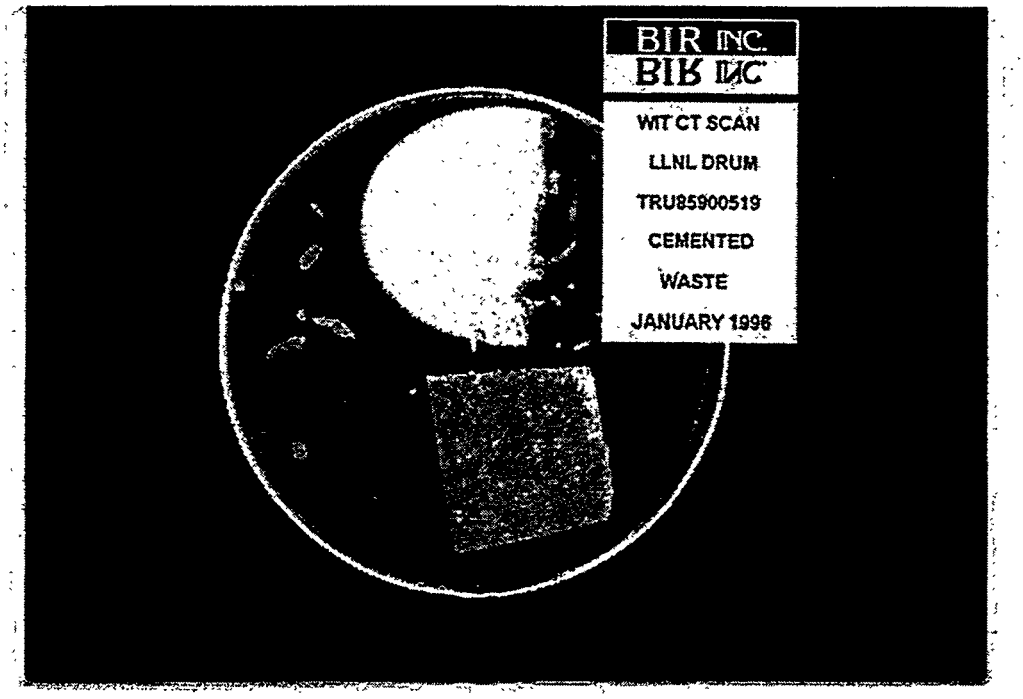

Figure 2 - 2 MeV 10 mm thick CT slice, through LLNL cemented TRU waste with varying density.

Up to 90 CT slices can be stacked by WIT to form a volume rendering of drum content, light shaded and cutaway, such as the one shown in Figure 3. Each volume rendered view requires 45 seconds of post processing. WIT processes up to 50 views at equal drum rotation angles to provide a cinematic presentation of rotating drum content.

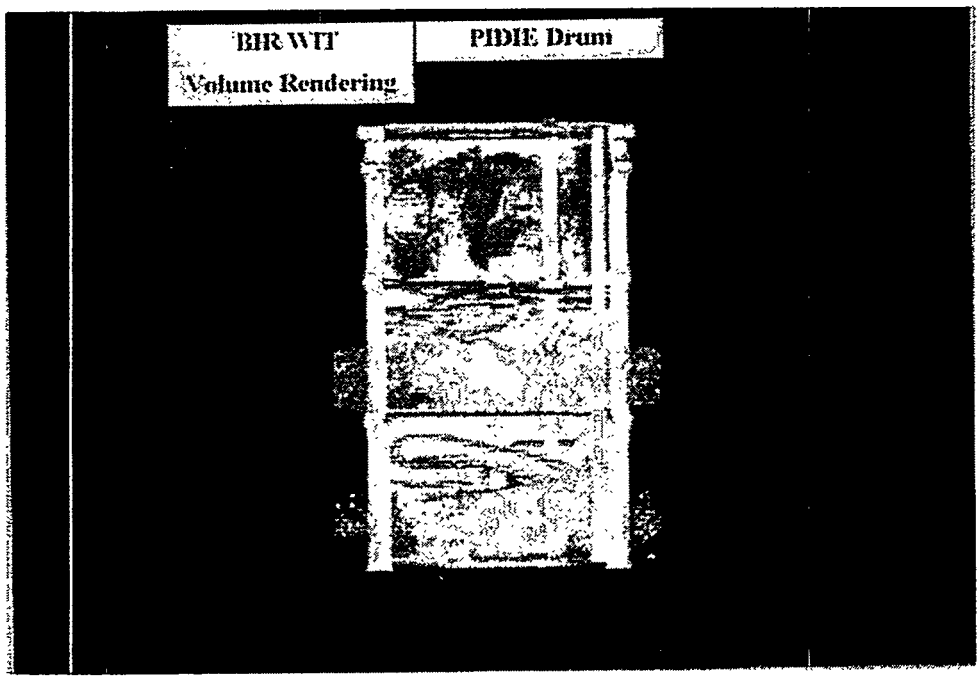

Figure 3 - Volume rendered image from WIT CT of a LLNL phantom drum, showing combustibles, metals, and cement matrices.

With a cinematic presentation of rotating drum contents, volume rendered CT could possibly replace invasive visual examination for verification of drum contents with radiography.

Two emission imaging techniques are employed on WIT for characterizing gamma emitting materials in waste containers. The first of these is gamma emission tomography, commonly called single-photon emission computed tomography (SPECT). Rather than measuring gamma-rays from an external radiation source, SPECT measures the gamma-ray emission inherent in the radioactive waste from within the drum matrix. In this case, emission from actual nuclear waste within a container can provide three-dimensional volume or slice data of the radioactive source(s) within the container. SPECT uses large area sodium iodide crystals with a two-dimensional array of photo multiplier tube (PMT) detectors for rapid localization of gamma-ray emissions in two-dimensional space and in 3-D with SPECT. These area cameras are called Anger cameras. Figure 4 shows 32 gamma camera views of 5 gamma sources in the figure 3 drum. Each WIT SPECT view can require between 1 and 60 seconds of data collect time.

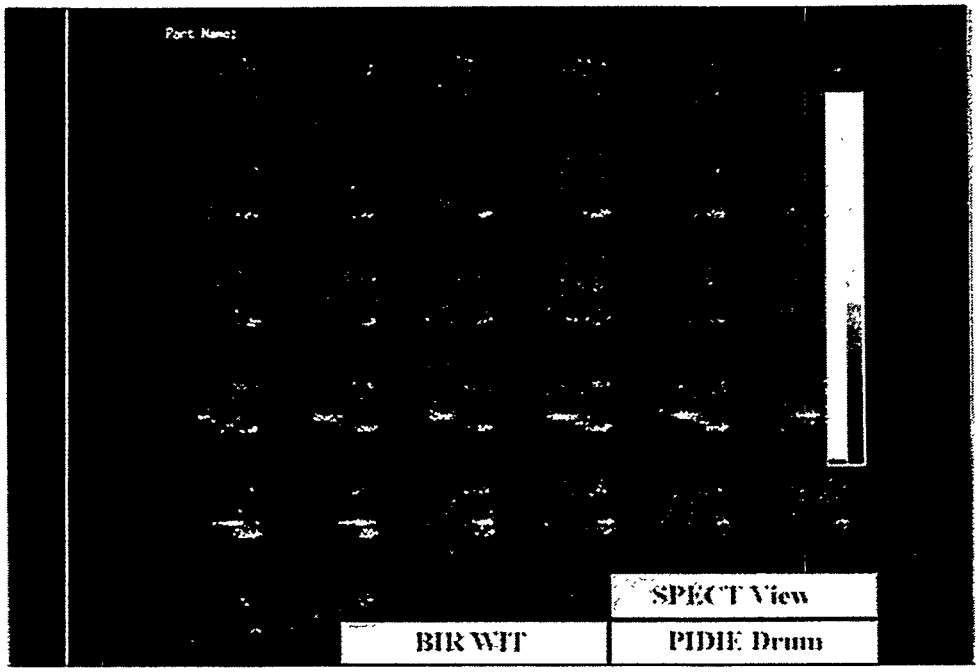

Figure 4 - WIT provides 32 gamma SPECT views of the LLNL PIDIE drum with a total of 1.5 gm ^{239}Pu. The "hottest source shown is only 0.131 gm ^{239}Pu in a cement matrix, with a total equivalence of 220 nanoCuries per gram in cement.

The gamma spectroscopy and assay techniques on WIT are called Collimated Gamma Scanning (CGS) and Active and Passive CT (A&PCT), both developed by LLNL. CGS is similar to SGS with a homogeneous matrix assumption. However, A&PCT corrects for a heterogeneous matrix. Active CT on WIT is somewhat similar to the conventional X-ray CT techniques. However, the differences are that a radioisotopic source and single-channel high-purity germanium detector are used with a first-generation active CT approach. Active CT data result in the absolute determination of the attenuation of the drum and its contents. As is shown in Figure 5, A&PCT provides for energy specific geometry and matrix corrections down to drum volume elements that are cubic with 50 mm sides to decrease assay uncertainty. Depending on the waste stream and activity, each WIT gamma assay, using either SGS or A&PCT could require between 0.5 and 65 hours per drum.

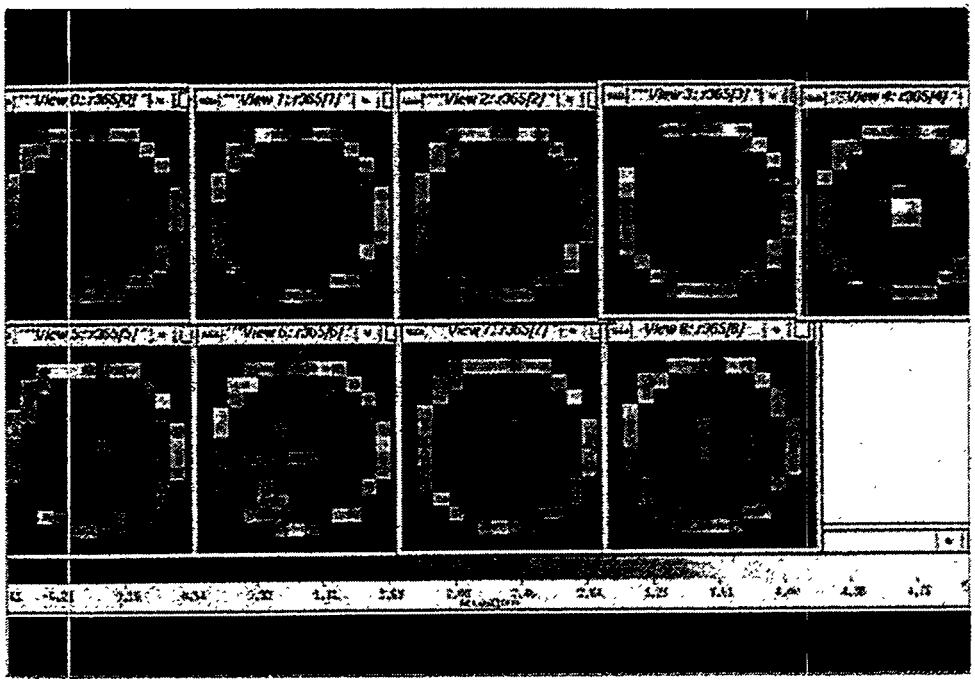

Figure 5 - Active CT from WIT showing energy specific attenuation in a drum with a 19.6 gm source of ^{239}Pu, with 9 slices, each 50 mm thick.

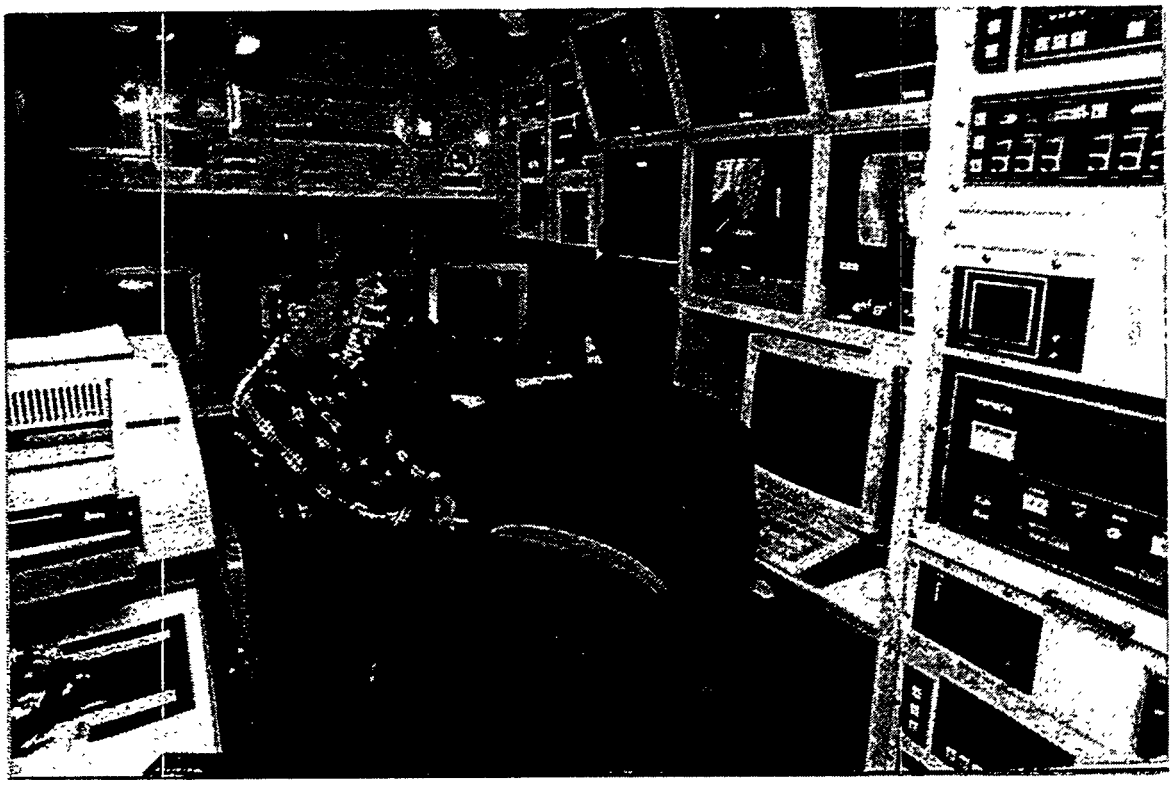

Figure 6 - The WIT control room.

A&PCT uses an energy sensitive single-channel high-purity germanium detector for gamma-ray nuclear spectroscopy. This technique, for nondestructive assay (NDA), can directly identify the emitting isotopic species and the total gram content of ^{239}Pu equivalent for drum assay.

Figure 7 - The trailer which houses the WIT system.

Applications

The mobile feature of WIT, shown in Figures 6 and 7, allows inspection technologies to be brought to the nuclear waste drum storage site without the need to relocate drums for safe, rapid, and cost-effective characterization of regulated nuclear waste. The combination of these WIT characterization modalities provides the inspector with an unprecedented ability to noninvasively characterize the regulated contents of waste drums as large as 416 liters (110 gallons), weighing up to 726 kg (1,600 lbs). Any objects that fit within these size and weight restrictions can also be inspected on WIT, such as smaller waste bags and drums that are 19 and 132 liters (5 and 35 gallons). WIT can inspect LLW, TRU, and MW for all DOE matrices from low density combustibles up through high density matrices like glass, cement, sludge, and metals, which includes most, if not all, DOE waste streams.

BIR has designed the trailer and multiple inspection techniques including DR, CT, SPECT, and area gamma-ray imaging. BIR has also developed the WIT operational software, the computer hardware, and the gantry mechanical systems. Lawrence Livermore National Laboratory (LLNL), as a subcontractor to BIR under a Work-for-Others agreement with BIR, has developed the A&PCT scanning technique and is participating in WIT evaluation. Early BIR efforts prior to WIT involved investigating the feasibility of using CT to characterize nuclear waste between 1990 and 1993 under Small Business Innovative Research (SBIR) grants from DOE.

The data presented in this text are the initial phase 2 results from LLNL in early 1996. Throughout 1996 WIT is continuing demonstrations at Rocky Flats and Idaho National Engineering Laboratory, both DOE facilities. A summary of Phase 2 results up to INEL findings can be found at the end of this text.

Future Work

A second PRDA contract has been awarded to BIR to integrate Neutron based waste drum characterization capability with WIT. Though WIT's NDE and NDA systems can examine gamma emission sources, some dense TRU waste drums are poor gamma emitters. A semi-trailer assay system called Active Passive Neutron Examination Assay (APNEA) has been built by Lockheed Martin Specialty Components (LMSC) in Largo, FL. APNEA was originally developed by Oak Ridge. APNEA can measure transuranic fissionable isotopes even in the presence of dense matrices. In addition to imaging capabilities, APNEA makes both geometry and matrix corrections for heterogeneous waste. The first WIT-APNEA data fusion results are shown in Figure 8, where WIT volume rendered X-ray CT data of a sludge phantom drum is shown fused to APNEA data with one gallon volume elements. The gray scale number given to the APNEA volume elements is proportional to the ^{239}Pu gms in that volume.

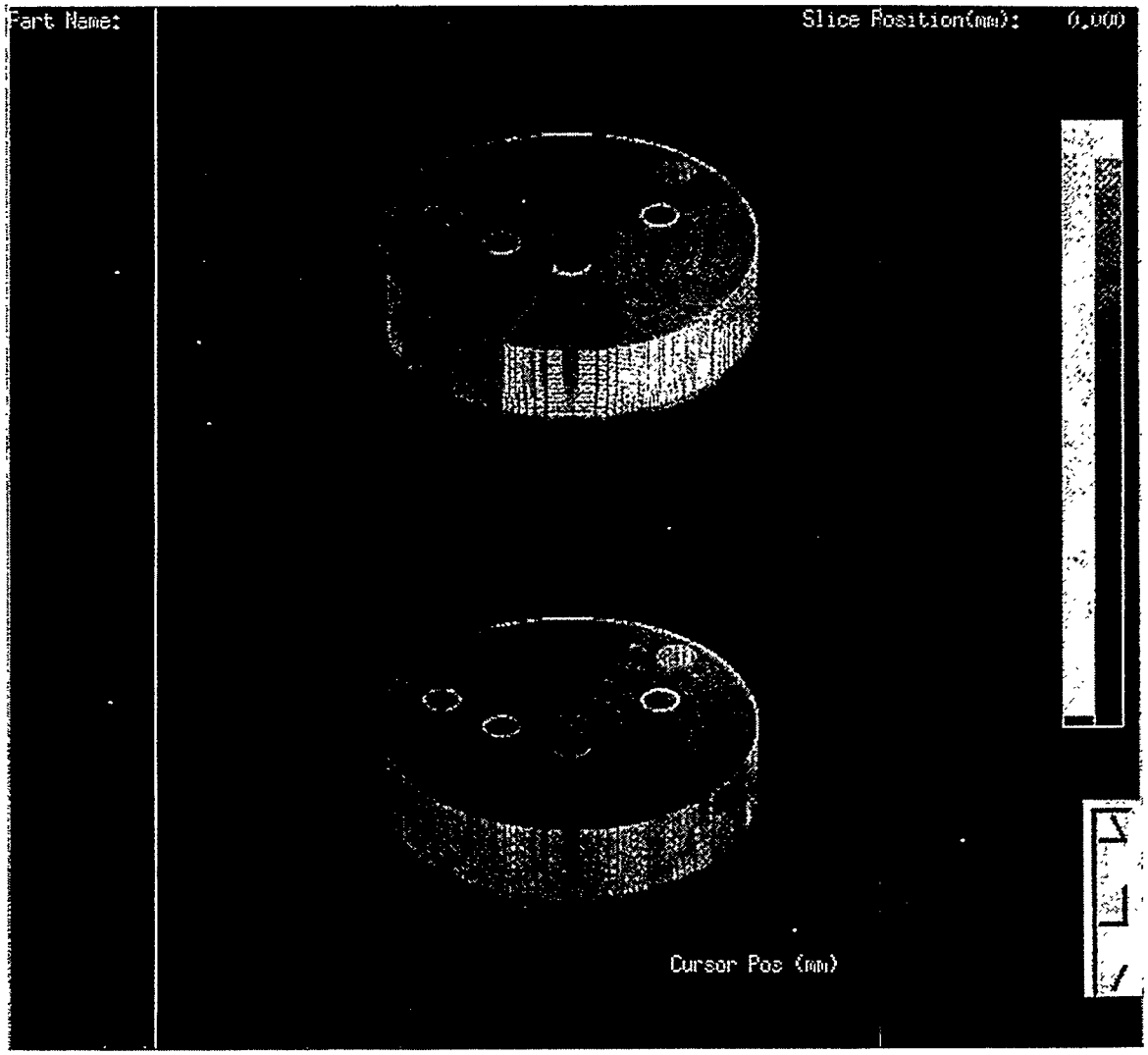

Figure 8 - WIT CT volume rendering of a phantom sludge drum of TRU waste fused to course (pie shaped) volume elements of APNEA data. The gray scale of each large volume element number is proportional to the total grams of ^{239}Pu in the drum.

Acknowledgments

WIT is a Program Research and Development Award (PRDA) contract number DE-AC21-93MC30173. The WIT PRDA is funded by Environmental Management's (EM) Office of Science and Technology (OST/EM-50) for the United States Department of Energy (DOE). The program is managed by the U. S. government from the DOE Morgantown Energy Technology Center (METC) in Morgantown, West Virginia. The METC COR is Steve Cooke, and the Contract Specialist is Mary Spatafore.

NOTE: Other WIT funding sources have been a second PRDA DE- AC21-96MC33127 and an RCI cooperative agreement 96-RCI-09, also managed by METC

BIR plans to commercialize WIT and plans to offer drum scanning/characterization services to DOE and other sites requiring mobile characterization capabilities.

PU-238 ASSAY PERFORMANCE WITH THE CANBERRA IQ3 SYSTEM

L. Booth, B. Gillespie and G. Seaman
Canberra Industries, Inc.

ABSTRACT

Canberra Industries has recently completed a demonstration project at the Westinghouse Savannah River Site (WSRC) to characterize 55-gallon drums containing Pu-238 contaminated waste. The goal of this project was to detect and quantify Pu-238 waste to detection limits of less than 50 nCi/g using gamma assay techniques. This would permit reclassification of these drums from transuranic (TRU) waste to low-level waste (LLW). The instrument used for this assay was a Canberra IQ3 high sensitivity gamma assay system, mounted in a trailer. The results of the measurements demonstrate achievement of detection levels as low as 1 nCi/g for low density waste drums, and good correlation with known concentrations in several test drums. In addition, the data demonstrates significant advantages for using large area low-energy germanium detectors for achieving the lowest possible MDAs for gamma rays in the 80-250 keV range.

INTRODUCTION

The goal of the mobile waste characterization service provided by Canberra was to demonstrate the capabilities of the assay system to meet WSRC requirements for characterizing "Suspect TRU" category waste. The IQ3 system contains three 45% relative efficient HPGe detectors and three large area Low Energy Germanium (LeGe) detectors for high sensitivity counting. Drums are loaded onto an automated conveyor system, moved to the counting chamber, loaded with a fork lift mechanism mounted on the shield door and placed on a turntable in a six inch thick steel shield counting chamber. Following completion of the count, the drum is unloaded onto the exit side of the conveyor system. All operations may be controlled from the operator's console in the control room. Results are computed and printed or displayed within two minutes of count completion.

The IQ3 was placed on a waste storage pad in the solid waste management area of the WSRC site. The pad is covered with a pole tent structure and is used for TRU waste drum storage. The pad is considered a Radiological Buffer Area (RBA) requiring both security and radiological controls. Canberra was required to provide all utilities and trailer services, while WSRC provided drum handling and safety support.

Two sets of drums were selected for counting, a group of unknown process drums, and a set of known test drums. The unknown drums were selected from low activity, low

Two sets of drums were selected for counting, a group of unknown process drums, and a set of known test drums. The unknown drums were selected from low activity, low density waste drums stored on site, and consisted of six drums marked "Pad Storage" and 14 drums designated as "Culvert Storage". The Pad Storage drums were known to have originated from process facilities, but were believed to contain very low level (or possibly no) activity. The Culvert Storage drums were so designated because of the possibility of containing more than 0.5 Ci TRU waste. All unknown drums had no detectable external radiation levels and weighed from 50 to 200 pounds. Drums were known to contain low density, low activity compactable waste such as protective clothing, plastic sheeting, breathing air line hosing, small hand tools and polyethylene bottles. The known test drums were prepared by WSRC personnel and contained known (to WSRC) amounts of Pu-238 in similar drum matrices.

All drums were counted on the IQ3 system for count times ranging from 15 minutes to one hour. Following the initial counting of all drums, system parameters were adjusted to account for WSRC specific conditions, and a second round of counting for selected drums was performed. Results are presented and discussed in the following sections.

Figure 1: Picture of IQ3 System

SYSTEM OPERATION

The IQ3 system contains three 45% relative efficient HPGe coaxial detectors for wide energy range detection and three 2800 sq. mm area LeGe detectors for low energy gamma/x-ray detection. The system is able to correct for non-homogeneous matrix distributions by employing photon transmission corrections, and identifies non-homogeneous source distributions by performing multi-spectral scaling as the drum rotates. The LeGe detectors can be used for Multi Group Analysis(MGA) when Pu or U isotopes are present. The system has a scale for weighing drums and calculates densities based on these weights. The data are analyzed with the standard Canberra Genie Waste Assay (GWAS) software.

The HPGe coaxial detectors are energy calibrated to about 0.5 keV per channel for a 4096 channel spectrum. Two drum analyses may be performed with these detectors: a sum of spectra analysis and an average segment analysis. The sum of spectra analysis sums the three detector spectra and analyzes the summed spectra for nuclide activity. This analysis assumes a uniform activity and matrix distribution throughout the drum and uses an efficiency which is interpolated from a set of calibration curves obtained from uniformly distributed activity in different density drums.

The average segment analysis routine uses the individual coaxial detectors and corrects each for matrix transmission. The transmission sources (Ba-133 is used to evaluate transmission in the 80 to 400 keV region) located opposite each coaxial detector are used to evaluate the matrix density in the region directly in front of the detector. Transmission peak intensities are compared to an empty drum transmission to develop correction factors for the matrix, using attenuation coefficients for lucite as the default values. The transmission corrected activity values for each of the three detectors are averaged to arrive at the total drum average segment activity.

The LeGe detectors are normally used to perform MGA on spectra with multiple Pu or U isotopes, and requires Pu-239 and Pu-241 to be present for Pu determinations. Since the demonstration project involved the measurement of Pu-238 only, MGA could not be used. As an alternative, the LeGe detectors were calibrated and configured to perform a sum of spectra analysis, as with the coaxial detectors, and were used as confirmation of HPGe coaxial detector results. The initial energy range for the LeGes was 0 to 300 keV, which was deemed optimum for Pu-238 measurements. Additional studies were performed to evaluate the LeGes when configured for use with transmission sources and for energies up to about 500 keV.

The GWAS software provides methods for assessing both source and matrix non-uniformity. The results of these analyses can be used to determine which analysis routine (sum of spectra or average segment) is optimum and to assign appropriate uncertainties due to non-uniformity. Multi-Spectral Scaling is used to determine radial source and/or matrix non-uniformities. For each detector, sample and transmission source counts are

collected in eight radial segments as the drum rotates. For sample counts, a high count rate in one segment indicates a concentration of activity in that segment. Likewise, a low transmission source count in one segment indicates a high matrix attenuation and a possible non-uniform matrix distribution.

Nuclide results and transmission corrections, per detector, may be used to infer vertical non-uniformity for both source and matrix. High activity results for one detector indicates a concentration of activity in a vertical segment of the drum, and a low transmission factor for a detector indicates high absorption, and probable matrix concentration or variation of matrix material, in a vertical segment.

SYSTEM CALIBRATION

The IQ3 analysis system was calibrated to measure radionuclide activities and/or concentrations in 55 gallon drums. Efficiency calibrations are made with uniform source and matrix distributions. A uniform source distribution is simulated with line sources placed vertically in the drum in the center of a series of equal volume cylinders such that a uniform distribution is approximated when the drum is rotated. The line sources consist of mixed nuclides with photopeaks at intervals sufficient to calibrate over the energy range of interest. Four drums with various density materials are used to obtain efficiency vs density calibrations. Calibration drums were standard DOT-17C containers, without liners. Due to license restrictions, Canberra is unable to possess sufficient Pu or U sources to perform calibrations or verifications with actual TRU materials, and must rely on customers to provide these verifications when possible.

DRUM COUNTING PROCEDURES

All drums were loaded on the conveyor and counted on the IQ3 system using the automated GWAS procedures. Count times were varied to obtain a range of detection limits. For the first round of counting, factory specified default parameters were used for data acquisition and analysis. Following review of this data, several modifications were made to address WSRC specific conditions. For example, initial Pu-238 quantification was accomplished using the 152 keV line only, since other lines were considered as likely to be interfered with by other nuclides or had abundances too low to be of use. Subsequent analyses also used the Pu-238 line at 99.9 keV, since it was determined that interfering nuclides were absent from the sample and test drums. Efficiencies were adjusted to account for WSRC drum liners, which were absent from Canberra calibration drums. The average segment analysis routine was selected for drum analyses, based on indications of non-uniformity of materials in drums. Correct tare weights for the WSRC drums were entered as required. Following these modifications, a second round of counting of selected drums was performed to establish final accuracy, precision and sensitivity values for the IQ3.

DRUM COUNTING RESULTS

Results of measurements of unknown drums are shown in Table 1. All six drums labeled as Pad Storage drums showed no detectable Pu-238 activity. The MDA levels ranged from 1.7 to 4.9 nCi/g Pu-238. The Culvert Storage drums contained from non-detectable to 2000 nCi/g Pu-238, but all had less than 0.5 Ci total activity, the requirement for Culvert Storage designation. In addition to Pu-238, several drums contained very low levels of Cs-137, K-40 and/or Ra-226 daughters Pb-214 and Bi-214 (these concentrations were on the order of a few pCi/g). These results confirmed that WSRC had been conservative when classifying and storing "Suspect TRU" waste, and that most of this category of drums could be designated as low level waste and dispositioned accordingly.

Table 2 shows the results of final accuracy, precision and sensitivity determinations using the WSRC prepared test drums. The values in Table 2 are those obtained following the initial round of counting and subsequent system realignment for WSRC specific conditions. Due to project time limitations, Canberra was unable to perform the complete set of replicate counts required by the TRU Quality Assurance Program Plan; however, the data collected indicates that the IQ3 easily meets the Quality Assurance Objectives(QAOs) for these drums. These results show that the system is accurate to better than +/- 10% for concentrations ranging from 50 to 200 nCi/g Pu-238. The precision (reproducibility) at 50 nCi/g was good, with a standard deviation of +/- 4.1 % and all measurements within the S.D. Detection limits on the order of a few nCi/g are achievable in a 30 minute count with the coaxial detectors. Counting uncertainties for these measurements are on the order of +/- 20% (95% confidence level) for a 30 minute count. Other uncertainties have been estimated at +/- 30%, based on review of all count parameters and estimated systematic uncertainties. Total propagated uncertainties are estimated to be in the +/- 50% range for these drums.

Note: The results for the initial round of counting showed that the system was biased low by -8% to -24% for the test drums, values which are still within the acceptable range for the QAO for accuracy. Realignment of the system resulted in increasing the response of the system by about 15%.

CONCLUSIONS

The results of the TRU waste characterization demonstration project verifies that the Canberra IQ3 system will measure Pu-238 activity in low activity, low density waste drums with high accuracy, precision and sensitivity. The system allows for segregation of TRU waste from low level waste for Pu-238 contamination and meets the QAOs for accuracy, precision, sensitivity and uncertainty for TRU waste characterization of these drums. Based on counting results, Canberra estimates the dynamic range of the standard IQ3 for counting Pu-238 to be from microgram quantities to approximately 1 gram Pu-238.

Table 1 Summary of TRU waste drum measurements on unknown drums.

All values are Pu-238 nCi/g concentrations. The error is a 2 sigma counting error

Pad Storage Drums	Pu-238 nCi/g	Culvert Storage Drums	Pu-238 nCi/g
557460	<4.6	608969	<8.3
557459	<4.1	608967	930 +/- 120
557475	<4.9	608970	1180 +/- 190
557521	<1.7	608971	<5.9
557439	<3.2	608974	1800 +/- 220
557454	<2.8	608979	220 +/-35
		608978	1950 +/- 260
		608975	80 +/- 12
		608968	<6.7
		608976	<2
		608973	1200 +/- 160
		608965	<5.3
		608977	430 +/- 80
		608972	510 +/- 65

Table 2a. Summary of TRU test drum measurements for accuracy.
The table shows measured vs actual activities for the three test drums. Errors are 2 sigma counting errors only. Drum 3b was prepared following CI reconfiguration and recounting of the original test drums.

Test Drum #	CI Result Activity (mCi)	Actual Activity (mCi)	CI Result Concen (nCi/g)	Actual Concen (nCi/g)
1	2.08 +/- 0.34	2.07	100 +/- 16	97.4
1	1.99 +/- 0.33	2.07	98 +/- 16	97.4
2	0.89 +/- 0.17	1.00	46 +/- 9	50.1
2	0.94 +/- 0.18	1.00	48 +/- 9	50.1
2	0.95 +/- 0.18	1.00	49 +/- 9	50.1
2	0.91 +/- 0.17	1.00	46 +/- 9	50.1
2	0.92 +/- 0.18	1.00	47 +/- 9	50.1
3	3.23 +/- 0.50	3.13	208 +/- 32	194.4
3	3.31 +/- 0.52	3.13	213 +/- 34	194.4
3	2.95 +/- 0.38	3.13	190 +/- 35	194.4
3b	1.41 +/- 0.23	1.30	41 +/- 7	37.4
3b	1.33 +/- 0.24	1.30	38 +/- 7	37.4
3b	1.38 +/- 0.23	1.30	40 +/- 7	37.4

Table 2b. Summary of TRU test drum measurements for precision.
Drum 2 counted five times for 20 min. each for reproducibility. All measurements fall within one S.D. of the mean.

Drum 2 Activity (mCi)
0.918
0.905
0.950
0.889
0.936

Mean = 0.919
S.D. = 0.038

Table 2c. Summary of TRU test drum measurements for sensitivity.
Drum 608965 recounted to obtain an a priori estimate of system sensitivity for different count times. Drum density is 0.08 g/cc.

Count Time (min)	MDA value Activity (mCi)	MDA Value Concen (nCi/g)
10	<0.161	<10.1
20	<0.112	<7.20
30	<0.088	<5.58
60	<0.062	<3.86

EXPERIENCE OPERATING LANL'S MOBILE PASSIVE/ACTIVE NEUTRON (PAN) ASSAY SYSTEM

D.P. Taggart, S.E. Betts, E.F. Martinez, J.L. Mendez, C.D. Rael , J.J. Vigil

Chemical Science and Technology Division
Mail Stop J594
Los Alamos National Laboratory
Los Alamos, NM 87544
(505)665-6149 (phone)
(505)665-8346 (FAX)

ABSTRACT

We present a summary of our operating experience with LANL's mobile PAN[1] assay system. This system was acquired from the Carlsbad Area Office in 1994, refurbished, calibrated and fielded for the first time on LANL's TRU waste in the winter of 1996. It is functionally identical to other PAN systems throughout the DOE complex and its software operating system is the same as that used at INEL.

Since January 1996, it has passed the first round of the Performance Demonstration Program (PDP)and has been used to assay several hundred drums of LANL's TRU waste. We will report on the difficulties experienced assaying homogeneous wastes with high (α,n) neutron fluxes. We will also report on our experience assaying debris waste in both the active and passive modes of PAN operation.

INTRODUCTION

Since the last NDA/NDE conference, we have had an opportunity to use LANL's Mobile Passive/Active Neutron Assay System for the first time to assay a variety of LANL TRU wastes

and to participate in the Performance Demonstration Program. We intend to use the PAN to begin certifying waste for shipment to the Waste Isolation Pilot plant along with our Tomographic Gamma Scanner (TGS) and newly acquired Canberra High Efficiency Neutron Counter (HENC). This past year's experience has been invaluable in pointing out the relative strengths and weaknesses of our various assay systems and has led to a clearer idea of how waste will be routed from storage to the correct instrument to perform the certifying assay.

WASTE ASSAY

National Transuranic Program Office Project

Our first experience using the mobile PAN on TRU waste at LANL was in support of a RCRA characterization project in the winter of 1995/1996. The goal of the project was to obtain RCRA characterization data of four LANL TRU waste streams to support WIPP's permitting process. The wastes selected for characterization were cemented sludges and pyrochemical salts.

The assay results were characterized by large uncertainties due to the very large (α,n) neutron signals produced in the low-Z waste matrix. An effect of these large (α,n) neutron signals is indicated in Figure 1. This plot of gross coincidence count rate (before correction for accidental coincidence events and dead time) versus totals count rate shows that the (α,n) contribution to the coincidence signal generally pushed the assay into a regime which most closely resembled a purely singles (i.e.- (α,n)) neutron source. In fact, the totals count rate generally greatly exceeded what would be expected from a drum

loaded with 200 grams WG-Pu (6% ^{240}Pu) metal. The resulting effect of high singles neutron detection rates on assay precision and accuracy has been observed and simulated by others[2,3].

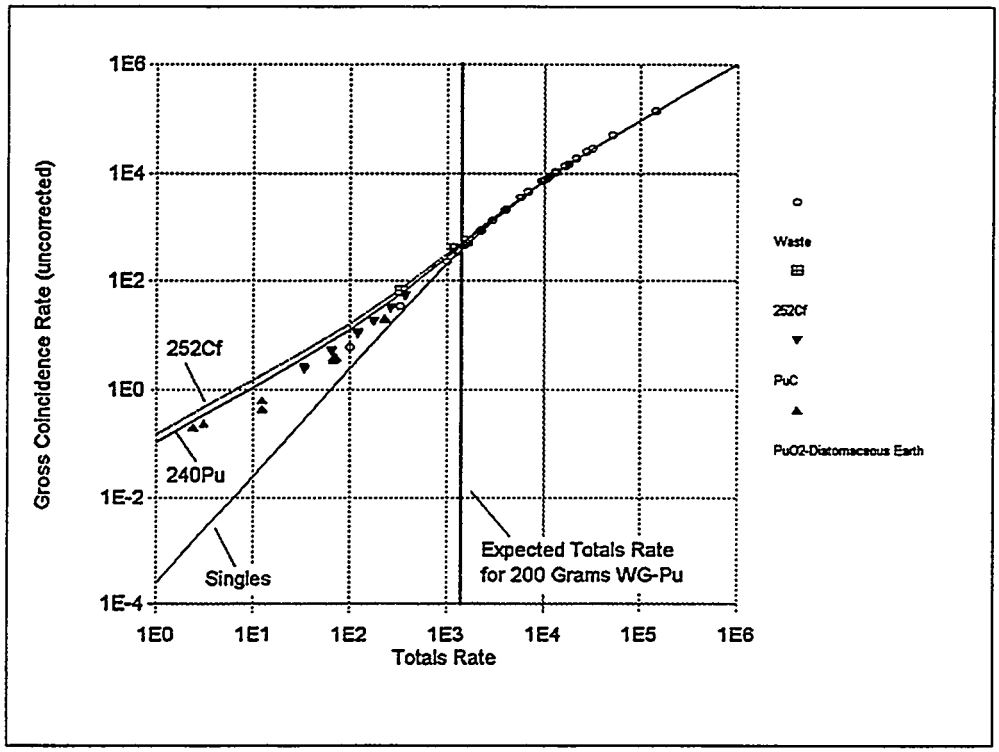

Figure 1 - Effect of High (α,n) neutron signal on assay results. Labeled lines are expected results from pure ^{252}Cf or ^{240}Pu fission events or pure single (i.e.- (α,n)) neutron events.

For these wastes, one of the basic limitations of our mobile PAN system was its electronics. It uses gated scalars (in the passive mode) which are limited in their ability to reject unwanted single neutron events when they are detected at high count rates. In fact, beyond event detection rates of about 1000 per second the gross passive coincidence count rate (uncorrected) begins to approach the totals count rate (the basic discrimination mechanism breaks down).

We have several options to circumvent this problem in the future. One is to use the Tomographic Gamma Scanner. We found

that we obtained quite reasonable results[4] using the TGS on these waste drums and others which were assayed during the summer of 1996. The TGS also provides a direct assay of the ^{241}Am which was present in non-equilibrium quantities (not due to ingrowth from the ^{241}Pu content of the waste). Another option is to assay these wastes using the High Efficiency Neutron Counter. This system has superior electronics for discriminating against unwanted (α,n) neutrons. Finally, we are planning to install shift register electronics on our existing PAN systems (following the lead of our colleagues at INEL) which also are intrinsically better able to discriminate against unwanted neutron signals.

Summer 1996 Debris Waste Assay

During the summer of 1996, we had an opportunity to assay several hundred drums of mostly debris waste. From the point of view of (α,n) neutron production, these wastes were far more benign and amenable to assay using our PAN than the cemented sludges and pyrochemical salts assayed during the winter. These assays provided us with information regarding the neutronics properties of LANL's debris wastes as well as a cleaner comparison of PAN assay results to declared Pu content than we obtained earlier.

During a PAN assay, the instrument "assays" the waste matrix as part of the process of quantifying Pu content. A global average quantity representative of the waste matrix moderating and absorbing characteristics is determined and subsequently used to correct for the effect of these processes on the final assay result. Figures 2 and 3 present the values for the "moderator index" and "absorber index" determined for the debris wastes. For comparison, the corresponding values of the same parameters

determined for the PDP test drums used to date are plotted as well.

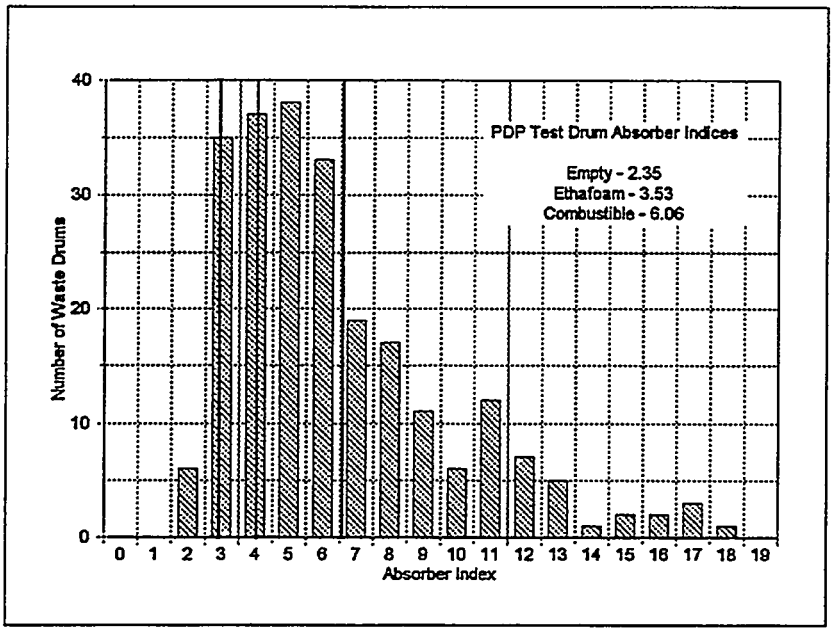

Figure 2 - Absorber indices of debris waste drums assayed using LANL's mobile PAN. Corresponding values for PDP drums used to date are indicated by heavy vertical lines.

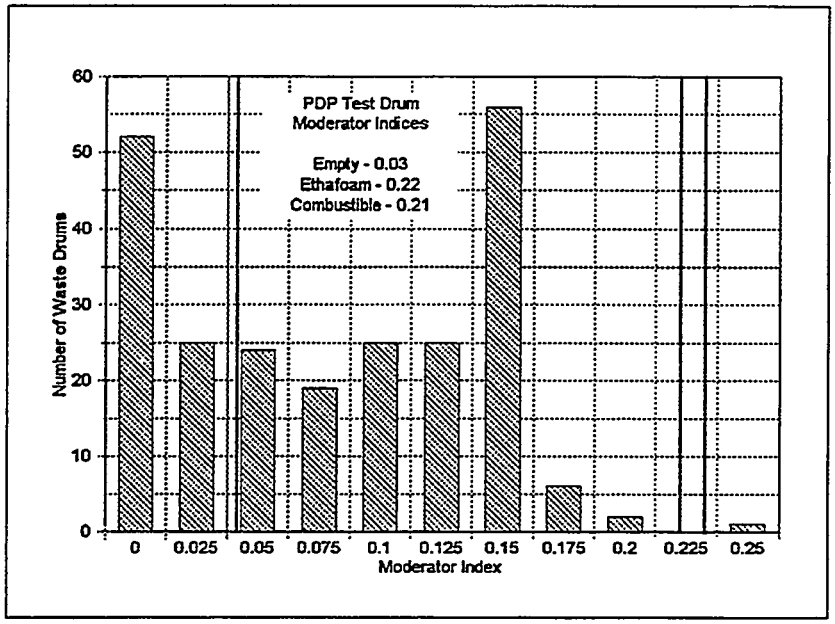

Figure 3 - Moderator indices of debris waste drums assayed using LANL's mobile PAN. Corresponding values for PDP test drums used to date are indicated by heavy vertical lines.

Figure 4 compares the PAN assay results obtained in the passive mode with the declared values from the waste generator. Generally the agreement is good. In fact, the sum of the assay values for this set of drums exceeds the declared value by only 3.5%. This may be fortuitous though. Closer inspection of the PAN assay results shows evidence of a slight bias (10-15%) low relative to the declared values with the majority of PAN assay results coming within 25-30% of the centroid of the distribution. In full production, outlyers would be reassayed on the TGS to pin down the cause of the apparent difference between the PAN assay result and generator's declared value.

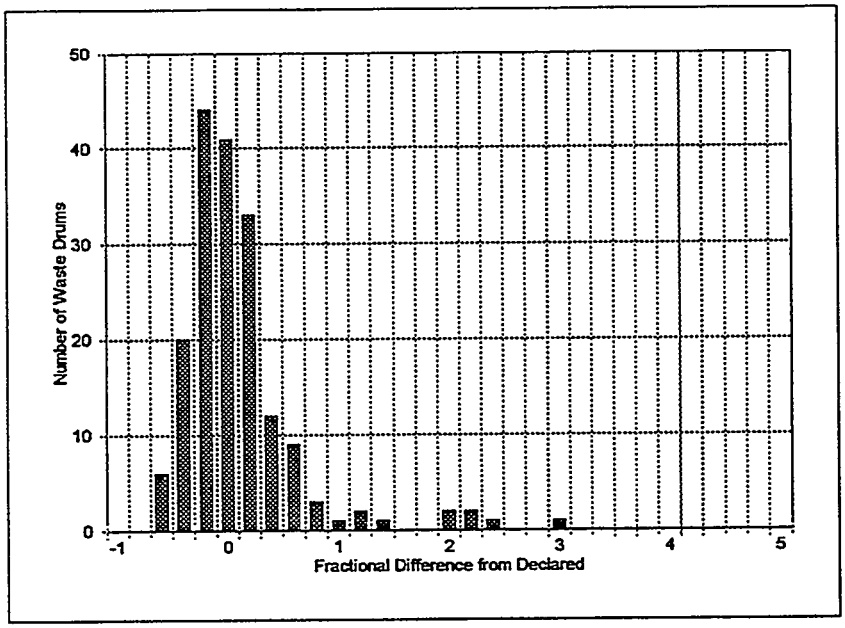

Figure 4 - Comparison of PAN assay results obtained in passive mode with generator supplied estimate (declared value) of Pu content of waste.

The active assay results (not shown) for the same waste drums do not exhibit the same behavior. Thermal (active) neutron assay results are more sensitive to matrix and self-shielding effects than passive assays. More analysis of the active data is required to explain the observed results.

PERFORMANCE DEMONSTRATION PROGRAM EXPERIENCE

Our PAN assay experience in the PDP tests to date is shown in Figure 5, along with the results of measurements made with the TGS and HENC. The PDP tests to date have concentrated on drum loadings in the range of 0 to 10 grams of weapons grade Pu (94% ^{239}Pu, 6% ^{240}Pu). A consequence of this is that the results reported so far have all been active assay results (the operating software forces this in its default mode). All of the results obtained with the PAN have been biased high. One reason why the PAN assay results are biased high may be that our calibration standard is too thick. We have used a depleted uranium bar provided with our fixed PAN system for active calibration. Unfortunately we have neglected to compensate for its ability to self shield. Self shielding would result in a reduced fission yield in our calibration standard for a given incident thermal neutron flux. Then, if the PDP standards are effectively "thinner" than our calibration standard we would obtain a larger fission yield for the same thermal neutron flux biasing our PDP results high. To test this possibility a series of Monte Carlo calculations will be run simulating neutron transport through the depleted uranium bar which we use to calibrate the active mode.

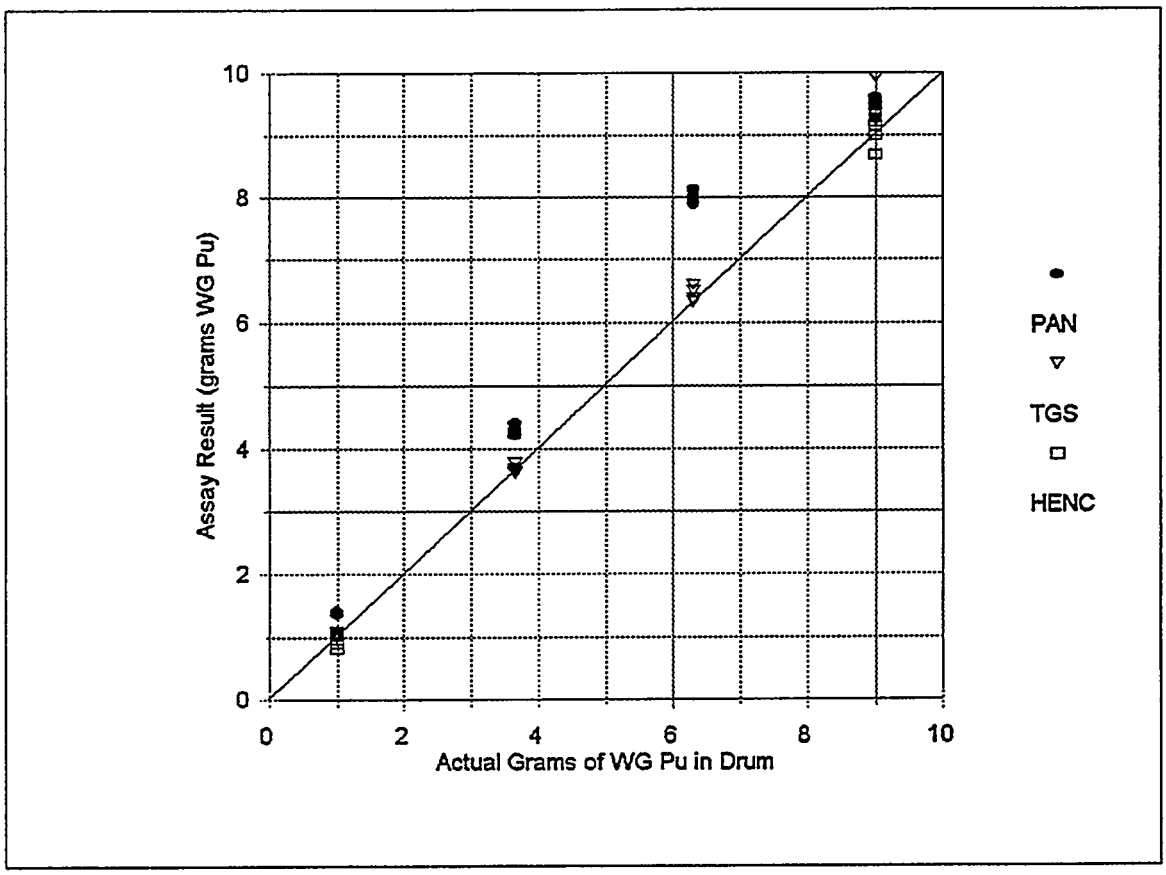

Figure 5 - Summary of PDP assay results for LANL's three assay systems. The data at actual grams equaling 1 and 9 grams are our best estimate (based on the concurrence of our three measurements) of what is in the drums. The data at 3.66 grams and 6.3 grams is accurately plotted based on the report of the first PDP round results.

This points to a general problem one has when assaying using the active mode. Without exact knowledge of the Pu particle sizes in actual waste, it is impossible to specify calibration standards which are equivalently self shielding.

The result of an active PAN assay is more strongly affected by moderation and absorption by the waste itself than passive assays are. At the same time as we are evaluating the ^{239}Pu equivalence of our active mode calibration standard, we will be revisiting these and other effects to arrive at the appropriate calibration.

CURRENT ACTIVITIES

We are currently reviewing the entire calibration of the mobile PAN both in active and passive modes. Our first calibration was made using ^{252}Cf for matrix corrections and PuC "pins" for zero matrix calibration in the passive mode. We plan to recalibrate using the PuC "pins" for matrix correction as well. The ^{239}Pu equivalence of our depleted uranium standard will be referenced to a "thinner" PuO_2 standard for active assay calibration.

As we are acquiring the data needed for passive mode calibration, we will be mapping out in some detail the PAN response to point sources at various positions in a set of mock waste drums. Our existing ^{252}Cf data indicates that in the course of acquiring this data, we will accumulate a fairly complete mapping of neutron coincidence count rate versus moderator index (Figure 6). A function can be fit to the distribution of results to correct for lost counts due to moderation of neutrons in the waste. This function can then be used to estimate the contribution from neutron moderation in the waste to the total uncertainty in a passive assay.

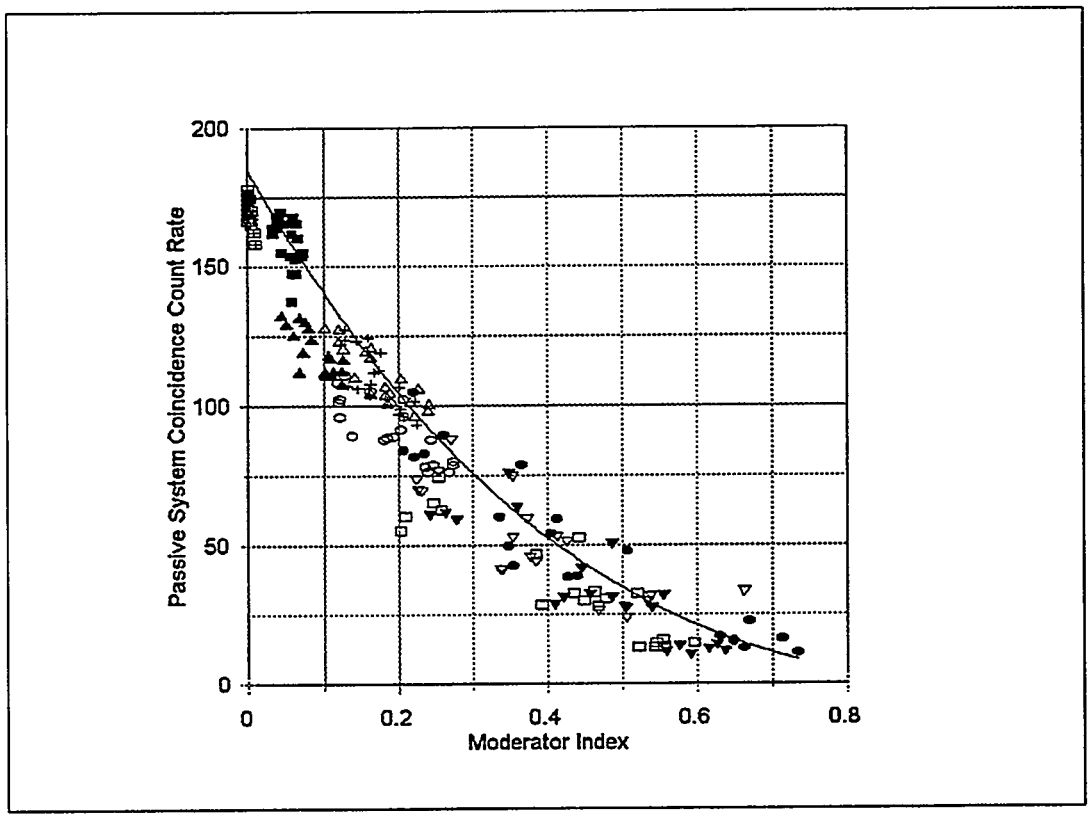

Figure 6 - Passive neutron coincidence count rate versus moderator index. The solid line represents what the PAN software is currently programmed to expect as the reduction in coincidence count rate due to moderation and correct for. Each symbol represents a particular mock waste drum.

FUTURE PLANS

Once we have re-evaluated our current calibration and made any indicated changes, we will begin assaying waste to meet the needs of a characterization audit scheduled for March 1997. After this audit we will complete implementation of an isotopics capability to support all three of our assay systems. This isotopics package will enable us to verify generator provided isotopics information, establish statistics on the variability of isotopics within a given material type and allow us to assay for ^{241}Am by establishing a scaling factor to the Pu content of the waste, then assaying the Pu on the PAN.

ACKNOWLEDGMENTS

This work is was supported by the U.S. Department of Energy.

REFERENCES

1. J.T. Caldwell, et al., "The Los Alamos Second-Generation System for Passive and Active Neutron Assays of Drum-Sized Containers," LA-10774-MS, Los Alamos National Laboratory, Los Alamos, NM, September 1986

2. L.V. East and G.K. Becker, "Experience Gained from Passive/Active Neutron (PAN) Assay Measurements on 12,600 TRU Waste Drums at INEL," Proceedings of the Nondestructive Assay and Nondestructive Examination Waste Characterization Conference, pp. 143-166, Idaho National Engineering Laboratory and Idaho State University, CONF - 940216, Pocatello Idaho, February 1994

3. N.J. Nicholas, K.L. Coop and R.J. Estep, "Capability and Limitation Study of the DDT Passive/Active Neutron Waste Assay Instrument," LA-12237-MS, Los Alamos National Laboratory, Los Alamos, NM, May 1992

4. D.P. Taggart, et al., "LANL's Mobile Nondestructive Assay and Examination Systems for Radioactive Wastes," Proceedings of the International Topical Meeting on Nuclear and Hazardous Waste Management, pp. 540-546, American Nuclear Society, La Grange Park, IL, August 1996

Neutron NDA Techniques/Design/Applications

COMPUTED NEUTRON COINCIDENCE COUNTING APPLIED TO PASSIVE WASTE ASSAY

M. Bruggeman, P. Baeten, W. De Boeck, and R. Carchon

Nuclear Research Centre, Mol, Belgium, B-2400

ABSTRACT

Neutron coincidence counting applied for the passive assay of fissile material is generally realised with dedicated electronic circuits. This paper presents a software based neutron coincidence counting method with data acquisition via a commercial PC-based Time Interval Analyser (TIA). The TIA is used to measure and record all time intervals between successive pulses in the pulse train up to count-rates of 2 Mpulses/s. Software modules are then used to compute the coincidence count-rates and multiplicity related data. This computed neutron coincidence counting (CNCC) offers full access to all the time information contained in the pulse train.

This paper will mainly concentrate on the application and advantages of CNCC for the non-destructive assay of waste. An advanced multiplicity selective Rossi-alpha method is presented and its implementation via CNCC demonstrated.

INTRODUCTION

Neutron coincidence counting in waste assay is generally applied to discriminate between the random neutron count-rate and the reals coincident count-rate from fission neutrons. Only the latter is directly proportional to the mass of the spontaneously fissioning material. Several coincidence counting electronic systems have been applied in the past,[1,2,3] but the shift-register (SR) technique is probably the most popular. It uses an electronic shift-register which acts as a memory element and keeps track of all the pulses within a predefined time gate. The gate length is defined by the frequency of the clock driving the SR and the number of flip-flops it contains. In this way each detected pulse opens a gate and at each clock pulse the SR content gives a snap shot of the number and position of the pulses detected in this time gate. Generally only the number of pulses present in the shift register are recorded and updated in a Reals + Accidentals, "R + A" and an Accidentals, "A" counter. In more sophisticated circuits also the detected neutron multiplicity is recorded with multiplicity counters.[4,5]

The information in all these counters finally composes the data used to calculate the assayed plutonium mass. When using the multiplicity data and appropriate interpretation models, it is also possible to measure the neutron multiplication or the detection efficiency via a three-parameter-analysis. [6,7]

None of these electronic systems however offers full access to the detailed time information contained in the pulse train representing detected neutrons. The commercial coincidence and multiplicity counters are often experienced as black boxes by the assayist and moreover they can only be tested using complex pulsers. Computed Neutron Coincidence Counting (CNCC) offers a new challenging alternative to the conventional electronics and also opens new dimensions in neutron assay. A CNCC system is composed of two main components: a data acquisition component and a computing component. The computing component, which may be actually a PC, is used for a software based processing of the data representing the pulse train. The processing of the data via software offers full flexibility with which different coincidence and multiplicity counting algorithms can be implemented. With CNCC the assayists can rely on user defined coincidence counting algorithms which can easily be tested just by studying their effect on simulated pulse trains of known characteristics.

First attempts to make use of a software based neutron coincidence counting method were already reported in the past.[8,9] The main limitation of the application of such an approach at that time was the lack of a powerful commercial acquisition system which can handle relatively high count-rates, up to 1 MHz, without influencing the quality of the data due to additional dead time effects caused by the data acquisition. Among the wide spread of commercial PC-based acquisition boards available today figure also multi-purpose Time Interval Analysers (TIA). A TIA is a high speed time and frequency measurement instrument which allows to accurately measure the time between pulses up to high pulse-rates. Data transfer via a PC-bus is generally limited to low count-rates, but the TIA board, however has fast on-board memory which momentarily stores the incoming data which are transferred to the PC memory at a much lower rate. These characteristics of the TIA board clearly makes it especially

suitable for use as the acquisition component for CNCC where it can be used to measure all time intervals between successive pulses in the pulse train.

This paper reports mainly on the technical feasibility of CNCC for waste assay. First a brief description of the main characteristics of the TIA board will be given. An example of CNCC based on a multiplicity selective Rossi-alpha technique is demonstrated and advantages of CNCC, in general and realised with this TIA, are discussed.

MEASUREMENT PRINCIPLE AND MAIN CHARACTERISTICS OF THE TIME INTERVAL ANALYSER

In this section the main features and modes of operation of the TIA acquisition board which are especially important with respect to its use for neutron coincidence counting are first discussed. The TIA referred to in this section is the commercial 16 channel model GT659-TIA Time Interval Analyser manufactured by Guide Technology, Inc., San Jose, USA. This TIA board plugs into the ISA slot of an ordinary PC. The standard 128 kB on-board memory however was upgraded to 2 MByte in order to have bigger buffer capacity.

The GT659-TIA allows to continuously measure the arrival times of pulses up to pulse-rates of $2x10^6$ pulses/s until memory is full (while accepting bursts of 50×10^6 pulses/s). All arrival times are stored in a fast First-In-First-Out (FIFO) memory. The maximum allowable pulse-rate applies to the total rate obtained by adding the pulse-rates at all individual channels. The time-base of the TIA board is 50 MHz which sets the maximum time resolution at 0.02 μs which is equal or superior to the resolution commonly obtained with a SR.

The 16 channels of the TIA board can be used as 16 independent inputs for the detection chains of a neutron assay detection assembly. The same time-base is applied to the 16 channels, which makes it possible to measure the time between pulses arriving at different channels. The triggering levels of each channel can be software set. The arrival

times of all triggering pulses are represented as 32-bit-numbers in the on-board memory. From these 32 bits, 16 times one bit is used to identify the channel at which the pulse was detected. If two pulses arrive simultaneously or in a time interval smaller than the time resolution of the TIA in respectively two different channels then their detection will generate a single time tag and the bits corresponding to those channels are set high. The ORing of pulses from different channels to one pulse train, realised in this way with the TIA is similar to the one obtained with special pulse mixers build for reducing pulse pile-up.[10,11] The remaining 16 bits are used to represent the time at which pulses were detected or for dummy time tags which indicate overflow of the 16 bit clock counter when no pulses are detected. The FIFO memory records the time intervals according to a back-to-back principle. This means that there is no dead time between the recording of the end of one time interval, storing the information, and the beginning of the next time interval. This is very important in neutron coincidence counting because dead time effects severely influence the coincidence and multiplicity counting. When using the software drivers of the TIA board, the bookkeeping of dummy time tags and the time calibration, is completely managed by the driver and invisible to the programmer. We used the C-drivers and subroutines coming with the board to write a measurement programme running under DOS.

Two different operation modes of the TIA's memory can be used. One is the memory-wrap mode in which the on-board memory is continuously read by the PC while acquiring data. This mode is only applicable if the combined PC read-rate, and the data processing-rate is higher than the actual count-rate. If the data reading and processing-rate is too low, memory will wrap around and an error message will result. When the count-rate is too high for the memory wrap mode, the no-wrap mode should be used. In the no-wrap mode data acquisition and processing is performed as a series of cycles in which for each cycle data acquisition stops when memory is full. In the no-wrap mode, data acquisition and the memory reading and data processing still occur in parallel. The main difference between both operation modes is that in the wrap mode a pulse train is recorded without interruption, while in the no-wrap mode only sequences of the pulse train are recorded. The recorded time sequences however cover a sufficiently long period.

Once data is transferred form the FIFO memory of the TIA to the PC memory, software modules can process these data. Table 1 gives an idea of the CPU time necessary to perform the reading of the data with respectively 16 or 1 channel(s) enabled. To calculate the Central Process Unit (CPU) time actually needed to make a measurement, the CPU time of the data-processing step also has to be taken into account. The CPU time devoted to data processing, however is function of the specific user defined coincidence counting algorithms implemented by the software.

PC-type	PC reading time (s) (per 1024 pulses) 16 channels	PC reading time (s) (per 1024 pulses) 1 channel
386/40 + coprocessor	0.228	0.142
Pentium/75	0.050	0.034
Pentium/200	0.021	0.016

Table 1 *Comparison of CPU time devoted to the transfer of data between TIA and PC memory for different PC types for respectively 16 channels enabled and 1 channel enabled, and for a pulse-rate higher than 2000 pulses/s.*

A ROSSI-ALPHA TECHNIQUE FOR MULTIPLICITY SELECTIVE COINCIDENCE COUNTING WITH THE TIA

In this paragraph we will discuss the particular use of the TIA for neutron coincidence counting based on an advanced Rossi-alpha method. The theoretical background of this multiplicity selective Rossi-alpha method has already been explained in another paper [12] and only the main principles will be repeated here while major attention will be paid to experimental aspects of the proposed method. By multiplicity selective we indicate the ability to measure quantities which give information on the neutron multiplicity.

The time intervals recorded with the TIA board allow to compute and visualise what is known as the Rossi-alpha distribution for the detected pulse train. The Rossi-alpha distribution gives the distribution of time intervals between each pulse, which is assumed to arrive at time zero, and all its neighbour pulses coming at later times and laying in a predefined time window *W*. Under the assumption that the neutron population decay is mono-exponential, it has the following form:

Equation 1

$$S_1(t) = A_1 + R_1 e^{-t/\tau} \qquad (t \geq W)$$

in which A_1 is the time independent component expressing the accidental coincidence count-rate and R_1 is the amplitude (count-rate) due to real coincidences.

The "R + A" and "A" counts commonly measured with a shift register, are time integrated quantities obtained from the distribution described by the equation 1. The SR electronics however does not allow to visualise $S_1(t)$ nor to analyse the detailed time behaviour of this function. To obtain the value of the time constant τ with SR electronics, several time windows of a different length are used to measure count-rates from which τ, can be calculated. From the Rossi-alpha distribution recorded with the TIA the real coincidence count-rate can be obtained in a similar way as with the SR via time integration, but can also be computed by mathematically fitting the curve $S_1(t)$. Via a non-linear fitting, the parameters A_1, R_1 and τ can be directly determined. The acquisition with the TIA and the fitting of $S_1(t)$ clearly offers several advantages compared to the SR:

- one can control if the actual neutron population decay is indeed mono-exponential;
- there is no need to choose a pre-defined pre-delay as is the case with the SR, because the range of $S_1(t)$ to be used to determine the reals-rate can be chosen at the time of fitting;
- the variances of the estimators obtained from the fitting of $S_1(t)$ also give directly a way to deal with the uncertainty of the quantities A_1, R_1.

In quite a similar way a two-dimensional Rossi-alpha distribution can be defined and computed for an actual pulse train. The two-dimensional Rossi-alpha distribution records only detected pulse multiplets with a pulse multiplicity equal to or higher than 3. The time distribution of the pulse multiplets is recorded with two time axis and two equal time windows W. A pulse multiplet will only be recorded when the condition is met that the time interval between a triggering pulse and a second pulse is smaller than W and the time interval between this second pulse and a third pulse is also smaller than W. The first condition is measured on a time axis t_1, the second on a time axis t_2. The mathematical expression for the two-dimensional Rossi-alpha distribution as a function of the time parameters t_1 and t_2 is -under the assumption of a mono-exponential decay of the neutron population- given by:

Equation 2

$$S_2(t_1,t_2) = A_2 + C_2(e^{-t_1/\tau} + e^{-t_2/\tau} + e^{-(t_1+t_2)/\tau}) + R_2\, e^{-2t_1/\tau}\, e^{-t_2/\tau}$$

with:

A_2 : the count-rate due to accidentally correlated pulse multiplets;

C_2 : the count-rate due to pulse triplets or higher order pulse multiplets of mixed origin e.g. containing a correlated pulse pair accidentally time-correlated with a singlet;

R_2 : the count-rate due to real coincident pulse multiplets;

τ : the die-away time as given in equation 1.

A two-dimensional Rossi-alpha distribution is also calculated from the TIA data and represented as a two-dimensional distribution. This distribution is analysed making use of the value of τ obtained from the analysis of $S_1(t)$ and a least squares fitting of the parameters A_2, C_2 and R_2 from $S_2(t_1,t_2)$.

The quantities R_1 and R_2 together with the measured total count-rate allow to build a system of 3 equations from which the fission-rate, the actual detection efficiency and the (α,n)-neutron production-rate can be inferred.[12] To be generally applicable, the quantities R_1 and R_2 and the total count-rate have to be corrected for counting losses first. In practice the distributions $S_1(t)$ and $S_2(t_1,t_2)$ are corrected for counting losses due

to dead time and the quantities R_1 and R_2 are derived from the dead-time-corrected distributions. The outlined approach based on the Rossi-alpha distributions and the determination of the parameters R_1 and R_2 lead to a set of equations. From these equations a three-parameter-analysis similar to the one obtained via Time Correlation Analysis TCA can be derived. [6,7]

The formulas for correction for counting losses of the quantities R_1 and R_2 and the total count-rate have been reported in another publication.[13] Connected to dead time correction there is another interesting feature of the TIA: its 20 ns time resolution allows to directly monitor the effect of counting losses due to dead time. For this purpose Rossi-alpha distributions are measured with a high time resolution with a random neutron source e.g. an AmLi source. The dead time parameter can then be derived from the recorded distribution without knowing the actual source intensity as will be demonstrated next.

EXPERIMENTAL SET-UP AND EXPERIMENTAL RESULTS

In this paragraph, the experimental set-up used in conjunction with the TIA board is briefly described and experimental data, showing the possibilities of CNCC based on the before mentioned Rossi-alpha method, is discussed.

The detection assembly of our neutron waste assay system consists of 20 equal detection blocks each containing 3 detectors of 1 meter active length. These detection blocks are fixed to a modular hexagonal frame currently dimensioned to hold 220 l drums. The inner walls of the assembly can be lined with a Cd sheet of 1 mm thick. The 3 detectors of each detector bank are connected to a Model A-111 hybrid amplifier/discriminator manufactured by AMPTEK, Inc., of Bedford, Massachusetts. All the TTL-outputs of the Ampteks are directly connected to the channels of the TIA. The use of a 16 channel board in our case, however only partially omits the use of a mixer for "ORing" the pulses of the different channels. The existing mismatch between 20 outputs and only 16 inputs obliged us to OR 8 channels two by two to obtain finally a total of 16 counting chains which are then connected to the 16 inputs of the TIA.

Applications which for experimental reasons would require more channels could make use of two or more synchronised TIA boards giving 32 or more individual channels. In our system the channels are taken in such a way that 12 channels allow to monitor the radial count-rate distribution while the remaining 4 channels give information of the count-rate of respectively top and bottom detectors. The TIA board is currently plugged in a 200 MHz Pentium computer. A less performing PC may also be used, although a fast computer is to be preferred for its computation speed and for its fast graphical display. The 16 input channels of the TIA board are available via a 40-pin high density D-type connector. The main measurement programme allows to calculate the one- and two-dimensional Rossi-alpha distributions for a user defined combination of channels. Some experimental results based on Rossi-alpha distributions are discussed next.

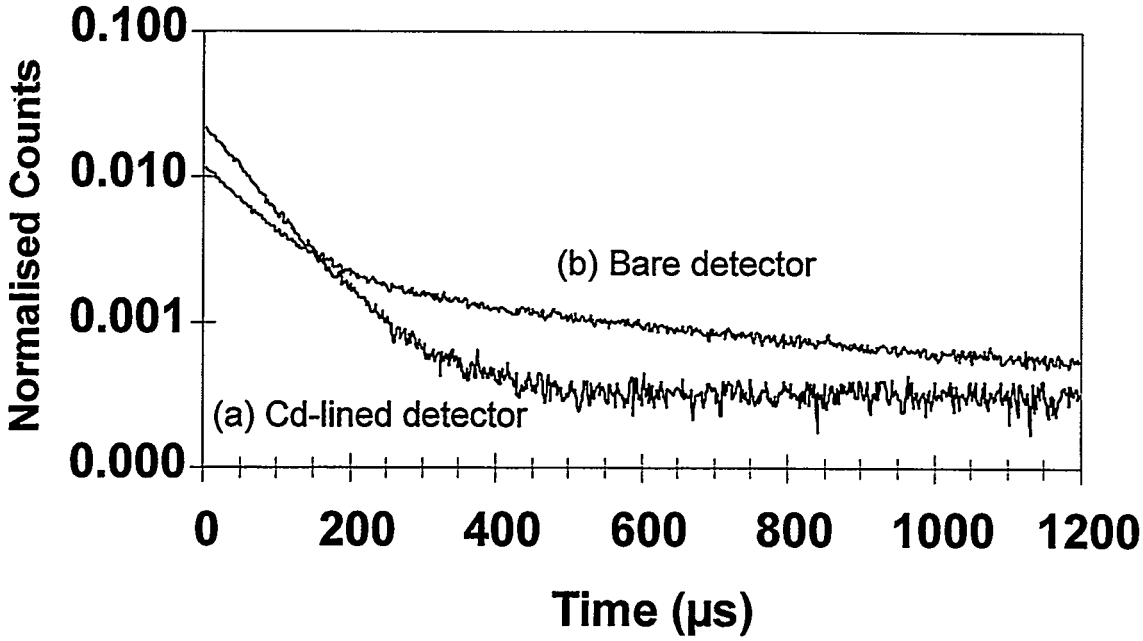

Figure 1 *Recorded Rossi-alpha distributions for (a) a cadmium lined detector assembly and (b) the same bare detector assembly*

Figure 1 shows recorded one-dimensional Rossi-alpha distributions on a log-lin scale of a weak ^{252}Cf point source positioned in the centre of a 220 l drum with a cellulose matrix with a density of 0.4 g/cm^3. Figure 1, curve (a) gives the Rossi-alpha distribution for a cadmium lined detector assembly, while curve (b) gives the Rossi-alpha distribution for the same detector assembly without cadmium lining. A cadmium lined detector assembly clearly shows a mono-exponential decay of the observed

neutron population. The recorded Rossi-alpha distribution for the detection assembly without cadmium lining is not mono-exponential but shows a fast and a slow decaying component. The cadmium lining is sometimes removed to take profit of a higher detection efficiency. The non-mono-exponential die-away then is dealt with by taking a gate time sufficiently short to exclude the slow decay component. The Rossi-alpha distributions recorded with the TIA in this case clearly gives the possibility to chose the most appropriate gate times.

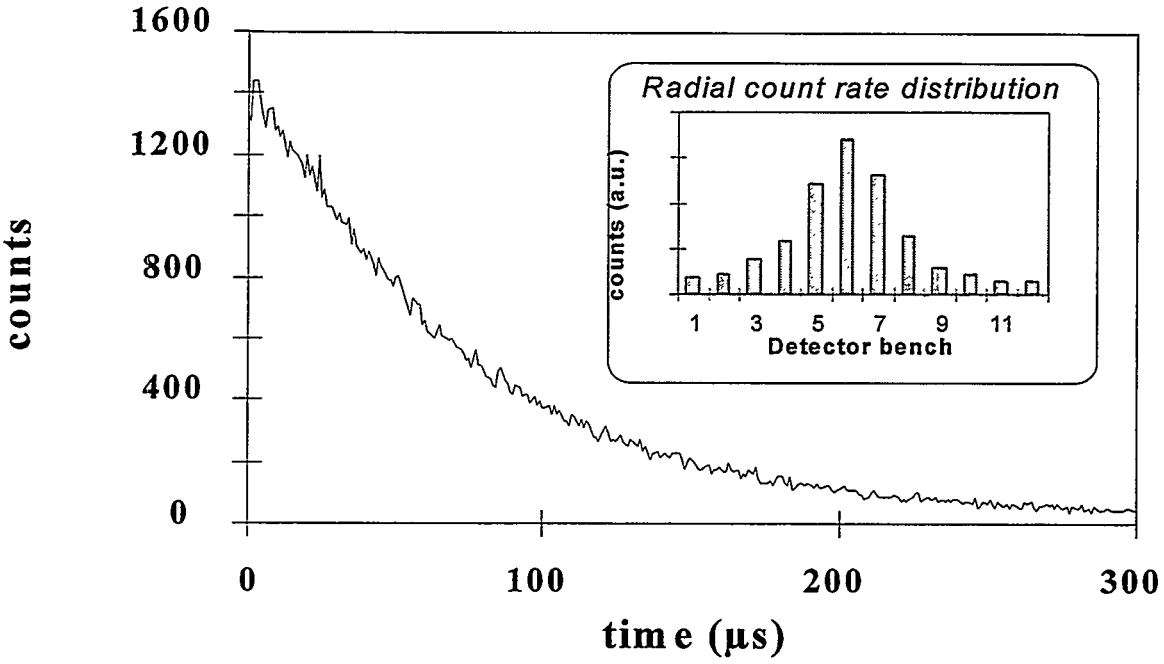

Figure 2 *One-dimensional Rossi-alpha distribution used to perform the three-parameter-analysis*

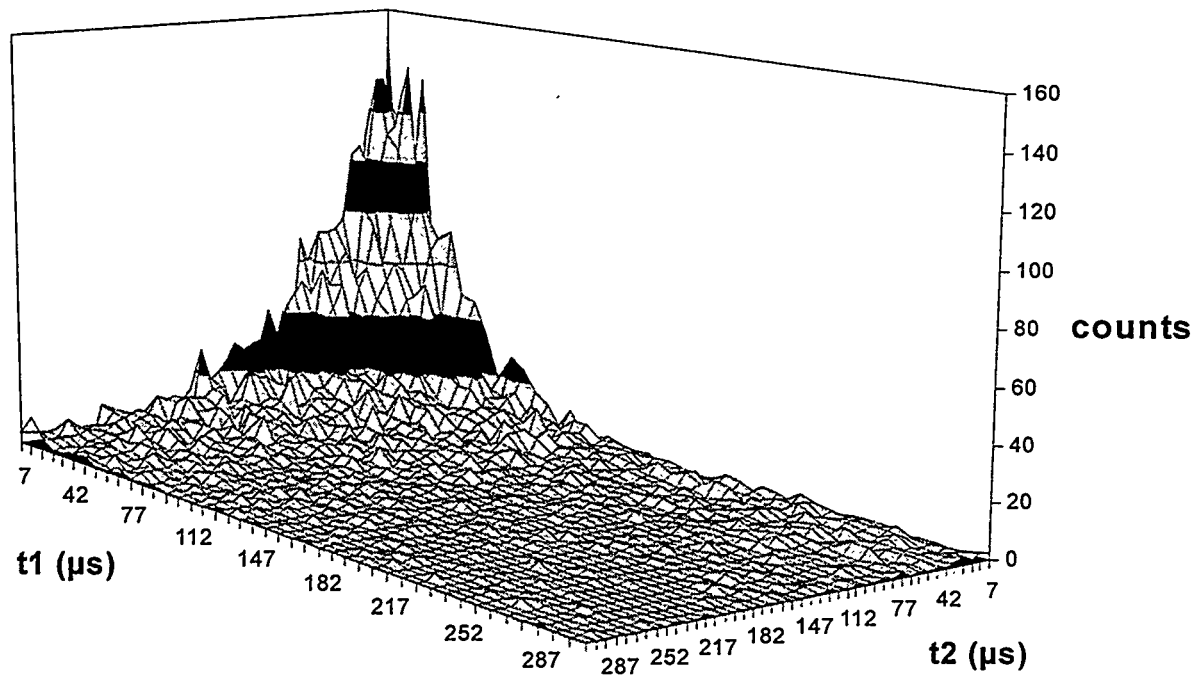

Figure 3 *Two-dimensional Rossi-alpha distribution used to perform a three-parameter-analysis.*

The figures 2 and 3 show one example of a one- and two-dimensional Rossi-alpha distribution recorded with a weak ^{252}Cf source in a 220 l drum with a cellulose matrix of a density 0.4 g/cm^3. The measurement time is 8 hours. The insert of figure 2 shows the measured count-rate distributions measured with the radial detectors with the source placed 18 cm out off-center. The data of this experiment and of similar measurements with the source in other positions were used to perform a three-parameter analysis from which the spontaneous fission-rate and the detection efficiency were determined. The results of these analyses are summarised in Table 2. For these preliminary measurements, only detection efficiency and the fission-rate of the source were determined for three different radial positions in the mid-height section of the 220 l drum. From table 2 we see that the Reals-rate increases with 73% when the point source is displaced from the centre to a position 17.9 cm from the center, while the calculated efficiency increases from 8.3 % to 10.7 %. Taking into account the uncertainty on the fission-rate, this parameter does not show a significant increase, and should under ideal conditions remain constant. The relatively high standard deviation reported for the fission-rate is due to the very low count-rate (which is less than 4 reals/s), and the bad statistics with which the multiplicity parameters are determined for such a weak source. This is however a general problem in multiplicity measurements, which only work well

for sufficiently high count-rates of real pulse doublets and triplets. Since the neutron activity of the californium source used in these experiments is not calibrated we can not compare the reported values for the fission-rate with the actual value.

Source position	Efficiency (%)	Fission-rate (1/s)	Reals-rate (1/s)
centre	8.3±0.7	49±10	2.06±0.06
13.7 cm	9.3±0.6	58±9	3.00±0.07
17.9 cm	10.7±0.6	52±7	3.57±0.07

Table 2 *Results obtained with the three-parameter-analysis for a ^{252}Cf point source of low neutron intensity at different positions in a 220 l waste drum.*

In figure 4, three one-dimensional Rossi-alpha distributions are shown for a random neutron source. The time resolution of the time axis is 0.1 μs. The spectrum indicated by the letter (a) is recorded with only 1 detector bench and 1 channel enabled. The onset of this distribution clearly shows the influence of counting losses. From this Rossi-alpha distribution, the mean dead time parameter δ_M which can be associated with the detection of that particular channel can, in a first approximation, be determined using the formula:

Equation 3

$$\delta_M = \left(1 - \frac{\int_0^t S_1(t,\delta)\,dt}{S_{1M}(\delta)\,t}\right) t$$

in which $S_{1M}(\delta)$ is the mean value of the dead time affected Rossi-alpha distribution measured in a data region sufficiently far away from the time origin and in the constant part of the distribution. The time t in this formula has to be taken just at the beginning of the constant part of the distribution. Better approximations of δ_M can be obtained by iteratively replacing the value of $S_{1M}(\delta)$ by $S_{1M}(\delta_M)$, the value obtained by using the latest value δ_M. The distributions indicated by (b) and (c) in figure 4 are Rossi-alpha distributions recorded with all the radial detectors connected and the respective channels

enabled. Counting losses due to dead time effects are clearly reduced when multiple counting channels are used. The difference between the curves (b) and (c) is caused by a different source and neutron intensity distribution seen by the detectors. The curve (c) is for a point source in the centre of the measurement cavity while the curve (b) is for a point source positioned off-centre. The enabled channels experience different count-rates in these two cases and Figure 4 clearly indicates that the actual dead time parameter is function of the count-rates in the different channels. For this reason we developped a dead time correction formalism which uses the count-rate distribution, as shown in the inset of figure 2, to calculate the actual dead time parameter to be used in the correction formula.

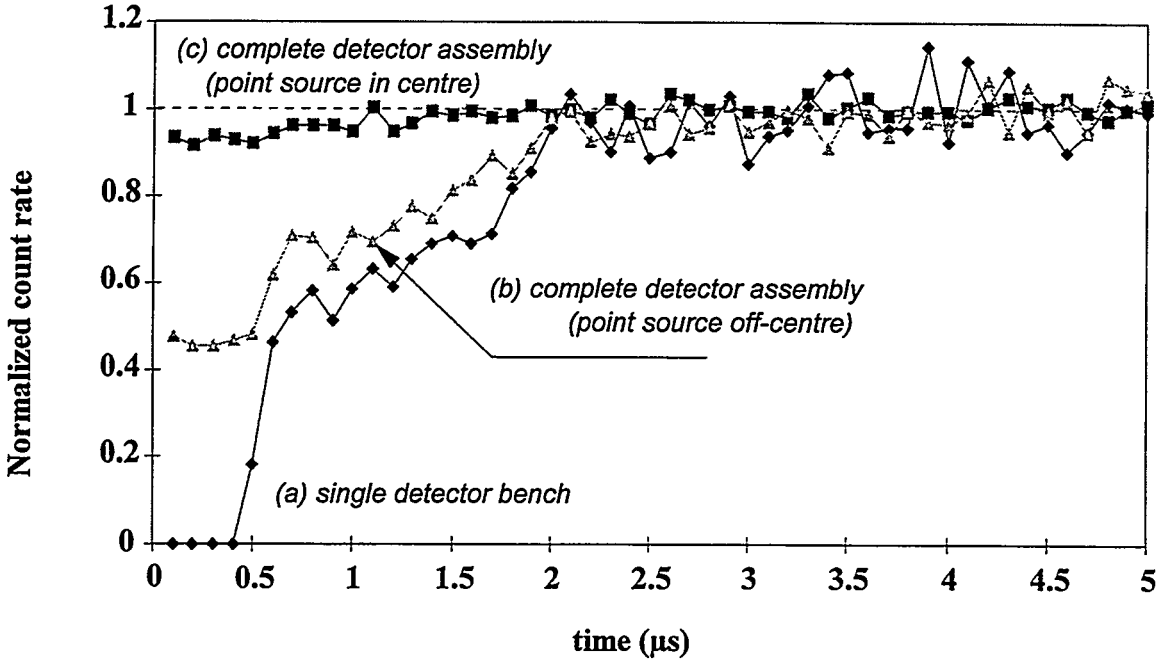

Figure 4 *Rossi-alpha distributions for a AmLi source showing dead-time effects as function of measurement conditions.*

CONCLUSION

The general concept of CNCC using a TIA for data acquisition and software modules for computation of coincidence parameters has been outlined. The main advantages of CNCC , discussed and demonstrated in this paper, can be summarised as follows: a maximum of flexibility for implementation and easy testing of user defined coincidence counting algorithms; access to the most detailed time information in the pulse train; a maximal choice of parameter settings, most of which can be defined even

after the measurement; on-line graphical display of parameters of interest; no need for complex derandomizing buffers or OR-gates; direct measurement of dead time parameters; possibility of multi-channel coincidence counting.

The feasibility of CNCC has been demonstrated through on the implementation of an advanced multiplicity selective Rossi-alpha method which was used for the measurement of a ^{252}Cf point source at different locations in a waste drum with a cellulose matrix. The presented Rossi-alpha method allows to perform a three-parameter-analysis from which three unknowns can be determined. In the case of waste assay these unknowns are commonly chosen to be the spontaneous fission-rate, the (α,n)-rate and the detection efficiency.

ACKNOWLEDGEMENTS

The authors want to thank Mr. A. Mészàros from the Technical University of Boudapest for designing and programming the coincidence counting, graphical display and analysis modules.

REFERENCES

1. G. Birkhoff, L. Bondar, and N. Coppo, "Variable Deadtime Neutron Counter for Tamper-Resistant Measurements of Spontaneous Fission Neutrons", EUR-4801e (1972).
2. M. M. Stephens, J. E. Swansen and L. V. East, "Shift Register Neutron Coincidence Module", LA-6121-MS, Los Alamos scientific laboratory (December 1975).
3. L. Bondar, "Passive Neutron Assay", IAEA-SM-260/5A (1982).
4. J. A. Mason, L. Bondar, W. Hage, B. Pedersen," Neutron Multiplicity Drum Monitor using the Time Correlation Analyser", *Proceedings of the 17th Annual ESARDA Symposium*,EUR16290EN, pp 433-436, Aachen, Germany, (1995).
5. D. G. Langner, M. S. Krick, N. Ensslin, G. E. Bosler, and N. Dytlewski, "Neutron Multiplicity Counter Development," *Proceedings of the 13th Annual ESARDA Symposium*, Vol. 24, pp 285-290, Avignon, France, (1991).
6. L. Bondar, F. Girardi, "A 'waste' Instrument for classifying of Pu-Contaminated Wastes based on Passive Neutron Assay", Radioactive Waste Products - Suitability for Final Disposal (Proc. Int. Sem. Jülich, (1985).
7. R. J. Sharpe, C. J. Addison, C. H. Orr, R. D. Gunn, J. C. B. Simpson, B. Pedersen, L. Bondar, "Experience with Assay of Simulated Plutonium Bearing

Drummed Waste Applying Neutron Correlation Techniques", *Proceedings of 17th ESARDA Sypmosium*, EUR16290EN, Aachen, Germany, (1995).

8. Eyrich, W. D. Klotz and G. G. Simon, "Neue Auswertemethode für Neutronen-Messungen zur Plutoniumbestimmung in Fässern mit heterogenen und schweren Abfällen, KfK 4999 / PWA 39/91 (1992).
9. G. Birkhoff, L. Bondar, "Computerized System for the Application of Fission Neutron Correlation Techniques in Nuclear Safeguards", EUR-4799 e (1972)
10. S.C. Bourret and M. S. Krick,"A Deadtime Reduction Circuit for Thermal Neutron Coincidence Counters with Amptek Preamplifiers", Nucl.- Mater. Manage. **XXIII** (Proc. Issue), 646-650 (1994)
11. A. Fazzi, V. Varoli, D. Rozzi, V. Vocino, R. Jaime, "A Cost-Effective Circuit for Dead-Time Reduction in Neutron Multiplicity Counters", *Proceedings of the 17th Annual ESARDA Symposium*, pp 567-570, (Aachen, Germany), (1995).
12. M. Bruggeman, P. Baeten, W. De Boeck, R. Carchon,"Neutron coincidence counting based on time interval analysis with one- and two-dimensional Rossi-alpha distributions: an application for passive neutron waste assay", to be published in *Nuclear Inst. and Methods in Physics Research, A*
13. P. Baeten, M. Bruggeman, R. Carchon, "Single- and Multi-Deadtime Parameter Corrections of One and Two Dimensional Rossi-alpha Distributions for Time Interval Analysis in Neutron Coincidence Counting, submitted to *Nuclear Inst. and Methods in Physics Research, A*

APPLICATIONS OF A VERSATILE NEW INSTRUMENT MODULE

G. S. Brunson and G. J. Arnone
Los Alamos National Laboratory, Los Alamos, NM 87545

ABSTRACT

We have found a number of interesting applications for the Pulse Arrival Time Recording Module (PATRM). This CAMAC module is capable of recording the arrival time of up to 4 million pulses. The result is a list of 32-bit binary numbers in which each number represents the arrival time of a single pulse, expressed in terms of the number of "ticks" of a 10-Mhz clock which have elapsed since the beginning of the count. Versatility arises from the fact that the data list can be analyzed by whatever algorithm we can put into software and because we can "play it back" as many times as we like. We already have the following applications:

1. Neutron multiplicity counting in waste assay.
2. Study of dead-time recovery and double pulsing in individual channels.
3. Autocorrelation analysis for Rossi-α measurements in critical systems.
4. Variable channel-width multichannel scaler for delayed neutron counting.
5. Cross-correlation analysis and conventional multiscaling.
6. Time-dependent multiplicity measurements during neutron interrogation.

We expect in the coming year to test an updated version of the PATRM which will incorporate a 100-Mhz clock and label each pulse with the channel from which it came. The device will be configured as a single PC card installable in any high-performance IBM-type computer.

INTRODUCTION

The Pulse Arrival Time Recording Module (PATRM) is extremely simple in principle. It records the arrival time of each pulse up to total of 4 million. The result is a list of 32-bit binary numbers, each of which records the arrival time of a particular pulse (in 10-Mhz "ticks" since the beginning of the count). The "Swiss-Army-Knife" versatility arises from the fact that the list file records a particular segment of the data stream; we can analyze that data with any algorithm for which we can write the software. Moreover, we can "play it back" and try different algorithms on exactly the same data. Physically, the PATRM is a double-wide CAMAC module with 15 independent pulse inputs (see Fig. 1). If several pulses happen to arrive on the same tick of the clock, none is lost. They will be recorded in sequential locations in the list with their arrival times differing by just one tick. The electronic details of the PATRM have been described elsewhere.[1] In all cases, the signal sources were ^{3}He-filled proportional counter tubes, except where specifically noted.

This paper deals primarily with passive measurement, meaning that there is no interrogating burst of neutrons. Active measurement with interrogation by bursts of neutrons has been discussed elsewhere

and is the subject of a paper by Hollis, et al., in these proceedings. There was also an earlier paper by Hollis, et al.[2]

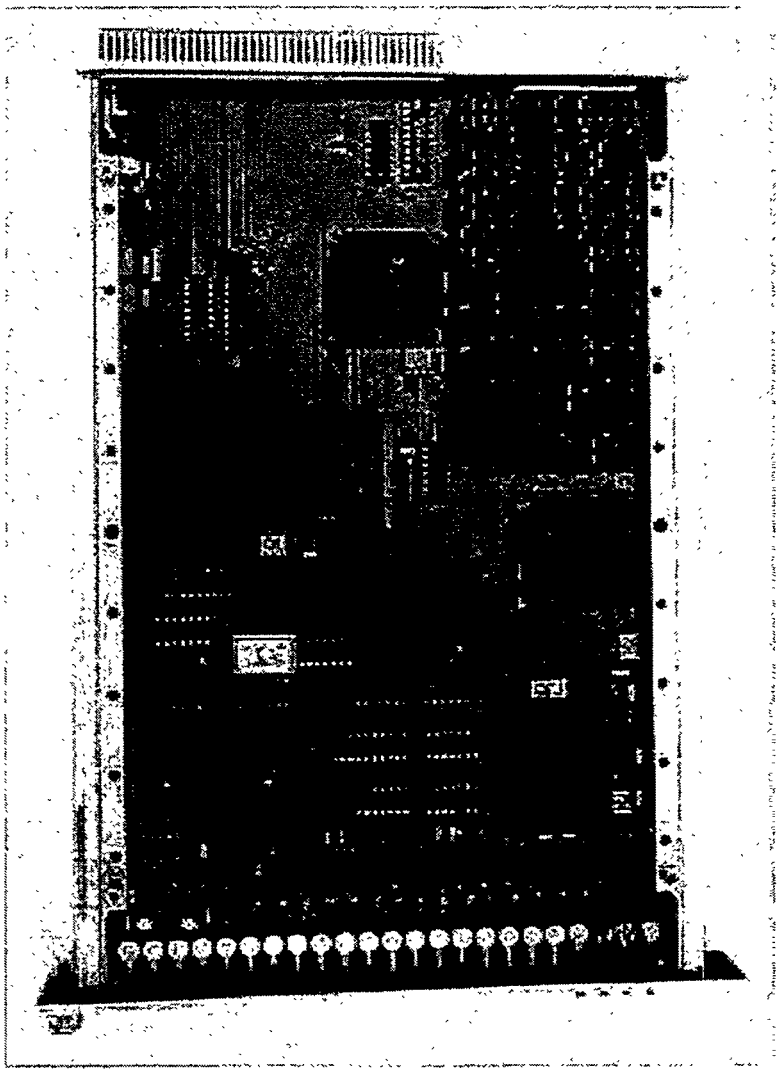

Fig. 1. Pulse Arrival Time Recording Module (PATRM).

PHANTOM SHIFT REGISTER

The original rationale for this device came from Ken Coop of Los Alamos, who anticipated that it would be a significant improvement to the shift register which we had been using for neutron coincidence counting of transuranic waste. Earlier methods of multiplicity analysis counted neutron events in a gated scaler or the number of pulses remaining in a shift register just after a pulse has exited. Both of these methods require that the analysis parameters (window width, clock rate, etc.) be set before collecting data. To try different parameters required rerunning the entire experiment. Using the PATRM to record the raw

data list, we can "play it back" with different parameters or even a completely different algorithm for comparative analysis.

The term "phantom shift register" refers to a software analog to the usual hardware shift register. Starting with the first pulse arrival time ($t1$), we add the window width (say, 100 μsec = 1,000 ticks of the 10-Mhz clock) to that time to get the far boundary of the first window. We scan the list between $t1$ and ($t1$+1,000) to count the number of pulses in that interval. We find n pulses in the window (n can be 0) and we increment by one the nth bin in our triggered window histogram. We move on to the second pulse at $t2$ (which may or may not have fallen in the preceding window) and inspect the list for events between $t2$ and ($t2$+1,000), again tallying the result in the histogram, and so on to the end of the list. When done, we have a histogram which represents the number of times that exactly n pulses (n=0,1,2...) have been observed in a triggered window. This is normalized to unity so that each bar in the histogram represents the probability that exactly n pulses will be observed in a given window.

Next we do another scan of the entire list using arbitrarily placed windows of the same 1,000-tick width. We scan the list for pulses between t=0 and t=1,000, between t=1,000 and t=2,000, and so on. Each time we tally the result in a separate histogram which represents the number of times that exactly n pulses (n=0,1,2...) have been observed in an arbitrary window. This is also normalized to give the probability for n pulses in such a window. Figure 2 illustrates the two histograms obtained by counting a 10-gram sample of plutonium metal in a counter of ~32% sensitivity with a 100-μsec window. Note the logarithmic vertical scale. Higher multiplicities occur rarely; and triggered windows are much more apt to see higher multiplicities.

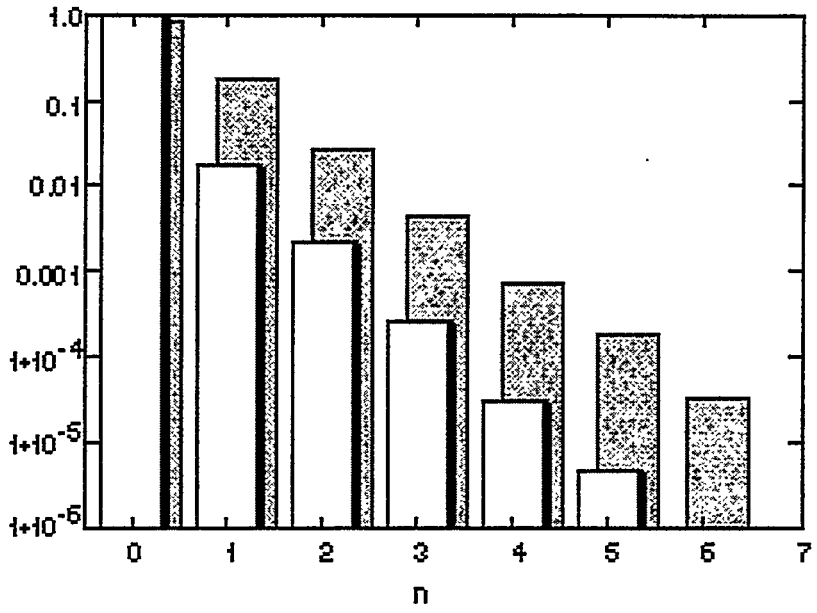

Fig. 2. Probability histogram obtained with the "phantom shift register." The sample was 10 g of plutonium metal (~5% ^{240}Pu). In each pair of bars, the one on the left represents the probability that exactly n pulses will be counted in an arbitrary 100-μsec window. The bar on the right corresponds to the probability that n pulses will be found in a 100-μsec window triggered by a neutron pulse. Logarithmic vertical scale.

These two probability histograms are the input to the multiplicity analysis algorithm, whether it be the Hage[3] technique or the one used in this group.[4] These algorithms are not discussed here since they have been covered in the cited documents. A major advantage of the PATRM is that while assembling the above histograms, we can exclude from analysis any single window which has too many pulses in it and therefore might be attributable to a cosmic-ray event. The multiplicity level at which we exclude is set by the operator. For a relatively low-sensitivity counter, we might set n=5. For a more sensitive counter, or for multiplying samples, it might be n=10 or more. If we are uncertain, we can play it back with a different criterion. Typically, this requires about one minute.

Another feature of the software permits us to "capture," and set aside for later analysis, a segment of the data stream with a very large number of pulses. In a large counter such as CTEN,[5] we occasionally observe a cosmic-ray shower which can register 50 or more events in a window. The threshold of interest is set by the operator. Figure 3 illustrates such an event. The upper plot depicts the pulses as distributed in a 500-μsec window. Below this plot, the same events are binned in a histogram. This feature is helpful in diagnosing electronic noise since, in general, noise will not exhibit the die-away characteristic of neutrons in the counter.

At our elevation (~6,750 feet), we see large cosmic ray events in CTEN from a few times a night to a few times per hour, depending on the criterion for capture. In Fig. 3, we see a few pulses at the leading edge of the window, a small gap, and then the decay of neutron pulses in a manner commensurate with the time characteristics of the detector. We see this consistently with large events and we think such a data pattern is triggered by mesons. The interval between the triggering events and the rest of the pulses can vary considerably. Figure 4 illustrates an unusual case in which the interval is ~ 15 μsec.

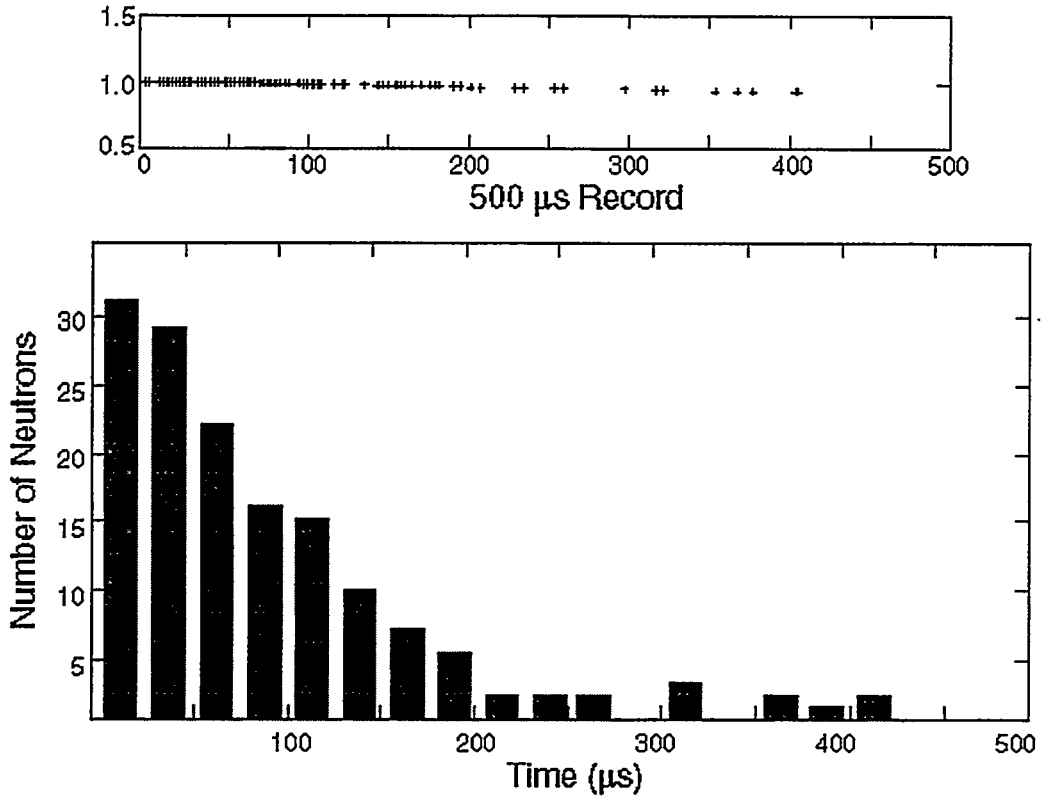

Fig. 3. Cosmic-ray shower in the CTEN counter. Upper figure shows the distribution of events in a 500-μsec segment of the data list. There is a small gap between the meson events that triggered the window and the following neutrons. In the lower figure, the events are sorted into 25-μsec time bins, showing the characteristic decay of a neutron burst.

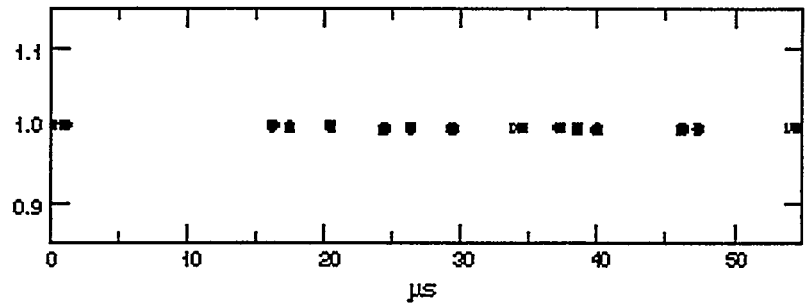

Fig. 4. Cosmic ray shower with unusually long interval (15 μsec) between mesons and neutrons.

AUTOCORRELATION

While executing the shift-register algorithm described above, we can also perform autocorrelation on the same data. As we examine each window (in the first pass), we count not only the number of pulses in the window, but we also sort them, one by one, into 100 bins[a] depending on where each one fell in the window. This generates an autocorrelation distribution spanning whatever time the operator specified for the window width. Figure 5 is an example of such a distribution derived from the same data list as Fig. 2. Autocorrelation makes a number of useful things possible.

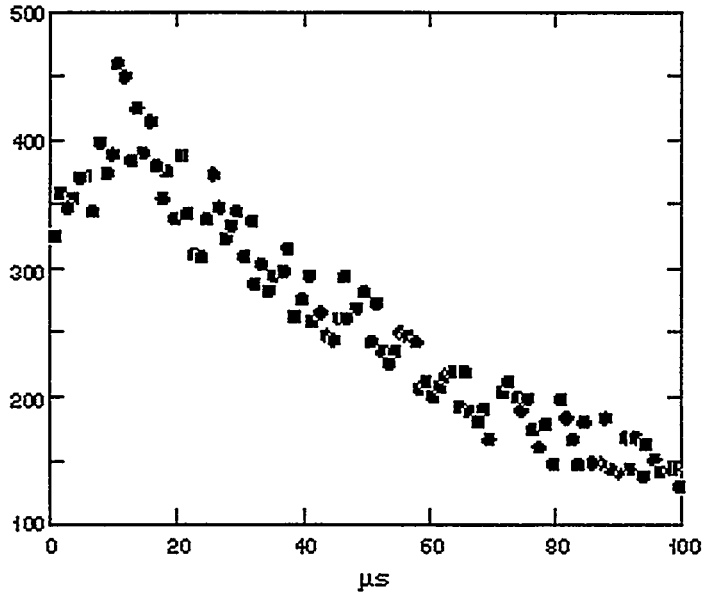

Fig. 5. Autocorrelation distribution of neutron pulses. This is from the same data list as the probability histogram in Fig. 2.

---

[a] This is set by the software and could be any reasonable number. For our purposes 100 is convenient.

Examination of Dead-Time Recovery in Counting Channels

This section is more detailed than the others for two reasons: Dead-time recovery and double pulsing are vital factors in multiplicity counting, and the other applications mentioned in this paper have been, or will be, described elsewhere.

Figure 6 illustrates the autocorrelation observed in a single channel when counting a large AmLi (α,n) source. The counter module consisted of three 2-in. x 40-in. 4 atm ^{3}He detectors in parallel. The source was random, and except for dead-time effects, should show no correlation. This data was obtained while we were comparing a new pulse channel design with a conventional channel which we have been using for a number of years. The new unit, (PADEM),[6] including in each a Preamplifier, Amplifier, Discriminator, ECL Driver in a single Moduleincorporates four independent channels (The time constant in each channel can be set at 0.5, 1, 2, or 4 μsec. In Figure 6, the five curves represent, respectively, from the left, the response of the PADEM at 0.5 μsec, PADEM at 1 μsec, the conventional channel at nominally 1 μsec, PADEM at 2 μsec, and PADEM at 4 μsec. For the several ^{3}He counters that we have examined in this way, we find that the dead-time recovery can best be modeled by a linear term. Figure 6 differs from Fig. 5 in two distinct ways:

1. Figure 6 is uncorrelated; Fig. 5 shows a strong correlation.

2. In Fig. 6, the count goes to 0 at 0 time. In Fig. 5, the count is depressed by only ~20% because the data represents the output of five roughly equal channels of which only one is affected by the dead-time of the pulse which triggered the window.

All five of the curves in Fig. 6 show a hump just at the end of dead-time recovery. We conjecture that this represents interactions between two neighboring pulses in which the tail of the first pulse boosts over the discriminator threshold a small pulse which would not otherwise have "made the grade." This attribution is supported by the fact that the probability of an extraneous pulse is (within statistics) proportional to the count rate, that is, proportional to the proximity of pulses to each other.

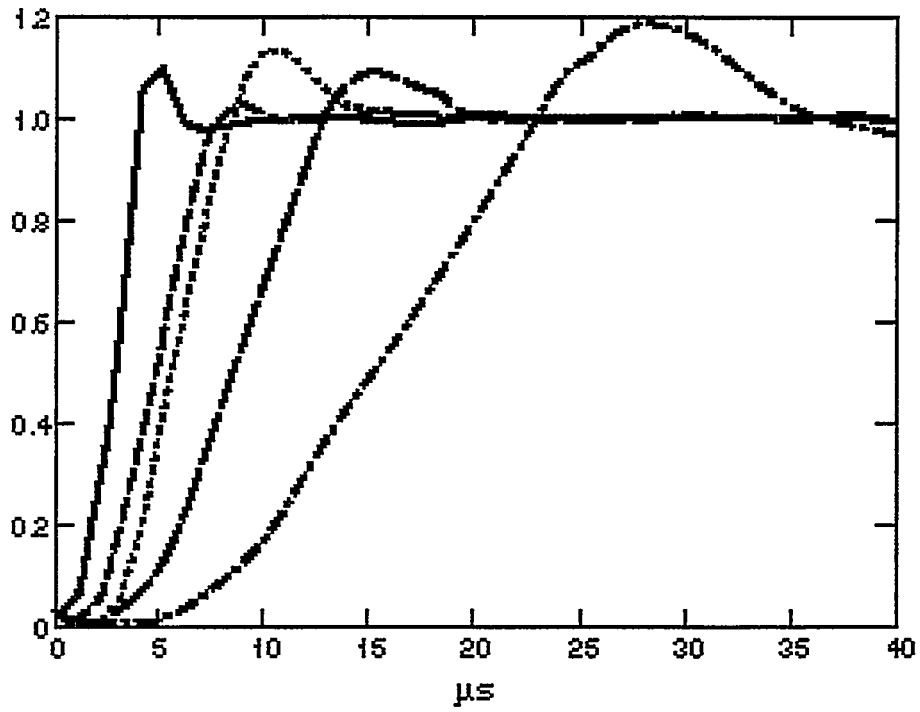

Fig. 6. Autocorrelation of pulses from an uncorrelated source (AmLi) using different preamplifier time constants. The traces are (1) PADEM @ 0.5-μsec time constant, (2) PADEM @ 1.0 μsec, (3) conventional counter channel at nominal 1 μsec, (4) PADEM @ 2 μsec, and (5) PADEM @ 4 μsec.

Figure 7a shows the autocorrelation curves for the same counter module connected to a PADEM channel with 1-μsec time constant. The three curves (normalized to compare shapes) correspond respectively to the three discriminator levels indicated on the pulse height spectrum in Fig. 7b. The detectors and cabling in this module have a combined capacitance of ~ 80 pf. Normally we connect these modules in groups of three (nine detectors in all). When we connected three modules to the same channel (~275, pf including a few additional feet of cable), there was no perceptible effect due to the additional capacitive load. In any event, the anomalous counts represent a small effect, as seen in the following table which refers to the data in Fig. 7.

Curve	Discriminator	Count Rate	Anomalous Fraction
1	0.400	2760	0.13%
2	0.600	2720	0.09%
3	0.800	2700	0.04%

We emphasize here that the different count rates in the above table refer to different discriminator settings at the same neutron intensity, whereas the proportionality to count rate mentioned in the preceding paragraph applies to different neutron intensities at the same discriminator setting.

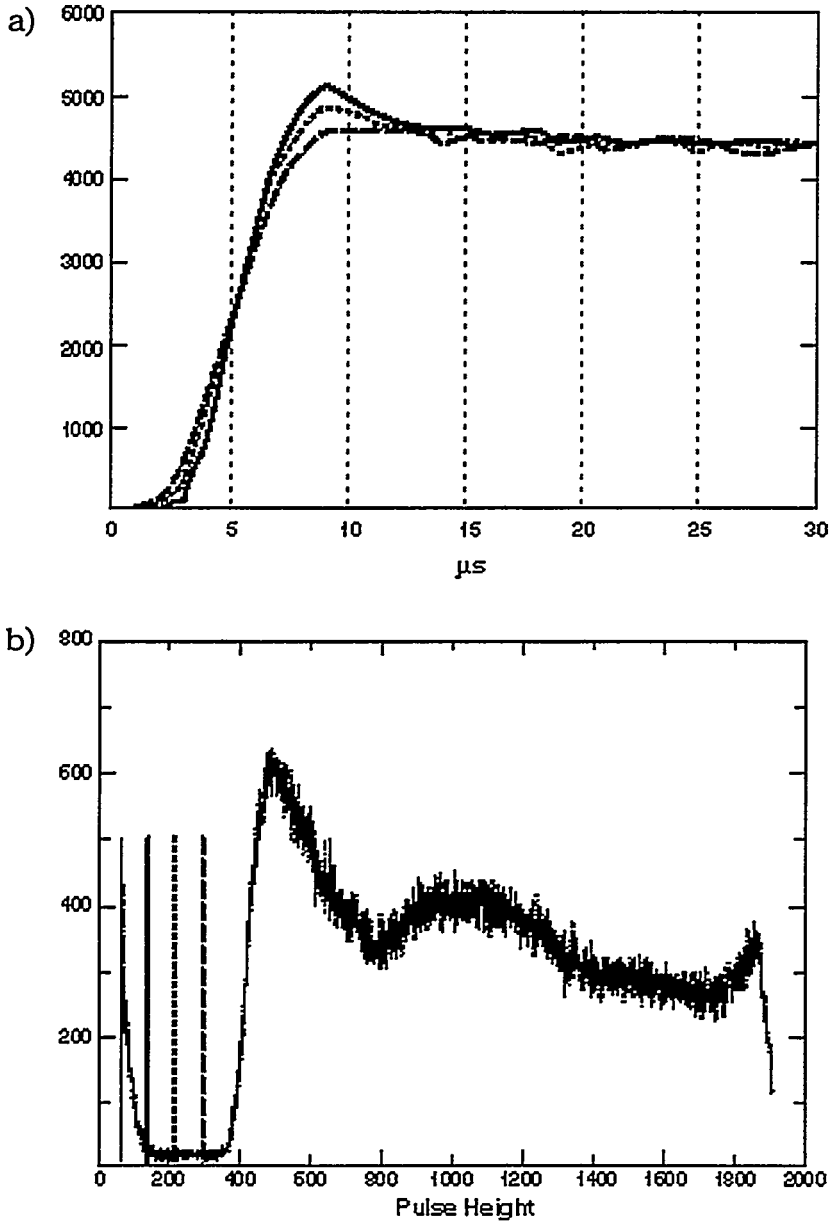

Fig. 7. Autocorrelation distribution obtained in counting an uncorrelated source (AmLi) with a pod of three 2-in. x 40-in. ^3He detectors at three different discriminator settings. The respective settings are displayed on a plot of the pulse height spectrum in the lower figure.

In contrast to the ^{3}He detectors discussed above, Fig. 8a illustrates double pulsing in a 2-in. x 20-in., 15-atm ^{4}He detector also connected to a PADEM channel with 1 μsec time constant. All curves are normalized to 10^{6} events. The upper curve shows data taken at ~1,430 counts/sec. The second curve was made at ~440 counts/sec (same discriminator setting, reduced neutron intensity). The fact that the anomalous counts are essentially the same for the two instances indicates that they arise from double pulsing (interaction of pulse with discriminator rather than with another pulse). The other two curves illustrate the effect of raising the discriminator level. The following table shows the trade-off between sensitivity and double-pulsing.

Curve	Discriminator	Counts/sec	% Double Pulsing
1	0.200	1430	11.3
3	0.300	680	3.3
4	0.400	420	0.67

Curve 2 is not tabulated because it was made at reduced neutron intensity. However, it showed 11.8% double pulsing, which is comparable, as it should be, to Curve 1.

For completeness, we include in Fig. 9a the autocorrelation data for a Westinghouse fission chamber loaded with about half a gram of ^{235}U. The PADEM channel was at 1 μsec time constant. The discriminator was set as shown on the pulse height spectrum in Fig. 9b. This data was taken at 1,000 volts, but there was no perceptible difference in the recovery characteristic when the voltage was reduced to 50.

a)

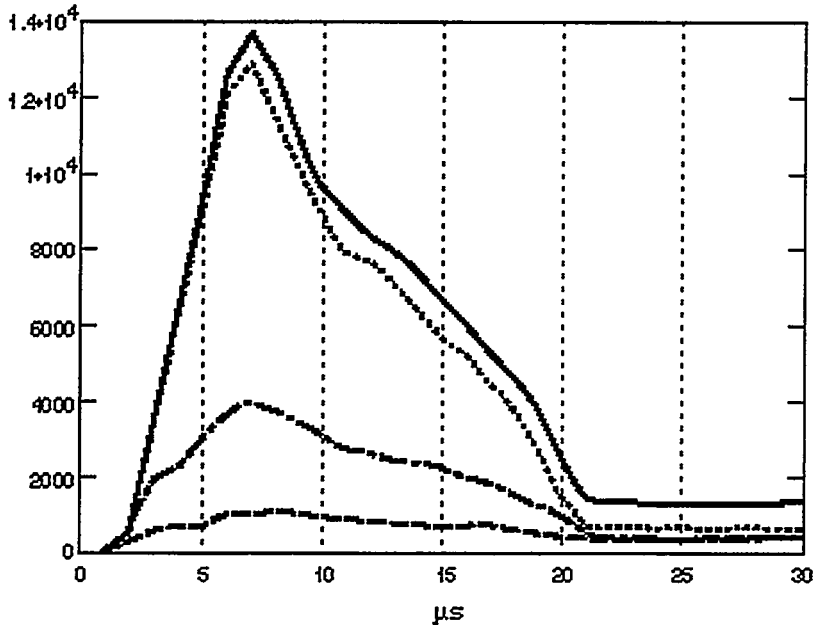

b)

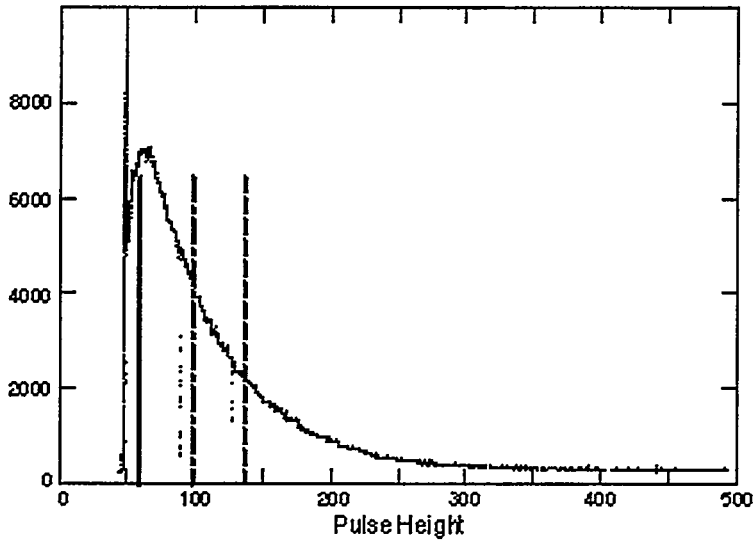

Fig. 8. Autocorrelation distribution obtained in counting an uncorrelated source (AmLi) with a ^{4}He (2-in. x 20-in., 15-atm) detector at three different discriminator settings. The top two curves were made at the same setting, but with the neutron intensity decreased by moving the source away. See the table. The discriminator levels are shown on the pulse height spectrum in the lower graph.

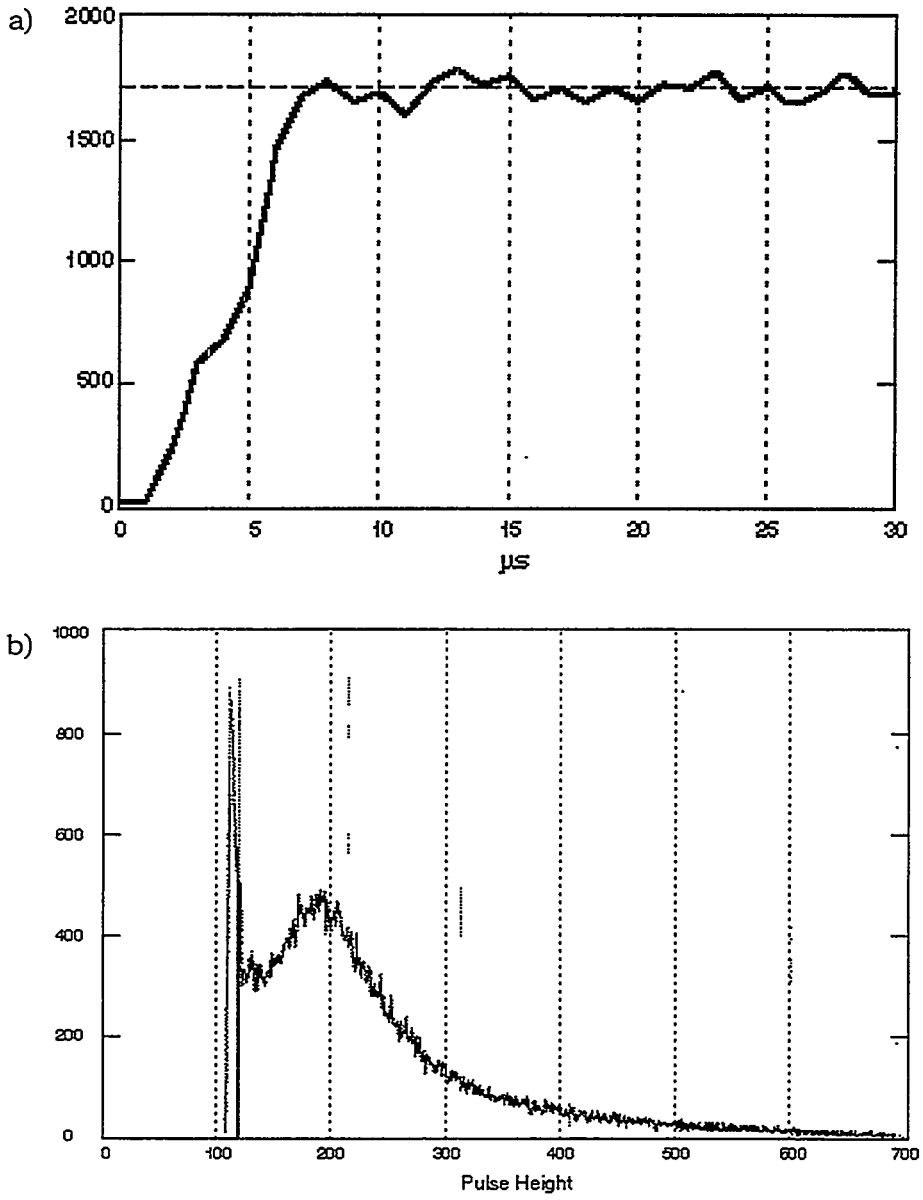

Fig. 9. Autocorrelation distribution obtained in counting an uncorrelated source (AmLi) with a fission chamber loaded with about 1/2 g ^{235}U. Discriminator level shown in lower graph.

Dead-Time Correction in Multiplicity Counting

In multiplicity counting, dead-time losses are much more severe than they are in counting in the general case. We take the autocorrelation distribution and use the Levenberg-Marquardt[7] algorithm to fit a single exponential function plus a background. This is modified by a linear dead-time recovery term spanning (for this detector) 10 μsec. Figure 10 shows such a fit on the data of Fig. 5. To restate what was said above, the *n*th data point in the figure represents the number of times that a pulse was found to be *n* μsec behind another pulse. The triangular area between the two smooth curves represents the actual number of pulses lost in dead-time. These losses amounted to 726 counts. The total count was 112,005 in 500 sec, for a count rate of 224 s^{-1}. Thus, the actual losses were

726/112,005 = 0.65%.

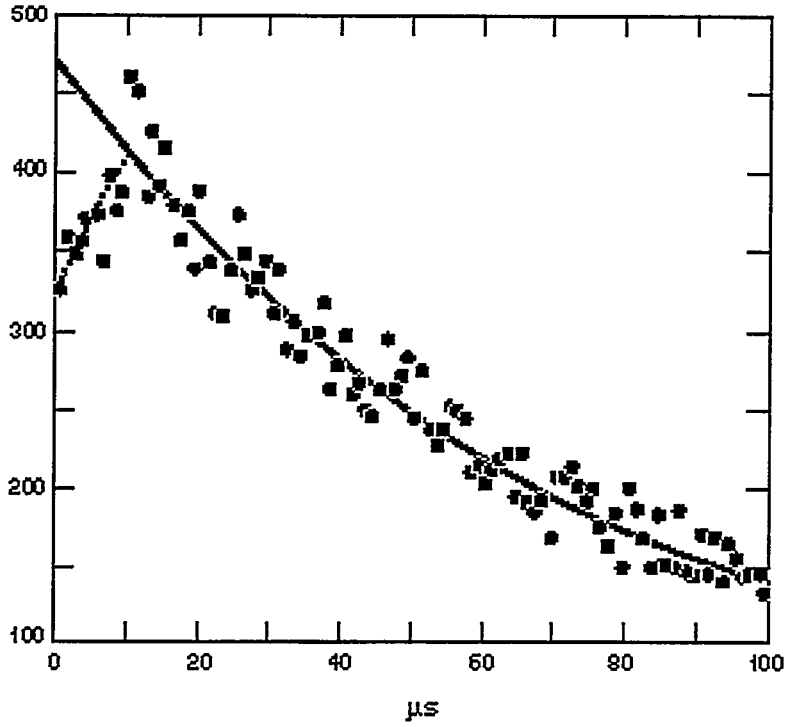

Fig. 10. Autocorrelation distribution (the same as in Fig. 5) fitted with a single exponential plus background. This is modified with a linear dead-time recovery term for the first 10 msec. The smooth curve represents the distribution inferred for an ideal counter with no dead-time.

On the other hand, if we estimate losses based merely on count rate, the result is quite different. Assume a system dead-time of 1 μsec (a five-channel system with a nominal dead time of 5 μsec per channel), we have losses of

$$.000001 \times 224 = 0.022\% ,$$

which would be low by a factor of ~30.

One approach we have taken on the dead-time problem is to "put back" the lost pulses. We have written a Monte Carlo routine with which we scan the data list and insert, in a random but realistic way, the lost pulses. Figure 11 is the autocorrelation curve obtained when we process the "dead-time-corrected" list. From this, we generate another pair of histograms (slightly different from Fig. 2) which serve as input to the multiplicity algorithms mentioned above.

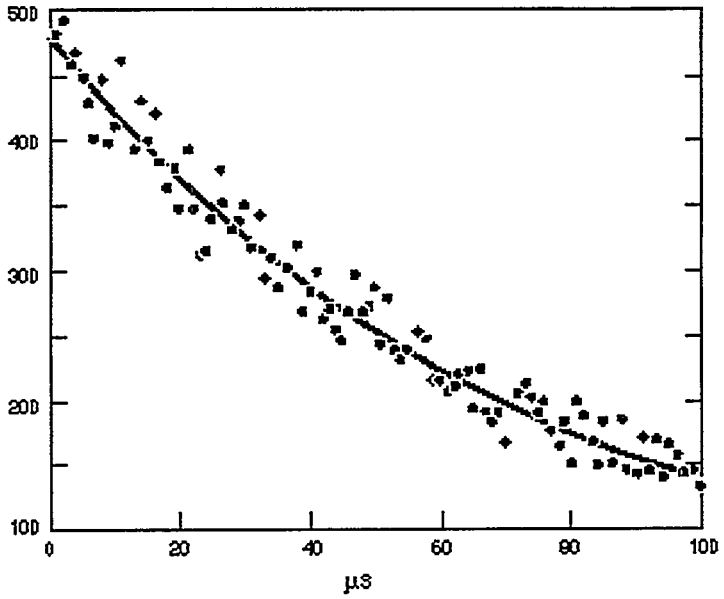

Fig. 11. Autocorrelation distribution of the data in Fig. 10 after the dead-time losses have been "put back" with a Monte Carlo routine.

Rossi-α

Rossi-α is a measurement routinely made on many critical or near critical nuclear systems.[8-11] In its simplest form, we do an autocorrelation on the pulse train coming from neutron detectors located (preferably) deep within the assembly. From the autocorrelation distribution, we obtain an exponential curve which characterizes the average time behavior of neutron chains in that system. This enables us to infer a prompt neutron lifetime as well as examine other aspects of the system near critical.

Rossi-α measurements are currently being made on SHEBA[b] at this installation. The neutron pulses are obtained from four small, high-pressure ^{3}He detectors located in a well near the center of the tank. To reduce dead-time losses, we lead the signals independently to four separate channels of the PADEM module described above.

Figure 12 displays a Rossi-α distribution observed in SHEBA by Rene Sanchez[12] of Los Alamos using the list module (PATRM). The system was about $3 below delayed critical. The coincidence distribution has been fitted with two exponential terms plus a background continuum. These components are plotted individually in the graph. The longer exponential represents the fundamental characteristic of the

[b] SHEBA is a uranyl fluoride solution system. The solution contains ~1 g/cc of uranium (~5% enriched). The cylindrical tank with vertical axis has an ID of 19.25 in. Delayed critical is reached when the tank is filled to a depth of ~20 in.

system, while the short one is due to higher mode(s). For data taken nearer delayed critical, the shorter exponential becomes almost invisible.

SHEBA, having only one region, is a simple system. In other systems having reflectors and possibly more than one multiplying region, Rossi-α measurements can yield information regarding time characteristics of the various regions and neutron communication between regions. For this purpose, we do the measurements by cross-correlation between detectors located in different regions.

The improved PATRM[13] now being designed will make this very easy, because every pulse will be tagged with the channel of origin. With this additional information, any conceivable cross-correlation can be written into the software. We have, however, been able to do limited cross-correlation with the current PATRM even though the pulses, per se, are not tagged.

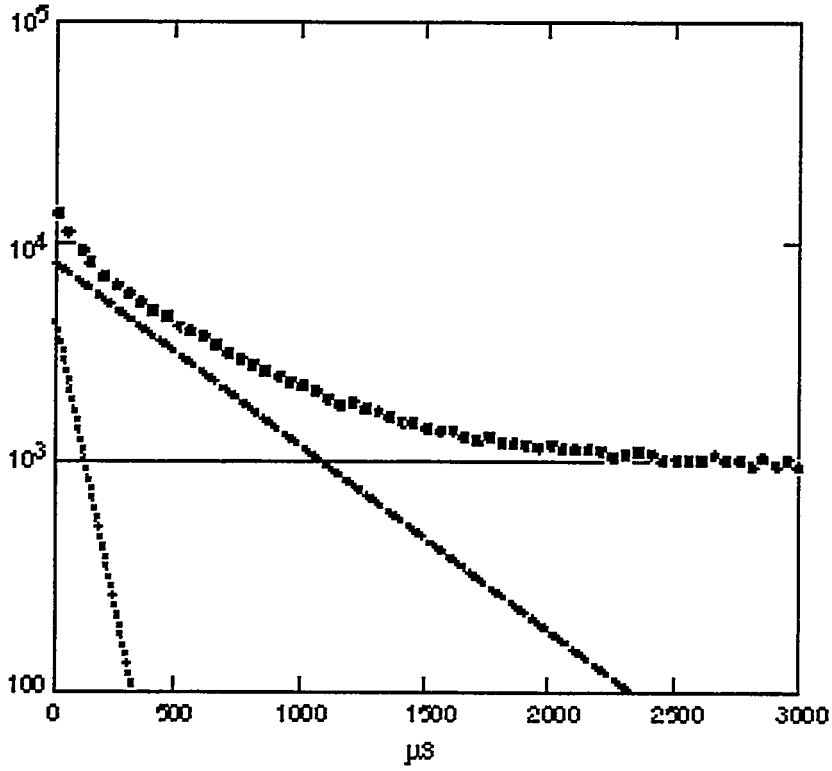

Fig. 12. Autocorrelation in SHEBA to measure Rossi-α logarithmic vertical scale. The three straight lines represent the components of the fitting model.

As mentioned above, if multiple pulses arrive on the same tick, they will be recorded as having arrived on successive ticks. We choose a specific counter channel to serve as the "trigger" channel to be cross-correlated with all the other channels. We "fan out" the pulse from the trigger channel into three separate inputs to the PATRM. Figure 13 shows a short segment of a data list made in this way. The

triplets in the list (indicating the occurrence of a trigger) are bracketed. In scanning the list, the software opens a window only when it encounters a triplet; it ignores triplets within any window. Of course, there is the possibility of a triplet really occurring during a count. This can only occur in the unlikely event of three independent pulses arriving within the span of 0.3 μsec. With plausible count rates the chance of this happening is on the order of 10^{-6}.

116	604512094
117	604512095
118	604512096
119	607419312
120	614714039
121	614714040
122	614714041
123	620633913
124	622708885
125	630862798
126	630862799
127	630862800
128	641781411
129	642078284
130	658867118
131	658867119
132	658867120
133	660739288

Fig. 13. Short segment of a data list illustrating the "triplets" which mark trigger pulses.

MULTICHANNEL SCALING

The PATRM can be used as a conventional multichannel scaler if the cross-correlation software is modified slightly. We merely ignore any triggers until after a window has been closed and start another window with the next following trigger. We have complete control, in software, of the number and width of the time channels. A feature of the PATRM not now used is the capability of scaling the clock frequency down by 2^n where n can range up to 7. In principle, time channels can be set from 10^{-7} sec to several

minutes and the number of channels from a few to thousands. The only restriction is capacity of the memory: 4 million events.

With a somewhat different application of multiscaling, David Loaiza[14] of Los Alamos is currently doing measurements of delayed neutrons at this installation. To this end, we have written special software to use the PATRM as a single-pass multiscaler with variable-width time bins. The execution of the experiment entails three steps:

1. Neutron irradiation of a small sample of fissionable material with the GODIVA critical assembly. The sample may be exposed over a period of time long enough to saturate the population of delayed neutron precursors, or it may be exposed to a burst irradiation. Both are used.
2. The sample is transported pneumatically to a well-shielded neutron counter. Transport time is ~150 msec.
3. Counting follows for ~5 minutes, during which time the count rate diminishes from 5×10^4 s^{-1}, or higher, to a background (<10 s^{-1}).

The software for taking data under these conditions does the following:

1. Starts the clock in the PATRM when a sensor detects the departure of the sample from the irradiation position. This means that the time reference in the list is tied to a well-defined and reproducible event.
2. Does not enable neutron inputs to the PATRM until another sensor detects the arrival of the sample at the counting station. This avoids recording neutrons not associated with the sample.
3. Scans the data list with windows (bins) of increasing width to accommodate the four orders of magnitude change in count rate during the decay of the sample. Currently, we start with time bins 20 msec wide and double the width every 50 bins.

Figure 14 shows the data (used by permission) resulting from such a counting routine. Figure 14a plots the entire run; the ordinate (log scale) is the count rate; the abscissa is time in seconds since the irradiation. Time is reckoned to the midpoint of each bin. The four smaller figures (linear ordinate scale) present the same data piece-wise for a more detailed view.

NEUTRON BURST INTERROGATION AND AUTOCORRELATION

Charles Hollas of Los Alamos has developed software to utilize the PATRM in correlation measurements of TRU waste when it is interrogated by bursts of neutrons from a small D-T neutron generator. He is discussing this in a separate paper in this meeting.

CONCLUSION

We want, by the foregoing examples, to emphasize the versatility of the present PATRM and the even greater potential of the new design. The improved version will record all that can ever be known from a given signal stream. Whatever data treatment is desired can be written into the software, and alternative analyses can be applied to exactly the same data.

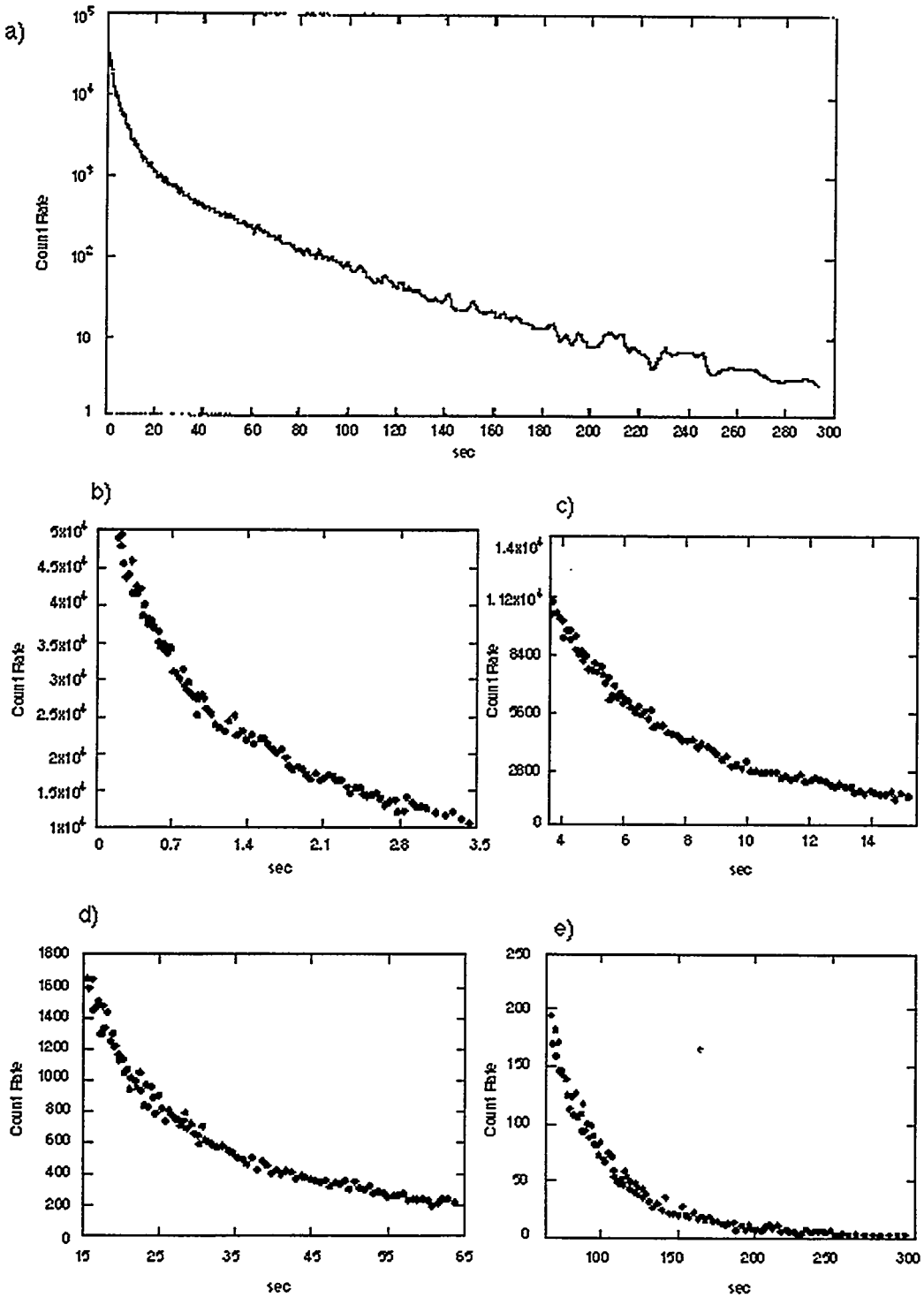

Fig. 14. Using the PATRM as a single-pass multichannel scaler with variable-width time bins to record the delayed neutron die-away. Top graph (log vertical scale) shows a complete run. The other four curves display (with linear vertical scale) segments of the whole. We begin with 20-msec bins and double the bin width after every 50 bins, using 5.12-sec bins toward the end of a 5-min count.

REFERENCES

1. G. J. Arnone, G. S. Brunson, and K. L. Coop, "A Pulse Arrival-Time Recording Module for Analyzing Neutron Multiplicities," *1992 IEEE Nuclear Science Symposium*, Los Alamos National Laboratory report LA-UR-92-3460 (October 1992).

2. C. L. Hollas, G. J. Arnone, G. S. Brunson, and K. L. Coop, "Determination of Fission Neutron Transmission Through Waste Matrix Material Using Neutron Signal Correlation from Active Assay of ^{239}Pu," *Institute of Nuclear Materials Management (INMM)*, Los Alamos National Laboratory report LA-UR-96-2574 (October 1996).

3. M. S. Krick and W. C. Harker, "Multiplicity Neutron Coincidence Counting User's Manual," Los Alamos National Laboratory report LA-UR-93-1394 (1993).

4. G. S. Brunson and N. J. Nicholas, "Shift-Register Neutron-Coincidence Counting and the Gray Barrel Problem," Los Alamos National Laboratory report LA-12414-MS (October 1992).

5. K. L. Coop and C. L. Hollas, "Epithermal Neutron Interrogation of Fissile Waste," submitted to *Institute of Nuclear Materials Management (INMM)*, Los Alamos National Laboratory report LA-UR-96-2573 (October 1992).

6. G. J. Arnone, "A Preamp-Amplifier-Discriminator Module Developed for the CTEN Waste Assay System," Los Alamos National Laboratory report LA-UR-96-3877 (1996).

7. W. H. Press, S. A. Teukolsky, W. T. Vetterling, and B. P. Flannery, "Numerical Recipes in C," *The Art of Scientific Computing, Ed. 2*, pp 683-688, Cambridge University Press, (1992).

8. F. deHoffman, "The Science and Engineering of Nuclear Power," Vol. II, pp. 116-119, Addison-Wesley, Cambridge, 1949.

9. J. D. Orndoff, "Prompt Neutron Periods of Metal Critical Assemblies," *Nuclear Science and Engineering*, **2**, pp 450-460 (1957).

10. G. S. Brunson et al., "A Survey of Prompt-Neutron Lifetimes in Fast Critical Systems," ANL-6681, Argonne National Laboratory (1963).

11. G. D. Spriggs, R. D. Busch, and J. G. Williams, "Two-Region Kinetic Model for Reflected Reactors," Los Alamos National Laboratory report LA-UR-96-533 (February 1996).

12. Personal communication with Rene Sanchez, (November 1996).

13. G. J. Arnone, "A New Pulse Arrival-Time Recording System," Los Alamos National Laboratory report LA-UR-96-3878 (1996).

14. D. Loaiza, G. Brunson, and R. Sanchez," Measurement of Delayed Neutron Parameters for U-235," Trans. Am. Nucl. Soc., Vol 75, 353 (1996).

MATRIX EFFECTS CORRECTIONS IN DDT ASSAY OF ^{239}PU WITH THE CTEN INSTRUMENT

Charles L. Hollas, Gaetano Arnone, Glenn Brunson, and Kenneth Coop
Advanced Nuclear Technology, NIS-6, Los Alamos National Laboratory
P.O. Box 1663, Mail Stop J562, Los Alamos, New Mexico, 87545, USA
Telephone (505)-667-0677, Fax (505)-665-3657
Sheila Melton
Y-12, Oak Ridge, Tennessee

ABSTRACT

The accuracy of transuranic (TRU) waste assay using the differential die-away technique depends upon significant corrections to compensate for the effects of the matrix material in which the TRU waste is located. We have used a new instrument, the combined thermal/epithermal neutron (CTEN) instrument for the assay of TRU waste, to develop methods to improve the accuracy of these corrections. Neutrons from a pulsed 14-MeV neutron generator are moderated in the walls of the CTEN cavity and induce fission in the TRU material. The prompt neutrons from these fission events are detected in cadmium-wrapped ^{3}He neutron detectors. We have developed methods of data acquisition and analysis to extract correlation in the neutron signals resulting from fission during active interrogation. This correlation information, in conjunction with the total number of neutrons detected, is used to determine the fraction of fission neutrons transmitted through the matrix material into the ^{3}He detectors. This determination allows us to cleanly separate the matrix effects into two processes: matrix modification upon the neutron interrogating flux and matrix modification upon the fraction of fission neutrons transmitted to the neutron detectors. Recent results indicate that for some matrix systems, corrections for position dependent effects within the matrix are possible.

1. The CTEN Instrument

A new instrument for the assay of ^{239}Pu and ^{235}U waste contained in 208- and 314- liter (55- and 83-gallon) drums has recently been constructed at the Los Alamos National Laboratory. This instrument designated CTEN, for combined thermal/epithermal neutron, actively and passively assays waste containers. The active interrogation method uses thermalized neutrons from a pulsed 14-MeV neutron source to irradiate the drum. Prompt neutrons from thermal neutron induced fission are detected by cadmium-wrapped ^{3}He neutron detectors. The detector signals are amplified and converted to logic pulses by leading edge discriminators.

*This work supported by the U.S. Dept. of Energy, EM-50, Mixed Waste Focus Area.

These logic pulses are input to a custom electronics module, the pulse arrival time recording module (PATRM) (Ref. 1), which sequentially records their arrival times. Located inside the cavity are three small ^{3}He detectors that are enclosed within cadmium lined cylinders. A small circular opening in the cadmium pointing to the axis of rotation of the drum from the axis of the detector allows thermal neutrons exiting the drum to be detected. These designated on-drum flux monitors provide a relative measurement of the magnitude of the thermal neutron flux at the outer surface of the drum. In addition to interrogation of the drum with thermal neutrons, the CTEN instrument also interrogates with epithermal neutrons to provide an estimation of the presence of self shielding effects in the thermal interrogation (Ref. 2). A passive assay is also performed by recording the neutron detection signal arrival times with the PATRM, and performing multiplicity analysis (Refs. 3, 4) to determine the ^{240}Pu mass.

2. Experimental Procedure

The 39 cadmium-wrapped or "shielded" ^{3}He neutron detectors of the CTEN instrument are used to detect neutrons from fission events induced by the interrogating thermal neutrons. Signals from these detectors are configured into 15 channels of logic signal input to 15 channels of the PATRM. The PATRM uses a logic pulse, designated VETO, to control data acquisition in the active mode assay. At the onset of the VETO pulse, the PATRM disables all data inputs, writes a code marker to its next available internal memory location, stops the internal clock counter, and resets this counter to zero. Upon lifting of the VETO, the clock counter and all data inputs are enabled. The result of the measurement is a history of the signal arrival times relative to the end of the VETO pulse. The clock frequency is set at 5 megahertz, allowing the signal arrival time to be measured with an accuracy of 0.2 μs. The VETO input used in the active assay is a logic pulse of length 500 μs derived from the trigger pulse from the neutron generator. Thus the PATRM is disabled during the neutron pulse and for most of the time in which the "shielded" ^{3}He detectors are able to detect interrogating neutrons from the neutron generator. The majority of pulses recorded by the PATRM are from fission events produced by the interrogating thermal neutron flux. The neutron generator provides neutron pulses at a rate of 100 hertz and duration of about 20 μs. Up to a million events can be recorded in the PATRM memory before transferring the data to a small computer for analysis and archiving. The number of neutrons detected by the on-drum flux monitors between 800 to 4000 usec is recorded to provide a first order estimate of the magnitude of the interrogating thermal neutron flux.

A 620-mg metallic foil of ^{239}Pu is used as a standard mass for all of the active measurements reported. A 100-g metallic cylinder of plutonium containing ~ 6% ^{240}Pu is used for passive measurements to determine the fraction of fission neutrons transmitted through the various matrix configurations into the "shielded" ^{3}He detectors. The mock 208 liter waste drums contain aluminum tubes located at radii of 12 cm, 20 cm and 25 cm. Measurements are made at three locations within each tube, at 24 cm, 40 cm and 56 cm from the top of the tube. At each location, both an active measurement with the 620-mg metallic foil of ^{239}Pu and a passive measurement of the 100-g metallic cylinder of plutonium are performed. In the active measurement the neutron arrival time history for signals from the shielded ^{3}He detectors is recorded following 19992 pulses from the neutron generator, (approximately 200 seconds measurement time). The passive measurements are performed for a 300 second time period. During the measurements the mock matrix drum is rotated once

through 360 degrees. Measurement are also made with the CTEN chamber empty to record background effects.

3. Experimental Results

We have applied the Feynman reduced variance method developed initially by Feynman, deHoffmann, and Serber (Ref. 5), and used by other investigators (Refs. 4,6) for the analysis of spontaneously fissioning systems. In Ref. 7 our method of applying this method to active thermal neutron induced fission systems is discussed. The time history of the neutron events, recorded in the PATRM module, is used to construct the Feynman variance parameters N1, the total number of neutrons, and N2, the number of "correlated" neutrons, from Feynman or "random" triggered distributions. In Ref. 7 we showed that the ratio N2/N1 can be used to determine the fraction of fission neutrons (TRAN) from the thermal neutron induced fission events that are transmitted through the matrix into the "shielded" ^{3}He detectors. The variation of N1, N2 and 100*N2/N1 as a function of time after the neutron beam burst (from Ref. 7) for a 7-g sample of plutonium oxide located at the central position of the empty CTEN chamber, using 6000 neutron bursts is illustrated in Fig. 1. The N1 and N2 distributions, both exhibit an exponential decrease over the region of

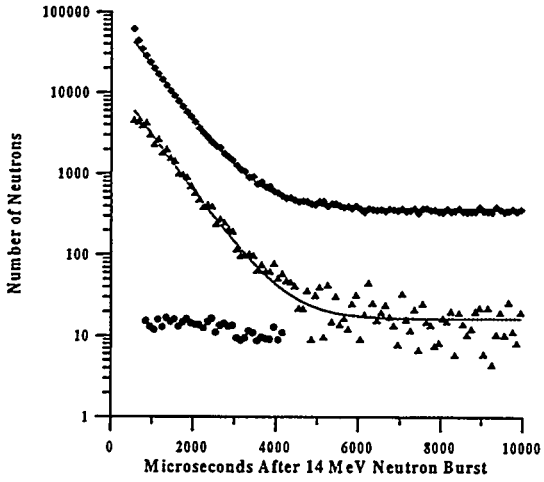

Fig 1. The time distributions for the N1 (diamonds), N2 (triangles) and ratio of 100*N2/N1(circles) for the 7-g plutonium sample obtained with 6000 neutron generator pulses.

~800 to 3000 μs, with a time constant that is representative of the thermal neutron die-away time in the CTEN chamber. A sharper exponential decrease is observed at the earliest times measured, from 500 μs to the start of the second exponential near 800 μs in the N1 distribution. This early region still contains neutrons from the neutron generator burst that have not yet been completely cleared from the ^{3}He detector packages. The solid lines represent the results of least square fits to the data for times greater than 800 μs, obtained with the function

$$Y(t) = A*\exp(-0.693*t/\Psi) + C. \qquad 1)$$

Here Ψ is the thermal neutron die-away half-life time constant at the location of the plutonium sample, A is proportional to the number of neutrons detected from thermal induced fission events, and C is a constant dependent upon background neutrons, which include neutrons from cosmic ray events, neutrons from spontaneous fission events from the ^{240}Pu, and delayed neutrons from fission products..

B. The position dependent variation of N1

Measurements of N1 were obtained for two homogenous matrix materials, one containing 0.9 kg of borax powder dispersed in vermiculite (BV matrix), and one containing pieces of polyethylene tubing (CH_2 matrix) with a total mass of 46 kg. The BV matrix contained boron at a density of ~0.00052 gm/cm^3. The CH_2 matrix contained hydrogen at a density of ~0.033 gm/cm^3. The values for N1 obtained at nine location are shown in Fig. 2 for the BV matrix and in Fig. 3 for the CH_2 matrix. These two matrix types are representative of the two different processes which alter the thermal flux. The predominant effect of the BV

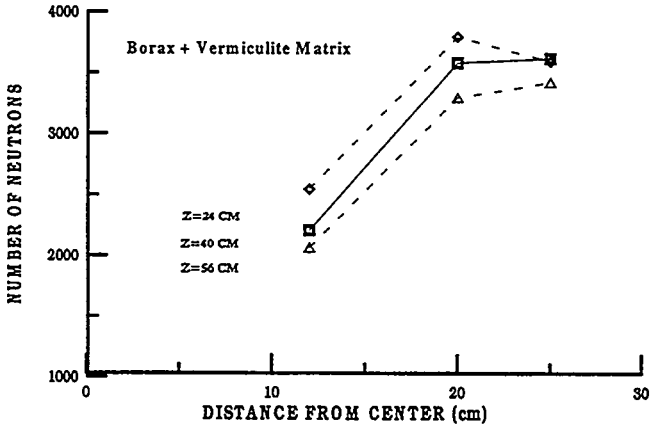

Fig. 2. The variation of the values for N1 as a function of position for the BV matrix.

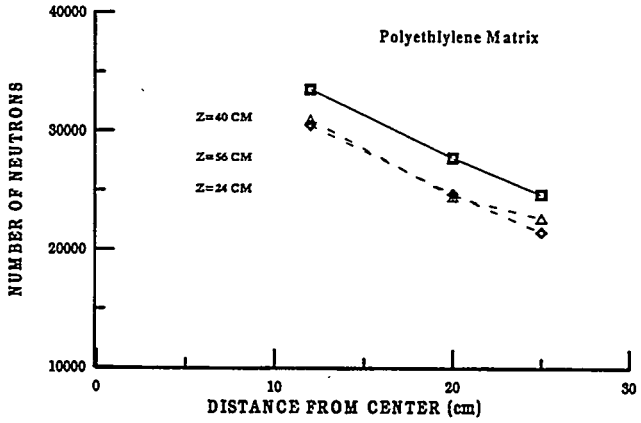

Fig. 3. The variation of the values for N1 as a function of position for the CH_2 matrix.

matrix is to reduce the thermal flux by means of the absorption of thermal neutrons by the large thermal neutron absorption cross section (~ 3843 barns) of the boron contained in the borax. The predominant effect of the CH_2 matrix is to increase the number of thermal neutrons within the matrix through the moderating properties of the hydrogen nuclei contained in the polyethylene. Of secondary importance is the removal of thermal neutrons by the thermal neutron absorption cross section of hydrogen (~ 0.33 barns). Another significant effect is the reduction of fission neutrons transmitted through the matrix, resulting from the moderating effect upon these neutrons.

The largest difference observed between the two matrix systems is the nearly order of magnitude larger values of N1 for the CH_2 matrix compared to the BV matrix. This large effect is also observed in the values for the thermal flux monitor, $THFLX_0$, obtained from the sum of the three on-drum flux monitors. In Figs. 4 and 5, the values of N1 have been divided by the values for $THFLX_0$. This normalization to $THFLX_0$ greatly reduces the difference in response between the two matrices; however these normalized responses still vary significantly with position in the two matrix materials. For the BV matrix, in general, the deeper into the

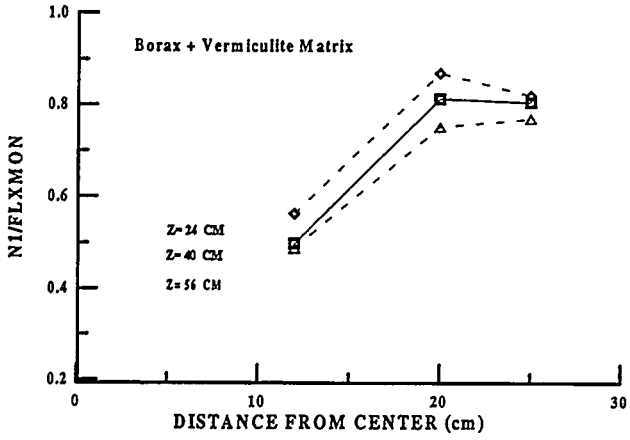

Fig. 4. The variation of the values for $N1/THFLX_0$ as a function of position for the BV matrix.

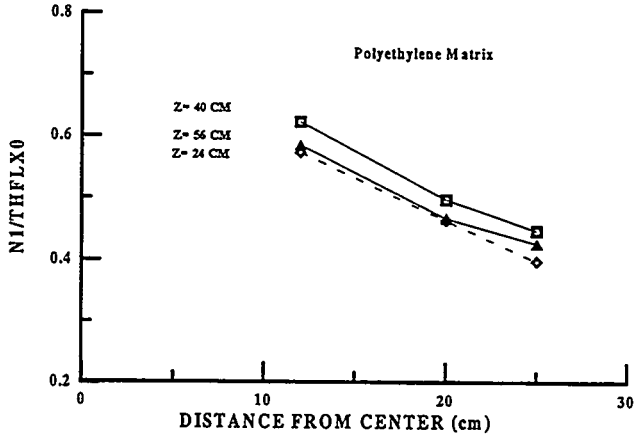

Fig. 5. The variation of the values for $N1/THFLX_0$ as a function of position for the CH_2 matrix.

matrix the smaller the values of N1, whereas for the CH_2 matrix, the deeper into the matrix the larger are the values of $N1/THFLX_0$. The $N1/THFLX_0$ values change by approximately a factor of 2 for positions near the surface of the drum (radius = 25 cm) compared to those nearer the center (radius = 12 cm) in both matricies.

C. The determination of the ^{239}Pu fissile mass

We assume that the number of fission neutrons N1 detected in the shielded ^3He detectors, can be described by the following expression:

$$N1 = C1*Mass*Mult*TRAN*\varepsilon*THFLX \qquad 2)$$

where

C1 = A calibration constant which relates the value of the thermal neutron flux at the drum surface to the number of neutrons detected by the on-drum thermal flux monitors, the cross section for thermal neutron induced fission, and the number of neutrons emitted per thermal neutron induced fission. C1 is determined with a measurement of a plutonium calibration standard of known mass located at the center of the empty CTEN chamber,

Mass = the plutonium mass,

Mult= Self multiplication,

TRAN = the fraction of fission neutrons transmitted through the matrix into the neutron detectors; for an empty drum TRAA is defined to be identically 1.0.

ε= fission neutron detection efficiency for an empty drum,

THFLX = the value of the thermal flux at the location of the plutonium sample.

In this study, we assume that the self multiplication is identically 1, which should in general be the case for TRU waste material. The value for TRAN is obtained from the measured N2/N1 ratio. The efficiency is always a constant and for the shielded ^{3}He detectors of CTEN, ε is equal to 0.10. The thermal flux THFLX, we assume, can be obtained to first order from the value of the on-drum thermal flux monitors $THFLX_0$, with a correction for the variation of the thermal flux $THFLX_I$ within the matrix , i.e.

$$THFLX = THFLX_0 * THFLX_I. \qquad 3)$$

With the above assumptions N1 can be expressed

$$N1 = C1 * Mass * TRAN * \varepsilon * THFLX_0 * THFLX_I. \qquad 4)$$

In this expression the position dependent variations observed in $N1/THFLX_0$ are contained in TRAN and $THFLX_I$ .We have observed that the value of the thermal flux lifetime Ψ, varies in a similar manner to $N1/THFLX_0$ as a function of position for the BV matrix. For this matrix TRAN is ~ 1.0 for all locations. This variation is apparent in the Fig . 6 for the BV matrix system. where $N1/THFLX_0$ is plotted with respect to Ψ. A linear relationship also is exhibited for the CH_2 matrix, but the dependence upon Ψ is opposite to that

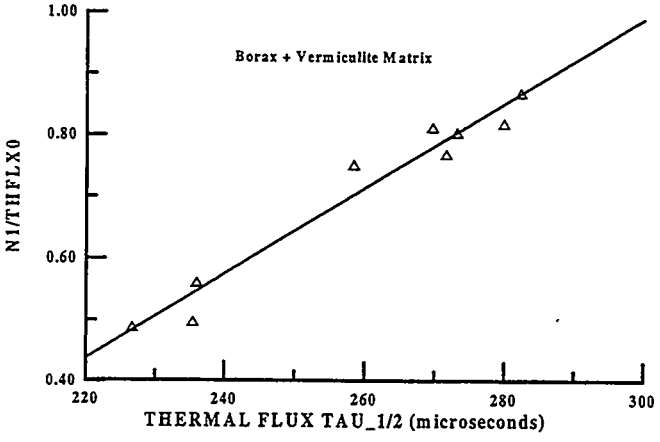

Fig. 6. The variation of the values for $N1/THFLX_0$ as a function of thermal neutron lifetime for the BV matrix.

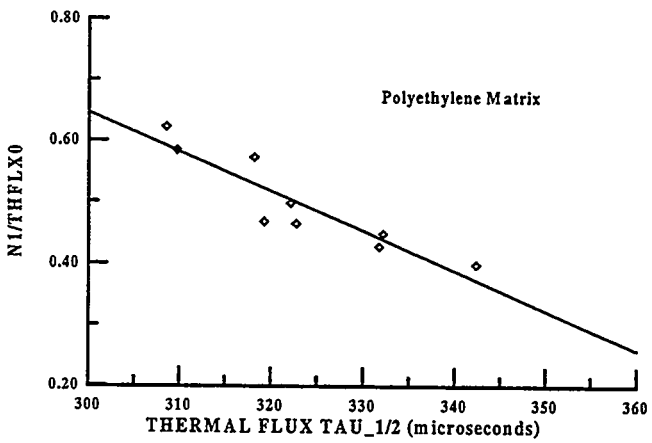

Fig. 7. The variation of the values for $N1/THFLX_0$ as a function of thermal neutron lifetime for the CH_2 matrix.

for the BV matrix. A possible interpretation is that the magnitude of the thermal flux is increasing toward the center of the drum due to the moderating effect of the hydrogen in the polyethylene, the life time is decreasing due to the thermal neutron absorption of the hydrogen. For this matrix system, TRAN is not a constant, but ranges in values from ~0.6 to ~0.4. For these results, the variation in N1/ $THFLX_0$ is due to both $THFLX_I$ and TRAN. A more complex, non-linear dependence of (N1/ $THFLX_0$ *TRAN) upon Ψ is observed. The straight lines through the data sets represent the results of linear fits. Using the parameters extracted from the fits, a value of mass is calculated from the measured values of N1, $THFLX_0$ and Ψ for each of the data points. These results are listed in Table I. The simple linear relationship improves the mass estimate from the estimates obtained without using the additional information contained in Ψ. These

Table I. The estimated mass values and percentage differences from the stated mass of 0.620 grams obtained with the linear parameterization illustrated in Figs. 6 and 7 for the BV and CH_2 matrix systems.

Borax + Vermiculite Matrix									
N1/THFLX$_0$	0.562	0.498	0.488	0.869	0.813	0.751	0.82	0.805	0.769
TAU	235.94	235.40	226.64	282.33	269.66	258.39	279.90	273.13	271.62
Mass	0.649	0.579	0.644	0.617	0.645	0.666	0.594	0.619	0.599
% Diff	4.7	6.6	3.9	0.5	4.0	7.4	4.2	0.2	3.4
Polyethylene Matrix									
N1/THFLX$_0$	0.497	0.447	0.622	0.572	0.463	0.398	0.584	0.466	0.427
TAU	322.13	332.15	308.50	318.15	322.74	342.35	309.70	319.25	331.73
Mass	0.625	0.645	0.665	0.684	0.587	0.675	0.633	0.566	0.612
% Diff	0.8	4.0	7.3	10.3	5.3	8.9	2.1	8.7	1.3

uncorrected variations track the values of N1/ $THFLX_0$. At this stage of our study, we have determined that position dependent effects for a single mass sample of ^{239}Pu in homogeneous matrix systems can be corrected with matrix specific algorithms. The algorithms differ considerably for the two types of matrix systems investigated. We speculate that this difference is dominated by the moderation effects of the hydrogen. In our study of transmission (Ref. 7) we observed that TRAN to first order is an exponential function of the average path length and average hydrogen density. We are currently studying the variation of N1/ $THFLX_0$ in a broad range of homogeneous matrix systems containing differing amounts of neutron absorption and moderating materials to determine if a parameterization of N1/ $THFLX_0$ as a function of both Ψ and TRAN, the fraction of fission neutron transmission, can adequately describe the variation.

References

1. G. J. Arnone, G. S. Brunson, and K. L. Coop, 1992 IEEE Nuclear Science Symposium, Orlando, Florida.

2. K. L. Coop and C. L. Hollas, Proceedings 37th Annual Meeting of the Institute of Nuclear Materials Management (INMM), Naples, Florida (July 1996) and Los Alamos National Laboratory report LA-UR-96-2573, (July, 1996).

3. G. S. Brunson Los Alamos National Laboratory report LA-11701-MS, (November, 1989).

4. D. M. Cifareli and W. Hage, Nucl. Instr. and Meth. **A251**, (1986) 550.

5. R. P. Feynman, F. DeHoffmann, and R. Serber, Journal of Nuclear Energy, **3**, (1956) 64.

6. A. A. Robba, E. J. Dowdy, and H. F. Atwater, Nucl. Instr. and Meth. **215**, (1983) 473.

7. C. L. Hollas, G. J. Arnone, G. S. Brunson, and K. L. Coop, Proceedings 37th Annual Meeting of the Institute of Nuclear Materials Management (INMM), Naples, Florida (July 1996) and Los Alamos National Laboratory report LA-UR-96-2574, (July, 1996).

APNEA LIST MODE DATA ACQUISITION AND REAL-TIME EVENT PROCESSING

R. A. Hogle and P. Miller,
GE Corporate Research & Development Center, Schenectady, NY. 12301

R. L. Bramblett,
Lockheed Martin Specialty Components, Largo, FL, 34649

ABSTRACT

The LMSC Active Passive Neutron Examination and Assay (APNEA) Data Logger is a VME-based data acquisition system using commercial-off-the- shelf hardware with application-specific software. It receives TTL inputs from eighty-eight ^{3}He detector tubes and eight timing signals. Two data sets are generated concurrently for each acquisition session: 1) List Mode recordings of all detector and timing signals, timestamped to 3 microsecond resolution; 2) Event Accumulations generated in real-time by counting events into short (tens of microseconds) and long (seconds) time bins following repetitive triggers. List Mode data sets can be post-processed to: 1) determine the optimum time bins for TRU assay of waste drums, 2) analyze a given data set in several ways to match different assay requirements and conditions and 3) confirm assay results by examining details of the raw data.

Data Logger events are processed and timestamped by an array of 15 TMS320C40[1] DSPs and delivered to an embedded controller (PowerPC604) for interim disk storage. Three acquisition modes, corresponding to different trigger sources are provided. A standard network interface to a remote host[2] system (Windows NT or SunOS) provides for system control, status, and transfer of previously acquired data.

INTRODUCTION

The LMSC APNEA system is a transportable measurement device used to perform TRU assay of 55-gallon and 85-gallon overpack waste drums. It includes an measurement chamber, embedded neutron detectors, and associated data logging electronics and computers. The measurement chamber is approximately 6' x 6' square and 8' high. A central cavity in the chamber contains a rotary stage upon which drums are turned at 3 RPM for examination. The cavity is surrounded by eighty-eight ^{3}He neutron detectors. The neutron detector signals arise from seventy-nine main detectors used for detection of fission neutrons and nine neutron flux monitors. Events from these detectors and eight additional special channels (external-clock,

[1] All products mentioned are the trademarks, service marks, or registered trademarks of their respective holders.
[2] J.H. McClelland, B.H. Storm, Jr., J. Ahearn, H. W. Hazzard, A. Rubin, K. Fernandez, F. Gulledge, N. Javagal and A. Yadav, "Operation and Control Software for Apnea", these proceedings.

barrel-position, azimuth timing pulse, etc.) are delivered to the data-logger. The detector electronics generate a TTL-compatible logic pulse for each neutron event. The data logger captures events as rising-edge change-of-state (i.e., low-to-high digital signal) transitions. APNEA processes neutron event temporal-spatial relationships to produce assay results[3] of drum contents.

The fundamental job for the APNEA Data Logger (APNEA-DL) is to record the following information for three acquisition modes:

- For any event signal, record the identification of the detector or special channel source and the time at which the event occurred. This is basic LIST-MODE data;
- Within time intervals following each trigger, count the number of events that occur on a given channel. For all triggers within a rotational segment of the drum, sum the counts for events that occur in the specified time interval following the trigger. The time intervals may range from microseconds to milliseconds. Rotational segments are delimited by an externally generated azimuthal timing pulse.
- Anomalous situations such as might be created by cosmic ray events, instrumental effects, or other outside influences.

ACQUISITION MODES

There are three acquisition modes: Active, Passive and EMP (External Matrix Probe). In each mode, the drum is rotated and timing pulses indicating the azimuthal starting point and rotary stage azimuthal position are generated. In Active mode, a neutron generator source (Zetatron) produces 100 Hz, 20 microsecond pulses, and neutron events are recorded for about 40 seconds. The start of the Zetatron pulse is the trigger signal. During Passive measurement, events are recorded for about 400 seconds, with no externally generated neutrons. In Passive mode there are two trigger sources: 1) the logical "OR" of inputs from the main neutron detectors, such that if any event is detected, a trigger is declared, and 2) an external 5 KHz clock pulse. During EMP measurement a ^{252}Cf neutron source is indexed through six vertical positions. At each position, events are recorded for 20 seconds. In this mode, each azimuthal timing pulse is a trigger point. A typical "run" for each drum being scanned involves all three of these acquisition types.

[3] B. H. Storm, Jr., R. L. Bramblett, D. C. Hensley, "Identification of the Fast and Thermal Neutron Characteristics of TRU Waste Drums", these proceedings.

LIST MODE RECORDING

The time resolution of APNEA-DL (2.72 μsec) is short enough to not degrade the timing information intrinsic in ^{3}He detectors (5 μsec) and, for Active mode, the Zetatron pulse (20 μsec). Each event is encoded as a two byte integer. One byte identifies the source of the input device and the other gives the time (in APNEA-DL ticks) since the last timing code. Timing codes. also two bytes, are recorded every 256th data logger time interval (2.72 μsec). The size of the list mode data set for one drum is about 200 MBytes. The list data are archived, so that details of the measurement may be reconstructed later to incorporate improvements in the assay analysis or evaluate the presence of anomalies. These data and the results of assay analysis are archived on one CD per drum.

REAL-TIME EVENT ACCUMULATION

The time to process a 200 MB list mode data set to generate assay results might be several minutes, where such processing would include the generation of accumulation records and the detection of anomalous events. To avoid this delay, the APNEA-DL pre-processes the event data in real time. The pre-processed data is then input to analysis codes to produce assay results. Preprocessing consists of accumulating the events, much the same as has been done in earlier differential die-away systems by scalers or scalers plus shift registers. Under operator control, APNEA-DL parameters can be set to modify the accumulation intervals. the time resolution, and the trigger events. These same, or modified. parameters may be used during off-linc accumulation of the list mode data, for testing or for new analysis procedures.

SYSTEM DESCRIPTION

Figure 1. is a top-level diagram of APNEA. The APNEA Host provides the operator interface, monitors and displays various system parameters, and coordinates data acquisition with the APNEA-DL. The Host also provides archival services (to CD-Recorder or other long term storage device) for the acquired data sets.

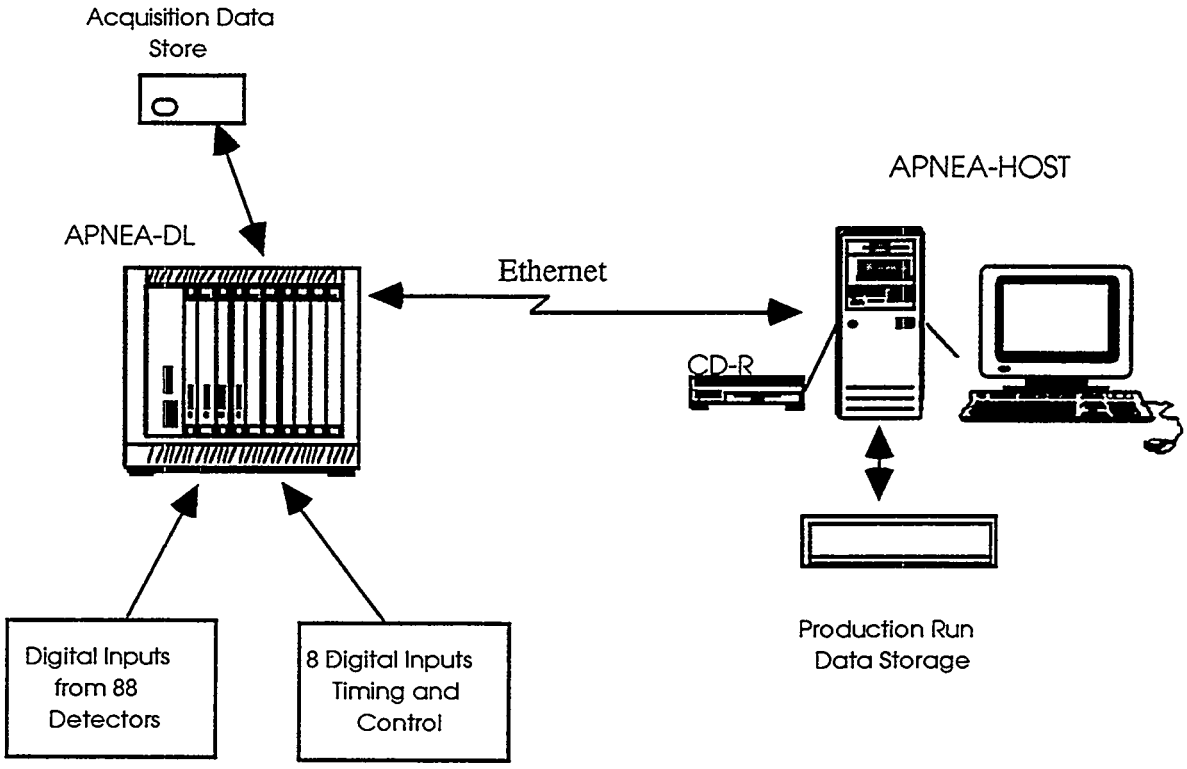

Figure 1. APNEA System Components

The APNEA-DL is responsible for acquiring the event and count data and logging it to a local disk file. APNEA-DL responds to Host requests to start and stop recording for the different measurement modes, and to transfer data from its local storage to the Host.

The purpose of the data logger is two-fold: 1) to detect neutron and special channel events from an array of 96 signal inputs and to record these events as channel-number/time pairs, and 2) to count the occurrence of events on each channel, and record these counts in time-segments following a trigger, as specified by the operator. At the end of an acquisition, three primary data sets are produced: 1) an *event* file, containing the channel/time pairs, timing marks, and special codes; 2) *accumulation* files, containing event counts divided into time segments; and 3) a *drum-position/azimuth-timing-pulse* file, which records times related to the rotation of the scanned drum. For Passive mode runs there are two accumulation files: One file, containing auto-correlated neutron counts, uses neutrons as the trigger source. The second accumulation

file uses an external clock as the trigger source. The data in this second file is used to determine the auto-correlation background measured concurrently with the auto-correlation measurement.

APNEA-DL SYSTEM ARCHITECTURE

The APNEA-DL is a VME-based system using commercial, off-the-shelf hardware. A block diagram of the system configuration is shown in Figure 2. A 6U 21-slot VME chassis with an embedded disk system contains the 14 processing and memory cards required to acquire event data. Eighty-eight channels from the detection chamber and eight control bits (96 bits total) are tied to the input lines on six standard digital I/O IndustryPack modules. The channel signals, ninety-six total, including the special channels, are:

- 88 ^{3}He Neutron Detector Outputs
- 1 Azimuth Timing Pulse with an adjustable period, nominally 2.5 sec
- 1 Drum Reflector Pulse
- 1 Zetatron Trigger (Neutron source)
- 1 Input to veto accumulation during background caused by interference from other NDA systems.
- 1 Cosmic Ray Detector input
- 1 External Clock Input (200 μsec period)
- 2 Spare

During a typical acquisition session, the Host transfers a configuration file to APNEA-DL describing the triggering sequence, the event accumulation parameters[4], the channel map[5] and the length of the acquisition. APNEA-DL is then armed and begins polling input words, looking for detector events and control bits. Every 1.36 microseconds, three 32-bit input words are read by the APNEA-DL, for an input data rate of approximately 9 MB/sec. All ninety-six bits must be examined and processed after each read cycle. Fortunately, the number of events observed at any given instant is relatively low. During the most demanding acquisition mode (Active), the peak event rate seen at the APNEA-DL system is about eight million events per second, while the average event rate is 0.2 million events per second. After processing and List Mode data generation, the total output data rate to the local disk system is a sustained 3

[4] Trigger channels, the number of time segments following each trigger, and the duration of each segment.
[5] A channel map describes how the signal wires are connected to the APNEA-DL input channels.

MBytes/second. Also, in practice, the inputs are polled twice before data are processed, yielding a List Mode timestamp resolution of 2.72 microseconds.

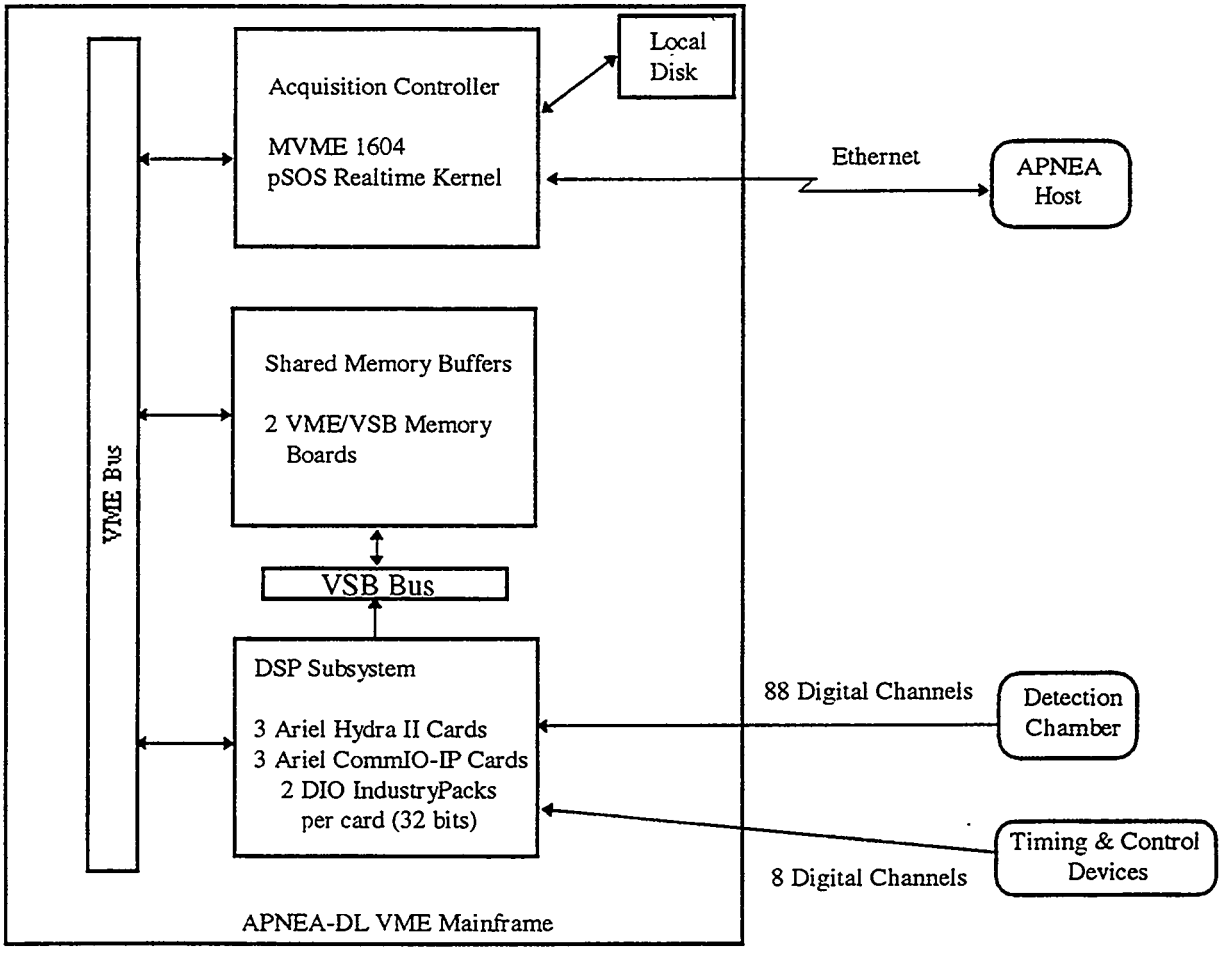

Figure 2. APNEA-DL Hardware Architecture

There are two distinct hardware and software subsystems which cooperate to acquire, process. and store the List Mode and Event Accumulation data sets. The Acquisition Controller interacts with the Host system to configure and execute an acquisition session. The DSP Subsystem is responsible for actually catching timing and neutron detector events and generating List Mode data. During an acquisition, the DSP Subsystem and the Acquisition Controller cooperate to generate Event Accumulation data sets and to log the data to local disk storage. Following a session. the Acquisition Controller delivers the data sets to the Host system for post-processing and long term storage.

Acquisition Controller

The APNEA-DL Acquisition Controller coordinates the flow of data, status, and control information among the various APNEA subsystems, as well as providing the interface to the Host. This single board computer (Motorola MVME-1604) is a double-wide VME module equipped with a 100 MHz PowerPC 604, 8 MB DRAM, 16-bit Fast-Wide SCSI interface, AUI and 10BaseT Ethernet connections, and a PCI bus with one PMC slot available. The APNEA-DL application software is layered on top of Integrated Systems Inc.'s pSOS+ real-time kernel which provides standard multitask synchronization and communication tools, as well as substantial network support. APNEA-DL uses the NFS client/server capabilities of pSOS+ and ONC RPC functionality for interacting with remote host systems. In this environment, the Host operating system and underlying architecture are independent of APNEA-DL. To date, APNEA-DL has been controlled and run from Windows-NT, Solaris, and SunOS host systems. List Mode and Accumulation data are written to a local disk for interim storage prior to transfer to the APNEA Host. Acquisition data set size is limited only by the available APNEA-DL disk space - currently four gigabytes on a Fast-Wide SCSI device (Quantum).

DSP Subsystem

The DSP Subsystem is responsible for monitoring ninety-six digital channels for detector and timing events. During an acquisition, it will generate the List Mode and Event Accumulation data sets according to configuration information supplied by the Acquisition Controller. The DSP Subsystem consists of three Ariel Hydra II Quad TMS320C40 (50 MHz) Processor boards and three Ariel CommIO-IP IndustryPack carrier boards, each with a single TMS320C40 processor. Using the C40 CommPort communications pathway, the signal processors are arranged in stages, as shown in Figure 3.

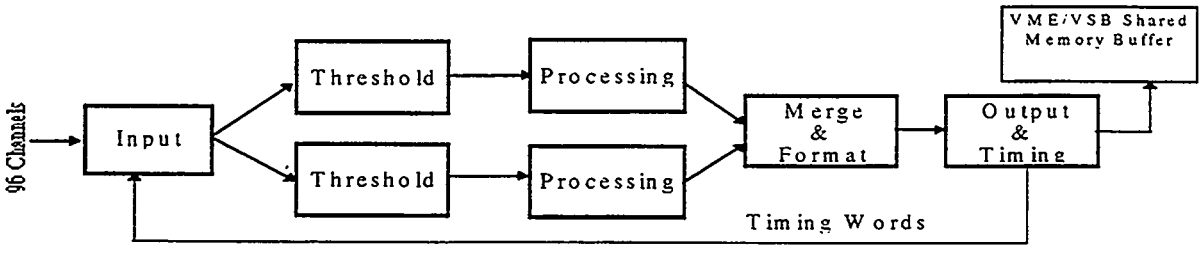

Figure 3. DSP Processing Stages

An acquisition is started at the Output & Timing stage where an internal clock is running with a user-specified period (i.e., 1.36 microseconds). At each time interval, a timing word is sent to the Input Stage.

Upon receipt of the timing word, the Input Stage, using three CommIO-IP modules, each with digital I/O IndustryPacks, reads the input channels, initiating the data stream as a 96-bit bit pattern. The input data stream is divided (to enhance system throughput) and passed to the Threshold Stage which sums the total count of events at each time step for anomalous event[6] tracking. The Threshold Stage also determines the starting point of the acquisition by monitoring the data stream for the configured trigger condition. Once triggered, the input data stream, along with control information is passed to the Processing Stage.

The Processing Stage converts the raw input change-of-state bit patterns into lists of channel numbers, and accumulates event counts for each of the 96 input channels. These accumulation counts are placed into "bins" or "interval-segments" determined by azimuth timing pulse and trigger times, Figure 4. If a blanking segment is specified, then only special channel events are accumulated for that time period, i.e. detector events are blanked. This is useful in situations where the detectors are saturated, for instance, immediately following a Zetatron pulse.

---

[6] An anomalous event occurs when pre-set event count threshold has been exceeded, or when the Cosmic Ray Detector bit is on. This is an indication that more than the expected number of events has been seen in a given sampling period. In this case, APNEA-DL records the current state of all 96 inputs and may invoke a blanking period for a short time.

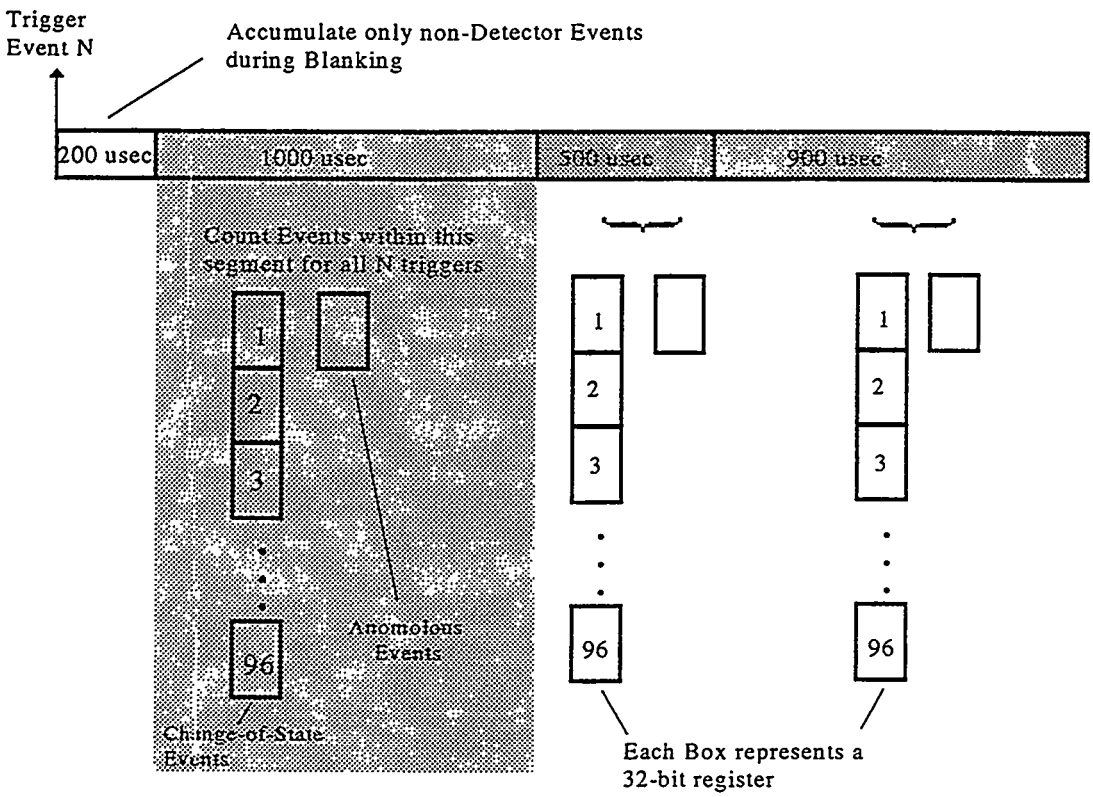

Figure 4. Accumulation Set with Three Signal Segments and One Blanking Segment. The time following a trigger event is divided into time segments, the duration of which is configurable. There are ninety-seven registers associated with each segment, one for each input channel and one to count anomalous events. When an event occurs, the associated register in the proper time segment is incremented. Note that APNEA-DL provides an Accumulation Set for each azimuthal time period during an acquisition.

There is one accumulation set for all of the trigger events that occur within the same azimuthal time period, and each azimuth has its own accumulation set. In addition, some acquisition modes can have more than one trigger event (e.g. external clock and neutron event). In that case, each trigger type will have a set of accumulations associated with it.

The Merge and Format stage accepts the dual stream of channel numbers from the Processing stage and merges them according to channel number and time occurrence and adds the timestamp to each item. This formatted data stream is passed to the Output stage which handles the shared buffering mechanism used to transfer data to the Acquisition Controller. When a data buffer is ready for transfer, the DSP Subsystem use a VME interrupt signal to inform the Acquisition Controller that data available.

DEVELOPMENT ENVIRONMENT

The APNEA-DL software was developed in a hosted cross-platform environment using tools from Integrated Systems Inc., Ariel, and Texas Instruments. The Acquisition Controller, which executes wholly within the MVME-1604, is written entirely in the 'C' programming language. Source code editing, cross-compilation and linking, and source level debugging are all hosted on a Solaris-based UltraSparc workstation. The DSP Subsystem is composed of two parts: 1) device drivers and test applications, executing (and developed) as part of the Acquisition Controller; and 2) the DSP executables, which are written in assembly language and downloaded to the DSPs via the Acquisition Controller. No operating system is used within the DSP Subsystem. All source code and documentation are kept under configuration control, facilitating a product release mechanism and feature tracking.

During initial development, and prior to integration with the detector electronics, the APNEA-DL system was tested using a multi-channel digital pattern generator which was programmed to deliver signals at precise timing intervals. The List Mode and Accumulation data sets generated by APNEA-DL were compared to the expected results to verify correct operation. In addition, software tools to generate Accumulation data sets from an existing List Mode file were developed to verify that event accumulations are consistent with the acquired data. Now, prior to each software release, these tools are used to ensure that the system continues to produce consistent results.

PERFORMANCE

Figures 5 and 6 show results with APNEA-DL of a nominal passive and active acquisition for a Rocky Flats sludge drum. Figure 5 shows the auto-correlation signal as a function of time after the neutron trigger and shows the auto-correlation background measured concurrently using a clock trigger. In both cases the statistical range is indicated by plotting the measured value plus and the measured value minus the counting statistical standard deviation. The results in Figure 6 are total main detector count rates as a function of time after the Zetatron pulse. There is an initial blanking interval of 200 μsec followed by fourteen unequal accumulation intervals. The heavy lines are for a Rocky Flats sludge drum. The lighter lines are for a surrogate drum with the same nominal composition but no Pu. In this figure the background determined from the thirteenth (from 5 to 8 milliseconds) interval has been subtracted from the curves.

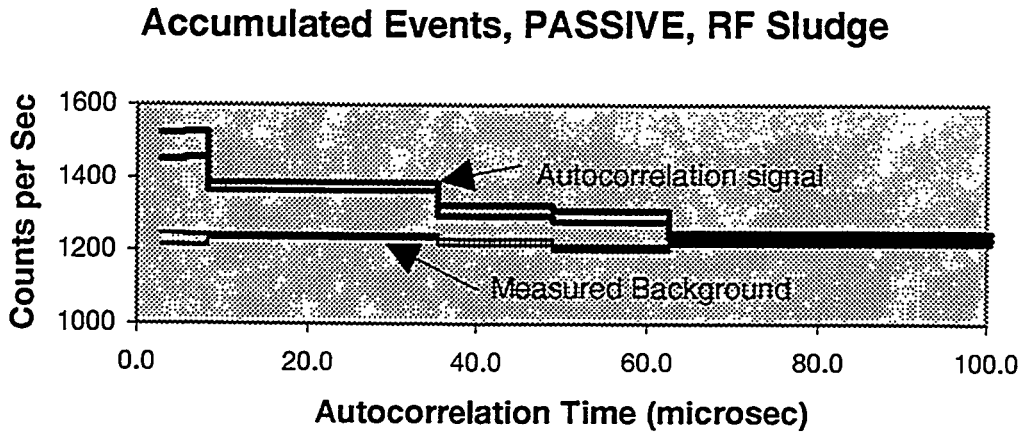

Figure 5. Example of passive mode data. Accumulated count rates following two types of triggers are shown: 1) auto-correlation signals that result from neutron triggers and 2) auto-correlation background measured using an external clock trigger. This concurrent background measurement is accurate, even if the neutron background changes during the assay. For both cases, the effect of counting statistics is indicated by plotting the measured value plus one standard deviation and the measured value minus one standard deviation. Over the time interval shown, the background is constant to within counting statistics.

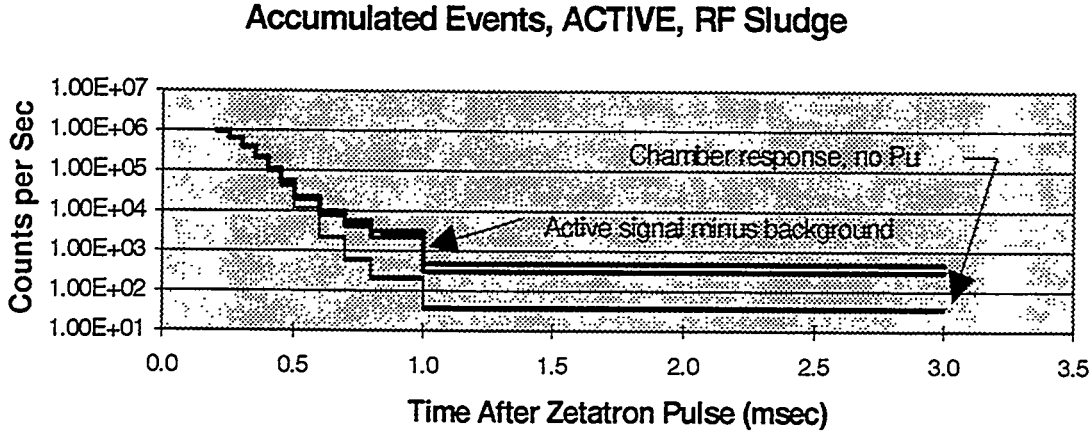

Figure 6. Example of active data acquired with APNEA-DL. The active signal from a TRU waste drum , corrected for background, is compared with the background corrected active signal from a simulated drum with no Pu. For both cases, the effect of counting statistics is indicated by plotting the measured value plus one standard deviation and the measured value minus one standard deviation.

STATUS

The LMSC APNEA is presently undergoing testing at INEL The test data will be used to optimize the parameters used for event accumulation.

ACKNOWLEDGEMENTS

The authors would like to thank D.K. Steinman and E. Wegman of Lockheed Martin Specialty Components for their support, suggestions, and comments during the development of APNEA, and R. Filkins and A. Schmitz of the GE Research & Development Center for their technical contributions to the APNEA-DL system.

APPLICATION OF NEUTRON MULTIPLICITY COUNTING TO WASTE ASSAY

M. M. Pickrell and N. Ensslin
Los Alamos National Laboratory
Safeguards Science and Technology
Group NIS-5, MS E540
Los Alamos, NM 87545 USA
505/665-5098, Fax: 505/665-4433

T. J. Sharpe
North Carolina State University
Raleigh, NC 27607 USA

ABSTRACT

This paper describes the use of a new figure of merit code that calculates both bias and precision for coincidence and multiplicity counting, and determines the optimum regions for each in waste assay applications. A "tunable multiplicity" approach is developed that uses a combination of coincidence and multiplicity counting to minimize the total assay error. An example is shown where multiplicity analysis is used to solve for mass, alpha, and multiplication and tunable multiplicity is shown to work well. The approach provides a method for selecting coincidence, multiplicity, or tunable multiplicity counting to give the best assay with the lowest total error over a broad spectrum of assay conditions.

INTRODUCTION

Passive neutron multiplicity counting has been very effective at reducing bias errors in neutron assays. In the hierarchy of neutron counting, the simplest approach is singles counting, which measures neutrons from any source. Next is doubles (or coincidence) counting, which is specific to fission events. The most complex approach is triples (or multiplicity) counting, which is specific to fission and which can also determine multiplication. Neutron multiplicity counting measures singles, doubles, and triples events. From these three measured parameters, it is possible to obtain sample ^{240}Pu mass, the (alpha,n) reaction rate, and sample net leakage multiplication. Or, the three parameters can be used to obtain sample ^{240}Pu mass, (alpha,n) reaction rate, and detector efficiency.

The assay of plutonium metals, oxides, scrap and residues can be significantly improved by using the three measured parameters—single, double, and triple neutron events—to solve for sample mass, (alpha,n) reaction rate, and multiplication. Two recent publications that show good performance obtained during IAEA inspections of excess weapons materials are for cans of impure oxide[1] and for cans stored in 30-gal. drums.[2]

Application of neutron multiplicity counting to waste assay is suggested because of the significant success of multiplicity counting for safeguards applications. The additional information (compared to conventional coincidence counting) could directly improve assay accuracy by correcting for detector efficiency variations caused by waste drum matrix effects. However, multiplicity counting should only be used if it is more effective in the waste application than coincidence counting. Waste measurements are nominally made under different conditions than typical for safeguards. Waste is typically stored in larger containers, with lower plutonium mass and near unity multiplication. Also, passive neutron coincidence counting assay of waste drums using the segmented add-a-source method has demonstrated the capability for correcting for matrix effects.[3]

In multiplicity counting, singles are measured with the best precision, doubles with moderate precision, and triples with the least precision. Coincidence counting will always have better precision than multiplicity counting because of the additional variance from the triples measurement. On the other hand, waste drum counters have now been designed with high absolute neutron detection efficiencies on the order of 30%.[4,5] With such high detection efficiencies, measurement precision of 1 to 5% can be obtained for triple coincidence events.[6] The basic issue is that for safeguards assay, the small additional error from triples counting is insignificant compared to the improvement in bias error from the multiplicity analysis. For waste applications, the situation may be reversed.

When should coincidence counting be used rather than multiplicity counting? This paper examines this question using a new figure of merit code that calculates both bias and precision for these two techniques, and determines the optimum regions for each. Also, a "tunable multiplicity" approach is described that uses an appropriate combination of coincidence and multiplicity counting to minimize the total assay error. The tunable multiplicity approach is used to predict the total assay error as a function of plutonium mass for typical waste drum applications.

THE POINT MODEL EQUATIONS FOR NEUTRON MULTIPLICITY COUNTING

The point model for neutron multiplicity counting assumes that sample self-multiplication, (alpha,n) reaction rate, detection efficiency, and die-away time are constant across the sample volume, as though the sample were a point. Under these assumptions, the detected singles, doubles, and triples count rates (with room background removed) are given by the following equations:[7, 8,9]

$$S = F\varepsilon M\nu_{s1}(1+\alpha) \tag{1}$$

$$D = \frac{F\varepsilon^2 f_d M^2}{2}\left(\nu_{s2} + \left(\frac{M-1}{\nu_{i1}-1}\right)\nu_{s1}(1+\alpha)\nu_{i2}\right) \tag{2}$$

$$T = \frac{F\varepsilon^3 f_t M^3}{6}\left(\nu_{s3} + \left(\frac{M-1}{\nu_{i1}-1}\right)\left[3\nu_{s2}\nu_{i2} + \nu_{s1}(1+\alpha)\nu_{i3}\right] + 3\left(\frac{M-1}{\nu_{i1}-1}\right)^2 \nu_{s1}(1+\alpha)\nu_{i2}^2\right) \tag{3}$$

where F = sample fission rate,
ε = detector efficiency,
f_d = double gate fraction,
f_t = triples gate fraction,
M = sample net leakage multiplication,
α = ratio of (alpha,n) to spontaneous fission neutrons,
ν_{si} = spontaneous fission moments,
ν_{Ii} = induced fission moments.

Equations (1), (2), and (3) relate the mass, alpha, efficiency, and leakage multiplication to the statistical measure of:

- single neutrons (uncorrelated),
- doubles or coincidences (2 neutrons),
- triples (3 neutrons).

Also note that the statistical differences between the measured count rates are increased by the rate of accidental coincidences.

Equations (1), (2), and (3) are inverted to obtain mass, alpha, and detection efficiency as shown in Eqs. (4), (5), and (6) below. Or, they can be inverted to yield sample mass, alpha, and multiplication as shown in Eqs. (7), (8), and (9) below:

$$\alpha = \frac{3ST\nu_{s2}^2}{2D^2\nu_{s1}\nu_{s3}} - 1 \tag{4}$$

$$F = \frac{2f_d D^3 \nu_{s3}^2}{9T^2\nu_{s2}^3} \tag{5}$$

$$\varepsilon = \frac{3T\nu_{s2}}{f_d D\nu_{s3}} \tag{6}$$

$$F = \frac{\frac{2D}{\varepsilon f_d} - \frac{M(M-1)\nu_{i2}S}{\nu_{i1}-1}}{\varepsilon M^2 \nu_{s2}} \tag{7}$$

$$\alpha = \frac{S}{F\varepsilon\nu_{s1}M} - 1 \tag{8}$$

$$a + bM + cM^2 + M^3 = 0 \tag{9}$$

The constants a, b, c in Equation (9) are defined in Ref. 6. Finally, the sample ^{240}Pu effective mass m = F/479.

APPLICATION OF MULTIPLICITY COUNTING TO WASTE

The calculations presented in this paper were obtained using a new figure of merit code developed for multiplicity counting analysis, based on an earlier variance code developed by Ensslin, et. al.[7] The new code described in this paper is able to evaluate both bias and precision for multiplicity and coincidence counting. The code determines assay variance from the reduced factorial moments of the neutron multiplicity distribution, which may be thought of as single, double, and triple neutron coincidences. The multiplicity distribution does not need to be

measured, but is predicted from pre-selected sample and detector design parameters. The procedure can be summarized as follows:

1. Input the mass, multiplication, alpha, count time, and detector parameters such as efficiency.
2. Calculate the point model neutron moments: singles, doubles, and triples.
3. Calculate the emitted and detected factorial moments of the neutron distribution function.
4. Calculate the variance in the singles, doubles, and triples.
5. Calculate the sensitivity of the measurement to errors in the singles, doubles, and triples.
6. Calculate the total assay variance from this sensitivity.
7. Calculate the assay mass and the bias in the assay (by using Eqs. 4-9).

One example of the use of the new figure of merit code is given in Fig. 1. This figure compares precision, bias, and total error for multiplicity and coincidence counting for nominal values in safeguards and waste applications. In the safeguards application, the sample mass is assumed to be 1 g ^{240}Pu, with multiplication of 1.2, α of 1, counted for 100 seconds in a neutron counter with 30% detection efficiency. For coincidence counting, assay precision is about 1%, bias is about 280%, and total assay error is about 280%. For multiplicity counting, assay precision is about 5%, bias is close to 0%, and total assay error is 5%. These error estimates assume that it is not feasible to use a non-linear calibration curve to remove the bias in the coincidence count due to (alpha,n) induced fissions, and that the multiplicity assay removes this bias entirely. Therefore, in this case multiplicity has a much lower error, 5%, than coincidence counting, 280%. Multiplicity counting is the better choice in this instance. In the waste application, the sample mass is assumed to be 0.01 g ^{240}Pu, with multiplication of 1.0, α of 1, counted for 100 s in a low-background neutron counter with 30% detection efficiency. For coincidence counting, assay precision is about 15%, bias is nearly 0%, and total assay error is about 15%. For multiplicity counting, assay precision is about 25%, bias is nearly 0%, and total assay error is 25%. In this case, there is no benefit to multiplicity counting; coincidence counting has the lower net error. This figure demonstrates the general issue we wish to address. In some assay regimes (for example, nominal safeguards) multiplicity counting is clearly superior to coincidence counting. In other assay regimes, there is no benefit to multiplicity counting.

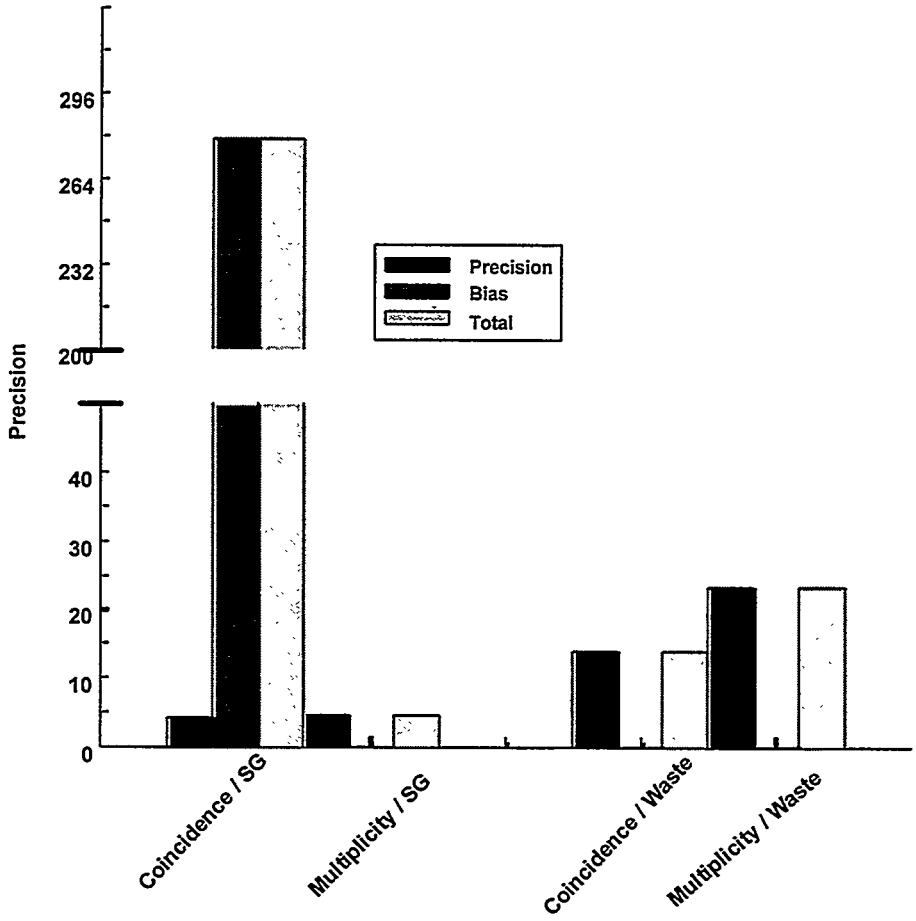

Fig 1. Measurement errors calculated by the figure of merit code for four cases: coincidence and multiplicity counting for a nominal safeguards (SG) measurement of 1 g ^{240}Pu, multiplication of 1.2, alpha of 1, counted for 100 s in a neutron counter with 30% efficiency. The error for these two measurements is dominated by the bias error in the coincidence measurement. The multiplicity case has a slightly larger precision, but the dominant bias error is gone. The second two cases are the same measurement conditions as the first except the mass is 0.01 g ^{240}Pu and the multiplication is 1; this is nominal waste assay conditions. In these cases the bias error is negligible and the dominant error is the precision. The multiplicity measurement has a slightly degraded precision because of the addition of the triples measurement.

Figure 2 demonstrates the comparison between multiplicity and coincidence counting again. The figure of merit code is used to determine the total assay error in % by scaling over the range of ^{240}Pu effective from 0.01 to 10.0 g and sample multiplication from 1 to 1.05, with $\alpha = 1$. The sample multiplication is scaled to the sample mass with a quadratic equation. This range of parameters covers most typical waste applications, except for high-alpha wastes such as

fluorides. The total error in the coincidence assay is the counting precision and the bias error in quadrature. The total error in the multiplicity assay is just the statistical precision, which is dominated by the poor precision in the triples count rate (the bias is added in quadrature but it is zero). Note that the

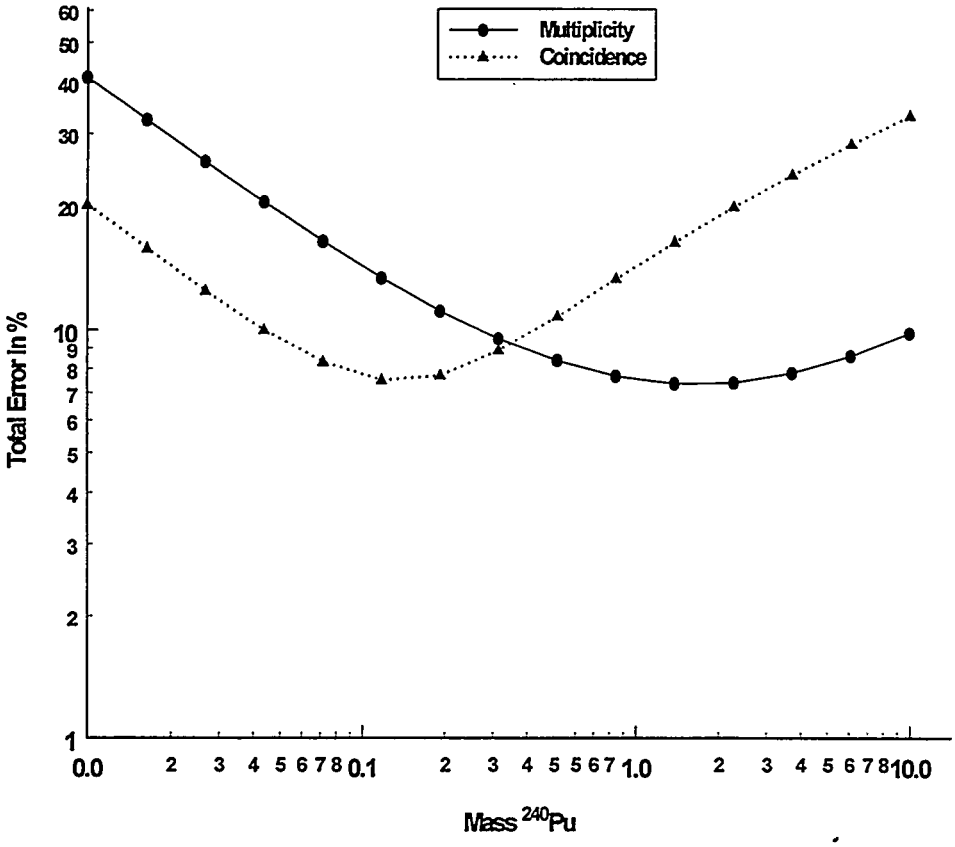

Fig. 2. Application of the new figure of merit code to scale the total error in coincidence and multiplicity counting over the range of ^{240}Pu effective from 0.01 to 10.0 g and sample multiplication from 1 to 1.05 with $\alpha = 1$, for waste assay with 30% detection efficiency.

coincidence assay has a lower total error for low masses with low multiplication, whereas the multiplicity assay has a lower total error for higher masses with higher multiplications.

The individual coincidence components of error, including the bias, precision, and total error are detailed in Fig. 3 for coincidence counting and the same measurement conditions as above. This figure shows how the coincidence bias increases with increasing multiplication, as the induced fission rate increases and biases the coincidence count upwards. The coincidence counting precision improves with increasing mass, eventually leveling off. The bias and precision components combine in quadrature to give a total error with a minimum near 0.10 g ^{240}Pu effective.

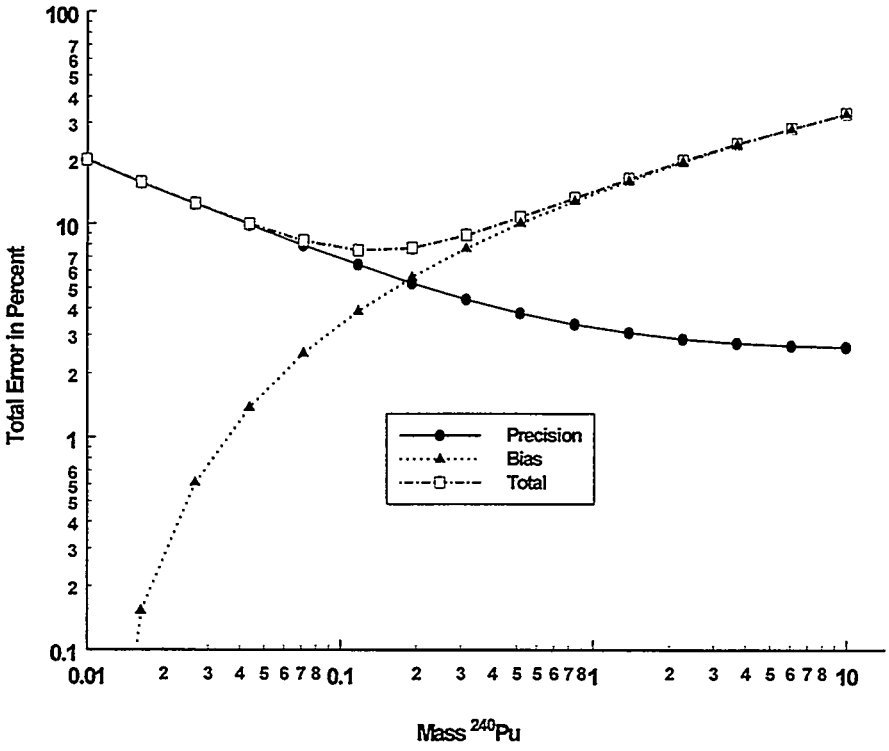

Fig. 3. The coincidence bias, precision, and total error over the range of ^{240}Pu effective from 0.01 to 10.0 g and sample multiplication from 1 to 1.05 with α = 1, for waste assay with 30% detection efficiency.

By way of comparison, Fig. 4 illustrates the error sources that make up the total multiplicity error. Only counting statistics error sources are shown, although multiplicity counting can also exhibit bias for actual samples if the assumptions of the point model are not valid. Figure 4 shows the contribution to the variance from singles, doubles, and triples for

safeguards applications with ^{240}Pu mass of 1 g, multiplication of 1.2, and alpha of 1 for a neutron counter with 20% detection efficiency; also for waste applications with multiplication = 1.0. The triples counting precision dominates the total error, as expected from the significantly lower triples count rate. Note that the curve of total error for multiplicity counting shown earlier in Fig. 2 also has a minimum, although it is caused only by counting precision, because the accidental overlap rate of multiplicity events increases with increasing sample mass.

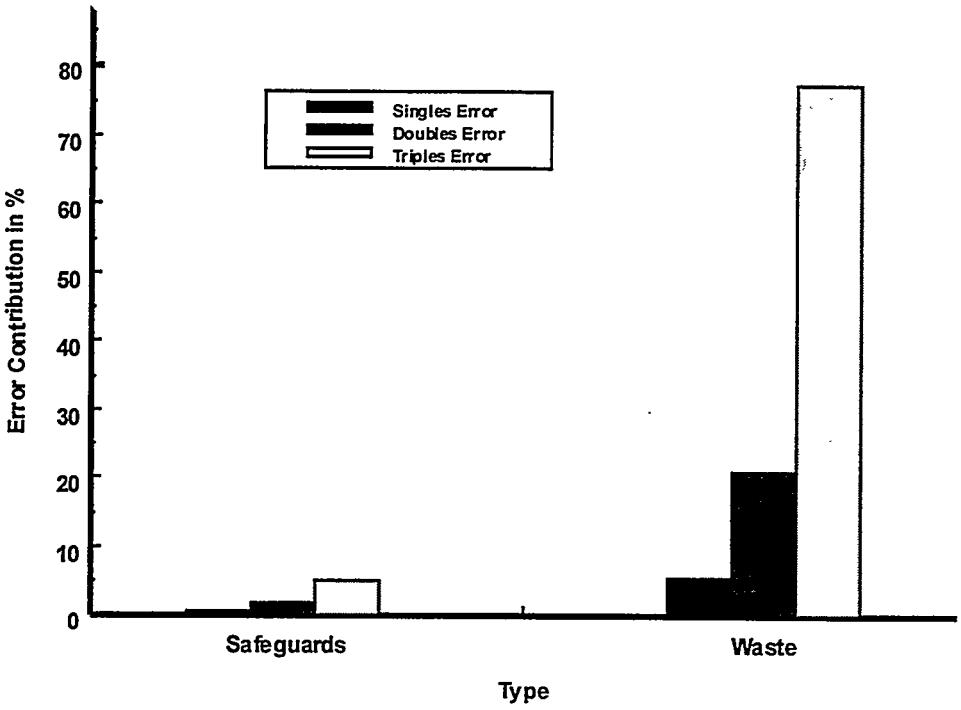

Fig. 4. Multiplicity error sources from singles, doubles, and triples counts for nominal safeguards and waste assay applications, with 20% detection efficiency.

COMPARISON OF CALCULATED AND OBSERVED PRECISION

To benchmark the figure of merit calculations described above, we compared observed and calculated assay precision for a series of small plutonium samples. Each sample contained 10 g of plutonium, but the plutonium was intimately mixed with an impurity element that was a source of (alpha,n) neutrons. The impurity elements were pure metal (no impurities), oxide, aluminum, silicon, magnesium, and fluorine. These sample matrices simulate the range of neutron-emitting impurities that can be found in actual transuranic waste drums. Observed assay precision was obtained by placing the samples in the center of empty 55-gal. waste drums

and carrying out a series of passive neutron coincidence and multiplicity measurements using the waste drum counters described in Ref. 4 and 5. Each sample was measured for a long series of short runs, typically 30 to 100 runs of 100 s each.

Observed variances (normalized to 1000-s counting times) ranged from 1 to 16% for coincidence analysis, from 2 to 22% for multiplicity analysis solving for sample multiplication, and from 11% to 39% for multiplicity analysis solving for detection efficiency. The observed RSD was larger than the calculated RSD by about 30% for conventional coincidence counting and 35% for multiplicity counting. These results are consistent with past benchmarking studies, and are due to the fact that the effects of correlations between detected neutron events are not included in the computation of variance in the calculated multiplicity distributions. When these correlations are taken into account, we can expect the figure of merit calculations in this paper to be accurate to about 10 to 15%, which is sufficient for observing the effects of parameter variations.

NEW INVERSION OF THE MULTIPLICITY EQUATIONS

A comparison of the error structure in Fig. 2 shows that multiplicity is better when the bias is high and the precision is good. On the other hand, coincidence is better when the bias is low, as is the case in many waste applications. Figure 2 suggests the potential benefits of a new approach that could minimize assay error by selecting either coincidence or multiplicity counting, as appropriate. Is there a heuristic system that can determine from the data when to use coincidence and when to use multiplicity?

Equations (4) through (9) in Section II show a discrete change in the mathematics from coincidence to multiplicity. There is no gradual shift from one to the other, the choice is either coincidence or multiplicity. We also observe that the multiplicity equations are inverted algebraically. In the inversion, no distinction is made between singles, doubles and triples. All three parameters are used equally. The inversion does not weight the relative errors in the singles, doubles, or triples, even through the triples variance is typically higher, as was shown in Fig. 4.

These observations suggest another approach: a perturbation expansion inversion of the point equations. The singles, doubles, and triples could be weighted according to their variance. In this way we could include "partial" multiplicity, and we could move continuously between

coincidence and multiplicity. This approach will be called "tunable multiplicity." The tunable multiplicity approach will use a perturbation expansion of the equations, and then linearize them by keeping only first order terms. The perturbation can be adjusted with a multiplicative constant to move from zero perturbation (coincidence counting) to full perturbation (multiplicity counting to first order). Two cases will be solved, inverting the multiplicity equations for mass, α, and efficiency and inverting for mass, α, and multiplication.

To solve for efficiency, the efficiency is expanded about ε_0, the unperturbed detection efficiency of the waste drum counter with no sample matrix present. The triples to doubles ratio T/D is used as the expansion parameter and only first order terms are kept. The resulting inverted equations are

$$\varepsilon\left(S,D,{}^{T}\!/_{D}\right) \cong \varepsilon_o + \frac{\partial\varepsilon}{\partial\left(\frac{T}{D}\right)}\left[\left(\frac{T}{D}\right) - \left(\frac{T}{D}\right)\Big|_{\varepsilon=\varepsilon_o}\right] \tag{10}$$

Use of Eq. (10) results in the following new inverted equations:

$$\alpha = \frac{3ST\nu_{s2}^2}{2D^2\nu_{s1}\nu_{s3}} - 1 \tag{11}$$

$$F = \frac{2D}{f_d\nu_{s2}\varepsilon_o^2} - \frac{4D}{f_d\nu_{s2}\varepsilon_o^3}\left(\frac{3\nu_{s2}T}{f_d\nu_{s3}D} - \varepsilon_o\right) \tag{12}$$

$$\varepsilon_1 = \frac{3\nu_{s2}T}{f_d\nu_{s3}D} - \varepsilon_o \tag{13}$$

To solve for multiplication the equation for multiplication will be expanded about $M = 1$, again using T/D as the expansion parameter:

$$M\left(S,D,{}^{T}\!/_{D}\right) = M_o + \frac{\partial M}{\partial\left({}^{T}\!/_{D}\right)}\left[\left(\frac{T}{D}\right) - \left(\frac{T}{D}\right)\Big|_{M=1}\right] \tag{14}$$

Use of Equation (14) results in the following new inverted equations:

$$F = \frac{2D}{\varepsilon_o^2 f_d \nu_{s2}} - \frac{M_1}{\varepsilon_o \nu_{s2}} \left[\frac{4D}{\varepsilon_o f_d} + \frac{S\nu_{i2}}{(\nu_{i1} - 1)} \right]^{\beta} \tag{15}$$

$$\alpha = \frac{S}{F\varepsilon_o \nu_{s1}(1 + M_1\beta)} - 1 \tag{16}$$

$$M = 1 + M_1\beta \tag{17}$$

$$M_1 = \frac{2D(\nu_{i1} - 1)\left[\varepsilon_o f_d \nu_{s3} - 3\nu_{s2}(T/D)\right]}{\varepsilon_o f_d \left[3S\nu_{s2}\nu_{i2}(T/D) - 2D(\nu_{i1} - 1)\nu_{s3} - 6D\nu_{s2}\nu_{i2} - S\nu_{i3}\nu_{s2}\varepsilon_o f_d\right]} \tag{18}$$

The parameter β in equations (15), (16), and (17) represents the ability to tune the amount of the multiplicity contribution. A β factor of 0 is zero perturbation (coincidence only) and a beta factor of 1 is full perturbation (multiplicity counting to first order). The optimization of the tunable multiplicity is illustrated in Fig. 5, which plots precision, bias, and beta as a function of ^{240}Pu effective mass. The figure of merit code is used to scale the mass and multiplication and calculate the total error in % over the range of ^{240}Pu effective from 0.01 to 10.0 g and sample multiplication from 1 to 1.05, with α = 1, detection efficiency = 20%, and counting time = 100 s. The sample multiplication is again scaled to the sample mass with a quadratic equation. As the figure of merit code steps through the values of sample mass and multiplication, the beta factor is also varied to find the value that gives the lowest total error. Note that at very low mass, where coincidence counting has a lower total error (ref. Fig. 2), the beta factor is only about 10 or 15%, which is nominaly consistent with coincidence counting. At high mass, where multiplicity counting has a lower total error, the beta factor is 70 or 80%, so that more multiplicity information is being tuned in to reduce the total error.

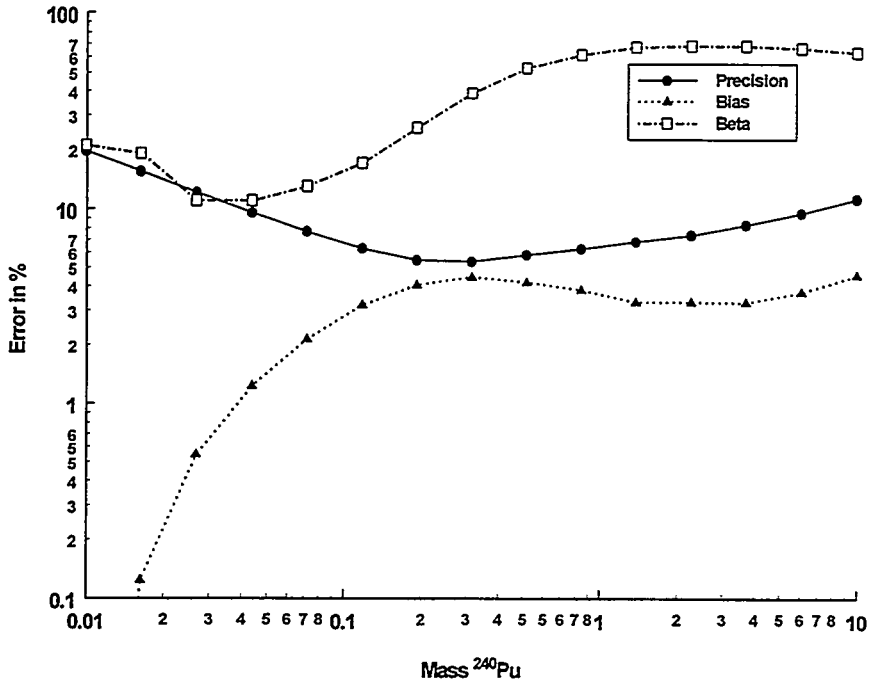

Fig. 5. Optimization of the tunable multiplicity using the new figure of merit code. The percent error in precision and bias, and the beta factor in percent, are scaled over the range of ^{240}Pu effective from 0.01 to 10.0 g and sample multiplication from 1 to 1.05, with α = 1, detection efficiency = 20%, and counting time = 100 s.

Figure 6 compares the total error calculated from the figure of merit code for three cases: coincidence, multiplicity, and tunable multiplicity for the same measurement parameters (mass, multiplication, α, etc.) as Fig. 5. Note that as the sample mass and multiplication vary over the allowed range, the tunable multiplicity approach yields the lowest total error for most mass values, and is close to the lowest for the others.

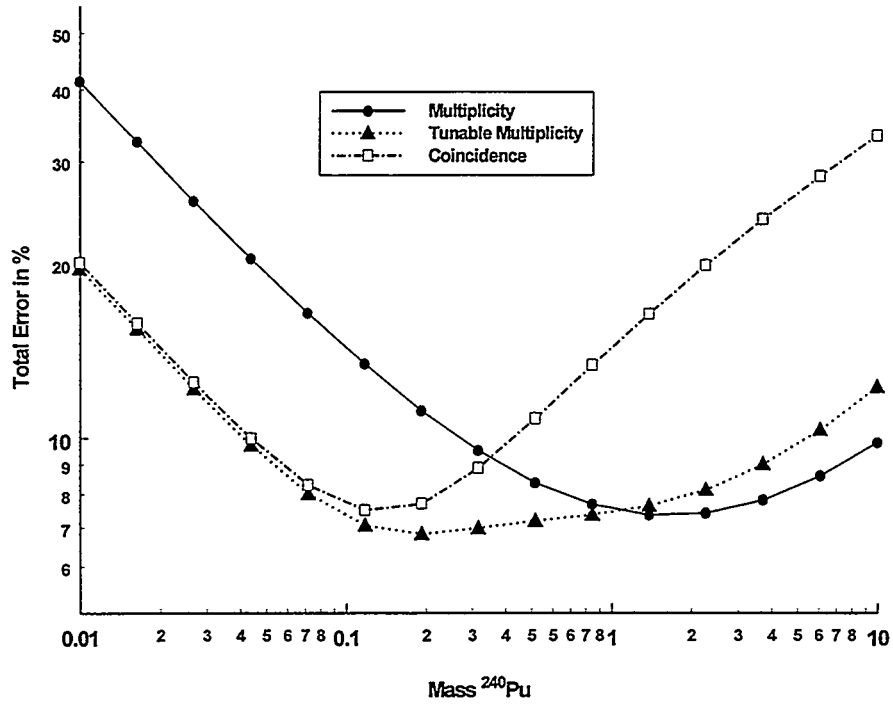

Fig. 6. Comparison of the total error in tunable multiplicity with coincidence and multiplicity counting using the figure of merit code, for the same range of measurement parameters as Fig. 5.

CONCLUSIONS

1. It has been possible to develop a tunable multiplicity approach for combining coincidence and multiplicity analysis for waste drum assay. A new figure of merit code has also been developed to evaluate the tunable multiplicity approach.

2. For the case where multiplicity analysis is used to solve for mass, alpha, and multiplication, the tunable multiplicity approach works well. We are able to move continuously between coincidence counting and multiplicity, and obtain the optimal lowest total error in most cases. The cusp observed in Figs. 2 and 6 at the transition from coincidence to multiplicity is smoothed out, and a total error less than the cusp value is obtained. As assay bias increases, the multiplicity "turns on," as expected.

3. A method for choosing the beta factor from actual measurement data in a field environment needs to be developed.

4. The tunable multiplicity approach described above needs to be extended to the case where multiplicity analysis is used to solve for detection efficiency.

5. The approach described in this paper leads directly to a heuristic method for selecting coincidence, multiplicity, or tunable multiplicity counting as the best assay approach with the lowest total error.

ACKNOWLEDGMENTS

We would like to thank Howard Menlove for valuable discussions on waste assay using Add-a-Source and multiplicity techniques, and Merlyn Krick for his review of this paper.

This work is supported by the US Department of Energy, Office of Nonproliferation and National Security, Office of Safeguards and Security.

REFERENCES

1. J. E. Stewart, M. S. Krick, J. Xiao, and R. J. Lemaire, V. Fotin, L. McRae, D. Scott, and G. Westsik, "Assay of Scrap Plutonium Oxide by Thermal Neutron Multiplicity Counting for IAEA Verification of Excess Materials from Nuclear Weapons Production," Proc. of the 37th Annual Meeting of the Inst. of Nuclear Materials Management, Naples, FL, July 28-31, 1996.

2. D. G. Langner, J. B. Franco, J. G. Fleissner, V. Fotin, J. Xiao, and R. J. Lemaire, "The Performance of the 30-Gallon-Drum Neutron Multiplicity Counter at the Rocky Flats Environmental Technology Site," Proc. of the 37th Annual Meeting of the Inst. of Nuclear Materials Management, Naples, FL, July 28-31, 1996.

3. H. O. Menlove, "Passive Neutron Assay of Heterogeneous Waste Drums Using the Segmented Add-a-Source Method," *Nucl. Mater. Manage.* **XXIV**, 972-975 (1995).

4. H. O. Menlove, D. H. Beddingfield, M. M. Pickrell, D. R. Davidson, R. D. McElroy, and D. B. Brochu, "The Design of a High-Efficiency Neutron Counter for Waste Drums to Provide Optimized Sensitivity for Plutonium Assay," Proc. of the 5th Nondestructive Examination Waste Characterization Conference, Salt Lake City, Utah, January 14-16, 1997.

5. M. M. Pickrell, "Development of a High-Efficiency Neutron Counter Using Novel Materials," Proc. of the 5th Nondestructive Examination Waste Characterization Conference, Salt Lake City, Utah, January 14-16, 1997, Los Alamos National Laboratory document LA-UR-96-4821.

6. N. Ensslin, M. S. Krick, and H. O. Menlove, "Expected Precision of Neutron Multiplicity Measurements of Waste Drums," *Nucl. Mater. Manage.* **XXIV**, 1117-1124 (1995).

7. N. Ensslin, N. Dytlewski, and M. S. Krick, "Assay Variance as a Figure of Merit for Neutron Multiplicity Counters," *Nucl. Instr. and Meth. in Phys. Research* **A290** (1990) 197-207.

8. K. Boehnel, *Nucl. Sci. and Eng.* **90** (1985), p. 75.

9. D. M. Cifarelli and W. Hage, "Models for a Three-Parameter Analysis of Neutron Signal Correlation Measurements for Fissile Material Assay," *Nucl, Instr. and Meth. in Physics Research* **A251** (1986) 550-563.

THE DESIGN OF A HIGH-EFFICIENCY NEUTRON COUNTER FOR WASTE DRUMS TO PROVIDE OPTIMIZED SENSITIVITY FOR PLUTONIUM ASSAY

H. O. Menlove, D. H. Beddingfield, and M. M. Pickrell
Los Alamos National Laboratory
Safeguards Science and Technology
Group NIS-5, MS E540
Los Alamos, NM 87545 USA
505/667-2182, Fax: 505/665-4433

D. R. Davidson, R. D. McElroy, and D. B. Brochu
Canberra Industries
800 Research Parkway
Meriden, CT 06450 USA
202/238-2351

ABSTRACT

An advanced passive neutron counter has been designed to improve the accuracy and sensitivity for the nondestructive assay of plutonium in scrap and waste containers. The High-Efficiency Neutron Counter (HENC) was developed under a Cooperative Research and Development Agreement between the Los Alamos National Laboratory and Canberra Industries. The primary goal of the development was to produce a passive assay system for 200-L drums that has detectability limits and multiplicity counting features that are superior to previous systems. A detectability limit figure of merit (FOM) was defined that included the detector efficiency, the neutron die-away time, and the detector's active volume and density that determine the cosmic-ray background. Monte Carlo neutron calculations were performed to determine the parameters to provide an optimum FOM. The system includes the ^{252}Cf "add-a-source" feature to improve the accuracy as well as statistical filters to reduce the cosmic-ray spallation neutron background. The final design gave an efficiency of 32% for plutonium with a detector ^{3}He tube volume that is significantly smaller than for previous high-efficiency systems for 200-L drums. Because of the high efficiency of the HENC, we have incorporated neutron multiplicity counting for matrix corrections for those cases where the plutonium is localized in nonuniform hydrogenous materials. The paper describes the design and performance testing of the advanced system.

INTRODUCTION

The measurement of plutonium content in waste containers is required prior to long-term storage and disposal. Measurement accuracy should meet the requirements of safeguards, material accountancy, criticality control, and environmental regulations. It has long been recognized that the passive neutron coincidence assay of typical waste containers is intrinsically more accurate than active neutron techniques because of the excellent penetrability of the passive spontaneous fission neutrons. However, the signal level of the spontaneous fission neutrons is low, which limits the sensitivity, and it is necessary to know the plutonium isotopics to convert the measured ^{240}Pu-effective to total plutonium.

We have developed a passive neutron counter with advanced design features to improve the detectability limit and to make the system accurate for a large range of matrix materials. To improve the detectability limit, the efficiency was increased, the cosmic-ray background was decreased, and external shielding was increased to reduce the room background neutron rate.

The dependence on the waste matrix was reduced by incorporating the ^{252}Cf add-a-source correction and multiplicity counting to make corrections for localized shielding.

Joint development of the advanced passive neutron assay system was accomplished under a cooperative research and development agreement (CRADA) between Canberra Industries and the Department of Energy. Table I lists design goals for successful completion of this CRADA. The relative weighting and prioritization of these goals was determined by Canberra, based on market considerations. The parameters that can be used to meet these goals include sample cavity size, active detector volume, detector efficiency, die-away time, shielding (both internal and external), moderator materials, electronic background rejection, and add-a-source.

Table II lists some of the design parameters that can be used to optimize the system design. The cavity size for the system was set to be the same as the Model WM3100 to take advantage of the existing mechanical system. Smaller cavity dimensions would give higher efficiencies and less expensive fabrication costs. However, the requirement to accommodate samples somewhat larger than 200-L drums dictated the WM3100 cavity size.

The design goals that are based on counting statistics, such as precision, can be met by higher efficiency and a lower die-away time as well as by smart software that terminates a measurement based on the statistical error rather than a preset run time.

In general, multiplicity counting will require higher efficiency than simple doubles counting, and calculations have been performed to provide the statistical error in multiplicity counting.[1]

Competitive cost criteria determine many of the design parameters (e.g., number of He tubes, number of detector banks, and shielding). A modular design is the key in meeting competitive pricing factors, and the WM3100 provides a good design platform to allow a modular approach.

TABLE I. Design Goals for the Waste Drum Counter.

1. Low detectability limit
   (good sensitivity at low mass)

2. Ability to meet Performance Demonstration Program (PDP) requirements
   a. High (α,n) backgrounds
   b. Variable Pu distribution
   c. Accuracy requirements

3. Matrix independence
   a. Pu distribution independence
   b. Accurate matrix corrections

4. Modular detector design
   a. high/low efficiency
   b. high/low shielding
   c. with/without add-a-source
   d. with/without multiplicity
   e. flexible software

TABLE II. Design Parameters for the Waste Drum Assay System

1. Cavity size
2. Active detector volume
3. Detector efficiency
4. Detector die-away time
5. Internal shielding
6. External shielding
7. Moderator materials
8. Statistical background rejection
9. Multiplicity counting
10. Add-a-source

DETECTABILITY LIMIT

Optimization of the detectability limit was one of our primary design goals. To obtain a low detectability limit, we need a high counting efficiency as well as a small active detector volume, a large coincidence gate fraction, and a small neutron background rate from the room.

Two of these design parameters work in opposition to each other. That is, the higher-efficiency designs require a larger active volume for the detector. The problem with the large active detector volume is that the cosmic-ray spallation background increases as detector volume and density increase. A detector with three rings or layers of ^{3}He tubes will have a larger detectability limit than a two-ring or one-ring detector because of the increased detector volume for three rings. Also, a large detector volume displaces the external neutron shielding, resulting in an increased measured background from room source neutrons (e.g., drums stored near the detector).

The detectability limit can be obtained from totals counting or coincidence counting. In general, the totals-based limit is lower than the coincidence-based limit because of the high totals counting efficiency. However, variable room background rates and unknown sample (α,n) rates make the totals results difficult to interpret so we will use the coincidence rate for our detectability limit calculation. The limit based on totals neutrons is still a useful screening tool to pass uncontaminated samples and to set an upper limit on the plutonium contamination. The totals neutrons also provide a good measurement of any alpha decay in the waste because of the (α,n) reactions in the waste materials.

The detectability limit d (in grams of ^{240}Pu) at 3 standard deviations above background can be calculated for the counter using the equation

$$d \cong (3/a) \bullet \left(\frac{B + ad}{t} \right)^{1/2} , \qquad (1)$$

where

a = response of counter in counts/(s • g ^{240}Pu)
B = room background rate (based on a counting time much greater than t), and
t = counting time.

Equation (1) is an approximation based on a long counting time for the cosmic-ray background and a negligible accidental background from the room totals rate. The detectability limit is a function of the neutron coincidence background; we can reduce the background by eliminating the cosmic-ray spallation events with high multiplicity by using a statistical filtering technique.[2]

For coincidence counting, both the calibration constant a and the background B are coincidence rates that depend on the efficiency squared. Thus, from Eq. (1) we get

$$d \sim \frac{\sqrt{\varepsilon^2}}{\varepsilon^2} = \frac{1}{\varepsilon} . \qquad (2)$$

However, the background term is complex and it contains two primary components—the cosmic-ray spallation rate and the accidental coincidence rate from the room source totals rate.

The cosmic-ray spallation neutrons increase with the active volume and density of the ^{3}He tube area moderator. Thus, if we double our detector volume or density, we will approximately double our cosmic-ray spallation background. The additional cosmic-ray background from spallation reactions in the sample drum is negligible for hydrogenous drums because the drum absorbs as many neutrons as it creates. Of course, if the drum contains high-density materials or metals, it becomes a background source of cosmic-ray coincidence neutrons. Figure 1 shows the cosmic-ray coincidence background as a function of drum loading.[2] We see that most hydrogenous (combustibles) loadings and concrete rubble have the same background as the empty case. Pure polyethelene reduces the cosmic-ray background because the CH_2 matrix absorbs more neutrons than it creates by spallation reactions.

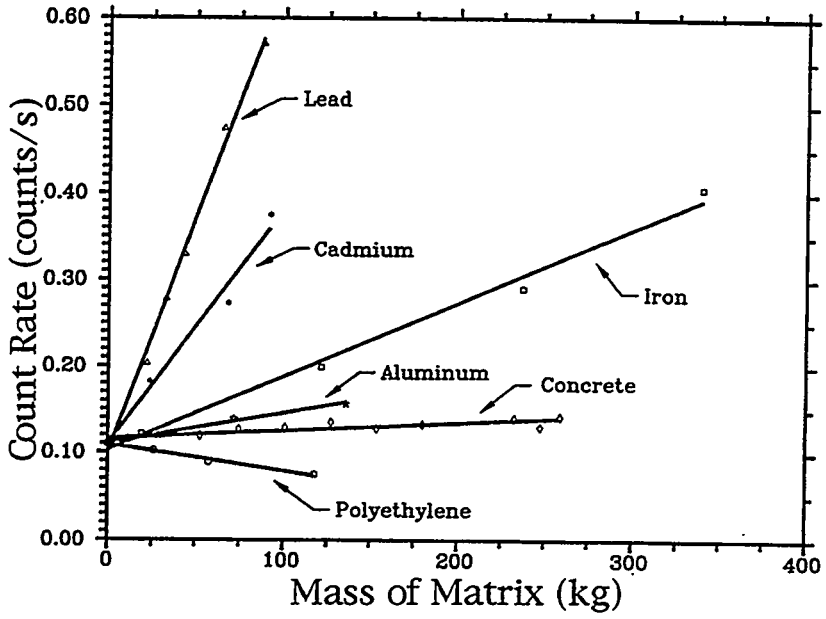

Fig. 1. Cosmic-ray coincidence backgrounds as a function of matrix materials in the shielded JCC-21. Most combustibles give no change in the background rate.

The accidental coincidence rate from room source totals neutrons can be calculated from

$$A = T^2 G \ , \tag{3}$$

where

A = accidental coincidence rate,
T = totals background rate, and
G = gate width(s).

The coincidence background can be written as

$B = B$ (cosmic ray) + B (room accidentals)

and

B (cosmic ray) ~ ε^2 • volume • density.

As a first step in the design optimization, we removed all of the cadmium and heavy metal in the detector to reduce the cosmic-ray spallation rate. The room source neutrons are relatively easy to remove with external shielding; however, the cosmic-ray background is several orders of magnitude harder to reduce.

The detector's active volume can be estimated by the ^{3}He tube and moderator thickness as shown in Fig. 2. The back edge (away from the sample) boundary merges with the CH_2 used for the external shielding. The distance from the edge of the back tube to the shielding boundary was defined as one diffusion length (2.73 cm) of a thermal neutron in CH_2.

Figure of Merit

To aid in the design optimization based on the detectability limit, we defined a figure-of-merit (FOM) as follows:

$$FOM \sim \frac{1}{d} \sim \varepsilon^2 \left[\frac{f_g}{\varepsilon^2 \bullet t \bullet \rho} \right]^{1/2}, \text{ or} \tag{4}$$

$$FOM = \varepsilon \left(\frac{f_g}{t \bullet \rho} \right)^{1/2}, \tag{5}$$

where

ε = totals counting efficiency (%),
ρ = moderator density,
t = moderator thickness (cm), and
f_g = the fraction in the gate for a 128-μs gate length.

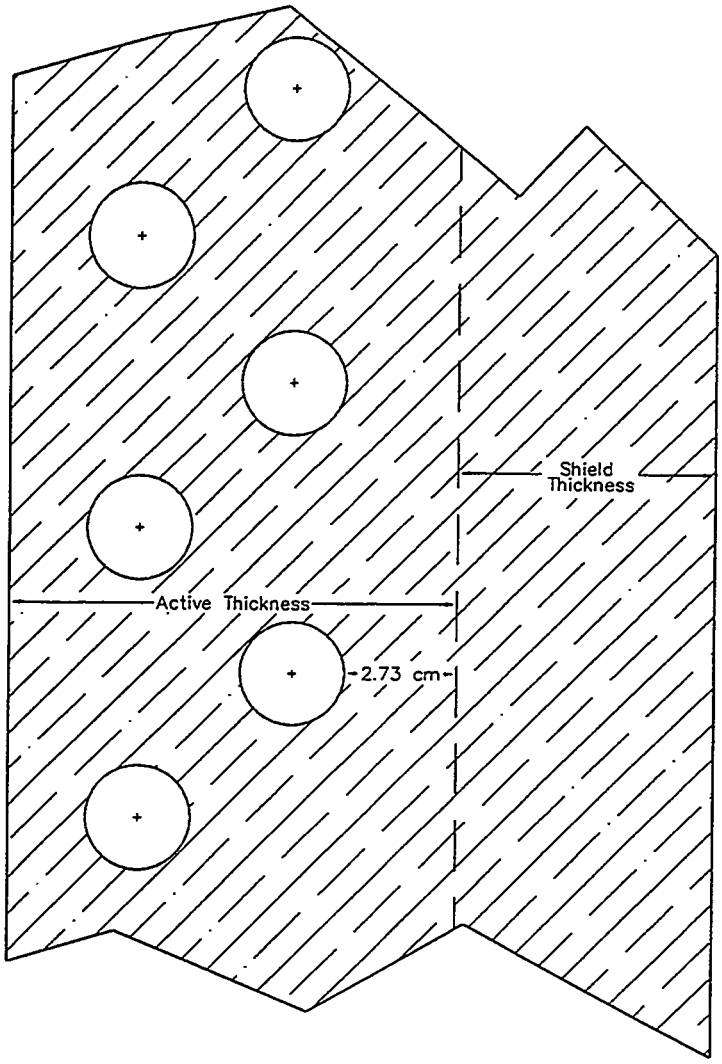

Fig. 2. A two-row tube detector geometry used to calculate the FOM.

The reals coincidence counting efficiency is a function of the number of time correlated neutrons that fall within the coincidence time gate. The fraction in the gate for a 128-μs gate length is defined as

$$f_g = \frac{\sum_0^{128\mu s} T}{\sum_0^{\infty} T} \quad , \tag{6}$$

where

T = the totals counts.

The ε was determined from the unnormalized results of Monte Carlo N-Particle Code (MCNP)[3] calculations. The moderator thickness was determined to be the distance from the inner face of the detector cavity to 1.0 diffusion length (2.73 cm in poly and longer for low-hydrogen plastics) beyond the edge of the back tube row as shown in Fig. 2. The fraction in the gate can be determined from the unnormalized output tallies produced by MCNP.

The FOM equation given above does not include the effect of the moderator thickness on the room source neutrons. Thus, this source of background neutrons must be negligible or there will be additional thickness penalties. The largest values for the FOM give the smallest detectability limit. Thus, the counting efficiency is only one of the parameters that go into the optimization of the detectability limit. A detector design with two rows of ^{3}He tubes or 5-cm-diam tubes is inherently less desirable for the detectability limit (or FOM) optimization because of the added detector thickness caused by the second row of tubes. In effect, the second row of tubes can increase ε by a factor of ~1.5 but it also increases t by ~1.7 so the FOM improves only by $1.5/\sqrt{1.7}$, or ~1.15, and we doubled the number of tubes by adding the second row. The optimized design will have a high number of ^{3}He tubes located near the sample cavity to obtain a high efficiency, a small detector volume, and a small neutron die-away time.

SHIELDING AND BACKGROUND REDUCTION

We have investigated several methods to reduce neutron backgrounds for passive counting. The backgrounds have several components including neutrons from

1. external-area radiation sources (for example, waste-drum storage areas),
2. external-area cosmic-ray sources (for example, spallation reactions in the room),
3. spallation reactions between cosmic rays in the sample or the detector body, and
4. radioactive alpha or beta decay in the walls of the detector tubes.

Items 1, 2, and 4 produce only single neutrons, whereas item 3 produces both single and coincidence neutrons.

The detectability limit of a passive system varies approximately as the square root of the background rate (B). Thus, a factor-of-10 decrease in B results in about a factor-of-3 decrease in d. Different methods can be used to reduce the background for the different source terms listed above. These background reduction methods include the following:

1. External shielding such as CH_2 and concrete
   a. 10 cm of CH_2 gives a factor-of-10 reduction for items (1) and (2),
   b. 100 cm of concrete gives a factor-of-4 reduction for item (3), and
   c. the reduction in atmospheric shielding in going from an altitude of 2200 m to 300 m gives a decrease in items (2) and (3) by a factor of ~5.

2. Underground shielding locations
   70 m of dirt gives ~10^3 reduction for items (2) and (3).

3. Removal of high-mass-number elements in the detector and shield
   a. cadmium liners on both sides of the waste-drum detector banks increase the coincidence background by a factor of ~2 because of item (3), and
   b. the exterior cadmium liners on the ^{3}He detector banks decrease items (1) and (2) by only ~15%.

4. Statistical filter for the rejection of cosmic-ray spallations. The statistical outlier test can reduce item (3) by a factor of ~1.8 for coincidence counting and ~1.1 for singles counting in a well-shielded location. Short runs of 10 s each are used to add sensitivity to the statistical test.

5. Choice of the tube wall and an energy window on the thermal-neutron peak of the ^{3}He detector.
   a. After large reductions in the true neutron background in the detector, there is a residual background of counts from the radioactive alpha and beta decay products from the interior wall of the ^{3}He tube. We have measured these background levels to be

      1. 2.8×10^{-4} counts/s • inch for a 1-in.-diam aluminum tube and
      2. 4.3×10^{-5} counts/s • inch for a 1-in.-diam stainless steel tube.

      A 200-L-drum assay system might contain 100 tubes (36 in. long) giving 0.16 counts/s of this type of background (1.0 counts/s for aluminum tubes). For 2-in.-diam tubes, these backgrounds would approximately double.

6. Active cosmic-ray veto counters. Plastic scintillator "paddles" can be placed over the ^{3}He detector system to operate in the anticoincidence mode. Background item (3) can be potentially reduced using this technique; however, for a large drum counter, the deadtime would be excessive.

The combination of all of these background-reduction techniques can reduce the measured background rate by orders of magnitude.

DESIGN OPTIONS

The design options focused on an HDPE moderator and on a composite moderator (H, C, O, and F). For both options, the number of tubes, gas pressure, and tube placement can be varied to increase the FOM at the expense of tube and fabrication costs. In general, there is a performance saturation effect so that the initial cost increments produce more gain than the final cost increments as we approach saturation. Parametric studies of the variables are needed to make the final parameter selections.

Moderator Materials

Two sets of MCNP design calculations were performed, the first for a moderator that was 100% HPDE and the second for a composite moderator containing layers of HPDE and other plastics. These plastics contain less hydrogen and more C, O, and F than does CH_2.

In general, as the neutrons penetrate deeper into the moderator, the role of hydrogen for thermalizing the neutrons is less essential than at the surface. In the moderator, the thermalized neutrons are absorbed by hydrogen before they reach the ^3He tubes so it is desirable to replace H with C, F, and O in moderator locations away from the front surface and near the ^3He tubes. The primary benefit of this substitution is in the second row of ^3He tubes where the neutrons are well moderated. The drawback of this substitution is that the detector active volume gets larger and the average density gets larger. Both of these factors hurt the FOM and can wipe out the efficiency gain.

Modular Design

The WM3100 platform and the HPDE moderator make it possible to add or subtract performance capability with only minor changes in the electro-mechanical design. The number of tubes in the detector bank can be decreased to save tube costs and the shielding thickness can be decreased to save CH_2 costs. The MCNP design study was be used to select the desired FOM and efficiency.

This modular design allows the fabrication of a system with reduced cost and reduced performance with very minor mechanical changes.

Multiplicity Counting

We have assumed that the dominant consideration in the design optimization was the detectability limit. A high efficiency is also needed for multiplicity counting. The multiplicity counting uses the singles, doubles, and triples rates and high efficiency is required to get reasonable counting statistics for the triples counts. The ratios of the triples : doubles : singles varies as $\varepsilon^3 : \varepsilon^2 : \varepsilon$ so changes in the efficiency can be detected by changes in the ratios. The efficiency measured by multiplicity counting has the advantage that it directly tracks the actual efficiency for each neutron escaping the drum. Thus, localized shielding and nonuniform plutonium distributions are not a problem. The primary problem is that low plutonium mass samples have poor counting statistics.

DESIGN RESULTS

HDPE Moderator Design

The design work included the normal HDPE moderator as well as the more complex composite moderators made of HDPE combined with different types of plastic and Teflon. The added efficiency from the composite moderators needs to be balanced against the increased material and fabrication costs. The efficiency can be increased by using a composite moderator or by adding additional ^{3}He tubes. Both of these activities increase the cost and the best approach is an economic decision.

HPDE Design Results

The MCNP calculations were performed for the HDPE case using the as-built JCC-21[4] as the benchmark case. Figure 3 shows the geometry used in the calculations. The JCC-21 has 10 tubes on a side, giving a total of 60 tubes. In the study, we evaluated the tube pitch, depth in CH_2, gas pressure, and number of rows. Spontaneous fission source spectra for ^{252}Cf and ^{240}Pu were modeled. The ^{240}Pu neutron spectrum was used for the final FOM analyses.

The key parameters that were used to estimate the performance include the efficiency, the moderator thickness, and the gate fraction (128-μs gate). The efficiency as a function of gas pressure and tube depth in the HDPE is shown in Fig. 4. We see that the optimum depth is about 35 mm from the inside face of the moderator to the center of the ^{3}He tubes. This distance reduces to ~31 mm for the 10-tube case.

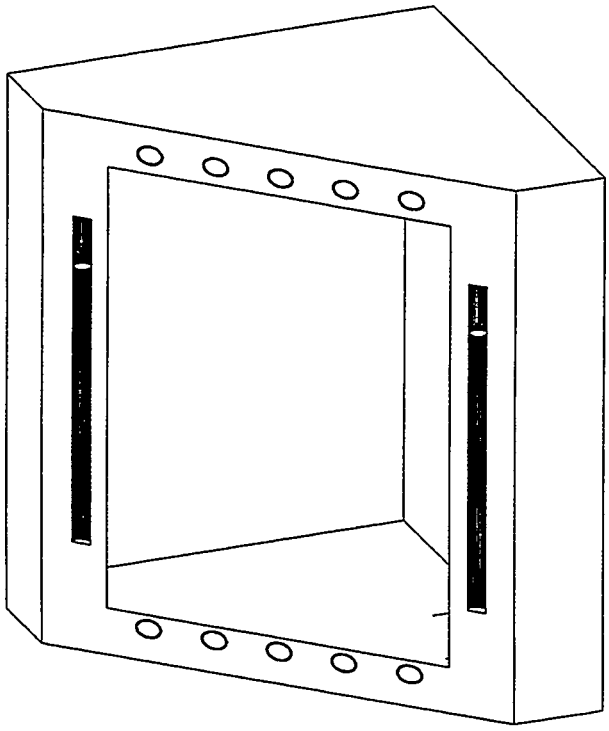

Fig. 3. Diagram of the detector geometry that was used for the MCNP calculations.

Figure 5 shows the data for the FOM; we see that the two-row design gives a low FOM. The selection of the number of tubes is a tradeoff between the desired FOM and the cost. Figure 6 shows the calculated ε vs the number of tubes for different gas pressures. The cases with and without cadmium are shown and a two-row (staggered) configuration is shown. For one row of tubes and no corner leakage, the ε tends to saturate at 37% for 20 tubes on a side. However, if the tubes are staggered to make two rows as shown in Fig. 2, the ε is increased to ~46%. The second row of tubes significantly increases our room background (from shielding displacement) and our cosmic-ray background (from volume increase).

5-cm-Diameter ^{3}He Tubes

For large detector systems of the type described in this report, higher counting efficiencies per detector can be obtained with 5-cm-diameter tubes compared with 2.54-cm tubes. However, the FOM for the larger tubes is worse than for the smaller tubes because the detector body thickness

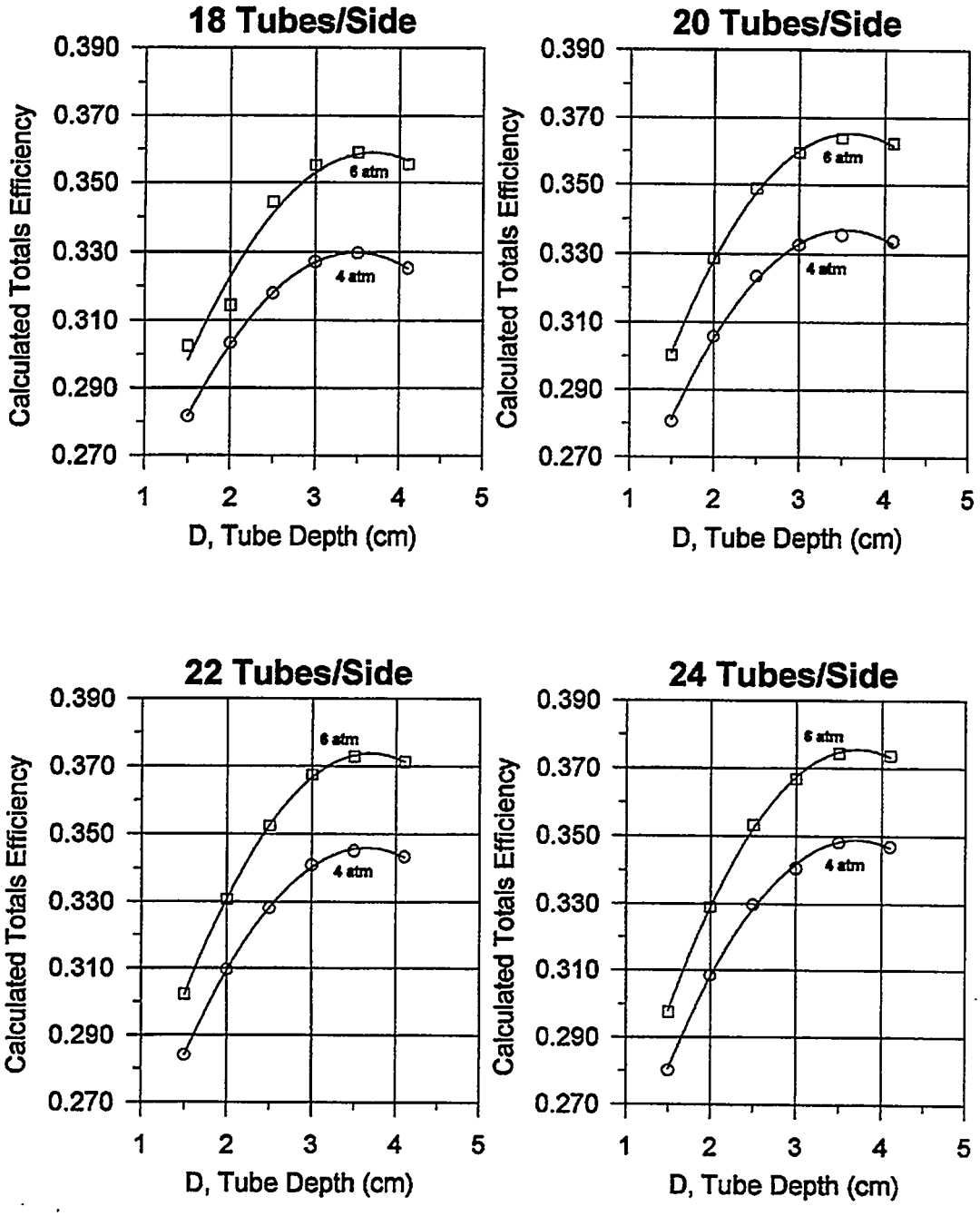

Fig. 4. Calculated efficiency for ^{240}Pu neutrons as a function of ^{3}He tube depth in the CH_2 and as the number of tubes per side.

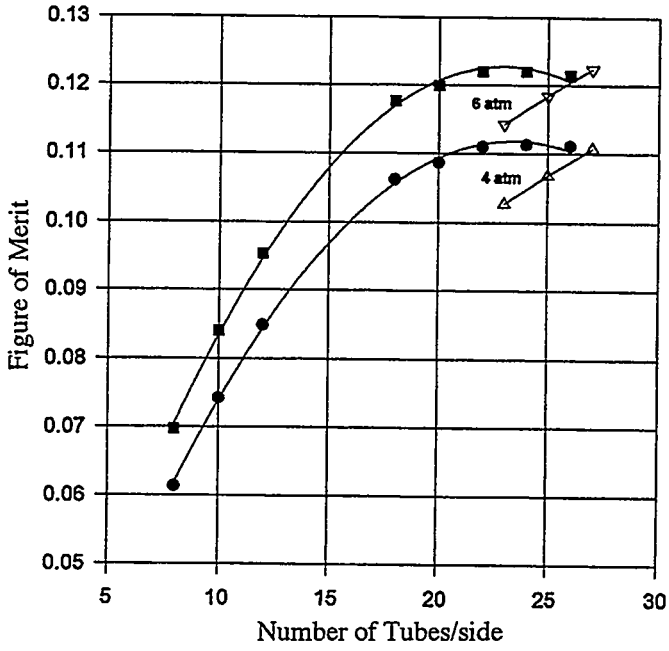

Fig. 5. Calculated FOM as a function of the number of tubes per side (triangle symbols represent a two-row design).

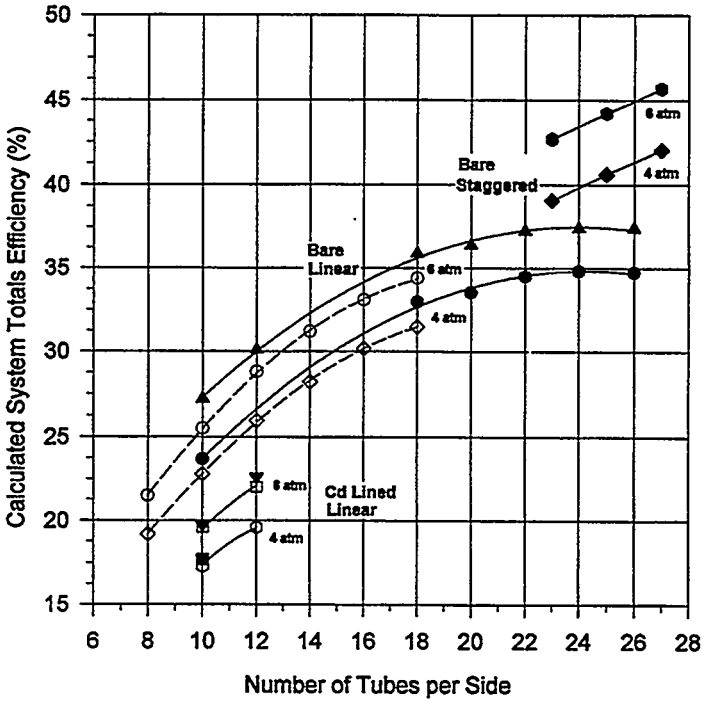

Fig. 6. Calculated efficiency for ^{240}Pu neutrons as a function of the number of tubes per side and the ^{3}He gas pressure. The highest efficiencies are for the staggered (two-row) design.

increases for the larger tubes. The larger-diameter tubes also have the problem that the AMPTEK amplifiers have: time constants that are too short for the 5-cm-diameter tubes. The use of amplifiers with long time constants makes the 5-cm tube system much more sensitive to gamma-ray backgrounds. The smaller-diameter tubes with the AMPTEK amplifiers are roughly an order of magnitude less sensitive to gamma-ray pileup than the 5-cm-diameter tubes.

For high-efficiency systems, the 2.54-cm tubes would use 6 atm pressure and the 5-cm tubes would use 3-atm ^{3}He pressure. The larger tube has an efficiency that is ~1.7 larger than the smaller tube; however, the cost of the larger tube is ~1.6 times larger so the economics are similar for the two options.

Composite Moderator Results

Composite moderators were evaluated using the MCNP calculations. Plastics other than HDPE were chosen to get more scattering atoms such as C, O, N, and F in place of the H in the CH_2 or moderator. The composite moderators gave results with a higher efficiency per ^{3}He tube than the pure HDPE moderator; however, the FOM for the composite materials was no better than the HPDE moderator. A separate paper[5] in this conference will give the detailed composite moderator results.

System Performance

The High-Efficiency Neutron Counter (HENC) was fabricated using design guidance from the MCNP calculations. The HDPE option was used to obtain a good FOM and to use standard fabrication methods. A single row of ^{3}He tubes was used with a pitch of 3.95 cm. The performance specifications are listed in Table III. The design was optimized for a moderated ^{240}Pu neutron spontaneous fission energy spectrum.

The 30-cm-thick HDPE neutron shield on the outside of the HENC reduces the room source neutron rate by 3 orders of magnitude; however, it gives only a small reduction (<10%) in the cosmic-ray coincidence neutrons. To reduce the cosmic-ray background, a large quantity of overhead shielding, such as concrete, is required.

TABLE III. Performance Specification for the HENC	
Parameter	Value
Neutron efficiency for ^{240}Pu	32%
Neutron die-away-time	50 μs
Deadtime (a)	0.50 μs
(b x 10^{-6})	0.161 μs
Multiplicity deadtime	171 μs
correction coefficient c	0.147 μs
correction coefficient d	0.147 μs
Coincidence gate	128 μs
Predelay	3.0 μs
Doubles calibration coefficient	53.8 counts/s•g ^{240}Pu
Multiplication constant (ρ_0)	0.178

The minimum mass detectability limit for the HENC depends on the location of the system and whether totals or reals are used for the assay. At sea level, the detectability limit (3 σ) is ~1.7 mg ^{240}Pu-eff. for doubles assay and 0.48 mg ^{240}Pu-eff. for singles neutron counting. At the high elevation of Los Alamos (2200 m), the cosmic-ray background is 4 to 5 times higher than at sea level and the detectability limit approximately doubles.

The HENC was calibrated using plutonium standards including MOX pellets and small PuO_2 powder samples. Figure 7 shows the linear doubles calibration fit to the standards. The neutron multiplication was negligible for the calibration standards.

Figure 8 shows the triples calibration line for the HENC with a slope of 5.83 counts/s•g ^{240}Pu. This calibration demonstrates that the triples rate can be used down to sub-gram quantities of ^{240}Pu-eff. In general, the triples rate will be used to make matrix corrections.

The HENC was used in the second round of the PDP drum measurement test and the results of this test should be available in early 1997.

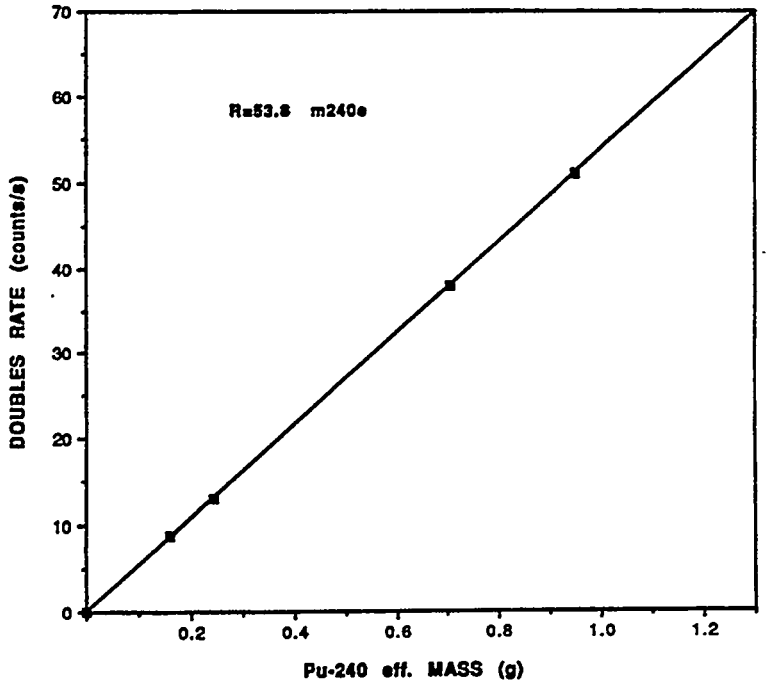

Fig. 7. The linear doubles calibration curve for the HENC.

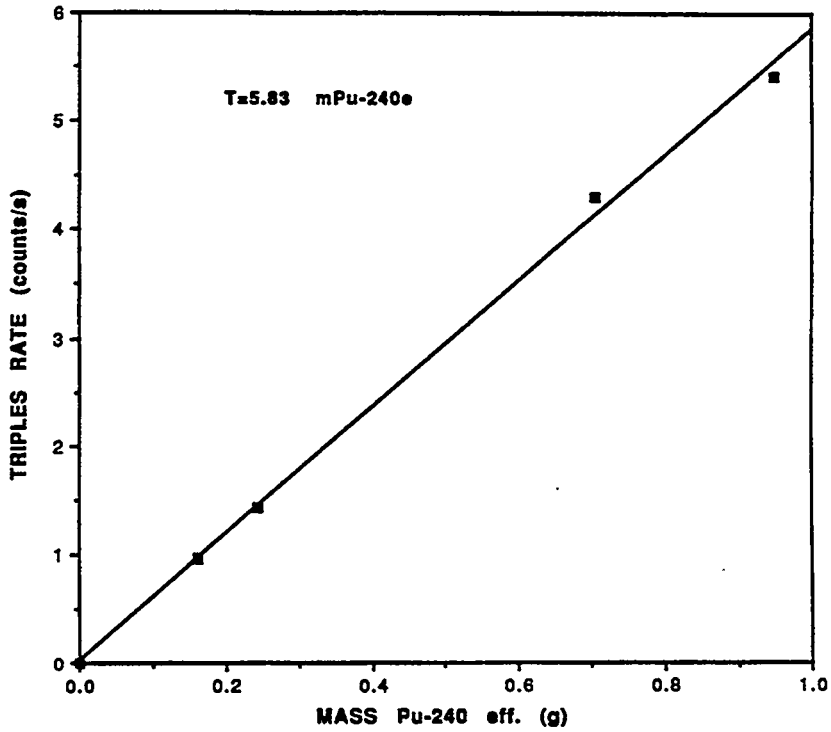

Fig. 8. The triples rate calibration curve for the HENC.

ACKNOWLEDGMENTS

This work was supported by the US Department of Energy, Office of Nonproliferation and National Security, and by Canberra Industries

REFERENCES

1. N. Ensslin, M. S. Krick, and H. O. Menlove, "Expected Precision of Neutron Multiplicity Measurements of Waste Drums," *Nucl. Mater Manage.* **XXIV** (Proc. Issue) 1117-1124 (1995).

2. D. H. Beddingfield and H. O. Menlove, "Statistical Data Filtration in Neutron Coincidence Counting," Los Alamos National Laboratory report LA-12451-MS (November 1992).

3. J. F. Briesmeister (ed.), "MCNP - A General Monte Carlo Code for Neutron and Photon Transport," Los Alamos National Laboratory report LA-7396-M, Rev. 2 (1991).

4. H. O. Menlove, J. Baca, W. Harker, K. E. Kroncke, et al., "WDAS Operation Manual Including the Add-A-Source Function," Los Alamos National Laboratory report LA-12292-M (April 1992).

5. M. M. Pickrell, "Development of a High-Efficiency Neutron Counter Using Novel Materials," to be presented at this meeting.

IDENTIFICATION OF THE FAST AND THERMAL NEUTRON CHARACTERISTICS OF TRANSURANIC WASTE DRUMS

B. H. Storm, Jr., R. L. Bramblett,
Lockheed Martin Specialty Components, Largo FL

C. Hensley,
Oak Ridge National Laboratory, Oak Ridge, TN

ABSTRACT

Fissile and spontaneously fissioning material in transuranic waste drums can be most sensitively assayed using an active and passive neutron assay system such as the Active Passive Neutron Examination and Assay. Both the active and the passive assays are distorted by the presence of the waste matrix and containerization. For accurate assaying, this distortion must be characterized and accounted for. An External Matrix Probe technique[1] has been developed that accomplishes this task. Correlations between in-drum neutron flux measurements and monitors in the Active Passive Neutron Examination and Assay chamber with various matrix materials provide a non-invasive means of predicting the thermal neutron flux in waste drums. Similarly, measures of the transmission of fast neutrons through various matrix materials are shown to be correlated with the probability of detecting fast neutrons emitted from sources in the drum. Results obtained using the Lockheed Martin Specialty Components Active Passive Neutron Examination and Assay system are discussed.

INTRODUCTION

The Lockheed Martin Specialty Components (LMSC) Active Passive Neutron Examination and Assay instrument (APNEA) is the heart of a transportable system capable of performing nondestructive assay of TRansUranic (TRU) waste drums. The system provides

---

[1] D.C. Hensley, "Autonomous Matrix Identification by the APNEA System", *4th Nondestructive Assay and Nondestructive Examination Waste Conference*, Salt Lake City, Utah (October 24, 1995).

imaging of spontaneous and induced neutron emission from within the drum and quantification of the activity in equivalents of ^{239}Pu and ^{240}Pu.

The APNEA utilizes seventy-nine main ^{3}He detector tubes, seven cavity neutron flux monitors, and two neutron generator output monitors. A detailed description of data acquisition is given by Hogel *et al.*[2] The primary use of the main detectors is to provide spatial and temporal information describing fast neutron emission from materials in the drum. These detectors are encased in polyethylene and enclosed in cadmium packs which shield them from incident thermal neutrons. Cadmium collimators on some of the cavity flux monitors provide them a preferential view of the thermal neutron flux from either the cavity wall or the drum. Neutron generator monitors are embedded in polyethylene at 14.5″ and 20″ from the neutron generator. These provide a measurement of the neutron generator output that is independent of drum matrix materials.

Plan and elevation views of the LMSC APNEA are presented in Figures 1 and 2. Two coordinate systems are used to describe the system. The first is a cylindrical system whose azimuthal axis corresponds to the drum center with z = 0 defined at the drum bottom. The drum is divided into eight azimuthal segments which are described by segment number (rather than angle) for ease of handling by the analysis algorithms. The notation adopted to describe this system will be (r,φ,h) representing the radius, segment number and height. This second is a right-handed Cartesian system whose z -axis is collinear with that of the cylindrical system. The x-axis extends through the center of segment 3, and the y-axis through segment 1. The Zetatron is located at (-20″,0,18″) in the Cartesian system, as indicated in the figures. The N2 detector group consists of three 48″ long vertical detector tubes whose responses are summed in software.

---

[2] R. A. Hogle, P. Miller, and R. L. Bramblett, "APNEA List Mode Data Acquisition and Real-Time Event Processing", submitted to the *5th Nondestructive Assay and Nondestructive Examination Waste Characterization Conference*, Salt Lake City, Utah, (January 1997)

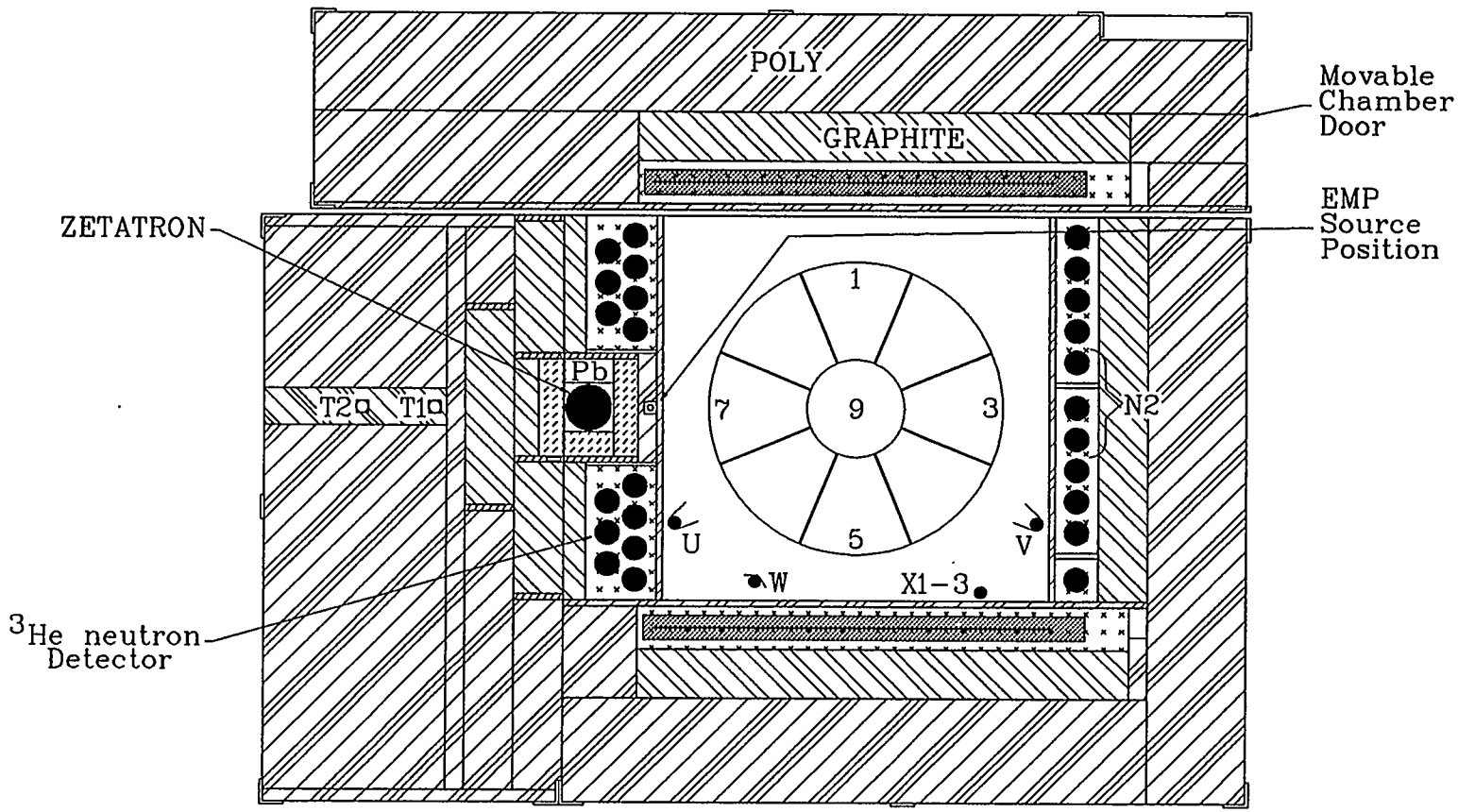

Figure 1. Plan view of the APNEA chamber and detector configuration.

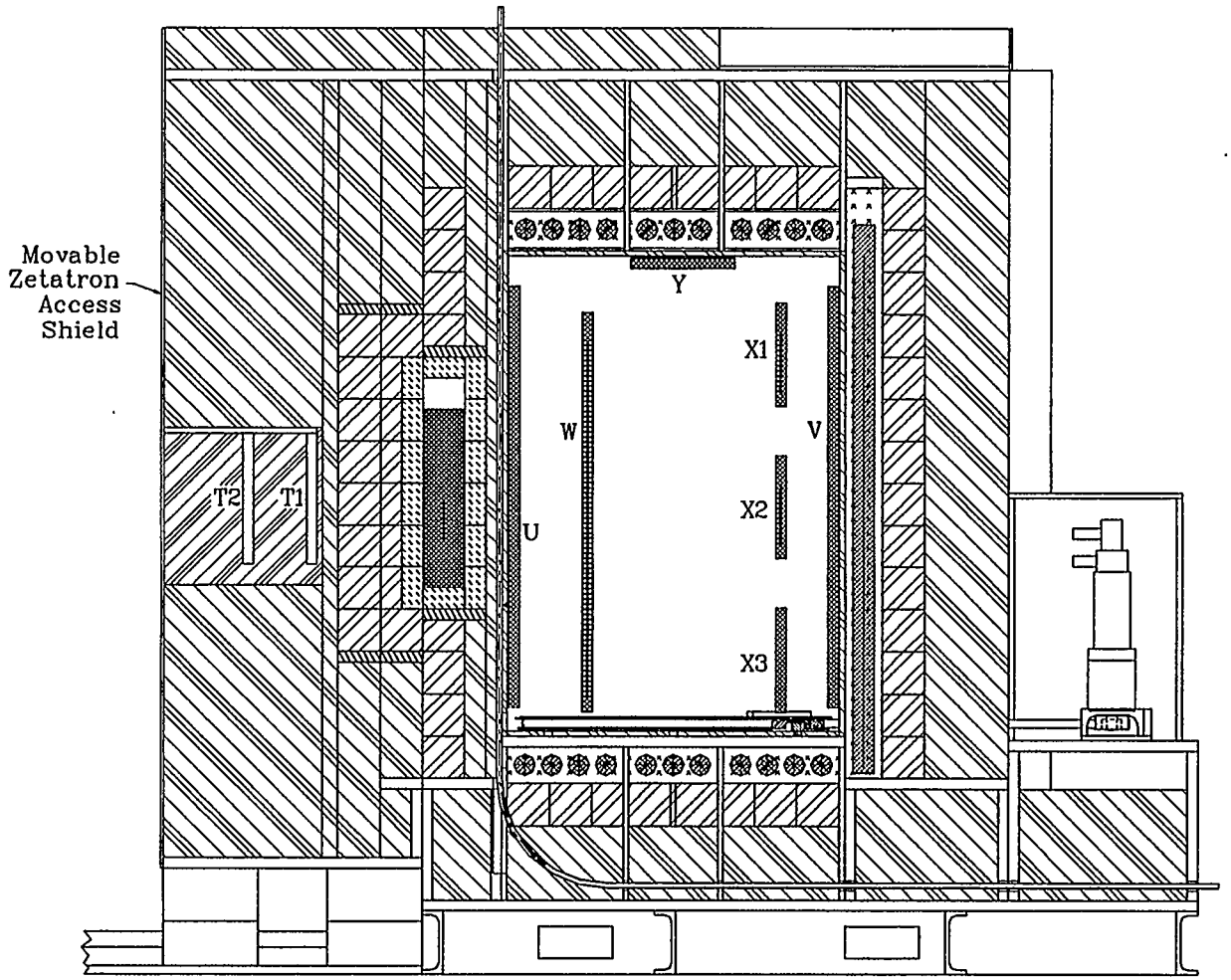

Figure 2. Elevation of the APNEA chamber and detector configuration.

The middle tube of this group is centered at (18″, 0″, 20″). The tubes in this group are separated by about 3″.

The location of a ^{252}Cf external matrix probe (EMP) source is also indicated. This source is moved from a shielded container to (-16.5″,0,z), where the z-position ranges from 0 to 30″. These measurements are used to determine the fast neutron scattering and transport characteristics of the drum matrix.

The behavior of the system is modeled by two basic equations. These have been discussed in detail by Hensley.[3] Passive mode (spontaneous fission) measurement of singles neutron emission is described by equation 1,

$$Y(det) = \sum_{r,\varphi} \varepsilon\,(det,r,\varphi,z)\rho\,(r,\varphi,z) \quad . \qquad (1)$$

The singles yield (Y) measured by a detector (det) is given by the accumulated product of the efficiency (ε) for detection of a neutron emitted from the virtual volume element centered at radius r, azimuthal segment φ, and height z, and the source density (ρ) in neutrons/second/volume element at the virtual volume element centered at (r, φ, z). The measurement of neutrons in an active (induced fission) measurement is described by equation 2,

$$Y_f(det,t) = \sum_{r,\varphi} \varepsilon\,(det,r,\varphi,z)\rho_{\,f}(r,\varphi,z)Flux(r,\varphi,z,t) + A(det)Fast(det,t) \quad . \qquad (2)$$

Here the density, $\rho_f(r,\varphi,z)$, is an array representing the production and emission of fission neutrons. It accounts for the fission cross section and quantity of fissile material. The thermal neutron flux in a given matrix material at position (r, φ,z) and time t following the neutron

[3] D. C. Hensley, "Source Imaging of Drums in the APNEA System", *4th Nondestructive Assay and Nondestructive Examination Waste Characterization Conference*, Salt Lake City, Utah, (October 1995)

generator burst is described by $Flux(r, \varphi, z, t)$. The response of the main detectors to the neutron generator burst is given by the product of $Fast(det, t)$ and $A(det)$ as described in reference 3. The subscript f is used to reference an induced fission event.

DETECTION EFFICIENCY AND THERMAL NEUTRON FLUX CALIBRATION STANDARDS

In order to best quantify fissile material in a waste drum, the neutron transport characteristics of the drum matrix material must be determined. The pertinent properties are the transmission of fast neutrons through the matrix material, the shape and amplitude of the thermal neutron flux in the drum, and the response of the main detectors to fast neutrons produced by the neutron generator. To determine the efficiency and flux arrays which are to be applied to an unknown matrix, the responses of cavity flux monitors and main detector monitors to the unknown matrix are compared to a library of responses from known matrix materials in calibration drums. An efficiency and flux profile are then chosen from the standard or standards whose responses best match those of the unknown matrix.

Calibration drums have been constructed containing fixtures that allow placement of neutron sources, fissile materials, or neutron flux monitors at various heights and radial positions in the drum. This allows a drum to be partitioned into a number of virtual volume elements for which the efficiency and flux are determined. The drums are filled to various heights with a variety of materials whose properties are expected to span the range of those encountered in actual waste drums. These include water, soil, concrete, ethafoam, a mixture of polyethylene and stainless steel (poly-steel), simulated Rocky Flats sludge, and an empty drum. Each drum also contains a polyethylene liner. Efficiency and flux measurements have been obtained for the above at radii from 0″ to 10″ and heights from 2″ to 30″.

THERMAL NEUTRON FLUX RESPONSE IDENTIFICATION

The amplitude and shape of the observed thermal neutron flux is modified in a different manner by each of the matrix materials. This is to be expected from the different physical densities of the matrix materials, and the different neutron scattering and absorption cross sections of their constituent elements. The relative flux as a function of location along a diameter in several matrix materials is shown in Figure 3. The flux has been normalized to the matrix independent flux monitor (T2) so that differences observed depend only on the interaction of neutrons with the matrix material and not on fluctuations in the neutron generator output.

Figure 4 shows the relative flux as a function of time following the neutron generator pulse as measured by flux monitors inside calibration drums. The top figure shows the distribution measured by a monitor located in the volume element at (10,3,12), the bottom shows the flux measured at (10,7,12) (adjacent to the neutron generator). The coordinates (r, φ, h) refer to the radius, segment, and height of the monitor. There are eight discrete segments as indicated in Figure 1. As expected, the flux in each matrix material varies as a function of both position in the drum and time following the neutron burst. While it is sometimes difficult to distinguish among similar matrices based on data at a single location and time following the neutron burst, examination of the spatial and temporal distributions indicate that differences in the flux profile due to the matrix material can be recognized. For instance, while the flux distribution measured by the monitor at (10,3,12) in the poly-steel and concrete are quite similar, the distributions at (10,7,12) clearly differ. Corresponding spatial variations in the flux are indicated by the external monitors.

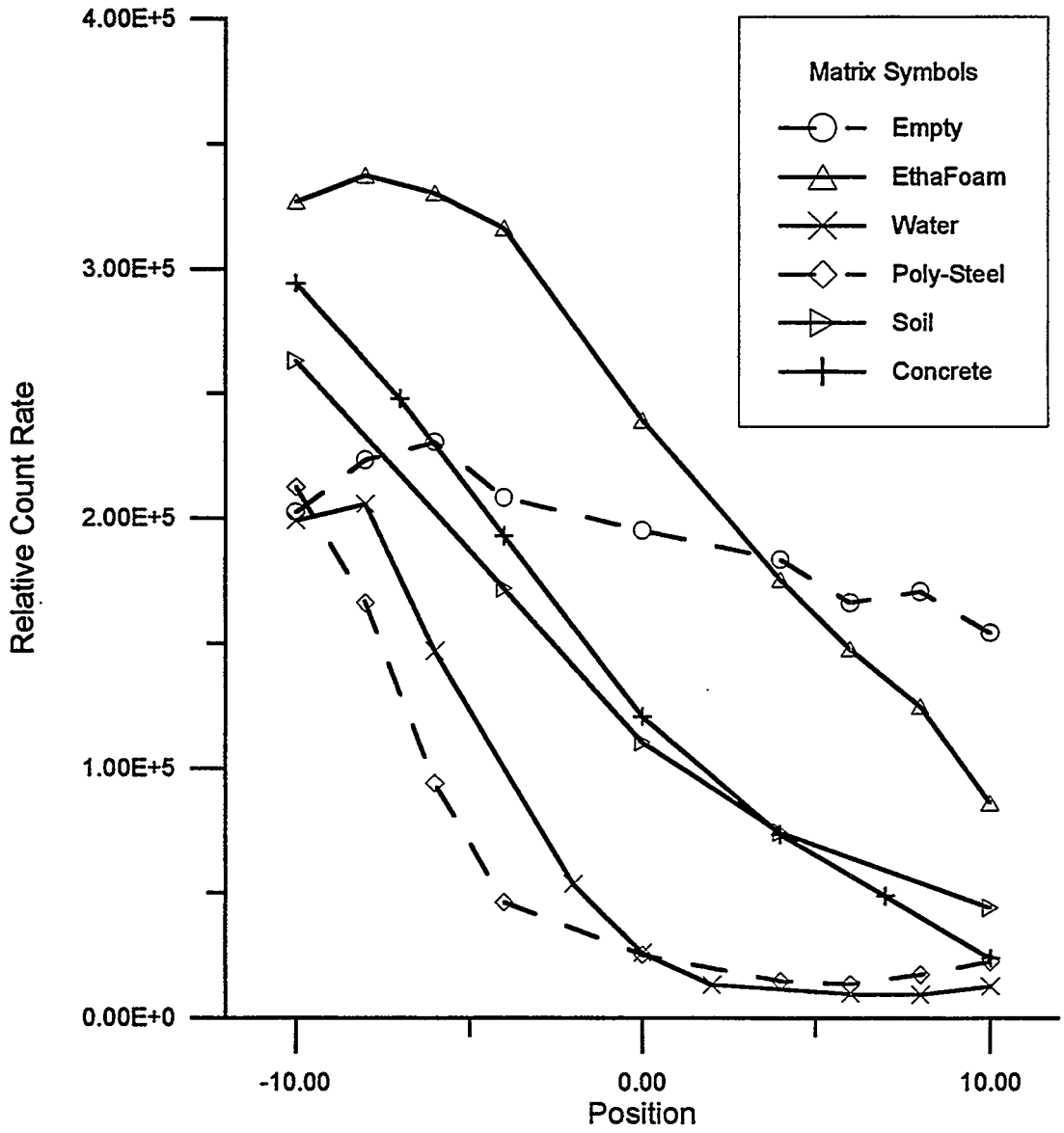

Figure 3. Relative counting rate in the 350 - 400μsec time bin as measured by a monitor 12″ from the drum bottom and at the indicated position inside the drum.

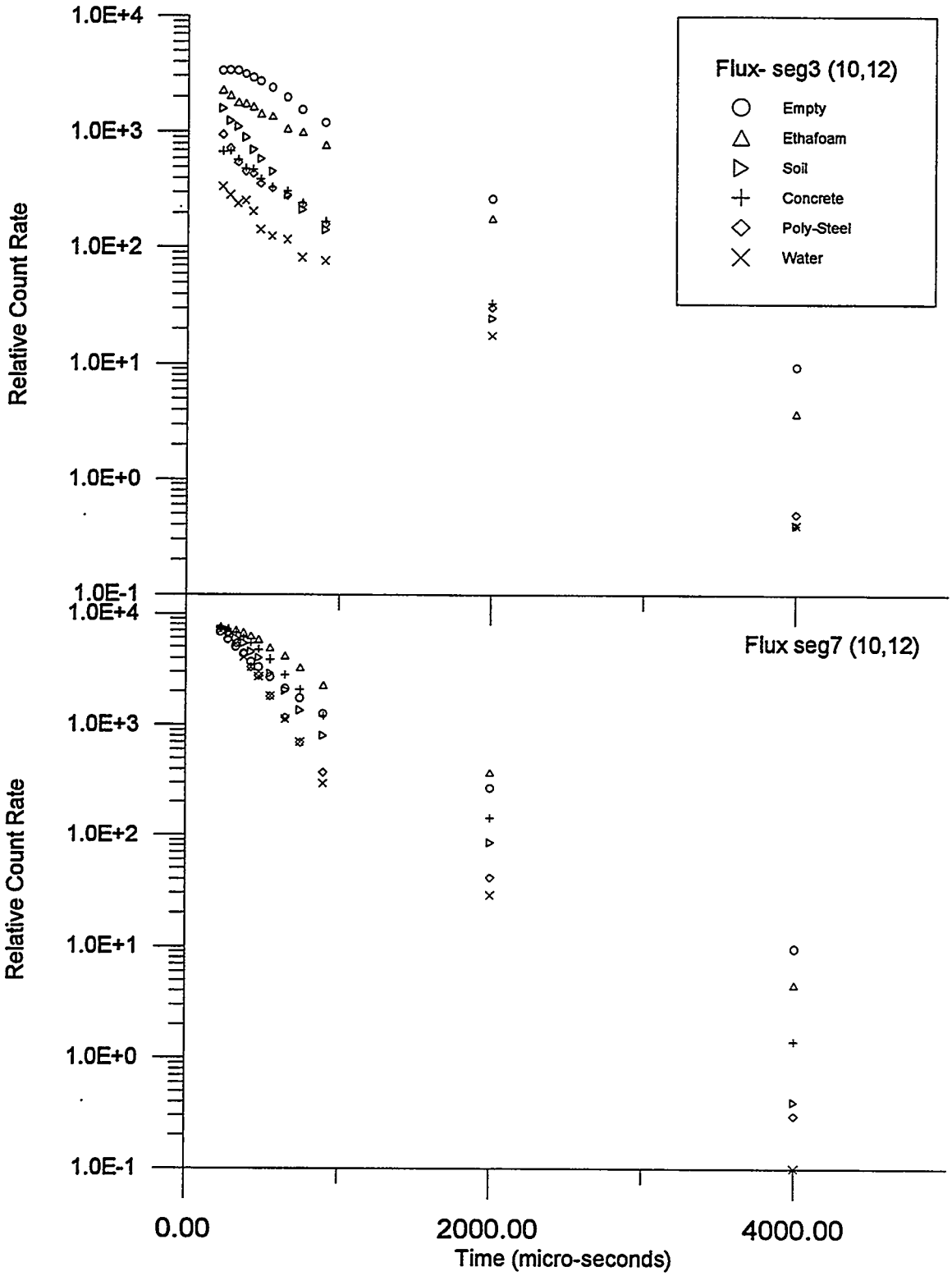

Figure 4. Relative counting rate in segments 3 (opposite Zetatron) and 7 (adjacent to Zetatron) at 10″ radius and 12″ from the drum bottom.

It is necessary to determine the flux inside a drum matrix material by a measurement external to the drum. Each of the cavity flux monitors gives a piece of information about the spatial distribution of the thermal neutron flux which is used to properly identify the matrix material in the drum. Some of these employ cadmium shields designed to give them a preferential view of a portion of either the cavity wall or the drum. The flux in monitors U and V are shown as a function of time following the neutron generator burst in Figure 5. As indicated in Figures 1 and 2, these monitors have a preferential view of the side of the drum facing and opposite the neutron generator, respectively. Figure 6 shows the flux in three oriented vertically detectors with an active length of 6″. The center of the active areas of X3, X2 and X1 are 6″, 20.5″ and 35″, respectively, from the bottom of the chamber. These are used in EMP and active measurements to provide information about the vertical variation of the neutron flux.

This approach requires a means of normalization which, while sensitive to the neutron generator output, is independent of the matrix material in the cavity. As Figure 7 indicates, T2 provides such a measurement. Data presented for concrete, soil, and ethafoam were acquired at LMSC, Largo, FL in September 1996. Those for the empty and poly-steel drums were acquired at the Idaho National Engineering Laboratory (INEL) in late November 1996 using the same neutron generator but a different pulse forming network assembly. The difference in the T2 response is attributed to differences in the source voltage supplied by each assembly.

In order to identify an 'unknown' matrix, the response measured by the cavity flux monitors is compared to the library of responses for known matrix materials. In each case, the flux is normalized by the total counts measured by the T2 monitor in the same acquisition. Amplitude and shape information allow identification of the known matrix material which best matches the 'unknown' matrix. An automated method is being evaluated which identifies the calibration drum whose EMP signals are nearest, in a weighted least squares sense, to those of the drum being assayed. The unknown drum is compared with each calibration drum by computing a

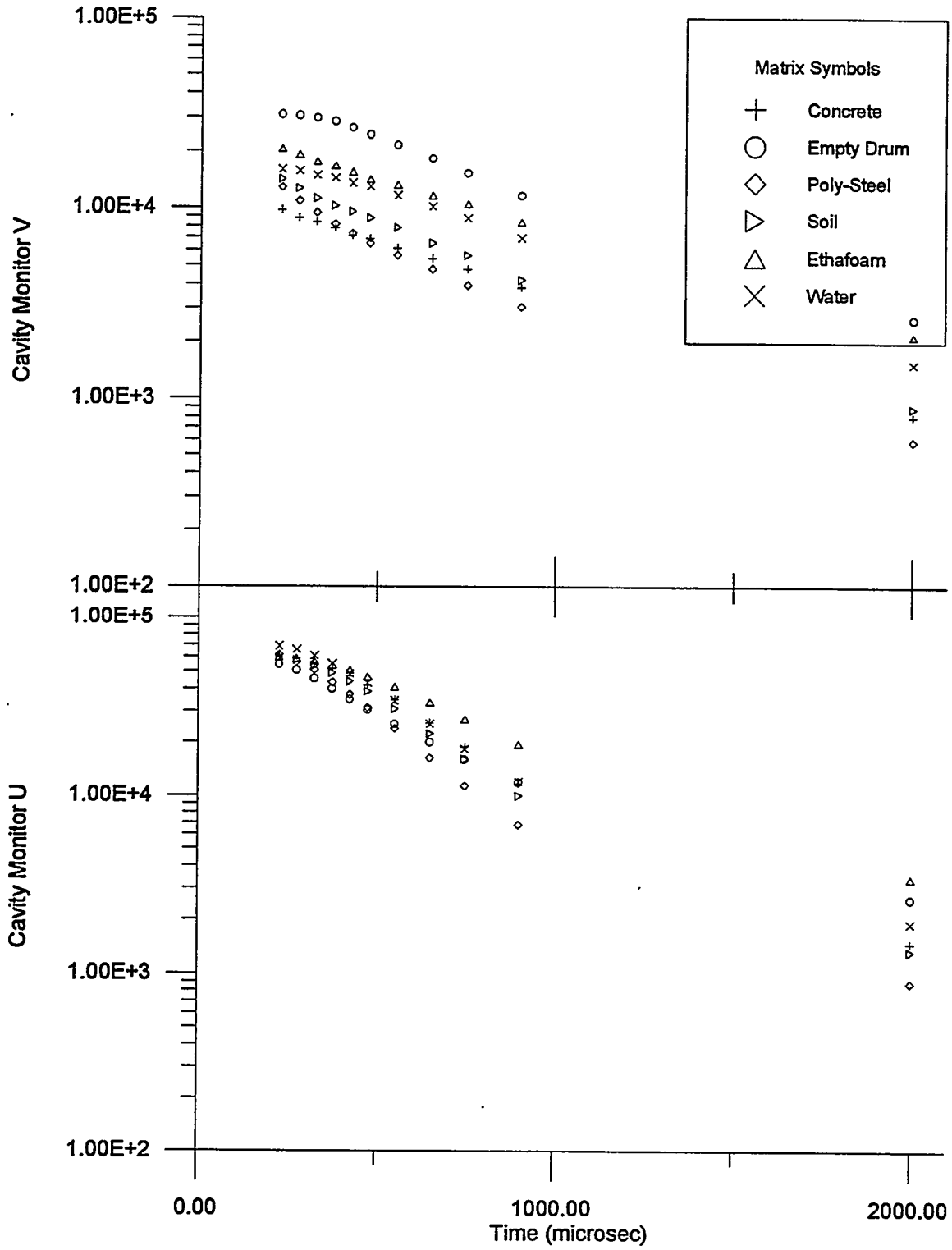

Figure 5. Relative counting rates in cavity flux monitors V (opposite Zetatron) and U (near Zetatron).

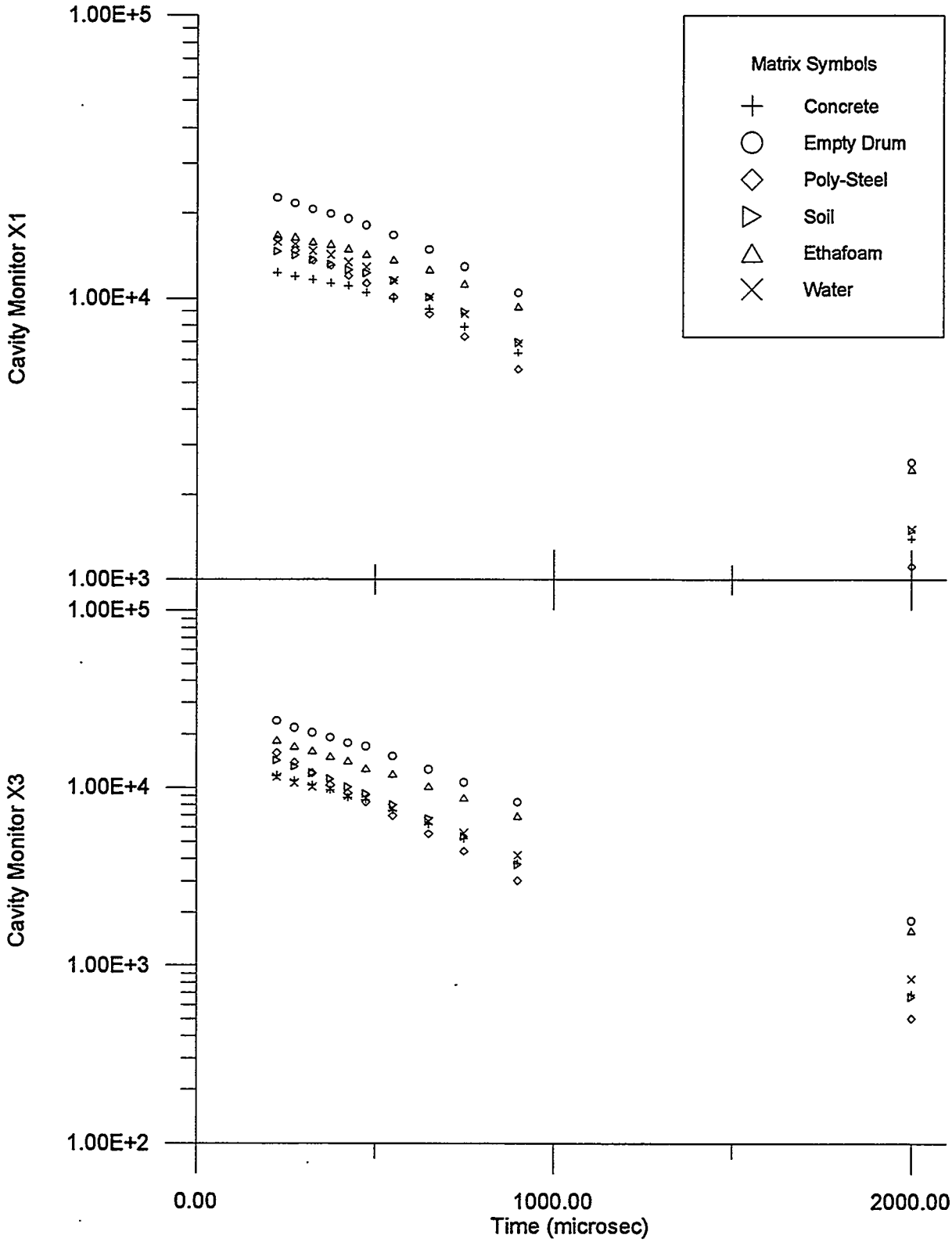

Figure 6. Relative counting rates in the height sensitive vertical monitors X1 (upper) and X3 (lower).

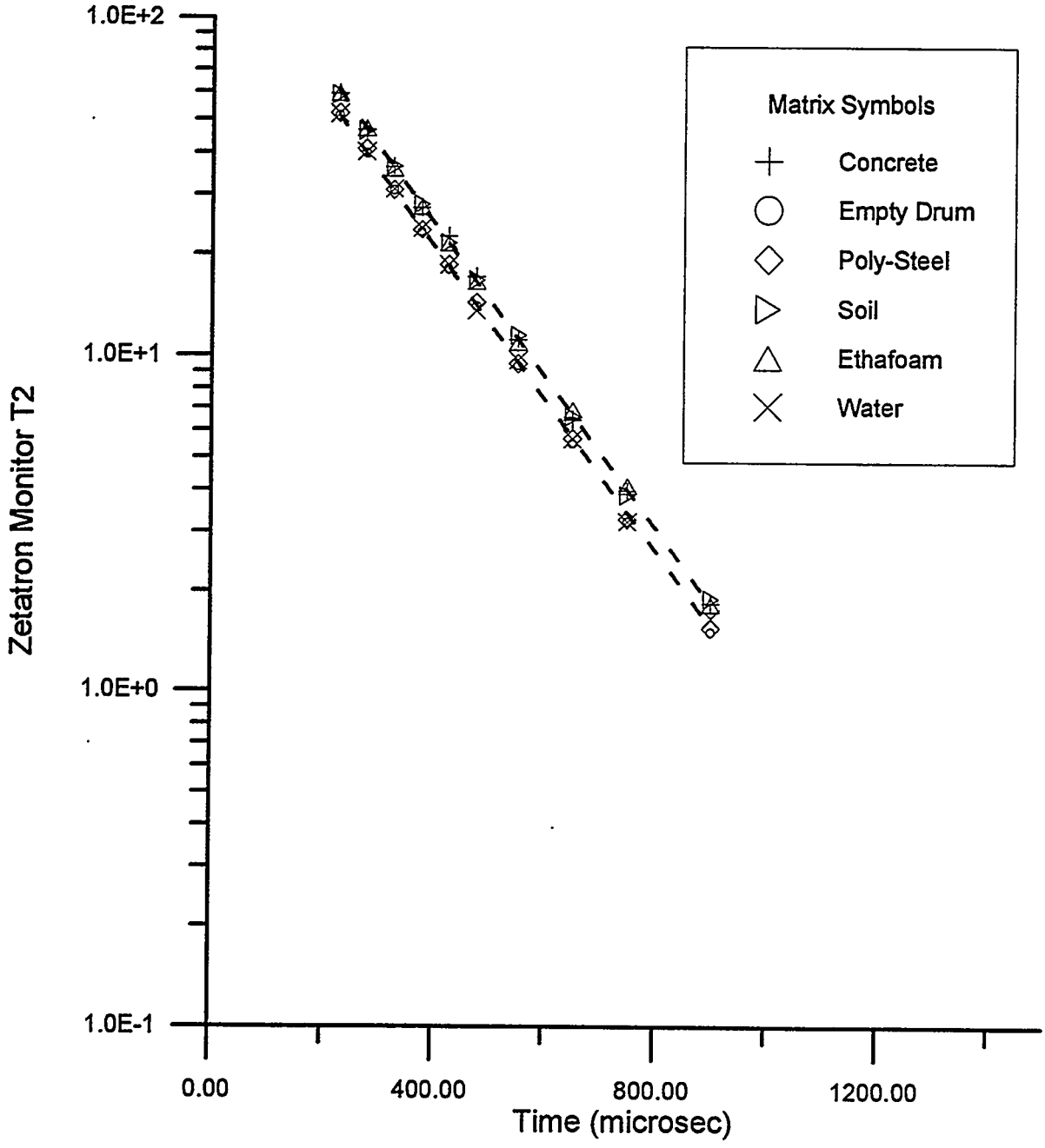

Figure 7. Relative counting rate in the Zetatron Monitor T2. The dashed lines are drawn through data acquired with different neutron generator electronics systems.

weighed sum (WSS), of the squared differences of EMP signals between unknown and calibration drums. The calibration drum with the smallest value of WSS is the best match. Weight factors are based on the measurement standard deviation of each parameter are used so that, for a perfect match, WSS is the reduced chi squared statistic. This process is applied separately for the determination of the calibration drums to use for neutron flux and detection efficiency. For neutron flux, the monitor signals during active acquisition are used. For detector efficiency the data from the Cf matrix probe source are used. Figure 8 shows WSS for the case where the INEL graphite calibration drum is used as an unknown. Six active runs were made. As expected, the minimum value of WSS (approximately 1) is for the response of the graphite calibration standard. More important, the next higher WSS, that for ethafoam, is around 75, so it is statistically very significant. Similar results are shown in Figure 9, where the LMSC sludge calibration drum is used as the unknown. The minimum WSS is about 1 for the sludge calibration drum and the next WSS (15) for the two thirds filled water calibration drum. As may be observed from the plots of the repeated runs or the values of WSS, the distinction between sludge and concrete calibrations is statistically very significant.

When the unknown is a real waste drum, the value of WSS, even for the best match, is much greater than 1. This obviously depends on how well the best calibration matches. Figure 10 shows the results of the WSS analysis on four Rocky Flats (IDC=001) waste drums. In each case, the minimum WSS is about 16 for the two thirds full water calibration drum and the next smallest value is about 36 for the sludge calibration drum. The sludge calibration drum was designed to match these drums, but water is a better match for the neutron flux response. It is observed that there is a large variability in neutron transport properties within a given waste type. For this reason the best match is not always provided by a surrogate drum of the same nominal type as the 'unknown'. This illustrates the importance of a technique that determines the properties of each drum by matching measured responses.

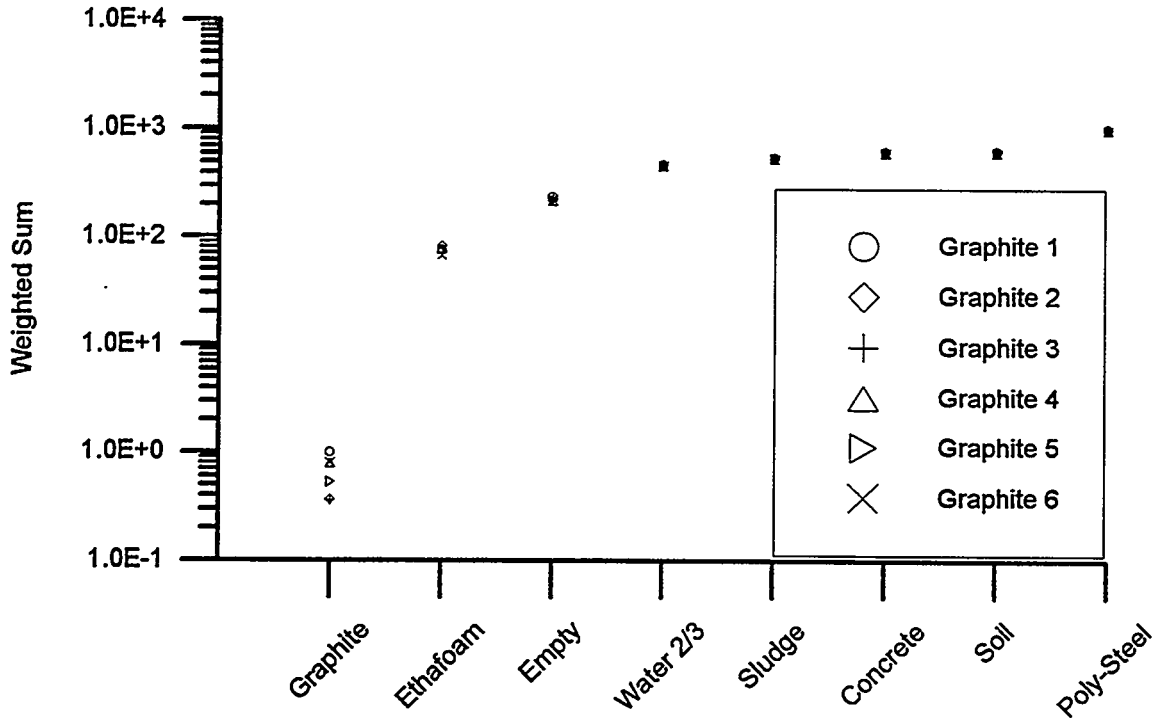

Figure 8. Fit of repeated runs of the graphite calibration drum to the library of thermal neutron flux responses for calibration standards.

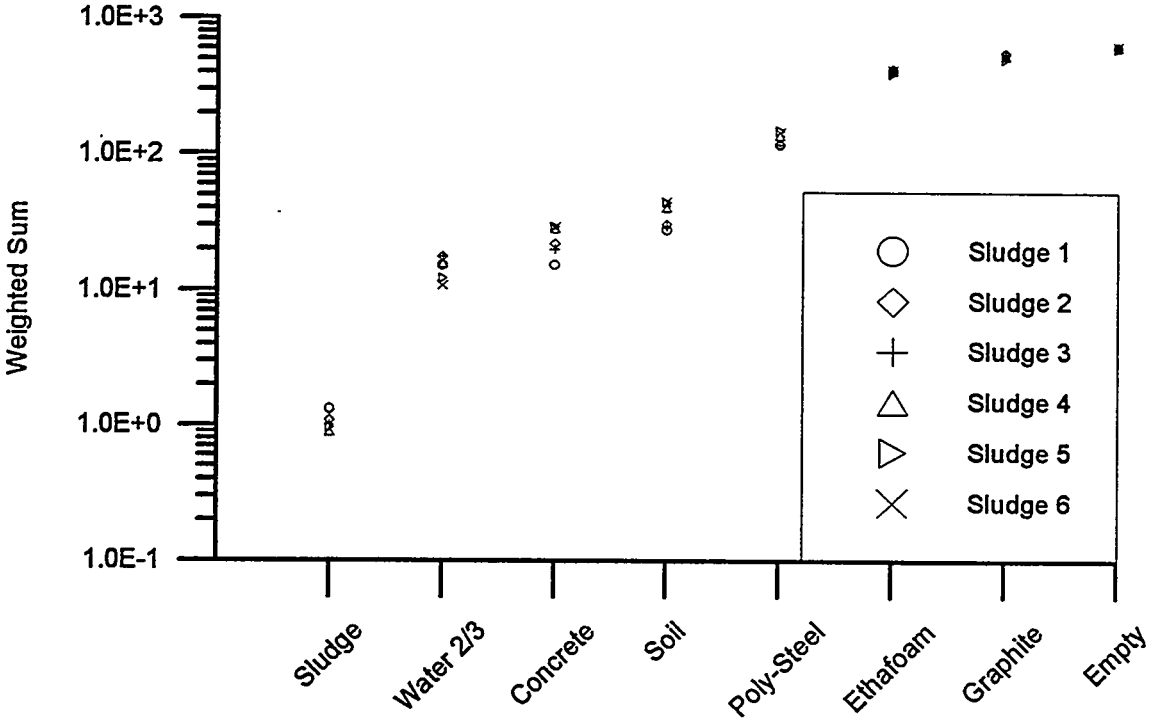

Figure 9. Fit of repeated runs of the sludge calibration drum to the library of thermal neutron flux responses for calibration standards.

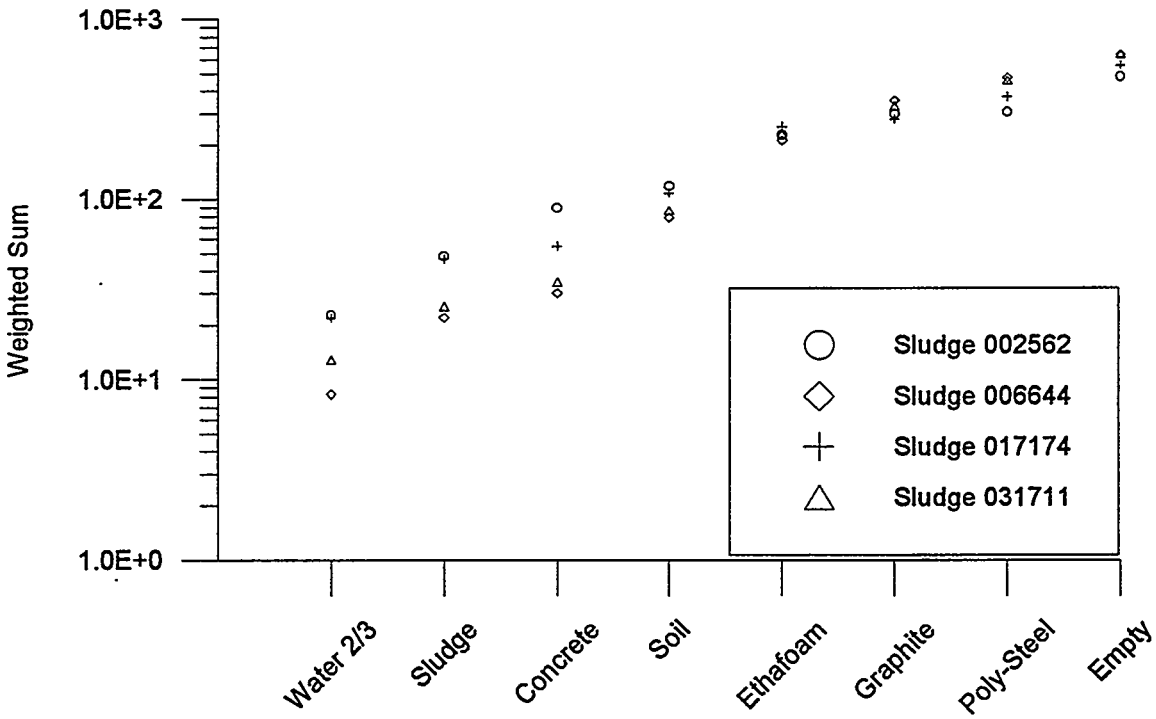

Figure 10. Fit of real sludge waste drums to the library of flux responses of calibration standards.

In the imaging algorithm, the array comprised of the internal flux monitor results identified with the best fit matrix material is applied in a fitting routine. These data are normalized by the ratio of the total counts in the cavity flux monitor (V) in the 'unknown' to that in the known matrix material. Thus, both the shape and the amplitude of the actual flux in the 'unknown' are determined.

DETECTION EFFICIENCY RESPONSE IDENTIFICATION

The relative efficiencies vs. position of a ^{252}Cf source in various calibration drums as measured by the N2 detector group are shown in Figure 11. The abscissa is referenced to the drum center at 0″ with the N2 detector at +18″. Each matrix material has different fast neutron transport properties, as evidenced by differences in the measured efficiencies. Near the outside of the drum the effects of back-scattering become important for matrix materials containing heavy elements. This is observed as an enhancement in the efficiency from about 7″ to 10″ and is particularly apparent in the poly-steel as compared to the empty drum. The observed efficiency is dependent on the physical density of the material and the magnitude and angular distribution of the scattering cross sections of the constituents, resulting in a system which is difficult to describe with a simple model.

Since the efficiency for detection of fission neutrons differs for various matrix materials, a non-invasive measurement is required which allows this property to be predicted for actual waste drums. The LMSC APNEA uses a nominal 10^7 neutrons/second ^{252}Cf source as an EMP in an automated series of measurements to determine fast neutron transport characteristics of unknown drums. Applying a similar technique as for the active responses, comparison to a library of known matrix materials allows selection of the known matrix material(s) whose transport characteristics most closely match those of the unknown matrix.

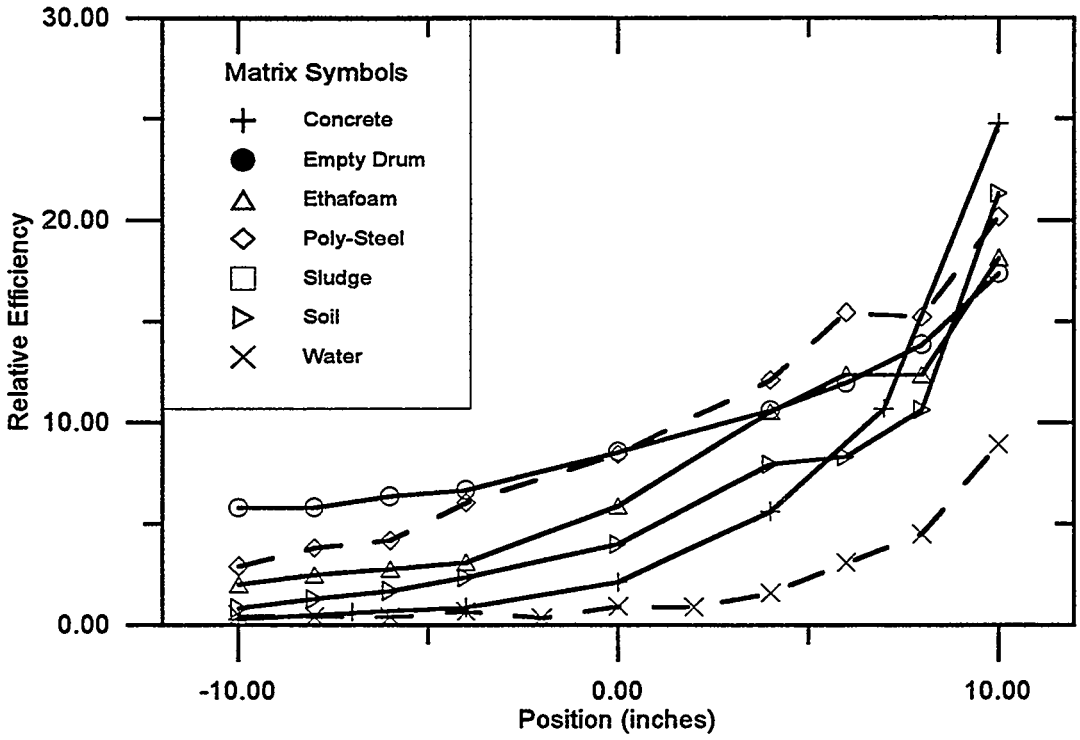

Figure 11. Relative efficiency measured by the N2 detector pack. The drum center is at 0" and the N2 detector pack is at 18".

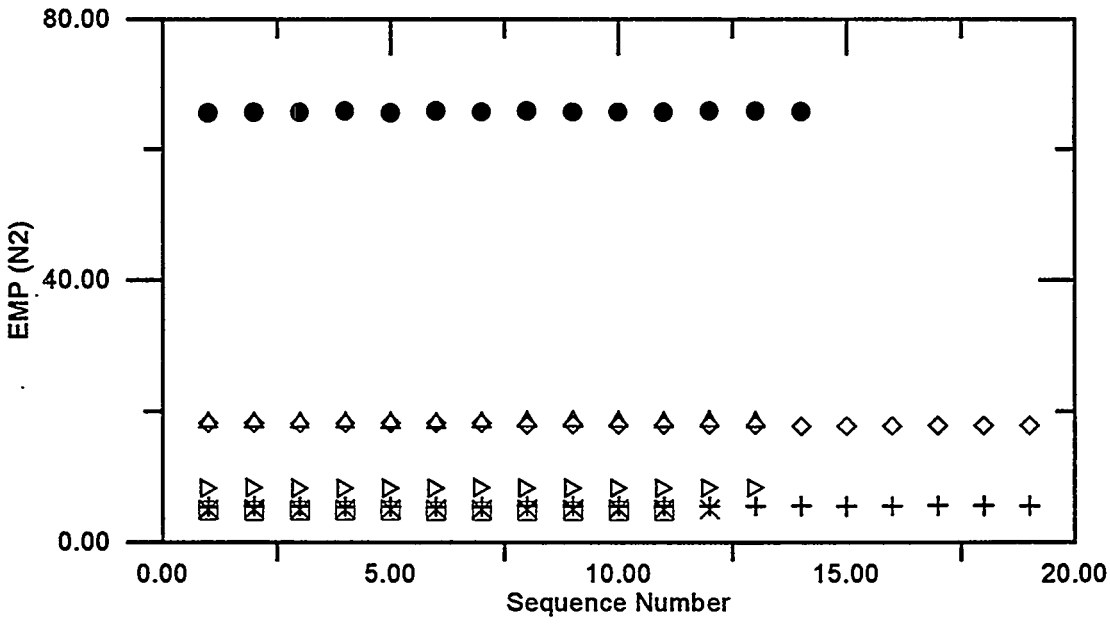

Figure 12. Response of the N2 detector pack to the EMP source at a height of 18".

The efficiencies for each volume element of the known matrix material are then applied in the analysis of the unknown matrix.

Figure 12 shows the response (relative to the empty cavity) of the N2 detector group to the EMP ^{252}Cf source at a height of 18″ for a variety of matrix materials. This series of measurements was repeated a number of times on each matrix material with each measurement denoted by sequence number. EMP results based on N2 transmission alone are expected to be most closely correlated with the efficiency measurements at -10″. Both may be described as measurements of the transmission of fast neutrons through the matrix material. Comparison of Figures 11 and 12 indicates qualitative agreement. The efficiency at -10″ and EMP(N2) normalized to the empty drum response are presented in Table 1. While the EMP(N2) measurement may not be sufficient in and of itself to predict the associated efficiency, when combined with data acquired by other detector groups and cavity monitors (e.g. back scattering into the S1 and S2 detector groups, or vertical distinction by use of X1, X2, and X3) a reasonable prediction can be obtained.

Table 1. N2 Detection Efficiency for ^{252}Cf (-10″,0,18″,) and EMP responses for calibration standards.

Matrix Material	Efficiency / Empty	EMP(N2) / Empty
empty	1.00	1.00
poly-steel	0.48	0.27
ethafoam	0.35	0.29
soil	0.13	.013
water	0.022	.070
concrete	0.05	0.08

SUMMARY

An APNEA was built by LMSC under license to Lockheed Martin Energy Research. This instrument has several enhancements for data acquisition, processing and storage compared to that described by Hensley.[3] As a consequence of the instrumental flexibility, the characteristics of the response to different matrix materials in actual waste drums can be quantified more completely. It is necessary to characterize the neutron transport properties of the drum non-invasively in order to process the active and passive measurements to produce assays. In the present work that correlation is extended to other matrix materials, and, because of the normalization using the Zetatron source monitor, other detectors in the cavity provide independent information for use in the analysis.

The response of APNEA type instruments to fissile and spontaneously fissioning material in the plethora of matrix types and geometric configurations is described by a multi-variable analysis. Neutron transport characteristics of the homogeneous materials (e.g. sludge, soil, concrete) and various debris filled drums (e.g. graphite, combustibles) cannot be characterized by two or three simple neutron measurements. The analysis shown here demonstrates a new approach that exploits the variety of signals available. This weighted sum method allows rapid classification of the response of any drum in to a space defined by the set of characterization drums constructed to span the materials and geometric configurations expected of actual waste.

ACKNOWLEDGMENTS

Thanks to D. K. Steinman for many hours of stimulating discussions and shared insight. His editorial oversight is greatly appreciated. The majority of the data presented were collected by G. C. Bischoff, L. Godbee, M. D. Rubin, J. Grizzell, H. W. Hazzard, and J. A. Austin. Special recognition goes to G. C. Bischoff and L. Godbee for their willingness to endure the Idaho winter at the INEL. The assistance of W. S. Forshay in both developing data manipulation routines and analysis of data is much appreciated. His consistent ability to quickly understand and perform complex operations has been an invaluable asset.

This work was supported in whole or part by the Technology Deployment Center, a cooperative agreement between the University of South Florida, Pinellas Plant Stakeholders, Lockheed Martin, and the Pinellas County Industrial Council under agreements #DE-FC04-95AL85816 and #7903-035-LO-A.

DEVELOPMENT OF A HIGH-EFFICIENCY NEUTRON COUNTER USING NOVEL MATERIALS

M. M. Pickrell
Los Alamos National Laboratory
Safeguards Science and Technology
Group NIS-5, MS E540
Los Alamos, NM 87545 USA
505/665-5098, Fax: 505/665-4433

ABSTRACT

Neutron detection efficiency is an important figure of merit for waste assay applications that must measure small quantities of material. It is also important for neutron coincidence counting and multiplicity counting because the detection of double- and triple-correlated events scales as the detection efficiency squared and cubed, respectively. Conventional thermal neutron detection systems typically employ ^{3}He detector tubes embedded in polyethylene. The polyethylene moderates the neutrons so they can be detected by the ^{3}He tubes. However, the hydrogen in the moderator also absorbs neutrons and reduces the diffusion length. We have extensively explored alternate designs that use both polyethylene and other industrial plastics with lower concentrations of hydrogen. In MCNP studies, we have achieved higher detection efficiency by using both polyethylene and other plastics in a hybrid design. In this paper we will present the design of a nominal 30%-efficient, 200-liter neutron counter that uses a hybrid design. We will show comparison results of this design compared to a standard polyethylene design. Finally, this counter has been constructed and tested, and was used in the Los Alamos waste assay course. We will show comparisons of the experimental results from this counter to the MCNP predictions.

INTRODUCTION

The design of modern neutron counters is a sophisticated process generally involving extensive modeling with Monte Carlo codes, such as MCNP.[1-6] Depending on the particular application, different parameters will be optimized, including the neutron detection efficiency, the thermal neutron die-away time, the neutron energy dependence of the detector, and even the detector volume (for cosmic-ray considerations). These requirements must be balanced against economic issues as well.

The basic design of most neutron detectors consists of ^{3}He detector tubes embedded in a polyethylene plastic moderator.[1-3,7] Energetic neutrons enter the polyethylene and are moderated in the plastic. After moderation, the neutrons diffuse to the ^{3}He tubes where they are absorbed

and detected. The diffusion length for thermal neutrons in polyethylene is roughly 1.8 cm, so that neutrons outside of this distance from a detector tube will generally not be detected. Although polyethylene is an excellent moderator of neutrons because of the high hydrogen content, hydrogen also absorbs neutrons and reduces the detection length and detection efficiency.

For this research we designed and built a novel neutron detector. The application was a 200-liter drum counter that is capable of both passive neutron counting with the add-a-source correction and active neutron interrogation as a californium shuffler.[1,7,8] The purpose of the counter is to provide a data set for studies of data integration. We wish to explore the concept of combining multiple different measurements of the same sample and combine the results into a single, robust assay value. Much of the research into data fusion will be empirical, so it was necessary to obtain a data set of multiple measurements. This counter is providing that data set and was designed to make two different measurements. Although it has a single neutron counting chamber, it has both add-a-source and shuffler mechanisms.

The counter was built to assay 200-liter drums, as these commonly have significant matrix interference problems and therefore are a natural application for the data fusion concept.[7] In order to be cost-effective, the instrument was built into a shield cell. The shield-cell walls were used for the californium source storage. A picture of the counter is shown in Fig. 1.

Fig. 1. The drum neutron counter with both shuffler and add-a-source capability.

DESIGN CONSIDERATIONS

The design requirements for the counter were derived from the anticipated measurements. The counter was designed to measure mostly waste drums. Nominal plutonium loadings in waste drums may be quite low, approaching the 100 nCi/ gram low-level waste/transuranic (LLW/TRU) waste cutoff. In order to extend the capabilities of the waste assay, we wished to explore multiplicity neutron counting (as an extension to the more conventional coincidence counting). The nominal low plutonium levels require a small value for the lower limit of detection for the counter. The minimum detectable limit depends on several factors including the efficiency, a short die-away time, and rejection of the cosmic-ray induced neutron background. The short die-away time mitigates the effect of accidental coincidences. The accidentals rate contributes to the loss of precision, since it must be subtracted from the reals plus accidentals signal. The contribution to the background from cosmic rays may be reduced by decreasing the volume of the detector. The specification that the counter is capable of multiplicity counting requires also that the efficiency must be high (nominally 30% or better). The detection of neutron multiplicity "triples" scales as the detection efficiency cubed. Therefore, a low detection efficiency quickly compromises the multiplicity measurement.

A figure of merit function was derived to optimize the counter design for the lowest possible limit of detection. The details are given by Menlove,[9] in these proceedings and by others.[10] The final functional form for the figure of merit function was:

$$\text{FOM} = \varepsilon \left(\frac{f_g}{t\rho} \right)^{1/2} ,$$

where

ε is the totals counting efficiency,

ρ is the moderator density,

t is the moderator thickness, and

f_g is the gate fraction for a 128-ms gate length.

The counter design was optimized by improving the figure of merit function value. However, the design was strongly constrained by economic considerations as well. To contain costs, existing ^{3}He detector tubes were used rather than purchasing new ones. The existing ^{3}He

tubes had a fill pressure of only 4 atmospheres rather than the 6-atmosphere pressure that was desirable.

DESIGN PROCEDURE

The mechanics of the detector design optimization involve an iterative procedure of creating or modifying an MCNP model, evaluating the model with MCNP, and using the results to calculate the figure of merit. Then a design change is made and the process is repeated. Design changes that improve performance are kept, others are discarded. The process is repeated iteratively for all design variables. Typically, we would choose a particular variable and vary it over a range using 10 evenly spaced values in the model. These would be evaluated using MCNP, and the optimal value would be selected. Then the process would move to the next variable to optimize.

The typical parameters for detector optimization include the dimensions of the counter, the location and number of ^{3}He detector tubes, the number of rows of tubes, the spacing between the tubes, and the thickness of the polyethylene between the rows and between the tubes and the assay-chamber wall. These dimensions provide only a limited suite of adjustments that can be used to optimize detector performance. The total number of detector tubes provides an additional, very effective method of improving detector performance, but the cost of ^{3}He detectors is quite high so their excessive use must be balanced by economic considerations. With unlimited funding for detector construction it is possible to design a counter with extremely high performance but it may not always be practical.

We chose to explore other methods for increasing counter performance that are cost-effective. Our approach was to increase the number of design variables. The intent was that a more flexible design (one with more design variables) might achieve a better optimum. One aspect of neutron detector design that has not been explored extensively has been the choice of moderating material.[11,12] Polyethylene is essentially the only material used. The benefit of polyethylene is that it is the most effective practical moderator because of a very high hydrogen content. However, it also has a short neutron diffusion length for the same reason. Hydrogen absorbs thermal neutrons and the high hydrogen content reduces the diffusion length and decreases the number of neutrons detected. By contrast, other commercial plastics have a lower hydrogen concentration. These are less-effective moderators, but they have a larger diffusion length for thermal neutrons because they absorb fewer thermal neutrons.

The basis for this design was to judiciously select plastics other than polyethylene for the detector moderator material. Because moderation is important, we chose a layered design that could accommodate polyethylene and other plastics in subsequent layers. We selected a representative sample of commercial plastics to test with this design. The plastics were selected to have varying hydrogen concentrations, from a high of 0.137 grams/cm^3 for polyethylene to a low of zero for Teflon. In this fashion, the hydrogen content could be varied as a parameter by selecting the appropriate plastic. Table I lists the plastics we used and includes the hydrogen concentration in gm/cm^3 for each one. Also listed are the stoichiometric elemental compositions. The hydrogen concentrations for each of the plastics is also plotted in Fig. 2.

A base-case MCNP model was constructed for the counter. Each of the variables was optimized in a sequential fashion. Included with the optimization of the counter dimensions were the material types used for the moderator. The results from each cycle were tabulated in the figure of merit function and used to select the optimum value. Each of the design variables was optimized sequentially. Included were the number of tubes in each row, the material type

TABLE I. A Listing of the Different Types of Plastics Tested, Including the Elemental Composition and the Hydrogen Density. Elemental Composition is Listed Stoichiometrically by Fraction. Hydrogen Density is Listed by grams/cm^3.

Material Type	Density	Hydrogen	Carbon	Nitrogen	Oxygen	Fluorine	Other	H density
Polyethylene	0.96	0.667	0.333	0	0	0		0.137
Polypropylene	0.91	0.667	0.333	0	0	0		0.129
Nylon	1.14	0.578	0.316	0.053	0.053	0		0.111
Composite Nylon/Kevlar	1.16	0.558	0.335	0.053	0.053	0		0.105
Delrin	1.42	0.5	0.25	0	0.25	0		0.095
Acetal Copolymer	1.4	0.5	0.25	0	0.25	0		0.093
Polystyrene	1.05	0.515	0.485	0	0	0		0.085
Phenolic Paper	1.45	0.452	0.354	0	0.193	0		0.084
Polystyrene	1.05	0.5	0.5	0	0	0		0.081
Polybutylene Terephthalate	1.31	0.428	0.428	0	0.143	0		0.071
Lexan	1.2	0.424	0.484	0	0.091	0		0.066
PVDF Fluropolymer	1.78	0.333	0.333	0	0	0.33		0.056
PVDF Fluropolymer Composite	1.78	0.307	0.333	0	0	0.36		0.055
Polyetherimide	1.27	0.351	0.534	0.029	0.086	0		0.052
Polysulfone	1.24	0.333	0.5	0	0.125	0	.04 Sulfur	0.049
Teflon	2.16	0	0.357	0	0	0.643		0

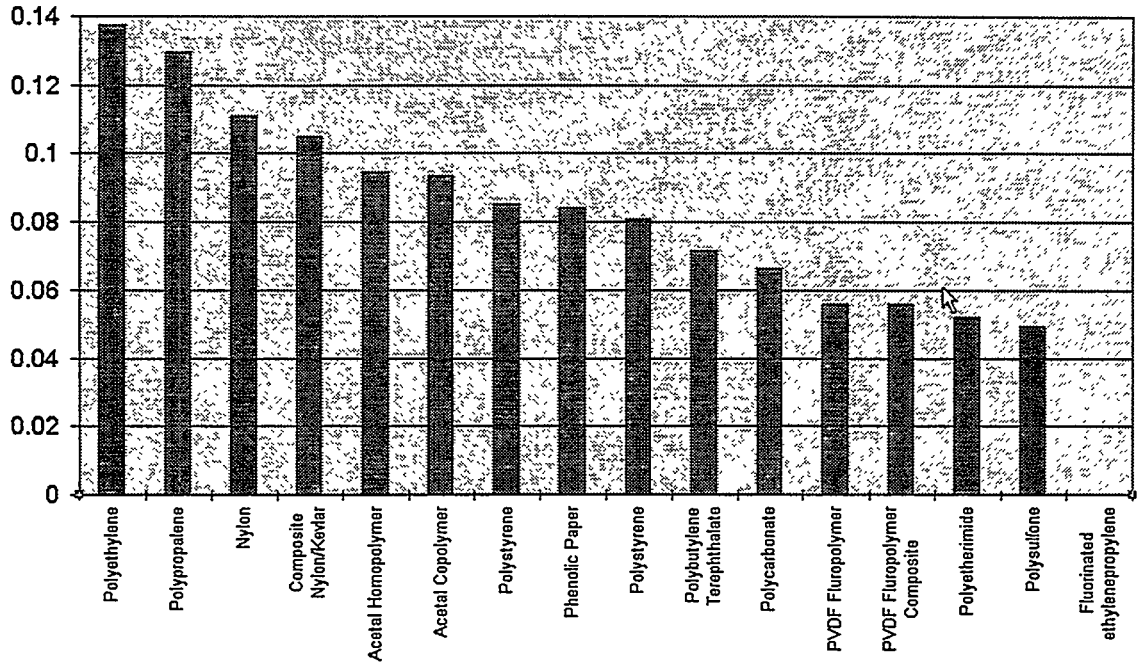

Fig. 2. The hydrogen content for each of the plastics in gram/cm^3.

for the first three layers, the distance between tubes, the separation between rows, and the separation from the tubes to the inside surface of the detection chamber. Some judgment was used in the interpretation of the results. This design differed from the counter described by Menlove[9] in these proceedings, because this system was limited to 4-atmosphere tubes. Also, the system described by Menlove was designed to be a commercial unit and the design was somewhat more conservative. This design was for a research instrument; therefore, we allowed greater risks in the design.[9,10]

COUNTER DESCRIPTION

The results of this design optimization were a new counter design that includes other plastics in addition to polyethylene. Once the design was complete, the counter was fabricated as shown in Fig. 1. The results of the MCNP design simulations agreed quite closely with the experimental results obtained when calibrating the instrument. It achieved a detection efficiency of 30% and a nominal die-away time of 65 microseconds. Output plots from MCNP of the counter design are shown in Figs. 3, 4, and 5. The final design consisted of six banks of ^{3}He detector tubes, to cover all six faces of a cubical detection chamber. The system was sized to just accommodate a 200-liter drum. Drum rotation hardware was built into the bottom of the instrument to rotate the drum during active interrogation or during the add-a-source function.

Each detector bank consists of two rows of detector tubes. The second row of tubes has half the number as the first row because the neutron density is much lower at that depth into the

counter. There are essentially three layers to the counter design. The first layer is polyethylene, which is used to moderate the neutrons from the chamber. The second layer consists of polypropylene and a row of tubes. The polypropylene has a slightly lower hydrogen content than polyethylene. The third row consists of more detector tubes embedded in a plastic called Delrin, the trade name for a common industrial plastic. This plastic has an even lower hydrogen content than either polyethylene or polypropylene. All of the plastic layers were designed to be either a single flat layer or a layer with notches that were milled out for the ^{3}He tubes. The milling process was much easier than drilling out the holes, as is often done for monolithic polyethylene systems. Then the three layers were assembled, much as a sandwich, into the final bank assembly. Figure 3 shows the counter design cross section from the top view. The four side banks are shown, each with two rows of tubes. The top and bottom banks have an identical layout.

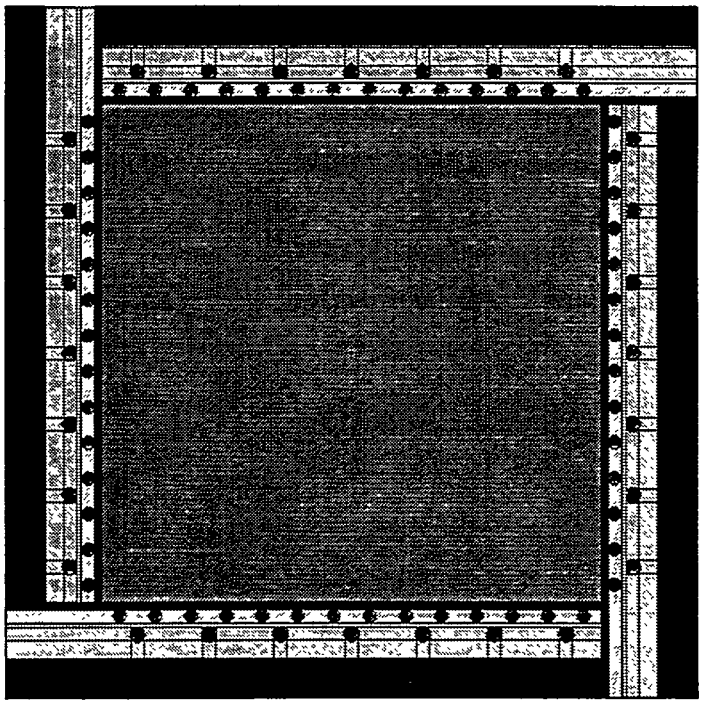

Fig. 3. MCNP output plot of the cross section of the drum counter. The four side banks are shown with two rows of detector tubes each. The inside is air, followed by polyethylene, then a layer of polypropylene and a row of tubes. The third layer consists of a row of tubes embedded in Delrin plastic.

Figure 4 shows the cross section of the detector side banks in greater detail. The three layers are seen. The first layer is polyethylene, the second is polypropylene, and the last is Delrin. In the third layer (second row of tubes) there are also annular rings of air around the detector tubes. This feature was also found to improve the efficiency. The simple fabrication of

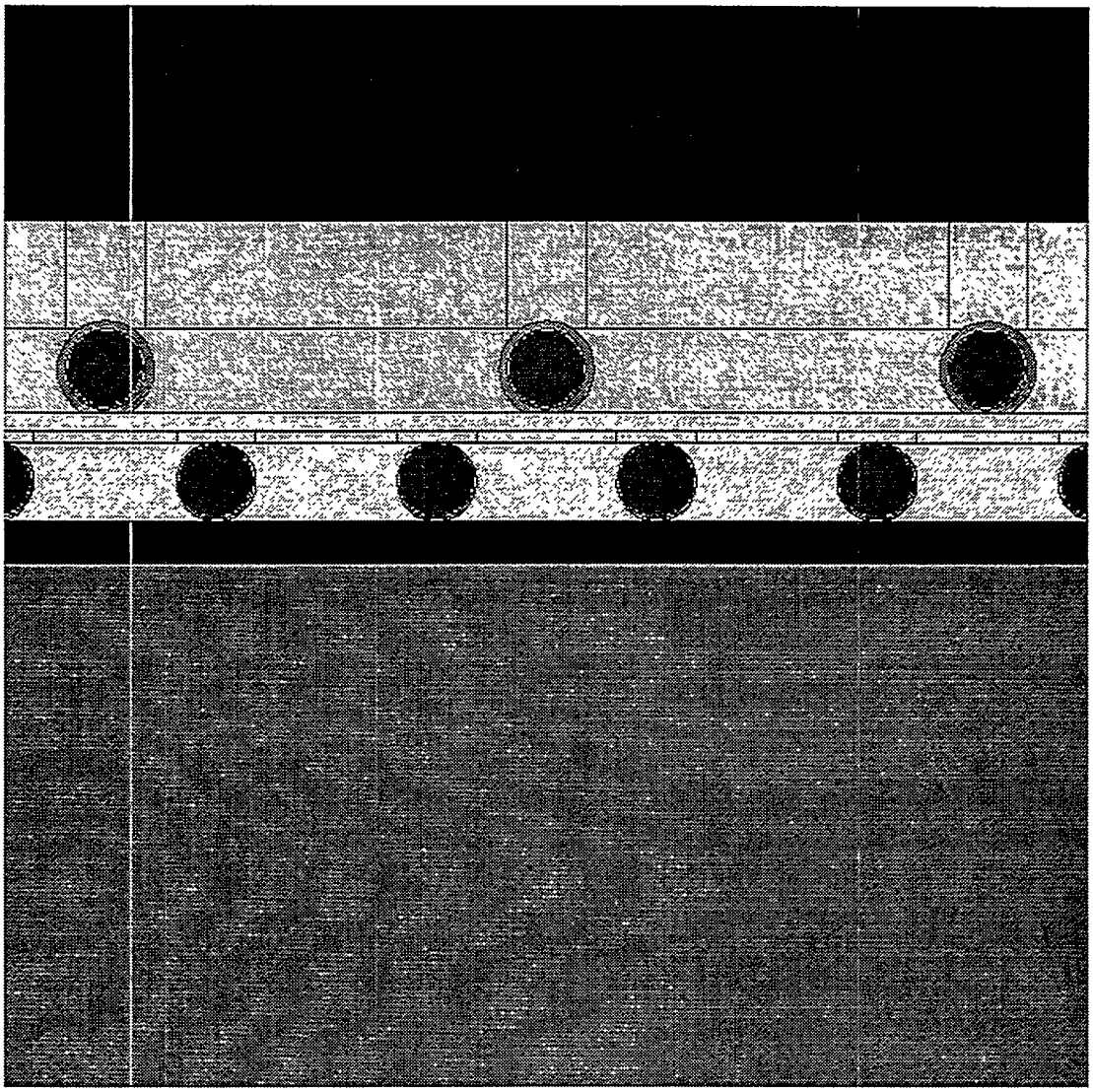

Fig .4. Close-up view of the detector design cross section. A single side bank is visible. The layers are polyethylene, polypropylene, and Delrin. Note the annular rings of air around the second row of tubes.

the detector can be seen in this diagram. The first layer of polyethylene is a straight slab of material. The second layer of polypropylene is also a flat slab, with channels milled out for the detector tubes. The milling process is significantly easier machining than drilling holes because it is easier to maintain alignment. The construction of the third layer, which is Delrin, is similar to the second. Channels are milled out of a flat piece of plastic.

The detector optimization involved varying many parameters, both the physical dimensions, which are conventional, and the material types. These variables included the number of tubes in each row (and concomitantly the spacing between tubes), the thickness of each of the layers, the fill pressure of the tubes, and the size of the annular ring of air around each tube.

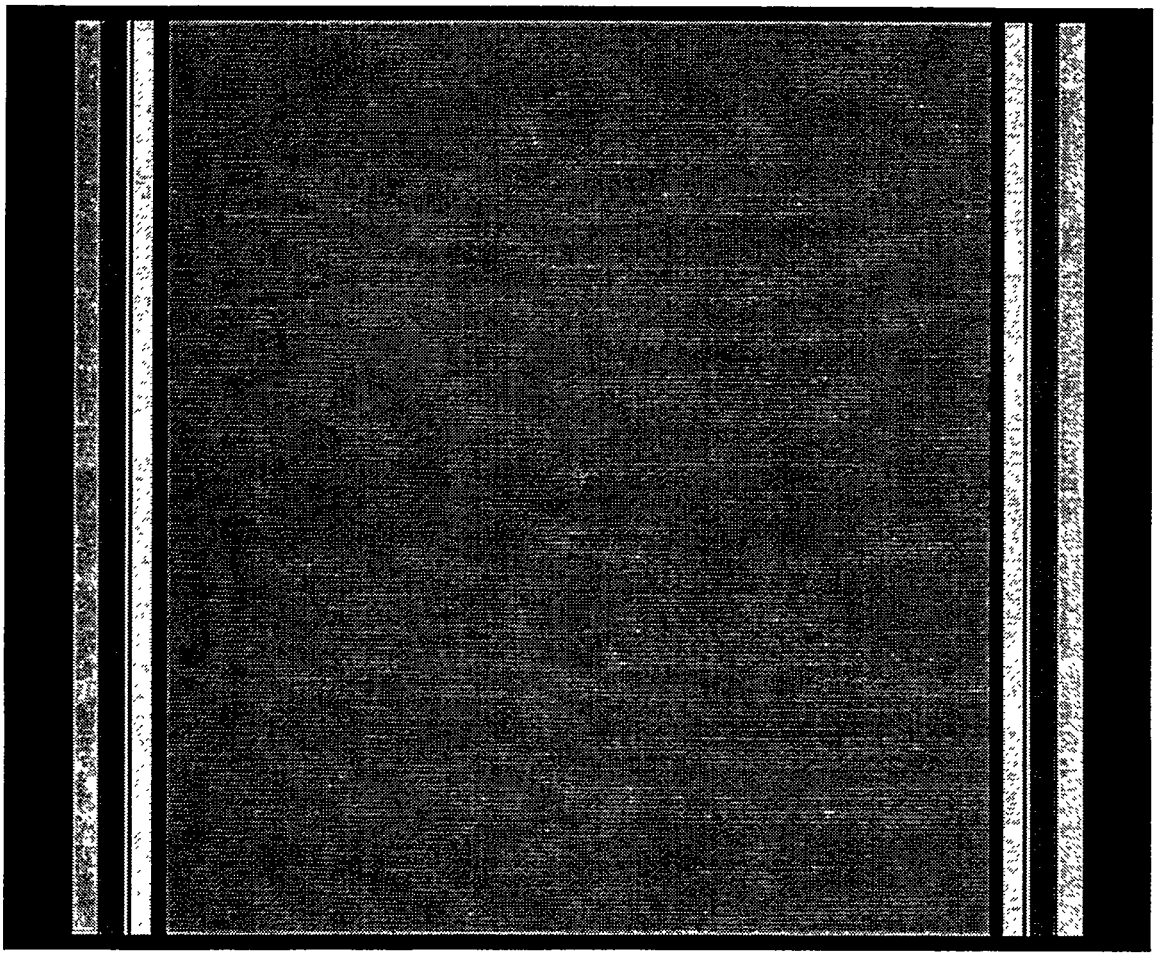

Fig. 5. Side view of the detector showing the detector tubes running vertically.

Ultimately, the fill pressure was selected at 4 atmospheres, because that was what was available. Finally, the material types were varied and the optimum value was selected in much the same way as the physical dimensions. A set of MCNP models were created that were identical in all respects except for the material type of one particular layer. The material type was different for each model. Then all (typically 15) models were processed using MCNP and the results were evaluated using the figure of merit function. The optimum material was selected and the optimization process proceeded to the next variable. The results of two typical scaling runs are shown in Figs. 6 and 7. Figure 6 plots both the efficiency and the figure of merit value for the suite of various material types used in the second layer (first row of tubes). The results show that polypropylene performs better than polyethylene: both the efficiency and the figure of merit are improved. There are two conclusions that can be drawn from these results (and they are consistent with the entire scaling study).

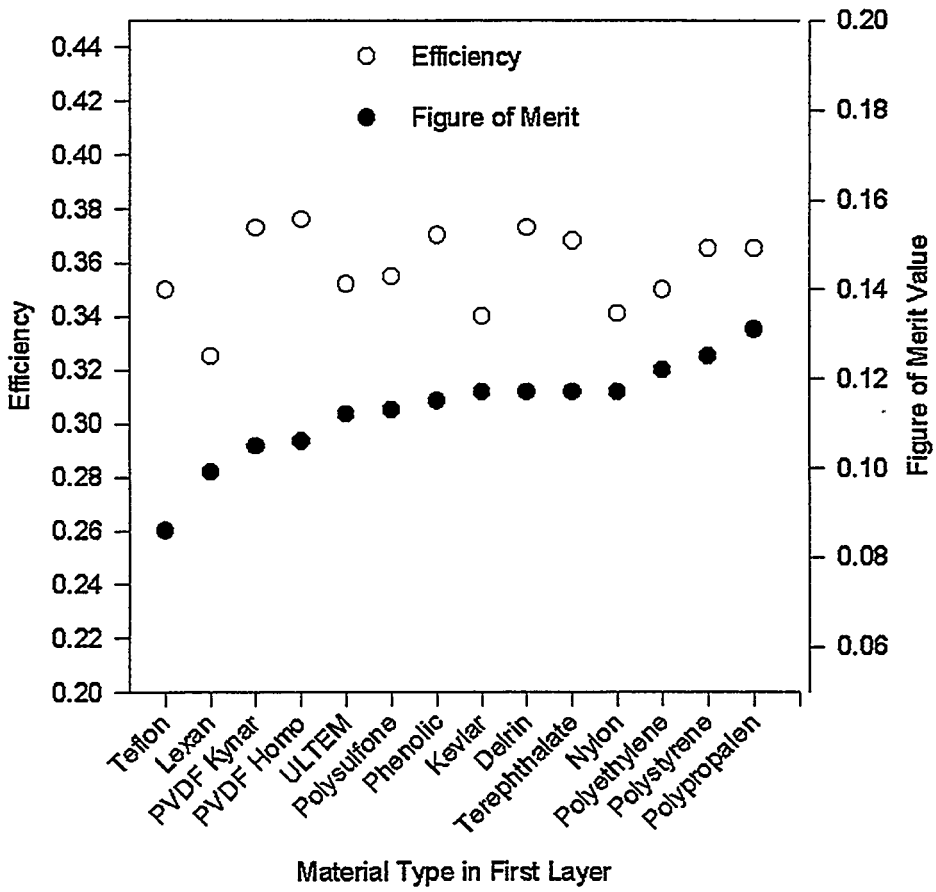

Fig. 6. Plot of the figure of merit and the efficiency for different material types in the first row of tubes.

- The selection of a different material type can improve detector performance measured both as efficiency and also the figure of merit.
- Just like any other design parameter, the improper selection of material can also degrade performance compared to polyethylene. These parameters are used for optimization, they don't necessarily guarantee improved performance.

These results were typical for the material scaling study. The results of Fig. 6 indicate that polypropylene was the optimum choice, and it was the one selected. A similar scaling was done for the material in the third layer. These results are shown in Fig. 7. We find the same effect as for the second layer. The judicious choice of material can improve the detector performance, but the improper choice can also degrade it. In this scaling there were a few materials that had significantly improved performance. The one selected to be used in the actual construction was Delrin because it was much less expensive than the other possibilities. Therefore, the materials shown in Figs. 3, 4, and 5 are polypropylene and Delrin.

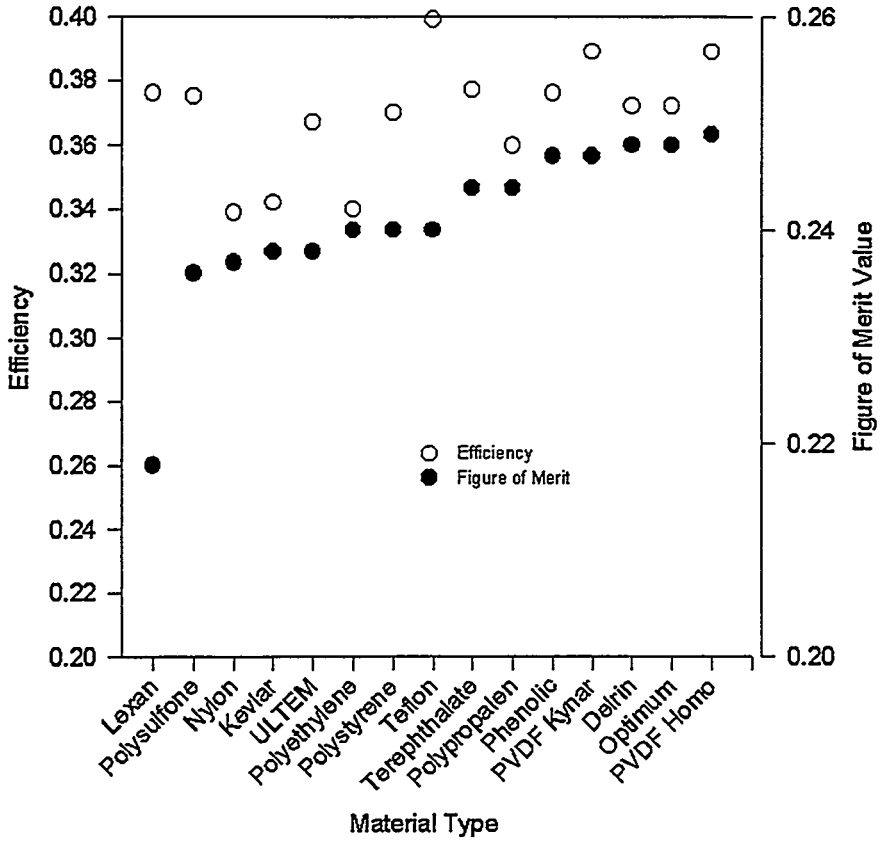

Fig. 7. Plot of the efficiency and figure of merit for various materials in the second layer of tubes.

Another observation that we draw from these results is the general pattern for optimum material selection. As the distance from the front surface becomes larger, the optimum material has a lower hydrogen concentration. For example, when the material optimization was done for the first layer, the optimum material was polyethylene; all of the new plastics had lesser performance. In the second layer, the plastic selected was polypropylene, which has only slightly lower hydrogen concentration than polyethylene (refer to Table I). Finally, in the third row, at the greatest depth into the detector from the chamber surface, the optimum materials were PVDF polymers and Delrin. These have a lower hydrogen density yet. Note that none of the optimum materials were from those with the absolute lowest hydrogen concentration, such as Teflon. Some hydrogen content is necessary for optimum performance.

One interpretation of these results is that as the neutrons transport in from the front surface of the detector, they are moderated by the moderating plastic. At the front surface they are at their highest energy, where they are incident to the detector. As they transport in, the average energy drops. Therefore, at the front surface the detector requires the greatest amount of

moderating power to moderate the energetic neutrons. However, in subsequent, deeper layers, the average neutron energy is less, and less moderation is needed. In these layers a lower hydrogen content is optimum because the moderation is not as necessary and the longer diffusion length is beneficial. Therefore, the average hydrogen content drops for layers deeper in the detector, in the optimum configuration.

These results also show that material choice can improve detector performance, but there is an important caveat. These results are strongly dependent on the nature of the figure of merit function. The potential improvement in the raw efficiency was considerably larger than the improvement in the figure of merit. With another figure of merit function, the improvement possible with different materials might be larger, or there might be none at all. The improvement achieved for this figure of merit was worthwhile for the case of the 4-atmosphere tubes. However, the benefit was diminished for the 6-atmosphere case. For the case of this research counter, the improvement achieved by using the new materials was worth the risk of a novel and untried system. However, for the commercial counter described by Menlove,[9] which used 6-atmosphere tubes, the benefit was considerably less and the conditions were different. It was a commercial counter and the design was more conservative. The outcome of whether these materials improve performance will depend largely on the figure of merit function chosen. However, the significance is that varying the material type offers another degree of freedom that offers the possibility of improved performance.

As a last test of this concept we compared several designs, with and without the new materials. A conventional polyethylene design was chosen. Then both the second and third layer material were changed as one type. This evaluation did not include the figure of merit, only the detector efficiency. The comparison is to the nominal, conventional polyethylene design. These results are shown in Fig. 8. The improvement available from the other materials is clear. The conclusion is not that material selection will always improve detector performance, but that it is a very valuable additional variable that can improve the performance relative to many figure of merit functions.

CONCLUSIONS

The conclusions from this study are as follows:

1. We have designed and built a novel neutron counter for waste assay that uses new materials. This counter will be used for data combination studies, combining active shuffler

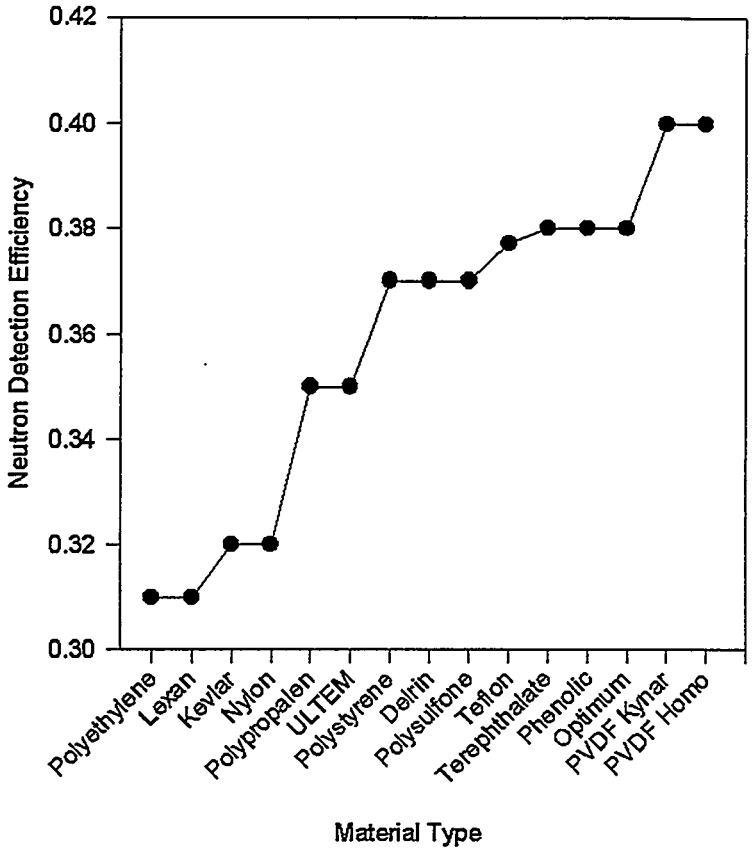

Fig. 8. The efficiency of the detector as a function of various material types. Note that this is not the figure of merit. Comparison is to polyethylene, which is the worst case. This test varied the materials in both the second and third layers.

measurements with passive neutron counting. An efficiency of 30% was achieved using 89 detector tubes with a 4-atmosphere fill pressure.

2. A novel design approach was used that included industrial plastics other than polyethylene. These plastics reduced the moderating strength but increase the diffusion length for thermal neutrons. The judicious use of these plastics increases the detection efficiency and in some cases can improve the detector performance for a particular figure of merit.
3. The use of different materials is another design variable, not a guarantee of better performance. It allows another degree of freedom in the optimization, but may improve or degrade performance depending on the conditions.
4. The general pattern for the use of materials with lower hydrogen concentration is that the hydrogen concentration drops at increasing depths into the counter. The apparent reason is that the neutron population is more moderated at the greater depths, and less moderating power is necessary.

ACKNOWLEDGMENT

This work was supported by the US Department of Energy, Office of Nonproliferation and National Security.

REFERENCES

1. P. M. Rinard, E. L. Adams, H. O. Menlove, and J. K. Sprinkle, Jr., "Characterization and Improving Passive Active Shuffler for Assays of 208-Liter Waste Drums," in Proceedings of the 14th Symposium of Safeguards and Nuclear Material Management, Salmanca, Spain, May 4-8, 1992, Los Alamos National Laboratory document LA-UR-92-1252.
2. Howard O. Menlove and George W. Eccleston, "High Sensitivity Measurements for Low Level TRU Wastes Using Advanced Passive Neutron Techniques," in Proceedings of the Transuranic Waste Characterization Conference, Pocatello, Idaho, August 10-13, 1992, Los Alamos National Laboratory document LA-UR-92-2563.
3. Norbert Ensslin, Doug Reilly, Hastings Smith, Jr., and Sarah Kreiner, eds., *Passive Nondestructive Assay of Nuclear Materials* (U.S. Regulatory Commission, Washington, D.C., March 1991).
4. Diana G. Langner, Nicholas Dytlewski, and Merlyn S. Krick, "Pyrochemical Multiplicity Counter Development," *Nucl. Mater. Manage.* XX (Proc. Issue), 438-442 (1991).
5. Harl'O M. Fisher, "A Nuclear Cross Section Data Handbook," Los Alamos National Laboratory report LA-11711-M (December 1989).
6. Judith F. Breismeister, "MCNP-A General Monte Carlo Code for Neutron and Photon Transport, Version 3A," Los Alamos National Laboratory report LA-7396-M (September 1986).
7. Howard O. Menlove, "Passive Neutron Assay Heterogeneous Waste Drums Using the Segmented Add-A-Source Method," in Proceedings of the 36th Annual Meeting of the Institute of Nuclear Materials Management, July 9-12, 1995, Los Alamos National Laboratory document LA-UR-95-1989.
8. N. Ensslin, M. E. Abhold, K. L. Coop, T. H. Prettyman, P. M. Rinard, G. A. Sheppard, and H. A. Smith, Jr., "Results from the First Waste and Residue NDA Measurements School," in Proceedings of the 37th Annual Meeting of the Institute of Nuclear Materials Management, July 28-31, 1996, Los Alamos National Laboratory document LA-UR-96-2601.
9. H. O. Menlove, D. H. Beddingfield, M. M. Pickrell, D. R. Davidson, R. D. McElroy, and D. B. Brochu, "The Design of a High Efficiency Neutron Counter for Waste Drums to Provide Optimized Sensitivity for Plutonium Assay," in Proceedings of the 5th Nondestructive Assay and Nondestructive Examination Waste Characterization Conference, Salt Lake City, January 14-16, 1997, Los Alamos National Laboratory document LA-UR-96-4585.
10. D. H. Beddingfield and H. O. Menlove, "Parametric Optimization of Neutron Drum Counter," *Nuclear Instruments & Methods in Physics Research*, A, 369 (1996) 205-214.

11. M. M. Pickrell, "Development of a Uranium Oxide Canister Counter for the Rokkasho Reprocessing Plant," in Proceedings of the 37th Annual Meeting of the Institute of Nuclear Materials Management, Naples FL, July 28-31, 1996, Los Alamos National Laboratory document LA-UR-96-2604.
12. M. M. Pickrell and H. O. Menlove, "Development of High Efficiency Neutron Counters," in Proceedings of the 34th Annual Meeting of the Institute of Nuclear Materials Management, Scottsdale, AZ, July 8-21, 1993, Los Alamos National Laboratory document LA-UR-93-2668.

PASSIVE ACTIVE NEUTRON RADIOASSAY MEASUREMENT UNCERTAINTY FOR COMBUSTIBLE AND GLASS WASTE MATRICES

Larry G. Blackwood
Yale D. Harker
Teresa R. Meachum
Woo Y. Yoon

Idaho National Engineering Laboratory, Idaho Falls, ID 83415

ABSTRACT

Using a modified statistical sampling and verification approach, the total uncertainty of the Idaho National Engineering Laboratory's Passive Active Neutron (PAN) radioassay system was evaluated for combustible and glass content codes. The waste structure and content of 100 randomly selected drums in each of the waste categories were computer modeled based on the review of real-time radiography video tapes. Specific quantities of Pu were added to the drum models according to an experimental design. These drum models were then submitted to the Monte Carlo Neutron Photon code processing and subsequent calculations to produce simulated PAN system measurements. The reported plutonium masses from the simulation runs were compared with the corresponding input masses. Analysis of the measurement errors produced uncertainty estimates. This paper presents the results of the uncertainty calculations and compares them to previous reported results obtained for graphite waste.

INTRODUCTION

At last year's NDA/NDE conference, we reported on the methods and results from a total uncertainty analysis of a Passive Active Neutron (PAN) radioassay system at the Idaho National Engineering Laboratory's (INEL) Stored Waste Examination Pilot Plant (SWEPP)[1]. That analysis was specific to the measurement of graphite molds. Since that time, similar uncertainty analyses have been completed for an additional two waste forms: combustibles and glass.

The combustible waste form includes Item Description Codes (IDC) 330 (dry paper and rags) and 336 (moist paper and rags). Upon review of real time radiography tapes of combustible filled waste drums it became clear that those drums contained numerous types of combustible material in addition to paper and rags, as well as some noncombustible items. Thus this waste form comprises considerable heterogeneity.

The glass waste analyzed consists of IDC 440, 441, and 442 drums. IDC 440 waste consists primarily of broken glass vials and related products. The code 441 and 442 drums both contain raschig rings, the only difference being that the code 442 waste has been leached while the code 441 waste has not. Compared to the combustible waste form, the glass wastes are considerably more homogeneous.

The particular methods used to perform the uncertainty analysis for the combustible and glass wastes paralleled that previously described for graphite waste. Some changes and enhancements to the methods used for graphite were implemented. Details of the procedures used are available elsewhere[2-3]. This paper provides a brief overview of the methods employed and a description of the major changes in the methods from those applied for graphite waste. The primary purpose of this paper is to present the uncertainty findings for the combustible and glass waste forms. The results for these two waste forms are compared with each other as well as with the previous findings for graphite. These comparisons will point out the broad effects of waste matrix on radioassay performance and re-emphasize the importance of including matrix effects in any system performance assessment.

PASSIVE ACTIVE NEUTRON ASSAY SYSTEM

The SWEPP PAN system is a second generation passive active neutron system developed in the early 1980's by Los Alamos National Laboratory (LANL) for the U. S. Department of Energy (DOE) and delivered to the INEL in 1983. This system was designed to assay drums containing transuranic contaminated waste.

The PAN assay system consists of a shielding housing which surrounds the drum on all four sides, top and bottom. Each side of the housing contains moderator, thermal and low-energy neutron shielding and He-3 neutron detectors. There are two types of detector assemblies contained in each side of the assay system; i.e., bare detectors (sensitive to all neutrons) and shielded detectors (sensitive to fast neutrons and insensitive to thermal and low-energy neutrons).

The assay system operates in two modes, passive and active. In the passive mode the detector assemblies (bare and shielded) are detecting neutrons produced by spontaneous fission and (α,n) interactions in the waste matrix. Differentiation between the fission neutrons and the (α,n) neutrons is accomplished by coincidence event counting. In addition to the coincidence counting, single event counting is also accumulated during the passive mode. The single event counting data are used to derive chance coincidence corrections to the coincidence data and also to arrive at a Moderator Index (MI).

In the active mode the shielded detectors are used to detect neutrons produced by stimulated fission resulting from thermal neutron interrogation. The interrogation neutron source for the active mode is a Zetatron 14 MeV neutron generator located at one corner inside the system shield enclosure. The high energy neutrons are moderated to thermal via the graphite moderator in the enclosure walls and varying amounts of moderator in the waste matrix. Also during the active mode two monitors are used to monitor the interrogation neutron flux (cavity monitor) and the effective transmission of interrogation neutrons through the contents of the drum (barrel monitor). The ratio of the cavity monitor to the barrel monitor count during active mode is referred to as the Absorber Index (AI).

The Moderator Index (from the passive mode count) and the Absorber Index (from the active mode count) are used in the analysis algorithm to arrive at correction factors which are intended to correct for moderator and absorber effects on the measured responses (both active and passive responses). The corrected responses are used to determine the measured plutonium mass. Therefore, both the active and passive counts must be completed to obtain the needed correction factors. Three measured mass values are obtained by the system for each measurement; i.e., a mass value determined from the active mode count, a mass value determined from the passive short-gate coincidence count and a mass value determined from passive long-gate coincidence count. However, not all three values are valid over the mass range and waste forms covered in SWEPP waste. A set of selection algorithms is included in the system software to determine which of the three assay values should be used in the waste certification documentation. For most waste, only the two passive mass values are considered for selection as the reported mass. The selection criterion for the reported mass is based on which of the short-gate and long-gate coincidence mass values has the smaller relative error.

MATRIX EFFECTS AND TOTAL UNCERTAINTY

The PAN system itself reports a counting statistics error based on the detector response values and an assumed Poisson distribution for counts. Beyond the counting statistics errors, there are various other contributors to the total uncertainty of a measurement. These include

- Source isotopic/chemical composition variability
- Non-uniform matrix absorption
- Non-uniform matrix moderation
- Non-uniform source distribution
- Variations in source particle size
- Significant voids in the matrix
- Shadow shielding of one region by high neutron absorption in another region
- Waste elemental composition not addressed by the calibration routine
- (α,n) source interference

Properly designed, a total uncertainty analysis will include the effects of these factors in addition to the counting statistics.

Some waste matrix effects on the system response were studied during the original calibration series and an algorithm for determining correction factors was developed by LANL. The correction factors were determined empirically using simulated waste drums in which generic materials (e.g., vermiculite, boric acid, sand, and metal scraps) were used to simulate the waste matrix. The basic assumption in the development of the simulated waste was that the matrix was uniform, the source distribution was uniform and that each waste drum was filled to near the volume capacity of the drum. Over the years, there have been small changes made to the correction factor algorithm, but the basic premises; i.e., uniform matrix and uniform source distributions, have not changed. Because the PAN reported counting statistics error does not reflect the uncertainty associated with the calibration derived matrix correction factors, and because those correction factors themselves were based on simplified assumptions regarding waste types and configurations, a more thorough analysis is required to assess the system's total uncertainty.

UNCERTAINTY ANALYSIS APPROACH

The large number of parameters with potential significant effects on assay quality precludes evaluating the PAN system's uncertainty by actual physical experimentation. Instead a calculation/simulation method was used. This computer intensive approach involves three main components: an input data set consisting of statistically generated waste drum and related measurement parameters, a computer model for the physical processes associated with each PAN assay measurement (neutron transport and temporal response), and a set of computer programs duplicating the PAN system's data processing routines (from which counting data and final mass values are obtained). The neutron transport and temporal response calculations are performed using a benchmarked neutron transport model based on the Monte Carlo Neutron Photon (MCNP) transport code[4].

The idea behind this approach is to simulate a process in which total uncertainty is established by comparing data from PAN measurements on representative drums with known contents. By analyzing the differences between the known and measured Pu quantities for the sampled drums, both the bias and precision of the system's measurements for the waste form of interest can be established. The basic steps in performing the uncertainty analysis are as follows:

1. Perform a content code specific review of probable causes of error in the PAN measurements to identify those factors which need to be included in the uncertainty analysis.
2. Review real-time radiography (RTR) video tapes, a data base of previous PAN assay results, and information provided by the waste shipper to establish either statistical distributions or appropriate values for factorial design settings for the parameters considered to have an effect on the assay results.
3. Develop a composite statistical model incorporating the variances and correlations of the distribution-based parameters identified in (1) and (2).
4. From the statistical model developed in (3), generate sets of simulated values for the distribution-based parameters by random sampling. Combine these values with assigned values for the factorial design variables to produce a complete set of parameter settings for each of 100 simulated waste drums.
5. For each simulated waste drum in the set from (4), apply the MCNP model of the PAN assay system to determine the basic efficiencies and temporal responses of the assay system.

using the same basic approach as that for the simulated waste drums. Comparison of the simulated PAN results to the known PAN results for the calibration runs thus provides a check on the validity of the simulation process.

Other major differences between the approach used for combustible and glass wastes compared to that used previously for graphite include the number of drums simulated and the use of factorial design factors. The graphite analysis was based on 50 simulated waste drums; 100 cases were used for combustibles and glass. Adding cases was made possible by increased calculation efficiencies and has the benefit of giving more accurate results. Factorial design parameter settings were not used in the graphite analysis. For combustibles and glass, Pu quantity, Pu in chunks vs. fines, and moisture content (combustibles only) were determined according to a factorial experimental design. Treating moisture as a factorial effect was necessitated by the inability to detect it in the RTR reviews. The same is true for Pu in fines vs. chunks. Pu quantity was treated as a factorial effect primarily to gain better control over the quality of the uncertainty estimates at particular Pu levels.

While the PAN system operates in both active and passive modes, the current uncertainty analysis considers only the passive system response. Work on assessing the active mode uncertainty is ongoing.

UNCERTAINTY ANALYSIS RESULTS FOR COMBUSTIBLE WASTE

For brevity, the Pu quantity specified for each simulated drum will generally be referred to in this section as the "actual" or "true" quantity, and the simulated PAN system measurement result as simply the "PAN Pu" quantity. The true vs. PAN measured Pu quantities are plotted in Figure 1. The line of perfect agreement specified in the plot indicates where the data would fall if there were no measurement bias and/or precision error. The second line in the plot is a regression line fit to the data using the method described below. That the regression line falls below the line of perfect agreement indicates a negative bias exists in the PAN system results. The degree of the scatter in the points about the regression line is an indicator of the degree of precision in the measurements.

Bias and precision in the results can be quantified by considering the following basic mathematical model for the data in Figure 1

6. For each case in the set from (4), input the results from the MCNP model produced in (5) and other parameters from the statistical model into the simulation routine of the assay system response to determine the basic counting data that would be produced by the PAN assay system under the conditions specified.
7. Apply the PAN assay system analysis algorithm to the set of counting data produced in (6) to determine the measured plutonium mass. Compare that mass to the mass used as input to the simulation process (i.e., the true plutonium mass).
8. Analyze the results from all the specified cases to arrive at the total uncertainty which can be assigned to the measured plutonium mass for the waste form being studied.

In the previous analysis of graphite waste, the statistical model used to produce the simulated drum parameters (steps 3 and 4 above) was established by sampling strictly from theoretical distributions for all relevant parameters. The distributions assigned to each of these parameters as well as their correlations with one another were based on the statistical analysis of data from previous PAN assay results. That is, the theoretical distributions were obtained from data pertaining to actual waste drums and then used to generate a specific computer simulated representative sample of drum characteristics. For the combustible and glass waste forms a more direct method of creating most of the matrix characteristics for the representative computer simulated drums was used. A random sample of RTR tapes was obtained and the sampled drums were modeled directly (instead of assigning theoretical distributions to each matrix characteristic). This assures a realistic representative sample of each characteristic's values and their correlations with one another without the necessity of fitting theoretical distributions and sampling from them. (In effect we are using an empirical model for the statistical distributions and correlations of parameters). For characteristics not obtained from the RTR tape reviews (e.g. background radiation levels, (α, n) singles counts, etc.), theoretical distributions were still used. This change in methodology is more straightforward and more easily accommodates the more heterogeneous configurations found in combustible and glass wastes as compared to graphite.

As a check on the validity of the simulation approach for a particular content code, the simulation process is benchmarked against actual measurements on a calibration drum. The calibration drum is an actual drum built of known contents to approximate the matrix configuration found in a typical drum of the waste form under study. Measurements of the calibration drum using the PAN system are obtained with Pu sources with known properties placed in the drum. The quantities and locations of the Pu sources are varied from run to run. The calibration runs are also computer modeled

$$y_i = \alpha + \beta(x_i) + \varepsilon_i \quad (1)$$

where y_i is the PAN system Pu measurement for drum i and x_i is the true Pu quantity in the drum. The parameters α and β relate to the bias in the measurement process. If $\alpha \neq 0$ and $\beta = 1$, then there is a constant bias in the measurement system. If $\alpha = 0$ and $\beta \neq 1$, then there is constant relative bias in the system. It is also possible to have both constant and relative bias terms at the same time. The term ε_i in the model is the random error component of the measurement. Precision of the measurement system is evaluated by considering the variance (or equivalently the standard deviation) of the ε_i values.

Figure 1. PAN Pu measurements vs. true Pu quantity for the simulated combustible waste drums

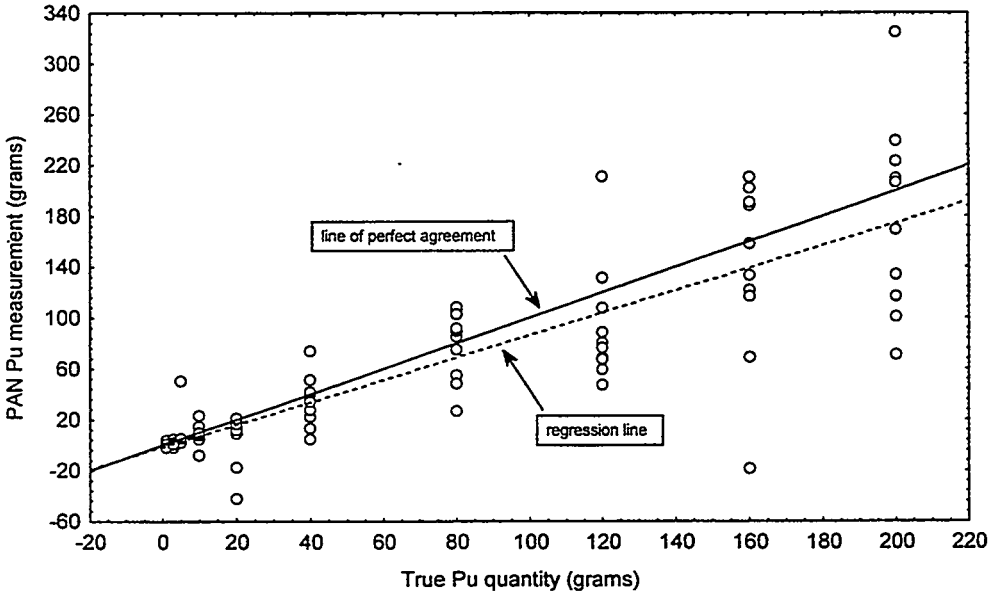

Using this basic measurement model for the PAN system, bias and precision can be evaluated by applying appropriate statistical analysis to the data from the simulations. These calculations are described in detail below.

Bias

Simply defined, bias is the expected difference between the measured and actual Pu quantities. Thus it can be assessed more directly by subtracting the true Pu quantity x_i from both sides of Equation 1 to give:

$$y_i - x_i = \alpha + \beta(x_i) - x_i + \varepsilon_i$$
$$= \alpha + \beta^*(x_i) + \varepsilon_i \qquad (2)$$

where $\beta^* = \beta - 1$. The meanings of α and ε_i remain the same as before. β^* still relates to relative bias, but now no relative bias results in a value of 0 for β^*. Based on this equation then, the bias in a PAN measurement of x grams Pu is simply $\alpha + \beta^*(x)$, the expected value of Equation 2. Since the parameters α and β^* are not known they must be estimated using regression techniques applied to the simulated waste drum data.

The data for the revised model in Equation 2 are plotted in Figure 2. If there were no bias in the measurements, the data in Figure 2 would be centered around the line of perfect agreement. (Variability about the line represents the random error or precision of the measurements.) That the data points tend to fall below this line indicates once again a negative bias in the PAN measurement system.

Figure 2. Bias in the PAN system measurements for the simulated combustible waste drums

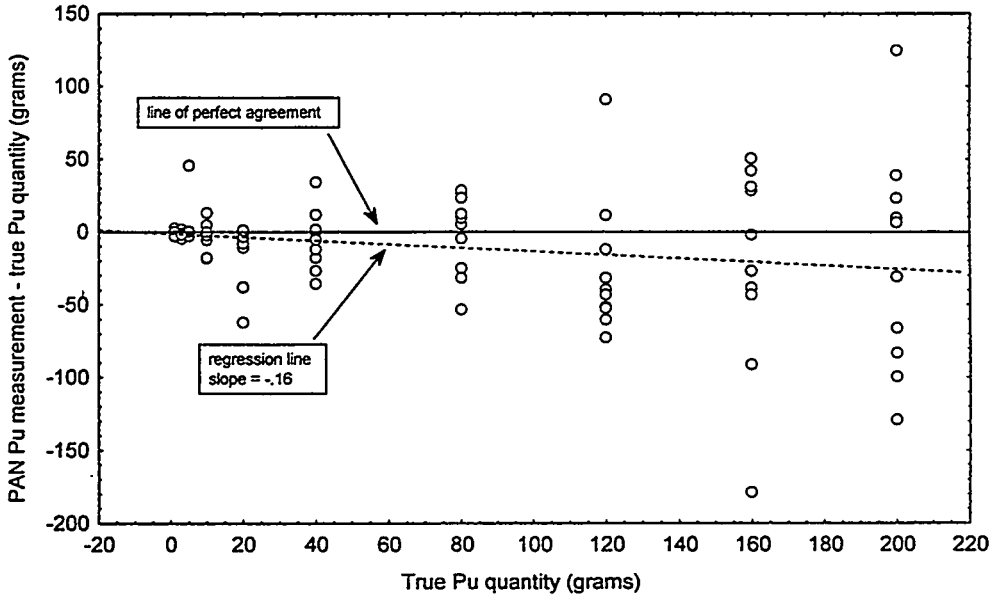

A regression analysis was performed to estimate the parameters α and β^* in Equation 2. Since the variability of the data increases with increasing true Pu quantity, a weighted least squares analysis was performed[5]. Ideally, weights should be $1/\sigma_x^2$ where σ_x^2 is the variance of ε for a given value of x.

Note that these variances are also the desired precision estimates for the PAN system (as defined in Equation 1). Since these values are not known, they must be estimated. The method of estimation is described in the section on precision below.

Weighted Least Squares Results

Using the weights defined by the precision estimates, a weighted least squares analysis of the model in Equation 2 was performed. The first test in the analysis was to consider the presence of a quadratic effect in the bias trend as a means of assessing the validity of the linear model stated in Equation 2. The test for a quadratic effect had a p-value of .45. Hence there is no indication of significant departure from linearity in the bias trend (i.e., Equation 2 is an appropriate model for the data).

Fitting a strictly linear equation to the data produced an estimate of α that was not significantly different from zero ($p = .89$), hence that parameter was dropped from the model. In the reduced model with α set to zero, the effect of β^* was highly significant ($p = .01$). Substituting 0 for α and the estimated value of -0.16 for β^* into Equation 2 and taking expectations of both sides gives the following simple model for bias in the PAN system for combustible waste.

$$\text{Bias}_{\text{combustible}} = -0.16(\text{true Pu mass}). \quad (3)$$

In other words, for combustible waste the PAN system produces measured values that are 16% lower than the true Pu quantities. The standard error of the estimated value for β^* is .062, so an approximate 95% confidence interval on the -16% relative error value is (-28%, -4%). The large inaccuracy in the bias estimate is due to the large variability in the data.

Precision

As indicated in Figure 2, variability of the PAN response for the combustible measurements increases with increasing Pu mass. Hence precision was estimated by fitting an appropriate smooth function to standard deviations calculated for each of the 10 sets of 10 replicate Pu mass measurements (1, 3, 5, 10, 20, 40, 80, 120, 160, and 200g). These data are plotted in Figure 3.

Figure 3. Standard deviations of replicate data for the simulated combustible waste drums

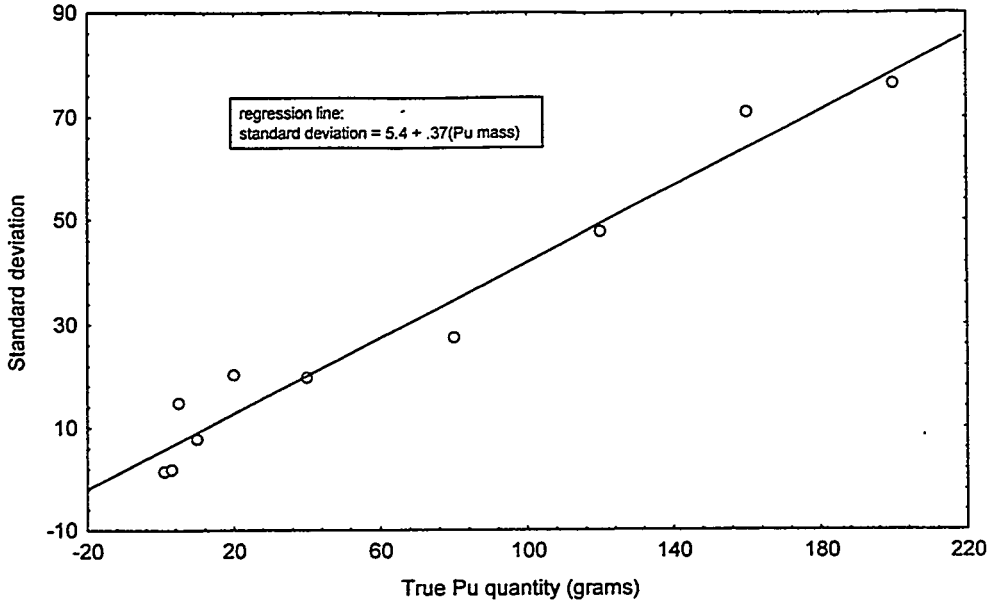

A linear regression line fit to the data produced the following equation for expressing precision of the PAN system for combustible waste drums:

$$\text{standard deviation}_{\text{combustible}} = 5.4 + .37(\text{true Pu mass}). \quad (4)$$

The intercept term in the equation did not quite meet the .05 level of significance ($p = .06$), but was left in because of the known fact that a certain amount of variability will occur even in repeat measurements on an empty drum. (Excluding an intercept term would produce zero variability at zero grams Pu). A test of a quadratic effect was non-significant, indicating the appropriateness of representing the relationship with a linear function. In addition to its use as a representation of precision for combustible drum measurements in the PAN system, Equation 4 was also used to derive the weights used in the weighted least squares regression for bias estimation in the previous section.

Comparison to Counting Statistics Error

It is of interest to compare the precision estimates obtained from Equation 4 to the standard deviations reported automatically by the PAN system. The PAN system estimates of standard deviations include variability due to counting statistics only. Since standard deviations obtained from Equation 4 also include matrix effects etc., they should in general be larger than the PAN reported values. The PAN

reported standard deviations are plotted in Figure 4. A weighted least squares fit to the PAN data is also plotted and compared to the formula in Equation 4. The plot shows the values from Equation 4 exceed the PAN fitted value line over the entire range plotted. The distance between the line increases gradually with Pu quantity. The amount of this increase in standard deviation due to matrix effects varies from approximately 5g at low Pu quantities to 10g at 200g Pu.

Figure 4. Comparison of Equation 4 results and PAN reported standard deviations for the simulated combustible waste drums

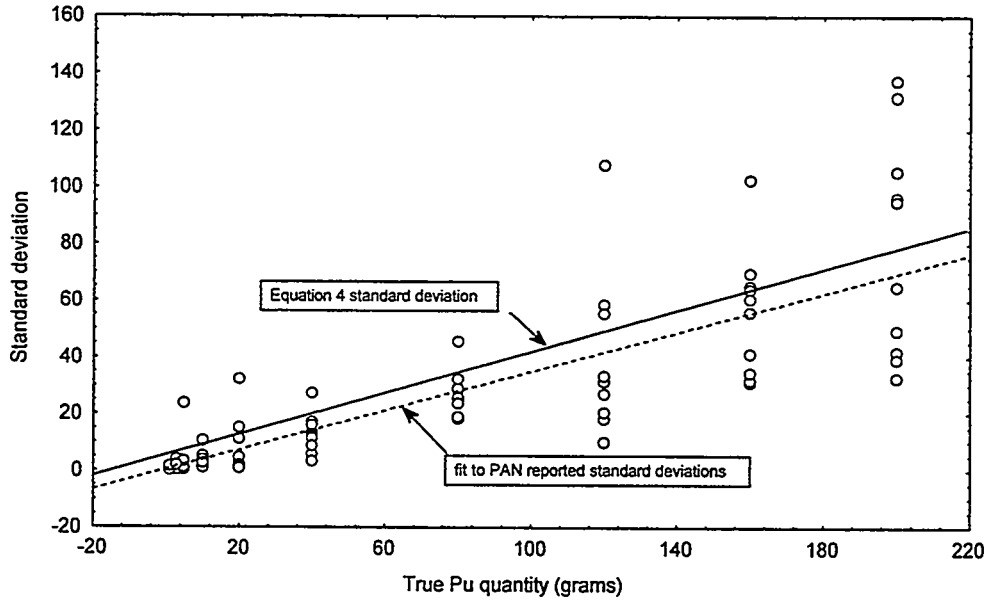

It should be noted that one major matrix-related parameter contributing to the precision error is the (α,n) singles rate. The variability in this rate also affects the counting statistics error reported by the PAN system. So in that regard the reported counting statistics error actually already contains some additional variability (i.e. that due to (α,n) interference).

Matrix Parameter Effects on Uncertainty

The analysis of data related to Equations 1 and 2 established a relationship between the error in a combustible waste measurement and the Pu quantity being measured. It is also of interest to consider whether any of the matrix parameters have consistent effects on the measurement error $y_i - x_i$. This was accomplished by performing a statistical analysis using key matrix parameters determining the simulated combustible waste drum configurations. These include dichotomous design parameters (presence or

absence of added moisture and whether or not the plutonium occurs in fines or chunks) and continuous modeled parameters (absorber index, fill height, the shielded and system (α, n) singles rates, Pu-240 mass fraction, and the mass fractions of the 25 other elements making up the matrices in the drums).

Note that effects of the various parameters, especially the elemental mass fractions are not independent (because of the requirement that the mass fractions sum to unity, when one percentage goes up, the remaining ones must go down). To specify the effects in detail, a complicated mixture model analysis of variance would be needed. But for the purpose of this analysis (i.e., to get a general idea of which parameters have noticeable effects), examination of the individual effects using t-tests, correlations, and other methods, interpreting them in light of the known dependencies, is sufficient.

Parameter Effects on Bias

Because Equations 2 and 3 specifies a known effect of Pu quantity on the error, the quantities $y_i - x_i$ were adjusted prior to the analysis of parameter effects using the formula:

$$\text{adjusted value} = y_i - x_i + .16(x_i). \quad (5)$$

In regression terms the adjusted values are the residual values remaining from the regression analysis of the model in Equation 2. The residuals are essentially measurement errors adjusted for the bias due to Pu quantity. Hence the results below refer to the effects of other matrix parameters after the previously identified effect of Pu quantity has been taken into account. The result is that any significant effects identified will indicate bias effects of the matrix parameters that are in addition to the bias due to Pu quantity.

Neither of the dichotomous design parameters had significant effects on the bias of the PAN measurements. For added moisture vs. no added moisture, the t-test for differences in bias had a p-value of .30. The p-value for the t-test of Pu in chunks or fines was .37.

Effects of the continuous scale parameters were tested using Pearson's r correlation coefficient. Parameters with significant ($p < .05$) or nearly significant ($.05 < p < .10$) are listed in Table 1. The p-values given are for the test of the null hypothesis that the correlation is zero. Thus, low p-values (e.g., $p < .05$) indicate statistically significant correlations.

Table 1. Significant or near significant correlations of matrix parameters with adjusted deviation data (indicating effects on bias) for simulated combustible waste drums.

Matrix parameter	Correlation	p-value
Fill height	-.36	.00
System (α,n) singles rate	.18	.08
Shielded (α,n) singles rate	.18	.07
Mass fraction, lead	-.48	.00
Mass fraction, sulfur	.35	.03

As might be expected due to lead's shielding properties, the strongest correlation with bias was a negative correlation with lead mass fraction. While the correlation of bias with lead mass fraction is strong, it is largely due to one drum with a very high lead content (mass fraction = .54 for a drum containing a large quantity of lead tape). The range of lead mass fractions for the remaining 99 drums (0.0 to .20) had little systematic effect on bias. A similar situation exists for the correlation with sulfur, in that it was also due to a single outlier among the 100 cases, without which the correlation is not significant. Fill height's negative correlation with bias is in contrast to the significant positive correlation found previously with graphite waste.

The equality of the system and shielded (α,n) correlations is due to the high correlation of these values with each other. The average effect on the adjusted bias due to (α, n) count ranges from about -4 grams Pu for smaller (α, n) count values to 30 grams for the largest (α, n) count values.

The (α, n) interference is an inherent problem with coincidence systems as used in the PAN passive mode. In order to get sufficient sensitivity with the He-3 detectors mounted inside polyethylene moderators it is necessary to operate the coincidence units with relatively wide gate widths (i.e., 35μs for short-gate coincidence and 250μs for long-gate coincidence). Normal coincidence systems used in nuclear physics applications operate with gate widths which are much smaller (e.g., 5μs or less). Therefore, the probability for chance coincidence counts are much higher with the wider gate widths. Obtaining the real coincidence rate with the PAN gate widths becomes a problem of taking the difference between two large statistically varying numbers and therefore the difference will be highly uncertain. This effect is expected to be more pronounced on the precision of a coincidence measurement as shown in the next section. However, it does affect the bias as well.

Parameter Effects on Precision

To assess the effects of the categorical experimental design parameters on precision in the combustible measurements, standard deviations of the adjusted difference values given in Equation 5 were calculated and compared using F-tests. Since there were no replicate measurements of PAN results for specific values of the continuous scale parameters, their effects were examined by considering correlations with the absolute values of the adjusted differences calculated in Equation 5. The absolute value of a difference can be interpreted essentially as a standard deviation estimate based on a single observation. Thus, parameters with large effects on precision errors should show significant correlations with the expected magnitude (i.e., absolute value) of the differences between measured and observed values. Because the standard deviation of differences is known to vary by Pu quantity as described earlier, the difference values obtained from Equation 5 were normalized prior to analysis by dividing by the standard deviation for the relevant Pu mass as calculated in Equation 4. Thus the correlations represent effects of the parameters on precision in excess of that attributable to Pu mass.

The difference between standard deviations of the adjusted absolute deviations for drums with and without added moisture was small and not statistically significant ($p = .69$). For drums with Pu in fines vs. chunks, the difference in standard deviations was considerable and highly significant ($p = .000$). For drums with Pu fines, the standard deviation was 25 compared to a value of 47 for drums with chunks.

Significant ($p < .05$) correlations of matrix parameters with the adjusted and normalized absolute deviations are given in Table 2. The (α, n) singles rates show the largest correlation with precision error. (As, with the bias correlations, the values for shielded and system counts are equal due to their high correlation with each other.) All the correlation values, except for copper mass fraction, show positive correlations.

Table 2. Significant correlations of matrix parameters with adjusted and normalized absolute deviations (indicating effects on precision) for simulated combustible waste drums.

Matrix parameter	Correlation	p-value
System (α,n) singles rate	.43	.00
Shielded (α,n) singles rate	.43	.00
Mass fraction, copper	-.26	.02
Mass fraction, iron	.40	.01
Mass fraction, manganese	.24	.04

The (α, n) interference effect was expected as explained in the previous section. However, the effect of the metals (copper, iron, and manganese) are somewhat surprising considering they are minor constituents in combustible waste. This points to the fact that their transport properties (i.e., elastic scattering, inelastic scattering and absorption) must be considered in any simulation of system performance.

Propagation of Total Uncertainty for Measured Mass Values

In the previous sections, bias and precision estimates for the combustible drums are reported relative to the true Pu mass (i.e., the mass specified in the simulation). It is also helpful to convert these estimates so that they are relative to the measured Pu mass. Then, given the measured mass, we can calculate a confidence interval (based on the total uncertainty) within which the true mass is expected to fall. These calculations were obtained as follows.

Based on Equation 3, the expected bias can be restated as

$$\text{(measured Pu mass) - (true Pu mass)} = -.16\text{(true Pu mass)}. \tag{6}$$

Solving for the true Pu mass gives

$$\text{true Pu mass} = 1.19\text{(measured Pu mass)}. \tag{7}$$

The applicable precision for a particular measured Pu mass is the standard deviation specified in Equation 4 applied to the bias corrected mass value:

$$\begin{aligned}\text{standard deviation} &= 5.4 + .37(1.19\text{(measured Pu mass)}) \\ &= 5.4 + .435\text{(measured Pu mass)}.\end{aligned} \tag{8}$$

To get approximate 95% uncertainty bounds on a measured mass value, consider propagation of error for Equation 7, acknowledging that both the measured Pu mass and the bias parameter have associated precision error. Treating the bias as a parameter, Equation 7 can be restated as

$$\text{true Pu mass} = (1 + b)^{-1}(\text{measured Pu mass}) \tag{9}$$

where $b = -.16$ with standard error $s_b = .062$.

Let s_{true} be the standard deviation obtained from Equation 8. Taking partial derivatives of Equation 9 with respect to b and the measured Pu mass, and applying standard propagation of error formulas yields the following equation for the standard deviation of the adjusted measured Pu quantity:

$$s_{adjPu} = [((1+ b)^{-1})^2(s_{true})^2 + ((\text{measured Pu mass})(1 + b)^{-2})^2(s_b)^2]^{1/2} \tag{10}$$

Substituting the previously estimated values for b, s_{true}, and s_b for combustibles gives

$$\begin{aligned} s_{adjPu(combustible)} &= [((1 - .162)^{-1})^2(5.408 + .365(1.193(\text{measured Pu mass}))^2 \\ &\quad + ((\text{measured Pu mass})(1 - .162)^{-2})^2(.062)^2]^{1/2} \\ &= [41.6 + 6.71(\text{measured Pu mass}) + .278(\text{measured Pu mass})^2]^{1/2}. \end{aligned} \tag{11}$$

(Note for precision in calculation, more decimal places than previously shown are given for the parameter estimates in Equation 11.) An approximate 95% confidence interval for the true mass is:

$$1.19(\text{measured Pu mass}) \pm 2s_{adjPu(combustible)}. \tag{12}$$

Using the results of this evaluation we can make comparisons with performance criteria as established in Table 9-1 of the TRU Waste Characterization Quality Assurance Program Plan (QAPP) (DOE, 1995). The parameter of interest in this table is "Total Uncertainty" which is what has been evaluated in this report. The performance criteria are given in terms of total alpha activity, but we can make limited comparisons based on Pu mass. Shown in Figure 5 is the confidence interval for the true Pu mass plotted against the measured Pu mass. Also shown on this figure are the upper and lower limits as contained in the Table 9-1 of the QAPP. This figure shows that the performance criteria (based on Pu mass only) cannot be met for PAN measurements on drums containing combustible waste.

Figure 5. Uncertainty bounds for combustible drum measurements
(bias adjusted and accounting for uncertainty in bias estimate)

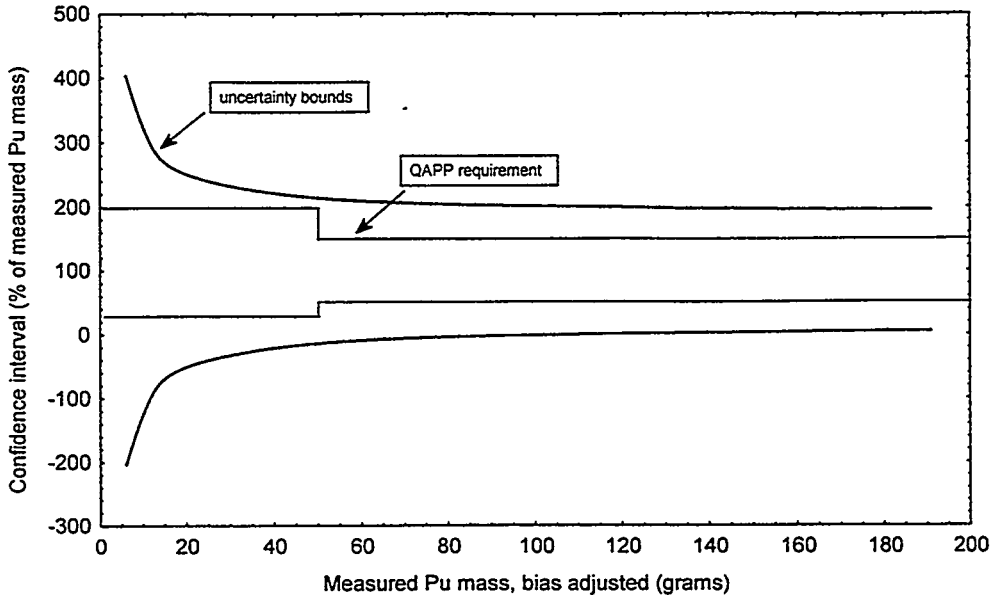

New criteria have recently been proposed for Table 9-1 of the QAPP. These criteria only impose restrictions on the bias component of the total uncertainty. These criteria vary by activity level. The most restrictive of these criteria indicate that the smallest allowable lower limit on the 95% confidence interval for relative bias is -33% and the maximum allowable upper limit is 150%. As stated above, the expected bias for combustibles is -16% with a standard error of 6%. An approximate 95% confidence interval for the true bias is then (-28%, -4%). This interval applies to all mass levels. Hence the new criteria for Table 9-1 can be met.

In order to be critically safe, there is a safety limit requiring that the measured Pu mass plus $2s_\varepsilon$ (i.e., the upper bound in Figure 5) must not exceed 200g. Based on the equations used to derive Figure 5 the measured mass must be below 83g in order to meet this criterion for drums containing combustible waste. This requirement does not present much of a limitation for combustible waste drums as only two of the over 900 drums in the PAN data base used for this study exceeded 83g.

UNCERTAINTY ANALYSIS RESULTS FOR GLASS WASTE

The uncertainty analysis for the simulated glass waste drums followed the same procedures as that for the combustible waste. Thus presentation of the results for the glass drums given below closely

follows that for the combustible drums, except that the development of the modeling and analysis methods is not repeated.

The true vs. PAN measured Pu quantities for the glass waste drums are plotted in Figure 6, and their differences in Figure 7. As observed previously with the combustibles, the regression line for the glass data falls below the line of perfect agreement, indicating a negative bias exists in the PAN system results. The glass data exhibit greater bias but less variability than the combustible data.

Bias

Using the weights defined by the precision estimates given below, a weighted least squares analysis of the model in Equation 2 was performed for the glass data. The first test in the analysis was to consider the presence of a quadratic effect in the bias trend as a means of assessing the validity of the linear model stated in Equation 2. The test for a quadratic effect had a p-value of .90. Hence there is no indication of significant departure from linearity in the bias trend (i.e., Equation 2 is an appropriate model for the glass data).

Fitting a strictly linear equation to the glass data produced an estimate of α that was not significantly different from zero ($p = .43$), hence that parameter was dropped from the model. In the reduced model with α set to zero, the effect of β^* was highly significant ($p < .001$). Substituting 0 for α and the estimated value of -0.24 for β^* into Equation 2 and taking expectations of both sides gives the following simple model for bias in the PAN system for glass drums

$$\text{bias}_{\text{glass}} = -0.24(\text{true Pu mass}). \qquad (13)$$

In other words, for glass waste the PAN system produces measured values that are 24% lower than the true Pu quantities. The standard error of the estimated value for β^* is .028, so an approximate 95% confidence interval on the -24% relative error value is (-30%,-18%).

Figure 6. PAN Pu measurements vs. true Pu quantity for the simulated glass waste drums

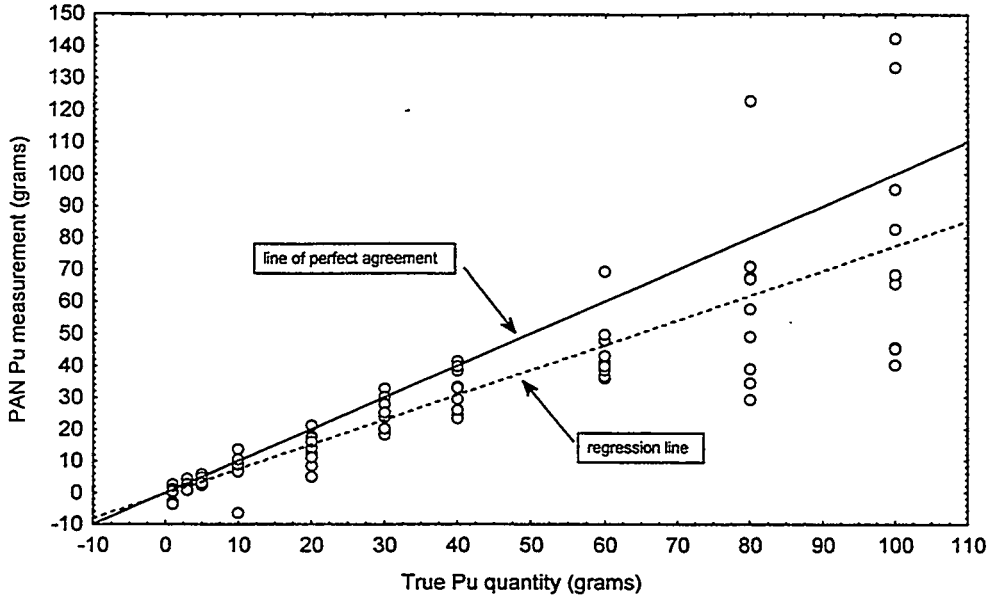

Figure 7. Bias in the PAN system measurements for the simulated glass waste drums

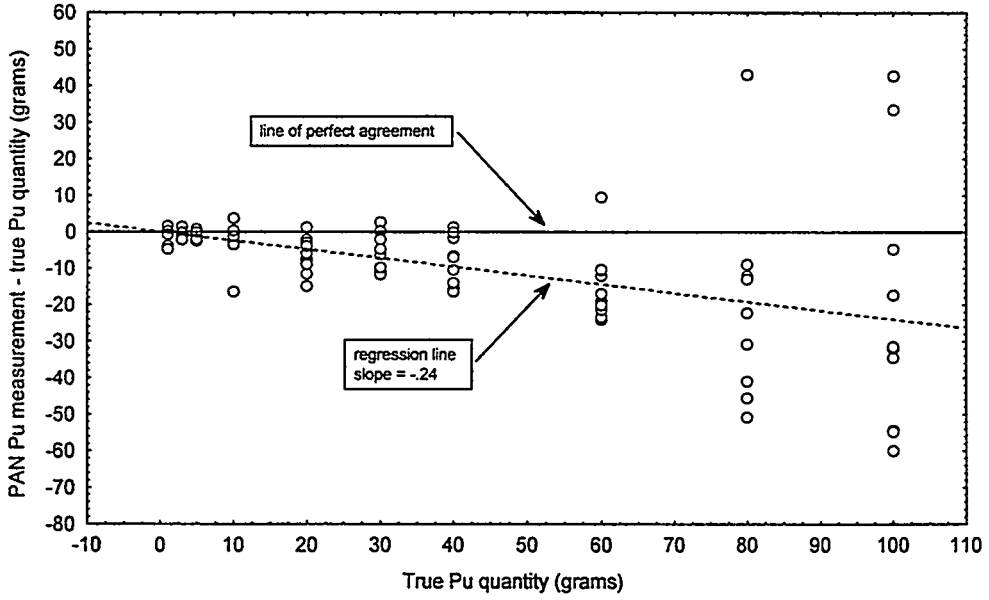

Precision

As indicated in Figure 7, variability of the PAN response increases with increasing Pu mass. Hence precision was estimated by fitting an appropriate smooth function to standard deviations

calculated for each of the 10 sets of 10 replicate Pu mass measurements (1, 3, 5, 10, 20, 30, 40, 60, 80, and 100g). (These gram quantities were different than that used for the combustible waste to better reflect the cover the range of Pu quantities found in glass waste.) These data are plotted in Figure 8.

Figure 8. Standard deviations of replicate data for the simulated glass waste drums

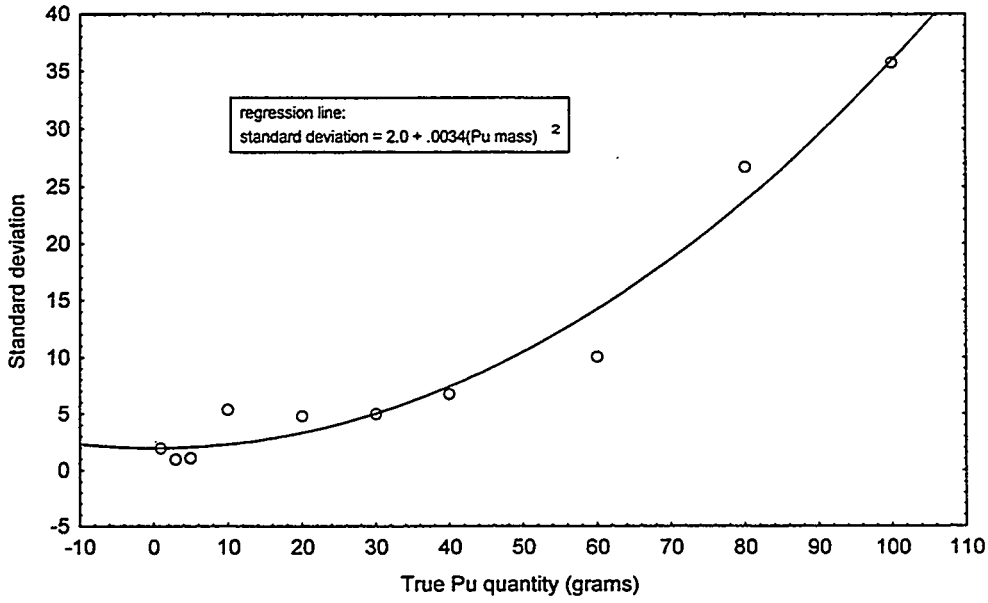

A regression analysis of these produced the following quadratic equation for estimating precision for the glass waste:

$$\text{standard deviation}_{glass} = 2.0 + .0034(\text{true Pu mass})^2. \quad (14)$$

The linear term in the quadratic regression was clearly not significant ($p = .65$) so was eliminated from the model. The intercept term in the equation did not quite meet the .05 level of significance ($p = .054$), but was left in because of the known fact that a certain amount of variability will occur even in repeat measurements on an empty drum. (Excluding an intercept term would produce zero variability at zero grams Pu.) In addition to its use as a representation of precision for glass waste drum measurements in the PAN system, Equation 14 was also used to derive the weights used in the weighted least squares regression for bias estimation in the previous section.

Comparison to Counting Statistics Error

Figure 9 compares the precision estimates for glass waste obtained from Equation 14 to the standard deviations reported automatically by the PAN system. A weighted least squares fit to the PAN reported data is also plotted to aid in the comparison. The analysis showed that a linear fit to the PAN reported data was appropriate. (The p-value for a quadratic term was .99). The plot shows the values from Equation 14 are actually less than the PAN fitted value line over the intermediate range of Pu quantities. This anomaly is to a large extent due to the amount of variability observed in the PAN data and the fact that the PAN reported values are positively skewed. Other methods of fitting a line to the PAN data produced different results. For example, a fit to the median PAN reported standard deviation values at each Pu quantity produced a line which always falls below the plot for Equation 14, as indicated in Figure 10. Additional work is planned to determine the best method of quantitatively comparing the two sets of results.

Figure 9. Comparison of Equation 14 results and regression fit to individual PAN reported standard deviations for the simulated glass waste drums

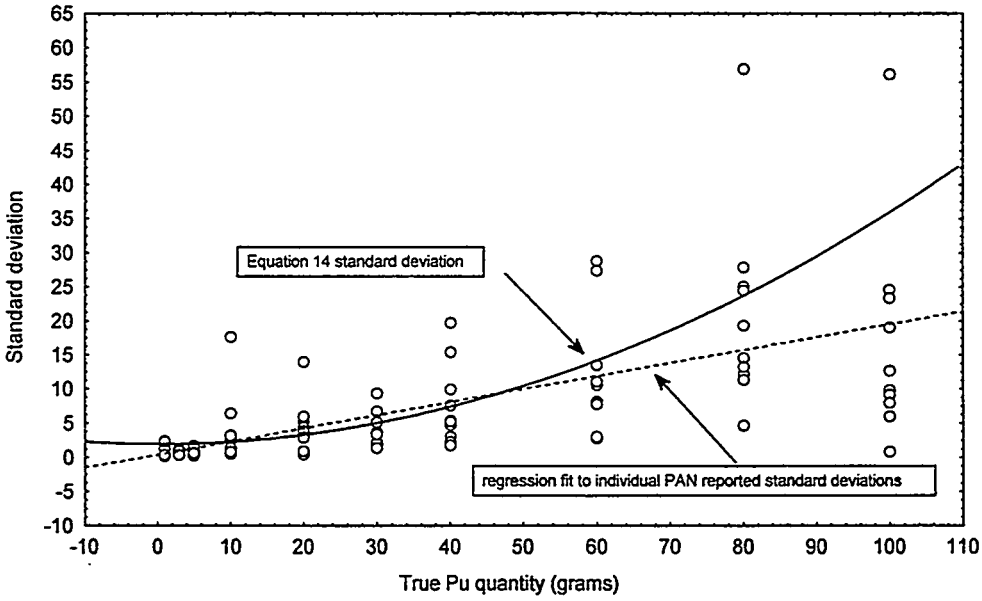

Figure 10. Comparison of Equation 14 results and regression fit to median PAN reported standard deviations for the simulated glass waste drums

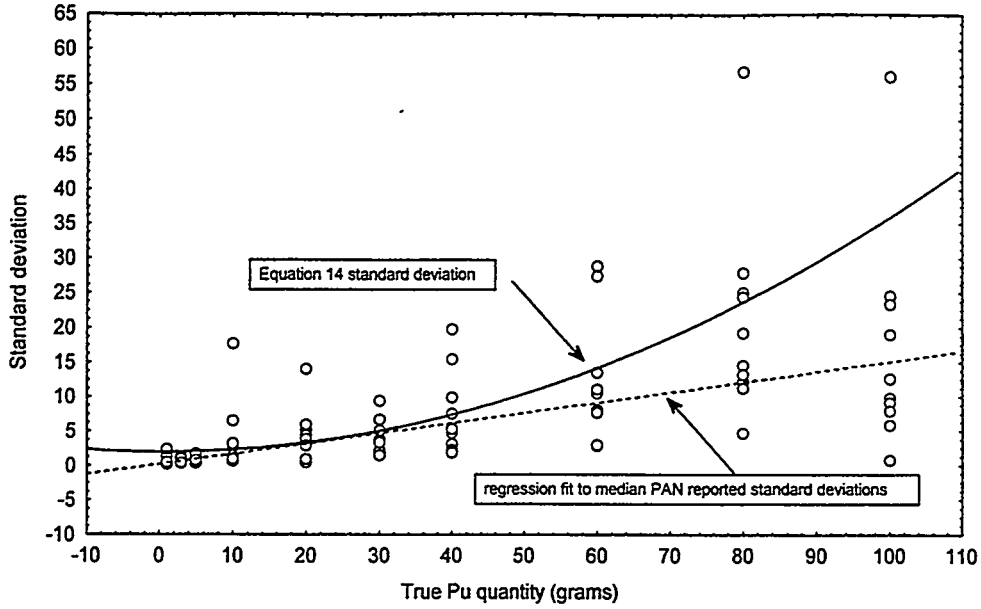

Matrix Parameter Effects on Uncertainty

Key matrix parameters for the glass matrix simulated waste drums include categorical parameters (number of fiber packs, content code, and whether or not the plutonium occurs in fines or chunks) and continuous modeled parameters (absorber index, average fill height, mass of the drum contents, the shielded and system (α, n) singles rates, Pu-240 mass fraction, and the mass fractions of the other elements making up the matrices in the drums).

Parameter Effects on Bias

As with the combustible data, the analysis for bias effects was performed on adjusted data to indicate bias effects of the matrix parameters that are in addition to the bias due to Pu quantity. The adjusted values were obtained from the equation

$$\text{adjusted value} = y_i - x_i + .24(x_i) \qquad (15)$$

which is the same as Equation 5 except that the bias estimate for the glass rather than combustible data is used.

Effects of the continuous scale parameters were tested using Pearson's r correlation coefficient. Parameters with significant ($p < .05$) or nearly significant ($.05 < p < .10$) are listed in Table 3. The p-values given are for the test of the null hypothesis that the correlation is zero. Thus, low p-values (e.g., $p < .05$) indicate statistically significant correlations.

Table 3. Significant or near significant correlations of matrix parameters with adjusted deviation data (indicating effects on bias) for simulated glass waste drums.

Matrix parameter	Correlation	p-value
Absorber index	.36	.00
Mass fraction of carbon	-.21	.00
System (α,n) singles rate	.17	.09

All three of the correlations in Table 3 are due to two or three outlier values, without which the correlations are not statistically significant. (The correlation with system (α,n) singles rate actually becomes negative without the two highest valued cases.) Thus, substantive conclusions can not be drawn from these data.

The categorical parameters were tested using analysis of variance (i.e., ANOVA) techniques. Both standard ANOVA techniques (which tests for differences between means) and nonparametric ANOVA techniques (which tests for differences between medians) were utilized. In terms of significance of effects the results were consistent between the two methods. Significant effects were found for the effects of Pu in chunks vs. fines, and content code. The mean adjusted difference for cases with Pu in fines was -4.5g while for cases with Pu in chunks it was 5.1g. The difference in medians was -1.4g for fines vs. 1.0g for chunks.

For content codes, the mean adjusted difference values were -1.6 for code 440, 23.1 for code 441, and -1.0 for code 442. The corresponding median values were 0.7, 5.8, and -0.5 respectively. Thus the biggest difference is between the code 441 drums and the others. There are only six code 441 drums in the simulated data. The significant difference appears due to only two of the six drums. These two drums were also two of the outlier cases identified earlier in the correlation analysis. Examination of the characteristics of these two drums did not reveal any single factor differentiating them from other drums.

Parameter Effects on Precision

The effects of the various parameters on precision were examined by considering correlations with the absolute values of the adjusted differences calculated in Equation 15. As with the combustible data, the absolute deviation values were normalized prior to analysis. For the glass data this was achieved by dividing by the standard deviation for the relevant Pu mass as calculated in Equation 14. Thus the correlations represent effects of the parameters on precision in excess of that attributable to Pu mass. To reduce the skewness of the data, the analysis was performed on the logarithms of the normalized deviation data. Correlations with elemental mass fractions were only considered when there were at least ten drums containing a particular element.

None of the categorical variables showed significant effects. Significant ($p < .05$) correlations of matrix parameters with the adjusted and normalized absolute deviations are given in Table 4.

Table 4. Significant correlations of matrix parameters with the logarithms of the adjusted and normalized absolute deviations (indicating effects on precision) for simulated glass waste drums.

Matrix parameter	Correlation	p-value
System (α,n) singles rate	.22	.00
Shielded (α,n) singles rate	.22	.00

Only the (α, n) singles rates showed significant correlations with precision error. The values for shielded and system counts are equal due to their high correlation with each other. The (α, n) interference effect has been seen in uncertainty analysis of other waste types (i.e., graphite and combustibles).

Propagation of Total Uncertainty for Measured Mass Values

Using the same propagation of errors procedure described above for combustibles, the standard deviation for an adjusted measured mass value for glass waste drums is

$$s_{adjPu(glass)} = [6.7 + .042(\text{measured Pu mass})^2 + .000060(\text{measured Pu mass})^4]^{1/2}, \quad (16)$$

and an approximate 95% confidence interval for the true mass is:

$$1.32(\text{measured Pu mass}) \pm 2s_{adjPu(glass)}. \quad (17)$$

Figure 11 compares the confidence intervals calculated using Equation 17 to performance criteria as established in Table 9-1 of the TRU Waste Characterization Quality Assurance Program Plan (DOE, 1995). This figure shows that the performance criteria (based on Pu mass only) can be met for measured PAN measurements of glass waste in the range from approximately 8g to 50g.

Figure 11. Uncertainty bounds for glass drum measurements
(bias adjusted and accounting for uncertainty in bias estimate)

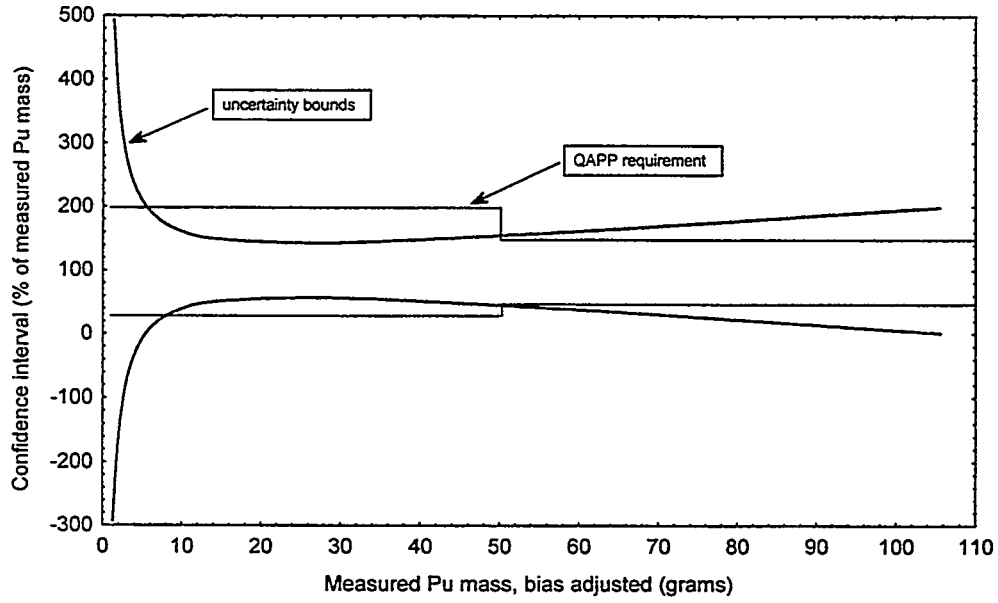

As mentioned before, new criteria have recently been proposed for Table 9-1 of the QAPP. These criteria only impose restrictions on the bias component of the total uncertainty. The expected bias for glass is -24% with a standard error of 2.8%. An approximate 95% confidence interval for the true bias is then (-30%, -18%). This interval applies to all mass levels. Hence, based on uncertainty for the PAN measured Pu mass, the new criteria for Table 9-1 can be met for glass waste, at least when only the uncertainty in the Pu mass is considered. (The final uncertainty must also include the uncertainty in the isotopic ratios used to convert the PAN computed Pu mass to curie content. The additional uncertainty may mean that the bounds are exceeded for some measurements, unless a bias correction is applied.)

In order to be critically safe, there is a safety limit requiring that the measured Pu mass plus $2s_\varepsilon$ (i.e., the upper bound in Figure 11) must not exceed 200g. Based on the equations used to derive Figure

11 the measured mass must be below 77g in order to meet this criterion for drums containing glass waste. (Again the uncertainty will be somewhat greater when isotopic ratios are considered.)

SUMMARY AND DISCUSSION

The glass data appear to indicate greater bias but less precision error than did the combustible data. The bias for combustible drums was estimated at -16% with an approximate 95% confidence interval covering from -28% to -4%. For glass waste drums the bias was -24% with a 95% confidence interval from -30% to -18%. The degree of overlap in the confidence intervals indicates that the difference in the bias for the two waste types is not statistically significant, but the broad confidence bands indicate that it is not necessarily safe to assume the bias values are in fact the same. The estimated difference between the glass and combustible drums is -8% with 95% confidence interval bounds of -21% and +5%, so there is the potential for a sizeable negative or moderate positive difference in the bias values.

Figure 12 compares the glass and combustible data to each other as well as to the graphite data previously analyzed. (Data for the glass content codes have been shifted slightly to the right in the plot to avoid obscuring the combustible data.) The graph shows that the least bias (-6%) occurred in the graphite measurements. The lower 95% confidence bound on the graphite bias was -8.6% (Harker, et al., 1995), which overlaps the interval reported above for combustibles, but not for glass (suggesting a statistically significant difference for the comparison with glass, but not for combustibles). More striking differences are evident in the amount of variability among the measurements for the three different waste codes. Graphite showed by far the least variability (i.e., the best precision). The glass waste showed considerably better precision than the combustible at low Pu quantities (60g or less) but approximately the same precision above that level. The more rapid increase in the variability for the glass data is reflected in the fact that the regression fit to the increasing trend in the glass standard deviation data was a quadratic equation while that for combustibles was only linear.

The combined results in Figure 12 clearly show that uncertainty patterns can vary considerably among waste types. Thus, for accurate assessment of a system's measurement uncertainty, it is essential to perform separate analyses for different categories of waste.

Figure 12. Combined waste form uncertainty analysis results

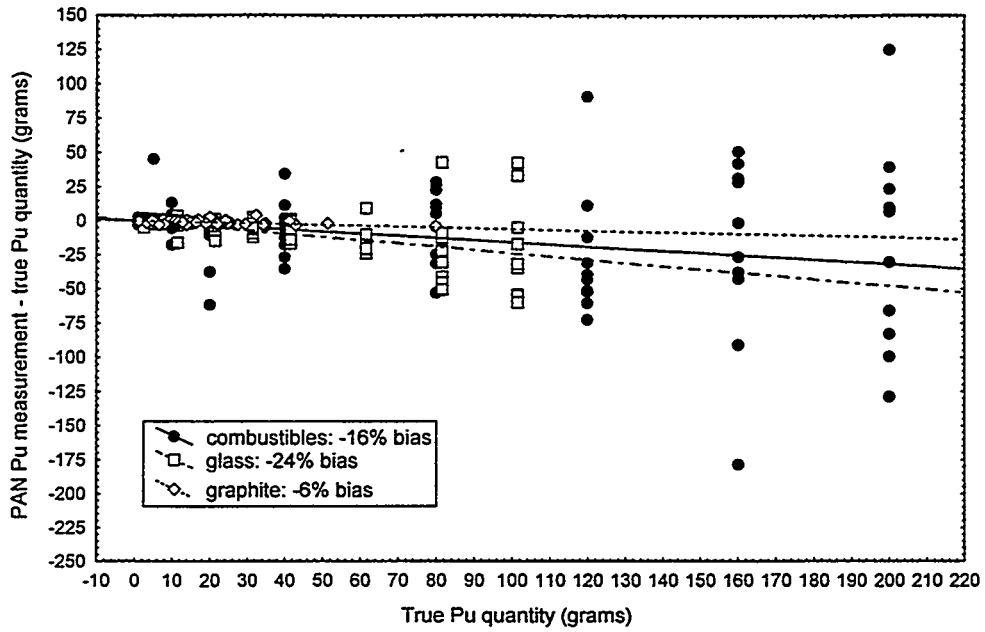

ACKNOWLEDGMENT

This document was prepared for the U. S. Department of Energy Office of Environmental Restoration and Waste Management under DOE Idaho Operations Office Contract DE-AC07-94ID13223.

REFERENCES

1. Harker, Y. D., Blackwood, L. G., Meachum, T. R. (1995). Uncertainty Analysis of the SWEPP Drum Assay System for Graphite Content Code 300. **Proceedings for the 4th Nondestructive Assay and Nondestructive Examination Waste Characterization Conference.** CONF-951091 Idaho National Engineering Laboratory.

2. Harker, Y. D., Blackwood, L. G., Meachum, T. R., and Yoon W. Y. (1996). "Uncertainty Analysis of the SWEPP PAN Assay System for Combustible Waste (Content Codes 330 and 336)," INEL-96/0257, Idaho National Engineering Laboratory, Idaho Falls, ID.

3. Blackwood, L. G., Harker, Y. D., Meachum, T. R., and Yoon W. Y. (1996). "Uncertainty Analysis of the SWEPP PAN Assay System for Glass Waste (Content Codes 440, 441 and 442)," INEL-96/0343, Idaho National Engineering Laboratory, Idaho Falls, ID.

4. Briesmeiser, J. F. (1986). "MCNP - A General Purpose Monte Carlo Code for Neutron and Photon Transport, Version 3A," Los Alamos National Laboratory manual LA-7396-M Rev 2.

5. Neter, J. and Wasserman, W. (1974). **Applied Linear Statistical Models: Regression, Analysis of Variance, and Experimental Designs**, Homewood, IL: Richard D. Irwin, Inc.

SWEPP ASSAY SYSTEM SOFTWARE – AN UPDATE

Larry V. East

Lockheed Martin Idaho Technologies Co.
Idaho National Engineering Laboratory, Idaho Falls, ID 83415

ABSTRACT

The development of a new software package to control data acquisition and perform data analysis for a Passive/Active Neutron Assay system was reported at this conference in 1994. The software has undergone additional development including improvements to the user interface, additional data integrity checks and support for a shift register coincidence analyzer. An overview of this additional work is presented in this report.

INTRODUCTION

The development of a Microsoft Windows® software package for use with the Passive Active Neutron (PAN)[1] assay system at the Stored Waste Examination Pilot Plant (SWEPP) at the Idaho National Engineering Laboratory's (INEL) Radioactive Waste Management Complex (RWMC) was described[2] at this conference in 1994. The PAN system is the primary nondestructive assay instrument used at SWEPP to determine the plutonium content of transuranic (TRU) waste packaged in 55 gallon drums. The software package is referred to as the SWEPP Assay Software, or simply "SAS". This paper presents an overview of enhancements that have been made to the SAS package and some "work in progress".

The initial release of SAS, Version 1.0, was installed at SWEPP in January of 1994 and replaced a FORTRAN program called "NEUT2". The NEUT2 code was originally developed at the Los Alamos National Laboratory and extensively modified by a commercial supplier of PAN systems and personnel at the INEL. The second release of SAS, Version 2.0, was put into routine operation in May of 1996. Version 2.0 contained enhancements to the user interface, additional data integrity checks, an algorithm to correct for the presence of ^{235}U, a revised analysis report format and corrections to several operational and technical problems that were discovered during approximately one year of production use. Work is currently in progress on a new SAS version that will contain support for a shift register coincidence analyzer and additional analysis capa-

bilities. If time permits, it will be converted to "32 bit native mode" for WindowsNT®. This version is scheduled to be installed at SWEPP in March of 1997.

The original object-model design of SAS has been retained with new objects added where necessary to accommodate additional functional requirements. The use of configuration files has been expanded to allow extensive customization of the program's behavior without requiring modification to the underlying coding instructions. Every effort has been made to keep the software highly maintainable yet flexible and a significant amount of effort has been expended on documentation. The documentation consists of a set of formal documents[3,4,5] and extensive comments within the C++ source, header and configuration files.

DATA INTEGRITY CHECKS

Examination of historical data from the PAN system revealed many instances of malfunctioning detectors, suspiciously high counts from one or more detector banks (indicating that the drum rotator was possibly not functioning) and bad background data.[6] The NEUT2 program included no checks on data integrity; it was assumed that the user would examine the data and determine whether or not it was valid. This type of approach does not work in a "production environment" such as SWEPP; the operators tend to just assume that any computer generated number is correct! Extensive off-line data validation procedures were therefore required to examine the data after the fact. This proved to be very time consuming and highly inefficient. It became obvious that implementing data integrity checks within the software in order to catch as many potential data problems as possible in real-time would greatly increase SWEPP throughput and efficiency. Unfortunately, Version 1.0 of SAS was almost completed before all of the problems in the historical data had been discovered.

One thing that stood out from examination of the historical data: There were many examples of the neutron counters within the door of the assay chamber malfunctioning; they would be intermittent over a period of several days and then cease to function entirely. This apparently resulted from flexing of the signal cables from the detector assemblies. (See Reference 6 for a description of the PAN counting chamber and detector assemblies.) An "eleventh hour" modifi-

cation was made to Version 1.0 of the software to check for consistency between count-rates observed from the detectors in the four sides of the assay chamber. Count-rates from the counters in the top and bottom of the chamber were not included because these rates vary relative to rates from counters in the sides from waste drum to waste drum. A note was added to the data display window indicating the amount of variation. Unfortunately, this note usually went unobserved by the PAN operators. In SAS Version 2.0, the side-counter consistency checks were expanded to take into account variations due to counting statistics and a prominent warning window is displayed, shown in Figure 1, when the variation exceeded what would be expected at the 99% confidence level. Data from the offending counters are also highlighted in the data display window as shown in Figure 2.

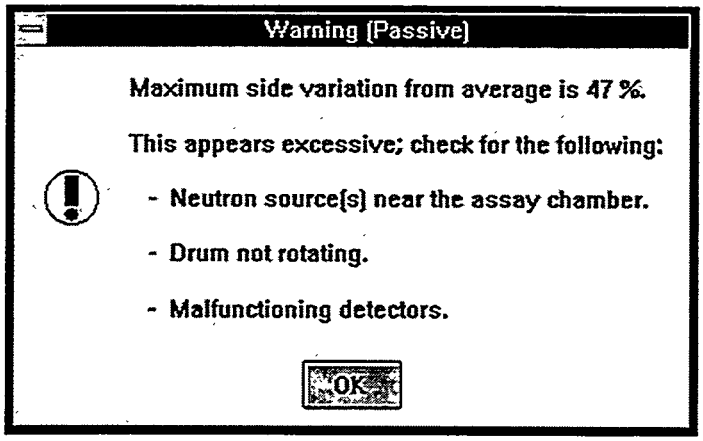

Figure 1. Warning message indicating a disparity between count-rates from detector banks around the sides of the assay chamber.

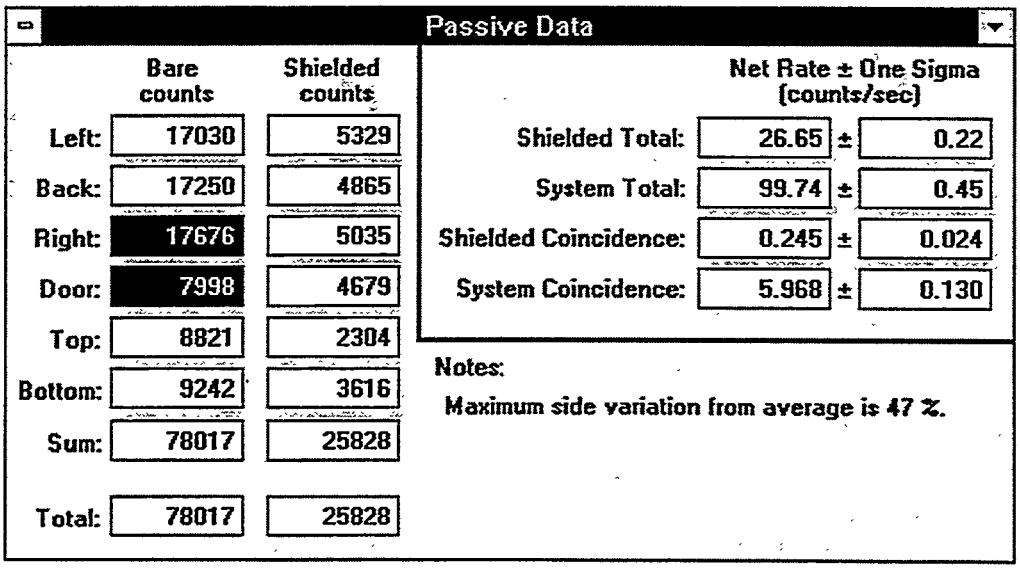

Figure 2. Questionable data are highlighted for ease of recognition.

Additional data integrity tests were added in Version 2.0. These include:

- Check for no counts from individual detector banks during a passive assay.
- Check for passive coincidence rates statistically less than zero (at a 95% confidence level).
- Check for unusually low flux monitor counts during active neutron interrogation indicating possible neutron generator malfunction or extremely high neutron absorption in the waste matrix.[a]
- Check background coincidence rates (passive) against "nominal" background rates read from a configuration file.

If any data integrity test fails, a prominent message is displayed on the screen and an acknowledgment is required from the operator in order to proceed. Serious problems such as no counts from one or more detector banks or high passive background rates are noted in a logging file along with the drum (or background) identification number, date, time of day and operator name.

AUTOMATIC HANDLING OF STATISTICAL UNCERTAINTIES

Like most high-level computer languages, the C++ language (in which SAS is written) has provisions for "user defined" data types. Somewhat unique, however, is the ability to also redefine how operations such as addition, subtraction, multiplication etc. are applied to specific data types. This capability is called "operator overloading". These capabilities of the C++ language – user defined data types (or "objects") and operator overloading – were put to good use in the original SAS development by defining a special data type to represent a measured value (e.g., detector count or count-rate) and its one standard deviation uncertainty. This data type was named "error_bar". Common arithmetic operations on error_bar data objects were "overloaded" to automatically perform error propagation. For example, if A and B are two error_bar objects,

---

a. Minimum acceptable flux monitor counts per 2000 neutron pulses are read from a configuration file.

then the result of adding *A* and *B* will be an error_bar object containing the sum of the "value" components of *A* and *B* and the uncertainties of *A* and *B* added in quadrature. Similar results are produced when error_bar objects are subtracted from, multiplied or divided by, or set equal to other error_bar objects or "normal" (floating point) numbers; the error propagation is taken care of automatically without the programmer having to explicitly code the error propagation equation for each operation. This is not only a tremendous time saver when error_bar objects are present in complex equations, but also eliminates a source of potential coding errors.

In SAS Version 2.0, operator overloading was expanded to include standard comparison operations (greater than, less than, greater than or equal to, etc.) involving error_bar objects. By default, the comparisons are performed using 95% confidence level statistics (the standard deviations are multiplied by 1.960).[7] A different confidence level can be set via a "member function" for any error_bar object. The following code segment illustrates how the "equal to" operator is implemented for comparisons between two error_bar objects:

```
int error_bar::operator == ( const error_bar &eb )
{
   return   (float)fabs( datum - eb.datum ) -
           CF * (float)sqrt( pow(error, 2) +
                 pow(eb.error, 2) ) <= 0.0;
}
```

In the above, "datum" refers to the value part of an error_bar object and "error" refers to the one standard deviation of the value. "CF" is the confidence factor, 1.960 by default.

INTEGRATION WITH SWEPP GAMMA-RAY SPECTROSCOPY SYSTEM

The SWEPP Gamma-Ray Spectroscopy System (SGRS) was just being brought on-line when the new PAN software was installed. This system is used to determine the relative abundance of selected nuclides within a waste drum. These relative abundances are reported as isotopic mass ratios. In the case of plutonium isotopes, the ratios are with respect to ^{239}Pu; ^{241}Am is also reported relative to ^{239}Pu. A data link was setup between the VAX computer controlling the SGRS and the PC controlling the PAN system using DECnet®. This link allows a disk directory on the VAX to appear to the PC as a local disk. The SGRS stores mass ratio results in files that can be accessed directly by the PAN PC. It was initially assumed that the SGRS generated mass

ratios could be used directly to correct for isotopic abundance variations in the plutonium and to determine the ^{241}Am content of waste drums. However, several problems were encountered:

- The SGRS was often unable to obtain a reliable value for the $^{240}Pu/^{239}Pu$ mass ratio – a fundamental quantity required to interpret PAN passive assay results.
- Many process sludge waste drums contained significant ^{241}Am but very little plutonium, making it difficult to obtain reliable $^{241}Am/^{239}Pu$ mass ratio values.
- SGRS measurements indicated that many waste drums contained enough depleted uranium to interfere with PAN active assay measurements of ^{239}Pu (due to the presence of ^{235}U).

The presence of large (multiple kilogram) quantities of depleted uranium in the TRU waste was entirely unexpected.[6] The presence of gram quantities of ^{235}U (present in the depleted uranium) and higher than expected ^{241}Am content caused a break-down in the algorithms used in the SGRS to determine plutonium mass ratios. In addition, ^{235}U was being falsely reported as ^{239}Pu by PAN system assays based on active neutron interrogation. The SGRS algorithms were modified to accommodate high ^{241}Am concentrations and the presence of ^{235}U. The SGRS software was also modified to report $^{235}U/^{239}Pu$ and $^{241}Am/^{235}U$ mass ratios when detectable quantities of ^{235}U were present. It soon became apparent that the SAS software required some major modifications in order to make more intelligent use of the mass ratio values generated by the SGRS.

The following changes were incorporated in SAS Version 2.0 to better utilize SGRS mass ratio results:

- SGRS $^{235}U/^{239}Pu$ values used to correct plutonium active assay results and calculate ^{235}U mass (included in output report and activity, etc. calculations).
- SGRS $^{241}Am/^{235}U$ values used to calculate ^{241}Am content when $^{241}Am/^{239}Pu$ value could not be determined or the ratio relative to ^{235}U has lower uncertainty.

- SGRS plutonium mass ratios used only to confirm that the plutonium isotopic composition is as expected for the waste stream.[a]

The new SAS software version currently nearing completion will report ^{238}U isotopic mass computed from the $^{235}U/^{238}U$ mass ratio that will be reported by a new version of the SGRS software. It will also treat ^{235}U as being the primary fissile isotope when SGRS results indicate that considerably more ^{235}U is present than ^{239}Pu. ^{239}Pu is currently assumed to be the primary fissile isotope and active assay results are corrected for any ^{235}U present; this results in large corrections and hence very large uncertainties when the fissile content is primarily ^{235}U. SAS computes the final assay results based on PAN and SGRS measurements and displays them on-screen (Figure 3), prints a "short form" report, saves raw counting data along with intermediate calculation results and the final assay results in a "long form" data file and, when operated in "Remote" mode, automatically uploads the assay results to a SWEPP database management system.

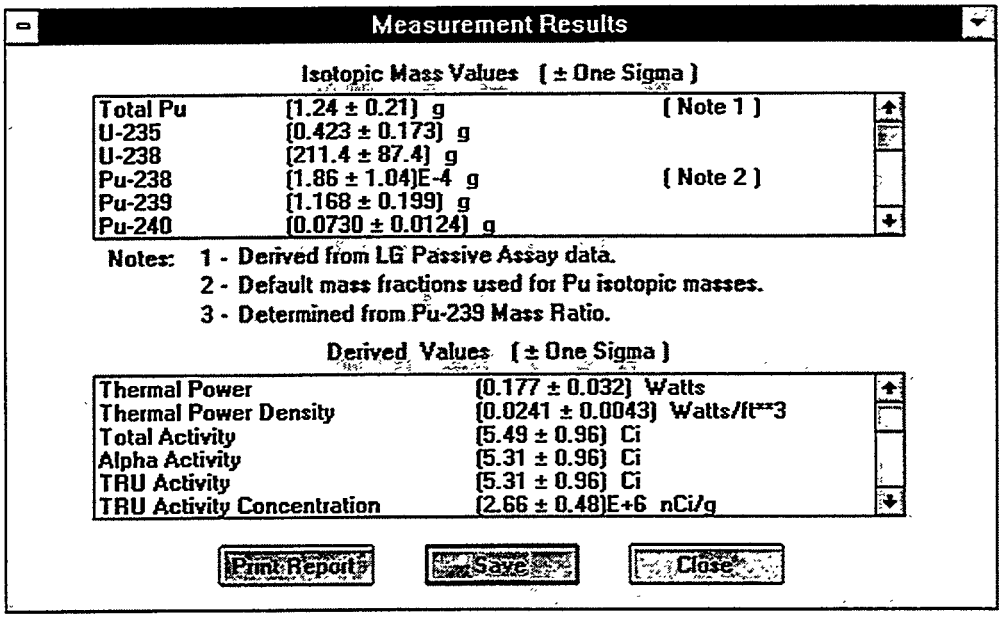

Figure 3. Integrated PAN/SGRS Measurement Results Window.

---

a. Configuration file parameters control how SGRS plutonium isotopic information will be used. The available options are: 1) Always use SGRS isotopic ratios to determine plutonium isotopic masses; 2) Use SGRS isotopic ratios to determine plutonium isotopic masses only if mass ratios are not within normal range; 3) Always use default plutonium mass ratios but indicate to the operator and on the output report when SGRS values are not within expected range; 4) Ignore SGRS results and use default plutonium mass ratios. The third option is the one currently in use at SWEPP.

SHIFT REGISTER COINCIDENCE ANALYZER SUPPORT

Many of the waste drums located at SWEPP contain significant amounts of ^{241}Am and chemical elements (F, B, etc.) that have high (α, n) neutron yields. The resulting high uncorrelated neutron flux from these drums severely interferes with passive neutron assay measurements performed by the PAN system resulting in large measurement uncertainties.[6] This situation can be improved by using a neutron coincidence technique based on "shift-registers" rather than the standard PAN coincidence technique that uses standard delayed coincidence logic.[8] The standard PAN coincidence system "saturates" at high count rates and only information from a set of "shielded" detectors can be used resulting in a loss of counting efficiency and accuracy. A shift-register coincidence system has much lower dead time losses and events from all detectors can be used at high counting rates resulting in much less measurement uncertainty.[6]

A model JSR-12 Neutron Coincidence Analyzer[a] which uses shift-register coincidence technology is scheduled to be installed in the PAN system early in 1997. The JSR-12 has an RS-232 interface that allows complete data acquisition control, parameter and data transfers to be performed by an external device. The new version of the SAS software scheduled for installation at the same time includes the necessary modifications to communicate with the JSR-12. The new software can use either the JSR-12 or the standard PAN coincidence unit (using standard CAMAC[b] modules) for data acquisition. "Long form" data files that do not contain shift register data can still be read and reanalyzed with new matrix or calibration parameters for complete backward compatibility.

Data integrity checks specific to the JSR-12 have also been implemented. For example, the JSR-12 directly measures the accidental coincidence rate and this measured rate is compared with the expected accidental coincidence rate based on the total count rate and the shift register

---

a. Manufactured by Canberra Industries, Inc., Meridian, CT.

b. Computer Aided Measurement And Control, specified in ANSI/IEEE Standard 583-1975.

gate width. A significant lack of agreement[a] between these two rates indicates a possible hardware malfunction or incorrect parameter setting.

On-line diagnostics can be used to exercise and verify parameter uploading, data acquisition and control functions via the JSR-12 / computer interface. These diagnostics are intended to be performed with a neutron source in the assay chamber so that agreement between measured and calculated accidental coincidence rates can be verified. Diagnostic results are displayed as shown in Figure 4. Hardware diagnostics are accessible only to users with "Physicist" access privilege[b] and are not part of normal assay procedures.

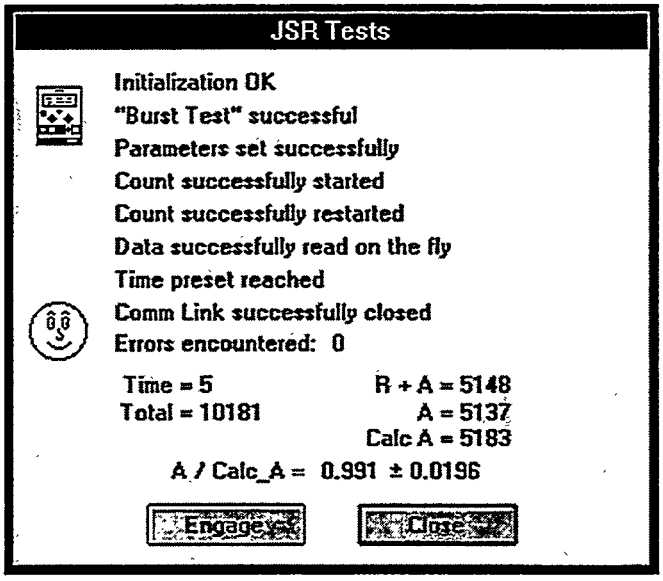

Figure 4.. Shift register diagnostics window.

ACKNOWLEDGMENTS

This work was supported by the US Department of Energy Assistant Secretary for Environmental Management under DOE Idaho Operations Office Contract DE-AC07-94ID13223. Project management was under the direction of the INEL Transuranic Waste Department in support if SWEPP Operations. Technical direction and support was provided by the INEL Radiation Physics Section. Valuable feedback and suggestions have been provided by SWEPP personnel and Radiation Physics personnel through out the SAS development effort. In particular, the author gratefully acknowledges the software testing efforts and valuable technical feedback pro-

a. This comparison is made at a 99.9% confidence level to reduce the chance of falsely indicating a failure. However, the test is still sensitive enough to catch most real failures.

b. The SAS software requires user log-in and recognizes three access levels: "Administrator", "Operator" and "Physicist". An "Administrator" can set/reset user passwords and print log and error files. An "Operator" can perform normal assay operations. A "Physicist" can access matrix, calibration and configuration parameters, perform hardware diagnostics, and perform "Operator" functions.

vided by G. W. Twedell. Operational requirements and technical oversight for the initial SAS development were provided by G. K. Becker.

REFERENCES

1. J. T. Caldwell, *et. al.*, "The Los Alamos Second-Generation System for Passive and Active Neutron Assay of Drum-Size Containers," Los Alamos National Laboratory Report LA-10774-MS (September 1986).
2. Earl S. Marwil, Scott D. Matthews and Greg K. Becker, "SWEPP Assay System Software," Proceedings of the NonDestructive Assay and NonDestructive Examination Waste Conference held in Pocatello, Idaho February 14-16, 1994 (CONF-940216), page 137.
3. S. D. Matthews, L. V. East, E. S. Marwil and J. J. Ferguson, "SWEPP Assay System Version 2.0 Software Requirements Specification," Lockheed Martin Idaho Technologies Co. Technical Report INEL-96/0056 (June 1996).
4. L. V. East and E. S. Marwil, "SWEPP Assay System Version 2.0 Software Design Description," Lockheed Martin Idaho Technologies Co. Technical Report INEL-96/0057 (August 1996).
5. J. J. Ferguson and T. K. Overlin, "SWEPP Assay System Version 2.0 Software Test Plan and Report," Lockheed Martin Idaho Technologies Co. Technical Report INEL-96/0058 (July 1996).
6. L. V. East and G. K. Becker, "Experience Gained from Passive/Active Neutron (PAN) Assay Measurements on 12,600 TRU Waste Drums at the INEL," Proceedings of the NonDestructive Assay and NonDestructive Examination Waste Conference held in Pocatello, Idaho February 14-16, 1994 (CONF-940216), page 143.
7. H. W. Coleman and W. G. Steele, *Experimentation and Uncertainty Analysis for Engineers,* Section 2-3, John Wiley & Sons, New York, 1989.
8. D. Reilly, N. Ensslin, H. Smith, Jr. and S. Kreiner, Eds., *Passive Nondestructive Assay of Nuclear Materials,* Chapter 16, US Nuclear Regulatory Commission, Washington, DC, 1991 (NUREG/CR-5550).

SCOPING STUDIES - PHOTON AND LOW ENERGY NEUTRON INTERROGATION

G. Becker, Y. Harker, James Jones
LMITCo, Idaho Falls, ID 83415

Frank Harmon
Idaho State University, Dept. of Physics, Pocatello, ID 83209

ABSTRACT

High energy photon interrogation of waste containers, with the aim of producing photo nuclear reactions, in specific materials, holds the potential of good penetration and rapid analysis. Compact high energy (≤ 10 MeV) photon sources in the form of electron linacs producing bremstrahlung radiation are readily available. Work with the Varitron variable energy accelerator at ISU will be described. Advantages and limitations of the technique will be discussed.

Using positive ion induced neutron producing reactions, it is possible to generate neutrons in a specific energy range. By this means, variable penetration and specific reactions can be excited in the assayed material. Examples using the $^{3}H(p,n)$ and $^{7}Li(p,n)$ reactions as neutron sources will be discussed.

INTRODUCTION

The detection of TRU materials by non-destructive means has a long history in the NDE/NDA community (1). The purpose of the work reported here is to examine the feasibility of various interrogation methods to quantify waste intrained TRU alpha activity at <1.0 nCi/g. The probe radiation penetration in intrained material is our chief concern. Conventional 14 MeV neutron systems suffer from problems of penetration and matrix effects.

Two approaches are described here; 1 - generating neutrons in a specific energy range to provide variable penetration and the excitation of fissile vs fertile reactions. Neutron generation relies on the proton reactions: ^{3}H (p,n) and ^{7}Li (p,n). The former reaction produced neutrons of energy ≤ 800 keV, the later neutrons of energy ≤ 230 keV.. Using a simple detector/source geometry, minimum detectible limits and penetrability were measured and evaluated. 2 - High energy photons offer excellent penetration and produce neutrons by photo-nuclear reactions. The neutron yield functions for these reactions have a threshold at γ-ray energies corresponding to the energy of the least bound neutron and/or the photo fission threshold, generally in the range of 6 to

8 MeV. The required high energy photons are generated by an electron linac, thus the photons have a continuous energy bremsstrahlung spectrum. Systems based on photon interrogation have been reported previously (2).

METHODS AND MATERIALS

The photon interrogation experiments were carried out using the Varitron variable energy 2-12 MeV pulsed electron Linac at ISU. This machine can be used to deliver a wide range of photon energies and intensities at various repetition rates. The neutron detector is a compact unit based on moderated ^{3}He tubes fitted with a special preamplifier (3). The detector can recover quickly from the γ-flash produced by the accelerator bremsstrahlung pulse. Prompt neutrons can be counted within 30 μs of the 3.5 μs long accelerator beam pulse. Typical acceleration repetition rates are ~ 100 Hz. Figure 1 shows a sketch of the measurement timing cycle. The TRU materials used in these experiments were in the form of small Cu covered ^{239}Pu foils, used in a former life as part of nuclear accident detectors (NADS). Figure 2 is a photograph of the experimental setup. The neutron detector is on top of the assembly, various numbers of NADS are in a cylindrical container just in front of the bremsstrahlung producing target and it's collimator. The NADS can be arranged in a cylindrical configuration to determine the absorption of the interrogation flux and neutrons generated as a function of Pu thickness. Bremstrahlung flux is determined by a gamma sensitive ion chamber placed at 1 meter from the bremsstrahlung target and in line with electron beam direction.

In the experiments involving low energy neutron interrogation, two neutron energies were used: $\leq$ 230 keV neutrons produced by 2 MeV protons on ^{7}Li and $\leq$ 800 keV neutrons produced by 1.7 MeV protons on tritium. The detectors used for these scoping tests were five 5 cm diameter, 10 atm, ^{4}He recoil detectors. The reason that these detectors were used in combination with the these particular neutron sources is because the ^{4}He tubes are relatively insensitive to the interrogating neutrons and yet are sensitive to the fast neutrons produced by fission. With this technique the detectors can be acquiring fission neutron counts while the interrogating neutrons are present. It was felt that this approach could lead to improved

sensitivity over the differential dieaway technique where the interrogating neutrons are produced in a pulse and the counting window is opened some time later when the interrogating neutrons have been thermalized.

RESULTS AND CONCLUSIONS

Figure 3 shows the decrease in γ flux as a fraction of the number of NADS. Figures 4 and 5 give the number of prompt and delayed neutrons as a function of NAD numbers. The linearity is remarkably good for both of these processes. The results demonstrate the high degree of penetration obtainable using photon interrogation. The ratio of delayed to prompt neutrons is consistent with previous measurements (4). In another experiment, the distance of five stacked NADS, was varied with respect to the distance from the bremsstrahlung target. Prompt and delayed neutrons were measured. Figures 6 and 7 display this data. These measurements demonstrate the collimation obtained using bremsstrahlung photons.

With respect to low energy neutron interrogation, it was found that with the detector/source configurations used, the sensitivities (in counts per gram Pu) of either $\leq$ 230 keV neutron interrogation or the $\leq$ 800 keV neutron interrogation were approximately the same. However, because ^{4}He detectors are more sensitive to the higher energy interrogating neutrons there was a higher background associated with the $\leq$ 800 keV neutron interrogation. As a result, the minimum detectible limit was a factor of three higher than that associated with the $\leq$ 230 keV neutron interrogation which for the system used was $\approx$ 0.2 g Pu. With a more efficient detector system and more intense neutron source it is felt that a minimum detectible limit of ~ 1 mg Pu could be achieved using the $\leq$ 230 keV neutron interrogation. There are several interrelated factors that play into this estimate so linear scaling with neutron intensity is not expected.

There is one major difficulty with neutron interrogation whether the interrogating neutrons are thermal or at a higher energy and that is penetrability into the matrix and particularly into sizeable pieces of Pu or U. In the cases examined in this paper it was found

that the non-linear effects due to neutron absorption in the Pu sources were quite apparent. Even though the bulk of the interrogating neutrons are well above thermal, the large thermal neutron fission cross section results in a large fraction of the fissions coming from thermal neutron interactions.

In summary, the results of the scoping studies presented in this paper would suggest that neither the photon interrogation nor the low energy neutron interrogation can achieve both sensitivity and penetrability. It appears that sensitivity is best achieved by neutron interrogation and penetrability is best achieved by photon interrogation.

REFERENCES

1. J.E. Lovett, Nuclear Materials - Accountability, Management and Safeguards, American Nuclear Society (1974).

2. R.L. Bramblett, et.al.. Proceedings of the AEC Symposium on Safeguards Research and Development, WASH-1147, 135 (1969).

3. J.L. Jones, et.al.. Proceedings of the Non-Destructive Assay and Non-Destructive Examination Waste Characterization Conference, Pocatello, ID, 1994.

4. T. Gozani, et.al., Trans. ANS 11, 659 (1968).

FIGURE CAPTIONS

1. Timing sequence for photon interrogation.

2. Experimental setup for photon interrogation penetration measurements.

3. Dose rate versus plutonium thickness (number of NADS) as measured by gamma sensitive ionization chamber located 1m downstream from bremsstrahlung target.

4. Prompt photo-neutron response (counts) versus plutonium thickness (number of NADS) as measured by moderated ^{3}He neutron detectors.

5. Delayed photon-neutron response (counts) versus plutonium thickness (number of NADS) as measured by moderated ^{3}He neutron detectors.

6. Prompt photon-neutron response (counts) versus distance from bremsstrahlung target to plutonium foils

7. Delayed photo-neutron response (counts) versus distance from bremsstrahlung target to plutonium foils.

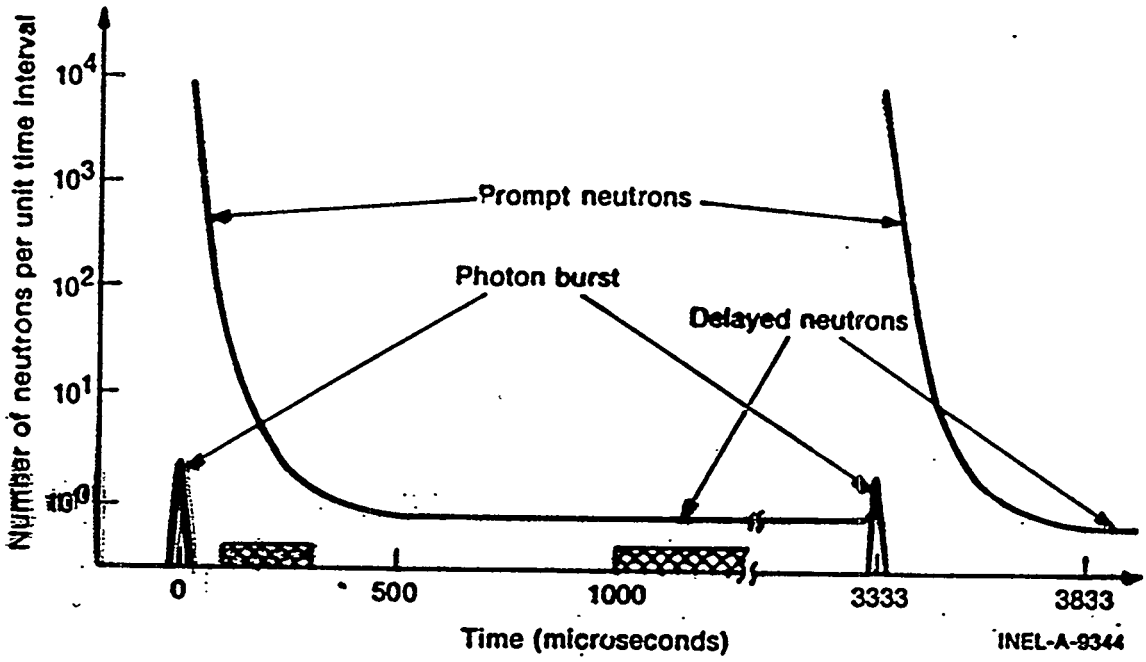
Number of neutrons per unit time interval
10^4
10^3
10^2
10^1
10^0
Prompt neutrons
Photon burst
Delayed neutrons
0
500
1000
3333
3833
Time (microseconds)
INEL-A-9344

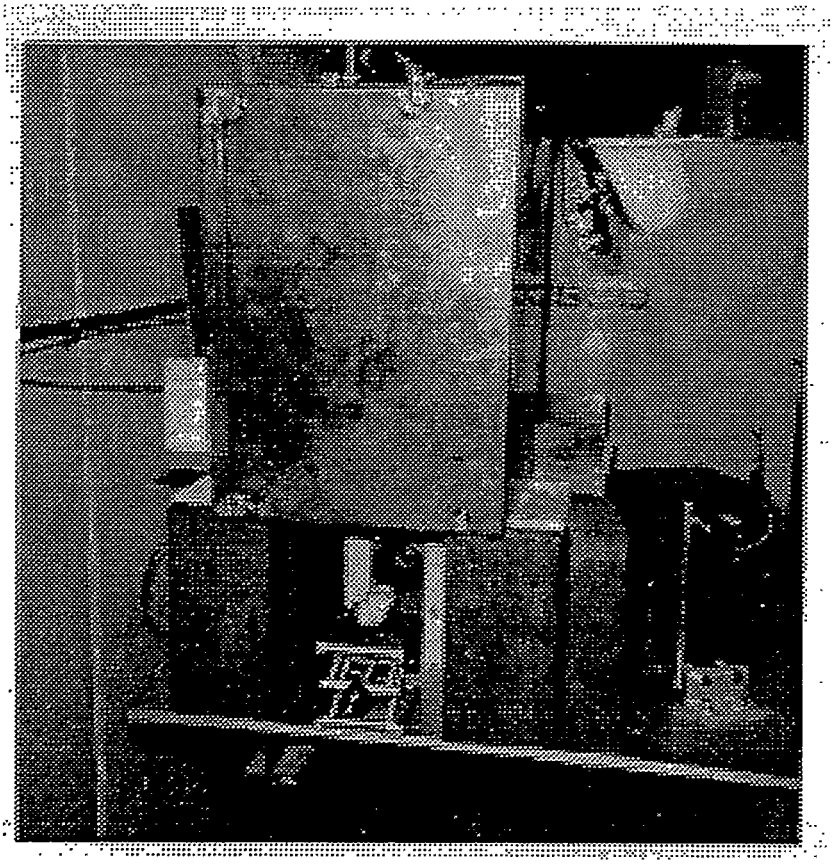

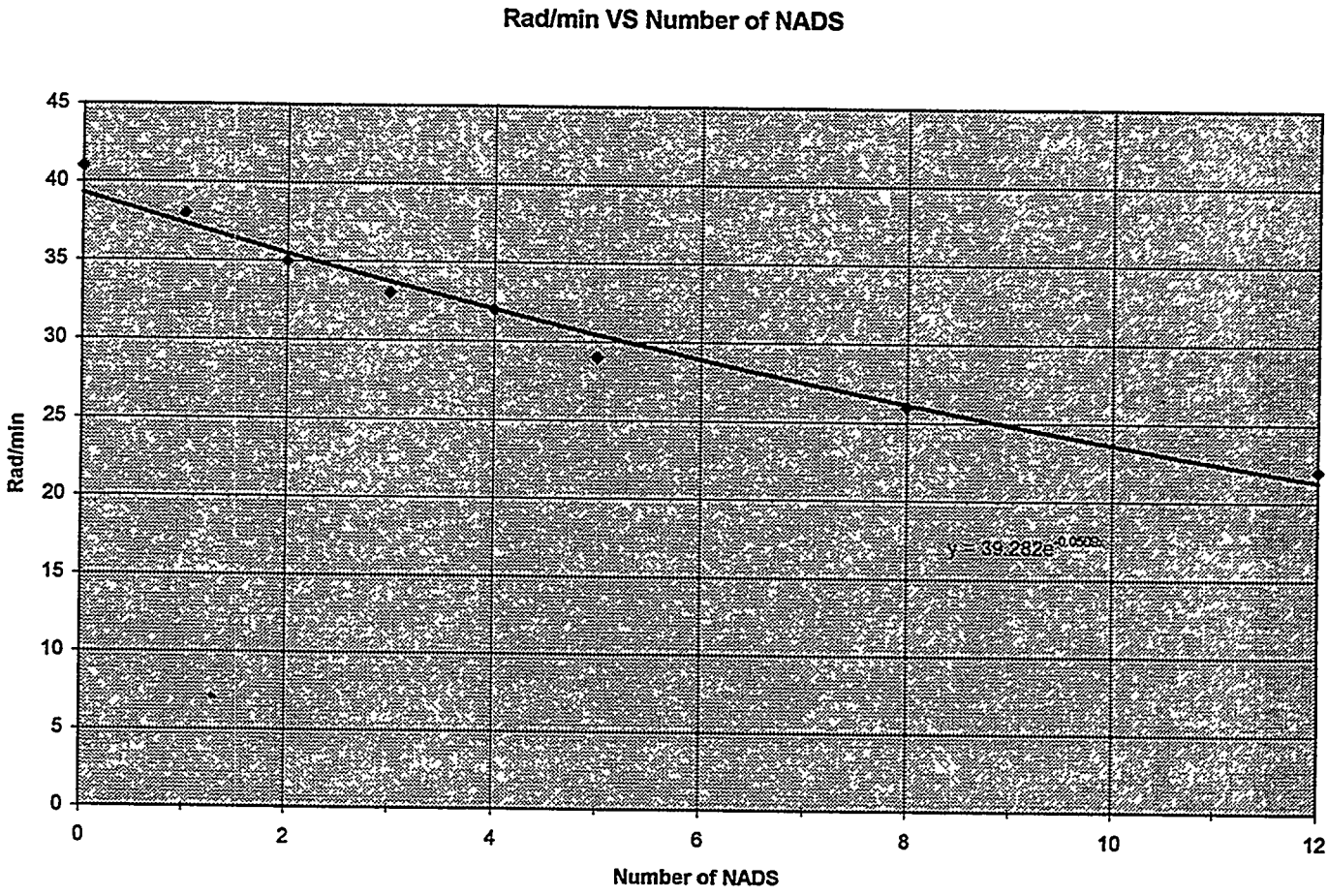
Rad/min VS Number of NADS
Rad/min
Number of NADS
0
5
10
15
20
25
30
35
40
45
0
2
4
6
8
10
12
y = 39.282e-0.050x

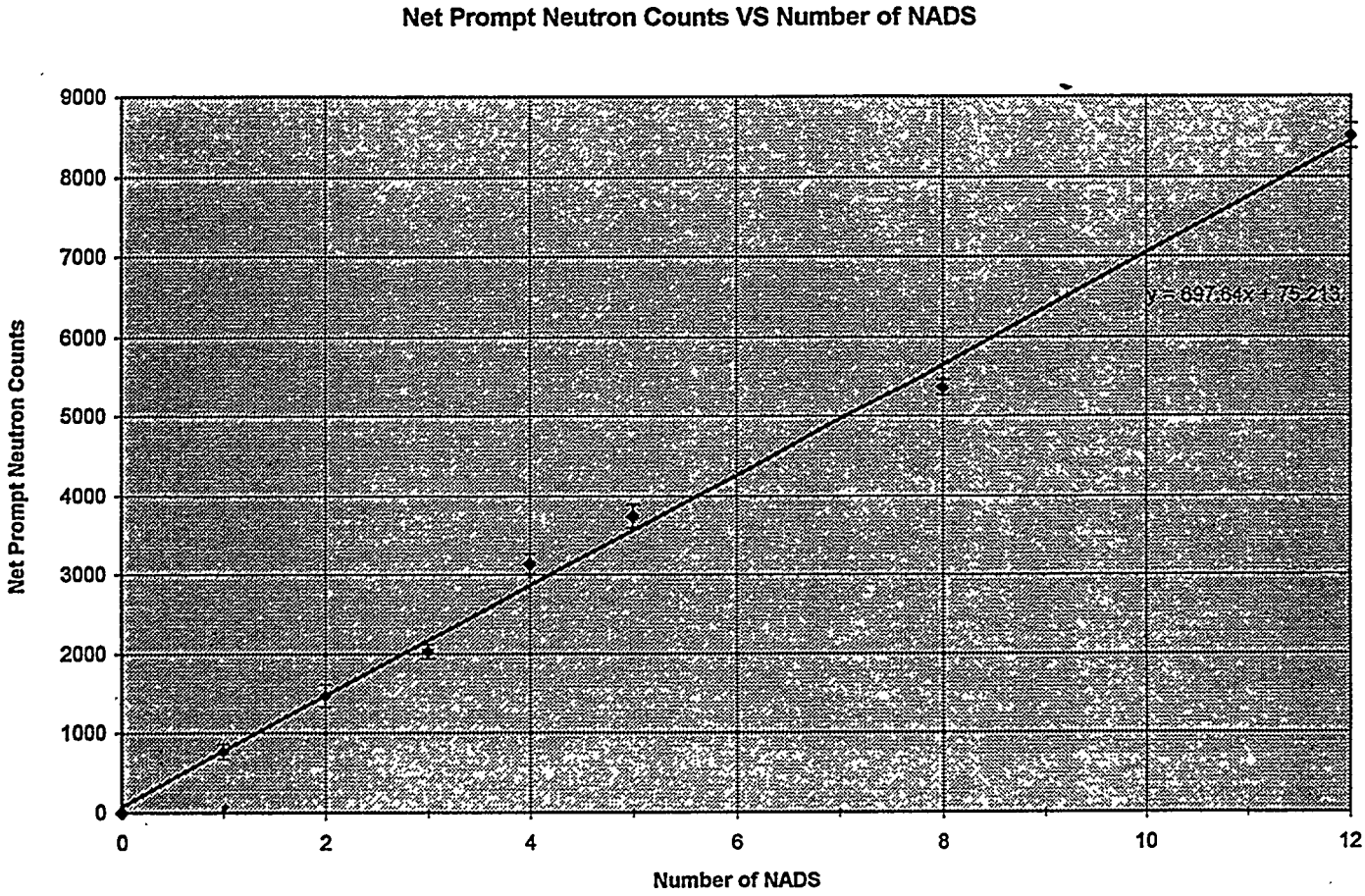
Net Prompt Neutron Counts VS Number of NADS
Net Prompt Neutron Counts
9000
8000
7000
6000
5000
4000
3000
2000
1000
0
0
2
4
6
8
10
12
Number of NADS
y = 697.64x + 75.213

Fig.

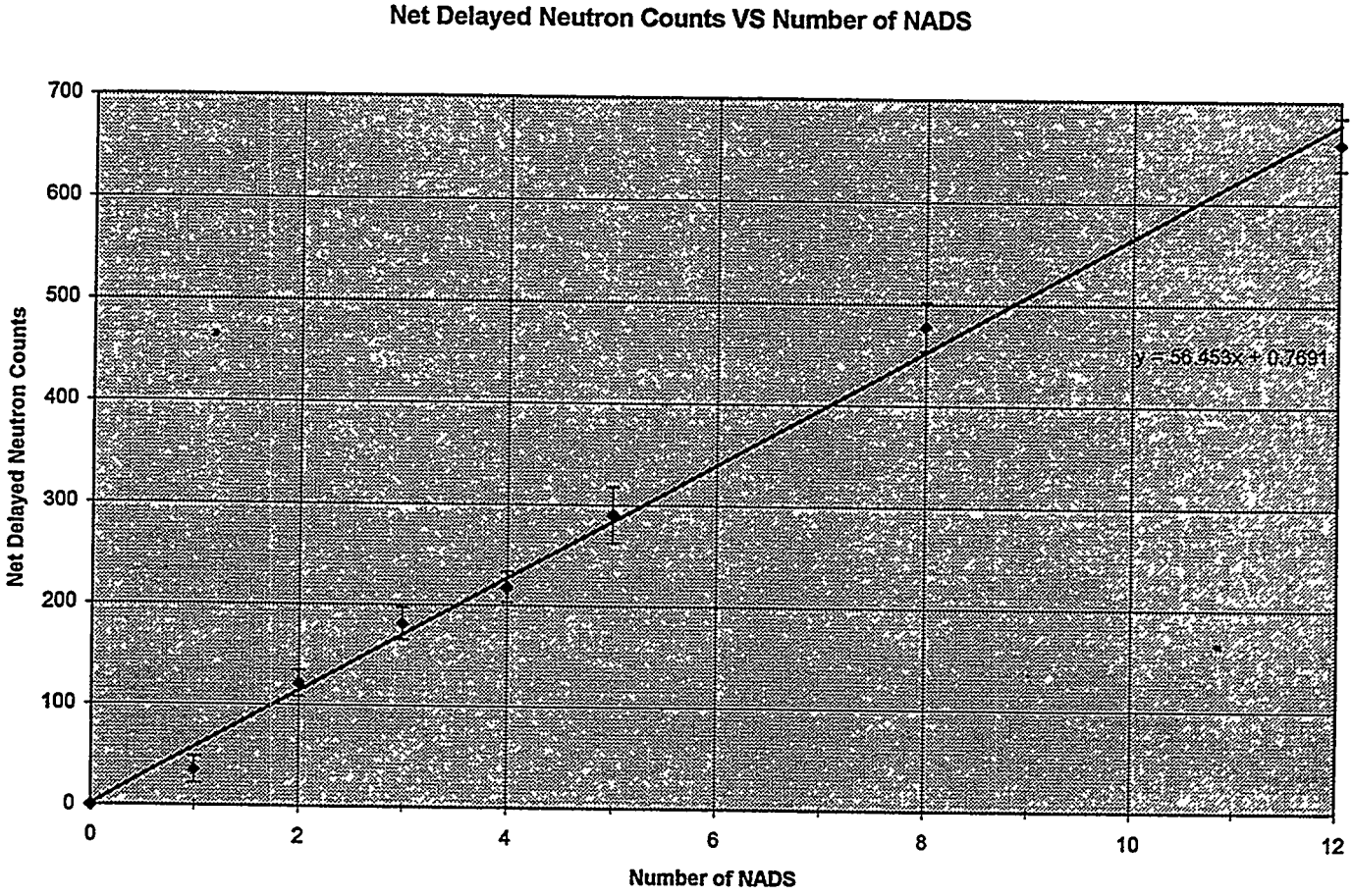
Net Delayed Neutron Counts VS Number of NADS
Net Delayed Neutron Counts
Number of NADS
y = 56.453x + 0.7691
0
100
200
300
400
500
600
700
0
2
4
6
8
10
12

Fig 6

Net Prompt Neutron Counts VS Distance From Target

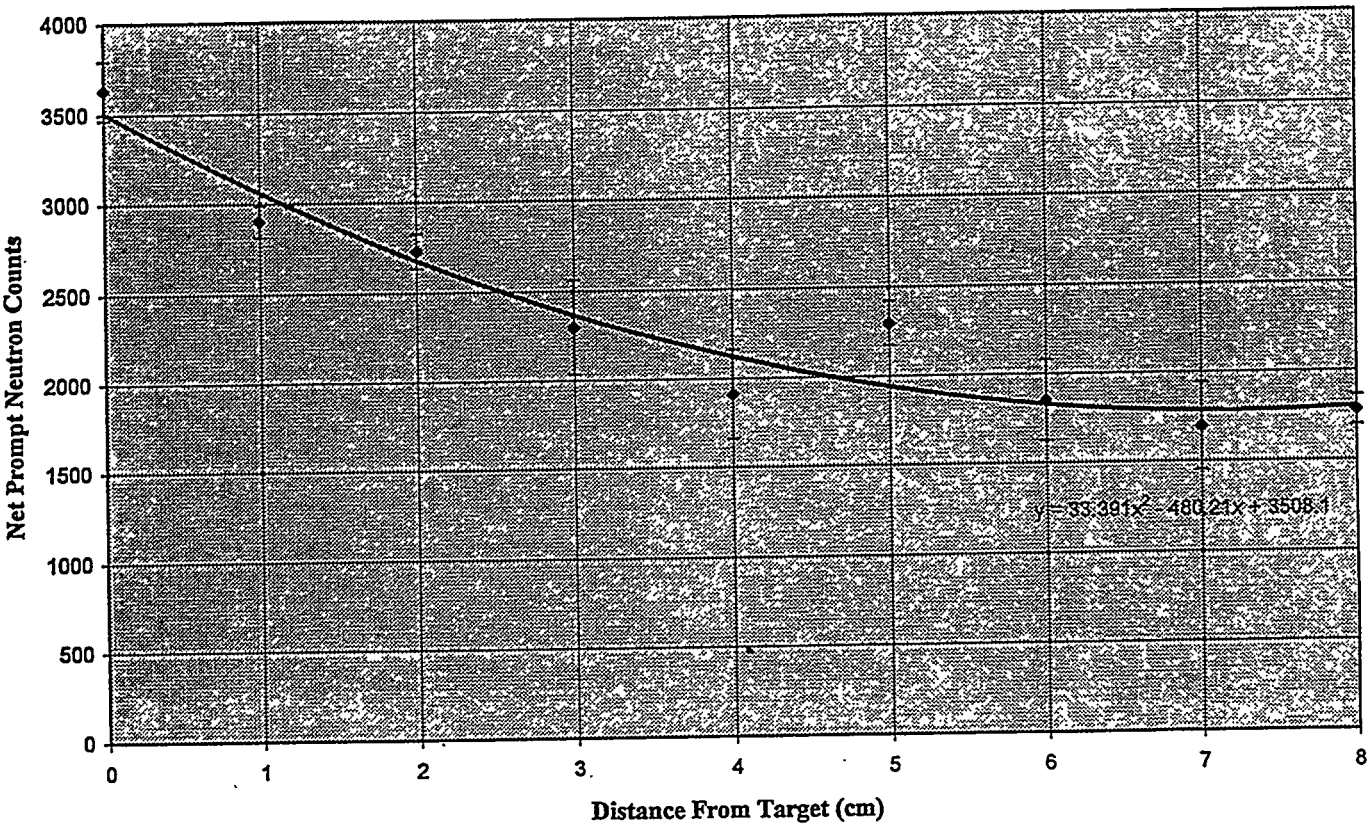

Fig. 7

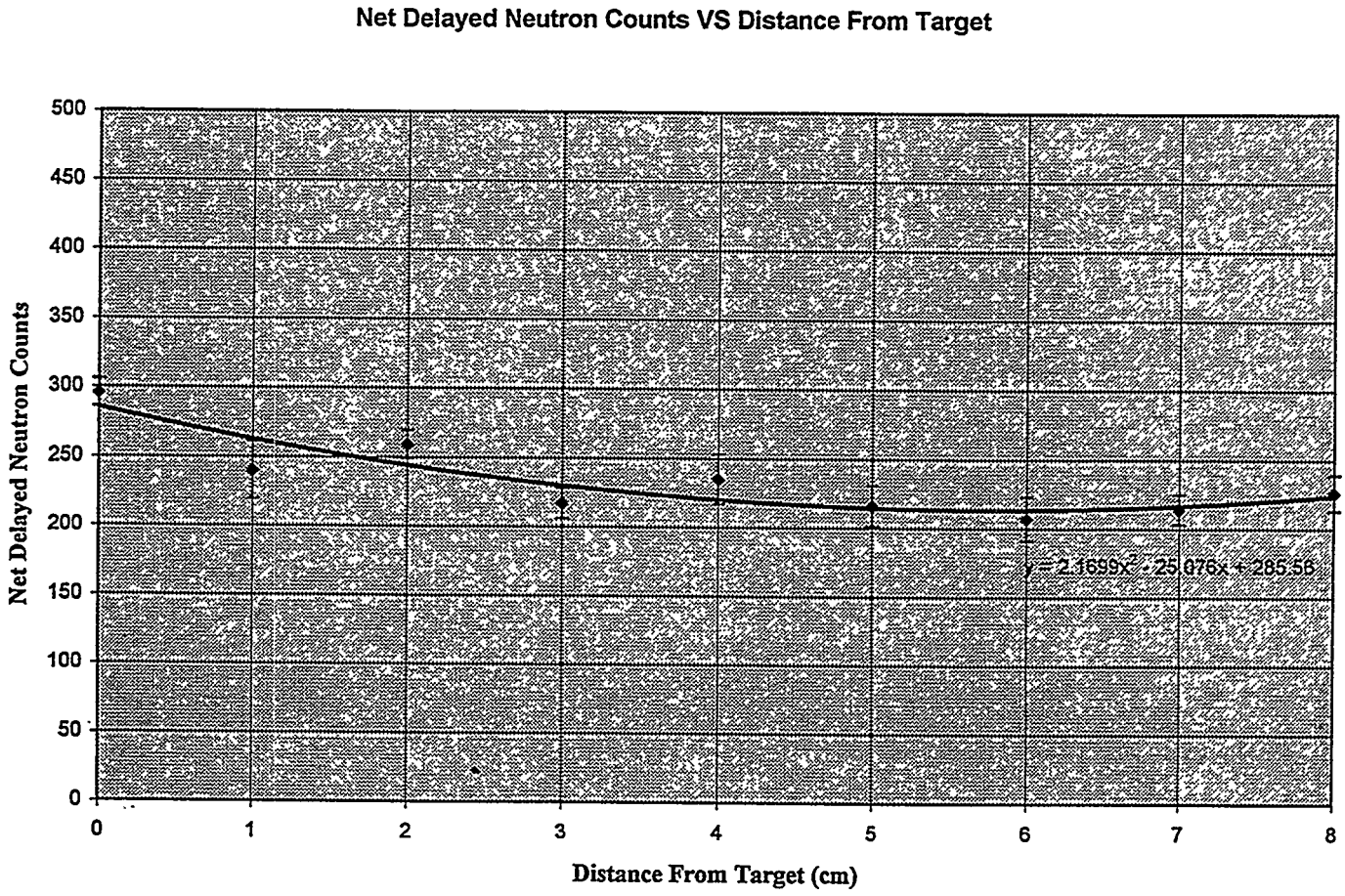
Net Delayed Neutron Counts VS Distance From Target
Net Delayed Neutron Counts
500
450
400
350
300
250
200
150
100
50
0
0
1
2
3
4
5
6
7
8
Distance From Target (cm)
y = 2.1699x² - 25.076x + 285.56

Self Shielding in Cylindrical Fissile Sources in the *APNea*[a] System

David Hensley
Oak Ridge National Laboratory, Oak Ridge, TN 37831

Abstract

In order for a source of fissile material to be useful as a calibration instrument, it is necessary to know not only how much fissile material is in the source but also what the effective fissile content is. Because uranium and plutonium absorb thermal neutrons so efficiently, material in the center of a sample is shielded from the external thermal flux by the surface layers of the material. Differential dieaway measurements in the *APNea* System of 5 different sets of cylindrical fissile sources show the various self shielding effects that are routinely encountered. A method for calculating the self shielding effect is presented and its predictions are compared with the experimental results.

Thermal neutron flux will be attenuated as it traverses a matrix because it is absorbed by the matrix; alternamtely, the flux can escape from the matrix. Both of these effects lead to a diffusion dieaway time of the thermal neutron flux. The *APNea* cavity is large enough that the diffusion time for thermal flux out of the cavity is of the order of $800\mu s$. When a matrix material (in a drum) is introduced, the dieaway time of flux in the drum matrix drops to $600\mu s$ for ethafoam, to $400\mu s$ for concrete, and to as little as $100\mu s$ for raschig rings.

But, there is a special concern for the measurement of fissile materials, such as ^{235}U and ^{239}Pu, which have large thermal-neutron-capture cross sections. The attenuation of the flux as it penetrates clumps of these fissile materials can be so severe that the fissile signal will be significantly reduced over that which would normally be hoped for. The purpose of this paper is to study the effect for a certain class of sources encountered by the *APNea* System and to assess the overall accomodation that must be made in measuring these materials. In particular the focus of this paper will be on fissile sources in the form of right circular cylinders, as all of the calibration sources for the *APNea* System have this form factor (or can be put into this shape). The strengths of the various sources are listed in the first three

[a] *APNea* — It takes your breath away!

tables.

Fissile Sources

Uranium Pins

# Pins	# Pellets	^{235}U(mg)	Factor
2	0	0	1.0
2	1	61	0.917
2	2	123	0.887
2	4	244	0.851
30	6	368	0.832
6	13	797	0.809
Enriched Uranium Pins			
2	3	803	0.634
2	5	1350	0.601
30	8	2150	0.580
20	17	4560	0.562

Table 1:

Fig. 1 shows the results of assaying two different sets of fissile sources in the *APNea* System. These sources were specially made for the *APNea* in order to form the basis of an absolute calibration for the active mode of the *APNea* System. The 98 pins which make up the calibration set are loaded with various numbers of uranium fuel pellets. One set of pins use natural uranium fuel pellets with a ^{235}U fraction of 0.76%; the other set uses fuel pellets with a ^{235}U fraction of 4.45%. The strengths of the sources vary as the number of fuel pellets in each pin assembly. Fig. 1a shows the *APNea* ^{235}U mass values versus the reported mass values for the various stacks of natural uranium fuel pellets. In this figure and in several of the following figures is included the contribution from a one inch cylinder of uranium metal (labeled **dU**) depleted to the 0.2% level. The actual amount of ^{235}U in this slug is somewhat in question, but it is used as the (relative) reference point for all of these active measurements of fissile sources. That is, the slug is measured along with whatever reference source so that the results from all reference sources can be correlated in the final analysis.

Fig. 1b is the equivalent plot for fuel pellets enriched in ^{235}U to 4.45%. It is seen in

these figures that the assay values deviate more significantly from the reported mass values for both sets of pins as the mass increases. 800mg of ^{235}U in natural uranium pins looks like 650mg but looks like only 500mg when it is in the 4.45% enriched uranium pins. This difference is essentially the self shielding distortion. Fig. 2a shows results for a set of small cylinders of pure ^{235}U dust. Here the self shielding is greater than 50% as 500mg of ^{235}U is barely 200mg in the assay.

Pure ^{235}U Powder

Pin ID	^{235}U(mg)	Factor
EU6	9.97	0.663
EU1	25.01	0.642
EU3	49.94	0.614
EU4	74.91	0.589
EU2	99.98	0.566
EU5	149.78	0.529
EU8	424.38	0.428
EU7	498.75	0.416

Depleted Uranium Slug

Height(in)	^{235}U(mg)	Factor
1.02	~500	0.794

Table 2:

Fig. 3 features the Quinby sources, a set of weapons grade plutonium cylinders. The roughly 20% deviation of the 2.96g source prompted a special study of the Quinby Sources plutonium distribution. These sources are cylinders of alumina, 7 inches in diameter and roughly 8 inches high — they are supposed to be uniformly doped with increasing amounts of weapons grade plutonium. In order for self shielding to account for the apparent 20% depletion of the 2.96g source, the plutonium would have to be crammed into a sphere with a radius of 1 inch. In fact, the γ-ray imaging of the Quinby Sources reported in a separate paper at this meeting indicates that the sources are reasonably close to being uniform, close enough that the factors indicated in Tab. 3 don't come anywhere close to explaining the active descrepancy.

Quinby Pu Sources

#	^{239}Pu(mg)	^{240}Pu(mg)	Factor
12	1	0.07	1.0
10	10	0.73	1.0
9	100	7.3	0.9993
12	1000	73	0.994
1	2940	213	0.973

Table 3:

Self Shielding in a Cylinder with Dimensions R,H

First Approximation

It is assumed that the fissile material does not appreciably attenuate the overall flux. This means that only effects within the calibration sample will be considered. The absorption within the sample will depend on the cross section for absorption of the materials in the sample. If several materials are present then the sum of the absorption probabilties should be used. Tab. 4 lists the relevevant parameters for both uranium and plutonium. The derivation assumes that the flux impinging on the sides of the slug is the same as that impinging on the top surface. The final form contains an integral which I could not put into closed form, necessitating a numerical integration.

$$\begin{aligned}
Fission &= Flux * \rho * Avagadro/A * \sigma_f \\
Absorption &= Flux * \rho * Avagadro/A * \sigma_a \\
Probability &= Avagadro/A * \sigma_a \\
&= 2.574\,(cm^2/g) \qquad ^{239}Pu \\
&= 1.802 \qquad ^{235}U \\
Flux(x) &= Flux(0) * e^{-x\lambda_a} \qquad \lambda = Probability * \rho
\end{aligned} \tag{1}$$

$$Fraction * volume = \frac{2H}{3}\int_0^{\pi/2} 2Rcos(\theta)d\theta \int_0^{Dcos(\theta)} e^{-\lambda x}\lambda dx + \frac{\pi R^2}{3}\int_0^H e^{-\lambda h}\lambda dh \tag{2}$$

$$Fraction = \frac{8}{3\pi\lambda D}\left[1 - \int_0^{\pi/2} cos(\theta)e^{-\lambda\, Dcos(\theta)}d\theta\right] + \frac{1-e^{-\lambda H}}{3\lambda H} \tag{3}$$

Cross Sections(barns)			
Isotope	Fission	Absorb	Elastic
^{235}U	584.4	683.21	15.04
^{238}U	0.0	2.717	9.360
^{238}Pu	17.89	558.19	28.54
^{239}Pu	747.4	1017.7	7.968
^{240}Pu	0.06	289.5	1.642
^{241}Pu	1012.0	1373.5	11.35
^{242}Pu	0.0	18.79	8.318
^{241}Am	3.02	603.4	11.14
^{16}O	0.0	0.0	3.87

Table 4:

Self Shielding Calculations

Internal Flux

The challenge at this point is to generate self shielding corrections sufficiently accurate that the various calibration sets can be used to form the absolute calibration for the *APNea* active mode. The first approximation formula listed above does fairly well for a squat cylinder but increasingly misses the mark as the cylinder becomes taller. The first term of Eq. 3 is independent of H, so all of the effect of having a taller cylinder is contained in the second term, which goes to zero as H becomes large. The measurements of the various pellet stacks in Fig. 1 indicate a much more gradual increase in the self shielding effect with increasing height. The focus of the next order calculation is to try to include and consider other aspects of the thermal flux.

The first insight was a simple one and was quickly included in the first order formula. Simply considering the fission capture cross section to calculate the flux attenuation neglects the fact that both 235U and ^{239}Pu have additional capture cross section which does not lead to fission. Therefore, in calculating the attenuation of the flux in the source material, the total absorption must be used. Surprisingly, it is the case for depleted uranium, a favorite calibration source material, that the ^{238}U contributes significantly to the absorption though

it contributes essentially nothing to the fission output. In natural uranium the absorption due to ^{235}U is less than twice that due to the ^{238}U — whereas this drops to less than 1 for depleted uranium. Thus, for the depleted uranium slug used with the *APNea* system, greater than half of the observed ($\sim$20%) self shielding is associated with the ^{238}U.

The next insight was a less obvious one for the author; essentially that the elastic scattering of thermal neutrons in the source medium must be included. This arises because, even though the elastic scattering does not deplete the flux, it does retard its penetrating a volume and it tends to hold some of the flux within the source volume where it has a further chance to interact with the fissile material. What this entailed was to do an integration through the source volume of the capture fission response, of the flux attentuation, and of the flux elastic scatter. A second integration integrated the fission response to the now internal flux and the attenuation and scatter of this internal flux. This procedure is continued until the internal flux dwindles to an uninteresting level. Again, one must include all of the materials in the source matrix which contribute to elastic scattering. For the fuel pellets which are in the molecular form of UO_2, the oxygen in the molecule ups the elastic cross section from 9 barns to over 16 barns. For the 100% enriched ^{235}U dust, the ^{235}U contribution is so large that the oxygen plays essentially no role.

The results of these more detailed calculation have been included in the *Factor* columns of Tabs. 1,2 and have been incorporated in several of the figures. It must be remember, however, that the point of the self shielding calculations is to provide the basis for an absolute calibration of the *APNea* active mode. Because this work is still preliminary, some of the observed deviations have to do with the absolute calibration and only indirectly with the self shielding calculation. In particular, some of the discrepancy of the enriched pin assays at 2.1g and 4.5g is surely related to the uncertainty in the absolute calibration.

It can be seen in the pin assay data of Figs. 1a,b that the self shielding calculation has the self shielding factor (SSF) falling too rapidly with increasing height of the pellet stack. It is likely that the calculation of the internal flux is still not detailed enough and more

experimental and calculational work is planned. The results for the enriched dust are hidden in Fig. 2b. Here the assay results are plotted as a function of the shielded mass calculations. Of interest is the result of the vertical/horizontal measurements. Since the source is in the form of dust, it takes on a truly cylindrical shape only when the tiny container is the the **vertical** position. Then the dust settles to the bottom and takes on the cylindrical shape of the container. When the container is in a horizontal position, the dust spreads out and increases its surface area. It turns out that the *APNea* measurements are sufficiently precise as to see the difference, as can be seen in the figure. There should be less self shielding in the horizontal position, and that is the case. The vertical measurements agree nicely with the self shielding calculations — there is no obvious effect of too much self shielding with increasing height (mass). Part of this may be the fact that the H/R never becomes too extreme, but it is also explained by the fact that there is little internal flux within the pure dust.

The Quinby sources are of special interest because they feature plutonium rather than uranium, and they also feature a fairly uniform distribution of a low density of the material. The self shielding factors from calculations based on the γ-ray imaging are listed in Tab. reft:quin. Here it can be seen that the factors are simply not large, in fact, small enough to be lost in the measurement uncertainties. The measurements of ^{240}Pu shown in Fig. 3b demonstate the general integrity of the sources. The discrepancy in the assay values over the recorded mass values is less than 2%. On the other hand, the experimental uncertainty in the ^{240}Pu vlues can be seen to be dominated by counting statistics, even for the hottest source.

An interesting aspect for the plutonium sources is that there are 3 independent measures. The active measurement of ^{239}Pu is one, the auto-correlation measurement of ^{240}Pu is another, and the third is the direct measurement of the neutron output from the source (**Singles**). Since all of the Quinby sources were made from the same batch of weapons grade plutonium, one would expect that the singles rate should correlate closely with the actual

plutonium loading. Fig. 4a shows both the assay and the report values for ^{239}Pu plotted against the singles rate. The separation of the two sets of values at 1 gram is largely due to the uncertainty in the absolute calibration, but the Quinby value at 2.96g clearly does not follow the singles as well as do the *APNea* active results. This is unfortunate, since the singles rate should not be affected by self shielding or source distribution, but it is pleasing that the active results do seem to follow the singles rate fairly closely. As a further insight into the problem, Fig. 4b shows the region near 1 gram in more detail. The vertical separation of the two data sets depends on the absolute calibration, but the overall agreement of the various results with the singles measurements clearly indicates that the Quinby results have a degree of error which is noticeable.

Conclusions

The method for calculating the self shielding correction for cylindrical sources clearly predicts too much shielding as the height and fissile mass of the source increases, but the deviation is relatively small. It does mean, however, that the quality of a fissile source is compromised if the actual fissile contribution in a particular differential dieaway device cannot be precisely predicted. In general, the quality of the current predictions is adequate to provide calibration points for the active mode the *APNea* System. The experience is sufficient, however, to indicate that etablishing the basis for the active mode calibration is not trivial and that correcting for the actual clumping of fissile material in waste will be difficult whenever significant clumping is suspected.

Acknowledgements

Oak Ridge National Laboratory is managed by Lockheed Martin Energy Research, Inc. for the U.S. Department of Energy under contract no. DE-AC05-96OR22464. The submitted manuscript has been authored by a contractor of the U.S. government. Accordingly, the U.S. Government retains a nonexclusive, royalty-free license to publish or reproduce the published form of the contribution or allow others to do so for U.S. Government purposes.

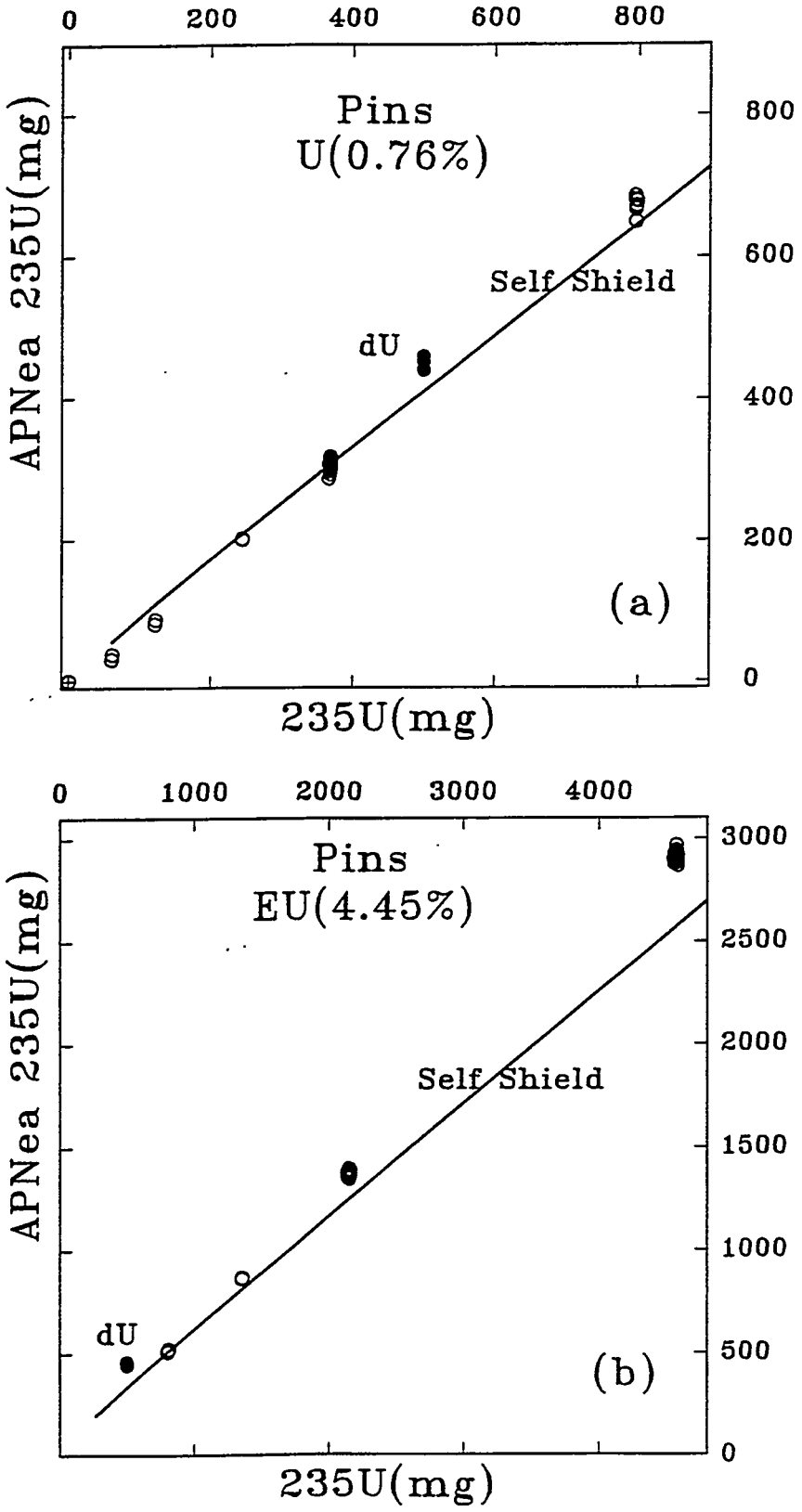

Figure 1: Pins of Fuel Pellets

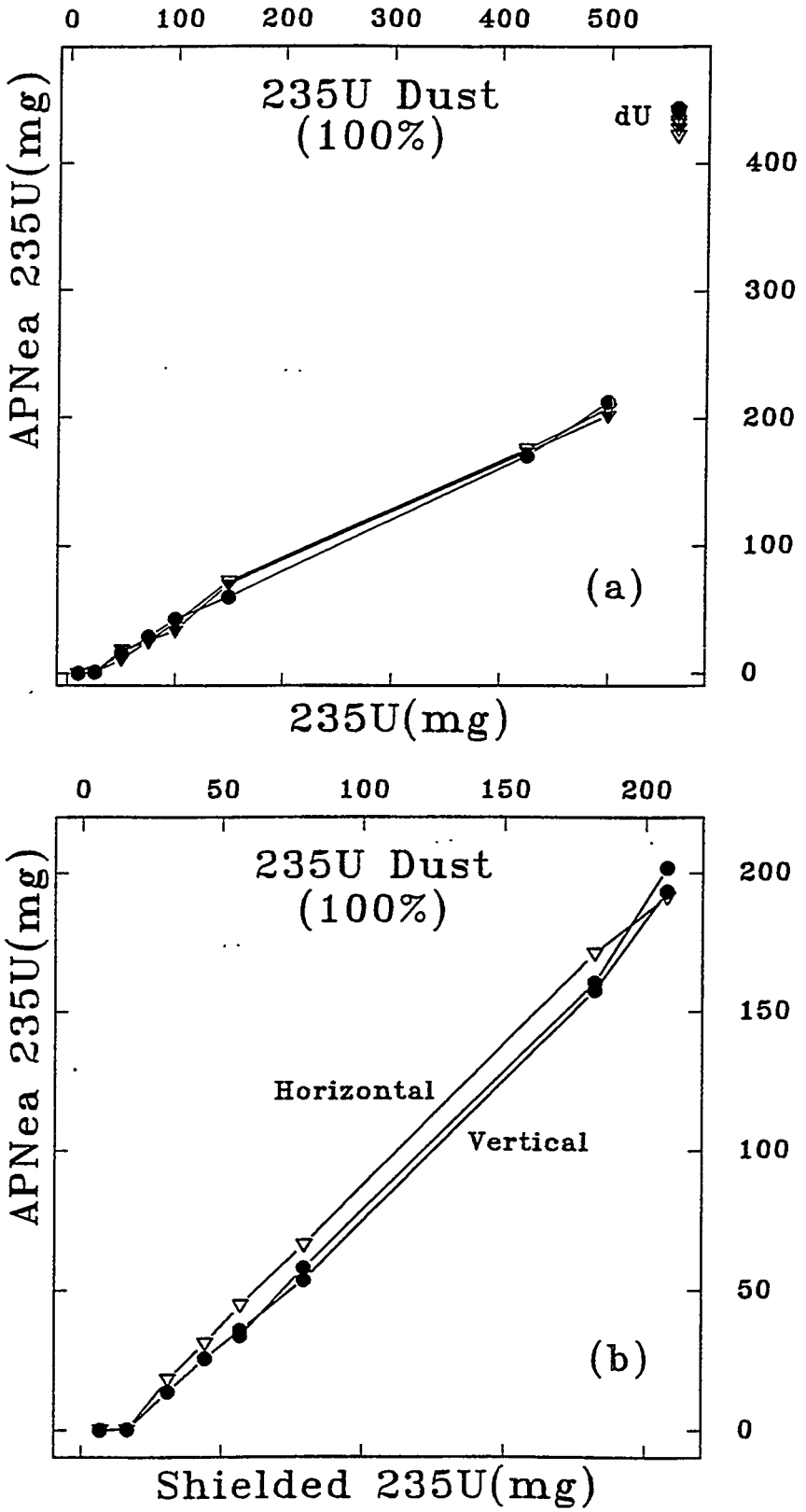

Figure 2: Pure 235U Dust

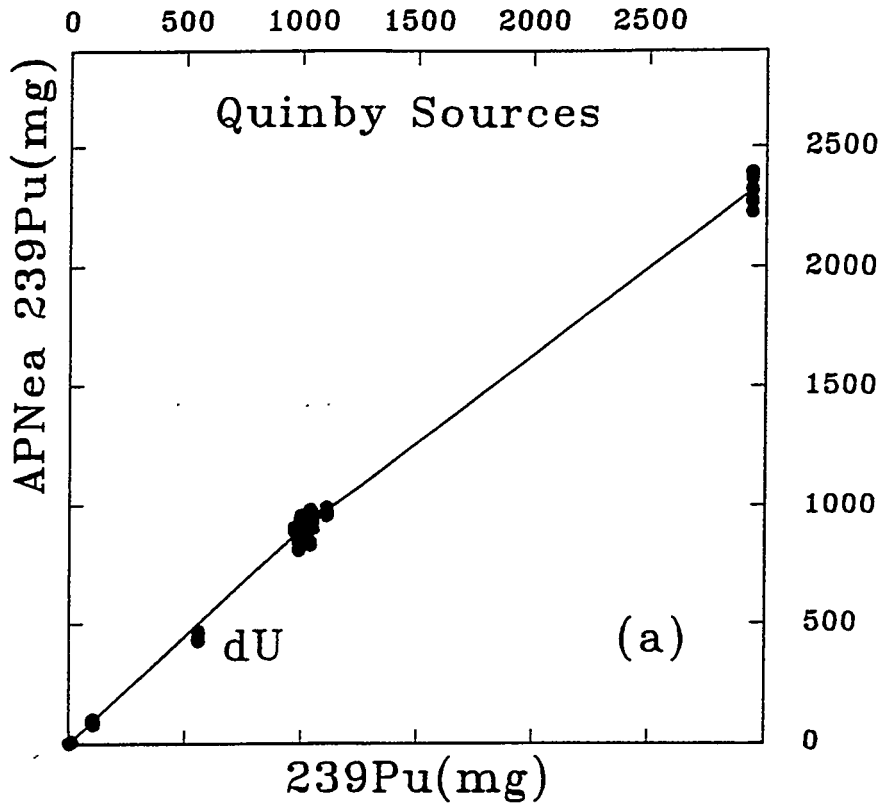

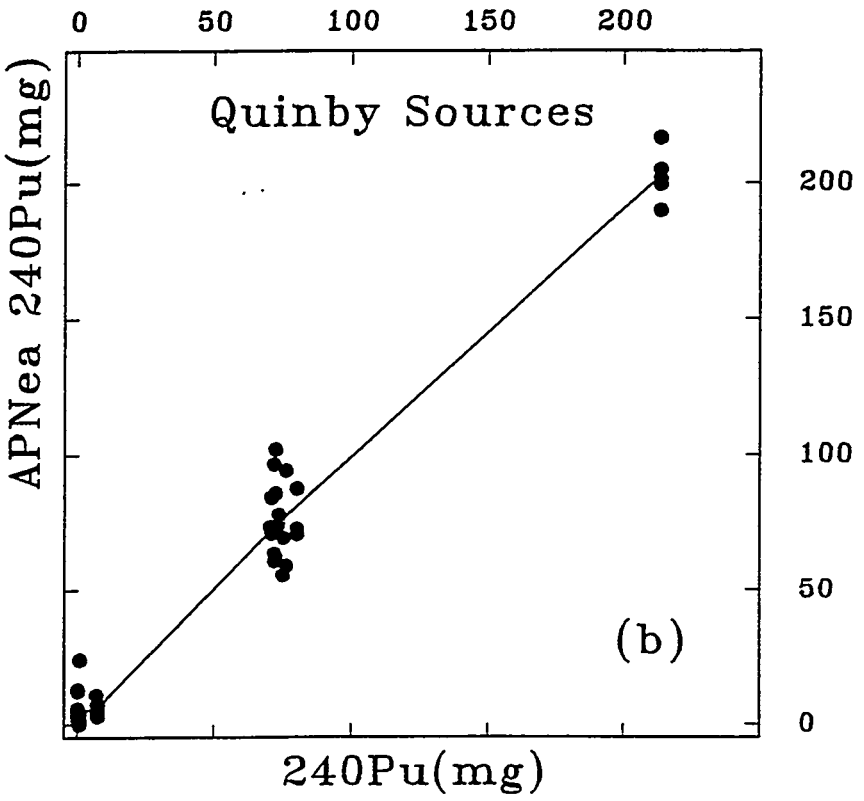

Figure 3: Quinby Sources

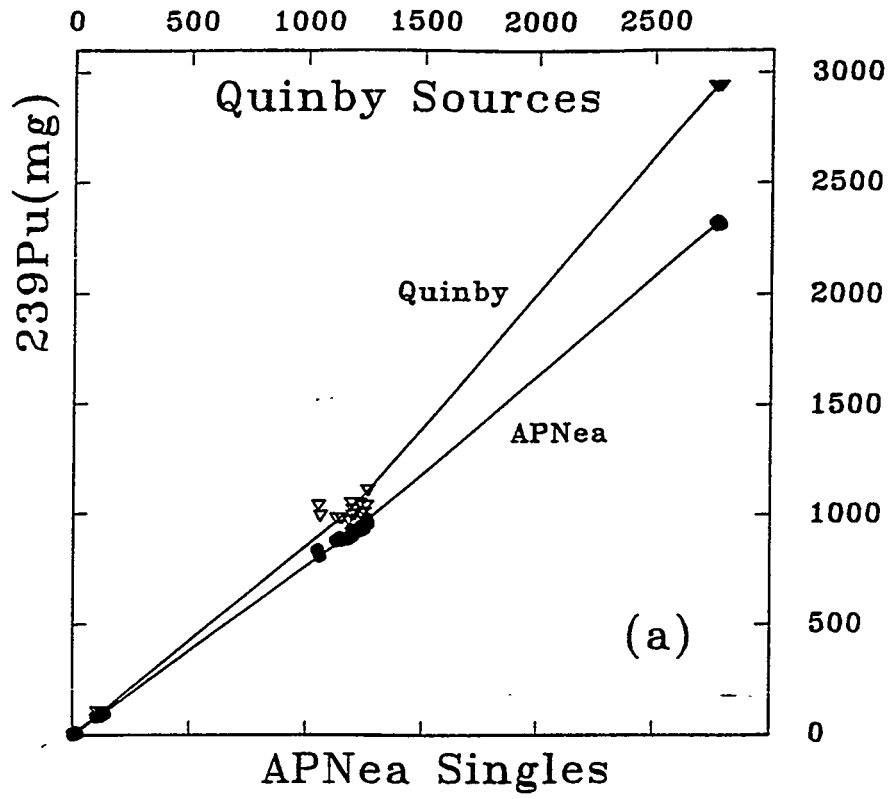

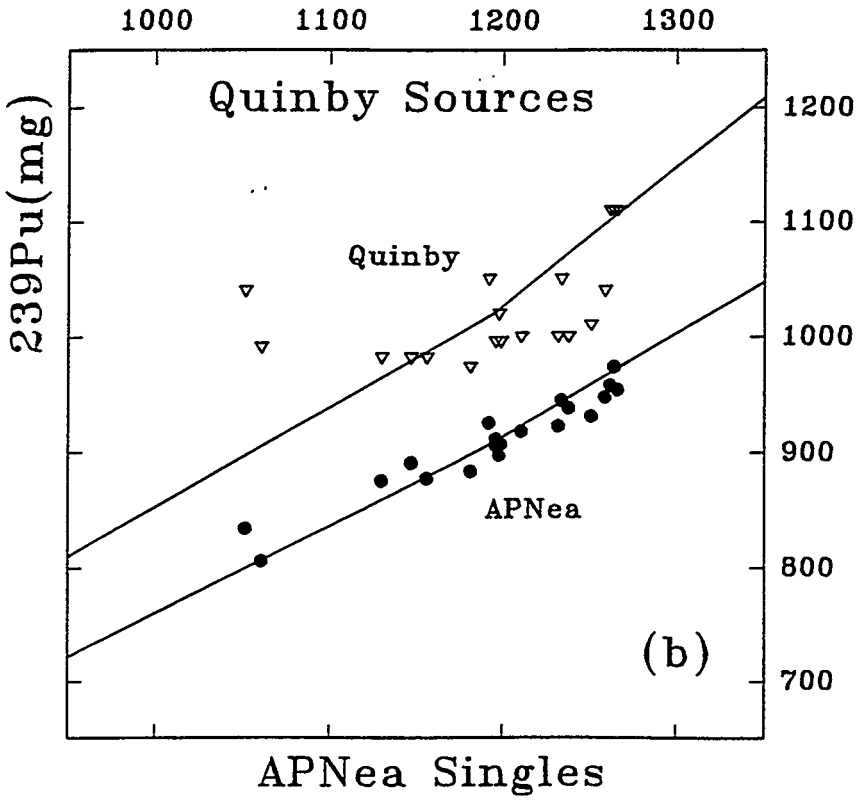

Figure 4: Quinby Singles

Technical -
Gamma NDA Techniques/Design/Applications

The Development of a New Edition of the Gamma-ray Spectrum Catalogues Designed for Presentation in Electronic Format

R. L. Heath
Idaho National Engineering Laboratory
Lockheed -Martin Idaho Technologies Co.

ABSTRACT

New editions of the original Gamma-ray Spectrum Catalogues are being prepared for publication in electronic format. The objective of this program is to produce versions of the Catalogues in CD-ROM format and as an Internet resource. Additions to the original content of the Catalogues will include integrated decay scheme drawings, tables of related decay data, and updated text on the techniques of gamma-ray spectrometry. Related decay data from the Evaluated Nuclear Structure Data File (ENSDF) are then added, and all data converted to the Adobe Acrobat (PDF) format for CD-ROM production and availability on the Internet. At a later date the catalogues will be expanded to include spectra representing the response of large-volume Ge detectors, alpha-particle spectra, prompt neutron capture and inelastic scattering gamma-ray spectra, and gross fission product spectra characteristic of fuel cycle waste materials.

Characterization of radioactivity in materials is a requirement in many phases of radioactive waste management. Movement, shipping, treatment, all activities which involve handling of mixed waste or TRU categories of waste at all DOE sites will require that measurements and assessment documentation utilize basic nuclear data which are tracable to internationally accepted standard values This program will involve the identification of data needs unique to the development and application of specialized detector systems for radioactive waste characterization.

INTRODUCTION

A program is presently underway at the INEL to produce new editions of the original Gamma-ray Spectrum Catalogues[1-3] for publication in electronic format. The objective of this program is to produce versions of the Catalogues in CD-ROM format and as an Internet resource. Additions to the original content of the Catalogues will include integrated decay scheme drawings, tables of related decay data, and updated text on the techniques of gamma-ray spectrometry. All of the original spectral plots for over 300 radionuclides, gamma-ray energy and intensity data, and text have been converted to digital format. Related decay data from the Evaluated Nuclear Structure Data File (ENSDF) are then added, and all data converted to the Adobe Acrobat (PDF) format for CD-ROM production and availability on the Internet from the Gamma-ray Spectrometry Center web

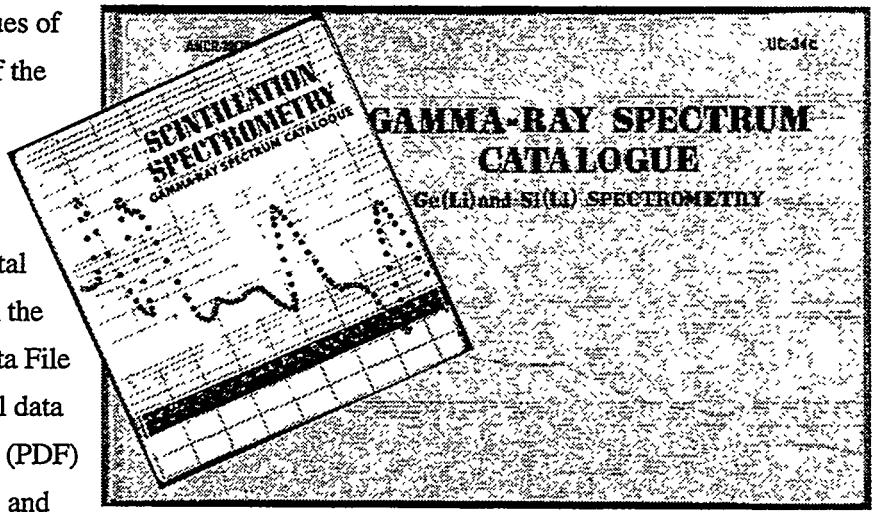

Fig. 1. The original published editions of the Gamma-ray Spectrum Catalogues which contain gamma-ray spectra for Ge semiconductor and NaI(Tl) scintillation detectors.

site at the INEL.. Major objectives of the program include: (a) production of a baseline CD-ROM version of the original Gamma-ray Spectrum Catalogues for NaI(Tl) Scintillation detectors and Ge semiconductor detectors (illustrated in **Fig. 1**) and, (b) development of enhanced content for follow-on expanded versions of the spectrum catalogues. Characterization of radioactivity in materials is a requirement in many phases of radioactive waste management. Movement, shipping, treatment, and activities which involve handling of mixed waste or TRU categories of waste at all DOE sites will require that measurement documentation utilize basic nuclear data which are tracable to accepted standard values. This program will target the identification of data needs unique to the development and application of specialized detector systems for radioactive waste characterization. To meet these needs, expanded versions of the Spectrum Catalogues are being developed which will include alpha-particle spectra, prompt neutron capture and inelastic scattering gamma-ray spectra, and spectra for relevant detector configurations.

CONTENT FOR THE BASELINE CD-ROM EDITION OF THE SPECTRUM CATALOGUES

In addition to the original gamma-ray spectra, the first version of the new edition of the Catalogues will be enhanced to include: (1) decay schemes in an integrated format designed for monitor display and, (2), the addition of decay data from the Evaluated Nuclear Structure Data File (ENSDF)[4]. Initially, the original data set, enhanced with decay data and decay schemes, will be available in CD-ROM format with outline content on the INEL web site in 1997. Examples of the content of the first edition of the new Spectrum Catalogues in CD-ROM format are presented in Figs. 2 and 3. **Fig. 2**

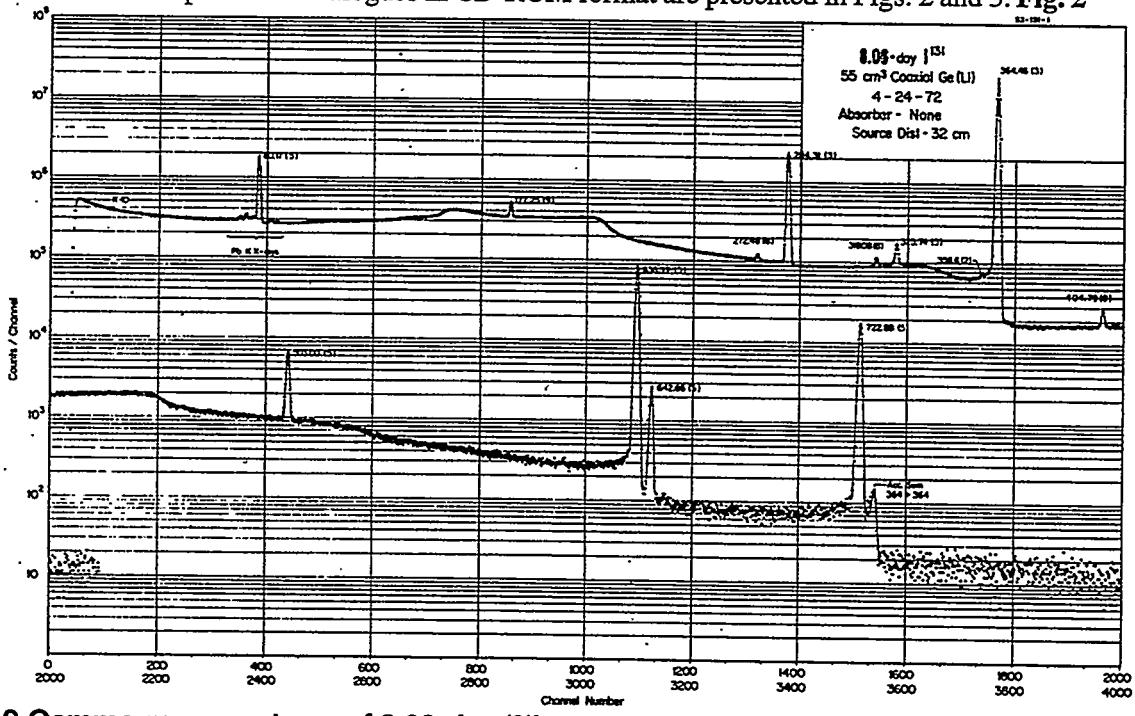

Fig. 2.Gamma-ray spectrum of 8.02-day ^{131}I. shown is a plot of a digital scan for version 1.0

shows the spectrum of ^{131}I from the Ge Spectrum Catalogue as it appears in the new Edition. **Fig. 3** illustrates decay schemes for 49 yr. ^{44}Ti and 2.14 min. ^{211}Bi and their associated decay products. These examples serve to illustrate the concept of the "integrated decay scheme" adopted for the new

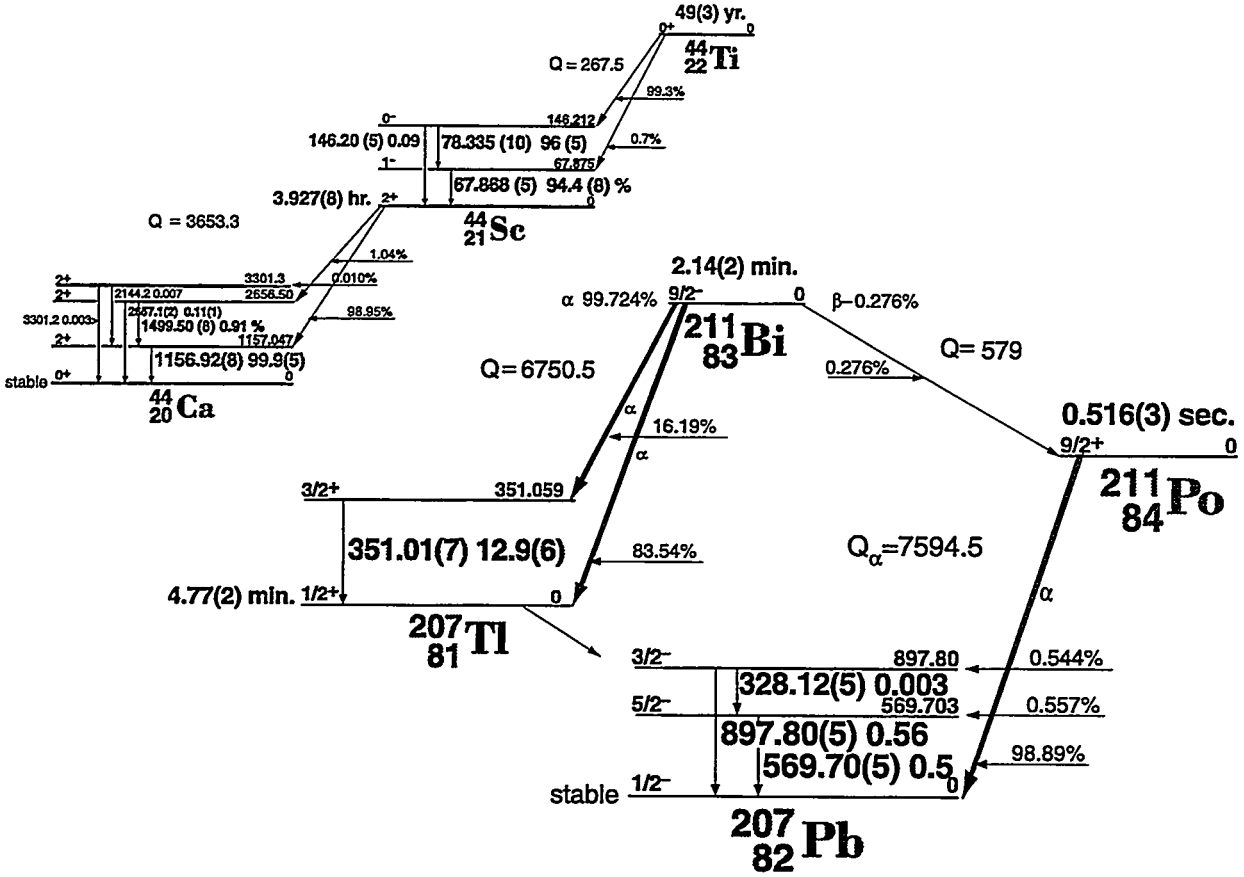

Fig. 3 Examples of decay schemes in the format adopted for the new Gamma-ray Spectrum Catalogues. These decay schemes include all radiations associated with the decay of a source of a given radionuclide, as would be observed in an experimental measurement.

Spectrum Catalogues. These decay schemes illustrate all modes of decay associated with a given nuclide, providing values for gamma-ray energy, absolute intensity, and half life with associated uncertainties. Color is used to highlight gamma-ray transitions which are significant in the interpretation of measured pulse-height spectra.

ENSDF DATA IN CATALOGUES

The original Ge Spectrum Catalogues contained plots of experimentally measured gamma-ray spectra, gamma-ray energies, and relative intensities. The new editions have incorporated values for absolute gamma-ray intensities obtained from the Evaluated Nuclear Structure Data File[4]. **Table I**, shown below, is an example of the data included with each spectrum in the catalogue. The

format followed in these data tables is as follows:

Header: Isotope, half -life, detector data, and method of source production

Column 1 Comments on source of gamma-ray line

Column 2 Gamma-ray energy (keV) - source of data indicated, e.g.[c] refers to the source as the orignial experimental values published in the Catalogue

Column 3 Experimental uncertainty for gamma-ray energy in Column 1

Column 4 Experimental value for Gamma-ray intensity (relative)

Column 5 Gamma-ray Intensity (Absolute) - data from ENSDF

Column 6 Sensitivity Index value for gamma-ray line in spectrum (S), where the quantity S is related to the magnitude of a given line above the underlying background. Thus a value of 1 for S indicates a gamma-ray peak exceeding the underlying "continuum" in the pulse amplitude distribution by more than one order of magnitude.

Table I - Decay Data Tables in Spectrum Catalogues

GAMMA-RAY ENERGIES AND INTENSITIES

Nuclide: ^{144}**Ce** - ^{144}**Pr** Half Life: 284.893(8) day - 17.28(5) min.
Detector 65 cm^3 coax. Ge(Li) Method of Production: U (n,f) chem

	E_γ(keV)[C]	ΔE	I_γ(rel)	I_γ(%) [E]	ΔI_γ[E]	S
^{144}Ce	53.34	± 0.02	6.64	0.10	± 0.01	3
^{144}Ce	**80.12**	**± 0.025**	**108.3**	**1.36**	**± 0.06**	**2**
^{144}Ce	99.96	± 0.035	2.67	0.040	± 0.003	3
^{144}Ce	**133. 53**	**± 0 .03**	**80.0**	**11.0**	**± 0.3**	**1**
^{144}Pr	**696.492**	**± 0.019**	**100**	**1.30**	**± 0.06**	**1**
	814.13	± 0.15	0.18	0.0032	± 0.(2)	4
	864.28	± 0.18	0. 21	0.0024	± 0.(2)	4
DE	**1163.73**	**± 0.05**	**3.56**		**± 0.25**	**2**
	1387.92	± 0.18	0.57	0.0087	± 0.(7)	3
	1489.124	**± 0.032**	**21.**	**0.28**	**±0.02**	**1**
SE	**1674. 59**	**± 0.080**	**3.53**		**±0.25**	**2**
	2185.608	**± 0.046**	**57.0**	**0.69**	**±0.03**	**1**

DEVELOPING CONTENT FOR EXPANDED VERSIONS OF CATALOGUES

The second phase of the Gamma-ray Spectrum Catalogue program will include several major additions which should enhance the Catalogues as laboratory reference material. These will include:

1. New digital plots of original gamma-ray spectra

2. **Spectra representing response of large-volume Ge detectors**
3. **A new tutorial text volume on gamma-ray spectrometry using Ge detectors**

NEW DIGITAL PLOTS OF ORIGINAL SPECTRA - Fortunately, due to a well established data archiving effort at the INEL, the original experimental data for all spectra in both the NaI{Tl} and Ge Catalogues are available in digital format. Using these data, a plot format has been developed for screen display, annotated with gamma-ray energies, absolute intensities, and half-lives with uncertainties. **Fig. 4** shows two Ge gamma-ray spectra for the radioisotope ^{133}**Ba**, comparing a digital scan of the spectrum appearing in the original Ge Catalogue and a new

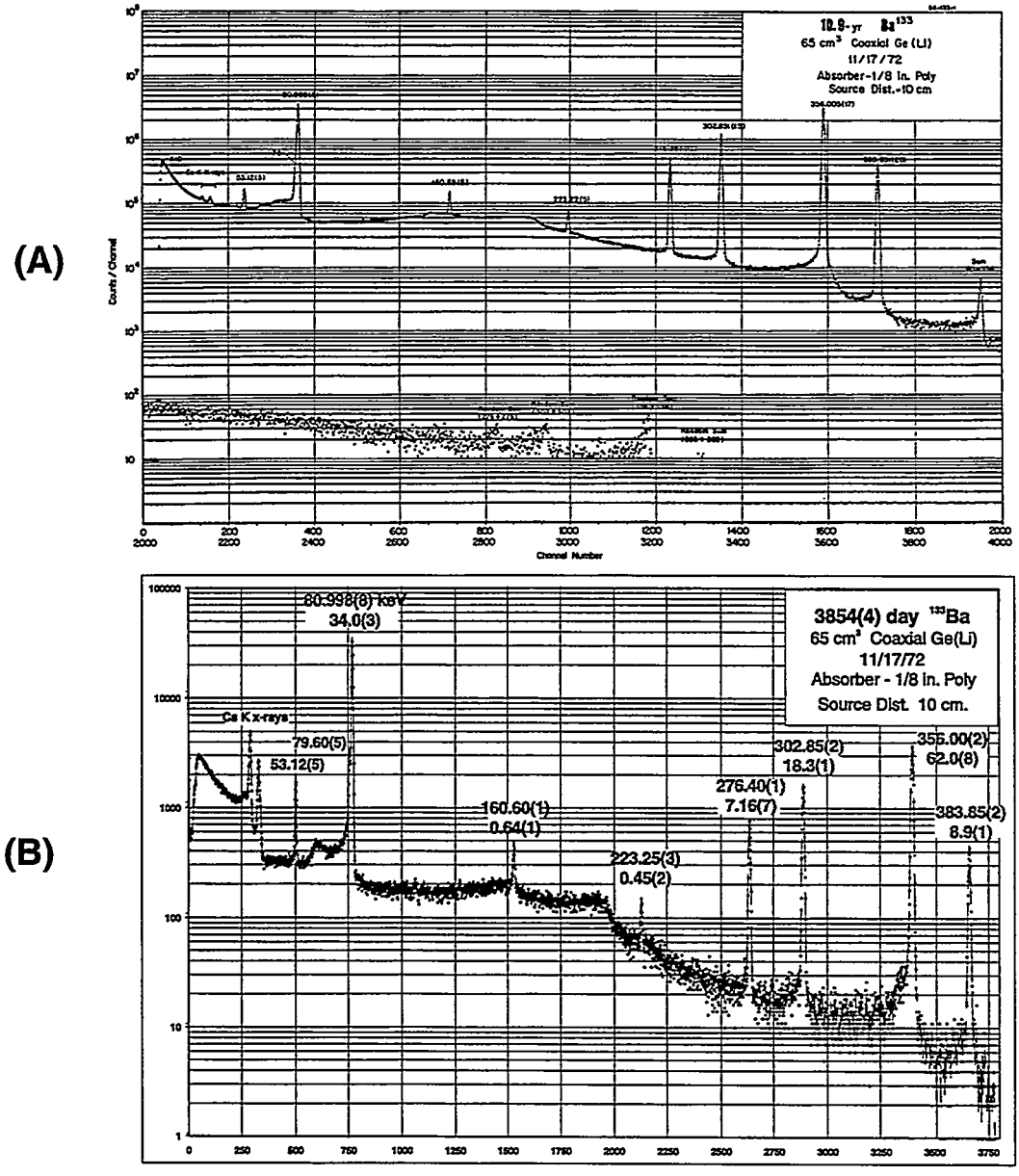

Fig.5. Examples of Ge gamma-ray spectrum of ^{133}Ba . Shown are (A) a digital scan of the spectrum from the original edition and (B) a new digital plot (vector) incorporating decay data from ENSDF.

digital plot incorporating evaluated decay data. The plan is to produce new plots for all spectra in the NaI(Tl) and Ge Spectrum Catalogues to be included in the second CD-ROM release.

SPECTRA FOR LARGE-VOLUME GE DETECTORS - Reviewing the state-of-the-art in gamma-ray spectrometry at the present time as compared with technology in use at the time the original Gamma-ray Spectrum Catalogues were produced leads us to the following conclusions. The experimental techniques have remained relatively unchanged. Some improvement has been made in precision of data available (gamma-ray energies and intensities) and during the past 10 to 15 years significant advances have been made in detectors, electronics, and computer data analysis techniques for field implementation. This has largely resulted from the development of the PC computer as a standard lab platform.

In the detector arena, improvements in material purity has made it possible to increase the volume of intrinsic germanium detectors from a few cubic centimeters to over 500 hundred cc. The availability of large-volume detectors produces many practical advantages. The detector response to monoenergetic radiation is greatly improved as the detector volume is increased. This results from more multiple events occurring after the initial interaction of high-energy photons with the detector material. The net result of this is that a larger fraction of the events result in total-energy absorption and the detector response is simpllfied. For radioactive sources emitting very complex photon energy spectra the ability to analyze complex spectra is enhanced. This is important in the assay of mixed fission products and similar complex radiation sources. The development of large-volume Ge detectors over the past several years has greatly improved the performance of these devices for the analysis of complex gamma-ray spectra. **Fig. 6** compares the response of two Ge semiconductor detectors to a ^{60}Co source. The upper curve, designated "1", is the spectrum obtained using a 65 cc. volume Ge(Li) coaxial detector. The lower curve, designated "2", is the response of a 450cc

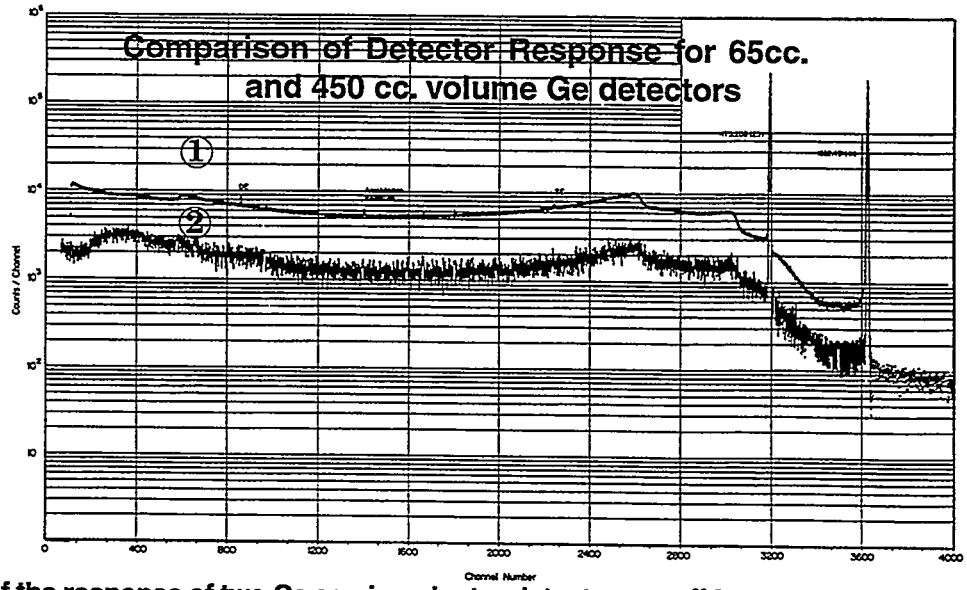

Fig.5 - Plot of the response of two Ge semiconductor detectors to a ^{60}Co source. Detector 1 has a 55 cc. volume and detector 2 a volume of 450 cc. The large detector has a much reduced fraction of pulses appearing in the "Compton electron distribution" which greatly increases the sensitivity of the device to low intensity, low-energy gamma rays.

intrinsic HPGe p-type coaxial detector. The spectrum obtained with the large detector indicates a significant reduction in the fraction of pulses appearing in the Compton-electron distribution, due to increased probability for total-energy absorption in events characterized by multiple Compton scattering and/or photoelectric events. The reduction of the Compton distribution, relative to the full-energy peak, will result in an increased sensitivity to low-energy, low-intensity gamma rays in complex gamma-ray spectra. For this reason the trend has been to utilize large-volume detectors. This leads to a need to provide new gamma-ray spectra from this class of detector in the Spectrum Catalogue database.

TECHNIQUES FOR THE CALCULATION OF SPECTRA

Techniques are presently under development to produce synthesized spectra representing the response of large-volume intrinsic Ge detectors (100% or greater relative efficiency) to isotopic sources. The method to be employed for the generation of spectra for radionuclides will utilize gamma-ray energies and intensities obtained from the evaluated nuclear decay database (ENSDF)[4] and detector response functions for monoenergetic gamma rays obtained using a combination of empirical modeling techniques, experimental spectra from monoenergetic gamma-ray sources, and monoenergetic detector response functions generated using Monte Carlo calculations. This will augment available experimental data.

The Monte Carlo calculational approach uses basic information on cross sections for the various processes occuring during the interaction of photons and secondary electrons with detector material and the geometry used for the measurement. All cascading events which occur following the primary interaction of each gamma ray with the detector material are followed, taking into account all mechanisms which deposit energy in the detector. Performing such calculations for a large number of primary events can produce a representation of the pulse-amplitude spectrum which would result from illuminating a detector with a monoenergeic source of radiation. For this approach to generating monoenergetic detector response functions we will apply the CYLTRAN Monte Carlo photon transport code[5] and the MCNP code [6]. Work is currently in progress to develop a method for calculating spectra in collaboration with Prof. Robin Gardner at North Carolina State U. and Russian scientists at the V. G. Khlopin Radium Institute in St. Petersburg, Russia. A summary description of the application of Monte Carlo techniques for the calculation of response functions is presented by Yin, Gardner, and Verghese[7]. To illustrate the capabilities of the Monte Carlo modeling approach to the calculation of detector response **Figure 6** presents a plot comparing an experimental spectrum of ^{60}**Co** obtained using a 39% HPGE coaxial HPGe detector with a spectrum generated using Monte Carlo calculated response functions for the two gamma rays emitted by this nuclide. Examination of the plot indicates excellent agreement between the two spectra.

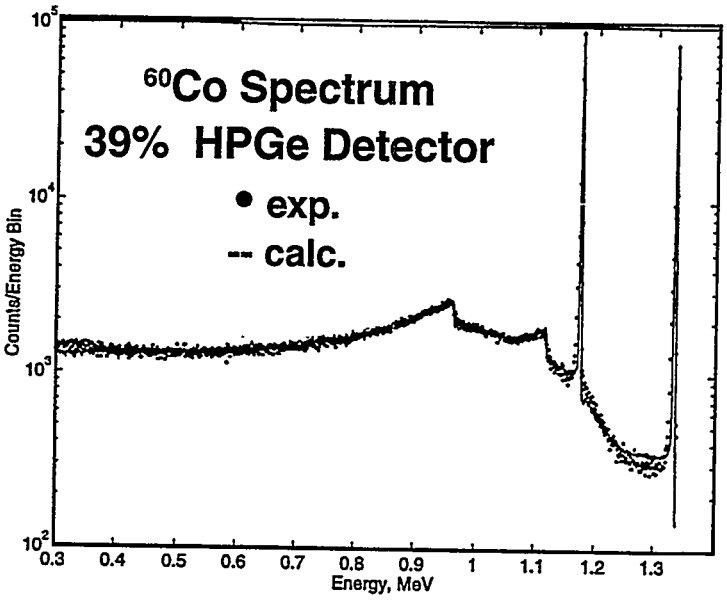

Fig.6- Comparison of experimental ^{60}Co spectrum obtained with a 39% HPGe detector with a spectrum generated from Monte Carlo calculated spectral shapes for monoenergetic gamma rays emitted in the decay of this nuclide.

GENERATION OF SPECTRA USING DETECTOR RESPONSE FUNCTIONS

Using experimental spectra obtained from monoenergetic gamma-ray sources and spectra calculated using the Monte Carlo calculational approach, the spectra will be treated with a modeling approach similar to that described by Heath, et. al. in Reference[8]. In this approach a 3-D surface is developed to define the detector response to a monoenergetic gamma ray of any energy by interpolation. With response functions obtained from this model for individual γ-rays and decay scheme data, an entire spectrum may then be generated. **Fig.7** shows a comparison of calculated and experimental spectra for the isotope ^{148}Pm

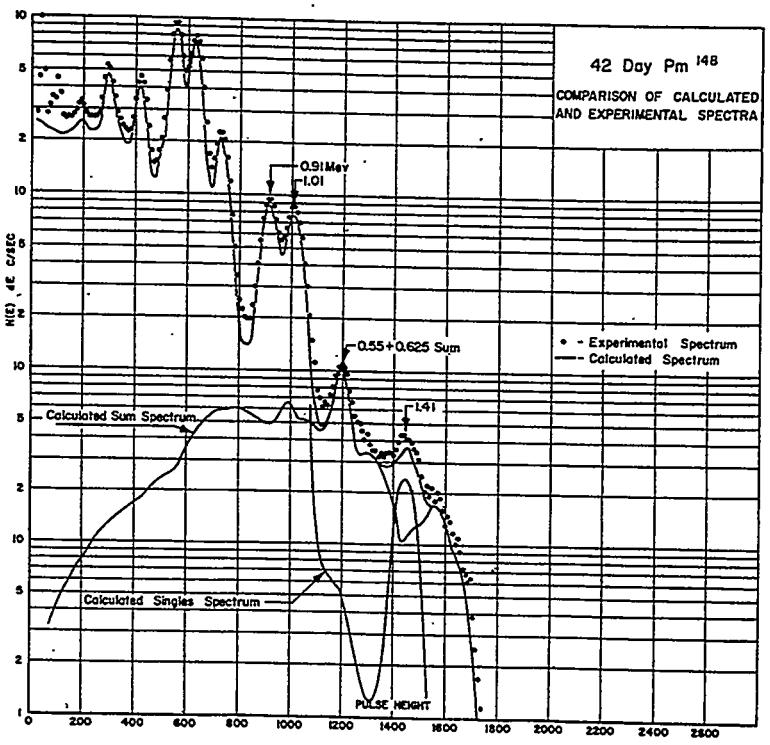

Fig. 7 Comparison of the measured spectrum obtained from a source of 42-day ^{148}Pm with a spectrum calculated by use of the spectral response surface for the standard 3" x 3" NaI detector..

for a NaI(Tl) detector. The result shows excellent agreement between calculated and experimental spectra, including coincidence summing effects. This methodology, in a refined form, will be used for the generation of both NaI and Ge detector spectra for selected detector configurations form and geometry.

ADDITION OF OTHER TYPES OF SPECTRAL DATA TO CATALOGUE DATABASE

Gamma-ray spectrometry as a major analytical tool is applied in many areas of basic and applied science. A review of the areas of application reveals the importance of prompt gamma ray measurments techniques which utilize the detection of reaction gamma rays emitted at the time the muclear reaction occurs. These "active interrogation" techniques involve the use of accelerator particle beams or neutron sources. Neutron sources employed include pulsed d,t generators which emit 14-MeV neutrons or spontaneous fission sources (e.g. ^{252}Cf) . The interaction of these neutrons with materials results in the emission of prompt photons which are characteristic of the nuclei being irradiated. In the area of nuclear environmental management we also have TRU materials which constitute fission neutron sources themselves, as a result of the emission of neutrons following spontaneous fission. Other reactions of interest in this area include the (α,n) reaction which can occur when intense sources of alpha particles are involved. In nuclear medicine more attention is being given to the use of particle accelerators as clinical irradiators. This serves to demonstrate the need for reference gamma-ray spectral data from these classes of nuclear reactions. To illustrate the complexity of prompt reaction gamma-ray spectra an example is presented in **Fig. 8**. This

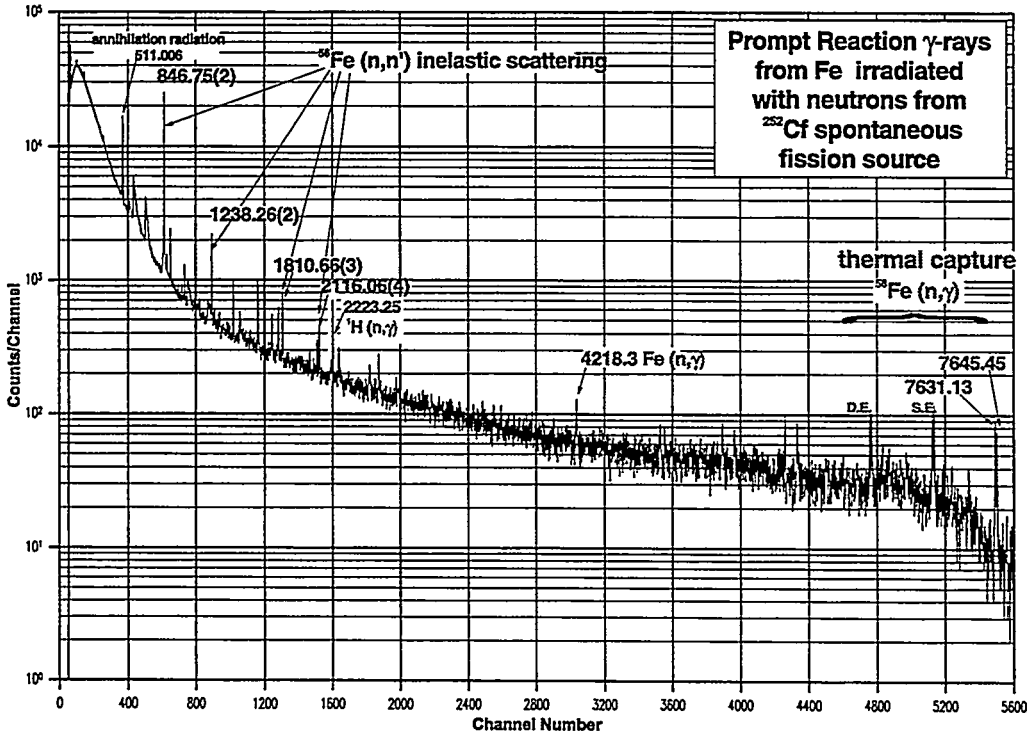

Fig. 8 Example gamma-ray spectrum of reaction gamma rays emitted by Fe object irradiated with fission neutrons emitted by ^{252}Cf source. Illustrates complexity of this class of spectral data.

figure shows the gamma-ray spectrum emitted from an Fe object during irradiation with fission neutrons emitted by a ^{252}Cf spontaneous fission source.

In view of the need for reference data in these areas, both experimental and calculated thermal neutron capture gamma-ray (n,γ) spectra, and inelastic scattering (n,n.γ) reaction gamma-ray spectra will be included as additional classes of spectral data in later editions of the Spectrum Catalogues. An experimental program is being developed to generate thermal neutron capture and inelastic scattering spectra for individual chemical elements. Neutron sources to be utilized for these experimental measurements will include the cold nedutron beam facility at the NIST reactor , D-T particle accelerators, and ^{252}Cf sources. Some data are currently being obtained to assist in defining data needs and planning an experimental program.

REFERENCES

1. R. L. Heath, "**Gamma-ray Spectrum Catalogue, Ge(Li) Spectrometry**", Report ANC-1000, 1974.

2. R. L. Heath, "**Scintillation Spectrometry, Gamma-ray Spectrum Catalogue**", 2nd Ed., 2 Volumes, Report IDO-16880 (1964).

3. R. L. Heath, , "**Scintillation Spectrometry, Gamma-ray Spectrum Catalogue**", 1st Ed., Report IDO-16408 (1957).

4. Evaluated Nuclear Structure Data File, generated by International Network for Evaluation of Nuclear Structure and Decay Data, compiled by National Nuclear Data Center, Brookhaven National Laboratory.

5. J. A. Halbleib and T. A. Mehlhorn, *Nucl. Sci. Eng.* **92,** 338 (1986)

6.. Briesmeiser, J. F., "**MCNP - A General Purpose Monte Carlo Code for Neutron and Photon Transport, Version 3A**", Los Alamos National Laboratory Report LA-7396-M Rev 2 (1986).

7. Y. Jin, R. P. Gardner, and K. Verghese, *Nucl. Instr. Meth.* **A242,** 416(1986)

8. R. L. Heath, R. G. Helmer, L. A. Schmittroth and G. A. Cazier, "**A Method for Generating Single Gamma-ray shapes for the Analysis of Spectra**", *Nucl. Instr. Meth.*, **47**, 281 (1967)

ACKNOWLEDGEMENT

This Program is currently supported by the Department of Energy Office of Environmental Management (Science and Technology) and Energy Research under DOE Idaho Operations Contract DE-AC07-94ID13223 with Lockheed-Martin Idaho Technologies Co.

Mathematical Calibration Of Ge Detectors, and the Instruments That Use Them

F. L. Bronson CHP and Brian Young, Ph.D.
Canberra Industries, 800 Research Parkway, Meriden, CT. 06450 USA

ABSTRACT

Efficiency calibrations for Ge detectors are typically done with the use of multiple energy calibrations sources which are added to a bulk matrix intended to simulate the measurement sample, and then deposited in the sample container. This is rather easy for common laboratory samples. Bu, even there, for many environmental samples, waste assay samples, and operational health physics samples, accurate calibrations are difficult. For these situations, various mathematical corrections or direct calibration techniques are used at Canberra. EML has pioneered the use of mathematical calibrations following source-based detector characterization measurements for *in situ* measurements of environmental fallout. Canberra has expanded this by the use of MCNP for the source measurements required in EML. For other calibration situations, MCNP was used directly, as the primary calibration method. This is demonstrated to be at least as accurate as source based measurements, and probably better. Recently, a new method [ISOCS] has been developed and is nearing completion. This promises to be an easy to use calibration software that can be used by the customer for *in situ* gamma spectroscopy to accurately measure many large sized samples, such as boxes, drums, pipes, or to calibrate small laboratory-type samples.

Mathematical Calibration Of Ge Detectors, and the Instruments That Use Them

F. L. Bronson CHP and Brian Young, Ph.D.
Canberra Industries, 800 Research Parkway, Meriden, CT. 06450 USA

INTRODUCTION

Calibration the Traditional Way

Canberra is probably the worlds largest supplier of gamma spectroscopy systems, and as such has had much experience in detector calibration technology. The traditional, and still most accepted method, is with the use of radioactive sources. Consider the simple case of a laboratory counting system to count a 1 liter container of water. All the user needs to do is create an exact duplicate of sample and container, but with the addition of several appropriate radioisotopes. These radioisotopes are chosen with the following characteristics:

- Energies to extend below and above the range of interest;
- Adequate activity:
  - High enough to not require a long count time;
  - Low enough to not disturb the instrument response;
  - Appropriate chemistry to not precipitate, plateout, absorb, or evaporate;
  - Long enough half-life to allow preparation and measurement;
  - Enough gamma rays to define the shape of the curve;
  - Well known energies and yields;
  - Decay chain without coincident emissions to preclude summing effects;
  - A suitable mix of nuclides and activities for a single mixed-gamma source.

Although it is essentially impossible to have a perfect calibration source, there are several widely accepted mixtures that are commercially available and that we use frequently at Canberra as shown in Table I.

Table I.
Typical Calibration Sources used at Canberra

Energy [keV]	Nuclide	Energy [keV]	Nuclide
60	Am-241	88	Cd-109
122	Eu-152	122	Co-57
244	Eu-152	166	Ce-139
344	Eu-152	279	Hg-203
779	Eu-152	392	Sn-113
1112	Eu-152	662	Cs-137
1408	Eu-152	898	Y-88
		1173	Co-60
		1332	Co-60
		1836	Y-88

These sources have generally proven adequate for routine calibration of samples for environmental measurement, or for health and safety measurements. With the purchase of proper quality calibration sources and with care in the preparation of the standard, very good efficiency calibrations can be obtained. Sources of error in this process for a typical laboratory include:

- Uncertainty in yield (generally <3%)
- Calibration source accuracy (3-5% typically)
- Counting statistics (generally 1-2%)

- Errors in dilution (1-2%)
- Losses from plating, precipitation and other mechanisms (can be a serious problem for Am, Pu, Hg, Sn)
- Coincidence losses (typically <5%)

From these uncertainties, it would seem that calibrations in the 5-10% range would be quite easy. And if all the laboratory did was to count small samples of water, life would be simple. But most of the environmental laboratory samples are somewhat different from the calibration conditions, or have other conditions that make the calibration not completely representative of the sample.

- Samples can have a density from 0.001 - 2 g/cc, which makes mixable bulk calibration sources and matrices much more difficult to find;
- Sample matrices can have a Z that is different than water, which can cause rather severe problems at low energies, unless this is also present in the calibration matrix;
- When a non-liquid matrix is used, then uniformity of the radionuclide throughout the calibration standard is difficult to obtain or prove;
- Sample containers sometimes change shapes in the calibration process [e.g. when curing epoxy matrices], or change shapes during use, and may not be representative of the assay container.

Because of these differences between the traditional calibration source, and the typical environmental, waste, or operational radiation protection measurement sample, this leads to the more realistic [in the authors opinion] calibration error estimate of 10-25%.

Actually, for most of these applications, a 25% error is not much of a problem, but it is still appropriate for the laboratory to minimize the measurement errors as much as practicable.

Unique calibration sources are sometimes manufactured for each of these special geometries, but this can be quite expensive. Alternately, empirical calibration correction techniques are frequently used to extrapolate in density and/in Z from a measured calibrations standard. But these are of limited use since they only apply to a specific geometry.

When the laboratory must measure large samples, then these simple laboratory calibration techniques are no longer economical to use. We manufacture a large number of instruments that measure samples of sizes of 50 liters, 100 liters, 200 liters, 1000 liters and even 20,000 liters. These instruments are most commonly used for measurement of radioactive waste, measurement of TRU waste, or measurements to prove that the sample is suitably "not-radioactive". For these samples, the cost of procuring a series of standards with sufficient activity, mixing those standards with a suitable matrix, and then ultimately disposing of the large sources as radioactive waste can be prohibitive.

For some simple geometries (rotating cylinders) we have had much success with a series of line sources. For example, for our Q^2 system, or Waste Assay System, we have constructed a set of four 200 liter drums, each with a different bulk matrix. The density of these are approximately 0.01 (foam), 0.3 (cellulose), 0.8 (wood), and 1.6 (sand). In each drum, six parallel holes are drilled from top to bottom. Each hole is in the center of six concentric equal area elements of the full drum. Six line sources of Am-241 and Eu-152 are inserted into the holes. When the drum rotates, these six line sources adequately simulate a uniform cylinder ($\leq \pm 10\%$). We have also done this for a 1000 liter cylinder, but matrix and construction costs are high.

For many other geometries, we have simulated a uniform concentration with a large number of point sources, as shown in Table II. While this was certainly successful at the time, it still was rather difficult and expensive, and problematic at low energies (<200 keV).

Table II.
Calibrations with Multiple Point Sources

Application	# Sources	Nuclides
Livermore Lung for U/Pu *In Vivo* Lung calibration	~1000	Am-241, Eu-152
Lamb/Sheep/Cow phantom	~100	Cs-137, Co-60
Person with variable weight (50-200 kg)	~1000	Eu-152
200 liter drum with variable density [0.2 - 1.6 g/cc]	~200	Am241, Eu-152

Most of the problems and/or expenses identified in this section can be avoided by the use of a properly implemented mathematical calibration procedure.

MCNP Mathematical Calculations

Having experienced the difficulties calibrating of these moderate sized samples, and planning to build systems to count even larger and more difficult samples, we started investigating full mathematical calibration tools about three years ago. Our goal was to have a design and development tool to help us optimize the number of detectors, their size, and the detector placement strategy.

A potentially useful tool would be Monte Carlo modeling. MCNP [1] is a well known general-purpose Monte Carlo code commonly used for neutron transport applications. It is also capable of modeling photon problems. There have been a few very useful publications describing the use of MCNP to model gamma ray spectra and efficiencies for Ge detectors [2, 3, 4, 5]. However, these have generally evaluated fairly simple detector-source geometries, or they have not performed direct efficiency calibrations. Important issues such as what are the critical parameters, how much detail is necessary in the model, etc. have not been studied, or reported.

During this evaluation, a series of experiments was conducted. Each experiment compared an efficiency computed with MCNP to another efficiency measured with a radioactive source in the same geometry. The most simple case was done first (point source on the axis for a Ge detector). Eventually, usually after several iterations, we achieved suitable agreement, and then went on to a more complex geometry. The sequences of events is shown in Table III. When there was initial disagreement between the two calibrations, the causes can be explained and solved as described in Table IV.

Table III.
MCNP Validation Sequence

MCNP Validation Experiments
Point source on axis of detector
Point source at 45 degrees
Point source at 90 degrees
Line source
Planar source
Heavily attenuated point source - various attenuator thickness
Small complex source - Marinelli beaker
Large complex source - 200 L drum, 4 densities, 3 detectors

Table IV.
Problems Discovered and their Solutions

Problem	Solution
Inadequate model of the detector	Increase the complexity of the Ge detector model. Ultimately, we used 23 dimensions to describe the detector, holder, and endcap
Inadequate model of the source	Increase the complexity of the source, the container, and all other absorbers
Human error; e.g. incorrect understanding of MCNP or incorrect data entry	Vigilant proofing, use of tools to visualize the geometry [where available], and benchmarking to know reference points
Poor quality reference sources; even though all were tracable to NIST and allegedly with errors of <5%, 3 of the 11 source geometries had errors from 10-30%	Benchmarking unusual geometry calibration sources against other sources

But we did certainly learn how to use MCNP and validated it as a useful calibration tool. It is now frequently used by Canberra in for a variety of equipment design, testing, and calibration purposes.

IN SITU GAMMA SPECTROSCOPY OF SOIL

One of the most common applications of mathematical efficiency calibrations is in *in situ* Ge gamma spectroscopy of radionuclides on the near surface of soils. This is performed by placing a Ge detector at a standard position [commonly 1 meter] above the soil. Then the "sample" is counted, as shown in Figure 1.

Because of the very large sample size, detection sensitivity is quite comparable to that of laboratory measurements. Typical detection limits easily obtainable with common equipment are listed in Table V. This used a 15 minute count time over typical New England soil. Additional advantages over the traditional sample collection and laboratory measurement are approximately 1/2 the cost [6], immediate results, and better accuracy with non-uniform radioactivity distributions.

Figure 1
Typical *In Situ* Environmental Measurement

Table V.
Typical *In Situ* Detection Limits

Nuclide	LLD pCi/g	LLD Bq/g
Co-60	0.05	0.002
Cs-137	0.05	0.002
Eu-152	0.2	0.007
U-238 [Th-234]	8	0.3
U-238 [Pa-234m]	3	0.1
U-235	1	0.04
Am-241	1	0.04

Conditions of measurement:
15 min. count time over typical New England soil
40% coaxial Ge detector at 1 meter above ground
Uniform radioactivity distribution in soil

The most common calibration methodology is that of EML-300 (originally HASL-300). This is not a purely mathematical calibration, but instead uses a combination of radioactive sources and mathematical conversions. The user measures a multiple energy calibration source at 1 meter on the detector axis. Then repeated measurements are made at 1 meter and in 5° increments from 0 to 90°. Finally, a mathematical conversion is used to integrate the energy and angular response function into an efficiency calibration equation.

This calibration method has been very widely used and demonstrated to adequately represent simple distributions of radionuclides in the soil under the following conditions:

- Detector at the calibrated distance from the soil (typically 1 meter);
- Soil in an infinite flat horizontal plane;
- Radionuclides uniformly distributed in all radial directions out to nominally 20 meters;
- Vertical distribution in the soil represented by a single exponential, with the maximum at the surface.

While these assumptions are generally valid for environmental measurements in open areas with fresh fallout, they may not be applicable for environmental mediation measurements. Old depositions generally have a maximum somewhere below the surface. Weathering of the soil likely has reduced the surface contamination levels, and/or clean dirt/sod/coverings may have been added to the top.

While the full EML-300 technique uses radioactive sources to individually characterize each detector, a simplified technique was developed by Helfer and Miller at EML [7] which required no sources. This is basically an empirical calibration that is based upon the individual EML-300 calibration of approximately 40 detectors. The required data is diameter and height of the Ge detector element. This generic calibration methodology is used in some commercial software [Ortec M-1]. For many applications, this calibration is sufficient, but the user must be aware of these limitations.

- All mentioned in previous section;
- Calibration validated only for detectors of <45% relative efficiency;
- Calibration validated only for energies >200 keV;
- Calibration validated only for detectors with diameters:height ratios close to unity.

Because these limitations are commonly considered too great by our customers, and because the required multi-energy calibrations sources and measurements are difficult and easily inaccurate, Canberra has developed a combined MCNP/EML method. Each detector is individually calibrated, thus avoiding the generic calibration problems noted above. The point source measurements are replaced by MCNP computations. A theoretical point source is placed at each of the 10 radial locations. Energies from 50 keV to 3000 keV are used in the point source "measurements". Then the data is integrated and converted following the EML-300 technique into the 32 different calibrations that are delivered to each customer.

To validate this methodology comparisons were done between full MCNP and the MCNP-EML technique. Figure 2 shows the results for the uniform distribution geometry. The agreement is within 1% average and within 11% worst case. Similar agreement was obtained for the other three vertical distributions

computed. The major advantage of the MCNP-EML technique is computer time. MCNP computations for large samples take much computer time. The data in Figure 2 required several days time for a fast AXP computer, even using the various speed tricks we have learned. And this is just for 1 of the 32 calibrations delivered with the *in situ* system.

Full MCNP Efficiency Calibrations

But most geometries are not suitable for the simplified techniques described in the previous section. They are not very easy to numerically integrate. For these, we use the full MCNP computation, even at the expense of multiple days of computer time per run. This code has been extensively tested by Canberra with a series of validation comparisons to mixed gamma energy calibration sources [8]. We have shown MCNP to be consistent with source based calibrations to within 10% for energies >200 keV and to within 15% for energies between 60-200 keV. A few of the calibrations that have been done with MCNP are described next.

In situ well logging detector

For this application, the Ge detector is placed in a water-tight housing, and lowered down a hole in the ground, as shown in Figure 3. Measurements are made at various depths. Sometimes the detectors are uncollimated. Other times, they have internal or external shielding to limit the field of view to a known area. Previously, Canberra has calibrated these with a fixture containing approximately 100 tubes of Eu-152 in a plaster matrix. But this isn't very traceable, so MCNP was used most recently.

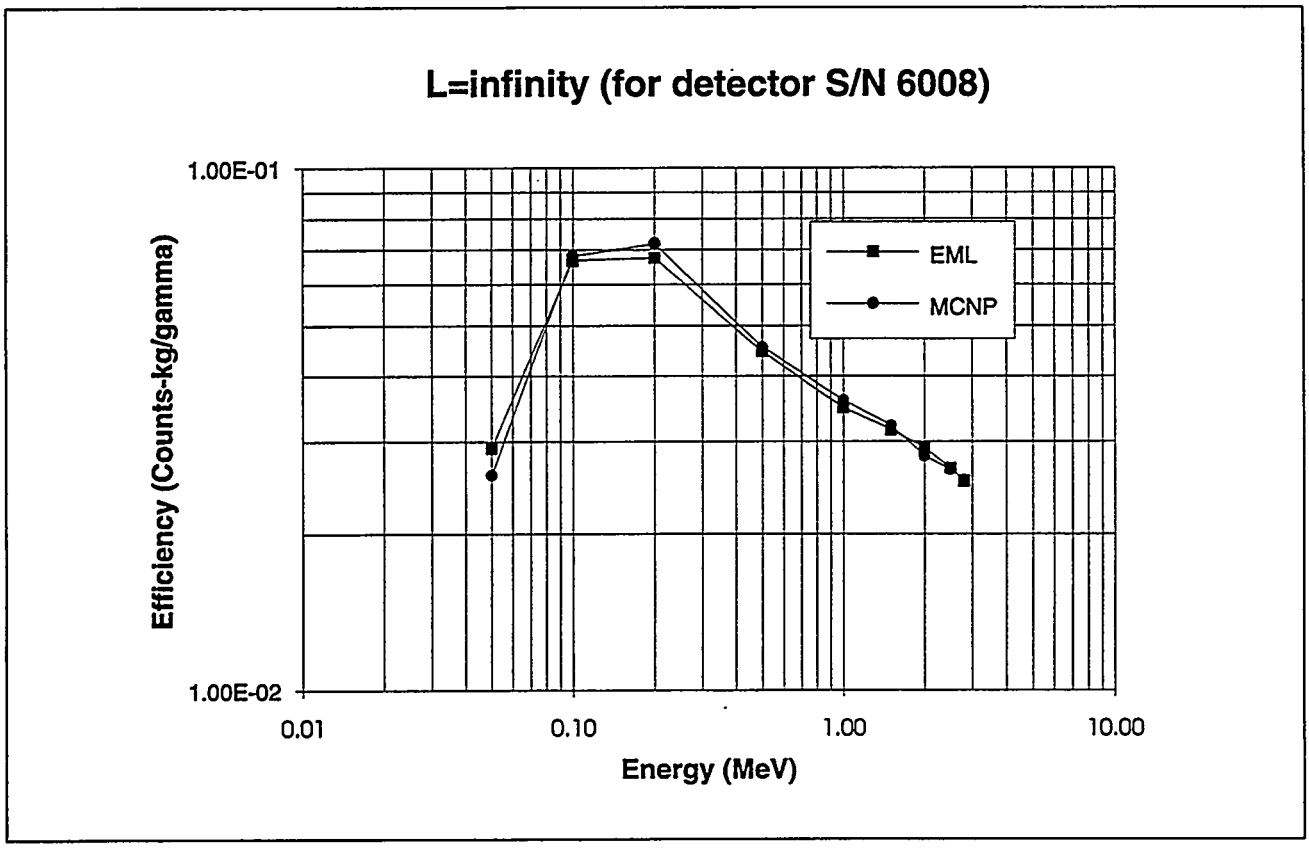

Figure 2.
Comparison Between MCNP and MCNP-EML In Situ Calibration

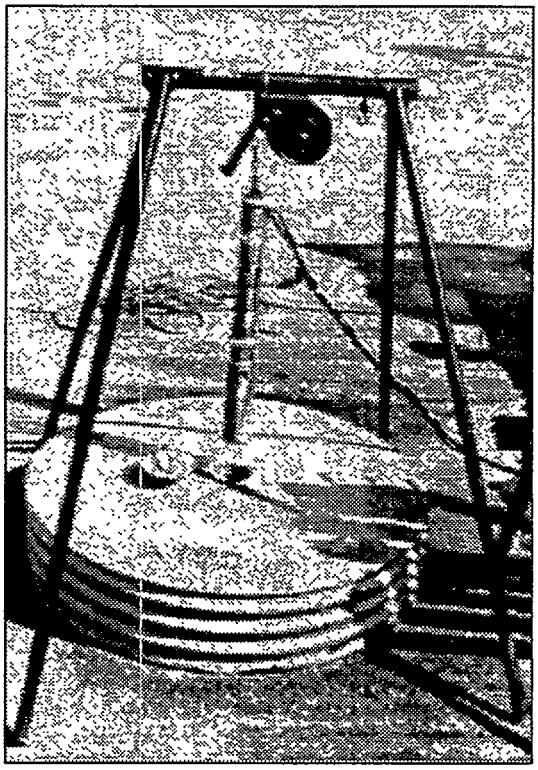

Figure 3.
Ge Detector being used in Well Logging Application

Large Box [and other] Counter

This product consists of four shielded and collimated Ge detectors, all counting the sample, but from different directions. Figure 4 is a composite showing the detectors of a manual box counter in the photos, and a drawing of the mechanism for an automatic system where the detectors move. The spectra are generally summed for analysis, but can be analyzed separately. The sample is a B-25 box, typically 4' x 4' x 6' in size. These were modeled with MCNP in four different densities to bracket the range of samples expected. Calibrations were also done for B-12 boxes [2' x 4' x 6'] and for a pallet of four 55 gal drums.

Portable Ge detector for B-25 Box field measurements

This customer is Canberra's Applications Services Group. They had a project to measure B-25 boxes of soil for Pu-238 to determine if they were TRU or not. A portable Ge detector with collimator was calibrated. Calibrations were done for the box with uniform radioactivity distribution. And to investigate the effect of non-uniform distributions or radioactivity, a variety of other point source distributions were also calibrated. Figure 5 shows the detector in use at the project site.

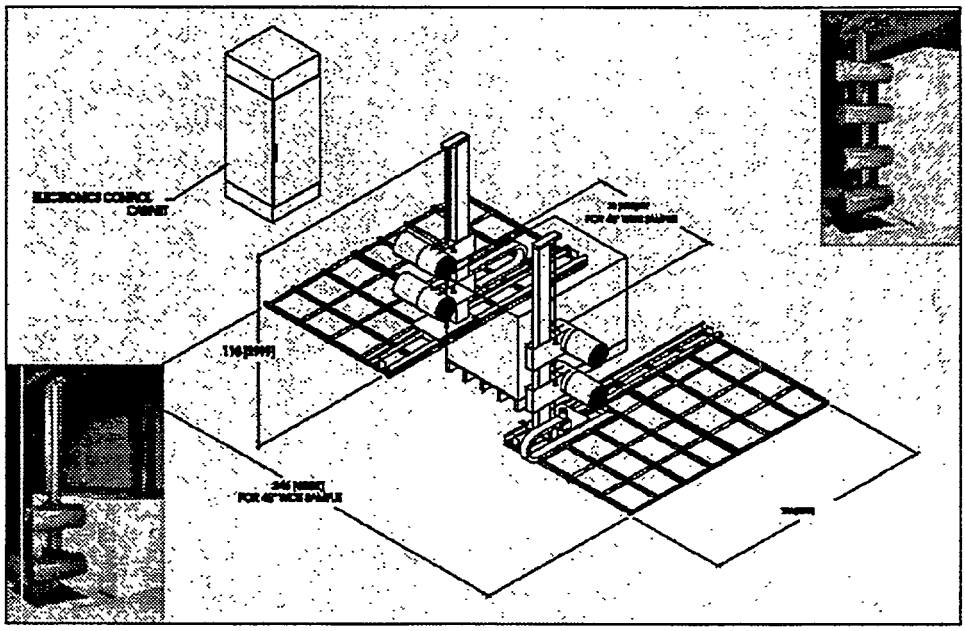

Figure 4.
Box Counter for Large and Very Large Samples

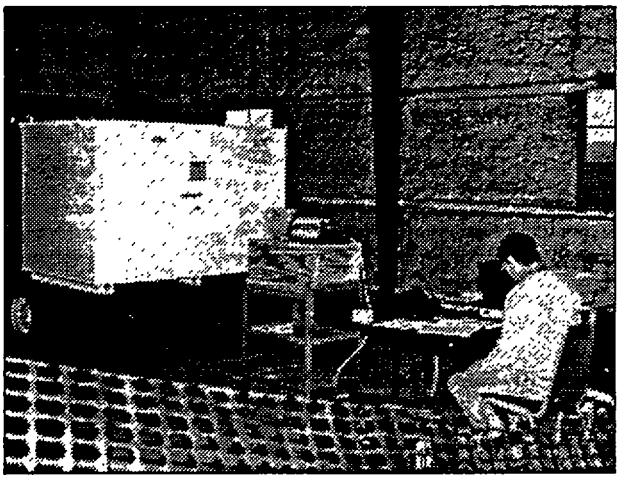

Figure 5.
Portable Ge Detector Counting B-25 Boxes

High Volume Soil Sorter System calibration and LLD determination

This system can count 50 tons of radioactive dirt per hour and is shown in Figure 6. The dirt is on a moving conveyor belt through a shield, where it is viewed by two large Ge detectors. A mathematical model was made of the dirt and of the shield. Efficiency computations were performed and used to determine the best placement of the detectors. Then, full energy spectral computations were done to determine the LLD of the system. MCNP is not yet suitable to model the cosmic contribution to background, but in this case, the background is nearly all from the natural Radium, Thorium, and Potassium in the sample itself. Therefore the background is from the Compton continuum of these radionuclides, which can be properly computed by MCNP. We have also developed a technique to modify the MCNP output to add noise, and make it statistically resemble the expected Ge peak shape. We then convert these spectra into our MCA format and analyze them with our Gamma Spectroscopy software. This gives a very reliable prediction of the actual instrument performance.

ISOCS, *In Situ* Object Counting System

This is a new product that is only practical because of mathematical calibrations. Various combinations of techniques now make it practical to do laboratory quality measurement of samples [small and large] in the field. This is an ideal instrument for decontamination surveys, environmental measurements, emergency response teams, light use waste assay measurement, and regulatory inspection teams.

The Ge detector is mounted on a portable cart to allow it to be transported and aimed at the sample to be counted. Various collimators and side shields and back shields can be added to reduce interference from

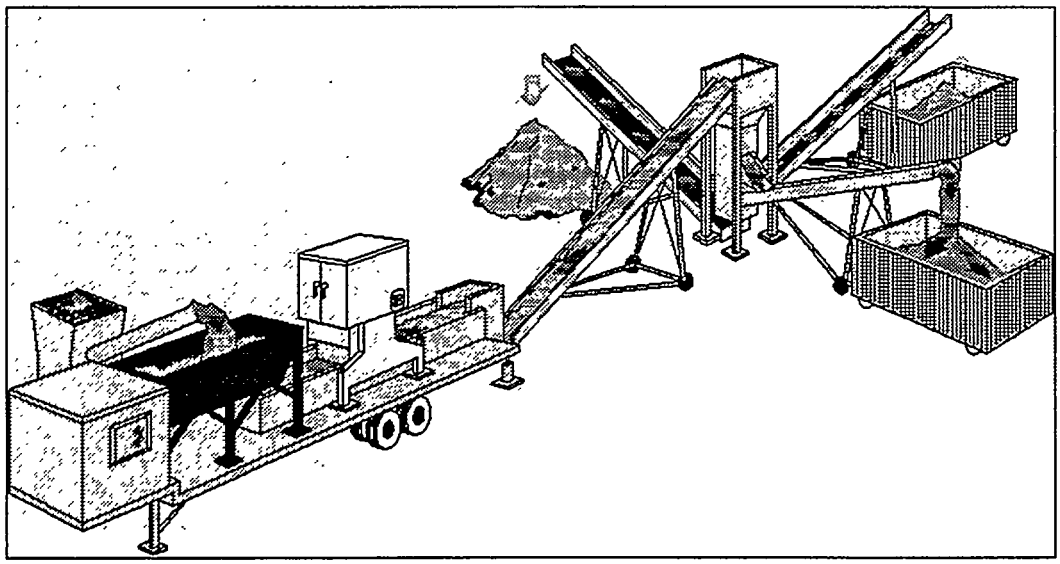

Figure 6.
High Capacity Spectroscopic Dirt Counter and Sorting System

other nearby radioactive items, and to define the field of view of the detector. Figure 7 shows the detector and shield and transportation cart.

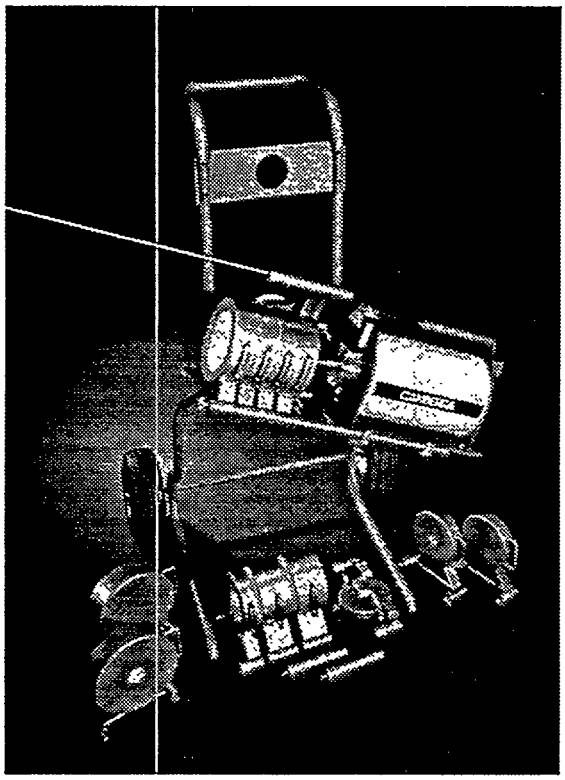

Figure 7.
ISOCS Shield System and Detector Carrier

Because of the very wide range of samples to be encountered in the typical use, the solutions before with pre-defined efficiency calibrations are not practical. So, for this product, the mathematical calibrations are performed by the customer. But, to make this process work accurately, each individual detector is first characterized by Canberra. The results of that individual detector characterization are delivered to the customer as a part of the calibration software. Multiple detectors can be characterized and selected for use by the customer. MCNP is used by Canberra for this characterization process. The output of the process is a series of equations that defines the detector response at any point from the endcap to 50 meters radius, at any energy from 50-7000 keV, and at any angle in all 4π directions.

When the user wants to do a calibration, it is a simple process taking only a few minutes. First, a template resembling the generic sample shape is chosen. Nine such templates are available:

- Simple box [basic box from point size up to many m^3]
- Complex box [allows various non-uniform source distributions]
- Simple cylinder [basic drum from point size up to many m^3]
- Complex cylinder [allows various non-uniform source distributions]
- Circular stacked planes [cylinders viewed on end, and *in situ* soil distributions]
- Rectangular stacked planes [walls, floors, ceilings]
- Pipe [source inside pipe in various locations]
- Marinelli Beaker or Well [detector inside source container]
- Sphere [basic object with source as volume or shell]

Each of these basic shapes has many parameters that can be used where necessary to create many variations. After selecting the template, the various critical parameters that define the sample-detector geometry are measured [or estimated] and entered.

If the detector is using one of the ISOCS collimators, then the appropriate one is selected, and the parameters defining it are entered into the software. Otherwise, the user can enter them.

All materials must be defined so that the proper attenuation corrections can be made. ISOCS contains the full cross-sections of all chemical elements. And it has a materials library containing common construction materials, and the tools for the user to create others not already defined.

Finally, the user instructs the ISOCS program to compute the efficiency vs. energy datapoints. This process takes from 10-30 seconds [normally] up to 5-10 minutes [large sources, multiple sources, and/or

narrow collimators]. The output is then converted into the Genie-PC efficiency curve and is now available for use in the analysis of the spectrum.

Currently underway is the validation of this efficiency calibration software. Comparisons are being made to MCNP computations for identical objects, and to source measurements. A few examples are shown in Figure 8.

The accuracy of the ISOCS efficiency computation method is nearly as good as the full MCNP computation for common and simple geometries, and perhaps a factor of 2-3 worse for very large sources and/or heavily collimated sources. But the accuracy is expected to be more than adequate for the field measurements where the primary use is expected. And, in our experience from the construction of these large radioactive calibration sources, the ISOCS calibrations probably just as accurate [maybe even better].

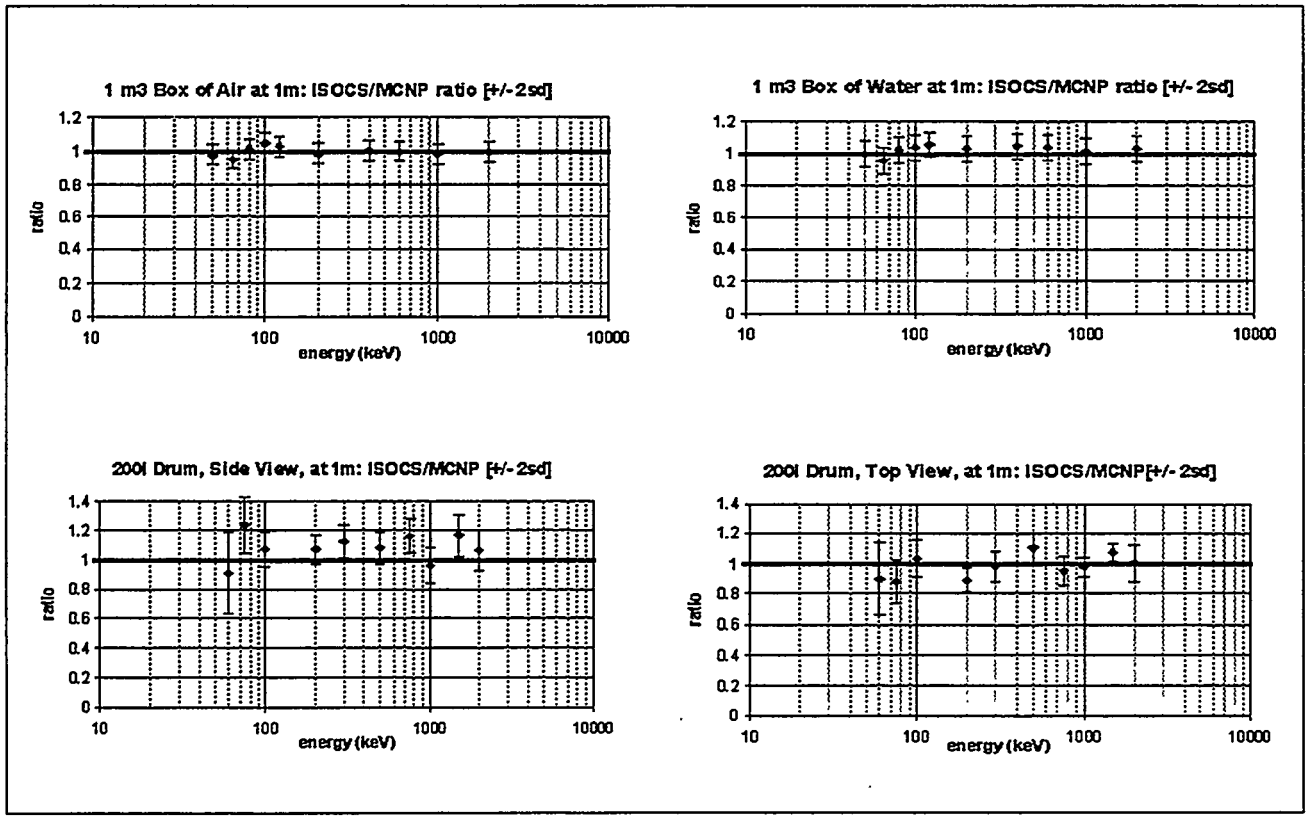

Figure 8.
Typical ISOCS Validation Testing Data

CONCLUSION

Mathematical calibrations have been shown to be a suitable alternative to the traditional method of duplication of the sample with multiple energy radioactive sources. For simple laboratory-sized samples containing water-equivalent samples, the use of radioactive sources is still the least expensive and most accurate method. However, when any of the following conditions is present,

- unusual densities
- unusual sample bulk matrix
- large sample
- sample to be counted in low efficiency position

the use of mathematical calibrations may well be more accurate, and will most likely be quicker and less expensive. The problem remains today, however, that mathematical calibrations are still not widely accepted, and must be well documented and proven to be acceptable to the ultimate customer and any of his reviewers. However, it is speculated that as the use becomes more common and more refined, that mathematical calibrations will be the preferred option a few years from now.

REFERENCES

[1] Briesmeister, J. F. (ed), November 1993, MCNP - A General Monte Carlo N-Particle Transport Code, Version 4a. Report LA-12625-M, Los Alamos National Laboratory.

[2] Wender, S. A., et. al. (1988). Nuclear Instruments and Methods, A265, 596.

[3] Moss, C. E. and Streetman, J. R. (1990). "Comparison of Calculated and Measured Response Functions for Germanium Detectors", Nuclear Instruments and Methods in Physics Research, A299, 98.

[4] Hsu, H. et. al. (1984). IEEE Transactions Nuclear Science, NS-31, 390.

[5] Hickman, D. P. et. al. (1984). Calibration of a Am-241 Wound-Monitoring System Using Monte Carlo Techniques, Vol. 66, 4. Health Physics, 400.

[6] NUREG-1496, Generic Environmental Impact Statement in Support of Rulemaking on Radiological Criteria for Decommissioning of NRC-Licensed Nuclear Facilities, Vol 2, Table 3.3. Aug, 1994.

[7] Helfer, I. K., and Miller, K. M. (1988). "Calibration Factors for Ge Detectors used for Field Spectrometry," Health Physics 55, 15-29.

[8] Bronson, F. L., and Wang, L. (1996), "Validation of the MCNP Monte Carlo Code for Germanium Detector Gamma Efficiency Calibrations," Proceedings of Waste Management 96, Tuscon AZ, Feb 1996.

GAMMA-RAY PULSE HEIGHT SPECTRUM ANALYSIS ON SYSTEMS WITH MULTIPLE GE DETECTORS USING SPECTRUM SUMMING

E. Wayne Killian
Idaho National Engineering Laboratory
Idaho Falls, ID 83415

ABSTRACT

A technique has been developed at the Idaho National Engineering Laboratory to sum high resolution gamma-ray pulse spectra from systems with multiple Ge detectors. Lockheed Martin Idaho Technologies Company operates a multi-detector spectrometer configuration at the Stored Waste Examination Pilot Plant facility which is used to characterize the radionuclide contents in waste drums destined for shipment to Waste Isolation Pilot Plant. This summing technique was developed to increase the sensitivity of the system, reduce the count times required to properly quantify the radio-nuclides and provide a more consistent methodology for combining data collected from multiple detectors. In spectrometer systems with multiple detectors looking at non homogenous waste forms it is often difficult to combine individual spectrum analysis results from each detector to obtain a meaningful result for the total waste container. This is particularly true when the counting statistics in each individual spectrum are poor. The spectrum summing technique adds the spectra collected by each detector into a single spectrum which has better counting statistics than each individual spectrum. A normal spectral analysis program can then be used to analyze the sum spectrum to obtain radio-nuclide values which have smaller errors and do not have to be further manipulated to obtain results for the total waste container.

I. INTRODUCTION

Gamma-ray spectrometers used to assay radio-nuclides from a large area sample form (55 gallon drums, large boxes, etc.) are typically configured with multiple detectors. This is usually done so that the radiation being emitted from all regions of the sample is measured (this is particular important if the source is nonhomogeneous). Of course, the same effect can be achieved with a single detector positioned at a large distance from the source. Sensitivity is then reduced unless long count times are used to compensate for the increased source to detector distance.

In spectrometer systems with multiple detectors looking at nonhomogeneous waste forms it is often difficult to combine individual spectrum analysis results from each detector to obtain a meaningful result for the total sample container. Usually the individual spectrum analysis results are combined using some type of an algorithm which takes into account the geometry of the detector array. The error propagation across these spectra are very difficult to do and usually result in large uncertainties, particularly if the count statistics in each individual spectrum are poor. Another technique, sometimes employed for multiple detector arrays, utilize an analog summing technique. In the cases where flat spatial sensitivity and high energy resolution is required each detector must be fairly well efficiency matched and the gain and zero of each detector system must be very stable and constantly monitored. Large changes in input rates for these types of systems can create difficulties.

This paper describes a software technique to sum the spectra collected from each detector to produce a single spectrum which is then analyzed to obtain a result for the total sample. This technique utilizes an INEL developed pulser system[1] (with subsequent removal), patent #4,968,889, and a spectrum analysis code VAXGAP[2]. The use of this particular spectrum analysis code is not a requirement for the spectrum summing technique, but is utilized to handle the data from the pulser system correctly. Briefly, pulser injection with subsequent removal requires the addition of a dual-amplitude pulser module to each detector. The pulser injects pulses into the test input of the detector preamplifier. Each Analog to Digital Converter used in the system has to be modified to intercept the digital address of each pulser pulse prior to storage in the MCA memory and route it to a high-energy region of the spectrum where the incidence of gamma-ray events is low and the storage of gamma-rays is forbidden. The result is a region of the spectrum above the normal gamma-ray region containing only the two pulser peaks. These two peaks can then be fit to determine their areas, widths, and centroids, all of which are useful indicators of spectrometer performance, but have particular importance in determining the energy scale of each component spectrum to the accuracy required to create a single summed spectrum.

Another advantage of summing individual spectra is improved spectrum statistics. The photo-peak shapes are better defined (not distorted by counting statistics) and the analysis of the

sum spectrum will produce smaller fitting errors. The counting times required to obtain a spectrum which can be effectively analyzed can be dramatically reduced. If there are n detectors being used then the count times can generally be reduced by a factor of n-1, which will result in a sum spectrum which has better counting statistics than any of the individual spectra.

II. SUMMING ALGORITHM DESCRIPTION

A series of spectra can be added together channel by channel if they have the same energy scale. For the technique described in this paper, the spectra collected from several detectors are normalized to a common energy scale and then added together channel by channel to produce a sum spectrum. The energy scale for a spectrum analyzed with the VAXGAP program is described by a parabolic energy function, E(x) where x is a channel number.

(1) $$E(x) = A+B*x+C* (x)^2$$

The coefficients A, and B are determined for each spectrum from the pulser information stored with spectrum. The coefficient C is determined during energy calibration using a multi-energy gamma source. The summing technique uses the energy coefficient parameters values determined for one spectrum as the normalization values. The channel contents of the other component spectra will be shifted such that the energy scale of all the spectra will be identical to the normalization spectrum. As a further illustration, suppose we have a 1332 keV photo-peak present in all spectra, when the channel contents of all spectra have been shifted, the 1332 keV photo-peak will have the same channel centroid.

In order to perform the shifting function we first convert the quadratic energy equation into a linear equation which has the same values for x=0, and x=L_c where L_c is the last channel in the spectrum. If the quadratic energy is defined by equation (1) the corresponding linear equation can be denoted by

(2) $$E_s(x) = A+(B+C*L_c) *x$$

Let the linear energy equation (2) be the equation to which we will normalize the component spectra, then for a component spectrum i with quadratic energy scale parameters of A_i, B_i, and C_i we can define a corresponding linear equation:

(3) $$E_i(x) = A_i+(B_i+C_i*L_c) *x$$

In order to gain and zero shift the component spectrum to match the normalization spectrum whose energy scale is defined by equation (2), we want to determine parameters R_i and Z_i such that

(4) $$E_i(\frac{X}{R_i}-Z_i) = E_s(x)$$

then

(5) $$A_i+B_i+C_i*L_c*\frac{x}{R_i}+Z_i = A+B*X+C*L_c*x$$

For x = 0 we have

(6) $$A_i+(-B_i*Z_i-C_i*L_c*Z_i) = A$$

therefore

(7) $$Z_i = \frac{A_i-A}{B_i+C_i*L_c}$$

Substituting Z_i in equation (5) we get:

(8) $$A_i+(B_i+C_i*L_c) * (\frac{x}{R_i}-\frac{A_i-A}{B_i+C_i*L_c}) = A+B*x+C*L_c*x$$

From which we get

(9) $$R_i = \frac{B_i + C_i * L_c}{B + C * L_c}$$

For the values of Z_i and R_i (equations (7) and (9)) we then shift the component spectrum using the following technique:

Define:

y(i) = contents of original spectrum at channel i

y'(i) = contents of gain and zero shifted spectrum at channel i

Then for every channel, i, in the original spectrum (which when gain and zero shifted lies within the boundaries of the new spectrum) we determine the corresponding gain and zero shifted channel contents, y'(i).

Let:

$$Xn = (i/R_i) - Z_i$$

where Xn is a floating point number. If we then define n to be the nearest integer to Xn. We can then determine the channel contents, y'(i), by performing a parabolic interpolation of contents of the original spectrum at channel n. The following equations are used to perform this interpolation:

$$A = \frac{1}{2}\left(y(n+1) - 2y(n) + y(n-1)\right)$$

$$B = \frac{1}{2}\left(-y(n+1) + 4y(n) - 3y(n-1)\right)$$

Then

$$y'(i) = \frac{A*(Xn-(n-1))^2 + B*(Xn-(n-1)) + y(n-1)}{R_i}$$

III. APPLICATION OF SUMMING TECHNIQUE

Lockheed Martin Idaho Technologies Company operates a multi-detector spectrometer configuration at the Stored Waste Examination Pilot Plant facility at the Idaho National Engineering Laboratory. The summing technique is presently being qualified to be used as one component of the analysis of gamma-ray data used to characterize the radionuclide contents in 55 gallon waste drums destined for shipment to the Waste Isolation Pilot Plant.

In order to demonstrate the use of the summing technique, a calibration source was placed in the center of a calibration drum and a spectrum was simultaneously collected on each of four detectors. The same channel regions of each of these component spectra are plotted in 4 graphs in Figure 1. The plots are a semi-log plot of counts versus channel. The computed sum spectrum is then plotted in Figure 2.

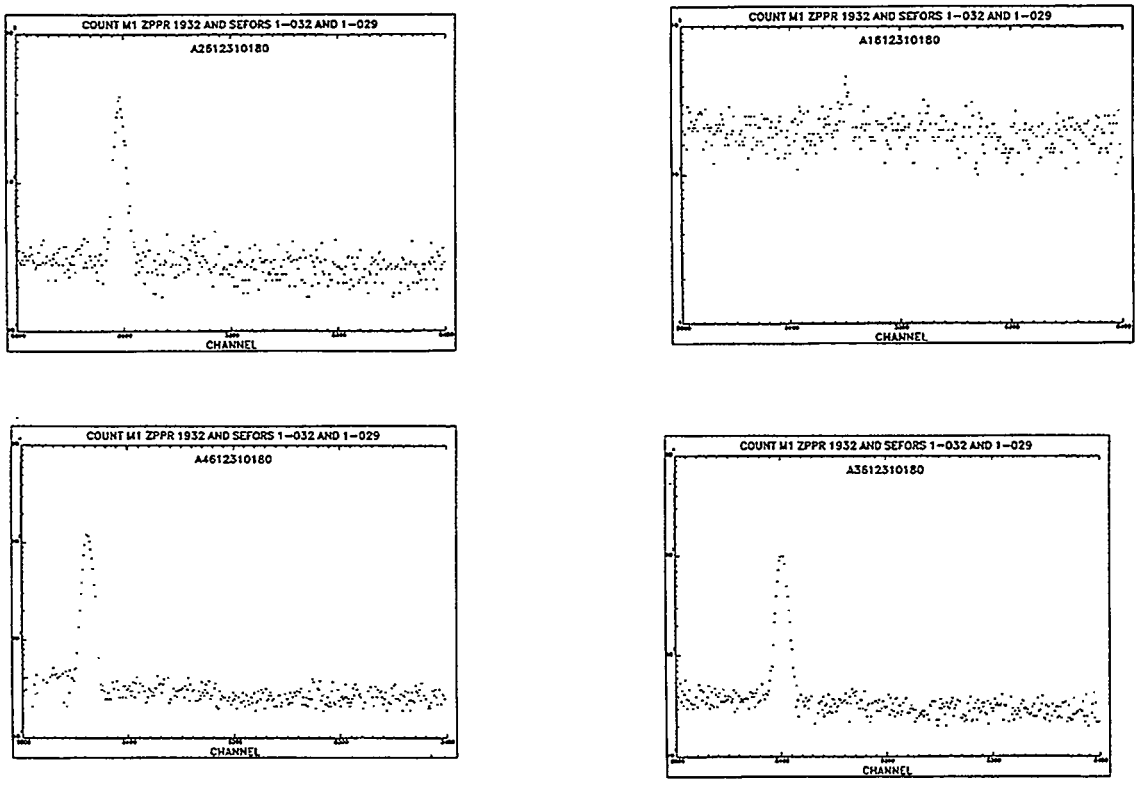

Figure 1. Spectra taken on four detectors

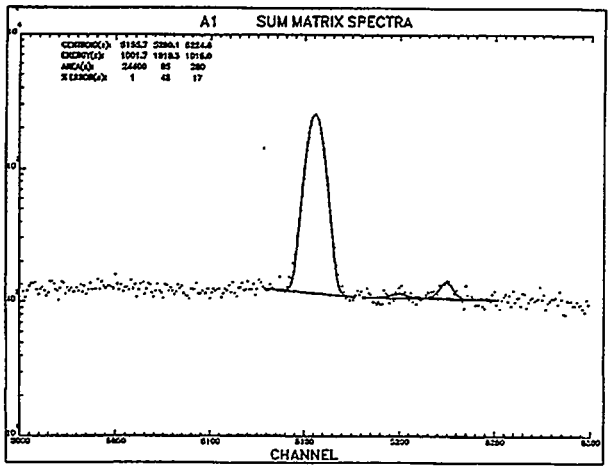

Figure 2. Sum spectrum computed from four individual component spectra

In the above plots the spectrum denoted as A1612310180 is the normalization spectrum (spectra collected on the other detectors are shifted to match the energy scale collected on this detector). The plot of the sum spectrum data is overlaid with the functional values of a gaussian function which has been fit to the data region containing three peaks. The sum spectrum plot illustrates two interesting facts:

1. The gaussian peak shape of the large peak has not been distorted by the summing process.
2. The third peak in each of the component spectra can not be readily identified in each of the component spectra, but becomes apparent in the sum.

Further analysis of the component spectra indicates that the photo-peak resolution has not been significantly degraded in the sum spectrum. For example, the full width at half maximum, FWHM, of a gaussian fit of the large peak shown in each of the plots, (A2612310180, A3612310180 and A4612310180) in Figure 1 are 9.4, 9.1, 9.1 channels respectively. The corresponding photo-peak FWHM in the sum spectrum is 9.4 channels. Our experience with the summing technique indicates that the FWHM of photo-peak in the sum spectrum will be no greater than the maximum FWHM from the corresponding photo-peak in each of the component spectra.

IV. CONCLUSION

The spectrum summing technique was developed to increase the sensitivity of a multi-detector spectrometer system, reduce the count times required to properly qualify the radio-nuclides present in the sample, and provide a more consistent methodology for combining individual spectrum analysis results to obtain a meaningful result for the total sample.

The summing technique adjusts the data in each component spectrum to a common energy scale. The adjusted channel contents of each component spectrum are added together on a channel by channel basis to produce a single spectrum. The technique utilizes an INEL developed pulser system (with subsequent removal), to determine the energy scale of each component spectrum to the necessary accuracy.

ACKNOWLEDGMENTS

Prepared for the U. S. Department of Energy Office for Environmental Restoration and Waste Management under Idaho Field Office Contract DE-AC07-94ID13223.

REFERENCES

1. "Pulser Injection with Subsequent Removal Implementation and Applications", IEEE Transactions on Nuclear Science 36 1, (February 1989).

2. Formal Report "VAXGAP: A Code for the Routine Analysis of Gamma-Ray Pulse-Height Spectra on a VAX Computer", E. Wayne Killian, Jack K. Hartwell EGG-2533 May 1988.

GAMMA-RAY IMAGING OF THE QUINBY SOURCES

J. Gregor
University of Tennessee, Knoxville, TN 37996–1301

D.C. Hensley
Oak Ridge National Laboratory, Oak Ridge, TN 37831-6388

ABSTRACT

The Quinby sources are alumina cylinders 7 inches in diameter and 8 inches high doped with weapons grade plutonium. We describe a computer tomography system for reconstructing three-dimensional images of these sources. Each reconstruction maps the spatial distribution of the internal ^{241}Am γ-ray activity and is computed using an iterative, expectation-maximization algorithm with detection efficiencies based both on a geometric model of the experimental set-up and attenuation corrections. Constructed about a decade ago, the Quinby sources were to contain uniformly distributed material. However, for some of the sources we have found regions where the plutonium solution tends to be concentrated. The ultimate goal of this work is to provide the basis for self-shielding corrections when analyzing differential dieaway neutron measurements.

INTRODUCTION

The Quinby sources are alumina cylinders 7 inches in diameter and 8 inches high doped with weapons grade plutonium. Constructed for calibration purposes about a decade ago, they come in several different strengths. We describe the design and development of a computer tomography system for reconstructing three-dimensional images that map the spatial distribution of the radioactive material of these sources. The ultimate goal of this work is to provide the basis for self-shielding corrections when analyzing differential dieaway neutron measurements using the *APNea* as discussed in a separate paper [1].

ORNL, Oak Ridge National Laboratory, managed by Lockheed Martin Energy Research Corp. for the U.S. Department of Energy under contract number DE–AC05–96OR22464.

In the following, we first describe the experimental set-up including the nature of the Quinby sources, the system design, and the data acquisition. Then we describe the algorithm used for the image reconstruction with emphasis on the computational model which incorporates detection efficiencies based both on the system geometry and attenuation corrections. Finally we present results from experimental work using synthetic data, point sources, and, of course, the Quinby sources themselves.

EXPERIMENTAL SET-UP

The plutonium used in the Quinby sources started with the isotopics (in percent by weight): ^{238}Pu(0.015), ^{239}Pu(92.8), ^{240}Pu(6.7), ^{241}Pu(0.27), ^{242}Pu(0.07), and ^{241}Am(0.09). Nearly one halflife of ^{241}Pu has passed since the sources were made, and the ^{241}Am has more than doubled – it is the 54.5 keV γ-ray from ^{241}Am that is sufficiently abundant to allow the source imaging to be done. On the other hand, its low energy means that the alumina matrix and the aluminum container contribute significantly to absorbing the γ-ray. The absorption effects were determined by moving two sources behind first an empty Quinby can and then behind a regular Quinby can with its alumina matrix; the two sources were ^{133}Ba (23.5, 80, and 155 keV) and ^{137}Cs (662 keV). This allowed for a very accurate determination of the attenuation in the can wall and within the alumina matrix of the ^{241}Am γ-rays since their energy is bracketed by the two lowest energy ^{133}Ba γ-rays.

The γ-ray detector was a standard 3x3 inch NaI detector enclosed in a 0.5 inch thick lead box to reduce background associated with the building. The inside of the box was lined with cadmium and copper sheets to provide a graded absorber for lead x-rays. The electronics started with a standard pulse shaping amplifier with 0.5μs shaping times. Although the amplifier was set for unipolar output, the fast decay time of the photomultiplier led to a bipolar output. This output was analyzed by an Ortec AD/811 CAMAC ADC with the trigger provided by a constant fraction descriminator set just above the noise, at about 15 keV, well below the ^{241}Am energy of 54.5 keV. Background count rates were about 15 c/s. Maximum count rates with the hottest Quinby source were about 500 c/s. Three sets of Quinby sources were scanned: a set of three sources containing about 0.1 g of plutonium, each; a second set of twelve containing about 1 g,

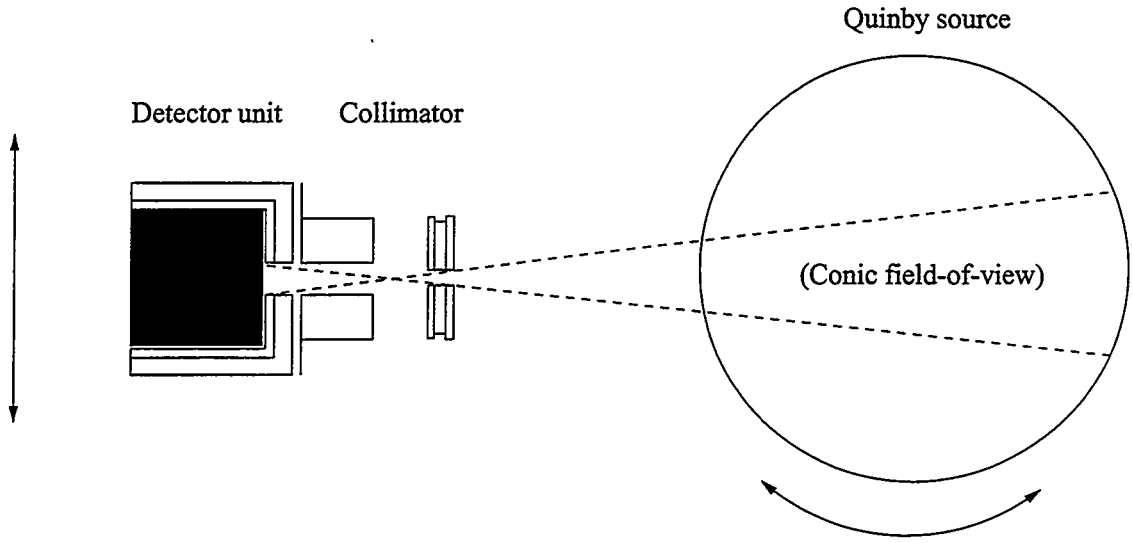

Figure 1. Topview of detector unit, collimator, and Quinby source (not drawn to scale). The conic field-of-view extends into the third dimension as well.

each; and a final (hottest) source containing 2.9 g.

With reference to Figure 1, the experimental set-up features a turntable that allows a Quinby source to be rotated 360 degrees about a vertical axis as well as translated in the horizontal and vertical directions. The vertical movement capability exceeds the height of the Quinby sources, but the horizontal movement is restricted to 5 inches. Since this is less than the 7 inch diameter of the sources, we chose to scan the sources horizontally from just outside the source can to somewhat more than 1 inch beyond its center. The front of the crystal views a Quinby source through a 0.5 inch diameter hole and through two separate lead collimators with apertures depicted in the figure. The collimator arrangement gives the detector a conic field-of-view. With a front collimator 0.25 inch in diameter, a cone is described with an opening angle of 3.2 degrees resulting in a viewing diameter of 0.46, 0.85, and 1.25 inches at the front, middle, and back, respectively, of a Quinby source.

In order to achieve a detailed image of the sources, an extensive data set was generated consisting of 26 horizontal steps, 49 vertical steps, and 24 azimuthal steps, for a total of

30,576 views. A 512 channel γ-ray spectrum was recorded for each view. Horizontal and vertical step sizes were 0.2 inches and the azimuthal steps were 15 degrees. For these measurements, the accumulated positioning time of the mechanical device was approximately 8 hours. Each 1 second of accumulation time amounts to about 8 hours of total time. Hence, the standard accumulating time per view of 7 seconds led to a total data acquisition time of just under 3 days. A few of the weaker sources were studied for over a week. The electronics were sufficiently stable that no significant drifts or changes were noticed during the data acquisition. The final data to be imaged were obtained by determining the background level on either side of the 54.5 keV peak and subtracting an appropriate background from the summed area under the peak. Fluctuations in the background were not a problem, even for the weaker sources.

As a step toward validating the imaging system, a point source mockup was generated. On the outside of a clean Quinby can, 4 inches up from the bottom, a ^{133}Ba source was attached. At the same height but 90 degrees away, a ^{137}Cs source was mounted. A one inch diameter hole was bored vertically through the center of the Quinby matrix, and in the center of this hole but at 3.5 inches up, a second ^{133}Ba source was mounted. Finally, also in the center but 4.5 inches up, a second ^{137}Cs source was mounted. A normal data scan was then initiated which scanned in 0.2 inch steps from 0.6 inches below to 0.6 inches above the 4 inch height. Because 4 different γ-rays were involved, each with a different attenuation response, four separate images can be studied, three for ^{133}Ba and one for ^{137}Cs. Background subtraction becomes an issue due to the relative weakness of the point sources.

IMAGE RECONSTRUCTION

Expectation-maximization (EM) is an iterative method for statistical parameter estimation. The EM algorithm is generally applicable when data must be sampled in one space, but maximum-likelihood (ML) estimates are required for parameters in a different space [2]. This is the case for the Quinby sources. We now describe details of the EM-ML algorithm that we have used to solve the image reconstruction problem at hand.

EM-ML Algorithm Basics

Let $\boldsymbol{n}^*$ denote the $D\times 1$ dimensional vector whose element n_d^* is the observed number of emissions recorded at detector position d, and let $\boldsymbol{\lambda}$ be the $B\times 1$ dimensional image vector whose element λ_b is the unknown (nonnegative) number of emissions from voxel b. Furthermore, define $\mathbf{E}$ as the $B\times D$ efficiency matrix whose element ξ_{bd} denotes the likelihood that a photon emitted from voxel b is detected by the detector when at position d. For ideal data, the image reconstruction problem can then be described by

$$\mathbf{E}^T\boldsymbol{\lambda} = \boldsymbol{n}^*$$

where T denotes the matrix transpose operation. This linear system of equations, however, may not have a solution for real data which tends to be noisy. While a constrained least-squares solution may suffice, the following EM–ML algorithm [3,4], which determines the maximizer of the Poisson likelihood $P(\boldsymbol{n}^*|\,\boldsymbol{\lambda})$, may be more suitable since the photon emissions can be modeled as independent Poisson processes.

Given $\boldsymbol{n}^*$ and $\mathbf{E}$, choose initial estimate $\boldsymbol{\lambda}^0$ and iterate through the sequence $\boldsymbol{\lambda}^1, \boldsymbol{\lambda}^2, \ldots$ using the multiplicative update rule

$$\forall b: \quad \lambda_b^{k+1} = \frac{\lambda_b^k}{\sum_d \xi_{bd}} \sum_d \frac{n_d^*}{\nu_d^{*k}} \xi_{bd}$$

where $\nu_d^{*k} = \sum_b \lambda_b^k \xi_{bd}$. It is easily shown that if $\boldsymbol{\lambda}^0$ is chosen to be a uniform, strictly positive distribution, then $\boldsymbol{\lambda}^k$ is nonnegative and $\sum_d \nu_d^{*k} = \sum_d n_d^*$ for any k. These properties facilitate quantitative studies.

Each step of the iteration consists of a forward-backward computation. The current image estimate $\boldsymbol{\lambda}^k$ is forward-projected into $\boldsymbol{\nu}^{*k}$ via matrix $\mathbf{E}$. Then $\boldsymbol{\nu}^{*k}$ is compared with $\boldsymbol{n}^*$ and the element-by-element ratios are back-projected via matrix $\mathbf{E}$ and used to form multipliers which are applied to $\boldsymbol{\lambda}^k$ to obtain $\boldsymbol{\lambda}^{k+1}$. Generally speaking, the first few iterations settle the 'low frequency' components of the image whereas later iterations fine-tune the 'high frequency' components.

Measured in terms of the Kullback distance [5], convergence is achieved when $D(\boldsymbol{n}^*, \boldsymbol{\nu}^{*k}) - D(\boldsymbol{n}^*, \boldsymbol{\nu}^{*k+1}) \rightarrow 0$. For ideal data, not only is monotonic convergence guaranteed but $D(\boldsymbol{n}^*, \boldsymbol{\nu}^{*k})$ is $o(k^{-1})$ meaning that $D(\boldsymbol{n}^*, \boldsymbol{\nu}^{*k}) \rightarrow 0$ faster than $k \rightarrow \infty$. For real data, we are only guaranteed that $D(\boldsymbol{n}^*, \boldsymbol{\nu}^{*k}) \rightarrow L$ where $L \geq 0$. A solution that yields $L = 0$ also solves the previously mentioned linear system of equations.

Finally, we note that the iteration scheme solves the image reconstruction problem even for the case of non-Poisson data [6] and that the EM-ML algorithm has been applied to solve problems quite similar to ours [7,8].

Computing Matrix E

The detection efficiencies represented by matrix **E** are based both on a geometric model of the experimental set-up and attenuation corrections. Specifically, we compute

$$\xi_{bd} = \frac{w_{bd}}{r_{bd}^2} a_{bd}$$

where w_{bd} denotes the relative volume of voxel b that can be seen by the detector from position d, r_{bd} is the Euclidean distance a photon emitted from b will travel before detection at d, and a_{bd} denotes the attenuation correction associated therewith.

The detector's conic field-of-view complicates matters substantially with respect to computing w_{bd} and we therefore take a numeric rather than analytic approach; each voxel is divided into a number of subvoxels and w_{bd} is taken to be the relative number thereof that lie inside the cone. Regarding r_{bd}^2, we compute it as the average of the square distance between the center of an included subvoxel and the center of the detector unit. Since each Quinby source contains nothing but the plutonium solution mixed in with the alumina, the attenuation correction is computed as

$$a_{bd} = \exp\{-(\theta_{bd}\alpha_C + \delta_{bd}\,\alpha_A)\}$$

where θ_{bd} denotes the effective thickness of the can-wall which varies with the penetration angle of an emitted photon, δ_{bd} is the distance a photon travels through the alumina before

exiting through the can-wall, and α_C and α_A are the associated coefficients. The tiny amount of plutonium has a negligible effect on attenuation and is ignored.

As may be apparent, matrix **E** is essential to the correct use of the EM-ML algorithm since it includes all the application-specific knowledge. Furthermore, matrix **E** is rather complicated to compute and it contains a vast number of elements which prohibits a simple brute-force implementation. Obviously, we can (and do) exploit its sparseness and store only the nonzero elements, but that alone is not sufficient. Consequently, we impose the constraint that the center of a voxel plane is always vertically aligned with the detector unit as it implies that explicit detection efficiencies need to be modeled for a single vertical detector position only. Finally, by making the number of view-angles divisible by four, geometrical symmetries lead to additional (proportional) computational savings. The reconstructed images are not affected by any of this.

Implementation Aspects

The EM-ML algorithm has been implemented in C on a Sun workstation. The entire scanner/image model is completely parameterized and everything is computed at runtime. The numerous parameters control the spatial resolution as well as the numerical accuracy of the computation. The default image dimension is $49 \times 38 \times 38$ voxels each of which is $0.2 \times 0.2 \times 0.2$ inches. Note that this produces an underdetermined system in that we have 30,576 measurements but aim to determine the emission activities for 70,756 voxels.

EXPERIMENTAL RESULTS

Synthetic Data

The first set of results we describe uses four synthetic data sets (SDS). With reference to Figure 2, the first is a disk with uniform activity (SDS 1), the second and third model disks with high center activity and low peripheral activity (SDS 2) and vice-versa (SDS 3), and the fourth is a disk with a linear increase in activity across the diameter (SDS 4). All four data sets have three active layers (as described) centered in a seven layer high cylinder. We simulate ideal scan data by forward-projecting each data set via matrix **E**.

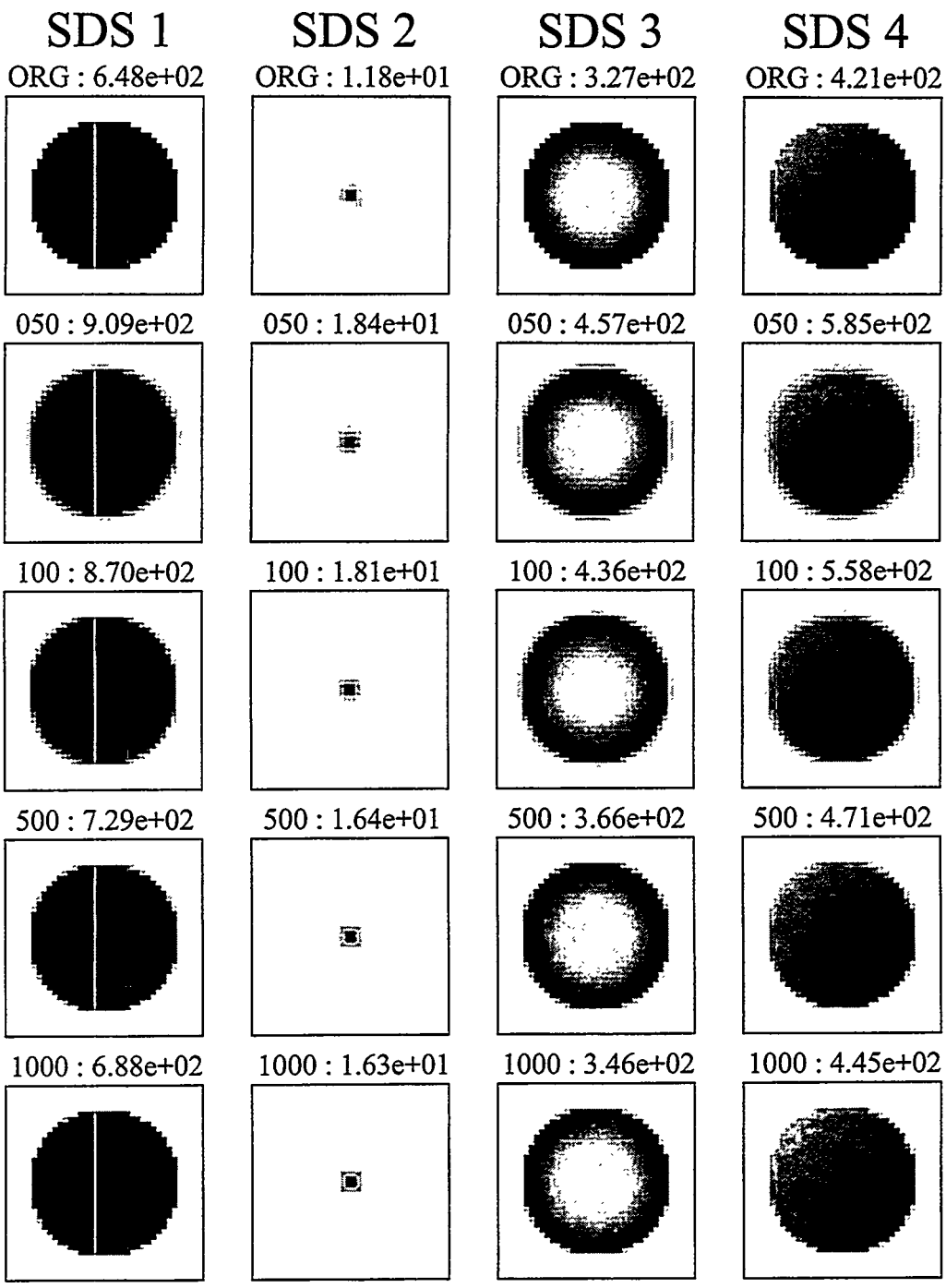

Figure 2. Synthetic data set reconstructions. Each column shows the images obtained for the center plane.

There are several things to be learned from this exercise. Figure 2 shows the image reconstructions obtained after 50, 100, 500, and 1000 iterations of the EM-ML algorithm. First, the reconstructions for SDS 1 and SDS 4 show evidence respectively of ring and crescent-shaped structures during the early phase of the computation. These artifacts tend to disappear as the iteration progresses. With respect to SDS 2, we clearly see the center emerge as such but also note the presence of a circular shadow. SDS 3 seems artifact free. Finally, the per-plane activity levels (the numbers given to the right, above each image) indicate that the center planes are assigned too much activity and that not even 1000 iteration are enough to restore the proper balance between the planes. Since observed here for ideal data, these radial and vertical artifacts should be expected to appear in the Quinby source reconstructions.

In order to study the effect of having somewhat limited horizontal scan capability, the experiment has also been carried out while simulating having full horizontal movement. We have not found this to improve the results in any significant way. Although more investigative work is required, we speculate that the cause of the artifacts described above are related to the conic shape of the detector unit's field-of-view.

Region-of-interest statistics computed for SDS 1 reveal that the mean is at 0.92 after a 50 iterations, grows to 0.97 after 500 iterations, and reaches 0.99 after 1000 iterations. The corresponding standard deviations are 0.34, 0.13, and 0.08, the maximum values are 1.56, 1.29, and 1.25, and the minimum values are 0.33, 0.51, and 0.57. Thus, if the region-of-interest can be determined, then especially the mean activity can be computed fairly accurately.

Point Sources

The next set of results is based on the point source measurements. Although the sources were weak, resulting in the scans being noisy, the images all show one or two dark voxels in the center and a single dark voxel on the periphery of the can. The position of these voxels coincide nicely with the position of the point sources. Table 1 lists relevant results for the point sources as a function of iteration index k. The maximum values take up to 500 iterations to settle whereas the average values computed for a $3 \times 3 \times 3$ neighborhood

Table 1

POINT SOURCE STATISTICS

Type	Iteration	Center		Periphery		Ratios	
		Max	Avrg	Max	Avrg	Max	Avrg
^{133}Ba	50	1.329	0.242	6.212	0.319	0.214	0.758
23.5 keV	100	1.974	0.248	6.935	0.319	0.285	0.779
	500	2.784	0.243	7.270	0.321	0.383	0.755
	1000	2.870	0.241	7.280	0.321	0.394	0.750
	1500	2.887	0.241	7.281	0.321	0.397	0.749
^{133}Ba	50	0.993	0.129	1.041	0.097	0.954	1.334
80 keV	100	1.424	0.131	1.208	0.097	1.179	1.352
	500	1.712	0.132	1.354	0.097	1.265	1.355
	1000	1.724	0.131	1.379	0.097	1.250	1.355
	1500	1.725	0.131	1.385	0.097	1.245	1.355
^{133}Ba	50	0.585	0.065	2.491	0.100	0.235	0.645
155 keV	100	0.846	0.064	2.688	0.101	0.315	0.637
	500	1.073	0.065	2.728	0.101	0.393	0.647
	1000	1.070	0.066	2.729	0.101	0.392	0.651
	1500	1.069	0.066	2.729	0.101	0.392	0.652
^{137}Cs	50	1.597	0.223	1.962	0.187	0.814	1.188
662 keV	100	1.990	0.226	2.234	0.184	0.890	1.226
	500	2.286	0.229	2.538	0.181	0.901	1.270
	1000	2.319	0.230	2.570	0.180	0.902	1.273
	1500	2.326	0.230	2.579	0.180	0.902	1.273

remain quite constant through-out the computation. Thus, while the shape of a point source image takes some time to settle, the strength of the image converges very quickly.

The ratios of the center-to-periphery activities were expected to have been the same for the three ^{133}Ba images. The results for the 23.5 keV and 155 keV images are close to each other but far from that of the 80 keV image. We speculate that the sources simply were too weak to get sufficient count statistics. Regarding the ^{137}Cs image, the expected ratio is close to 1.0 and we see that the ratio of the average activities comes quite close. In fact, it may even be correct although it probably is on the high side.

Quinby Sources

The final set of results involve the Quinby sources themselves. Figures 3–8 show image reconstructions obtained after 1000 iterations of the EM-ML algorithm with the 1% hottest voxels mapped to the same grey level. This number is listed to the right just below the Quinby source identifier; the overall maximum value is given to the left thereof. The two numbers seen above each image give the position (relative distance from the top of the can) and the integrated activity of the plane. The position of the planes shown are indicated by plus signs in the vertical profile illustrated at the bottom; T and B denote top-of-source and bottom-of-source, respectively, and the number listed is the maximum integrated activity of any plane.

Recall that the Quinby sources were supposed to contain uniformly distributed material. To a great extent that is true. However, there are also clear indications of regions with higher than average concentrations of the plutonium solution. For example, q3476 and q3509 show crescent-shaped hot structures toward the top of the cans, q3503 has a well-defined inner circle at about the same location, the top of q3504 looks more like a truncated cone than a cylinder, q3513 features a horseshoe-shaped structure, and q3514, which is the hottest of them all, has a layer of very hot voxels toward the bottom. The other Quinby sources are similar to q3476 and q3509. With respect to the vertical activity, we observe that a more or less ragged profile results for all the sources.

Clearly, some of these phenomena can be explained by the reconstruction artifacts observed for the synthetic data. The hot rings with cold centers probably correspond to regions of rather uniform activity. The same might be true for the crescent and horseshoe-shaped structures. We also speculate that the vertical profiles should have fewer peaks and valleys, i.e., be more smooth. But it is premature to draw too definite of conclusions without further experimentation with known sources.

When normalizing the total integrated activity computed for each Quinby source with respect to the scan time, we find that the average, relative strengths are 1.00 : 10.79 : 29.59 which corresponds quite well with the 0.1, 1.0, and 2.9 grams of plutonium.

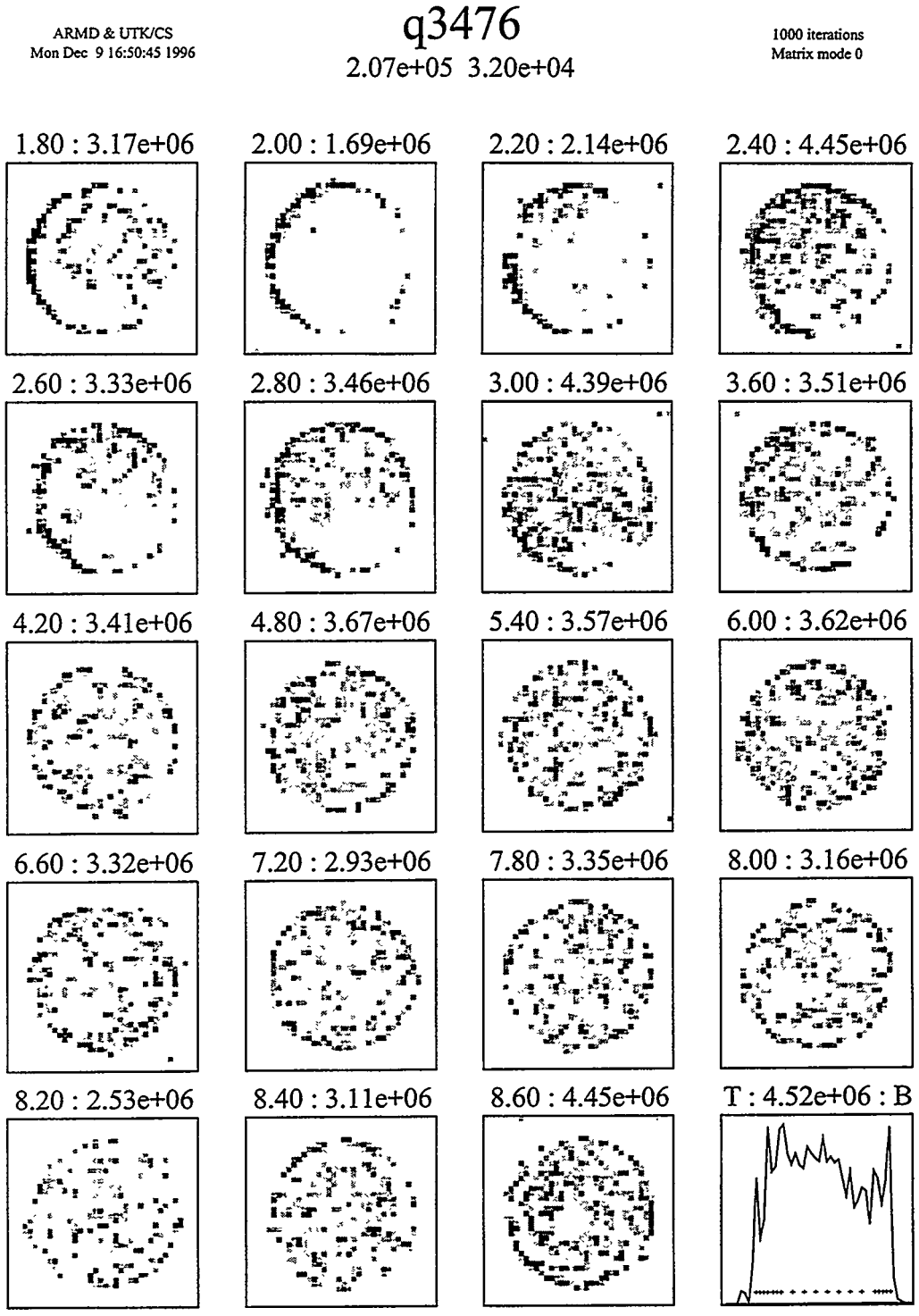

Figure 3. Reconstruction of Quinby source q3476.

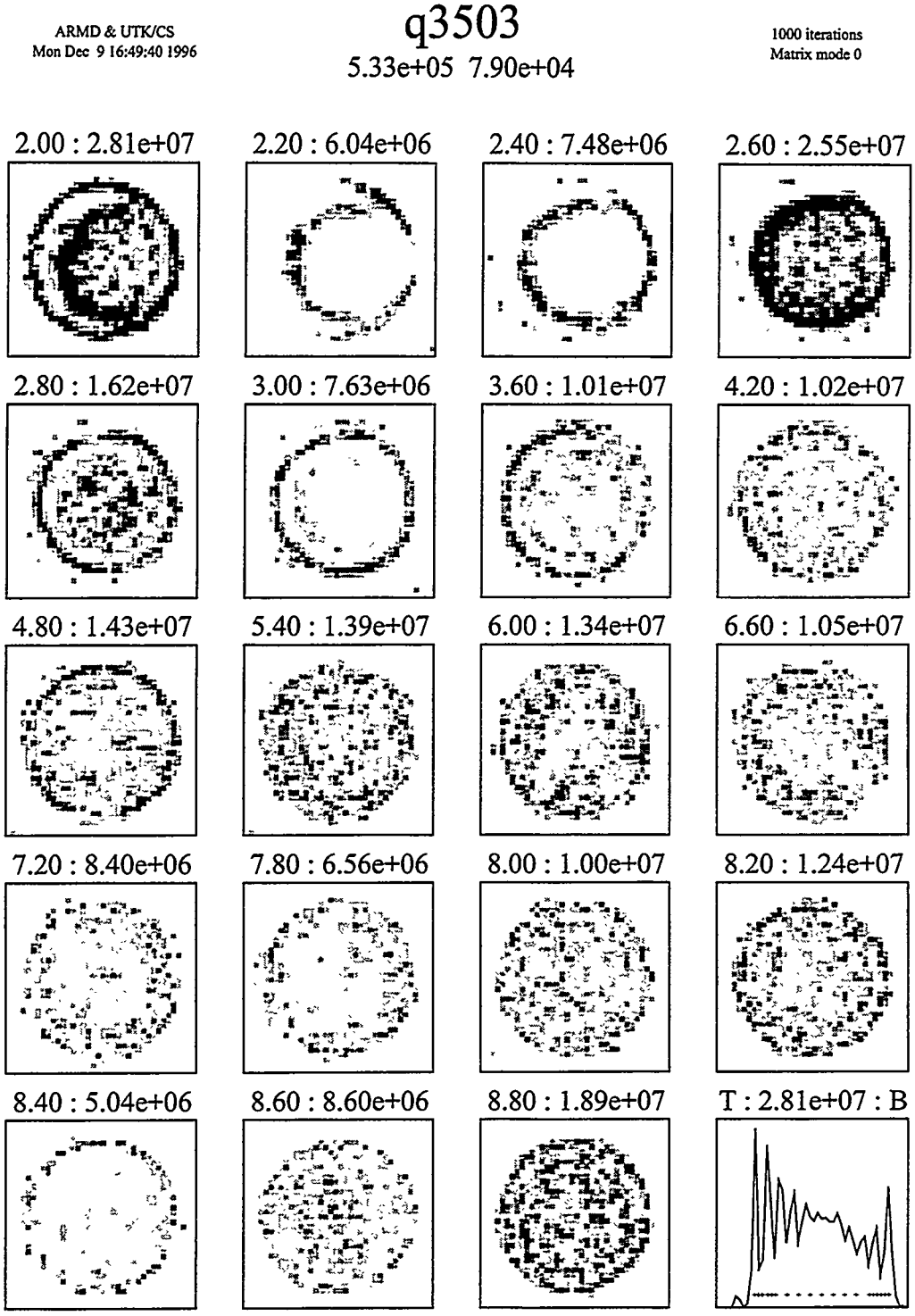

Figure 4. Reconstruction of Quinby source q3503.

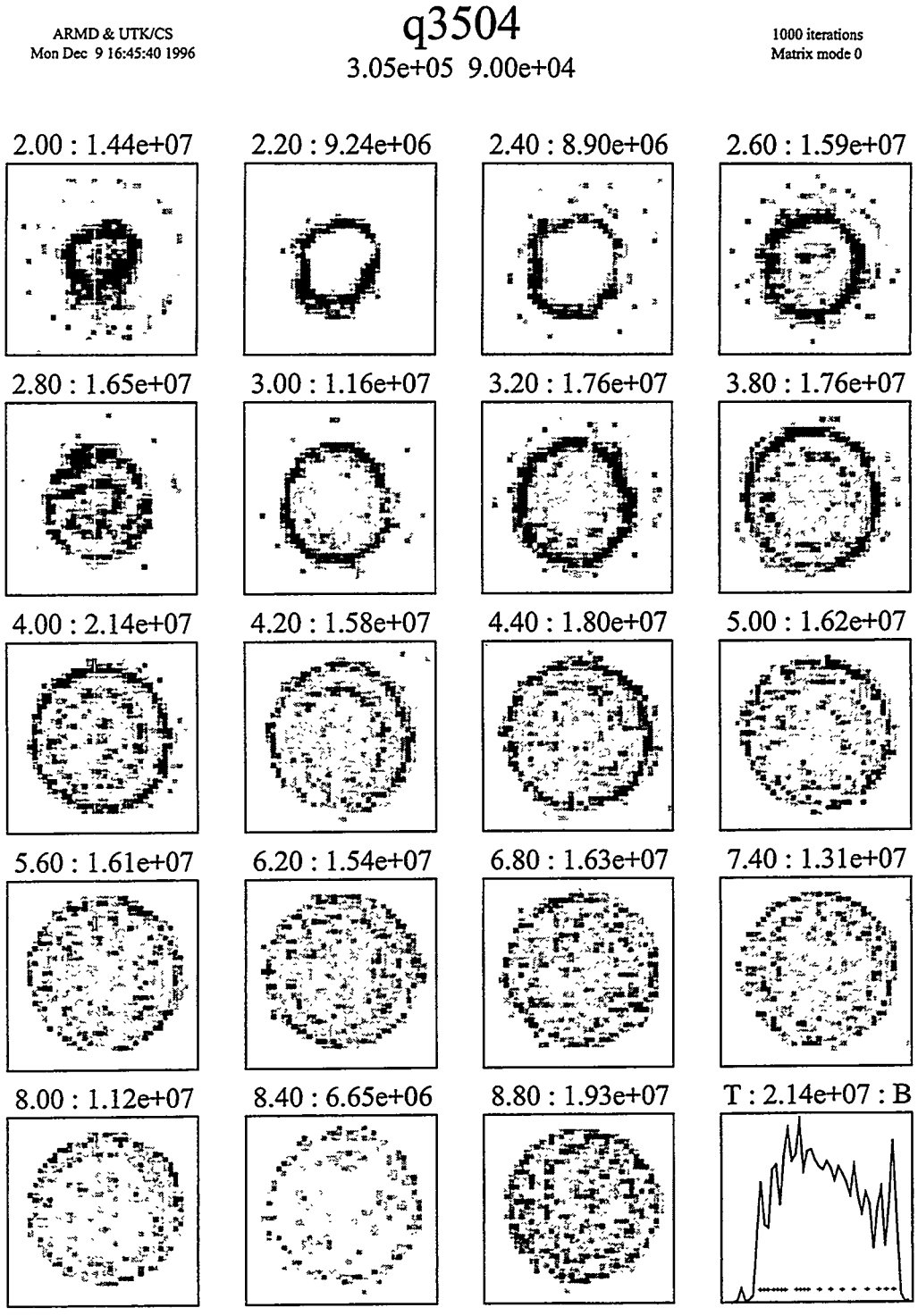

Figure 5. Reconstruction of Quinby source q3504.

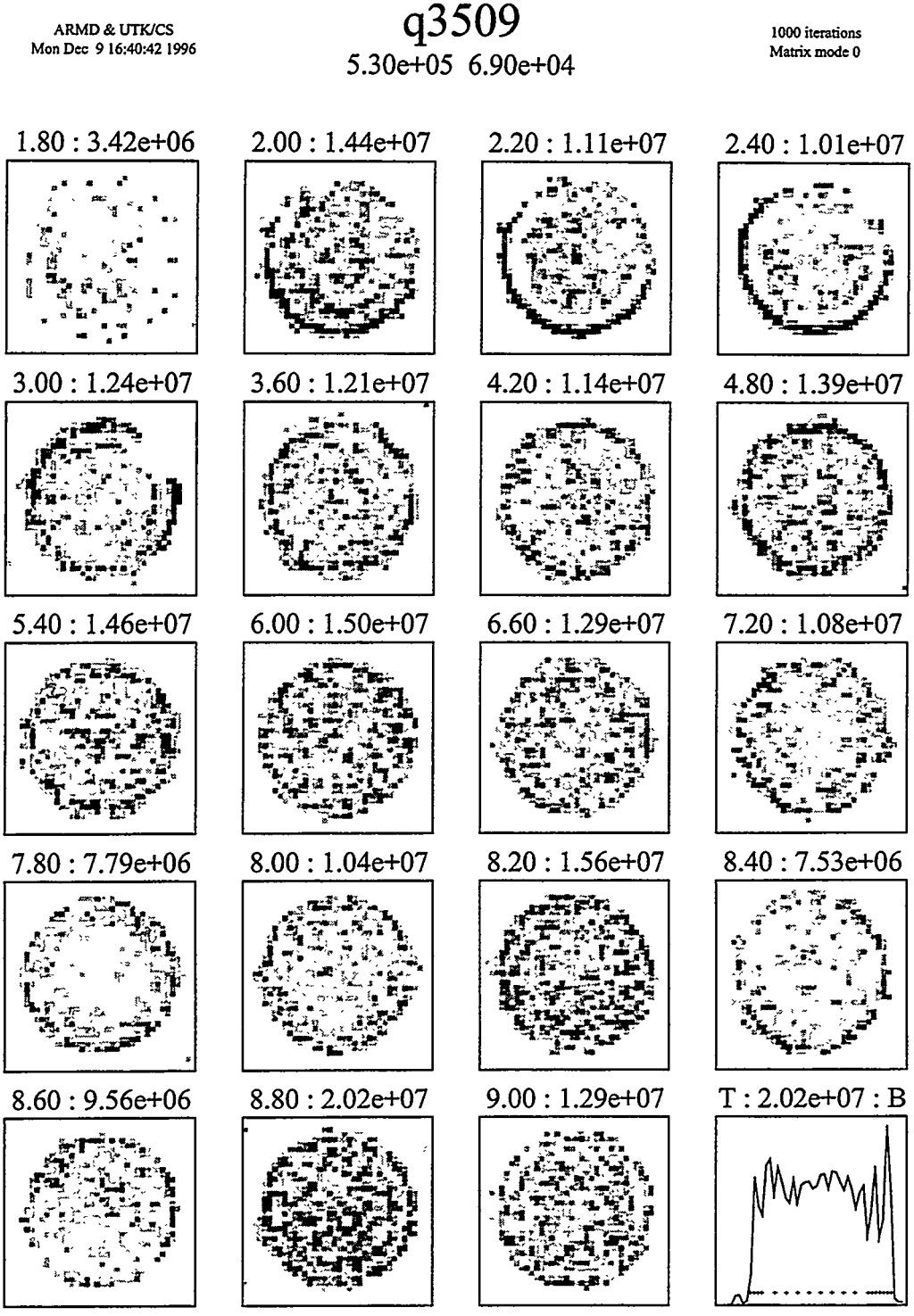

Figure 6. Reconstruction of Quinby source q3509.

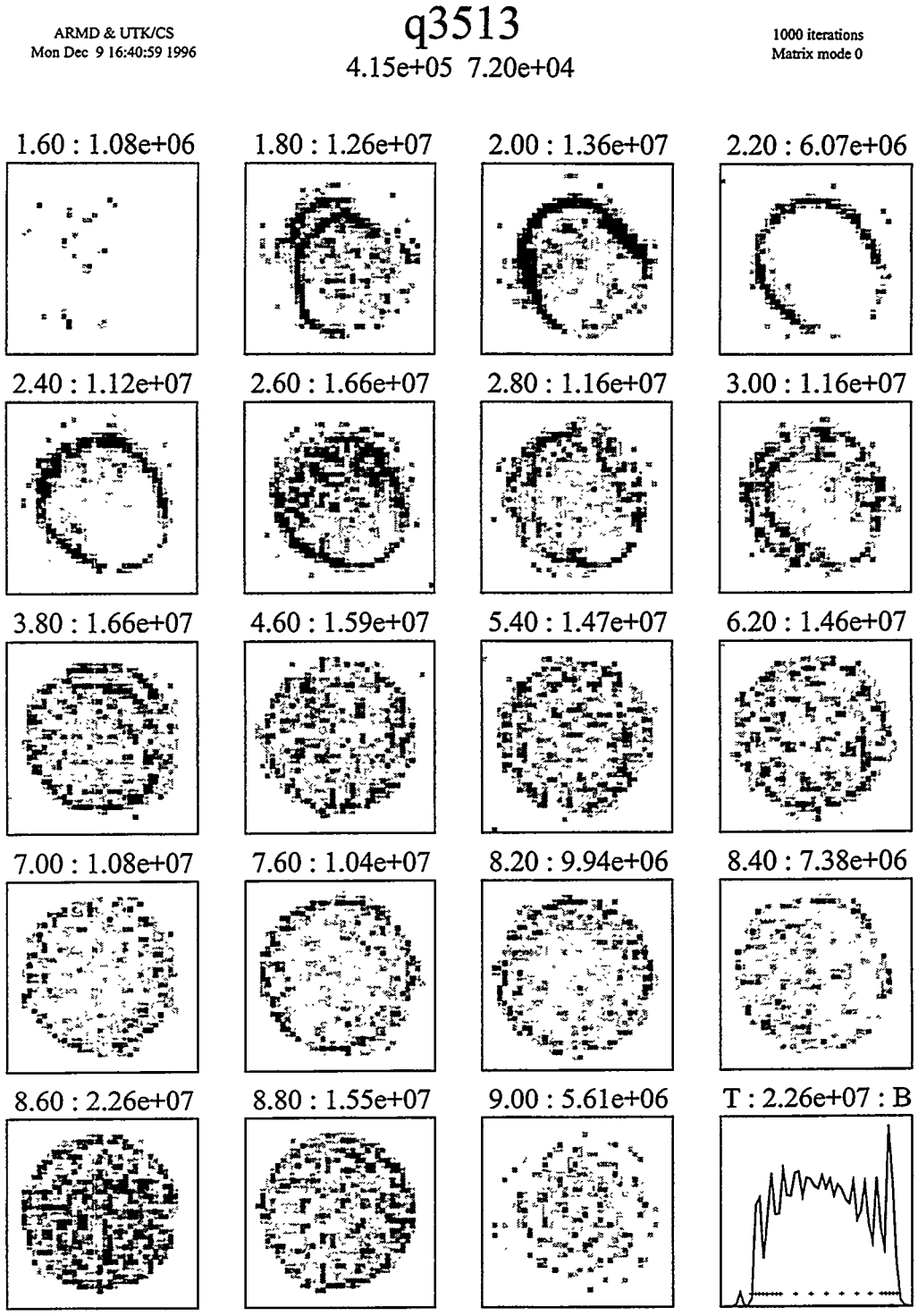

Figure 7. Reconstruction of Quinby source q3513.

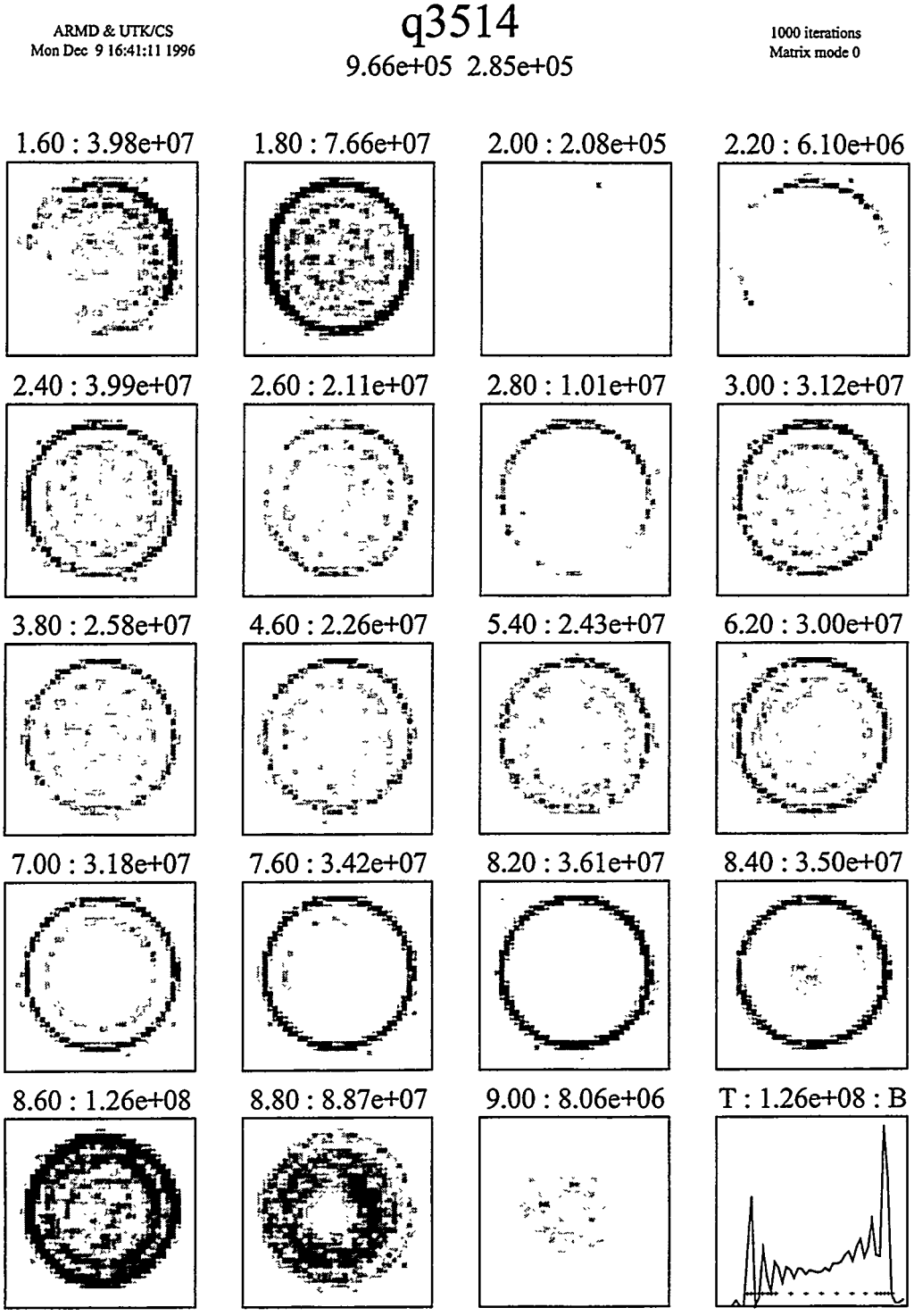

Figure 8. Reconstruction of Quinby source q3514.

CONCLUSION

We have described a computer tomography system for reconstructing three-dimensional images of the Quinby sources. The software includes a geometric model of the experimental set-up, attenuation correction, and numerous parameters that control the spatial resolution as well as the numerical accuracy of the computation. The image reconstructions are computed using an iterative technique for maximizing the Poisson likelihood of the externally recorded γ-ray activity and the unknown internal spatial distribution of plutonium. The experimental work indicates that most Quinby sources are close to being uniform but some have regions where the plutonium solution tends to be concentrated. On-going research is focused on eliminating radial and vertical artifacts observed for both synthetic data and the Quinby sources themselves.

ACKNOWLEDGEMENTS

This work was supported in part by Lockheed Martin Energy Systems, Inc., under subcontract MAR–11X–SV899V. Special credit is extended to Larry Pierce for construction of the scanning unit.

REFERENCES

1. D.C. Hensley, "Self-shielding correction calculations for the *APNea*" *5th NDA/NDE Conf.*, Salt Lake City, UT, 1997. These proceedings.

2. A.P. Dempster, N.M. Laird, and D.B. Rubin. "Maximum likelihood from incomplete data via the EM algorithm," *J. Royal Stat. Soc.*, vol. 39, pp. 1–38, 1977.

3. L.A. Shepp and Y. Vardi, "Maximum likelihood reconstruction for emission tomography," *IEEE Trans. Med. Imaging*, vol. 1, pp. 113–122, 1982.

4. K. Lange and R. Carson, "EM reconstruction algorithms for emission and transmission tomography," *J. Comp. Asst. Tomography*, vol. 8, pp. 306–316, 1984.

5. R.E. Blahut, *Principles and Practice of Information Theory*, Addison-Wesley, 1987.

6. L.B. Lucy, "An iterative technique for the rectification of observed distributions," *The Astronomical Journal*, vol. 79, pp. 745–765, 1974.

7. R.J. Estep, T.H. Prettyman, and G.A. Sheppard, "Tomographic gamma scanning to assay heterogeneous radioactive waste," *Nuclear Sci. Engr.*, vol. 118, pp. 145–152, 1994.

8. T.H. Prettyman, R.A. Cole, R.J. Estep, and G.A. Sheppard, "A maximum-likelihood reconstruction algorithm for tomographic gamma-ray nondestructive assay," *Nuclear Instruments and Methods in Physics Research*, vol. 356, pp. 470–475, 1995.

ROVER WASTE ASSAY SYSTEM

D. W. Akers, C. M. Stoots, N. C. Kraft, and D. J. Marts
Idaho National Engineering Laboratory, Idaho Falls, ID 83415.

ABSTRACT

The Rover Waste Assay System (RWAS) is a nondestructive assay system designed for the rapid assay of highly-enriched ^{235}U contaminated piping, tank sections, and debris from the Rover nuclear rocket fuel processing facility at the Idaho Chemical Processing Plant. A scanning system translates a NaI(Tl) detector/collimator system over the structural components where both relative and calibrated measurements for ^{137}Cs are made. Uranium-235 concentrations are determined from $^{137}Cs/^{235}U$ ratios measured using radiochemical methods. The system is currently in operation and is sufficiently automated that most functions are performed by the computer system. These functions include system calibration, problem identification, collimator control, data analysis, and reporting. Calibration of the system was done through a combination of measurements on calibration standards and benchmarked modeling. A description of the system is presented along with the methods and uncertainties associated with the calibration and analysis of the system for components from the Rover facility.

INTRODUCTION

Highly enriched ^{235}U fuel from the Rover nuclear rocket testing program was processed at the Idaho Chemical Processing Plant (ICPP) at the Idaho National Engineering Laboratory (INEL) from June 1984 through June 1985. This fuel was in a graphite matrix that contained a significant percentage of niobium. Fuel processing was prematurely stopped due to the formation of plugs in the process piping and vessels. The fuel present in the system at the time processing was stopped (nominally 160 kg) remained in the Rover hotcell facility until the defueling and decommissioning effort began in 1996.

The Rover fuel debris is present as a loose, powdery material on surfaces throughout the facility or as a physisorbed material on process piping that was deposited during the high-temperature reprocessing of the fuel. The method chosen for removal of the ^{235}U fuel from the facility to assure nuclear material accountability was to vacuum as much as possible of the loose debris from the exterior surfaces of the structural materials and then to perform nondestructive assay of piping and structural components as they were removed from the facility to assure that

criticality, nuclear material safeguards, and the INEL Radioactive Waste Management Complex (RWMC) radioactive waste disposal criteria were met.

A number of nondestructive assay techniques were evaluated to determine the most appropriate method for quantifying the amounts of ^{235}U present on the structural materials and piping to be removed from the facility. Acceptable methods were required to be compatible with the Rover facility and had to meet criticality and nuclear materials safeguards requirements for not removing unknown quantities of ^{235}U from the fissile material control area of the facility for assay. A number of assay methods were eliminated due to compatibility issues and because they may require dedicated operators that would significantly increase the cost of performing assays. Additionally, measurements through the hotcell wall were eliminated due to the counting times needed to obtain acceptable measurement data.

The method chosen for the assay system was to use a shielded and collimated gamma-ray spectrometer system that could be used to assay the quantities of ^{137}Cs associated with the nuclear fuel debris. The ratio of ^{137}Cs to ^{235}U was to be determined based on radiochemical analysis of representative samples from various parts of the Rover processing system. This system (the RWAS system) was initially to be installed in the Rover hotcell. This was later modified so that the measurements were performed in an glove box annex to the Rover hotcell as the debris was being removed for disposal. A description of the Rover Waste Assay System (RWAS) is presented along with the calibration methods used and the analysis of uncertainties associated with the measurement of structural and piping debris from the facility.

SYSTEM DESCRIPTION

The functional requirements for the Rover Waste Assay System (RWAS) dictated that the

system meet a number of prerequisites. Design specifications required that the system be portable for easy installation in the Rover hotcell and that it be capable of measuring samples with radiation fields ranging from a few mR/hr to 10 R/hr gamma. The initial analysis requirement for the RWAS, as defined by nuclear material safeguards personnel, was that the maximum disposable quantity of ^{235}U was 5 grams per assay that may contain multiple pipe or tank sections. Further, nuclear materials safeguards indicated that a minimum detectable quantity of 0.2 grams of ^{235}U per assay would be acceptable. Additional requirements were that the RWAS should have an automated control capability to minimize operator requirements and be sufficiently automated to assure that reproducible measurements were being performed. Further, due to the number of assays to be performed, a data analysis and reporting capability was to be included in the system.

To meet these requirements, a flexible design approach was taken that would allow software and hardware modifications to be made relatively quickly to assure that the system was user friendly, could be adapted to facility requirements, and could meet potential, rapidly changing reporting requirements. ANSI guidelines for nondestructive assay and control systems were used in the development of this system.[1,2] The control system chosen for the system was Labview 4.0, which would be used to control the four motors in the system, the horizontal and vertical axis and the two collimator control blocks and to provide control the data acquisition system, analysis, and reporting.

Figure 1 shows the general layout of the scanner system and Figure 2 shows the collimator system. The primary features of the scanner system that are important to the calibration process and accurate measurements are: 1) that the cart with the v-shaped tray centers calibration standards and unknowns under the collimator system in a fixed geometry (i.e., the scanner is bolted to the glove box system), and 2) that the cart has only two positions, up (30.48 cm from the detector) and down (49.8 cm from the detector). These locations provide fixed calibration locations when the collimator/detector is at the calibration distance where all calibration measurements have been performed. The primary feature of the collimator is that it

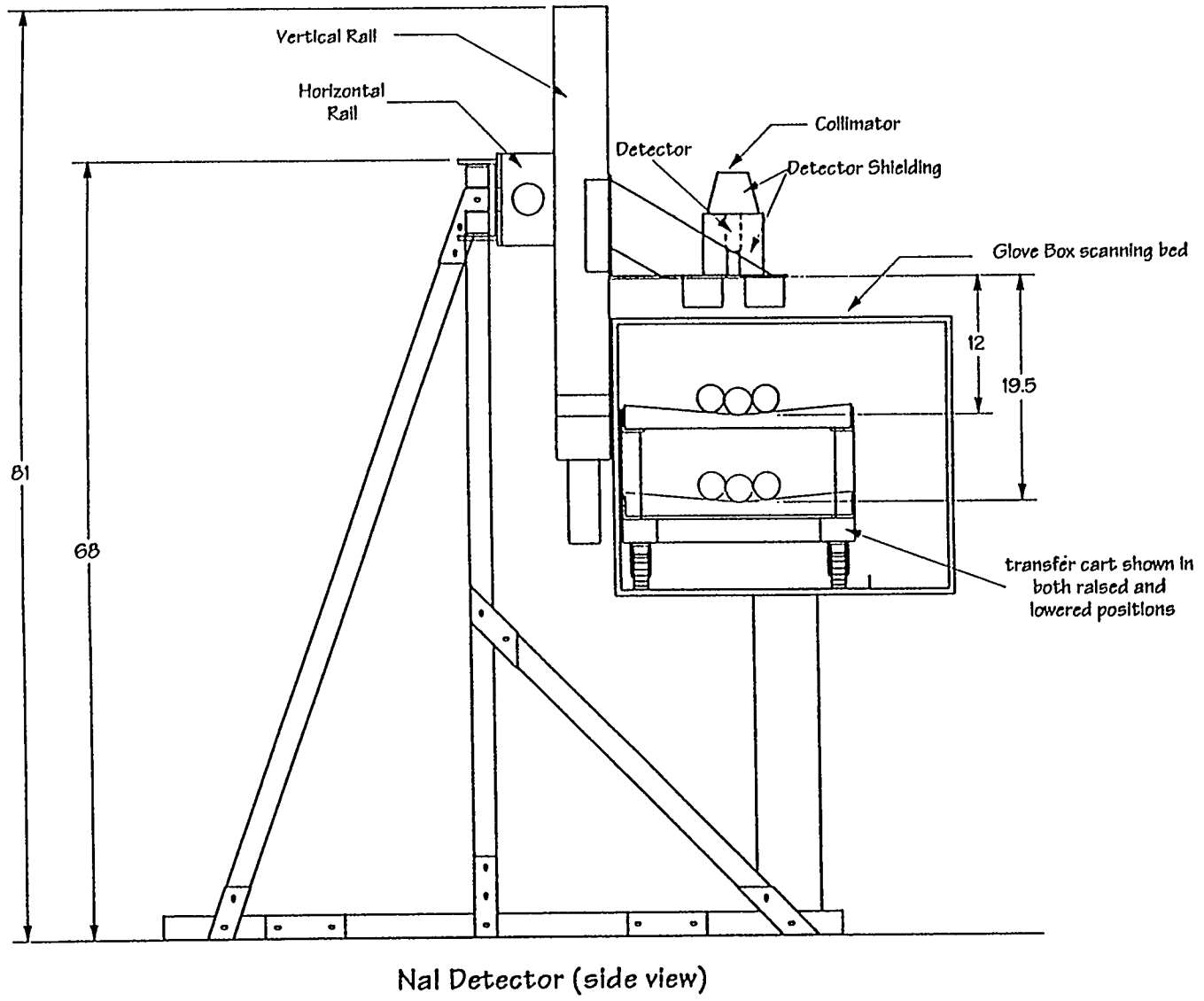

Figure 1. Rover Waste Assay System.

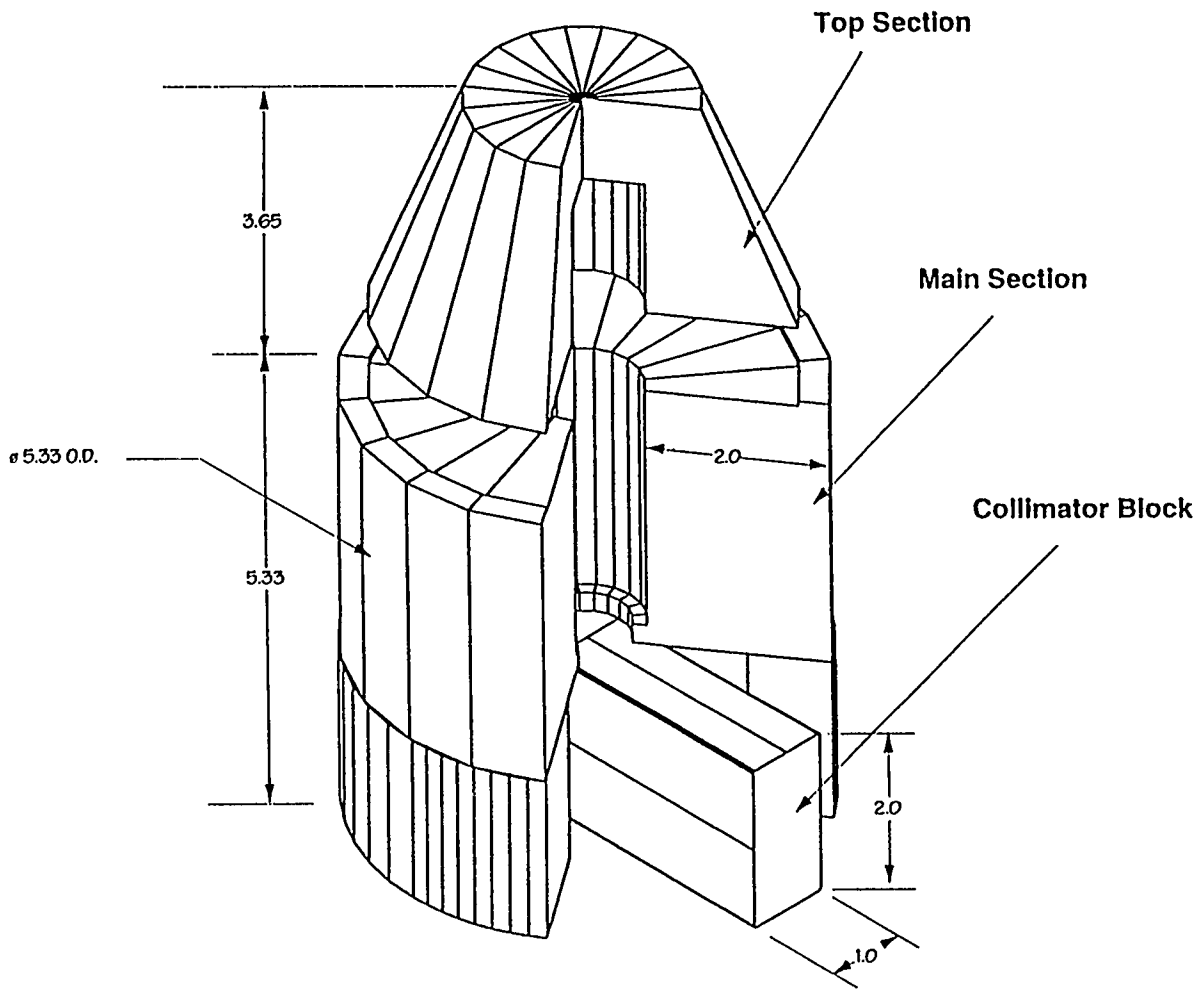

Figure 2. Collimator assembly.

provides a fixed collimator width (2.5 cm) and a variable collimator length (up to 2.5 cm) with a collimator thickness of 5 cm of tungsten. Two independently controlled collimator blocks are moved to vary the rectangular collimator aperture around the center line of the detector. This allows the length of piping or tank being scanned to be varied. Additionally, a calibration standard is located in one of the collimator blocks and provides the capability to locate the source under the detector and calibrate the system automatically. The nominal field-of-view for this collimator system with a 2.5 cm collimator aperture at the up calibration position (source-to-detector distance - 30.5 cm) if calculated using optical geometric calculations is about 29 cm. However, detection efficiency varies with distance from the point directly under the detector and near the edge of the NaI(Tl) crystal, the detection efficiency is poor. Measurement data indicated that the actual field-of-view was about 20.3 cm.

The gamma spectrometry analysis system used for the Rover WAS was the ORTEC Micromcb system, which was interfaced to the Labview 4.0 system. The gamma-ray spectrometer system is be a subsystem of the overall control system. The detector chosen for the Rover system is a 1 inch x 1 inch Teledyne Brown NaI(Tl) with a Hammamatsu photomultiplier tube that has been used previously in high rate applications. This detector has a resolution of approximately 7.5% at the 661 keV line of ^{137}Cs and has been tested and found to be stable at relatively high rates (and when collimated in fields up to 15 R/hr). The detector has been shown to operate at rates up to 50,000 c/s (vendor indicated 80,000 c/s). A Canberra 1481LA ratemeter with alarm has also been added to assure that any operator knows if he is exceeding the rate handling limits of the system.

In addition to the standard design of this detector, a source was included in the collimator block housing for direct calibration of the system. The sources used for this application are $^{57,60}Co$ which have gamma ray lines at 122, 1173, and 1332 keV. This provides a sufficient number of gamma ray lines for energy calibration and to assure that detector efficiency is not changing. These gamma-ray sources do not produce significant interferences with the ^{137}Cs

gamma-ray line

Specific operational functions performed by the Labview system with minimal operator control are the following.

- System calibration - The system performs a comparison of calibration data obtained at each startup and after each 20 analyses with peak area and Full Width at Half Maximum (FWHM) parameters that have been included in the Labview software for comparison purposes. System operation is stopped if these requirements are not met.

- Assess contamination in measurement area - Prior to beginning each sample analysis, a measurement is performed over the empty V tray and scanning bed to determine if the area under the detector has been contaminated with debris from the prior analysis.

- Define collimator aperture - A gross-scan of the structural debris is performed to determine the maximum count rate. This count rate is used to determine the collimator aperture for the analysis. A second scan is then performed to assure that the collimated count rate does not exceed the normal operational range (nominally 20,000 counts/sec).

- Quantitative analysis - Based on the measured field-of-view of the system, up to four gamma-ray spectra are obtained at 20.3 cm increments for count times of about 100 seconds each, which meets the minimum detection limit of 0.2 g of ^{235}U based on the calibration data that has been obtained. Appropriate geometry and calibration factors are applied to the ^{137}Cs results to obtain the quantity of ^{235}U present.

- Data analysis and reporting - The peak area and FWHM data from the ORTEC Micromcb analysis are abstracted from the ORTEC report format and the data are analyzed and reported in summary for the individual operator to sign showing the quantity of 235U present and in a summary format for the waste disposal box in which the debris is being

placed. Scaling factors from the radiochemical analysis data are used to determine to the quantities of other radionuclides in the waste (e.g. ^{94}Nb) that are needed for transportation and waste disposal purposes.

SYSTEM CALIBRATION

The calibration methodology used for the Rover wastes is summarized in this section. Measurement standards that are representative of major types of wastes (piping, etc.) found in the facility are used as primary calibration standards and for other items, detector efficiencies are calculated using the Microshield 4.2 code based on benchmarked measurement data. ANSI standard guidelines for standard and source preparation were used in the development of this system.[3,4] The calibration standards used for the Rover calibration measurements are listed in Table 1. Uncertainties are listed as 5% and are conservative as the uncertainties associated with the preparation of the sources are less than 5% (nominally 2-3%).

The calibration measurements that were performed were limited in number due to problems associated with source activities that were a factor of 10 less than those originally specified. An error in source preparation resulted in only 10% of the requested ^{137}Cs concentrations. Consequently, only a limited number of the calibration geometries were counted three times, and in most cases, the calibration efficiency is based on two measurements. However, as will be discussed, the measurements performed resulted in consistent results and provided the basis for the development of the calculated detector efficiencies using Microshield 4.2. The detector efficiency for a specific calibration source is determined using the following equation, which can be varied to provide calibrations in terms of count/second per microcurie or the inverse :

$$\text{Pk. Ct Rate (c/sec)} \times \text{Source activity } (\mu\text{Ci}^{-1}) = \text{Efficiency (c/}\mu\text{Ci)}$$

Where:

Pk ct rate = Total peak area divided by count time and decay corrected to the standard decay date

Source activity - Total source activity

Efficiency = Detection efficiency for that standard

Table 1 - Calibration Measurement Sources

Geometry/Number of Items	Dimensions	^{137}Cs Content [a] μCi/source)
2.0 in, Sch. 80 (3)	2.0 in OD x 8 inches	1.72 ± 0.09
1.5 inch Sch. 80 (3)	1.5 in OD x 8 inches	1.40 ± 0.07
1.0 inch Sch. 80 (3)	1.0 in. OD x 8 inch	1.56 ± 0.08
1 in tubing (3)	1.0 in O.D. x 8 inch	1.56 ± 0.08
0.5 in tubing (3)	0.5 in x 8 in.	1.56 ± 0.08
Large Planar (Tank) source (7 in. and 15 in. radius tank sections)	Nominal 21 in x 8 in	2.62 ± 0.13
Tray source	4 in. x 12 in.	3.05 ± 0.15
Personal Protective Equipment (large planar source)	20 in. x 20 in. X 20 in.	2.62 ± 0.13
^{137}Cs Point source [b]	CPP std. 450005	6.23 ± 0.31

The methodology used to determine calculated detector efficiencies was to calculate the gamma-ray flux (photons/second) at the face of the detector for a number of the geometric shapes for which measurements had been performed using the Microshield 4.2 code. These results are then compared with measured detector efficiencies to determine a ratio between actual and calculated efficiencies that accounts for the effects of intrinsic detector efficiency and variations in the collimator geometry. For the Rover waste assay system, calculated efficiencies were

compared with the measured efficiencies for four physical geometries: 1) a point source at 12 inches, 2) a point source at 19.6 inches, 3) a 0.5 cm tube at 12 inches, and 4) a 2.0 in Schedule 80 pipe at 12 inches. Table 2 lists the results of the comparison between the calculated and measured results.

Use of the pipe data and the uncertainties associated with all results resulted in a ratio of 13.9 $\pm$ 1.7 or about a 12% internal uncertainty (i.e., the standard deviation of the mean value). The pipe geometry data were used for determining the correction factor for other pipe geometries as they are extended sources that would be expected to fill the collimator view area completely and have lower efficiencies near the edge of the standard that would be more representative of other extended geometries (I.e., that is other pipe diameters, thicknesses, etc.). Uncertainties associated with the comparison are included in the errors associated with calculated detector

Table 2 Comparison of Measured to Calculated Detector Efficiencies

Source	Calculated Flux $\mu Ci/photons\ s^{-1}$	Measured Flux $\mu Ci/counts\ s^{-1}$	Calibration Factor Ratio	Error
Pt source (12 in.)	7.16E-2	7.25E-1	10.1	1.90E-1
Pt. Source (19.6 in.)	1.84E-1	1.99	10.8	1.86E-1
0.5 in tube (12 in.)	8.07E-2	1.20	14.9	2.34E-1
2 in. pipe (19.6 in.)	1.2E-1	1.54	12.9	1.92E-1
			average ratio pipe	average error
			13.9	4.03E-1

efficiencies. Additional modeling will be performed to better assess the uncertainties associated with this modeling technique. In addition, some comparison analyses will be performed with a Monte Carlo technique to better assess the uncertainties associated with the Microshield technique for determining detector efficiencies

The method used to determine the geometry for quantities of miscellaneous debris was to determine the average flux from a known source strength for items up to six inches in thickness that covered the entire 33.0 cm. wide debris tray, which is located at the lower tray location, and to determine an uncertainty associated with the sample distance that would account for samples ranging from 49.8 cm to 34.5 cm from the detector. The average flux associated with variations in distance was determined to be 1.35 $\pm$ 0.3 E+6 photons/sec which resulted in an average distance from the detector of 38.5 cm.

The effect of various thicknesses of iron up to 2.5 cm was also calculated for a slab geometry with the 33.0 cm width of the cart. This calculation resulted in an average flux of 5.6 $\pm$ 2.0 E+5 photons/s or an average metal thickness of 0.91 cm. The optimal thickness and distance were then reanalyzed using Microshield 4.2 to determine the expected flux rate from this geometry (8.72 E+5 photons/s) to which the errors associated with the metal thickness and distance measurements as absolute errors propagated in quadrature. This results in a flux rate of 8.7 $\pm$ 3.4 E+5 or about 39%. This uncertainty allows a variety of structural items from the facility to be analyzed and remain within the uncertainty associated with this geometry when two standard deviations are used to determine the waste disposal quantities at the INEL RWMC.

ROVER MEASUREMENT UNCERTAINTIES

An initial comparison between the assay results from the Rover Waste Assay System and radiochemical analysis results has been performed. The results of the ^{137}Cs and ^{235}U comparisons are shown in Tables 3 and 4. The comparison between the radiochemical data and the assay results for ^{137}Cs are shown in Table 3. The comparison for the samples analyzed, which included a 2.0 inch process pipe, a 1.5 in. process pipe, and a tank section indicates good agreement and probably better than might be expected. The efficiency used for the nonprocess pipe sample was

calculated based on the Microshield calculations that have been discussed.

Table 4 lists the comparisons for ^{235}U. The agreement is acceptable when using the average $^{137}Cs(\mu Ci)$ / $^{235}U(mg)$ ratios for both process and nonprocess piping materials. The propagated uncertainties indicate that all radiochemistry results agree well with the assay system results. The principal source of error in the Rover measurements is the uncertainty associated with the $^{137}Cs(\mu Ci)$ / $^{235}U(mg)$ ratio, as expected. If $^{137}Cs(\mu Ci)$ / $^{235}U(mg)$ ratios for the actual samples are used the agreement is quite good (within 10%). Additional sample analysis results will be used to reduce the uncertainties associated with the ratio; however, they have been accepted as being adequate for the purposes of accountability and waste disposal where inventories are not large. Additional sample analysis and assay system results are in the process of being obtained.

Table 3- Rover ^{137}Cs Comparison

Sample	Assay ^{137}Cs (μCi)	Radiochemistry ^{137}Cs (μCi)	Assay/Radiochem. (%)
process pipe	186 ± 35	192 ± 7	97
non process pipe	58 ± 7	52 ± 1.2	110
process tank	1.0 ± 0.29 E+3	1.00 ± .04 E+3	99.9
Debris	ND	3.3 ± 0.1	ND
	Average agreement - 102 %		

CONCLUSIONS

The RWAS system demonstrates that a flexible, user-friendly nondestructive assay system can be developed and placed into operation in a relatively short period of time and can meet facility-specific and operational requirements for assaying radioactive waste. The control system

Table 4- Rover ^{235}U Comparison

Sample	Assay System ^{235}U (mg)	Radiochemistry ^{235}U (mg)	Assay/Radiochem. (%)
process pipe	5.6 ± 2.3 E+2	380 ± 26	147
nonprocess pipe	3.2 ± 1.5 E+2	350 ± 12	91
process tank	3.0 ± 1.4 E+3	2.6 ± 0.3 E+3	115
Debris	ND	1.6 ± 0.13	
	Average agreement -- 118 %		

architecture developed for this system is highly flexible and adaptable to a range of potential assay problems. Specific comparisons with Rover waste indicate good agreement and uncertainties that are not significantly larger than those found for other types of nondestructive assay systems for radioactive materials.

Additional work has yet to be performed to complete validation of all measured and calculated efficiency data and some improvements in the operational and graphical user interface will be incorporated within the next few months.

ACKNOWLEGEMENTS

Work supported by the U. S. Department of Energy, Assistant Secretary for Environmental Management, under DOE Idaho Operations Office Contract DE-ACO7-94ID13223

REFERENCES

1. American National Standard Guide to the Automation of Nondestructive Assay Systems for Nuclear Materials Control, ANSI N15.37-1981, Institute of Nuclear Materials Management, August 1981.

2. American National Standard for Nuclear Materials - Nondestructive Assay Measurement Control and Assurance, ANSI N15.36-1983, Institute of Nuclear Materials Management, October 1982.

3. American National Standard Guide to Calibrating Nondestructive Assay Systems, ANSI N15.20-1975, American National Standards Institute, June 1975.

4. American National Standard for Nuclear Materials - Calibration Material for Nondestructive Assay Systems that Count Passive Gamma Rays - Guide to Preparing, ANSI N15.35-1983, Institute of Nuclear Materials Management, April 1982.

Tomographic Methods and NDE Systems

USING NAI DETECTORS FOR TOMOGRAPHIC GAMMA SCANNING

Robert J. Estep
Los Alamos National Laboratory, Los Alamos, NM 87545

Sheila Melton
Oak Ridge National Laboratory, Oak Ridge, TN 37830

ABSTRACT

We examined two approaches for using NaI detectors to perform transmission corrections used in the tomographic gamma scanner and segmented gamma scanner nondestructive assay methods. We found that a material-basis-set (MBS) fit using empirical logarithmic response spectra is quite accurate. Because this is a gross count technique, it gives sensitivities (for equal numbers of detectors) that are roughly ten times better than those obtained using Germanium detectors. We also found that simple continuum subtraction can be used in MBS fits using the energy-group-analysis technique only when the Pu transmission is greater than 10%. Both approaches for using NaI detectors require a knowledge of the Pu (or other) isotopics to obtain full accuracy.

INTRODUCTION

The objective of this study was to develop analysis methods that will allow arrays of NaI and other room-temperature gamma-ray detectors to be used in the tomographic gamma scanner (TGS)[1] and segmented gamma scanner (SGS) methods in place of high-purity-Germanium (HPGe) detectors. NaI detectors are widely used in detector arrays for medical and industrial imaging because of their low cost and simple operation, but they have not been used in TGS and other transmission-corrected gamma-ray nondestructive assay (NDA) methods because neither the ^{75}Se nor the Pu peaks used historically in SGS and TGS are resolved in NaI spectra and because the poor energy resolution of NaI introduces large statistical errors in measurements of continuum-subtracted (net) peak areas.

In this study we examine data analysis techniques for both the transmission and emission parts of TGS and SGS assays. One of the methods studied applies transmission corrections to gross Pu spectra from NaI detectors. The use of gross counts instead of net

counts dramatically improves the sensitivity of TGS assays, as is shown in Table I below. The table lists estimated low-burnup Pu assay sensitivities in a 30-minute emission scan for a TGS system with a varying number of NaI or HPGe detectors. The net area sensitivity estimates are based on a standard one-ROI linear continuum subtraction, while the gross count sensitivities are for assays using the total counts in the 332- to 452-keV peak group of Pu. It can be seen from the table values that the sensitivity using gross count methods with NaI detectors will be about ten times better than that for HPGe detectors using net area methods. In particular, a 120-detector NaI system using gross count methods would have the same sensitivity (5 mg of low-burnup Pu) as the differential dieaway technique.

TABLE I. Estimated TGS Pu assay sensitivities* for various array sizes

Number of detectors	HPGe net area sensitivity (mg Pu)	NaI net area sensitivity (mg Pu)	NaI gross count sensitivity (mg Pu)
1	600	1200	50
20	132	260	10
40	96	192	8
60	78	160	7
80	66	130	6
120	55	110	5

* estimates are for a non-attenuating matrix with a moderately high ambient background

EXPERIMENTAL DETAILS

To evaluate the effectiveness of the data analysis techniques considered here we performed transmission measurements on a series of attenuating materials. For each absorber we separately measured transmitted spectra from a 100-g metallic low-burnup Pu source, a ^{133}Ba source, a ^{137}Cs source, and a ^{60}Co source using a Bicron 2M2/2 (2-inch diameter by 2-inch thickness) NaI detector and a 35% Ortec GEM-type coaxial HPGe detector. This transmission source combination was recently shown[2] to be optimal for TGS assays of Pu. We then applied different analysis techniques to see how well the

transmission data could be used to correct the Pu data for attenuation through the absorbers. As is discussed below, the effectiveness of an analysis technique in estimating attenuation corrections in this simple geometry can be a good measure of its effectiveness in the TGS or SGS methods.

Table II lists the series of absorbers used. Also shown are the transmission values for the ^{239}Pu 414-keV gamma ray as measured using an HPGe detector as well as the gross count transmission of the 332- to 452-keV group of Pu peaks as measured with the NaI detector. The gross count Pu transmissions are influenced by geometric details that do not affect the 414-keV transmission measured using the HPGe detector. Side scattering of divergent gamma rays back into the detector is the most significant effect. It is observable with every absorber except those of Pb, and is particularly pronounced with the 10-inch polyethlylene absorber. That large-area absorber was composed of a stack of 2-inch-thick polyethlylene blocks with widths varying from 12 to 18 inches. The 4-inch polyethylene absorber, in contrast, was 4- by 6-inches in width, and shows correspondingly less side scattering.

TABLE II. Absorbers Used in Transmission Measurements

Absorber	414-keV transmission (HPGe)	332- to 452-keV gross transmission (NaI)
0.5" stainless steel	.400	.588
1" stainless steel	.156	.315
1" Cu	.162	.317
0.5" Al	.719	.861
1" Al	.521	.725
1.75" Al	.331	.547
0.25" Cd	.564	.614
0.5" Pb	.0534	.0405
10" polyethylene	.0671	.201
air (no absorber)	1.00	1.02
4" polyethylene	.352	.511
0.25" Pb	.225	.199
4" polyethylene plus 0.25" Pb	.0765	.101

To make transmission measurements we placed the NaI and HPGe detectors side by side facing the transmission source. The transmission source position was 18 inches from the detector faces. The absorbers were placed between the source and the detector. Some absorbers were placed closer to the detector, some closer to the source. For a given absorber we used the same placement with each transmission source so that side scatter and other geometric effects would be approximately the same. Using two detectors this way introduced a parallax difference of about 0.6% in the absorber thickness across the detector diameters, which we consider to be negligible.

A second set of absorbers composed of alternating layers of polyethylene and 1/16-inch Pb foils was used to construct empirical basis spectra for the response function methods discussed below. We used transmission spectra for 10 inches of polyethylene and 0.5 inches of Pb as basis spectra in a two-element material basis set[3] (MBS) approach. To determine the average spectrum shape of the side-scattered gamma rays we collected transmission spectra through the same absorber in configurations that alternately minimized and maximized side-scattering effects. We then subtracted the minimum-scattering spectrum from the maximum-scattering spectrum. As has been observed elsewhere, the shape of this scattered spectrum is fairly constant. Scattering spectra for several absorber combinations were averaged to create a composite scattering spectrum to be used as a response function. This approach characterizes only the excess scattering over the minimum observed; the minimum scattering cases still contain significant scattered counts, as is shown by the transmission values in Table II. Side scattering was characterized only for the ^{133}Ba and the Pu sources.

For measurements with all sources except ^{60}Co we used a weak ^{60}Co rate loss source to normalize spectra and eliminate rate loss effects. A weak ^{137}Cs source was used as the rate-loss source for ^{60}Co transmission measurents. Note that we are not recommending the use of rate-loss sources with NaI arrays in general, as they limit the sensitivity in high-efficiency counting applications. All NaI spectra were normalized to the rate-loss peaks by spectrum stripping. Because we used the transmission sources

separately instead of in combination, the stripping procedure produced clean spectra containing only counts from the transmission source.

ANALYSIS METHODS

We used two basic approaches for analyzing NaI spectra: (1) a method based on linear continuum subtraction to obtain net peak areas, and (2) an MBS empirical response-function method. Empirical or theoretical response-function or other peak-fitting methods could be used to extract net full-energy-peak areas from NaI spectra with better accuracy than can be obtained using linear continuum subtraction. We have chosen not to study those refined methods at this time. The response function technique described here is not aimed at obtaining net peak areas, but rather at obtaining gross count corrections. Aside from the elimination of excess side-scattering and emission components in the transmission spectra, the technique is fundamentally nonsubtractive. Thus, what we are really comparing is a net area method and a gross count method.

In the simple experiments described here, the Pu source represents the emission part of a TGS scan and the other sources the transmission part. We used the MBS method in both approaches to convert attenuation corrections from the transmission to the emission part of the problem. That is, we used the transmission data to compute partial density values (ρ_z) in a basis set of CH_2 and Pb, then we used the ρ_z values to compute attenuation corrections for the emission (Pu) attenuation loss. It is this intermediate conversion to the MBS that allows us to generalize from the simple source→absorber→detector geometry to the TGS geometry, in which a potentially large number of separate sources are mixed randomly with a potentially large number of separate absorbers. Not all methods that work with the simple geometry can be applied to TGS. For example, with the simple geometry one can use a response function technique to estimate the attenuation loss of the Pu source using just the Pu spectrum, eliminating the need for the transmission sources. This approach, however, cannot be generalized to TGS.

The analysis of NaI spectra can be greatly simplified by keeping the spectra as pure as possible. We recommend using the different transmission sources separately in different detector planes of the (linear) array. That is, the ^{133}Ba source transmission should be measured by one set of detectors, the ^{137}Cs source by another, and the ^{60}Co source by a third. Throughput can be maintained if the individual sources are each as strong as the single mixed source they replace. Emission gamma rays will contaminate the transmission spectra, so it is prudent with NaI detectors to perform emission measurements at every position used in the transmission scan so that the Pu or other emission spectrum can be stripped from the transmission source spectra.

If a rate loss source is used (as it is here), then its spectrum must also be stripped. Stripping a rate-loss-source spectrum will automatically strip the room background spectrum. If a rate-loss source is not used, then the room background must be stripped from every spectrum. Note that if region-of-interest (ROI) sum techniques are used, the channel-by-channel stripping of spectra can be replaced by a subtraction of ROI sums.

The data-fitting techniques used in this study are implemented in the LANL-developed TGS_FIT[4,5] image reconstruction software, which was used for the MBS, energy-group-analysis, and response-function fitting described below.

NET PEAK AREA METHODS

Figure 1 compares a gamma-ray spectrum of a mixture of ^{133}Ba, ^{137}Cs, and ^{60}Co taken with the HPGe detector to a spectrum taken with the NaI detector. One can see why NaI detectors are shunned in many applications: their energy resolution is 30-40 times worse than that of HPGe detectors. The four ^{133}Ba gamma-rays are easily resolved in the HPGe spectrum and can be separately measured and used as data for fitting MBS or Z-effective attenuation curves. They are not resolved in the NaI spectrum and cannot be separately measured. However, because of the wide energy separation between gamma

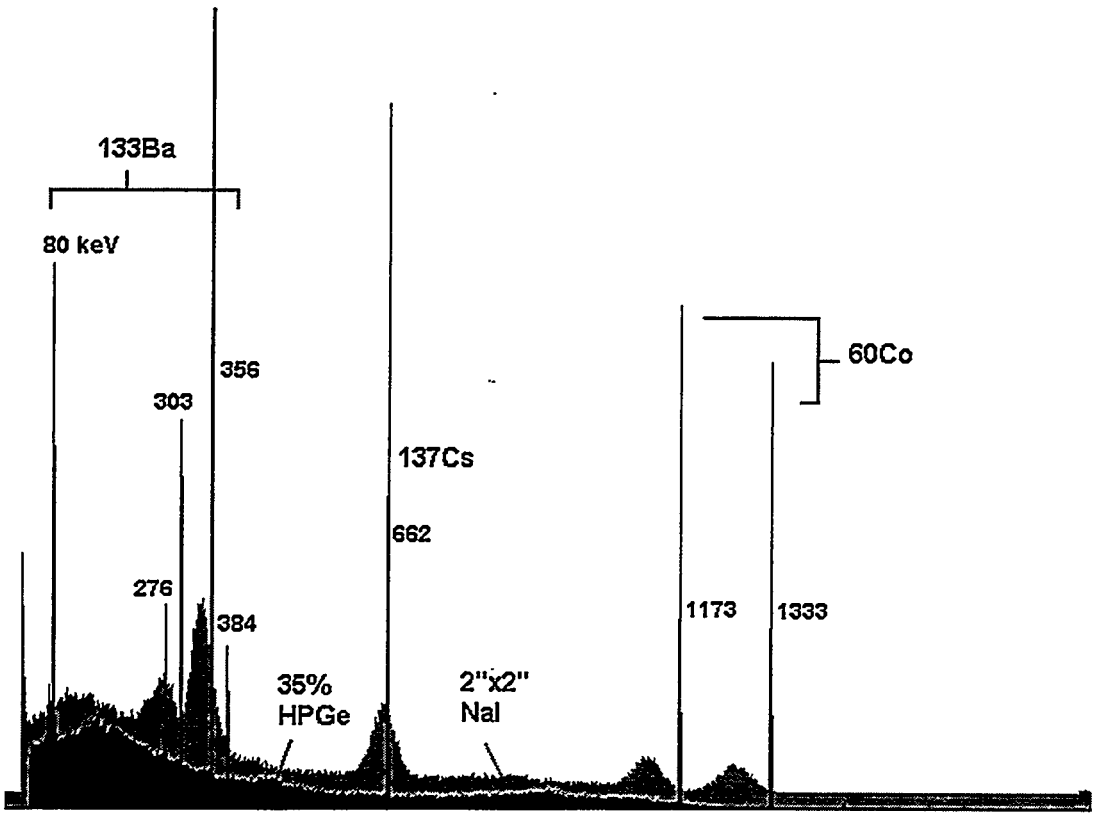

Figure 1. Comparison of HPGe and NaI spectra of a mixture of ^{133}Ba, ^{137}Cs, and ^{60}Co. Note the wide spacing between the groups of gamma rays emitted by these isotopes.

rays from the three isotopes, it is easy to resolve the ^{133}Ba gamma rays as a group from those emitted by ^{137}Cs and ^{60}Co. Also, the sum of the four ^{133}Ba gamma rays can be measured (approximately) from the NaI spectrum. Since the transmission values of all the transmission gamma rays must lie on the same monotonic attenuation curve, one might intuitively guess that the wide spacing and resolvability of the broad "energy groups" of gamma rays could be used to arrive at a good estimate of the individual gamma-ray intensities within the groups. This is in fact the case, and is the basis for what we are calling the energy-group-analysis method.

Energy-group analysis

The summed intensity of a group of gamma rays of different energies will not obey Beer's attenuation law and so cannot be used directly for transmission imaging or for attenuation-curve fitting with the linear MBS method. However, we have developed an iterative procedure that allows the relative intensities of the individual gamma rays in a group to be determined at each view. An initial guess is made of the relative transmissions of the gamma rays in the group, and these values are used along with the transmissions of the other energy groups to find an approximate MBS attenuation curve. The attenuation curve is used to make an improved guess of the transmissions, which are then used to make a second, improved MBS fit. This is repeated for a total of five iterations. The rapid convergence of this method is illustrated in Figure 2, which shows the attenuation curve for 0.25-inch of cadmium as fitted to the measured transmissions from a ^{133}Ba and ^{137}Cs transmission source combination. Even with a crude initial guess of the individual gamma-ray transmissions (i.e., all transmissions equal), the second estimate is already very close to the correct value.

Once the attenuation curve is known, applying an attenuation correction to a group of unresolved emission gamma rays is straightforward, provided that the isotopic composition of the emitting source mixture is known. In TGS, for each energy in the emission group, one sums the attenuation-corrected emission matrices, $F(E_i)$, for the individual gamma-ray energies E_i, to obtain the group-sum attenuation-corrected emission matrix, F(group). The group matrix is used to reconstruct the ^{239}Pu mass image vector, s. In the source→absorber→detector geometry used here, the Pu attenuation correction factor, CF, is given by

$$CF = \Sigma_e I_0(e) / \{ \Sigma_e I_0(e) \exp(-\mu_e) \} ,$$

$$\mu_e = \Sigma_z \rho_z U_{ez},$$

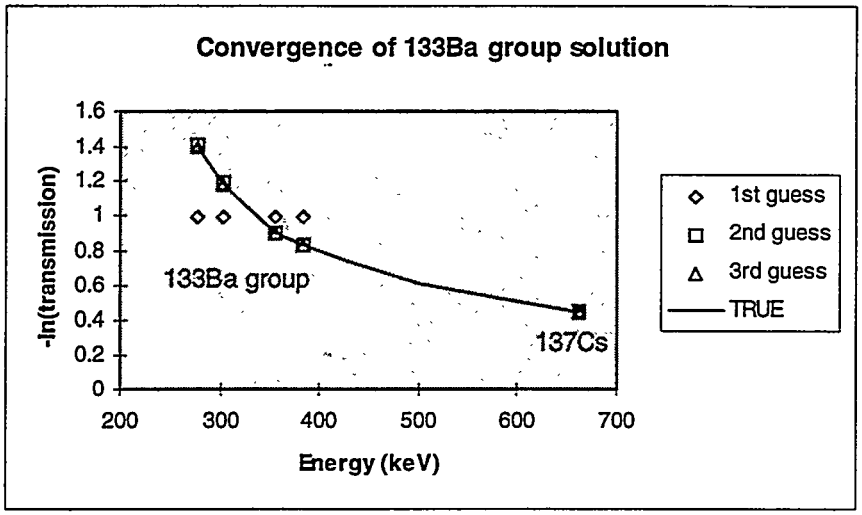

Figure 2. The rapid convergence of the estimated individual ^{133}Ba peak intensities in an energy-group-analysis iterative MBS fit. Although the initial guess for the ^{133}Ba transmissions is poor, the second guess is very close. By the third guess the estimated transmissions are within 0.5% of their true values.

where $I_0(e)$ is the unattenuated relative intensity of the e'th gamma ray peak in the group, ρ_z is the partial density of z'th basis material in the absorber, and U_{ez} is the attenuation coefficient for a standard amount of the z'th basis material at the e'th energy.

Figure 3 shows the ratio of the measured-to-true attenuation correction as a function of the transmission of the ^{239}Pu 414-keV gamma ray (measured with the HPGe detector) through the set of absorbers in Table II. The attenuation corrections estimated using the NaI detector with the linear continuum subtraction method were applied to the Pu transmissions measured with the HPGe detector (at 414 keV) and to the NaI detector (322- to 452 keV group net area, estimated using linear continuum subtraction). We can conclude from the figure that the net area method applied to NaI spectra gives good accuracy in determining attenuation corrections, but that the Pu peak net areas are less accurate and become completely unreliable at transmissions of less than 10%. To put the results in figure 3 in perspective, the standard deviation in the measured-to-true correction factor ratio was 3.5% when using HGPe data exclusively, 4.4% using Nai transmission

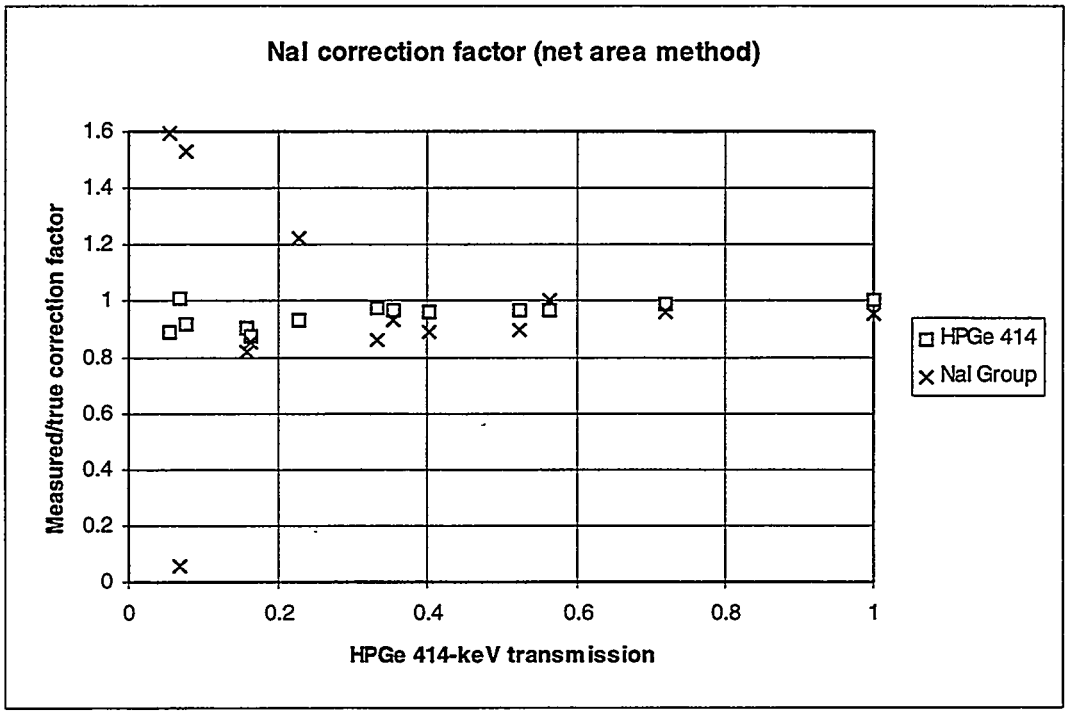

Figure 3. The measured-to-true attenuation correction as a function of the transmission of the ^{239}Pu 414-keV gamma ray (measured with the HPGe detector) through absorbers of varying composition and thickness. The attenuation corrections estimated using the NaI detector with the linear continuum subtraction method were applied to the Pu transmissions measured with the HPGe detector (at 414-keV) and to the NaI detector (322- to 452-keV group net area, estimated using linear continuum subtraction).

results to correct HPGe Pu emission data, and 11.5% (excluding points below 10% transmission) for using the net area NaI data for both.

AN EMPIRICAL RESPONSE FUNCTION APPROACH

We examined a simple empirical response function method that applies the MBS method directly to spectra rather than to transmissions computed from net peak areas. In this approach reference spectra of each transmission and emission source are measured after passing through air and through a set of basis materials and are then converted to logarithmic form to be used as a basis spectrum set. When the spectra of transmission

gamma rays passing through an arbitrary absorber are decomposed into component basis spectra, the coefficients in the decomposition are the partial densities (ρ_z). These are equivalent to the ρ_z values determined using net peak areas and can be used without modification to correct HPGe or NaI net area emission data.

A similar response function technique can be applied to emission spectra of Pu. In this approach the ρ_z values are used to create a "corrected" Pu spectrum. This spectrum represents the Pu spectrum that would have been obtained with no intervening absorbers, and in principle will have the same shape as the Pu reference spectrum through air but an amplitude that is proportional to the Pu mass. This is in fact a gross count technique. The only subtractions required (explicitly or implicitly as part of the fit procedure) are of the ambient background and of the rate-loss-source spectrum if one is used.

Side scattering must be treated in order to get accurate results in either the transmission or emission part of the problem. We used representative side-scattering spectra as a third MBS "material" for both parts of the problem. In the transmission method the solution vector becomes $\rho = [\rho_{Pb}, \rho_{CH2}, \rho_{scat}]^T$, where ρ_{scat} gives the amplitude of the scatter component. To subsequently use ρ to compute attenuation corrections for HPGe or NaI net-area emission data, the ρ_{scat} component can be ignored. To compute corrections in the emission response function method, ρ_{scat} is used as the amplitude of the scatter component in the Pu spectrum. Although the ρ_{scat} component is subtractive when fitting the transmission data, applying the correction to the emission data is not. This is true even when using several scatter-component spectra. One can say that if the ρ vector is determined with good accuracy and precision in the transmission part of the problem, then the scatter components in the Pu spectrum become useful tidbits of information that add counts to the assay and improve assay sensitivity.

Transmission analysis with MBS response spectra

Let $\{\mathbf{c}_z\}$ be a set of composite spectra measured after transmission through each of n_z basis materials. By composite we mean that if separate spectra are taken for different

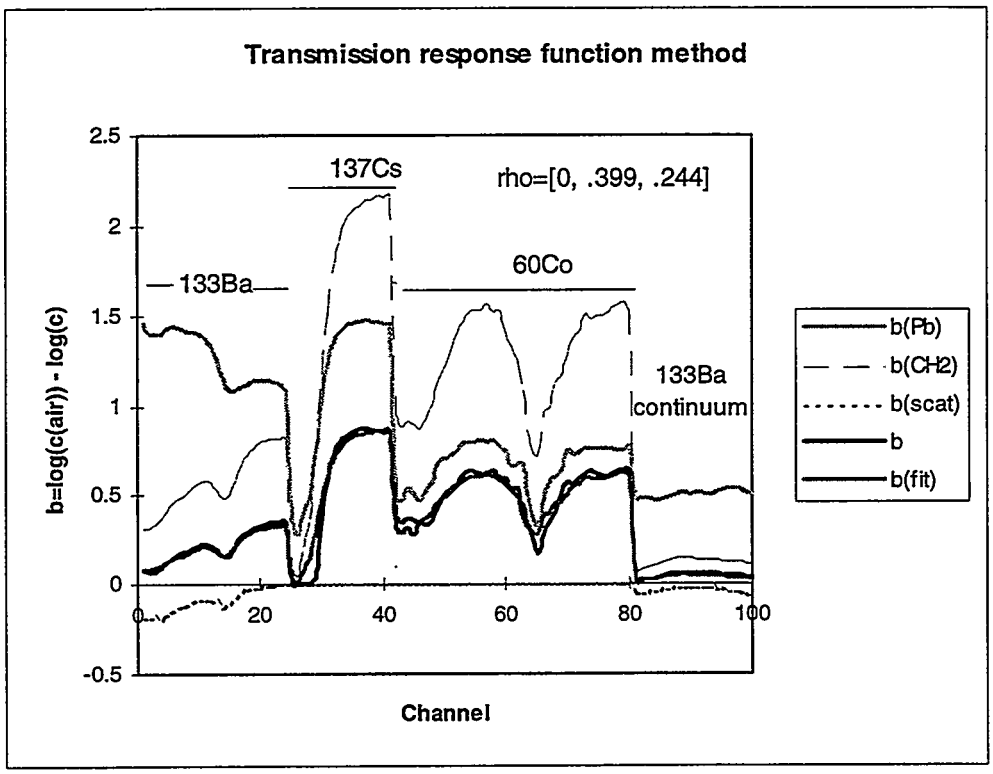

Figure 4. Illustration of the response function method applied to the composite transmission spectrum (**c**) for a 1.75-inch Al absorber. The logarithmic basis spectra are for 0.5-inches of Pb [**b**(Pb)], 10-inches of polyethylene [**b**(CH2)], plus a negative scatter component [**b**(scat)]. The best-fit combination of the basis functions to the curve **b** is given by **b**(fit) = 0 · **b**(Pb) + .399 · **b**(CH2) + .244 · **b**(scat), where the coefficients are the MBS ρ_z values for this basis set. The physical interpretation is that 1.75-inches of Al has attenuation properties equivalent to 3.99 inches of polyethylene, which is approx. true for gamma rays of these energies.

transmission sources, the interesting portions of each are extracted and arranged together into a single "spectrum" of counts. Figure 4 shows reference composite NaI spectra (in logarithmic form) created from separate ^{133}Ba, ^{137}Cs, and ^{60}Co sources transmitted through air and through our two basis absorbers (10 inches of polyethylene and 0.5 inch of Pb). The composite spectra contain the two ^{60}Co and the single ^{137}Cs peak, and the unresolved 276- to 384-keV peak group in ^{133}Ba. At the high end of the spectrum is a

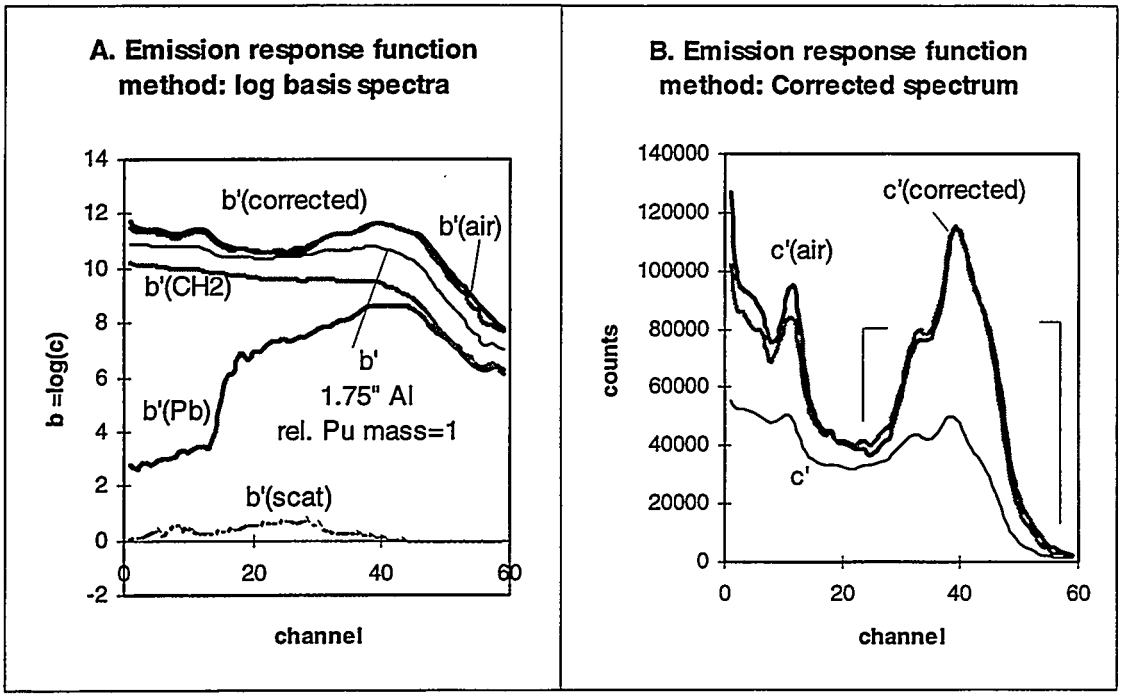

Figure 5. Illustration of the gross count response function method applied to the 100-g Pu source spectrum (**c'**) after passing through a 1.75-inch Al absorber. The ρ_z values determined for the transmission fit to the same absorber (see Figure 4) were used to create the corrected log spectrum, **b'**(corrected), which was converted to the normal corrected spectrum, **c'**(corrected). (A) Log spectra, including the basis spectra **b'**(Pb), **b'**(CH2), **b'**(scat), and **b'**(air). (B) Linear scale transmission spectra. The lines show the summation region used.

scaled-down portion of the lower-energy continuum from ^{133}Ba. The scaling of the different spectrum components determines their weight in least squares fits.

To construct basis spectra ($\mathbf{b}_{Pb}$, $\mathbf{b}_{CH2}$) we make the conversion

$$b_{Pb,i} = \log(c_{air,i}) - \log(c_{Pb,i}) \ ,$$

and

$$b_{CH2,i} = \log(c_{air,i}) - \log(c_{CH2,i}) \ ,$$

where $c_{air,i}$, $c_{CH2,i}$, and $c_{Pb,i}$ are the (normalized) counts in the i'th channels in the air, CH_2, and Pb transmission spectra, respectively. Figure 4 shows these logarithmic basis spectra. A spectrum **c** taken through an arbitrary absorber must be similarly converted to a logarithmic spectrum, **b**, i.e.,

$$b_i = \log(c_{air,i}) - \log(c_i) \quad .$$

The three-material MBS solution vector ρ ($=[\rho_{Pb}, \rho_{CH2}, \rho_{scat}]^T$) is computed by solving the linear system of equations

$$\mathbf{b} = U \cdot \rho \qquad , \qquad (1)$$

where U is an N-by-3 matrix whose columns are the N-channel spectra $\mathbf{b}_{Pb}$, $\mathbf{b}_{CH2}$, and $\mathbf{b}_{scat}$. We used the non-negative least squares (NNLS) fit option in TGS_FIT software to solve equation (1).

Figure 4 also shows fit results for a composite spectrum **b** measured through 1.75 inches of Al. The MBS solution was found to be $\rho = [\rho_{Pb}, \rho_{CH2}, \rho_{scat}]^T = [0, .399, .244]^T$. The physical meaning of this solution is that the absorber behaves like a material composed of (0)·(.5) = 0.0 inches of Pb and (0.399)·(10) = 3.99 inches of polyethylene, which is approximately correct for the energies involved.

Emission analysis with MBS response spectra

Figure 5a shows the basis spectra used for constructing a corrected Pu emission spectrum from the MBS partial density vector, ρ, determined by the response function method applied to the transmission data. The corrected Pu spectrum, $\mathbf{c}'_{corrected}$, and log spectrum, **b'**, are given by

$$\mu'_i = \rho_{Pb} \cdot b'_{Pb,i} + \rho_{CH2} \cdot b'_{CH2,i} + \rho_{scat} \cdot b'_{scat,i} \quad ,$$

$$c'_{corrected,i} = \exp(\mu'_i) \cdot c'_i,$$

$$b'_{z,i} = \log(c'_{z,i}) \text{ , and}$$

$$z = \text{Pb, } CH_2\text{, or scat,}$$

where the c'_z are the basis spectra for Pu and b'_z are the corresponding logarithmic spectra. The Pu mass (with whatever isotopic composition is represented by the basis spectra) is given by

$$\text{mass(Pu)} = \text{mass(reference)} \cdot \Sigma_i\, c'_{corrected,i} / \Sigma_i\, c'_{air,i} \qquad (2)$$

where "mass(reference)" is the mass of Pu represented by the basis spectra and $\mathbf{c}'_{air}$ is the Pu reference spectrum with no attenuation. The summations are all over the same range, which in this study was limited to the upper part of the spectrum bracketing the 332- to 452-keV peak group, as shown by the lines in Figure 5B. Note that because mass(Pu) here equals mass(reference) (they are the same source), the spectra $\mathbf{c}'$(air) and $\mathbf{c}'$(corrected) have the same amplitude.

As a matter of general interest, the Pu mass can be estimated for the simple source→absorber→detector geometry without using transmission sources by solving equation (1) for the Pu emission spectrum in the same manner as for transmission spectra, but with a constant term added to the basis set. That is, one uses the unit spectrum ($b_{unit,i}$ = 1, all i) as an additional basis spectrum. The amplitude ρ_{unit} of this constant term will be equal to the logarithm of the Pu mass relative to the reference mass.

Response function method results

Figures 6 and 7 show the results of applying the response function method to the series of absorbers in Table II. The results for correcting the HPGe detector 414-keV

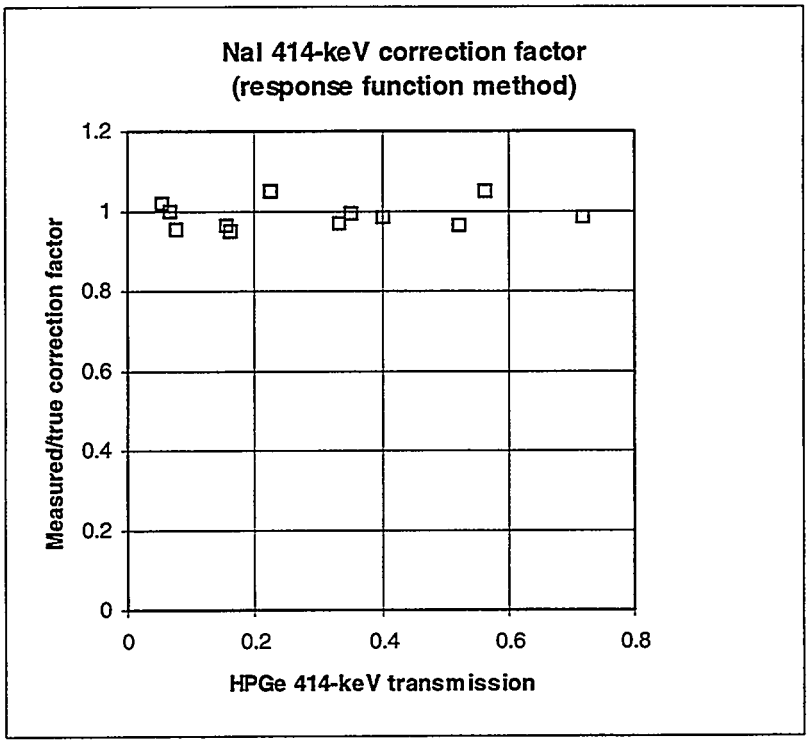

Figure 6. The measured-to-true attenuation correction as a function of the transmission of the 414-keV gamma ray through absorbers of varying composition and thickness. The attenuation corrections were measured using a NaI detector (response function method) and projected to 414 keV. The 'true' values were measured for the 414-keV gamma ray in ^{239}Pu using an HPGe detector.

gamma ray using the NaI transmission MBS solution are shown in Fig. 6. The results for correcting the NaI Pu gross spectrum using the same ρ are shown in Fig. 7. In figure 7, the results with and without the inclusion of side scattering are compared. The results are quite good overall, with a maximum mass error of only 3.5% when side scattering is included.

SUMMARY AND CONCLUSIONS

Table III summarizes our results as the average mass (relative to the true value) and standard deviation of the estimated masses in the absorber series for each of the analysis methods considered. The main conclusion we can draw is that all the methods

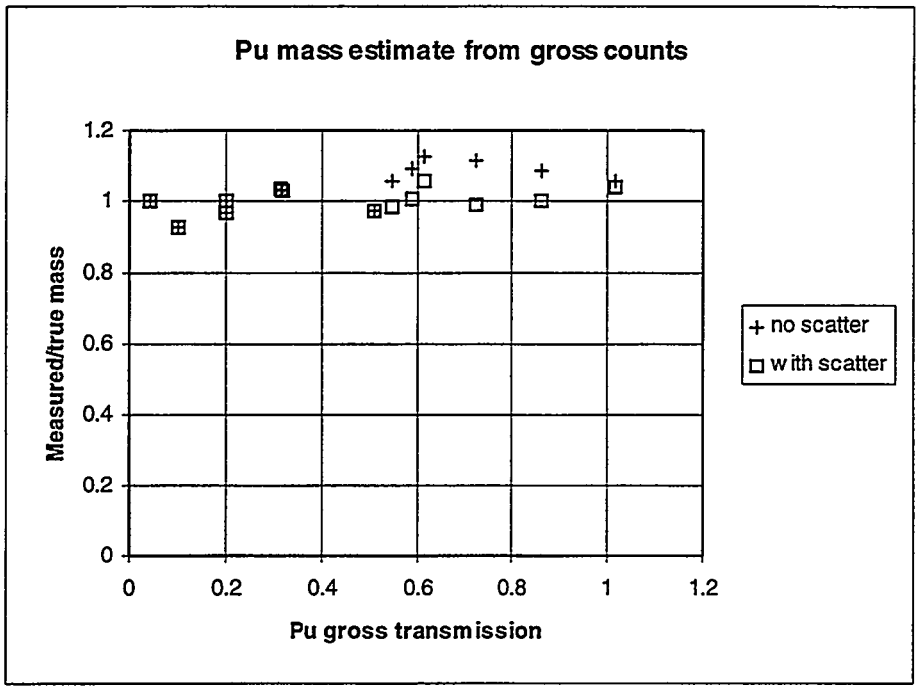

Figure 7. Pu mass estimate for a metallic 100-g Pu source transmitted through a range of materials. The masses were estimated using the empirical response function method for both the transmission and emission halves of the problem. Side scatter is ignored in the estimates plotted as '+' symbols, and is included in the estimates plotted as squares.

TABLE III. Summary of analysis results

Transmission source analysis method	Emission source (Pu) analysis method	Average estimated/true mass	Standard deviation (relative)
HPGe	HPGe	1.007	3.5%
NaI, continuum subtraction	HPGe	.95	4.4
NaI, continuum subtraction	NaI, continuum subtraction	.94*	11.5*
NaI, response function	HPGe	.990	3.4%
NaI, response function	NaI, response function	1.001	3.5%

*for transmissions >= 10%

studied worked well except for the linear continuum subtraction in Pu spectra. The problem in that case is that the Pu peak areas are not accurately extracted with linear continuum subtraction (the method worked well on the transmission peaks). It seems likely that more refined net area determinations (e.g., using a response function approach) will give good results.

NaI detectors worked very well when using the gross count response function method, but there are two important caveats concerning their application to TGS and SGS. The first is that the method requires accurate Pu response functions to give the best accuracy. This implies that the isotopic composition of the waste is well known . The second caveat is that we do not know yet how well the treatment of the scattered components will translate from the simple geometry studied here to TGS systems. If the method does not translate well, the scattered components will have to be treated using a response function analysis on the Pu spectra, which would introduce a subtractive element that would degrade the sensitivity. Even so, we believe that the dramatic improvement in sensitivity, along with the ability to image at higher resolutions without increasing the scan time, make NaI arrays an attractive option for the next generation of TGS systems.

REFERENCES

1) R. J. Estep, T. H. Prettyman, and G. A. Sheppard, "Tomographic gamma scanning to assay heterogeous radioactive waste," Nucl. Sci. and Eng. **118**, 145-152.

2) R. J. Estep, T. H. Prettyman, and G. A. Sheppard, "Comparison of atteuation correction methods for TGS and SGS: Do we really need selenium-75?" Proc. 37th annual INMM meeting, Naples, FL (July, 1996).

3) R. J. Estep, T. H. Prettyman, and G. A. Sheppard, "Reduction of TGS image reconstruction times using separable attenuation coefficient models," ANS Winter Meeting, San Francisco, CA (June 15, 1995). Also, Los Alamos Rept LA-UR-95-2013.

4) R. J. Estep, "TGS_FIT 3.0: Image reconstruction software for quantitative, low-resolution tomographic assays," to be published, Los Alamos National Lab.

5) R. J. Estep, "TGS_FIT: Image reconstruction software for quantitative, low-resolution tomographic assays," Los Alamos National Lab report, LA-12497-MS (1993).

LOS ALAMOS NATIONAL LABORATORY'S

MOBILE REAL TIME RADIOGRAPHY SYSTEM

Jack Vigil, Dan Taggart, Stephen Betts,
Jesse Mendez, Carlos Rael, Flavio Martinez
Chemical Science and Waste Technology
Los Alamos National Laboratory
PO Box 1663, MS J594
Los Alamos, New Mexico 87545

ABSTRACT

A 450-keV Mobile Real Time Radiography (RTR) System was delivered to Los Alamos National Laboratory (LANL) in January 1996. It was purchased to inspect containers of radioactive waste produced at (LANL). Since its delivery it has been used to radiograph more than 600 drums of radioactive waste at various LANL sites. It has the capability of inspecting waste containers of various sizes from <1-gal. buckets up to standard waste boxes (SWB, dimensions 54.5 in. x 71 in. x 37 in.). It has three independent x-ray acquisition formats. The primary system used is a 12- in. image intensifier, the second is a 36-in. linear diode array (LDA) and the last is an open system. It is fully self contained with on board generator, HVAC, and a fire suppression system. It is on a 53-ft long x 8-ft. wide x 14- ft. high trailer that can be moved over any highway requiring only a easily obtainable overweight permit because it weighs ~38 tons. It was built to conform to industry standards for a cabinet system which does not require an exclusion zone. The fact that this unit is mobile has allowed us to operate where the waste is stored, rather than having to move the waste to a fixed facility.

INTRODUCTION

The need to have mobile nondestructive assay/nondestructive examination (NDA/NDE) capabilities has been a vision and a necessity at the Department of Energy (DOE) complexes which produce radioactive waste for a number of years. The Radioassay Nondestructive Testing (RANT) Facility of the Chemical Science and Waste Technology at the Los Alamos National

Laboratory (LANL) has acquired and assisted in the development of three mobile NDA/NDE systems. The three are a mobile Passive Active Neutron (PAN) Assay system that was developed and built at LANL in the mid 1980s. This unit had been sitting in a salvage yard at Idaho National Engineering Laboratory (INEL) for a couple of years when it was transferred to LANL. We refurbished this unit and put it back into operation in 1995. The second mobile unit is a state of the art Segmented Tomographic Gamma Scanner (S/TGS) developed and built at LANL. The third and the topic of this paper is a mobile Real Time Radiography (RTR) system built by VJ Technologies of Long Island, New York. VJ built this unit with our input and requirements utilizing our past experience with our stationary RTR unit and knowledge of the waste streams that we would be inspecting. The mobile RTR took about a year to complete from design through construction before it was delivered to us in January 1996. The RTR system is built on a 51 foot trailer built by Ellis and Watts. Ellis and Watts has tremendous experience in building this type of trailers, having provided many to the medical industry for mobile labs. The mobile RTR has been used to inspect over 600 drums of various matrices and at different LANL locations. I would like report on some of the highlights, problems encountered and lessons learned using the mobile RTR.

MOBILE REAL TIME RADIOGRAPHY WASTE CONTAINER INSPECTION

The mobile RTR system was delivered to LANL the first week of January 1996. After a complete check, acceptance, and vendor-provided training, we were ready to take the mobile RTR on its maiden voyage. We made arrangements to take it into LANL's plutonium facility, TA-55, to determine the contents of five 55-gal. drums of unknown contents that had been stored at this facility for 24 years. The RTR was moved for us by our in house drivers. The RTR was parked outside an office building and the on

board generator was used to power the unit. Before any drums of waste were brought to the unit the host's radiological control technicians (RCTs) surveyed the unit for any possibility of radiation leakage. None was found. The x-ray enclosure was built to x-ray cabinet standards so we were confident that there would not be any radiation leakage. The beam stop wall contains 2 in. of lead and it tapers down to .5 in. to the control room side, additionally the x-ray head was also shielded in its own lead enclosure which contributes in reducing the amount of external radiation being emitted from the x-ray tube. The five drums were brought to the RTR and were also surveyed for external contamination prior to loading into the mobile RTR. These drums were named the EXXON drums because they originally came from EXXON Nuclear. When they were brought to LANL, apparently the contents were known but over the years that information was misplaced. The drums were radiographed and the inspection revealed that they contained mainly room-type trash such as filters, plastics, and paper. One of the drums did contain a container with approximately 1 L of liquid which surprised the owner of these drums because of the length of time that these drums had been in storage.

We used two methods of radiographic acquisitions on these drums. The 12-in. image intensifier was used first which is how the liquid was identified. Using the image intensifier allows us to view the contents of the drum in real time. The draw back to this is that only a 12 in. diameter field of view can be seen at any one time. The energies used to penetrate these drums using the image intensifier were about 150 kV and 3 mA. After completing the five drums using the image intensifier we radiographed them again using the 36 in. Linear Diode Array (LDA). By using the LDA although not real time we can scan the entire contents of a 55 gal. drum in 19 seconds and save the image to the computer's hard disc or to other media storage formats. This allows the image to be further scrutinized utilizing-off-the

shelf imaging software. The typical energies used to perform a LDA are 400 kV and 0.3 mA. The image produced is of the entire 55 gal. drum which can used to pin point areas of interest. The use of the LDA can be beneficial when time or production is of concern.

We completed this project and then moved the RTR to assist in the Transuranic TRU Waste Characterization Project. This project involved coring into cemented sludge drums and taking a sample for characterization. We radiographed 20 drums for this project. We knew that with the energies produced by the mobile RTR that we were not going to penetrate the contents of the drum. We concentrated on inspecting the top and bottom of the drums as well as the sides. We set the energy at 450 kV and 10 mA and proceeded to scan the drum using the image intensifier. We were searching for liquids that could have leached from the cement during the curing time. We were identifying weather the drum contained a liner. All of these drums contained a $1/16^{th}$ in. lead liner which made it that much more difficult to penetrate. We did not identify any liquid in these drums. When they were cored, no liquid was identified. This entire project was a success, it was also entirely quality assured.

Our next project took us to LANL's radioactive waste storage and disposal site TA-54 Area G. We were tasked with performing NDA and NDE on 500 drums of stored TRU waste. We started off with what we knew were going to be the more difficult drums to radiograph which were lead-lined cemented sludge drums of which we had prior experience from doing on our previous project. Some of cemented sludge was filled directly into the 55-gal. drum to approximately 80% to 95% full and some was filled into 1 gal. cans and the cans were stacked 5 high in the drum. The 55-gal. drums were then placed into 85 gal. overpack drums. Unlike the previous sludge drums, a good percentage of these drums were known to contain liquid. We set up

the unit and proceeded to work off these drums. We initially inspected 80 drums and did not identify liquid. We discussed this with the waste generator of this waste stream and it was discovered that a large percentage of these 80 drums that we had inspected were known to contain liquid. We decided that we would radiograph these drums again, but we needed to come up with another technique to see if we could identify the liquid in these drums. We knew that we could not count on the jogging motion of the drum rotator or the x-ray generator to give us more penetrating power because we had already used maximum power (450 kV and 10 mA) on the first attempt. We designed and built a wedge that would be placed under the drums when the drum was placed in the x-ray cabinet. The wedge was 1.5 in. tall at the high end. We were hopeful that with the drums being tilted at an angle that the liquid would seek its own level. This proved to be exactly what it did. We reexamined the 80 drums and located liquid in all the drums that were known to have liquid and identified liquid in drums that were assumed to be dry. Of the 200 plus cemented sludge drums that we radiographed we identified 123 to contain liquid. Most of the liquid was located at the bottom of the drum in the drums that contained the 1 gal. cans. In the drums that were directly filled with cemented sludge the liquid was located on the top of the sludge. We also located liquid in some drums between the lead liner and the drum. These drums were transported to the Waste Characterization, Reduction & Repackaging Facility (WCCRF) where they were opened and drained. The WCCRF identified one drum that we identified as dry to contain less than a liter of liquid and all the 123 that we identified as having liquid to contain liquid. We continued to work off the remainder of the 500 drums that were not cemented sludge and identified some liquid and some pressurized containers in the remaining drums. These drums were not as dense as the sludge drums and we did not require the use of the wedge to identify liquid in these drums.

Simultaneous to radiographing these drums they were being assayed with our mobile PAN and mobile S/TGS. The PAN Assay system cannot accommodate 85 gal. overpack drums and the S/TGS can assay overpack drums but the throughput is less. Due to the variances in drum sizes, throughput, and imposed requirements on the number of drums needed to be examined, we ended up radiographing 630 drums in this project in order to complete data packages for 500 drums radiographed and assayed.

I covered a couple of problems that we encountered during our first nine months operating the mobile RTR. These problems were not directly related to the unit itself but were more related to the waste stream. Some of the problems that we did encounter with the system were few and fairly simple to repair, reprogram, or redesign. As previously mentioned, we designed the unit to accept a wide range of waste containers. The 55 gal. and the 85 gal. drums require centering on the turntable in the x-ray enclosure when performing LDA acquisitions. This is achieved by the use of photo-electric sensors. As the drum enters the x-ray enclosure via a motorized conveyor system, the drum breaks the photo-electric beam causing the conveyor system to stop rolling. The problem we encountered was that when the conveyor would stop the drum would continue to coast which would cause it not to stop on the center of the turntable. This required the operator to open the lead enclosure door and manually center the drum. We designed and built mechanical stops that restricted the drum from coasting past the center of the turntable. Because of the design of this unit to accommodate various sizes of waste containers, a special roller cart to accept standard waste boxes (SWBs) was designed. The problem we encountered with this design was that we were limited to loading all waste containers on this cart before the container could proceed into the x-ray enclosure. This design worked for SWBs but was a nuisance for smaller containers. Once the

drum was centered on the turntable, the cart needed to be backed out in order for the x-ray enclosure doors to close. We discovered that it was more efficient to load drums directly into the x-ray enclosure using a forklift with a drum attachment than to use the cart, but the cart was interlocked to the entire drum movement sequence. We could store the cart next to the opening and override the limit switch but this posed a safety problem. Without the cart in place there was no electrical or mechanical stops to prevent the drum from falling off the trailer, which at that point measures 72 in. from the ground. We installed a positive mechanical stop and had the vendor come out and reprogram the programmable logic controller (PLC) to eliminate the need to have the cart tied into the drum movement sequence. It would continue to operate as designed when SWBs are loaded. The vendor reprogrammed the photo-electric sensor that was positioned at the end of the cart to operate at the entrance/exit of the x-ray enclosure causing the conveyor system to stop whenever a drum breaks the beam when exiting.

CONCLUSION

In conclusion the experience encountered using the mobile RTR has been of great value in the characterization of radioactive waste at LANL. With this experience, we are confident that we can continue to provide LANL the NDE capability that is required to prepare us to ship TRU waste to Waste Isolation Pilot Plant (WIPP) when it opens in 1997. We are presently scheduled to take the mobile RTR sometime in 1997 back to TA-54 Area G to assist in the TRU Waste Inspectable Storage Project (TWISP). This project consists of exhuming drums of TRU waste that have been buried under earthen berms for over twenty years. These drums will be characterized by NDA and NDE methods and then placed on inspectable arrays under weather proof domes, until they can be shipped to WIPP. The

mobility of this unit has proven to be a great asset in eliminating the need to move radioactive waste drums over public roads which pose safety concerns and are costly. If this unit were not available, we would not have been able to inspect the more than 600 drums that were completed, due to the cost of moving drums. We are delighted with the performance of our mobile RTR and are looking into a union between our mobile S/TGS and the mobile RTR. We are hoping to take the output image produced by the S/TGS and overlaying it to the output RTR's LDA image, which we feel would greatly assist in the characterization process.

Technical -
NDA Modality and Information Combination Techniques

THE DEVELOPMENT OF AN EXPERT SYSTEM FOR THE CHARACTERIZATION OF WASTE ASSAY DATA

Susan Bridges
Julia Hodges
Charles Sparrow
Bruce Wooley
Shiyun Yie

Diagnostic Instrumentation and Analysis Laboratory
Mississippi State University
Box 9550
Mississippi State, MS 39762-9550

ABSTRACT

Containers of transuranic and low-level alpha contaminated waste generated as a byproduct of Department of Energy defense-related programs must be characterized before their proper disposition can be determined. Nondestructive assay methods are the most desirable means for assessing the mass and activity of the entrained transuranic radionuclides. However, there are other sources of information that may be useful in the characterization of the entrained waste (e.g., container manifests, information about the generation process, and destructive assay techniques performed on representative samples).

This paper describes initial work on an expert system being developed to analyze and characterize containerized radiological waste. This system is being developed by scientists at the Mississippi State University Diagnostic and Instrumentation Laboratory (DIAL) in collaboration with scientists at the Idaho National Engineering Laboratory. The DIAL scientists are responsible for (1) the development of techniques to represent and reason with evidence from a variety of sources, and (2) the development of appropriate method(s) to represent and reason with confidence levels associated with that evidence. This paper describes exploratory versions of the expert system developed to evaluate four techniques for representing and reasoning with the confidence in the evidence: MYCIN-style certainty factors, Dempster-Shafer Theory, Bayesian networks, and fuzzy logic.

INTRODUCTION

The staff at the Idaho National Engineering Laboratory (INEL) Stored Waste Examination Pilot Plant (SWEPP) must analyze and characterize containerized radiological waste to determine if it meets the specifications of the *Transuranic Waste Characterization Quality Assurance*

Program Plan[1] and can be shipped to the Waste Isolation Pilot Plant (WIPP) in New Mexico[2]. They are developing a system called the Waste Assay Measurement Integration System (WAMIS) to "improve confidence in and lower the uncertainty of waste characterization data"[3]. One component of WAMIS is an expert system that can integrate data from multiple sources, reason with the uncertainty associated with the different types of data, characterize the waste material, and quantify the confidence in that characterization[4].

Scientists at the Mississippi State University Diagnostic and Instrumentation Laboratory (DIAL) are collaborating with scientists at INEL on the development of an exploratory prototype of the WAMIS expert system. We selected four different approaches to representing and reasoning with uncertainty in the data: MYCIN-style certainty factors, Dempster-Shafer Theory, Bayesian networks, and fuzzy logic. We have developed four initial versions of the prototype expert system, each using a different method for handling the uncertainty. We have conducted experiments to determine each method's strengths and weaknesses for this particular application. In this paper, we describe the four initial versions of the prototype expert system and the early results that we have gotten with each version.

DESCRIPTION OF THE PROBLEM

WAMIS is intended to improve the confidence in the characterization of containerized radiological waste based on a variety of data such as gamma spectra; radionuclide mass estimates; total alpha activity; thermal power; real-time radiography video; container attributes; and mass ratio estimates for americium, plutonium, and uranium isotopes. It is designed to consist of two major components: a data access/visualization component and a data interpretation component. The data access/visualization component will provide users with access to the various kinds of data. It will also have the ability to provide a variety of waste data reports. The data interpretation component will make use of artificial intelligence (AI) techniques to determine waste matrix and source material characteristics and the relationships among them to derive improved assays[3]. The waste characterization expert system that we are developing will be a part of the data interpretation component of WAMIS. Figure 1 illustrates the type of input data that the WAMIS expert system will process and the output that it will produce.

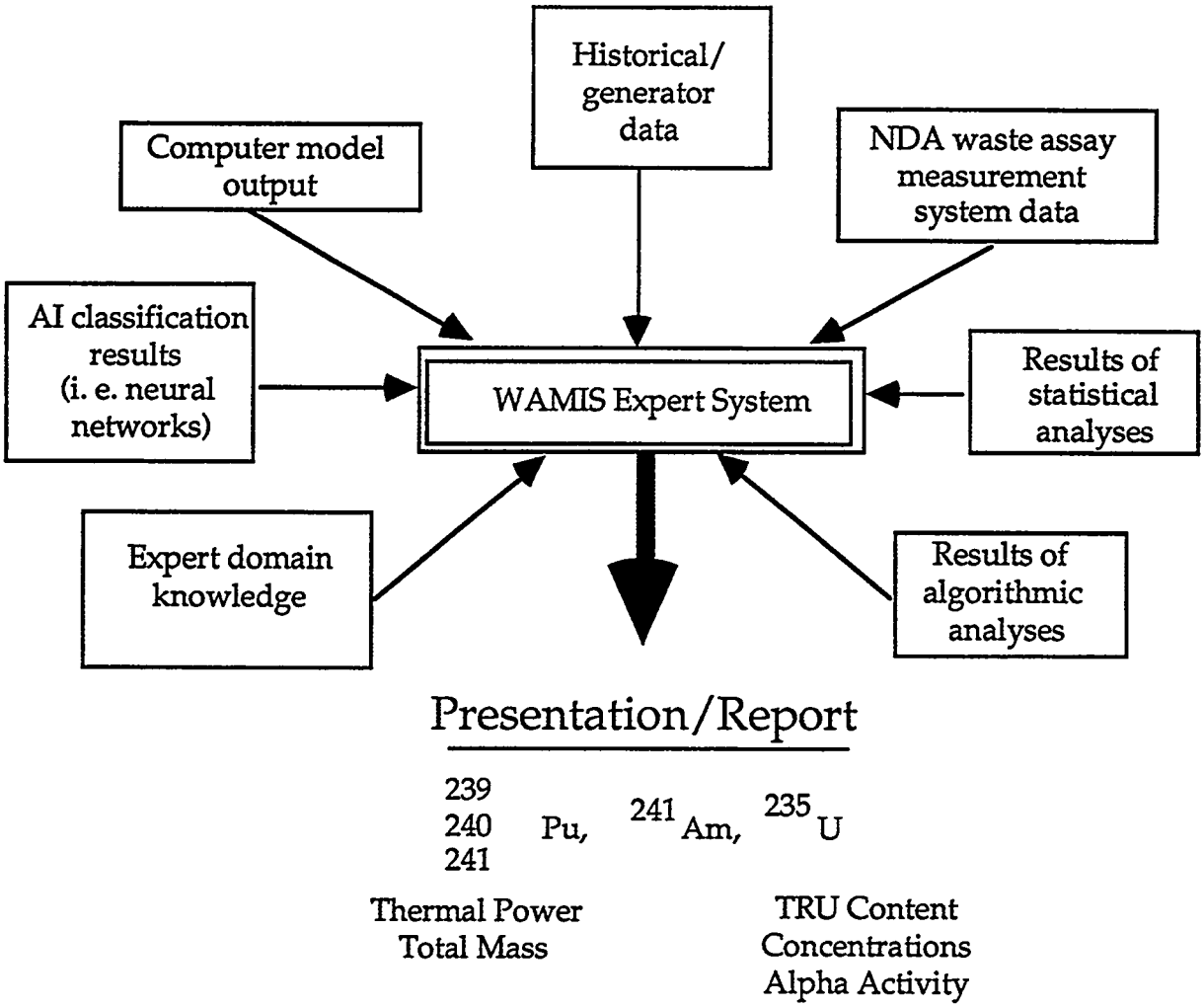

Figure 1. The Data Integration Process for the WAMIS Expert System

Scientists at DIAL are working with scientists at INEL to explore the use of different AI techniques to integrate information from multiple sources, to represent and reason with the uncertainty associated with the different types of knowledge, and to characterize the waste and quantify the confidence in the characterization. In consultation with scientists at INEL, we identified the initial problem to be addressed to be the synthesis of data from different sources and the characterization of the uncertainty of this data. The first step involved in this problem is the development of AI techniques to verify the consistency of data from a variety of currently available data sources.

BASIC APPROACH: AN EXPERT CLASSIFICATION TASK

In its simplest form, the problem being addressed in the development of the WAMIS expert system is the classification of containers of radiological waste into one of two categories: those that can be shipped to the WIPP site and those that cannot. Classification, which is a traditional task for knowledge-based systems, may be defined as identifying classes of data as solutions to a problem.[5]. For example, in our application, the data comes from a wide variety of sources that include simple measurements (e.g., the weight of a drum of waste), classifications based on human judgment (e.g., determination of the type of waste matrix based on real-time radiography), historical data (e.g., records describing the processes used to produce the waste), and the results of calculations based on data from nondestructive assay systems (e.g., the concentrations of radioisotopes based on neutron and gamma detectors).

In a classification task, the set of classes is known in advance as well as the necessary conditions for class membership. The necessary conditions for class membership for our problem are the characteristics of containers that may be shipped to the WIPP site as defined in the *Transuranic Waste Characterization Quality Assurance Program Plan*[1].

Many of the basic characteristics of containerized waste that are needed in order to determine if it can be shipped to the WIPP site have already been measured or computed. Some of this information was gathered at the time the waste was generated and is recorded in documents accompanying the waste. Other measurements have been made at INEL. Unfortunately, experience has demonstrated that the documentation accompanying waste may contain errors, and that some of the nondestructive assay systems may not be able to characterize the radioactive contents of the drums to the required level of accuracy. The initial task for our exploratory expert system was to check the consistency of existing data, to combine these sources of information to classify the containers, and to quantify a level of confidence in that classification.

Each waste container is labeled with a specific content code that specifies the category of the waste matrix. Proper identification of the waste matrix is an important factor in determining whether the drum can be shipped to WIPP and in interpreting the radioassay data. Initially, we limited our analysis to data from drums labeled with content codes that correspond to graphite, although we have recently begun to expand the system to include other content codes. We chose graphite for our initial analysis because there are many drums labeled as containing graphite (thus providing a large potential payoff for a successful classification), characterization of graphite was expected to be easier than for some other materials such as sludges, and we had access to the results of an extensive study that analyzed the uncertainty of the SWEPP Drum Assay System for graphite[6].

OBJECT-ORIENTED RADIOLOGICAL WASTE DATABASE

INEL has supplied us with a large collection of documents and data related to this project. They have also provided the data that was used in their neural network characterization system[7]. This data is in the form of Excel worksheets and includes sensor data from both the SWEPP Assay System (SAS) as configured at the SWEPP facility and shift register data.

We chose an object-oriented database system as a repository for the data to be used by the expert system in its decision process as well as the output produced by the system. We have developed a portion of this database system already, and we continue to expand its design to incorporate additional kinds of information. For the database design, we began with an object model of the different classes of data to be considered by the WAMIS expert system that had been included in the functional requirements of SAS[2]. The current design of the database is illustrated in Figure 2.

We are currently in the process of extending this design to include additional information such as descriptions of the assays that were conducted (the type of assay used, the samples used, the locations where the assay took place, etc.) and descriptions of the processes that produced the waste. We also expect eventually to include other data available through INEL such as data from the statistical analysis database and algorithmic data.

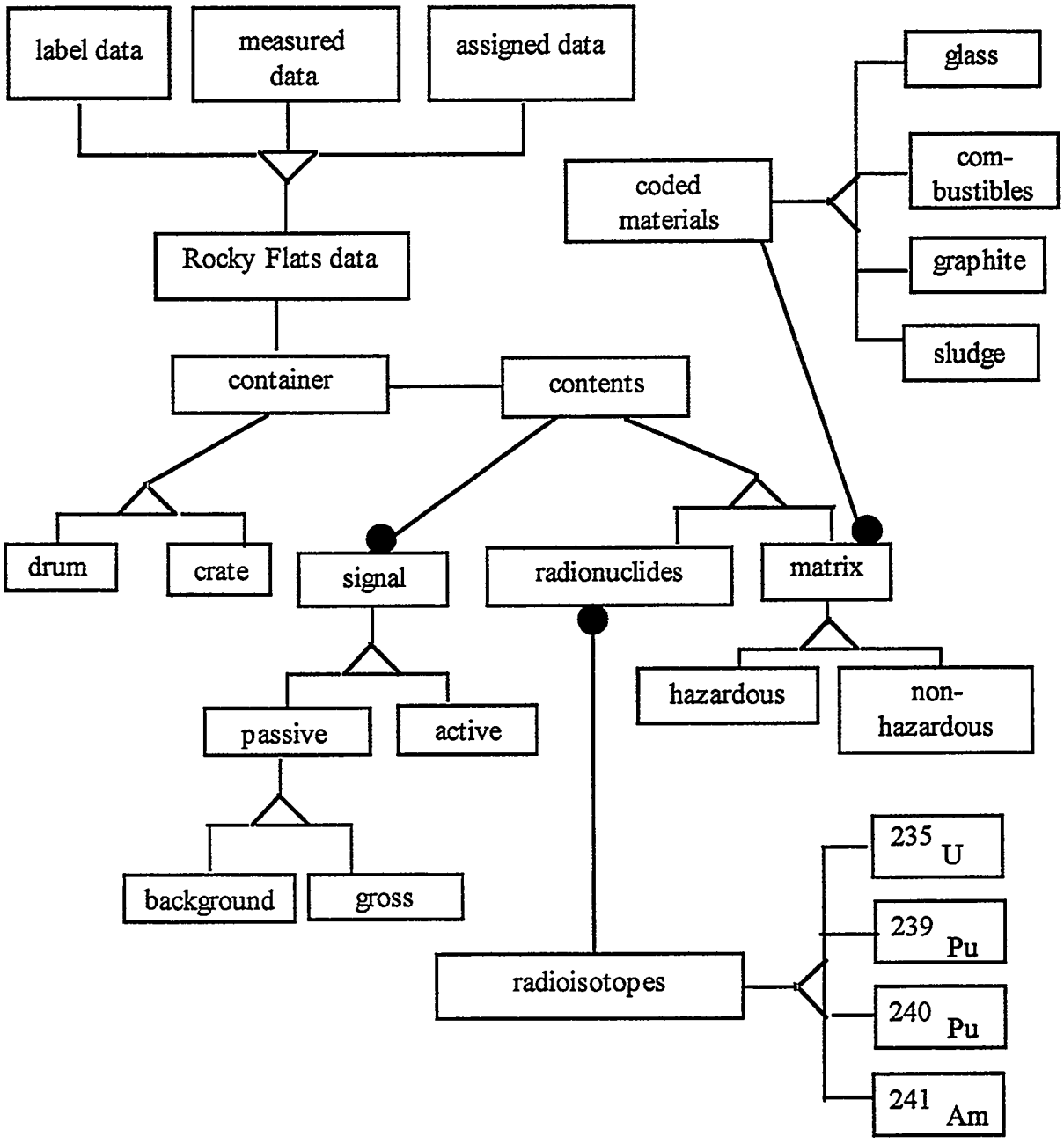

Figure 2. Object Model for the Radiological Waste Database

The notation used in our design of the database is the Object Modeling Technique notation[8]. A rectangular box represents a class, with the name of the class appearing inside the box. A triangular box connecting classes via arcs represents a generalization hierarchy, with the class at the point of the triangle serving as the superclass. For example, in our database model, the container class is a superclass of the drum class and the crate class. Also, the Rocky Flats data class is a superclass of the label data, measured data, and assigned data classes. The appearance of a filled circle on one end of an arc represents an association with a multiplicity of zero or more. For example, each instance of the radiosotopes class may be associated with zero or more instances of the radionuclides class.

A **container** may be either a 55-gallon **drum** or a **crate** in which radiological waste material may be stored. In our work, we are dealing only with drums. Each container is associated with one set of **Rocky Flats data**, which is data from the waste generator in Golden, Colorado. The Rocky Flats data associated with each container falls into one of three classes: **label data, measured data**, or **assigned data**. The label data consists of a unique label identifier and a barcode. The measured data includes the weight of the container, the waste weight, and nuclide information. (Although these values may actually appear on a label attached to the container, we have chosen to restrict our label data class to containing only identifying information about the container.) The assigned data includes the shipping date, the packing date, hazard codes, thermal activity information, surface dose, area, location, item description code, and an indicator as to whether the container was contact handled or remote handled. The assigned data also includes some calculated values such as TRU activity waste, TRU activity gross, non-TRU activity gross, TRU activity, and non-TRU activity, where TRU is an acronym for "transuranic".

Each container may have zero or more **contents** records associated with it. The contents records are divided into two subclasses: **radionuclides** records and **matrix** records. The radionuclides records contain inferred information about the **radioisotopes**. The matrix records contain inferred information about the coded materials. The matrix records may contain information about either **hazardous** or **non-hazardous** materials.

Each container is associated with one or more contents records. Each contents record may be associated with zero or more **signal** records. A signal, which can be either **passive** or **active**, is the SAS response to neutrons originating from transuranic materials extrained in the waste matrix. Passive measurements quantify the spontaneous fission neutron signal of weapons-grade Pu, which results primarily from ^{240}Pu , and/or ^{235}U via an external neutron source and quantifying the resultant fission neutron signal. A passive signal is further decomposed into **background** measurements and **gross** measurements. The background measurements are obtained with an empty container in the assay chamber, while the gross measurements are obtained with a contact-handled container in the assay chamber

The **coded materials** represented in our database are **glass, combustibles, graphite,** and **sludge**. Any given type of coded material may be found in a number of different matrices, as shown in the object model. The radioisotopes represented in our database are ^{235}U, ^{239}Pu, ^{240}Pu, and ^{241}Am. Any given type of radioisotope may be found in a number of different radionuclides records.

THE DECISION PROCESS

A flowchart in the *Transuranic Waste Characterization Quality Assurance Program Plan*[1] illustrates an idealized sequence of events used to determine if a given container of waste meets the requirements for shipment to the WIPP site. We adapted this flowchart to depict the initial decision process for the exploratory WAMIS expert system. This flowchart is shown in Figure 3. The exploratory system focuses on the decision points:

- Does the matrix parameter category still apply to the waste?
- Is the waste TRU waste?

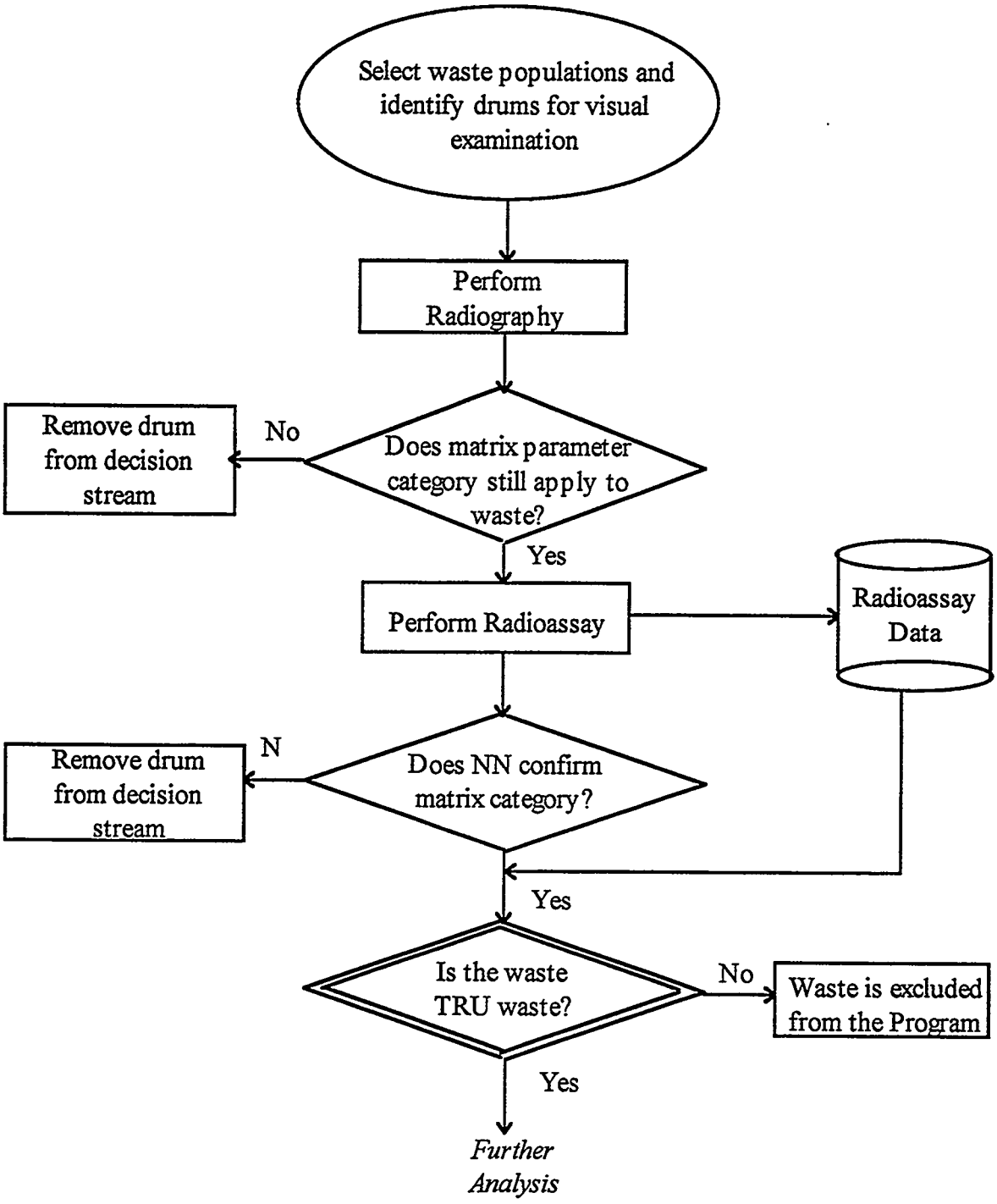

Figure 3. Initial Decision Process

This portion of the expert system verifies that the matrix category is consistent with the density computed from weight and observed fill height and with the matrix classification based on real-time radiography. If it finds that the category does not have a high probability of being correct, the assumption is that the drum will not be considered further at this time. The rationale for this decision is that it is likely to be quite difficult to identify the correct category for the matrix with a high degree of confidence if it is initially incorrect. Since one of our goals is to identify large populations of drums that can be characterized with a high degree of confidence and thus be eligible for shipment to WIPP, drums that are likely to be difficult to characterize will be removed for later consideration.

The expert system will also include the characterization provided by a neural network as part of the process of verifying the matrix category. The neural network identifies the matrix material based on neutronic data[7].

The decision point that determines if the waste is TRU waste will need to consider a much larger body of data and knowledge than considered for the matrix category determination. We have just begun the process of identifying the questions that must be asked at this point and expanding the design of the expert system to incorporate these questions. Examples of the questions that we anticipate as being a part of this decision point are:

- What is the level of confidence in the matrix category?
- How valid is the assumption of the ratios of the Pu isotopes in weapons-grade Pu?
- What are the isotopes that should be considered?
- Is the matrix uniformly distributed within the container?
- Is the source distribution uniform within the container?
- Does the Pu occur in chunks?
- Are there significant voids in the matrix?
- Is it possible to recognize and correct for (α, n) interference?
- Do the isotopes detected agree with written records about the processes used to produce the waste?
- Do the isotopes detected and their concentrations based on the SWEPP system agree with the values from Rocky Flats measurements?
- If the measurements at Rocky Flats and INEL disagree, which is more reliable for a particular waste form?

REPRESENTING AND REASONING WITH UNCERTAINTY

Some of the waste is relatively easy to characterize while other waste is much more difficult to characterize accurately due to a combination of complicating factors. It is imperative that any characterization of the waste must also have associated with it the level of confidence in that classification. In recognition of this, scientists at INEL recently applied traditional statistical techniques to sample collections of waste drums, quantified the total uncertainty associated with the SWEPP/PAN (Passive Active Neutron) measurements, and identified the factors which contributed to the uncertainty[6]. This study has been useful to us as we have developed appropriate AI techniques for representing and reasoning with the uncertainty associated with the data about the containerized waste.

In our approach, we will represent the level of confidence associated with each piece of relevant information about a particular waste container, then quantify the overall confidence associated with the characterization of that container. We have already done this for the data considered as evidence in the initial decision process illustrated in Figure 3, and we will continue to do so for other pieces of evidence as we extend the expert system. For the initial decision process, we developed four different versions of the expert system, each version using a different AI technique for handling uncertainty. The four techniques that we chose to use are: Bayesian networks, fuzzy logic, certainty factors (as used in the MYCIN expert system as well as a number of others), and Dempster-Shafer Theory. During the next year, a major task for us is to compare the results of the four different versions of the exploratory expert system to determine which method (or, more likely, what combination of methods) is most appropriate for our application.

In knowledge-based systems, certainty "refers to a **degree of belief**"[5]. In any decision-making process, there are various sources of uncertainty:

- The data may be unreliable or contain errors for some reason such as defective measurement instruments.
- The decision may have to be made in the absence of certain data.
- The data may be imprecise, e.g., the frequency with which a signal is sampled may limit the precision of the data.

In many knowledge-based systems, not only is there uncertainty associated with the data, but there is also uncertainty associated with the rules that manipulate the data in order to reach conclusions. Different AI techniques are intended to handle different kinds of uncertainty.

In the following sections, we describe the work done so far on each of the four versions and the results obtained using experimental data with each version.

Using Bayesian Networks to Handle Uncertainty

Although many early expert systems used methods based on probability theory to represent uncertainty, these methods have come under attack because of the *ad hoc* procedures used for combining certainties and because of the simplifying assumptions inherent in the systems. The development of Bayesian networks has caused renewed interest in the use of probability theory to represent uncertainty in expert systems because these networks provide a computationally feasible mechanism for representing and reasoning with a complete probabilistic model of a domain.

An Overview of Bayesian Networks

Bayesian networks are based on the **subjective Bayesian** view of probability rather than on the **objective** or **frequentist** view[9]. In the objective view, probabilities represent the likelihood of an event based on the observed frequency of occurrence of an event over many experiments. In the subjective view, probabilities represent an expression of a person's belief that a particular event will occur in a single experiment. The subjective view allows one to take all sources of information encountered to date into account when determining the probability of an event. This view of probability as a measure of personal belief is central to the use of probability theory in expert systems since it would be impossible to do the number of experiments necessary to determine all the probabilities needed in a large domain[10, 11].

A Bayesian network (or belief network) is a directed acyclic graph used to represent dependencies among random variables and to give a concise specification of the joint distribution function[12]. Each node in the network represents a random variable, i.e., a set of mutually exclusive and collective exhaustive states. The directed links between nodes represent a direct influence of the value of one random variable on the value of another. Associated with each node will be a conditional probability table that gives the probability of each value for the node given every possible combination of values for the parent nodes.

$P(X = x_i)$ represents the **unconditional** or **prior probability** that the random variable X has the value x_i. In the case of binary-valued random variables that represent propositions, P(X) means P(X = true) and P(~X) means P(X = false). In the case of multiple-valued random variables, **P**(Y) represents a vector of probabilities of all possible values of the random variable. For example, suppose that we define a random variable called *Experience* to indicate the experience level of a technician who will interpret the real-time radiography for a given drum. Then we could define the following:

P(Experience = high) = 0.6
P(Experience = medium) = 0.3
P(Experience = low) = 0.1

The statement **P**(Experience) = <0.6, 0.3, 0.1> defines a probability distribution for the random variable Experience. In other words, based on background knowledge, we know that 60% of the technicians are rated as highly experienced, 30% as having a medium level of experience, and 10% as inexperienced.

The prior probabilities represent probabilities based on background knowledge and in the absence of evidence. As evidence is gathered, the prior probabilities are replaced by **conditional** or **posterior probabilities** denoted as $P(X = x_i \mid Y = y_j)$. For example, we might express the relationship that the probability that a technician is highly experienced given that he/she has taken as special course in interpreting real-time radiography as the following conditional probability:

P(Experience = high | Attended-course = true) = 0.7

This indicates that the probability that the person is highly experienced given the evidence that he/she attended the course is 0.7. The **P** notation can also be used with conditional probabilities where **P**(X|Y) is a two-dimensional table that specifies $P(X = x_i \mid Y = y_j)$ for each possible value of X and Y.

Unconditional probabilities can be used to define conditional probabilities:

$$P(A \mid B) = \frac{P(A \wedge B)}{P(B)} \text{ where } P(B) \neq 0$$

It is generally much easier to determine prior probabilities of single variables and conditional probabilities than it is to determine the probability of a conjunction of variables. **Bayes's rule** eliminates the need to deal with probabilities of conjunctions. Bayes's rule is:

$$P(B \mid A) = \frac{P(A|B)P(B)}{P(A)}$$

If we have defined a domain with a set of random variables $\{X_1, ..., X_n\}$, then a Bayesian network is a representation of the joint probability distribution over those variables[13]. The Bayesian network consists of a set of local conditional probability distributions along with a set of conditional independence assertions that enable us to compute the joint probability distribution from the local distributions. The general idea behind Bayesian networks is that, for most of the random variables X_i, we will be able to define a subset Π_i that will be substantially smaller than the set $\{ X_1, ..., X_n\}$. A Bayesian network is defined in terms of these sets as a directed acyclic graph such that each random variable corresponds to a node in the graph and the contents of a node X_i will be the nodes corresponding to the variables in Π_i. Each node X_i will have an associated conditional probability table containing the probabilities of each value of X_i given the probability of each set of values for variables in Π_i.

The formal definition of a Bayesian network is based on the concept of conditional independence, but in practice, one usually uses expert knowledge of cause and effect relationships to determine the topology of the network. An arc drawn from one node to another generally indicates that the value of the source node has a direct effect on the value of the target

node. This method of constructing Bayesian networks almost always results in a network with accurate conditional independence assertions[13].

Bayesian Network for Confirmation of Graphite

The initial Bayesian network version of the WAMIS expert system confirms the content code of drums labeled as containing graphite. Figure 4 illustrates the design of the Bayesian network for this task. This network addresses the first decision point illustrated in Figure 3.

The network uses two basic types of evidence - evidence based on the computed density of the material in the drum and evidence based on identification of the matrix material by a technician using real-time radiography (RTR). The density computation is based on the weight of the drum and the volume of the material in the drum. The volume, in turn, is computed based on the fill height of the drum as observed using RTR. Different technicians (observers) have different levels of experience in reading RTRs. In addition, a technician may be able to determine the fill height or identify the material in some drums with more confidence than others.

Once the topology of the Bayesian network has been defined (i.e., the nodes to be included and the arcs connecting the nodes), it is necessary to obtain values for the required probabilities. Based upon knowledge acquisition sessions with one of the scientists at INEL who is serving as our domain expert, we defined the necessary conditional probabilities.

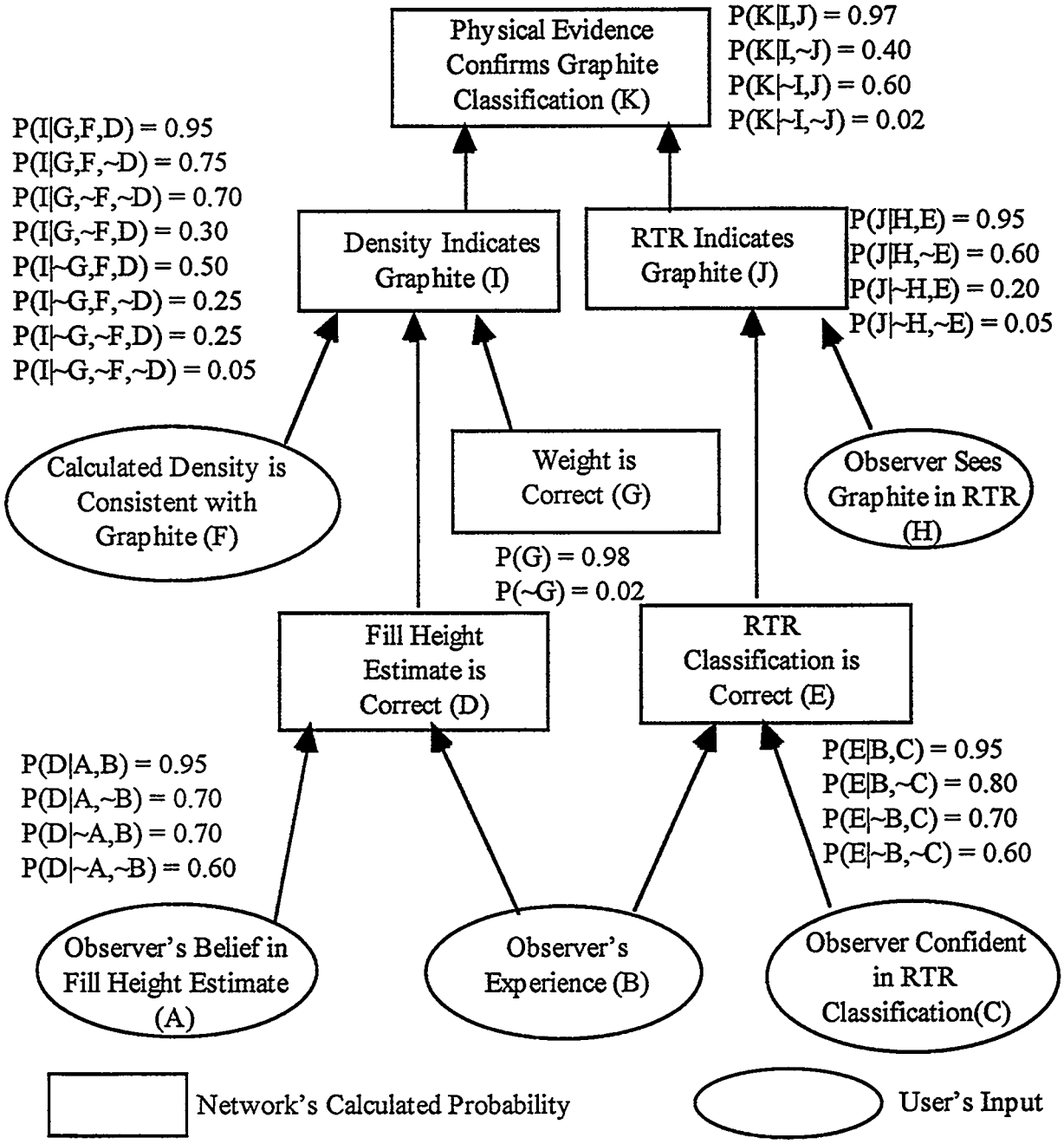

Figure 4. Bayesian Network

Test Run	Calculated density is consistent with graphite	Observer's confidence in fill height estimate from RTR	Observer's experience	Observer sees graphite	Observer's confidence in what he sees in the RTR	Domain expert's confidence in verification of graphite	System's confidence in verification of graphite
1	yes	high	low	yes	high	0.75-0.75	0.82
2	yes	low	high	yes	low	0.60-0.75	0.84
3	yes	high	low	yes	low	0.70-0.70	0.80
4	yes	high	high	yes	low	0.70-0.90	0.86
5	yes	high	high	no	high	0.40-0.60	0.41
6	yes	low	high	no	high	0.33-0.65	0.39
7	yes	high	low	no	high	0.40-0.45	0.41
8	yes	high	high	no	low	0.30-0.60	0.42
9	yes	high	low	no	low	0.35-0.60	0.41
10	yes	low	low	no	low	0.20-0.25	0.41
11	no	high	high	yes	high	0.20-0.75	0.75
12	no	low	high	yes	high	0.70-0.70	0.69
13	no	high	low	yes	high	0.65-0.65	0.65
14	no	high	high	yes	low	0.50-0.75	0.72
15	no	low	high	yes	low	0.50-0.70	0.67
16	no	low	low	yes	low	0.40-0.40	0.61
17	no	low	high	no	low	0.20-0.25	0.28
18	no	high	low	no	high	0.10-0.40	0.28
19	no	low	low	no	high	0.05-0.35	0.27
20	no	low	high	no	high	0.15-0.35	0.27
21	yes	high	high	yes	high	0.98-1.00	0.89
22	yes	low	high	yes	high	0.70-0.85	0.87
23	no	high	high	no	high	0.20-0.60	0.30

Table 1. Test Runs with Bayesian System

The Bayesian network has been implemented using the Hugin System. We have conducted a number of experiments to test the behavior of the system and compared the results to those provided by our domain expert. The results are given in Table 1. The values given as the domain expert's assessment of the final confidence value associated with a particular test case represent the range of values (lowest and highest) provided by the expert in different knowledge acquisition session. This illustrates the fact that human experts are not necessarily consistent in

their evaluations of test cases, so that evaluating an expert system by comparing it to the results provided by a domain expert can be a tricky business. We expect to continue to modify the conditional probabilities based upon further experimentation and the results that we get as we expand the Bayesian version of the system.

Using Fuzzy Logic to Handle Uncertainty

Fuzziness is related to "quantified degrees of knowing"[5]. We can think of it as a representation of **vagueness**. It allows us to represent classifications that include vagueness and degree. Unlike uncertainty, fuzziness is not related to degree of belief and probabilities. The source of the imprecision in a fuzzy system is different from the source of imprecision in an uncertainty system. Specifically, a fuzzy system's imprecision is caused by classifications for which the membership is a matter of degree. For example, suppose that it misted for an hour or so this morning, but was sunny for the rest of the day. Would we consider today to have been a rainy day? Fuzziness allows us to represent the day as having been somewhat rainy, or rainy to a degree. Similarly, fuzziness allows us to represent that a container partially or somewhat meets the requirements for shipment to WIPP.

Fuzziness and Fuzzy Sets

Most of the current work with fuzzy systems stems from a classic paper on fuzzy set theory by Lotfi Zadeh[14]. Fuzzy set theory, which was "created for use in pattern classification and pattern matching," allows gradual or partial membership in a set or class[5]. **Fuzzy logic**, or reasoning based upon fuzzy set theory, differs from traditional Boolean logic in that a statement need not be either **true** or **false**, but may have a **degree of truth**.

A **fuzzy set** is defined as a subset of some universal set, where each element in the fuzzy subset has associated with it a degree of membership in the subset. Let U represent a universal set. Then a fuzzy set or class A may be defined as a subset of U where each $x \in U$ is assigned a value between 0 and 1, inclusive, that represents the **degree of membership** for x in A. The

function f_A that assigns the degrees of membership to elements in A is called the **characteristic function** for set A.

A classic example is the determination of the "tallness" of a person[5]. We may define any person more than 6 feet tall as belonging to the set of tall people with a membership value of 1, and any person who is less than 4 feet tall as belonging to the set with a membership of 0. Anyone whose height falls between 4 feet and 6 feet would have a membership value between 0 and 1. The following figure illustrates a possible characteristic function for the fuzzy set of "tall people".

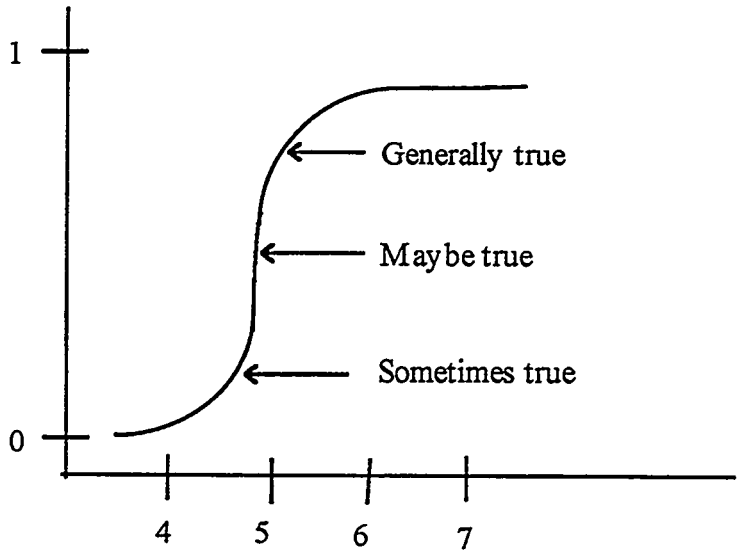

Figure 5. A Characteristic Function for the Set of Tall People

Another way to represent this information is to define "height" as a **fuzzy** or **linguistic variable**. Fuzzy variables are names that take **fuzzy adjectives** as values. Each fuzzy adjective is a fuzzy set. For example, the fuzzy variable "height" can take on values (or adjectives) such as "tall," "medium," or "short". Characteristic functions describe the fuzzy sets. The "height" example is represented using the piecewise linear characteristic functions in Figure 6. Modifiers may be used in our characterizations (e.g.: "*very* tall," "*somewhat* tall," "*very* short"). In fuzzy set theory, such modifiers for fuzzy variables are called **hedges**.

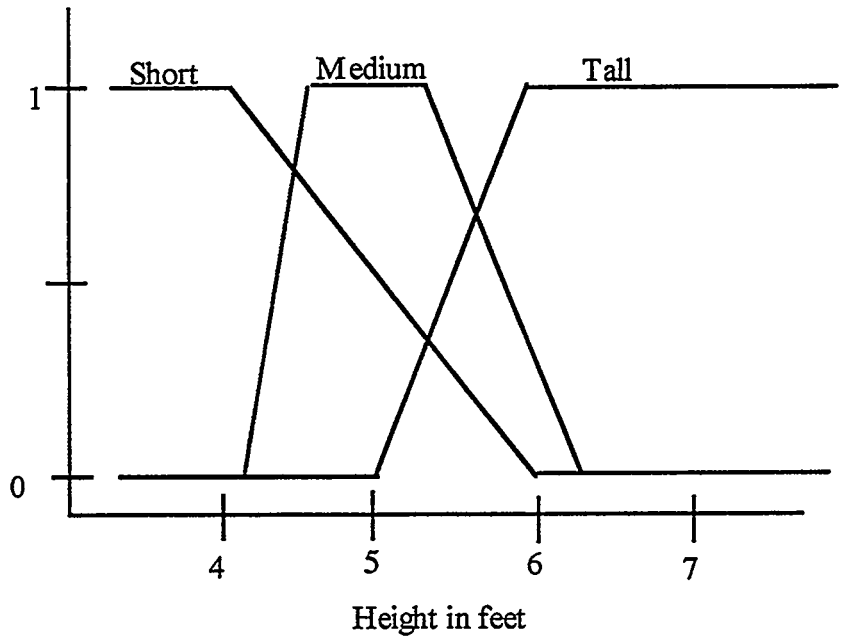

Figure 6. Three Piecewise Linear Characteristic Functions for the Fuzzy Variable "height"

Whereas in probability theory we deal with probabilities and probability distributions, in fuzzy logic we deal with **possibilities** and **possibility distributions**. For example, if we are told that John is "somewhat tall," then we can use fuzzy set theory to determine the possible values for John's height.

A statement that assigns a value to a fuzzy variable is called a **fuzzy proposition**. An example is the statement: John's height is tall. "John's height" is a fuzzy variable, and "tall" (which represents a fuzzy set) is the value for the variable. Fuzzy rules relate fuzzy propositions. Fuzzy inference techniques provide not only a conclusion, but also a degree of belief in that conclusion.

While fuzzy set theory provides a way of representing vagueness, fuzzy reasoning provides a way of combining fuzzy evidence. **Max-min inference** and **max-product inference** are the two most common methods used for fuzzy inference. The interested reader may refer to Stefik[5] for an explanation of these methods. Of these two approaches, max-min inference is generally preferred for discrete systems, i.e., systems that must make a distinct choice based on

the input data. The max-product inference is generally preferred for continuous systems, i.e., systems that must make a smooth transition in response to changing inputs.

Fuzzy Logic System for Confirmation of Graphite

The input fuzzy variables that we have defined for the exploratory expert system are:

- accuracy of the weight measurement
- degree to which the calculated density is consistent with graphite
- observer's experience
- observer's confidence that the RTR shows graphite

Each of these input variables and the output variable (confidence that container contains graphite) were defined as having values of high, medium, or low. Also, the same characteristic functions were used in defining the variables. The functions are illustrated in Figure 7. For example, a value of 0.1 for the fuzzy variable "observer's experience" places the variable in the fuzzy set "low" with a membership value of 1.0, the fuzzy set "medium" with a membership value of 0.0, and the fuzzy set "high" with a membership value of 0.0. The value of 0.4 for the fuzzy variable places it in the fuzzy set "low" with a membership value of 0.3, the fuzzy set "medium" with a membership value of 0.68, and the fuzzy set "high" with a membership value of 0.0.

Some examples of the rules contained in this version are:

If the consistency of the calculated density with graphite is high
And the accuracy of the calculated density is medium
Then the confidence that the density indicates graphite is high

If the consistency of the calculated density with graphite is low
And the accuracy of the calculated density is low
Then the confidence that the density indicates graphite is low

If the observer's confidence that the RTR shows graphite is medium
And the observer's experience is high
Then the confidence that the RTR shows graphite is low

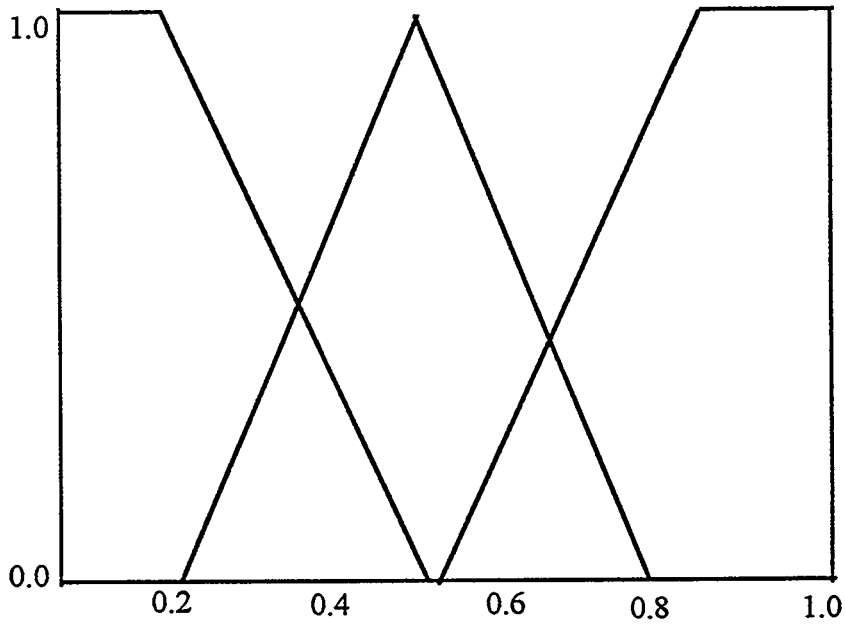

Figure 7. Characteristic Functions Used

The input fuzzy variables defined for this preliminary version of the fuzzy logic expert system were: accuracy of the weight measurement, degree to which the calculated density is consistent with graphite, observer's experience, and observer's confidence that the RTR shows graphite. Each of the fuzzy variables has associated with it ranges of values that define what is considered to be "low," "medium low," "medium," "medium high," and "high". These values were determined through a series of knowledge acquisition sessions with our domain expert.

Experimental Results with Fuzzy Logic System

We tested the fuzzy logic expert system with a series of test cases and compared the results to the assessments provided by the domain. The experimental results are shown in Table 2.

Test Run	Accuracy of weight	Observer's experience	Calculated density is consistent with graphite	Observer's confidence in RTR	System's confidence that contents are graphite	Domain expert's confidence that contents are graphite
1	0.98	1.00	1.00	1.00	0.86	1.00
2	0.98	0.80	0.80	0.80	0.78	0.90
3	0.98	0.80	0.20	0.80	0.54	0.60
4	0.98	0.40	0.40	0.80	0.51	0.30
5	0.98	0.40	0.60	0.80	0.51	0.40
6	0.98	0.20	0.80	0.80	0.25	0.70
7	0.98	0.80	1.00	1.00	0.86	0.90
8	0.98	1.00	0.00	0.80	0.51	0.20
9	0.98	0.00	0.00	0.00	0.25	0.00
10	0.98	1.00	1.00	0.20	0.25	0.30
11	0.98	0.20	0.60	0.20	0.25	0.40
12	0.98	0.40	0.60	0.20	0.25	0.10
13	0.98	0.80	0.20	0.20	0.08	0.20
14	0.98	0.60	0.40	0.20	0.25	0.20
15	0.98	0.20	0.80	0.20	0.25	0.50
16	0.98	0.80	0.80	0.20	0.25	0.40

Table 2. Results of Test Runs with Fuzzy Logic System

We found the system's results to be consistent with those of the scientist in most cases. In particular, the rankings of the test cases from those cases with the highest confidence value that contents are graphite to those with the lowest confidence value are quite similar. Consider a listing of the test cases in descending order according to the confidence values. Test cases enclosed in parentheses represent cases that had the same confidence value.

expert system's rankings: (1, 7), 2, 3, (4, 5, 8), (11, 16, 6, 10, 9, 14, 14, 12), 13

domain expert's rankings: 1, (7, 2), 6, 3, 15, (5, 11, 16), (4, 10), (8, 13, 14), 12, 9

In test case #6, there is a significant difference between the system's confidence that the contents are graphite and the domain expert's confidence. It is notable in this case that the confidence associated with all of the evidence was high except that the observer was considered to be inexperienced. The domain expert put much less confidence in the final confidence value because of this. We shall continue to modify the rules and the certainty factors associated with them to reflect such reasoning on the part of the domain expert.

Using Certainty Factors to Handle Uncertainty

The certainty factors (CF) approach to representing uncertainty in an expert system was originally developed for the MYCIN expert system[16]. In the CF approach to representing uncertainty in an expert system, each hypothesis made by the system (example: "Evidence is consistent with graphite in the container") and each piece of evidence considered by the system (example: "The technician thinks RTR indicates graphite in the container") has a certainty factor associated with it. This **certainty factor** indicates a degree of belief in that hypothesis (given all the evidence considered so far) or a degree of belief in that piece of evidence. Although this approach is somewhat similar to a probabilistic approach, in practice the certainty factor values are obtained from domain experts, not direct observation[5].

Consider the example:[5]

IF: 1) The stain of the organism is gram positive, and
2) the morphology of the organism is coccus, and
3) the growth of confirmation of the organism is chains
THEN: There is suggestive evidence (0.7) that the identity of the organism is streptococcus.

According to this rule, if the stated conditions regarding the stain, morphology, and growth of the organism are confirmed, then we can be 0.7 certain of the organism's identity. The value 0.7 is interpreted in the CF approach as being information about how to update belief rather than as a measure of absolute belief. The strength of a conclusion produced by a rule depends on both the CF associated with that rule and the degree of belief in the premise of the rule.

Belief, Disbelief, and Certainty Factors

The CF approach uses three measures of certainty: the **measure of belief** (MB), the **measure of disbelief** (MD), and the **certainty factor** (CF)[5]. MB(H,E) is a measure of increased belief in hypothesis H resulting from evidence E. MD(H,E) is a measure of increased disbelief in hypothesis H resulting from evidence E. Finally, CF(H,E) is the measure of belief decreased by the measure of disbelief. Let P(H) denote the subjective degree of belief in H. Let

P(H|E) denote the degree of belief in H given E. Then MB, MD, and CF are defined by the following formulas:

IF P(H) = 1 THEN MB(H,E) = 1
ELSE MB(H,E) = (max (P(H|E), P(H)) - P(H)) / (1 - P(H))

IF P(H) = 0 THEN MD(H,E) = 1
ELSE MD(H,E) = (min(P(H|E), P(H)) - P(H)) / (0 - P(H))

CF(H,E) = MB(H,E) - MD(H,E)

Both MB and MD range from 0 to 1; CF ranges from -1 to 1.

Combining Evidence to Update Beliefs

The rules for combining evidence in the CF approach in order to update the measure of belief and measure of disbelief, then determining the certainty factor, are defined such that it does not matter in what order the evidence is considered. A CF system simply stores the accumulative CF and continues to combine it with new evidence as the new evidence becomes available. The CF approach assumes modularity in the certainty computations. That is, this approach assumes that a rule can be used once its premises have been satisfied, no matter how the premises were derived or what other facts are currently in the knowledge base.

The rule for combining evidence for a single hypothesis is:

IF CF1 > 0 AND CF2 > 0
THEN CF(H,E_1 & E_2) = CF1 + CF2 (1 - CF1)
ELSE IF CF1 < 0 AND CF2 < 0
THEN CF(H,E_1 & E_2) = CF1 + CF2 (1 + CF1)
ELSE CF(H,E_1 & E_2) = (CF1 + CF2) / (1 - min (CF1, CF2))

where CF1 = CF(H,E_1) and CF2 = CF(H,E_2). What this rule says is that the certainty factor of a new piece of evidence should be applied proportionately to the remaining disbelief[5].

The rules for determining the certainty factor of a conjunctive hypothesis or a disjunctive hypothesis are:

CF($H_1 \wedge H_2$, E) = min (CF(H_1,E), CF(H_2,E))
CF($H_1 \vee H_2$, E) = max (CF(H_1,E), CF(H_2,E))

For a conjunctive hypothesis, the certainty factor is the certainty factor of the weaker piece of evidence. For a disjunctive hypothesis, it is the certainty factor of the stronger piece of evidence. The conclusion of one rule may be the evidence considered by another rule, so that the rules are chained together.

Advantages and Disadvantages of the CF Approach

An advantage of the CF approach is that it is not necessary to define the prior and conditional probabilities as must be done in probability-based approaches such as Bayesian reasoning. Instead, estimates of the certainty factors provided by the domain expert are used, then combined in a manner that assumes conditional independence, thus requiring far fewer numbers than in a probability-based approach. Although the CF approach is somewhat similar to a probabilistic approach, in practice the certainty factor values are obtained from domain experts, not direct observation[5].

However, the CFs tend to accumulate for multiple hypotheses as evidence is combined even though the evidence is quite weak (i.e., has a small associated CF). Thus this approach does not work well for applications in which many rules are used to derive conclusions. If the chains of reasoning are short, however, the CF approach can work well.

The CF approach uses a monotonic reasoning process. That is, a conclusion cannot be retracted (except manually, of course) once it has been derived. Therefore it may be necessary to define rules so that they include additional premises that serve as screening clauses. For example, consider the rule:

IF 1) the sidewalk is wet
THEN There is suggestive evidence (0.7) that it has been raining recently.

But one can begin to think of other reasons for the sidewalk being wet, so that we don't want to conclude that it has rained based only on this evidence. We could add a screening clause to the rule to produce the new rule:

IF 1) the sidewalk is wet, and
2) the sprinkler has not been on recently
THEN There is suggestive evidence (0.7) that it has been raining recently.

We can continue to think of other reasons for the sidewalk to be wet, thus continuing to add more premises to the rule. This could result in a rule containing premises that seem remotely related at best. It also requires us to anticipate all such conditions for complex situations.

Some of the disadvantages associated with the CF approach stem from the assumptions of modularity and independence made in this approach. In practice, however, the approach has been used successfully in a number of expert systems. Studies of the MYCIN expert system, for example, have shown that it is a highly competent medical diagnostician of infectious blood diseases.

CF Version for Confirmation of Graphite

In the CF version of the prototype expert system, a hypothesis made by the system (e.g., "Evidence is consistent with graphite as contents of the container") and any piece of evidence considered by the system (e.g., "Technician thinks real-time radiography indicates graphite in the container") has a certainty factor associated with it.

We implemented the CF version of the system using CLIPS. Some examples of specific instances of the rules, with specific certainty factors given, are:

If the calculated density is consistent with graphite (0.8)
And the calculation of the density is accurate (0.9)
Then there is evidence that the density is consistent with graphite (0.72)

If the observer is experienced (0.7)
And the observer is confident in seeing graphite in the RTR (0.9)
Then there is evidence that the RTR is consistent with graphite (0.63)

Experimental Results Obtained from the CF Version

The results of 16 test runs with this version of the expert system are shown in Table 3. Since the final values assigned to the hypothesis that the container contains graphite were defined from 0 (meaning that the evidence definitely does not support that hypothesis) to 1 (meaning that the evidence definitely does support the hypothesis), then the CF values obtained by this version of the expert system (which were from -1 to 1) were modified to fit this range.

Test Run	Weight accuracy	Observer's experience	Consistency of calculated density with graphite	Observer's confidence in RTR	System's certainty that contents are graphite	Domain expert's certainty that contents are graphite
1	0.98	1.0	1.0	1.0	1.0	1.0
2	0.98	0.9	0.8	0.8	0.83	0.9
3	0.98	0.8	0.2	0.8	0.46	0.6
4	0.98	0.4	0.4	0.8	0.47	0.3
5	0.98	0.4	0.6	0.8	0.64	0.4
6	0.98	0.2	0.8	0.8	0.66	0.7
7	0.98	0.8	1.0	1.0	0.99	0.9
8	0.98	1.0	0.0	0.8	0.28	0.2
9	0.98	0.0	0.0	0.0	0.0	0.0
10	0.98	1.0	1.0	0.2	0.3	0.3
11	0.98	0.2	0.6	0.2	0.3	0.4
12	0.98	0.4	0.6	0.2	0.3	0.1
13	0.98	0.8	0.2	0.2	0.26	0.2
14	0.98	0.6	0.4	0.2	0.32	0.2
15	0.98	0.2	0.8	0.2	0.3	0.5
16	0.98	0.8	0.8	0.2	0.36	0.4

Table 3. Results of Test Runs with Certainty Factors System

Using Dempster-Shafer Theory to Handle Uncertainty

The Dempster-Shafer approach (often called DS Theory) provides a method for representing and reasoning with numerical degrees of belief[5]. Unlike probabilistic approaches, it does not require a complete set of prior and conditional probabilities. The Dempster-Shafer approach also provides an explicit method for representing lack of knowledge (or **ignorance**) while other approaches provide no explicit way to distinguish lack of knowledge and conflicting knowledge. In DS Theory, one defines a **frame of discernment** (θ) - a mutually exclusive and exhaustive set of elements that correspond to ground propositions. When used with diagnostic systems, these elements typically refer to diagnostic hypotheses. A basic probability assignment (bpa) is associated with each possible subset of the frame of discernment, and the sum of all bpas is 1.0. In a typical scenario, all belief is initially associated with the complete set θ indicating complete ignorance. As evidence accumulates, a portion of the belief becomes associated with more refined subsets of hypotheses.

The set of all subsets of the frame of discernment is called 2^{Θ}. In DS Theory, measures of belief are represented by values in the interval [0, 1], and there is a basic probability assignment function, M, that assigns a number in this interval to every subset of the frame of discernment in such a way that the sum of the assignments over all subsets is 1.

$$\Sigma M(x) = 1 \quad \text{for } x \in 2^{\Theta}$$

The empty subset is always assigned a bpa of 0. In a rule-based DS system, the basic probability assignment represents "the degree to which belief in conclusions is altered by belief in premises"[5]. A rule in this type of system is of the form

If Premise$_1$ & Premise$_2$ & . . . Premise$_n$

Then Conclusion$_1$ & Conclusion$_2$ & . . . Conclusion$_m$ (M_1)

where M_1 is the basic probability assignment applied to the conclusions. Dempster's rule of combination provides a way to combine probability assignments of conclusions based on multiple rules. "Let M_1 and M_2 be two probability assignments. **Dempster's rule** computes a new M denoted $M_1 \oplus M_2$, for the combined effect. For every subset of θ Dempster's rule defines $M_1 \oplus M_2$ (A) as follows:

$$M_1 \oplus M_2 (A) = \Sigma M_1(X) M_2(Y) \text{ where } X,Y \subseteq 2^{\Theta} \text{ and } X \cap Y = A."[5]$$

The rule is commutative so that the order in which evidence is accumulated does not matter.

Dempster-Shafer System for Confirmation of Graphite

In our investigation of the application of DS Theory to the waste characterization problem, we first investigated structuring the DS solution for confirming graphite as the matrix material in a manner similar to that used for the other experimental systems. The frame of discernment in this case was {Graphite, Not-Graphite}. It soon became apparent that this approach did not allow us to make use of the strengths of DS Theory in this domain. We extended the problem to distinguish between multiple matrix materials. Figure 8 shows the frame of discernment and its subsets for the extended problem. All belief is initially associated with θ.

When the IDC code for the material is given, this pushes a substantial portion of belief to the node containing the single element for this material. The applicable rule for graphite is as follows:

If IDC Code = Graphite

Then Graphite is confirmed (M = 0.90)

Similar rules exist for all other content codes. Additional types of evidence such as density measurements and real-time radiography observations are used to further modify this distribution of beliefs.

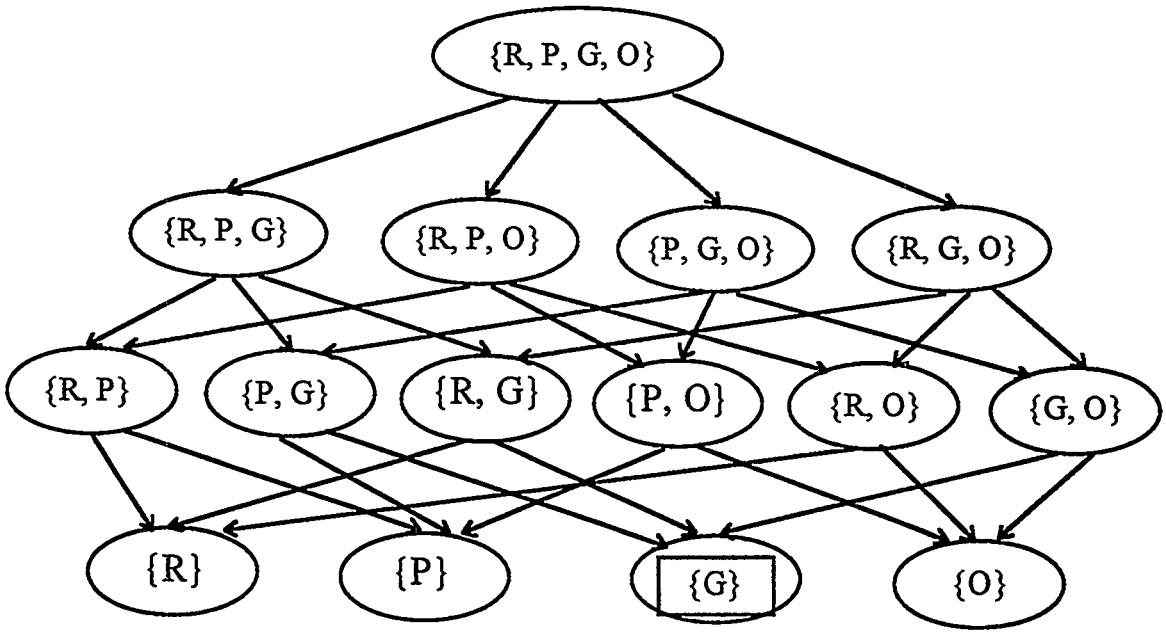

Frame of Discernment:

R	Raschig Rings
P	Paper and Rags
G	Graphite Molds
O	Other

Figure 8. The Frame of Discernment and its Subsets in the Dempster-Shafer System

Experimental Results with the Dempster-Shafer System

For purposes of comparison with the other methods for representing uncertainty, we compared the results using the DS system for confirming the content code as graphite with the domain expert results that had been acquired for the Bayesian network system. A characteristic of the DS approach is that a single piece of very negative evidence is overwhelmed by several pieces of positive evidence. In some cases, the effect of a single piece of negative evidence should outweigh any additional positive evidence. This effect has been easier to model using other methods (Bayesian networks for example).

Test Run	Calculated density is consistent with graphite	Observer's confidence in fill height estimate from RTR	Observer's experience	Observer sees graphite	Observer's confidence in what he sees in the RTR	Domain expert's confidence in verification of graphite	System's confidence in verification of graphite
1	yes	high	low	yes	high	0.75-0.75	0.97
2	yes	low	high	yes	low	0.60-0.75	0.98
3	yes	high	low	yes	low	0.70-0.70	0.96
4	yes	high	high	yes	low	0.70-0.90	0.98
5	yes	high	high	no	high	0.40-0.60	0.31
6	yes	low	high	no	high	0.33-0.65	0.31
7	yes	high	low	no	high	0.40-0.45	0.72
8	yes	high	high	no	low	0.30-0.60	0.64
9	yes	high	low	no	low	0.35-0.60	0.78
10	yes	low	low	no	low	0.20-0.25	0.78
11	no	high	high	yes	high	0.20-0.75	0.90
12	no	low	high	yes	high	0.70-0.70	0.98
13	no	high	low	yes	high	0.65-0.65	0.90
14	no	high	high	yes	low	0.50-0.75	0.71
15	no	low	high	yes	low	0.50-0.70	0.93
16	no	low	low	yes	low	0.40-0.40	0.90
17	no	low	high	no	low	0.20-0.25	0.35
18	no	high	low	no	high	0.10-0.40	0.44
19	no	low	low	no	high	0.05-0.35	0.52
20	no	low	high	no	high	0.15-0.35	0.11
21	yes	high	high	yes	high	0.98-1.00	0.99
22	yes	low	high	yes	high	0.70-0.85	0.99
23	no	high	high	no	high	0.20-0.60	0.02

Table 4. Test Runs with Dempster-Shafer System

ACKNOWLEDGMENTS

This work is supported by the Mississippi State University Diagnostic Instrumentation and Analysis Laboratory and by the U.S. Department of Energy.

REFERENCES

1. DoE, *Transuranic Waste Characterization Quality Assurance Program Plan,* U.S. Department of Energy, National TRU Program Office, Carlsbad Area Office, Report No. DoE/CAO-94-1010, Revision 0 (1995).
2. S.D. Matthews, G.K. Becker, E.S. Marwil, and G.V. Miller, *SWEPP Assay System Software Requirements Specifications,* U.S. Department of Energy, Office of Environmental Restoration and Waste Management (1993).
3. K.C. Mousseau, A.R. Hempstead, G.K. Becker, and T.J. Roney, "Waste Assay Measurement Integration System User Interface," *Proceedings of the 4th Nondestructive Assay and Nondestructive Examination Waste Characterization Conference,* pages 387-98 (1995).
4. Susan Bridges, Julia Hodges, and Charles Sparrow, *The Application of Artificial Intelligence Techniques to the Analysis of Waste Assay Data,* Mississippi State University Diagnostic Instrumentation and Analysis Laboratory, Technical Report No. MSU-960620 (1996).
5. Mark Stefik, *Introduction to Knowledge Systems,* Morgan Kaufmann Publishers, Inc., San Francisco, CA (1995).
6. Y.D. Harker, L.G. Blackwood, and T.R. Meachum, *Uncertainty Analysis of the SWEPP Drum Assay System for Graphite Content Code 300,* Idaho National Engineering Laboratory (1995).
7. G.K. Becker, C. Watts, J. Bennion, and T.J. Roney, "Utility of Neural Networks in Nondestructive Waste Assay Measurement Methods," *Proceedings of the 4th Nondestructive Assay and Nondestructive Examination Waste Characterization Conference,* pages 161-88 (1995).
8. James Rumbaugh, Michael Blaha, William Premerlani, Frederick Eddy, and William Lorensen, *Object-Oriented Modeling and Design,* Prentice Hall, Englewood Cliffs, NJ (1991).
9. Judea Pearl, *Probabilistic Reasoning in Intelligent Systems: Networks of Plausible Inference,* Morgan Kaufmann Publishers, San Mateo, CA (1988).
10. D. Heckerman, J. Horvitz, and B.N. Nathwani, "Toward Normative Expert Systems: Part I: The Pathfinder Project," *Methods for Information in Medicine,* Volume 32, Number 2, pages 90-105 (1992).
11. D. Heckerman and B.N Nathwani, "Toward Normative Expert Systems: Part II: Probability-Based Representations for Efficient Knowledge Acquisition and Inference," *Methods for Information in Medicine,* Volume 32, Number 2, pages 106-16 (1992).
12. S.J. Russell and P. Norvig, *Artificial Intelligence: A Modern Approach,* Prentice Hall, Englewood Cliffs, NJ (1995).
13. D. Heckerman and M. Wellman, "Bayesian Networks," *Communications of the ACM* 38: 27-30.
14. Lotfi Zadeh, "Fuzzy Sets," *Information and Control,* Volume 8, pages 338-53 (1965).
15. HyperLogic Corporation, *CubiCalc: The Third Wave in Intelligent Software,* HyperLogic Corporation, Escondido, CA (1990-3).
16. B.G. Buchanan and E.H. Shortliffe, *Rule-Based Expert Systems: The MYCIN Experiments of the Stanford Heuristic Programming Project,* The MIT Press, Cambridge, MA (1990).

APPLICATION OF EXPERT SYSTEM TECHNOLOGY TO NONDESTRUCTIVE WASTE ASSAY - INITIAL PROTOTYPE MODEL

G.K. Becker and J.C. Determan
Lockheed Martin Idaho Technologies Company
Idaho National Engineering and Environmental Laboratory, Idaho Falls, ID 83415

ABSTRACT

Expert system technology has been identified as a technique useful for filling certain types of technology/capability gaps in existing waste nondestructive assay (NDA) applications. In particular, expert system techniques are being investigated with the intent of providing on-line evaluation of acquired data and/or directed acquisition of data in a manner that mimics the logic and decision making process a waste NDA expert would employ. The space from which information and data sources utilized in this process is much expanded with respect to the algorithmic approach typically utilized in waste NDA. Expert system technology provides a mechanism to manage and reason with this expanded information/data set. The material presented in this paper concerns initial studies and a resultant prototype expert system that incorporates pertinent information, and evaluation logic and decision processes, for the purpose of validating acquired waste NDA measurement assays.

INTRODUCTION

The management and disposition of transuranic (TRU) waste forms necessitates a determination of entrained TRU and associated radioactive material quantities as per National TRU Waste Characterization Program requirements governing the use of NDA techniques. The technical justification and demonstration of a given NDA method in accordance with applicable transportation and program data quality requirements is a difficult task for many waste forms. Actual waste form configurations can manifest NDA system response complexities that diminish the reliability of established data acquisition, reduction and interpretation schemes. Examples include non-unique measurement system responses or waste type parameters for which the NDA system has no response. This situation has provided the impetus for investigation into alternate approaches to considering and managing NDA data/information, including exploration of expert system technology.

Useful aspects of expert systems relative to waste NDA include the ability to utilize supplemental waste characterization data/information and a reduced dependence on NDA personnel resources. Such advantages can be realized through the appropriate structuring of an expert system that utilizes and/or integrates conventional data acquisition/analysis techniques, existing waste container data/information, waste generation process knowledge, analytical and computational NDA data, statistical analyses, and empirical data-driven methods. These information and data sources are organized into a cohesive system via techniques for combining sources of evidence and their associated uncertainties. A variety of expert system modules with differing functions can be constructed for tasks ranging from data reviews, to validation checks, to fully integrated waste NDA data reduction systems.

As part of the effort to evaluate the utility of expert systems in waste NDA, a prototype has been developed that utilizes neutron assay measurement data and domain expert knowledge. The prototype is based on results derived from preliminary evidence representation and reasoning studies performed at the DOE Diagnostic and Instrumentation Laboratory (DIAL) at Mississippi State University. The prototype as developed at this stage, consists of a module that performs NDA measurement data preprocessing and reasoning by applying domain heuristics to data and information made available to the system. The prototype is configured to perform the specific task of identifying neutron based drum assays that have no significant indication of measurement interference. In effect, the expert system picks out good assays from a population of measurements and labels them as valid per the capability envelope of the neutron assay system.

EXPERT SYSTEMS OVERVIEW

Expert systems are computer programs that can represent and reason with knowledge in a defined domain. More specifically, expert systems employ heuristics to represent domain knowledge, and automated methods of reasoning to emulate the problem solving and decision making capabilities of human experts. Expert systems can serve as a repository for the collective knowledge of a single or multiple experts and provide immediate and reliable access to this knowledge, thereby relieving dependence on human experts to perform certain knowledge

intensive, yet mundane, activities such as those related to quality assurance. Expert systems can also be configured to provide explanation and justification for the answers they derive. Expert systems have been developed for many diverse applications, including medical diagnosis, geological data interpretation, and computer system configuration.

Another important aspect of expert systems is the ability to deal with uncertain data. In domains where expert systems are applied, data is often vague, uncertain or incomplete (note, for example medical diagnosis, where acquisition of data is frequently constrained by time, equipment availability, and cost). Nonetheless, humans are able to cope with such data to arrive at meaningful conclusions with a reasonable degree of certainty. Therefore, software that emulates the human problem solving capacity must also handle ambiguous data. Numerous approaches to dealing with uncertainty have been developed and employed in the context of expert systems including Dempster-Shafer theory, certainty factors, Bayesian networks and fuzzy logic.[1] The fuzzy logic approach has been determined suitable for this project based on the work done by our collaborators at Mississippi State University.

Fuzzy Logic

Generally speaking, the field of logic is concerned with the mathematical and logical operations performed on defined sets to arrive at conclusions. Fuzzy logic is concerned with the mapping of these mathematical and logical operators onto fuzzy sets. A fuzzy set is a set that allows graded membership for elements in the set. Fuzzy sets are representative of many real world situations, such as the set of sunny days, or the set of acceptable candidates. Fuzzy sets are represented mathematically by membership, or characteristic, functions, and logical operations on fuzzy sets are defined as mathematical operations on these membership functions.. The more traditional fields of logic, such as bi-valued and multi-valued logic, may be viewed as subsets of the more general theory of fuzzy logic.

Fuzzy Sets

Fundamental to the concept of fuzzy logic is the notion of a fuzzy set[2], as opposed to a crisp set with clearly defined boundaries. The crisp set fully includes those objects meeting certain specified criteria and fully excludes all other objects. For example, the set of all men whose height exceeds seven feet is a small enumerable set with distinct and objective membership criteria, and is therefore a crisp set.

The set of all tall men, on the other hand, is not a crisp set as there is no clear and universally accepted definition of membership implied by "tall." A six-foot tall man is generally considered tall but not in an occupation such as basketball. Even allowing that a six-foot tall man is tall, what is the status of a man just a quarter inch shorter? Clearly, both men would be considered tall in most contexts. It is possible that at a height of five-foot nine inches a man might still be considered "tall", but just a few inches shorter, a man might be labeled "tallish" or "medium tall". At a height of five feet, a man is very unlikely to be categorized as "tall." Therefore a more appropriate description of the set of tall men might be: The set includes all men whose height is greater than or equal to six feet, excludes all men whose height is less than five feet, and includes to a degree those men between the heights of five and six feet tall. The set of all tall men exemplifies the property of graded membership that is characteristic of fuzzy sets.

Mathematically, the degree of membership in a given set is encoded in a function called the membership or characteristic function, where a value of zero indicates exclusion from the set, one indicates complete inclusion, and a rational value between zero and one indicates partial inclusion. Figure 1 shows one possible membership function for the set of all tall men.

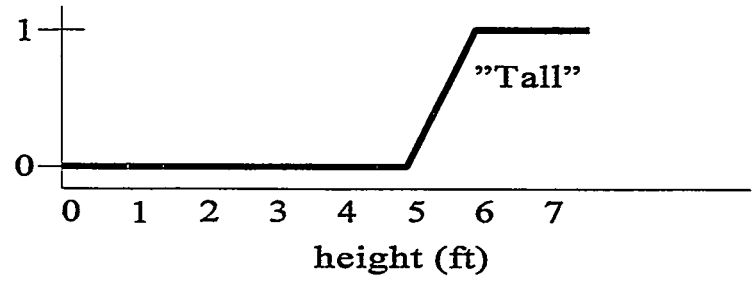

Figure 1. Fuzzy membership function for the set of all "Tall" men.

An example will be presented to clarify these ideas. Imagine a set of rules regarding a particular hypothetical chemical reaction:

Rule 1: "If the pressure is low then the yield is poor"

Rule 2: "If the pressure is medium and the temperature is hot then the yield is good"

where the fuzzy variables pressure, temperature and yield have the fuzzy values described by the membership functions shown in Figure 2. Also shown in Figure 2 are some pressure and

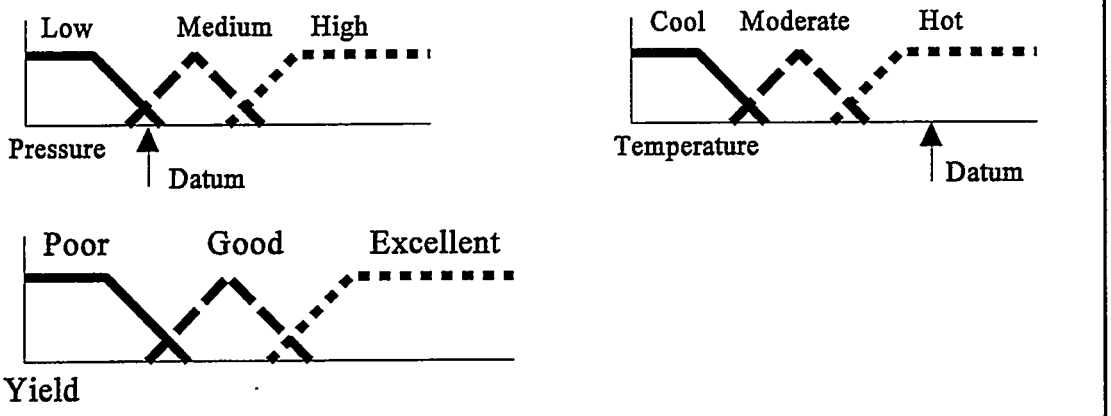

Figure 2. Hypothetical fuzzy membership functions for Pressure, Temperature, and Yield.

temperature data values. The temperature is such that it is considered to be definitely hot (membership value is one), while the pressure is low- to-medium (membership in each of the values low and medium is some small fraction). According to rule 1, and the fact that the pressure is low (to a degree), the fuzzy expert system will assert the fact that the yield is poor; but the membership function for the yield will be multiplied by the fractional degree of similarity between the pressure the fuzzy value "low". Likewise, the second rule will cause an assertion of the fact that the yield is good, but also qualified by the degree of similarity between the value of the pressure and the fuzzy value "medium pressure". The value of the temperature and the fuzzy

value "high temperature" form a complete match, and so this portion of the rule does not modify the resulting yield. Figure 3 shows the yield values produced by the two rules separately.

Figure 3. Separate membership functions for yield, due to rules 1 and 2.

To account for the fact that the actual yield for the given data is neither poor nor good but somewhere in between, the fuzzy expert system takes the union of the fuzzy sets representing yield as its final fuzzy answer for yield, as shown in Figure 4.

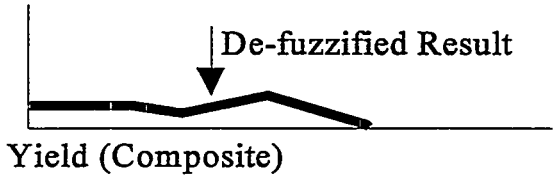

Figure 4. Composite membership for yield, and indication of de-fuzzified result.

The interpretation of the yield composite membership function is that there is roughly even possibility of getting poor or good yield, given the input data. The fuzzy expert system used offers two options for de-fuzzification, but the basic idea is to find a single number that best represents the distribution of area under the composite membership function. If, for example, the yield were composed only of "good" then the de-fuzzified yield would be the midpoint of the good range, or if the yield were composed of equal parts of the "poor" and "good" curves, the composite yield would de-fuzzify to the value half-way between the midpoints of the "poor" and "good" values. The relative importance of the "poor" and "good" values to the composite answer will determine where the de-fuzzified answer falls on the scale of "poor" to "good."

While this example indicates that the answer provided by fuzzy logic is a kind of "rough estimate" (yield is poor-to-good), the answer is within a context defined by the expert as being sufficiently precise to make meaningful decisions. According to Zadeh, a fuzzy system should "exploit the tolerance for imprecision" inherent in an application domain, because high precision is equivalent to high cost.[3] This statement is particularly appropriate to expert systems. An expert devises heuristics that yield a *sufficiently precise answer for his purposes*, quickly. Such heuristics are likely to be fuzzy (vague, imprecise) by their very nature. From this standpoint, fuzzy logic is more than just another method for dealing with uncertainty in expert systems. A fuzzy logic based expert system should be viewed as a formal framework for providing answers of limited, but sufficient, precision given that the knowledge base may be (inherently) incomplete, imprecise, or otherwise vague.

It has been argued, Zadeh, that fuzzy logic has an inherit advantage over rival methods for representing uncertainty in expert systems. The argument may be paraphrased as follows: Expert systems use heuristics to find a quick, approximate solutions (as an expert might do). Heuristics are likely to be fuzzy propositions (rather than statements of absolute truth or falsehood). The application of crisp probabalistic methods such as Dempster-Schafer theory or Bayesian networks to systems that are inherently fuzzy is unlikely to produce satisfactory results. Fuzzy logic offers a systematic approach to handling uncertainty that is inherent in the statement of the problem.

Fuzzy Expert System Implementation

Implementation of an expert system requires a software system that integrates the knowledge base, an inference engine and the knowledge representation. A commonly used package is the C-Language Integrated Production System (CLIPS)[4]. CLIPS is a multi-paradigm programming language developed by NASA to facilitate the development of expert systems. As its name would imply it can be compiled into C programs (and some other languages as well). CLIPS combines aspects of procedural programming, rule-based programming and object-oriented programming and is therefore a highly versatile tool for expert system development. At

the heart of CLIPS is the Rete Pattern Matching algorithm that efficiently matches fact patterns to rule antecedent patterns by keeping track of those facts and rules that have been recently changed or created. When a set of facts matches all of a rules antecedent patterns, the rule is said to "fire." When a rule fires, old fact patterns may be deleted or modified, and new fact patterns created. In this manner, a CLIPS module evaluates a set of facts and arrives at a set of conclusions.

FuzzyCLIPS[5] is an extension of CLIPS produced by the National Research Council of Canada. In FuzzyCLIPS, the patterns in both facts and rule antecedents may be represented by fuzzy variables. The Rete algorithm is extended to handle the partial matching of fuzzy variables, and the production system can produce fuzzy conclusions. Fuzzy variables can be "de-fuzzified," or transformed into a crisp representation if this representation is determined to be more appropriate.

PROTOTYPE EXPERT SYSTEM DESIGN AND LOGIC

The current version of the prototype expert system is designed to identify valid neutron assay measurements. The system logic is based on evaluating certain measured parameters with respect to the known capability of the neutron assay instrument. The system also employs heuristics that represent relationships in the problem domain to check consistency between the various system parameters. The process consists of conditioning the measured parameters into a form consistent with the rule specifications, classifying the measured parameters into fuzzy membership sets and applying the domain heuristics to arrive at an indicator of confidence in the measurement data. There are presently four different assay system output values for which a confidence is determined; the passive system neutron measure, passive shielded neutron measure, overall passive neutron measure and the active neutron measure. The set of confidence values output by the system is then used to classify the measurement data as either a valid measurement, within the capability of the neutron assay system, or a compromised measurement, not within the capability of the system.

By requiring that all measurement parameters be within the capability of the neutron assay system, and that they are all consistent with each other, the expert system in its present configuration selects assays whose measurement data indicate minimal or no measurement complication. Thus, the prototype system identifies assays with data that is clearly valid and consistent; this step is considered the first of many to be performed by the system under development. Observed complications of the measurement data that caused rejection of a given assay, will lead to a second, more focused phase of evaluation, during which it is expected that many assay measurements rejected in the first pass evaluation will now be found acceptable. In this manner, the system will be structured from multiple layers of increasingly focused evaluation. This type of process can be continued until it is clear that a rejected assay is truly invalid.

Prototype System Data/Variables

The prototype expert system processes measurement data with heuristics to determine a set of confidence values for an assay. Although there is a considerable amount of problem domain information/data that could be utilized via the expert system, only neutron measurement data and the container weight are used in the current version of the system. In terms of neutron assay data, it is intended that either raw data, e.g., neutron counts, derived figures of merit, etc., be selected as parameters that embody various aspects of system performance, and are pertinent to the quality of the assay. For neutron type systems in particular, such parameters must be indicative of the sources and magnitude of bias and/or imprecision present in the assay. For this reason indicators of neutron system bias and precision, such as the (alpha,n) neutron component, active neutron interrogation self-shielding, moderation, scattering and absorption are considered. The indicators do not have to be exact quantitative expressions of bias and precision sources, but must reasonably represent the magnitude of the effect, e.g. low, medium and high. Because density plays an important role in the majority of these parameters, the container weight is also a parameter of interest for use by the system.

A partial list of the neutron system measured and derivative parameters include: neutron

count rate, active shielded to total shielded counts ratio, flux monitor to barrel flux monitor count ratio and the system count to shielded count normalized to drum weight. The neutron count rate indicates the useful operability range of the system. For example, low count rates are indicative of uncertainty associated with being near or below the detection limit of the system. High neutron count rates indicate proximity to or degree of saturation of the coincidence counting circuitry and quality of dead time corrections. In a similar manner, the ratio of the active shielded detector count to the passive shielded count is an indicator of the degree of (alpha,n) interference that is important in assessing uncertainty associated with the passive neutron measurement. The values of several of the measurement parameters are a function of the waste type. In order to minimize the complexity of the prototype expert system rule base, those parameters related to the waste form were derived for the graphite type matrix. This is not a limitation if knowledge and data is available on a waste form basis.

Once the parameters of importance are defined, fuzzy set membership functions are defined for each parameter. The parameters in this form become the primary fuzzy variables of the system, where ranges of each variable are typically assigned low, medium, and high values. Each such range is represented as a fuzzy set using sigmoid type membership functions, as illustrated in Figure 5.

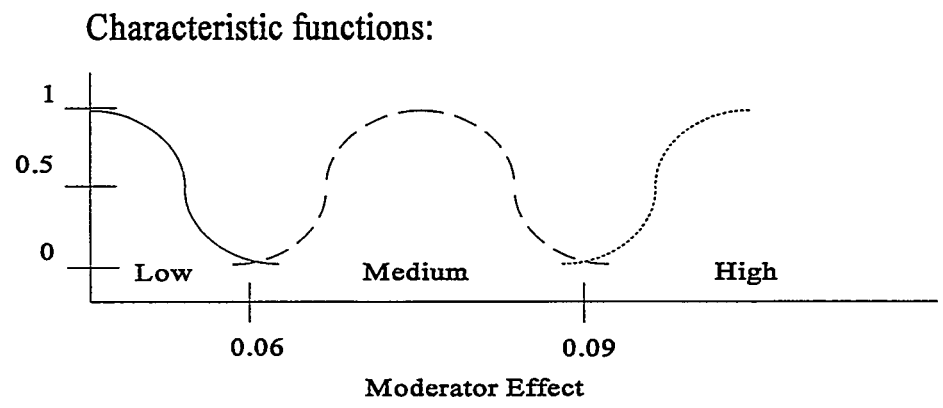

Figure 5. Typical fuzzy variable characteristic functions.

Prototype System Rules

The prototype system rules are defined to operate on the fuzzy variables with the ultimate purpose of assigning a set of confidence values to the neutron assay measurement. Hence the rules developed for the system represent heuristics and relationships an expert would utilize when considering the validity of an assay measurement. Because these rules yield confidence indicators, fuzzy variables were also used to define confidence values that ranged through five gradations "none", "minimal", "average", "good" and "excellent". An example of a rule employed in the system using an IF-THEN format is:

IF active shielded total/passive shielded total is *high*
and
index of moderation is *low*

THEN spectra is hard
and
self shielding insignificant

IF spectra is hard
and
self shielding insignificant
and
shielded total rate is *medium*

THEN passive shielded confidence is *good*

This particular rule set makes a confidence claim concerning the passive neutron shielded measure using values associated with the fuzzy variables "active shielded count/ passive shielded count ratio" and the "shielded total rate". As in the previously discussed example, where multiple rules produced assertions regarding the yield, the prototype system includes multiple

rules that produce assertions regarding any given confidence measure in the system. These assertions are then combined via the processes of fuzzy logic to arrive at a single (but fuzzy) confidence value for each system measure. These confidence values are subsequently de-fuzzified into crisp values between zero and one.

Prototype System Evaluation and Results

To evaluate the performance of the expert system, 524 actual neutron assays on graphite type waste containers generated at the Rocky Flats Plant were processed through the system. The system responded by dividing the population into two broad categories: those assays whose measurement data showed minimal or no complications, and could therefore be assigned a confidence value, and those assays for which the set of confidence values could not currently be assessed. Out of 524 graphite matrix neutron measurement assays processed by the system, about one quarter of the population fell in the first category. This is a reasonable result as the graphite waste form presents few significant bias and precision sources which interfere with the neutron assay modality.

To evaluate these results and gain some confirmation on the performance of the expert system, each assay selected as having a high confidence was manually reviewed to ensure that a human expert would arrive at a similar conclusion. In all cases the decision or assignment of confidence of the expert system was corroborated by the human expert. Likewise those assay which the expert system classified as unacceptable were also reviewed by a human expert where it was also determined that the classification was correct. It is noted that this is not a hard benchmark of performance thereby prompting another means to express performance.

Another confirmatory, albeit qualitative, measure of the prototype performance is derived from a statistical analysis of passive neutron assay uncertainty for the graphite waste form.[6] Results of the uncertainty analysis indicate an average negative measurement bias of roughly 6% for the passive system mode of the neutron counter for the graphite waste form. This is the same neutron assay measurement system from which the data was acquired for testing the expert

system. This being the case, the mass values for the 524 graphite assays determined via the passive neutron assay system are shifted low by roughly 6%. If the prototype expert system is properly selecting assays with little or no bias, one would expect to see the mass values for the population of assays classified as high confidence by the expert system shift upward on the order of 6%. In a qualitative manner this expectation is borne out. Figure 6 compares the relative frequency of occurrence for the passive neutron system measurement as a function of plutonium mass. The solid line represents the distribution observed for all 524 graphite drums, while the dashed line represents the distribution observed for the low-bias ("clean") drums picked out by the expert system, of which there were 129. As evident in the illustration, there is a shift upward giving further corroboration that the expert system is performing as intended.

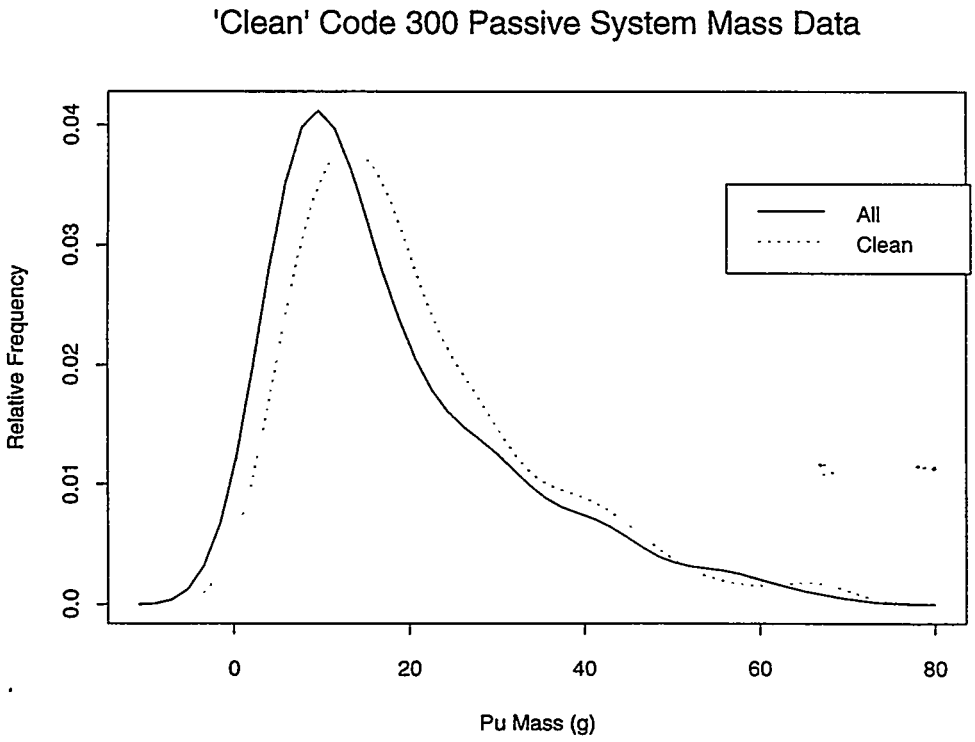

Figure 6. Comparison of passive system mass measurement for all and "clean" graphite drums.

CONCLUSIONS

Expert systems can be configured to perform the functions of human experts in a defined domain, in this case identification of valid measurement data. For the task of the prototype expert system discussed in this paper, classification of the 524 graphite drum population by the expert system was accomplished by the expert system in a matter of minutes. This same task, if performed by a human expert, would have consumed days of valuable time.

The performance of the system relative to other independent benchmarks, i.e., the graphite waste form uncertainty analysis, indicated correct function of the expert system. Certainly, more quantitative means of benchmarking and evaluating system performance are required using known input sources with quantifiable bias and precision elements. Such exercises have been planned and are to be performed in the near future. Future work with expert system technology includes expanding the knowledge base of the system to incorporate the use of process information, computational analyses, statistical data, and other acceptable information.

REFERENCES

1. S. Bridges, J. Hodges, C. Sparrow, The Appliaction of Artificial Intelligence Techniques to the Analysis of Waste Assay Data, Diagnostic and Instrumentation Laboratory (DIAL), Mississippi State University.

2. Ed. R.R. Yager et at, Fuzzy Sets and Applications: Selected Papers by L. A. Zadeh, John Wiley & Sons, New York, 1987.

3. IEEE, IEEE Video conferences, Seminars via Satellite, Fuzzy Logic: Applications and Perspectives, April 25, 1991.

4. JSC-25012, CLIPS Reference Manual, Software Technology Branch, Lyndon B. Johnson Space Center, June 15th 1995.

5. R.A. Orchard, FuzzyCLIPS Version 6.04 User's Guide, Knowledge Systems Laboratory, Institute for Information Technology, National Research Council Canada, June 1995.

6. Y.D. Harker, L.G. Blackwood and T.R. Meachum, Uncertainty Analysis of the SWEPP Drum Assay System for Graphite Content Code 300, INEL-95/0475, Lockheed Martin Idaho Technologies Company, September 1995.

A PRELIMINARY EVALUATION OF CERTAIN NDA TECHNIQUES FOR RH-TRU CHARACTERIZATION

J. K. Hartwell, W. Y. Yoon, and H. K. Peterson
Idaho National Engineering Laboratory
Idaho Falls, ID 83415

ABSTRACT

This report presents the results of modeling efforts to evaluate selected NDA assay methods for RH-TRU waste characterization. The target waste stream was Content Code 104/107 113-liter waste drums that comprise the majority of the INEL's RH-TRU waste inventory.

Two NDA techniques are treated in detail. One primary NDA technique examined is gamma-ray spectrometry to determine the drum fission and activation product content, and fuel sample inventory calculations using the ORIGEN code to predict the total drum inventory. A heavily shielded and strongly collimated HPGe spectrometer system was designed using MCNP modeling. Detection limits and expected precision of this approach were estimated by a combination of Monte Carlo modeling and synthetic gamma-ray spectrum generation. This technique may allow the radionuclide content of these wastes to be determined with relative standard deviations of 20 to 55% depending on the drum matrix and radionuclide.

The INEL Passive/Active Neutron (PAN) assay system is the second primary technique considered. A shielded overpack for the 113-liter CC104/107 RH-TRU drums was designed to shield the PAN detectors from excessive gamma radiation. MCNP modeling suggests PAN detection limits of about 0.06 g ^{235}U and 0.04 g ^{239}Pu during active assays.

INTRODUCTION

Remote handled transuranic (RH-TRU) waste is presently being retrievably stored at the Idaho National Engineering Laboratory (INEL). In compliance with Department of Energy (DOE) guidelines this waste has been stored in the Intermediate Level Transuranic Storage Facility (ILTSF) at the Radioactive Waste Management Complex (RWMC). This RH-TRU waste will eventually be retrieved and shipped to Waste Isolation Pilot Plant (WIPP) disposal facility, which is the located near Carlsbad, New Mexico. Each drum containing RH-TRU waste must be characterized and certified for shipment to and disposal at the WIPP repository.

This work evaluates selected nondestructive assay (NDA) technologies that may be able to characterize the primary INEL RH-TRU waste stream, Content Code 104/107 (CC104/107), in a cost effective manner. The NDA approaches evaluated are (1) direct gamma-ray spectroscopy for fission product content in combination with the calculation of fissile and other important nuclide contents using the ORIGEN fission product buildup and decay code; and (2) a combined passive-active neutron coincidence and dieaway measurement.

The bulk ((90%) of the INEL's RH-TRU wastes are CC104/107 wastes from Argonne National Laboratory-East (ANL-E) shipped in 30-gal DOT-17H drums. The contents of these are primarily alpha-gamma hot-cell wastes from ANL-E. They are primarily from metallurgical examination of Experimental Breeder Reactor II (EBR-II) irradiated fuel samples sent to ANL-E from ANL-West. The waste packages have a surface gamma radiation reading that does not exceed 30 R/hr. If a package reads greater than 30 R/hr, it is repackaged before shipment. These radiation fields arise from fission products in the irradiated fuel samples. The fuel material can be ^{235}U, ^{239}Pu as metal or ^{239}Pu as oxide. The Pu also contains ^{240}Pu and other Pu isotopes. The wastes are largely materials used in cleanup such as rags, paper, plastics, bits of metal, small tools or other contaminated hardware. Combustible materials are segregated from non-combustibles. No fuel sample materials are discarded as waste. All fuel remnants are returned to ANL-W. The TRU and fission products are simply contaminants in the waste from hot-cell cleanup after an examination campaign. The TRU arises from sawing and grinding operations and metallurgical mount preparation of samples. During the process, special effort is made to collect all grinding filings and saw cuttings. Also, as much material as possible is removed from grinding papers prior to discarding as waste. The cuttings and filings are NOT discarded as waste. For shipment of these wastes to the INEL's Radioactive Waste Management Complex (RWMC) the TRU content in the waste is estimated from process knowledge and historical loss rates (1½% of the TRU mass) with no direct assay or sampling of the waste. Typically these values are from 0.06 to 1.6 grams per 30-gal drum; however, in a few cases they can be as large as 16 grams.

The waste is generally placed into 7.5-gal containers (approximately 1 ft^3) and two of these stacked vertically in the center of a lined 30-gal drum. A given drum is loaded either with combustible or noncombustible wastes. The weight of the waste materials ranges from 11 to 66 kg (24 to 145 lb.), but is typically around 45 kg (100 lb.). Examination of the INEL storage records shows that 56% of the RH-TRU waste drums have surface radiation fields below 5 R/hr, 72% are less than 10 R/hr, and 84% are less than 20 R/hr. Only 27 drums have fields between 20 and 30 R/hr. None of the CC104/107 drums have a field above 30 R/hr.

Actual RH-TRU drum handling is expensive. This report relies on calculational models to evaluate the capability of the proposed NDA techniques, and to select systems for further development and testing. The modeling results are expected to provide a "road map" for future development and assessment measurements, and thus improve the cost effectiveness of the overall RH-TRU NDA characterization effort.

THE MODELING APPROACH

This work used the ORIGEN[1] code for fission and activation product inventory calculations; the MCNP[2] code for neutron and photon transport modeling; and the SYNTH[3] code for modeling of the gamma-ray spectral response. Since nearly 90% of the INEL's RH-TRU inventory is CC104/107 waste from ANL-E, this waste stream was chosen as the design basis case for NDA equipment evaluation.

Generally, waste packages with high surface dose rates present the greatest NDA challenge. Thus, the design basis drum was chosen to be an CC104/107 waste package containing 45 kg of homogeneously contaminated combustible waste with a density of 0.4 g/cm^3. The drum surface dose rate was chosen to be 30 R/hr, the maximum dose rate for this waste stream. The isotopic composition of the radioactive waste was presumed to be that of 15-year aged EBR-II fuel drawn from an ORIGEN inventory calculation computed for Pin DP-81 from a representative EBR-II irradiation.[a] The absolute drum content was that amount determined by MCNP calculations to yield a 30 R/hr gamma-ray dose rate at the exterior drum surface. The design basis drum contents are presented in Table 1.

Table 1. Radionuclide content of the RH-TRU design basis drum

Isotope	*Half-life (Yr)*	*Curies per drum*
^{54}Mn	0.85	3.72E-05
^{60}Co	5.27	1.91E-04
^{106}Ru(^{106}Rh)	1.02	6.69E-04
^{125}Sb	2.76	2.15E-02
^{134}Cs	2.07	3.35E-03
^{137}Cs	30.2	6.11E+00
^{144}Ce(^{144}Pr)	0.78	2.96E-04
^{152}Eu	13.5	3.12E-05
^{154}Eu	8.59	5.61E-03
^{155}Eu	4.71	5.24E-02

PASSIVE AND ACTIVE NEUTRON ASSAY

Neutron detection systems are generally the systems of choice for the direct measurement of fissile material content in bulk samples with a high gamma-ray dose rate. The INEL routinely uses a

[a] Inventory calculations were performed by K. Bunde (ANL-W) using ORIGEN-R, an ANL version of the ORIGEN code, and a proprietary set of EBR-II-specific libraries. Pin DP-81 was part of assembly S/A X-447 which accumulated 17.766 GWD from Nov. 1987 through Nov. 1988.

Passive/Active Neutron (PAN) assay unit to quantify the TRU content of contact-handled (CH)-TRU waste drums. A preliminary assessment suggested that the INEL's PAN system could possibly be used for the assay of RH-TRU waste drums.[4]

The INEL's PAN system is designed to assay TRU in 55-gal steel drums. It consists of an enclosed assay chamber, neutron shielding and moderator materials, ^{3}He neutron detectors, and a 14 MeV (D,T) neutron generator. The enclosure incorporates a motor-driven turntable that rotates a drum during assay. The system can be operated with the neutron generator running (Active Mode), or without the generator (Passive Mode).

Although the existing PAN system, since it uses ^{3}He neutron detectors, is quite tolerant of high gamma-ray backgrounds, the RH-TRU waste drums may require shielding in order to avoid an excessive accidental rate due to gamma-ray pile up events in the neutron detectors. Experience[4] suggests that the surface gamma-ray dose rate of a drum to be assayed should be below about 50 mR/hour. Since the PAN assay chamber is sized for 208-liter (55-gallon) waste drums, a shielded overpack was designed to reduce the dose rate of the 113-liter (30-gallon) RH-TRU drums to less than 0.05 R/hr. The thickness of lead shielding required to reduce the dose rate of the design basis RH-TRU drum (30 R/hr surface dose rate) to no more than 50 mR/hr was determined using the MCNP code. This model predicts that a 4.4-cm (1.75-in) thick lead shield provides the required dose rate reduction. A shield of this thickness can be accommodated within the PAN assay chamber. The PAN system turntable may require replacement to support the increase weight of drum and shield.

INEL researchers have developed a detailed MCNP model to predict the response of the PAN system.[5] This model was employed to estimate the detection sensitivity of the PAN system for assay of RH-TRU waste drums in a 4.4 cm lead overpack. Both active and passive assay modes were modeled; although, it was expected that only the active mode would be useful.

MCNP modeling estimated the response of the passive-mode PAN system to the design basis combustible matrix RH-TRU drum. The model assumed a waste density of 0.4 g/cm^{3} containing homogeneously distributed fissile material masses of 0.459 g ^{235}U, 0.068 g ^{239}Pu, and 0.008 g ^{240}Pu. These masses were determined from the typical CC104/107 RH-TRU drum inventories. The expected passive counting rate in the shielded detectors was 0.0157 counts per source neutron and 0.0955 counts per source neutron in the shielded plus unshielded (system) detectors. Converting these results to counts per gram of ^{240}Pu (using the neutron emission rate of 1.02E+03 n/s/g ^{240}Pu) and total Pu (using the assumed ^{240}Pu to Pu mass ratio of 11.7%) the expected shielded detector counting rates are 16 c/s/g ^{240}Pu and 1.9 c/s/ g Pu. In the system total detectors these values are 97 c/s/g ^{240}Pu and 11.4 c/s/g Pu. These

are total counting rates not coincidence counting rates. Only the neutron response was modeled. Photon interactions were not modeled.

The expected passive detection limit can be estimated from published values and the RH-TRU-specific MCNP modeling. For "benign" matrices, the existing PAN passive system has a detection limit of about 1g of weapons grade Pu in a 200 second count.[5] MCNP modeling of the existing system predicts a systems total counting efficiency of 0.127 counts per source neutron.[b] Assuming the same sample-induced background and a systems total counting efficiency of 0.0955 counts per source neutron, an estimated passive detection limit for the EBR-II-grade Pu would be about 0.8 grams.

The passive detection limit for Pu in the RH-TRU waste drums is greater than the usual estimated content. Additionally, this detection technique will not detect ^{235}U, often the highest concentration fissile isotope in these waste drums. To assay these drums will require active interrogation.

MCNP modeling of the overpack-shielded design basis RH-TRU drum predicts active mode counting rates in the time-correlated window of 0.38 c/pulse/g ^{235}U and 0.64 c/pulse/g ^{239}Pu. Thus, in a typical 2000 pulse assay, one expects 765 counts/g ^{235}U and 1280 counts/g ^{239}Pu. For comparison, similar sensitivity values for the 208-liter PAN assays, without the shielded overpack, are 1.6 to 1.9 c/pulse/g ^{239}Pu. The decrease of roughly a factor of three in detection sensitivity is believed due to neutron scattering in the shield, and the smaller geometry of the interrogated sample.

During the SWEPP PAN system performance demonstration testing, background rates in the accidentals gate were recorded for active assay of Pu-containing drums.[b] Six replicate runs were recorded on both a 208-liter waste drum empty except for the test sources, and on a drum containing Ethafoam©, a combustible matrix surrogate with a density of about 0.4 g/cm^3. Each run was for 40 second (2000 generator pulses). The mean counts in the accidentals gate were 502±34 counts for the empty matrix drum and 580±24 counts for the Ethafoam matrix drum. Scaling these to correct for the factor of five difference in gate time, suggests that a typical active assay background in the time-correlated channel would be about 110 counts in an assay period. The resultant detection limit[6] [(LD)] would be about 52 counts per assay period. Given the assay sensitivities calculated for the CC104/107 RH-TRU drums this would translate into reliable (95% confidence) detection of 0.06 g ^{235}U or 0.04 g ^{239}Pu. CC104/107 RH-TRU drums are typically said to contain between 0.06 to 1.6 g of TRU. These quantities should be reliably detected by PAN system assays in a shielded overpack. However, some caveats are in order.

---

[b] Y. D. Harker, *Private Communication*, September 9, 1996.

PAN system active assays are sensitive to a number of waste-form-specific parameters. Among these are sample self shielding (if the fissile material is in "hunks"), matrix absorption, and matrix moderation. From our understanding of the CC104/107 wastes, sample self absorption should not be a problem; however, little is know about the other two parameters. These parameters cannot be well modeled. Careful calibration of the PAN system for the specific waste matrix will be required.

DIRECT GAMMA-RAY SPECTROSCOPY (DGS)

Since the irradiation history, but not necessarily the total radionuclide content of the INEL's CC104/107 RH-TRU drums is well known, their radionuclide content might be sufficiently determined by a gamma-ray spectrometric assay of the major fission and activation product emitters in the drum along with calculations using the ORIGEN code to determine the total content. One uncertainty in the present knowledge of the CC104/107 RH-TRU drums is the fraction of the total activity that is due to activation (^{60}Co, for example) rather than fission products (^{137}Cs and ^{125}Sb are examples). By defining the relative amounts of the detected gamma-ray emitters and providing an estimate of the total content of a few radionuclides, a DGS system could improve the accuracy with which ORIGEN can calculate the total drum inventory. Additionally, certain fission product activity ratios and total activity estimates would be useful for confirmation of the declared burn-up and decay history on which the ORIGEN inventory values rely.

A cutaway drawing of the preliminary design for a direct gamma-ray spectroscopy (DGS) system for assay of RH-TRU drums is presented in Figure 1. The DGS incorporates a high-purity germanium (HPGe) detector with standard pulse height analysis electronics and a relatively common coaxial detector design. In order to allow the assay of the high activity waste drums, the system includes massive shielding and strong detector collimation. Since the collimator defines a source area that covers a thin strip from the top to the bottom of the drum, the system will require drum rotation to provide a full view of the drum.

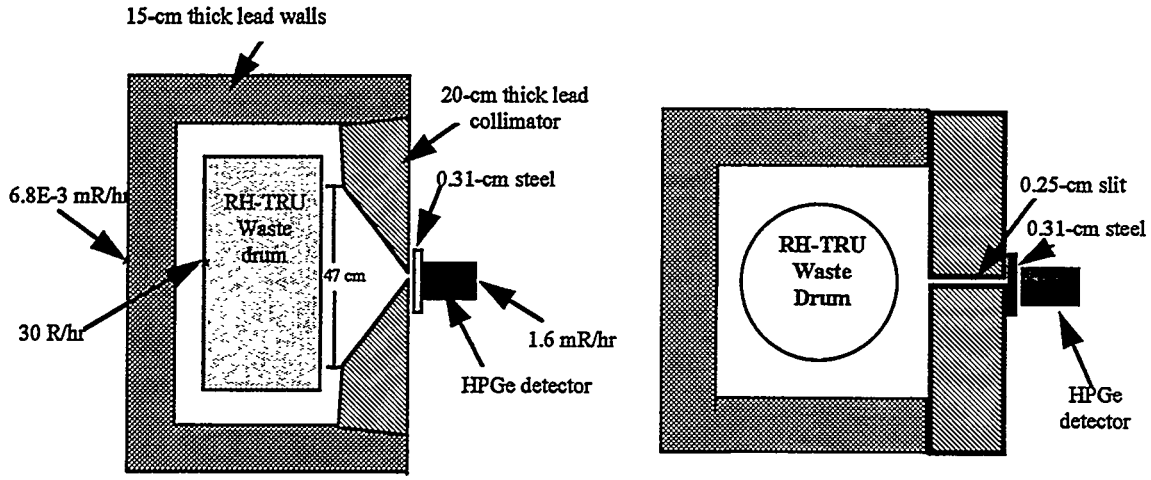

a. Vertical cross section b. Horizontal cross section

Figure 1. Cutaway drawings of the proposed DGS shield and collimator

The shielding and collimation design features were derived from MCNP modeling.[c] A system requirement was that the total counting rate in the HPGe detector be less than 50,000 counts per second (c/s) when a design-basis combustible matrix RH-TRU drum with a surface dose rate reading of 30 R/hr was assayed. This insures that the total system input rate is compatible with standard gamma-ray spectrometer component rate-handling capabilities. Figure 1 is annotated with the MCNP-calculated dose rates at critical points.

The DGS collimator defines the viewed source area and limits the HPGe detector counting rate to levels that can be reliably processed by readily available nuclear spectroscopy equipment. As depicted in Fig.1, a fan-shaped collimator with an entrance height of 47 cm was chosen to provide a view of a full vertical slice of the rotating RH-TRU drum. The collimator width and exit height were adjusted such that the MCNP model predicted a detector counting rate of 50,000 counts per second (c/s) for this highest activity drum. The collimator width and exit height that provided this modeled counting rate were both 0.25 cm (0.1 in), and a 0.31-cm (0.12-in) thick steel absorber was used to block low-energy gamma- and X-rays.

In any strongly collimated system, shield penetration can be a problem. If the detector counting rate from degraded photons that have passed through the shield is a significant fraction of the total system counting rate, then the signal-to-background ratio can be untenably small. Shield leakage was assessed by

[c] Private communication, W. Yoon to Y. D. Harker, J. K. Hartwell, and H. K. Peterson, Notegram of 4/23/96 "Preliminary HPGe Detection System for the R-H Waste Drum," and additional calculations performed 7/19/96.

comparing the calculated dose rate at the detector face for the collimated DGS with identical calculations performed for a solid shielding wall (these are normally termed "collimator open" and "collimator closed" results). For the proposed DGS design, the open-to-closed ratio was greater than 70,000, a fully acceptable result.

Accurate modeling of gamma-ray spectra requires that the spectral continuum be correctly predicted. In the DGS, the continuum will have two primary components 1) the Compton continuum from scattering events in the detector, and 2) photons scattered (and thus degraded in energy) during transport to the detector. MCNP has the capability to predict the complete gamma-ray spectrum for this DGS problem, and the modeled results would include both of the continuum components in addition to the full energy peaks. However, the computer time required for this calculation would be excessive. Consequently, an abbreviated MCNP model was used to predict the general shape of the scattered photon component reaching the detector and the total detector counting rate, and a recently developed code, SYNTH, [3] modeled the expected spectrum.

SYNTH requires that a source configuration, external absorbers, source radionuclide concentrations, detector configuration, and electronic settings be defined as input. From these input parameters SYNTH uses accepted parametric calculational techniques to predict the expected gamma-ray spectrum. Comparisons of measured and SYNTH-calculated spectra have been published.[3,7]

MCNP modeling predicted that the total detector counting rate would be 50,000 counts per second for the design basis 30 R/hr drum and the chosen collimator design. About half of the photon flux reaching the detector was predicted to be full energy (uncollided) source gamma-rays, and the remaining half degraded in energy (collided). Additionally, the MCNP model predicted the energy spectrum (152 bins) of the collided and the uncollided portion of the photon flux reaching the detector.

The isotopic distribution of the source used for the SYNTH calculations was drawn from the EBR-II inventory data provided. In order to emulate the expected attenuation in the RH-TRU waste, the source was described to SYNTH as a 10 cm^2 disk source with a thickness of 10 cm and a mass of 40 grams. (This description is not meant to reproduce the RH-TRU counting geometry, but rather to force a proper shape to the SYNTH-calculated detector efficiency curve.) The source composition was chosen to be 96% C_2H_2, 2% iron, and 2% uranium. The source-to-detector distance was arbitrarily set to 12 cm. To account for attenuation through the container walls and steel absorber plate, an external absorber of 0.65 cm of iron was selected. The detector was described as a standard HPGe detector with a diameter of 5 cm, a depth of 6 cm, and a relative efficiency of about 20%. The spectral gain and zero were chosen to be 0.36

keV/channel and 0 keV respectively. This provides an upper energy limit of 2950 keV in an 8192 channel spectrum.

From these parameters, SYNTH was used to calculate an absolute photopeak efficiency curve. As a check on the accuracy of this SYNTH prediction, an MCNP calculation of photopeak counts in the detector per source photon was performed. Since the SYNTH calculation was provided with an arbitrary source concentration (to be normalized later) the absolute photopeak efficiency values cannot be directly compared; however, the correctness of the SYNTH-calculated efficiency curve as a function of energy can be evaluated by comparing the relative efficiency curve determined by MCNP with the relative efficiency curve calculated by SYNTH. Relative photopeak efficiencies were computed in both cases by normalizing each curve to an efficiency of 1.0 at the 1332 keV line of ^{60}Co. The results are compared in Table 2. Throughout the energy range of interest, the SYNTH-calculated curve agrees very well with the MCNP values.

Table 2. Comparison of MCNP and SYNTH-calculated relative detector efficiencies as a function of energy

Energy (MeV)	*Rel Eff (MCNP)*	*Rel Eff (SYNTH)*	*SYNTH/MCNP Ratio*
1.3325	1.00	1.00	1.00
1.1173	1.13	1.08	0.95
0.6616	1.66	1.77	1.07
0.6359	1.71	1.79	1.05
0.6006	1.78	1.80	1.01
0.4634	2.17	2.15	0.99
0.4435	2.25	2.24	1.00
0.4279	2.31	2.40	1.04
0.3804	2.52	2.44	0.97

Since the shape of the SYNTH-calculated efficiency curve with energy seems correct, the next step was to define the total activity of the SYNTH-specified source. The relative radionuclide distributions were as specified for 15-year decayed material (Table 1). Again, the MCNP modeling results guided the total activity specification. MCNP calculations predicted a total detector counting rate of 50,000 counts/second with about half of these counts coming from uncollided photons and about half from collided photons. Thus, the SYNTH-specified source activity was adjusted to yield a spectrum containing about 25,000 total counts/second, simulating the "uncollided" portion of the modeled spectrum. The collided photon spectrum, an important component of the spectral background, was also determined from MCNP calculations. The MCNP results provided a binned energy spectrum of the collided photon flux impinging on the detector end cap. To conserve calculation time, the calculation used only 152 energy

bins. The MCNP results were smoothed, converted from counts/keV to counts per channel using the known spectral energy calibration of 0.36 keV/channel, and then interpolated into 0 to 4096 channels. (There is no significant collided photon flux above 1408 keV or channel 3920.) The channel contents of this interpolated spectrum were further smoothed and adjusted by a constant factor to yield a total of 25,000 counts/second. The SYNTH-generated source photon spectrum and the estimated collided photon spectrum were summed using the "background addition" function of SYNTH. (This procedure ignores the effect of the detector relative efficiency curve on the collided photon spectrum, thus the synthetic continuum will be over estimated at the higher energies.) Statistical fluctuations were then imposed on the channel contents (another SYNTH function) to produce a best estimate of the expected RH-TRU assay spectrum. The resultant spectrum with the two summed components identified is presented in Figure 2.

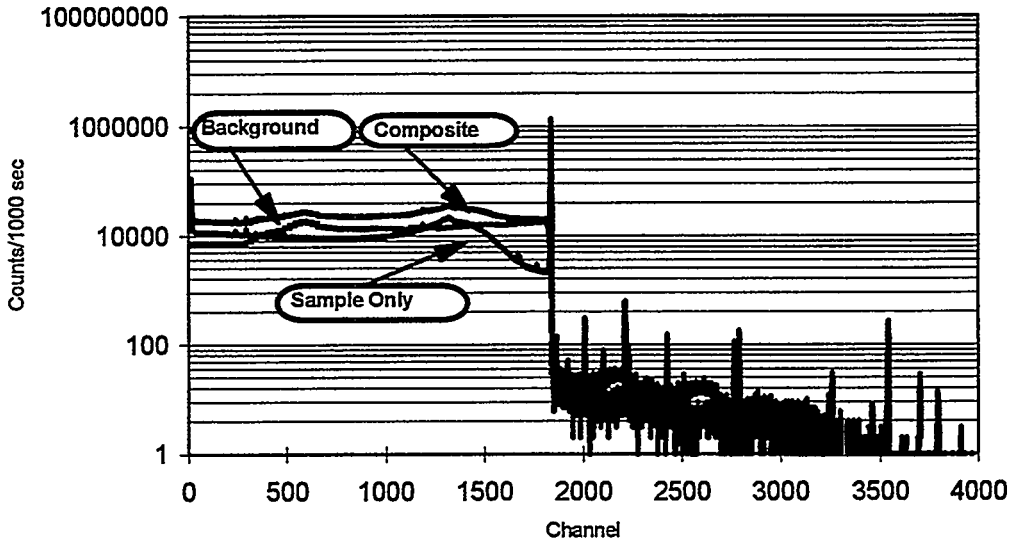

Figure 2. The simulated DGS spectrum detailing its components

The simulated DGS spectrum for the design basis RH-TRU drum was submitted to the commercial gamma-ray spectral analysis program *GammaVision.*© The analysis results provide the expected peak areas in a 1000 second count time spectrum, the uncertainties in these peak areas, and the total number of background (continuum) counts underlying each peak. These values were then used to determine the uncertainty in the spectral analysis results, and the expected system detection limits. Detection limits were computed following the technique of Currie.[6] Currie defines a critical level (L_C) and a detection limit (L_D). The critical level is the response that must be measured in a given spectrum in order to conclude "detected," while the detection limit is the response level that will result in a detected decision 95% of the time.

The expected peak areas, peak area uncertainties (as one relative standard deviation from counting statistics only), the spectral critical levels (L_C), and estimated detection limits at the 95% confidence level (L_D) are presented in Table 4. The detection limits are expressed both as peak area counts (in a 1000 second count time spectrum) and in terms of Curies of drum activity. Those spectral peaks for which the expected peak area exceeds the calculated L_D limit, and thus should be detectable 95% of the time, are identified as "Easily" detected.

It is important to note that the calculated detection limits are only correct for the design basis RH-TRU drum reading 30 R/hr at the drum surface and for a system assay time of 1000 seconds. The

Table 4. Spectral analysis results for the simulated DGS spectrum

Isotope	line energy (keV)	Est bkg (counts)	Est critical level LC (counts)	Est detection limit LD (counts)	Expected peak area (counts)	Relative Stand Dev	Detected?	Curies/ sample	Expected Counts/Sec per CI	Detectable limit (CI)
Co-60	1173	37	14	31	153	10%	Easily	1.9E-04	8.01E+02	3.9E-05
	1332	6	6	14	147	9%	Easily	1.9E-04	7.70E+02	1.8E-05
Mn-54	834	379	45	94	86	34%	Yes	3.7E-05	2.31E+03	4.0E-05
Rh-106	622	311675	1303	2608	621	127%	No	6.7E-04	9.28E+02	2.8E-03
Sb-125	176	229027	1117	2236	6577	10%	Easily	2.2E-02	3.06E+02	7.3E-03
	381	237029	1136	2275	914	75%	No	2.2E-02	4.25E+01	5.4E-02
	428	389703	1457	2916	12559	7%	Easily	2.2E-02	5.84E+02	5.0E-03
	463	421897	1516	3034	3801	24%	Easily	2.2E-02	1.77E+02	1.7E-02
	601	561290	1748	3499	4073	26%	Easily	2.2E-02	1.89E+02	1.8E-02
	636	293341	1264	2530	3098	25%	Easily	2.2E-02	1.44E+02	1.8E-02
Cs-134	563	608976	1821	3645	2038	54%	Yes	3.4E-03	6.08E+02	6.0E-03
	569	355548	1391	2785	3125	27%	Easily	3.4E-03	9.33E+02	3.0E-03
	605	338785	1358	2719	2628	31%	Yes	3.4E-03	7.84E+02	3.5E-03
	796	552	55	112	2992	2%	Easily	3.4E-03	8.93E+02	1.3E-04
	802	600	57	117	181	21%	Easily	3.4E-03	5.40E+01	2.2E-03
	1168	218	34	72	55	40%	Yes	3.4E-03	1.64E+01	4.4E-03
Cs-137	662	107790	766	1535	6.00E+06	0%	Easily	6.1E+00	9.81E+02	1.6E-03
Ce-144	133	205688	1058	2119	346	185%	No	3.0E-04	1.17E+03	1.8E-03
Pr-144	696	90	22	47	4	339%	No	3.0E-04	1.35E+01	3.5E-03
Eu-152	122	380290	1439	2881	1269	69%	No	3.1E-05	4.07E+04	7.1E-05
	344	252400	1172	2347	187	380%	No	3.1E-05	5.99E+03	3.9E-04
	779	83	21	45	5	262%	No	3.1E-05	1.60E+02	2.8E-04
	1408	6	6	14	8	56%	Yes	3.1E-05	2.56E+02	5.5E-05
Eu-154	123	365752	1411	2825	5217	16%	Easily	5.6E-03	9.30E+02	3.0E-03
	248	445642	1558	3118	613	154%	No	5.6E-03	1.09E+02	2.9E-02
	723	411	47	97	1174	4%	Easily	5.6E-03	2.09E+02	4.7E-04
	757	468	50	104	305	12%	Easily	5.6E-03	5.44E+01	1.9E-03
	873	226	35	73	673	5%	Easily	5.6E-03	1.20E+02	6.1E-04
	996	75	20	43	518	5%	Easily	5.6E-03	9.23E+01	4.7E-04
	1005	36	14	31	917	3%	Easily	5.6E-03	1.63E+02	1.9E-04
	1274	7	6	15	1468	3%	Easily	5.6E-03	2.62E+02	5.8E-05
	1596	5	5	13	60	14%	Easily	5.6E-03	1.07E+01	1.2E-03
Eu-155	86	177335	983	1968	7159	8%	Easily	5.2E-02	1.37E+02	1.4E-02
	105	178808	987	1976	11512	5%	Easily	5.2E-02	2.20E+02	9.0E-03

Compton continuum level and the scattered photon components will decrease as the source activity, and thus the total detector counting rate, decreases. A lowered continuum level will result in more sensitive detection of minor isotopic components. However, the expected peak areas will also decrease as the source activity declines. The measurement sensitivity increases with total counting time. For the design basis 30 R/hr drum the system detection limits would drop by factors of 7 to 10 with counting times of 50,000 seconds (14 hours) and 100,000 seconds (24 hours) respectively. For the limited number of RH-TRU drums to be processed, counting times of a day or so are probably not prohibitive.

In any NDA technique that uses gamma-ray spectral measurements to assay bulk samples, proper correction for gamma-ray attenuation in the assayed matrix can be critical to the success of the method, and can contribute strongly to the overall uncertainty of the assay. This is particularly true when the energy of the gamma-rays to be assayed is low (less than about 300 keV). Several approaches have been used successfully in similar situations,[8] including transmission source corrections, Monte Carlo modeling, relative efficiency calculations based on multiple detected gamma-ray lines, and geometric calculations. Since the actual waste packages for the CC104/107 RH-TRU wastes are small (1 ft^3), the contents relatively well defined, and the gamma-ray energies of primary interest are above about 600 keV, the contribution of the assumed attenuation corrections to the total DGS measurement uncertainty is expected to be acceptably low. The validity of this expectation is supported by the following scoping calculation.

For a different gamma-ray system for assay of TRU isotopic ratios in contact-handled (CH) drums, a review was conducted of the CH-waste drum contents, and a set of representative tables of gamma-ray mass attenuation coefficients calculated as a function of energy.[9] The waste matrix descriptions for the CH-handled combustible and mixed metals match closely our understanding of the CC104/107 RH-TRU waste. Thus the energy-dependent mass attenuation coefficients for these matrices were chosen for scoping calculations to evaluate the total magnitude and overall uncertainty contribution of the matrix attenuation correction for the design basis RH-TRU case.

The waste pails used to package CC104/107 wastes are 18.75 cm in radius. For an isotropic angular source distribution, this seems to be an appropriate attenuation pathlenght to use for correction calculations; however, the fan-shaped collimator suggested for the DGS allows a maximum path length through the matrix of 22 cm.

Although there are a number of techniques that could be employed to measure the effect of matrix attenuation on the DGS results, some initial calculations that assumed that no measured corrections to the DGS data were performed to guide the development of improved attenuation correction techniques. For these calculations it was presumed that each spectral result would be "blindly" corrected

using the mass attenuation coefficients of reference 9, the overall average waste density computed from INEL storage records, and a transmission path equal to the radius of the pails used to package waste in the 30-gal RH-TRU drums. The first set of calculations computed the appropriate attenuation correction for a set of gamma-ray lines ranging in energy from 600 keV (^{125}Sb) to 1332 keV (^{60}Co). Correction factors were calculated for the "average" set of waste densities and the assumed attenuation length of 18.75 cm, for a minimum waste density and an attenuation length of 18.5 cm, and for a maximum waste density and a maximum attenuation length of 22 cm. Attenuation correction factors were calculated both for the absolute correction of each gamma-ray to provide a total activity estimate, and for the correction of isotopic ratios relative to the 1332 keV line of ^{60}Co. The results are presented in Table 5.

Table 5. Calculation of matrix attenuation corrections for minimum, average, and maximum attenuation conditions for both combustible and noncombustible waste matrices

Combustible Matrix			*At Average Density*		*At Max Density*		*At Min Density*	
Isotope	*E (keV)*	*Att Coef*	*Corr Factor*	*Relative to 1332*	*Corr Factor*	*Relative to 1332*	*Corr Factor*	*Relative to 1332*
Sb-125	600	0.0919	1.24	1.06	2.27	1.22	1.07	1.02
	636	0.0879	1.23	1.05	2.20	1.18	1.07	1.02
Cs-137	662	0.087	1.23	1.05	2.19	1.18	1.07	1.02
Eu-154	723	0.0818	1.21	1.04	2.10	1.13	1.06	1.01
	1005	0.0726	1.19	1.01	1.96	1.05	1.06	1.00
	1274	0.0663	1.17	1.00	1.86	1.00	1.05	1.00
Co-60	1173	0.0663	1.17	1.00	1.86	1.00	1.05	1.00
	1332	0.0663	1.17	1.00	1.86	1.00	1.05	1.00

Noncombustible Matrix			*At Average Density*		*At Max Density*		*At Min Density*	
Isotope	*E (keV)*	*Att Coef*	*Corr Factor*	*Relative to 1332*	*Corr Factor*	*Relative to 1332*	*Corr Factor*	*Relative to 1332*
Sb-125	600	0.0758	1.49	1.12	3.16	1.34	1.15	1.04
	636	0.0739	1.47	1.11	3.09	1.31	1.14	1.04
Cs-137	662	0.0726	1.46	1.11	3.05	1.29	1.14	1.04
Eu-154	723	0.0696	1.44	1.09	2.94	1.24	1.14	1.03
	1005	0.0595	1.37	1.04	2.60	1.10	1.12	1.01
	1274	0.0528	1.32	1.00	2.38	1.01	1.10	1.00
Co-60	1173	0.055	1.34	1.01	2.46	1.04	1.11	1.01
	1332	0.0522	1.32	1.00	2.37	1.00	1.10	1.00

As expected, the differences between the assumed average correction and those at the minimum and the maximum attenuation conditions are greatest for the noncombustible matrix drums, and for the lower energy gamma-rays. For the maximum attenuation conditions the absolute attenuation correction factor for the ^{125}Sb 600 keV line would be underestimated by the average correction by a factor of about 2 (3.16/1.49) while at the minimum density conditions the absolute correction factor relative to the assumed

average would be overestimated by about 30% (1.15/1.49). (An overestimate of the attenuation correction factor would result in an overestimate of the absolute activity.) However, note that for this worst case scoping calculation, the correction for the ^{125}Sb to ^{60}Co activity ratios could be determined to within a factor of about 20%. For the combustible matrix drums the over and under estimates are of similar magnitude.

The results in Tables 5 and additional calculations using a Monte Carlo simulation[7] suggest that proper correction for matrix attenuation is not an overwhelming problem in the DGS measurements. If no attempt is made to calculate drum-specific attenuation corrections, other than to provide an estimated waste matrix density, the absolute correction for ^{137}Cs in the combustible matrix drums would have about a 1% high bias and a relative standard deviation of about 6%. The 95% confidence limits of this distribution are at about ±11%. As expected because of its higher gamma-ray energy, the results are somewhat better for ^{60}Co. The absolute correction for ^{60}Co in the combustible matrix drums would have about a 1% high bias (1.18/1.17) and a relative standard deviation of about 4%. The 95% confidence limits of the ^{60}Co distribution are at about ±9%. These results suggest that the ^{137}Cs/^{60}Co ratio can be determined with a bias of less than 1% and a relative standard deviation of about ±7%. The estimated results for the noncombustible matrix drums are somewhat less well predicted; however, the Monte Carlo simulation suggests that the attenuation correction for the137Cs/60Co ratio in these drums would have a high bias of about 2% and a relative standard deviation of about ±23%.[7]

The previous scoping calculations assumed that drum weight (and thus calculated matrix density) was the only drum-specific parameter used to predict the matrix attenuation correction factors. Although the results of these scoping calculations suggest adequate corrections can be made without additional measured data, there are techniques that can improve the estimated attenuation corrections for specific drums. Since the SYTH simulation predicts that a number of multiple lines from multi-gamma-ray emitting isotopes will be detected (for example the 123, 723, 873, 1005, and 1274 keV lines of ^{154}Eu) in the baseline drum, these results can be used to calculate a drum-specific attenuation correction directly. Since the gamma-ray emission probabilities for ^{154}Eu are well known, and the unattenuated detection efficiency will be determined, the multiple line results can be used to solve (probably most efficiently by iteration) the standard matrix attenuation equation for the product $\mu_i x_{eff}$ and the estimated standard deviation on this product. (To solve for both the value and its error requires a minimum of three points.) These measured results can then provide improved attenuation corrections; however, if the required multiple lines cannot be detected in certain drums then the previous scoping calculation defines the applicability of default corrections.

The uncertainty in the radionuclide results can now be estimated. The activity (A) in bequerels (d/s) in a waste barrel of isotope j computed from a gamma-ray line of energy i can be written as:

$$A_{ij} = \frac{(N_i)(C_{ai})}{(\varepsilon_i)(BR_{ij})}$$

where:

N_i = the measured photopeak counting rate at energy i (c/s)
C_{ai} = the matrix self absorption correction factor at energy i
ε_i = the detection efficiency of the system for a nonattenuating matrix (c/γ)
BR_{ij} = the gamma-ray emission probability for (i from isotope j

Using standard error propagation techniques, the standard deviation in A_{ij} can be estimated as (deleting the i and j subscripts for convenience):

$$\frac{\sigma_A}{A} = \sqrt{\left(\frac{\sigma_N}{N}\right)^2 + \left(\frac{\sigma_{C_a}}{C_a}\right)^2 + \left(\frac{\sigma_\varepsilon}{\varepsilon}\right)^2 + \left(\frac{\sigma_{BR}}{BR}\right)^2}$$

where the σ_i values are the estimated standard deviations of the parameters.

Estimated relative standard deviations and systematic errors for these parameters are available from experience, modeling, and nuclear data. Analysis of the SYNTH-generated spectrum provides estimates of N_i and σ_N (see Table 4). The matrix self-absorption correction values and their errors are available from the previous section. Experience with similar systems suggests that, in the energy range of interest, absolute nonattenuated detection efficiency values can be determined to an overall precision of less than 15%; while relative efficiency values (for the $^{60}Co/^{137}Cs$ ratio) can be much better determined, probably to ±3%. Gamma-ray emission probabilities and their associated errors are available from the nuclear literature. Their associated errors are generally 0.1% or less.

Similarly, for the isotopic activity ratios (R_{jk}) of isotope j to isotope k (using gamma-ray lines at energies of i and l respectively):

$$R_{jk} = \left(\frac{N_i}{N_l}\right)\left(\frac{C_{a_i}}{C_{a_l}}\right)\left(\frac{BR_{kl}}{BR_{ij}}\right)\left(\frac{\varepsilon_l}{\varepsilon_i}\right)$$ or, replacing $\frac{\varepsilon_l}{\varepsilon_i}$ with the relative efficiency $R\varepsilon_{il}$ and the ratio $\frac{C_{a_l}}{C_{a_i}}$ with the differential self absorption correction ratio DA_{il} then:

$$R_{jk} = \left(\frac{N_i}{N_l}\right)\left(\frac{BR_{kl}}{BR_{ij}}\right)\left(R_{\varepsilon il}\right)\left(DA_{il}\right)$$ and the estimated standard deviation computed as:

$$\frac{\sigma_{R_{jk}}}{R_{jk}} = \left[\left(\frac{\sigma_{N_i}}{N_i} \right)^2 + \left(\frac{\sigma_{N_l}}{N_l} \right)^2 + \left(\frac{\sigma_{DA_{il}}}{DA_{il}} \right)^2 + \left(\frac{\sigma_{R\varepsilon_{il}}}{R\varepsilon_{il}} \right)^2 + \left(\frac{\sigma_{BR_{kl}}}{BR_{kl}} \right)^2 + \left(\frac{\sigma_{BR_{ij}}}{BR_{ij}} \right)^2 \right]^{1/2}$$

Computing the estimated standard deviations for the absolute concentration of ^{137}Cs, ^{60}Co, and the activity ratio of $^{60}Co/^{137}Cs$ using the equations and data above yields an estimated relative standard deviation for the combustible matrix drums for the absolute concentrations of ^{137}Cs and ^{60}Co respectively of 18% and 17%, and of 12% for the activity ratio. For the noncombustible matrix drums these values are 24%, 20%, and 23% respectively.

ORIGEN INVENTORY CALCULATIONS

Whether the NDA technique of direct gamma-ray spectroscopy to quantify the fission and activation product content, or active neutron assay to determine the fissile material content are employed to characterize CC104/107 RH-TRU wastes, inventory calculations based on the known irradiation history of the fuel pins processed to produce the wastes in a particular drum will be required to specify total drum content. The expected uncertainty of these inventory calculations can be an important uncertainty contributor to the overall drum content determinations.

There is a paucity of published comparisons of calculated-versus-measured inventory results for the EBR-II reactor. While it is likely that such comparisons have been done, they do not appear in the open literature. Thus, all assumptions about the adequacy of ORIGEN fuel inventory predictions for EBR-II must be drawn by parallel to published data on light water reactors (LWRs). There can be a number of hazards in this approach. Just about every thing that one can think of that might affect inventory calculations -- fuel materials, fuel matrix, core size, neutron spectrum, flux and power densities, etc. -- of EBR-II are completely different from those of LWRs. However, the basic calculational techniques remain the same. Thus, *if the core neutronics of EBR-II are known at least as well as those for the LWRs studied, and this knowledge is translated into a proper cross-section library*, then inventory calculations for EBR-II should have uncertainties similar to those in the published set of LWR comparisons. Certain LWR comparison results are presented in this section. From the LWR data set uncertainty contributions to the characterization of CC104/107 RH-TRU wastes are estimated.

Inventory calculations performed using the ORIGEN-S code have been compared with radiochemically measured results for medium to high burnup fuel samples (nominally 30 GWD/MTU) from the US Yankee Rowe, Turkey Point, and H. B. Robinson LWRs.[10] In each case, the modeled power

level was adjusted to predict the radiochemically-measured atom percent burnup as determined from $^{148}Nd/^{235}U$ ratios. Comparison values for TRU inventories are reported for all three test cases; however, fission product comparisons are only reported for the H. B. Robinson assemblies. No inventory comparison results are reported for activation products. For all three reactors, the calculated ^{239}Pu concentrations were 3% to 6% greater than the measured. Conversely, the minor Pu isotopes (240-242) were generally under predicted 5% to 16%. The H. B. Robinson fission product comparison data is complicated by an analysis problem that biased the measured fission product concentration low by 15% to 25%. When corrected for a -20% analytical bias, the ORIGEN predictions agreed with the measured results to within -5.2% (for ^{137}Cs) to +14.9% (for ^{129}I). No measurement precisions were specified.

In the wake of the reactor accident at the Three Mile Island Unit 2 (TMI-2) power station a number of inventory calculations were performed to determine the core inventory.[11] TMI-2 shutdown occurred after very little fuel burnup (core average 3175 MWD/MTU). Inventory calculations were initially performed for the full core average, for each of three initial fuel enrichments, and for a set of multiple (1239) fuel zones grouped according to burnup and enrichment. When compared to measured concentration data on eight specific fuel pellets drawn from known positions on the core periphery (the core center having been destroyed), even the most detailed of these calculations differed from measurements by as much as 100%.[12] To better validate the inventory calculations, additional ORIGEN2 calculations were performed with the modeled power levels adjusted to match the radiochemically-measured burnup of each pellet. These results are reproduced in Table 6.

Table 6. Measured-to-calculated inventory ratios on eight specific fuel pellets from the TMI-2 reactor[12]

Isotope	*Measured/ Calculated*	*Stand Dev*[a]	*Isotope*	*Measured/ Calculated*	*Stand Dev*[a]
^{238}Pu	0.86	0.17	^{90}Sr	0.99	0.02
^{239}Pu	0.90	0.09	^{106}Ru	0.96	0.08
^{240}Pu	0.89	0.09	^{125}Sb	0.43	0.04
^{241}Pu	1.05	0.20	^{129}I	0.72	0.04
Total Pu	0.90	0.09	^{134}Cs	0.86	0.27
Total Kr	0.954	0.014	^{137}Cs	1.021	0.009
Total Xe	0.95	0.04	^{144}Ce	1.07	0.02
			^{154}Eu	0.63	0.06
			^{155}Eu	0.61	0.06

[a] The standard deviations reported are the standard deviations of the eight sets of analytical measurements.

For this set of fuel pellets, the actinides and the direct fission products (^{90}Sr, ^{106}Ru, ^{137}Cs, and ^{144}Ce) are generally well predicted when the measured pellet burnup is matched. The exceptions are ^{129}I and ^{125}Sb. Iodine-129 is extremely long-lived and was thus present in very small concentrations in these low burnup samples. The reason for the poor agreement on ^{125}Sb is not understood. Those nuclides with strong radiative capture coupling (^{154}Eu, ^{155}Eu, and to a lesser extent ^{134}Cs) are less well predicted,

probably due to differences between the modeled and actual neutron spectrum, since the neutron spectral shape is more important in capture than in fission.

Through unpublished communications, we are aware that the version of ORIGEN (ORIGEN-R) in use at ANL-E for calculation of EBR-II subassembly inventories has been tested against experimental results, and "compared favorably." Additionally, when used to predict inventories and decay heat generation rates for standard PWR and LMFBR problems, the ANL-E values agreed within about 5% with those published by ORNL using ORIGEN2. Thus it appears reasonable to assume that ORIGEN-based inventory calculations for EBR-II can be computed with uncertainties on the order of those published for LWRs. However, the apparent lack of open, peer-reviewed literature to support this view is disturbing.

Proper inventory calculations require careful attention to core neutronics and exposure considerations. Assuming that care is taken, reasonable estimates of the uncertainty contribution of ORIGEN inventory calculations to the overall uncertainty in RH-TRU characterization, drawn from published data on PWR comparisons are as follows. Direct fission product nuclides (such as ^{137}Cs) can probably be predicted to within ±5%. Specific TRU nuclides are generally predicted to ±20%, with ^{239}Pu and total Pu somewhat better predicted at ±10%. Strongly radiative capture coupled nuclides (such as ^{154}Eu and ^{134}Cs) may be less well predicted. Uncertainties of ±30% appear reasonable.

Although there is little direct comparison data to evaluate the uncertainty in the prediction of activation product inventories (^{60}Co for example), they will probably be determined less accurately than the strongly capture-coupled nuclides. An uncertainty estimate for activation product inventory calculations of ±50% will be used in this scoping work.

UNCERTAINTY ESTIMATES

Direct Gamma-ray Spectroscopy and ORIGEN

From estimates of the expected standard deviation for determinations by DGS and expected uncertainty estimates for the ORIGEN inventory calculations, an uncertainty in the determined contents of the design basis drum can be estimated. It is assumed that an ORIGEN inventory calculation has been performed that matches the measured $^{137}Cs/^{60}Co$ ratios, and further matches, within the expected calculational uncertainties, the ratios of other detected fission products to ^{137}Cs. These adjusted calculations then predict the fission and activation product content per gram of ^{235}U (or other fissile nuclide depending on fuel type). The ORIGEN calculations then predict the concentration of all the fission products and transuranics per gram of ^{235}U. Additionally calculated is the specific activity of ^{60}Co

per gram of activated stainless steel (SS) cladding. The DGS measurements provide the total activity of ^{137}Cs and ^{60}Co in the waste drum. The total drum contents are then determined from the calculated amount of ^{235}U and irradiated SS in the assayed drum. The relevant equations are:

$$G_{U-235} = \frac{(A_{Cs-137})}{(SA_{Cs-137})} \quad \text{and} \quad \frac{\sigma_{G_{U-235}}}{G_{U-235}} = \sqrt{\left(\frac{\sigma_{A_{Cs-137}}}{A_{Cs-137}}\right)^2 + \left(\frac{\sigma_{SA_{Cs-137}}}{SA_{Cs-137}}\right)^2}$$

and $$G_{SS} = \frac{(A_{Co-60})}{(SA_{Co-60})} \quad \text{and} \quad \frac{\sigma_{G_{SS}}}{G_{SS}} = \sqrt{\left(\frac{\sigma_{A_{Co-60}}}{A_{Co-60}}\right)^2 + \left(\frac{\sigma_{SA_{Co-60}}}{SA_{Co-60}}\right)^2}$$

where: G_i = grams of i in assayed drum
A_j = DGS-measured activity of j in Curies
SA_j = ORIGEN-calculated specific activity of j per gram of i
and the associated uncertainties are self explanatory.

Substitution of the uncertainty estimates from the previous sections into the simple error prorogation equations suggests the drum inventories of ^{235}U and SS can be predicted to about ±22% and ±55% respectively. These values are for noncombustible matrix drums; however, comparable values for combustible matrix drums are similar (±21% and ±53% respectively). To estimate the uncertainty for the determination of other unmeasureable nuclides the estimated relative error in the ^{235}U content would be propagated with the estimated error in the ORIGEN-calculated specific activity. For example, the estimated uncertainty in the waste drum content of ^{63}Ni, an unmeasureable beta-emitting nuclide induced in activated SS, would be about ±75%.

PAN Active Assays and ORIGEN Calculations

To characterize fully the content of RH-TRU drums using the PAN system will require DGS results for the $^{60}Co/^{137}Cs$ activity ratios, and active PAN assay, and an ORIGEN calculation that matches the DGS-predicted ^{137}Cs and ^{60}Co activity ratios. PAN system active assays provide the total fissile content of a waste drum in grams. ORIGEN inventory calculations then provide the fissile material ratios and the estimated fission and activation product concentration ratios. The total amounts of activated SS in a waste drum will rely on the measured $^{60}Co/^{137}Cs$ ratio.

During testing of the PAN system active assay on Pu-containing drums the total fissile contents were determined to relative standard deviations of about ±1.5%.[b] However, the effect of the waste matrix on these results can be substantial. For well-behaved waste matrices total uncertainties of ±10% have been determined.[5] For more difficult matrices disagreements between passive and active assay result of nearly a factor of 10 were noted. It seems reasonable that over the limited set of drums in inventory, and

the relatively benign matrices, PAN active assays could be performed to estimated uncertainties of ±15%. Using standard error propagation techniques the estimated uncertainties (1σ) in the various drum contents using this approach of ORIGEN, PAN, and DGS would be about ±18% in the total Pu and ^{235}U contents, and ±53% in the total SS content.

SUMMARY

A variety of modeling techniques were employed to estimate the expected performance of two NDA approaches to the characterization of the INEL's RH-TRU wastes. These techniques are 1) direct assay of the drum fissile material content using a Passive/Active Neutron (PAN) assay unit, and 2) determination of the fission and activation product content of the waste drums [direct gamma-ray spectrometry (DGS)], coupled with calculation of the fissile material content using the known irradiation history and any of several available fission product inventory codes (e.g. ORIGEN).

Passive/Active Neutron (PAN) Assay

MCNP modeling techniques investigated the usefulness of the INEL's passive/active neutron (PAN) assay system for the RH-TRU waste characterization. Both active and passive assay modes were evaluated. In order to avoid gamma-ray pile up events from interfering with the PAN system neutron counts, a shield was designed to limit the surface dose rate of the samples to ≤ 50mR/hr. This required a lead overpack for the 113-liter RH-TRU drums with a wall thickness of about 4.5 cm. This size of overpack can be accommodated within the existing PAN cavity; however, the existing drum rotator may need to be replaced to accommodate the increased weight of drum and shield.

The PAN passive mode assays lack the sensitivity required for RH-TRU characterization. Active interrogation modeling predicts detection limits of 0.06 g ^{235}U and 0.04 g ^{239}Pu. These appear adequate for the vast majority of the INEL's RH-TRU drums. However, variations in waste matrix and loading in actual rather than modeled drums can have an important effect on these estimated detection limits.

Direct Gamma-ray Spectrometry (DGS)

MCNP modeling aided in the design of a heavily shielded and collimated gamma-ray spectrometer for direct assay of the fission and activation product content of RH-TRU drums. The collimator was sized to yield a detector counting rate of about 50,000 counts/second when a design-basis RH-TRU drum with a surface dose rate of 30 R/hr was assayed.

Detection limit estimates, developed from a synthetic spectrum generated to reflect the modeled measurement conditions, suggest that ^{60}Co, ^{125}Sb, ^{134}Cs, ^{137}Cs, ^{154}Eu, and ^{155}Eu should be detected reliably (95% CL) in RH-TRU drums. The analysis predicts that multiple gamma-ray lines from ^{154}Eu should be reliably detected. These lines could be used to determine drum-specific matrix attenuation corrections.

Even without the presence of sufficient gamma-ray lines to allow drum-specific attenuation corrections to be determined, attenuation corrections can be calculated. With no more information than the matrix type (combustible of noncombustible) and the gross drum weight (from which the average matrix density is estimated), attenuation corrections can be calculated with a relative standard deviations of about 10% to 20% in combustible matrix drums, and 20% to 25% in noncombustible matrix drums.

The DGS modeling further predicted relative standard deviation expectations for the absolute concentrations of ^{137}Cs and ^{60}Co, and for the ratio of the $^{60}Co/^{137}Cs$ activity ratio. In a combustible matrix drum these respective values are 20%, 18%, and 16%. Comparable values for a noncombustible matrix drum are 24%, 21%, and 16%.

ORIGEN Inventory Calculations

There are no published data comparing ORIGEN inventory estimates with measurements for EBR-II problems. Assuming the EBR-II case can be calculated at least as well as those for LWRs, it seems likely that burnup-matched ORIGEN calculations can predict total TRU-to-uranium ratios to about ±10%, direct fission product-to-uranium ratios to about ±5%, and the activation product content of stainless steels to about ±50%.

CONCLUSIONS

The analysis in this report estimates that the content of a design basis RH-TRU drum could be determined by a combination of DGS, PAN system active assays, and ORIGEN inventory calculations to estimated relative standard deviations of ±18 to 25% in the total Pu and total ^{235}U content, ±20 to 25% in the direct fission product activities, and ±55 to 75% in the activation product content. This work suggests that both Direct Gamma-ray Spectrometry and Passive/Active Neutron Assay when coupled with ORIGEN inventory calculations show promise for the characterization of the radionuclide content of the INEL's CC104/107 RH-TRU wastes.

ACKNOWLEDGEMENTS

The authors gratefully acknowledge the assistance, support and attention provided this project by C. R. Tyler. This work was supported by the U.S. Department of Energy, Assistant Secretary for Environmental Management under DOE Idaho Operations Office Contract DE-AC07-94ID13223.

REFERENCES

1. M. J. Bell, "ORIGEN -- The ORNL Isotope Generation and Depletion Code," *ORNL-4626* (May 1973).
2. J. F. Briesmeiser, "MCNP -- A General Purpose Monte Carlo Code for Neutron and Photon Transport, Version 3A," *LA-7396-M Rev. 2* (1986).
3. W. K. Hensley, A. D. McKinnon, H. S. Miley, M. E. Panisko, and R. M. Savard, "SYNTH: A Spectrum Synthesizer," *Proceedings of the 35th Annual Meeting of the Institute of Nuclear Materials Management*, Naples, FL (July 17-20, 1994).
4. H. D. Killian and P. D. Randolph, "Stored Waste Examination Pilot Plant (SWEPP) Nondestructive Examination/ Assay (NDE/NDA) Capability Study for RH-TRU Waste Stored at the RWMC," *INEL-95/255*, October 1995.
5. W. Y. Yoon, G. K. Becker, and Y. D. Harker, "Monte Carlo Neutron and Photon Modeling and Verification Calculations for the Stored Waste Examination Pilot Plant Passive/Active Neutron Assay System," *CONF-940216, Proceedings of the NonDestructive Assay and NonDestructive Examination Waste Characterization Conference*, Pocatello, Idaho, February 14-16, 1994.
6. L. A. Currie, "Limits for Qualitative Detection and Quantitative Determination," *Analytical Chemistry, 25*, #3, March 1963.
7. J. K. Hartwell, W. Y. Yoon, H. K. Peterson, and C. R. Tyler, "A Preliminary Evaluation of Certain Candidate NDE/NDA Techniques for RH-TRU Characterization," *INEL-96/0233*, in preparation.
8. D. Reilly, N. Ensslin, H. Smith, Jr., and S. Kreiner, "Passive Nondestructive Assay of Nuclear Materials," *NUREG/CR-5550*, March 1991.
9. W. Serrano, "Drum Matrix Mass Attenuation Coefficients," *INEL Engineering Design File RWMC-EDF-722*, March 14, 1994.
10. J. C. Ryman et al., "Fuel Inventory and Afterheat Power Studies of Uranium-fueled Pressurized Water Reactor fuel Assemblies Using the SAS-2 & ORIGEN-S Modules of SCALE with an ENDF/B-V Updated Cross Section Library," *NUREG/CR-2397*, September 1982.
11. B. G. Schnitzler and J. B. Briggs, "TMI-2 Isotopic Inventory Calculations," *EGG-PBS-6798*, August 1985.
12. D. W. Akers and B. G. Schnitzler, "Verification of the ORIGEN2 Code Analysis for the TMI-2 Reactor Core," *EGG-34487*, 1982.

Poster Presentations

FABRICATING DEFENSIBLE REFERENCE STANDARDS FOR THE NDA LAB

R.N. Ceo and P.K. May
Analytical Services Organization
Oak Ridge Y-12 Plant[a]
Oak Ridge, TN 37831-8189

ABSTRACT

Nondestructive analysis (NDA) is performed at the Oak Ridge Y-12 Plant in support of the enriched uranium operations. Process materials are analyzed using gamma ray- and neutron-based instruments including segmented gamma scanners, solution assay systems, and an active well coincidence counter. Process wastes are also discarded based on results of these measurements. Good analytical practice, as well as applicable regulations, mandates that these analytical methods be calibrated using reference materials traceable to the national standards base.

Reference standards for NDA instruments are not commercially available owing to the large quantities of special nuclear materials involved. Instead, representative materials are selected from each process stream, then thoroughly characterized by methods that are traceable to the national standards base.

This paper discusses the process materials to be analyzed, reference materials selected for calibrating each NDA instrument, and details of their characterization and fabrication into working calibration standards. Example calibration curves are also presented.

INTRODUCTION

Standards for nondestructive analysis (NDA) are generally not available commercially due to the large quantities of special nuclear materials (SNM) involved. National standards organizations such as New Brunswick Laboratory and the National Institute of Science and Technology are also unable to handle large SNM quantities due to security and cost considerations. Operators of NDA facilities must calibrate their instruments using reference materials they have fabricated themselves. These reference materials are generally characterized by chemical analyses which are in turn calibrated with certified or standard reference materials. The "homemade" reference materials are therefore indirectly traceable to the national standards base.

At the Oak Ridge Y-12 Plant, enriched uranium operations generate several distinct process material streams. These process streams include pure and impure uranium oxides (UO_3, U_3O_8), uranium tetrafluoride (UF_4), aqueous and organic uranium-bearing solutions, combustible contaminated waste and

---

[a] The Oak Ridge Y-12 Plant is managed by Lockheed Martin Energy Systems, Inc. for the U.S. Department of Energy under Contract DE-AC05-84OR21400

used HEPA filters, ash, and acid-leached ash residue. The NDA Facility at Y-12 uses a complement of gamma-ray- and neutron-based instruments to analyze these materials. Materials such as UO_3, U_3O_8 , and UF_4 which are opaque to gamma radiation, are analyzed using the active well coincidence counter (AWCC), a neutron technique. Less-dense materials are analyzed using transmission-corrected gamma spectrometry.

For best results, it is important to use standards that are physically and chemically similar to the "unknowns." In Y-12's NDA Facility, the instruments are calibrated using selected process materials that have been thoroughly characterized by chemical methods. The reference materials are selected so that they represent the concentration range expected in the overall process stream. Because the reference materials are taken from the same process stream, they are chemically and physically similar to the items we wish to analyze.

URANIUM-BEARING SOLUTIONS

In Y-12 enriched uranium operations, process solutions contain uranium in aqueous acids or organic extractants. These solutions are routinely analyzed using the Solution Assay System (SAS), a form of transmission-corrected gamma spectrometer. The solutions to be analyzed by this technique do not contain any chemical species that are likely to interfere with gamma-ray analysis, so instrument response is assumed to be fairly matrix-independent. Suitable reference standards can be prepared from uranyl nitrate, $UO_2(NO_3)_2 \bullet 6H_2O$, dissolved in nitric acid and diluted to the appropriate concentrations.

A batch of pure uranyl nitrate highly enriched in ^{235}U was selected, thoroughly blended, and sampled in triplicate. Each sample was analyzed by thermal ionization mass spectrometry to determine its isotopic composition, and by Davies Gray titration and X-ray fluorescence to determine its total uranium content. A stock solution 0.23 g U/mL was prepared using nitric acid and diluted to make seven working solutions of appropriate U concentrations that are 4 M in HNO_3. All the working solutions were prepared as 500 ml batches to provide ample material for chemical analysis. Each working solution was divided into four equal parts -- three parts were submitted for X-ray fluorescence analysis and the fourth was reserved for use as a reference standard. Figure 1 shows the SAS instrument response curve for these reference solutions. As shown in the plot, the instrument is calibrated in the range between 9.3×10^{-4} and 2.2×10^{-1} g ^{235}U per mL.

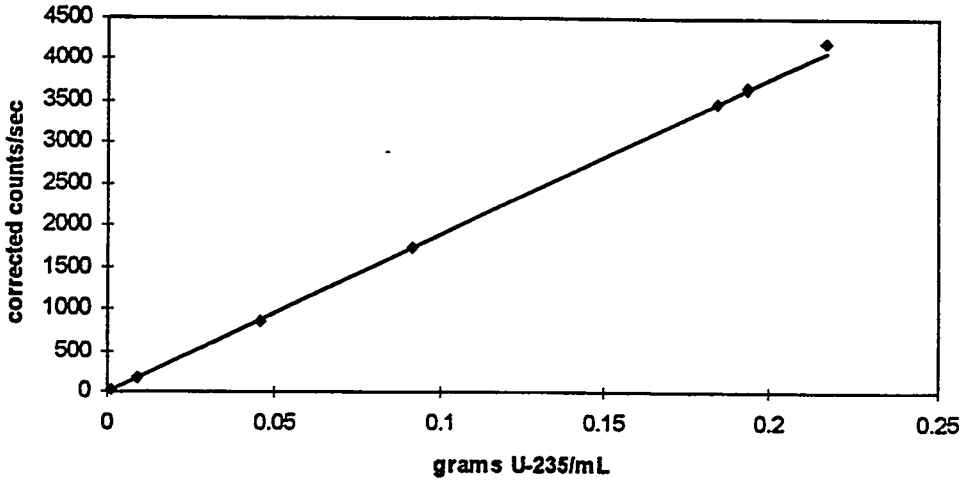

Figure 1: SAS Instrument Response Curve. The instrument is calibrated between 9.3 X 10^{-4} and 2.2 X 10^{-1} g U-235 per mL.

ASH AND RESIDUE

Ash and residue are generated from incineration of combustible contaminated wastes. NDA measurements are made on these materials to determine whether it is economically feasible to recover uranium from the ash by acid leaching. NDA measurements are also made on leached residues to verify that uranium recovery is complete. These measurements are made using the can scanner, a small segmented gamma scanner. The can scanner is calibrated using several containers filled with ash and residue which have varying uranium concentrations. These reference materials were selected because their uranium contents were similar to the expected contents of the "unknown" residues.

After the appropriate materials were selected, they were thoroughly blended and sampled in triplicate. The samples were analyzed by thermal ionization mass spectrometry to determine the isotopic composition, and by X-ray fluorescence to determine the total uranium content. Figure 2 shows the can scanner's instrument response curve for these reference residues. This instrument is calibrated for residues containing between 14 g and 398 g ^{235}U.

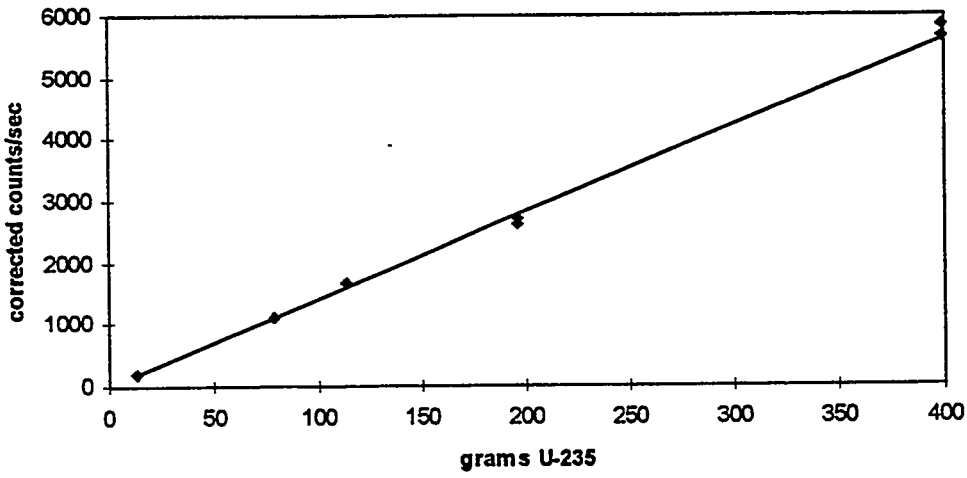

Figure 2: Can Scanner Instrument Response Curve. This instrument is calibrated for residues containing between 14 g and 398 g ^{235}U.

COMBUSTIBLE CONTAMINATED WASTE

Enriched uranium operations generate combustible contaminated wastes such as discarded protective clothing, paper towels, building materials, and used HEPA filters. Because these materials vary widely in composition, and because their uranium loading is never uniform, they are not suitable themselves as reference materials. Instead, we have constructed a set of surrogate contaminated wastes for use as calibration standards.

A batch of UO_3 , highly enriched in ^{235}U, was converted to U_3O_8 by heating to 900° C in the presence of steam. We converted UO_3 rather than using process U_3O_8 since the UO_3 is known to be free of contaminants. The resulting pure U_3O_8 was finely ground, passed through a #50 sieve, and sampled in triplicate. After grinding and sampling, weighed amounts of U_3O_8 were sprinkled onto blotter paper squares that had been coated with spray adhesive. A second sheet of blotter paper was fastened over the first so that the U_3O_8 was laminated between the blotter paper sheets producing a package 30.5 cm on a side. Several such laminated packages were fabricated, some with 5 grams of oxide and some with 25 grams. For the 5-gram packages, the uranium oxide areal density was 7.8 mg cm^{-2}, and for the 25-gram packages, the uranium oxide areal density was 39 mg cm^{-2}. Each package was put into a plastic bag and sealed with plastic tape. Each plastic bag was rolled and placed into a cardboard mailing tube so that each tube was loaded at the top, middle, or bottom with uranium.

During calibration, the cardboard tubes are arranged in a lightweight plastic rack within a 208-L steel drum. By varying the number and positions of the tubes, different loadings of uranium can be achieved. This technique allows us to simulate the random loading of uranium within drums of combustible process waste. Figure 3 shows a typical calibration curve for combustible wastes on the barrel scanner. The instrument is calibrated in the range of 3.8 grams ^{235}U to 196 grams ^{235}U.

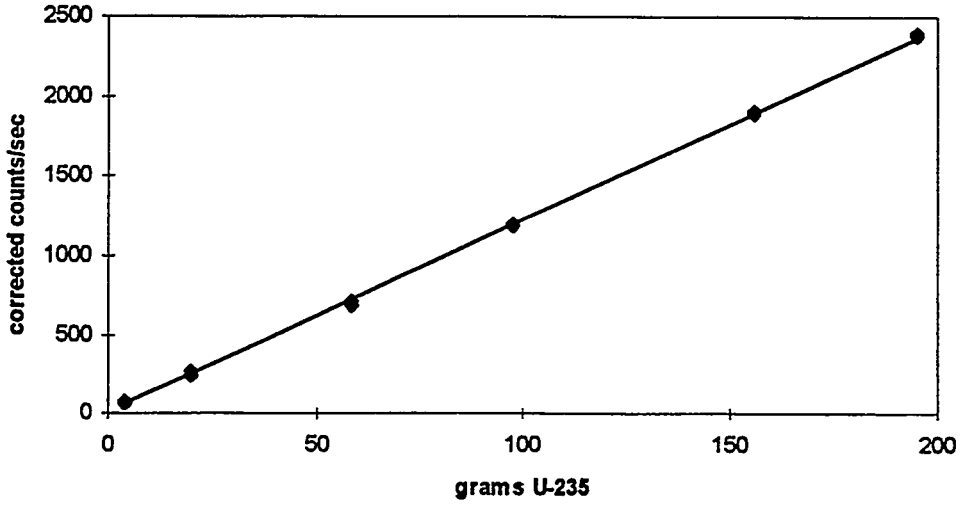

Figure 3: Barrel Scanner Calibration. The instrument is calibrated in the range of 3.8 grams ^{235}U to 196 grams ^{235}U.

URANIUM OXIDES

Uranium oxides are generated as recyclable process wastes during certain casting operations. These wastes are dense, opaque to gamma radiation, and generally contain significant levels of impurities. They may be lumpy and inhomogeneous. Because of these characteristics, process uranium oxides are analyzed using the active well coincidence counter (AWCC). AWCC instrument response is complex, and depends on several variables including material density, position in the detector chamber, and the presence of neutron-absorbing impurities. To properly analyze uranium oxides by AWCC, an item's fill height and mean density must be accurately known.

Eight batches of process U_3O_8 in full containers were selected with densities that are representative of the range of densities normally observed in U_3O_8 from the process stream. These materials were sieved and thoroughly blended. Approximately 500 cm^3 of material was removed from each container and transferred to a corresponding pre-weighed empty container, and a sample of each material was taken for chemical analysis. The new containers' weights and fill heights were determined, then they were placed in the AWCC and their contents measured. After the measurements were performed, another 500 cm^3 of material was removed from each container and transferred to the corresponding containers, more samples were taken, the weights and fill heights were redetermined, and the materials were remeasured. This process was repeated until all the material had been transferred from one container into the other; 10 batches for each container. The uranium content of each material was taken as the average of the 10 samples; the results verified that blending was effective. The mean densities of the materials were calculated from the weights, fill heights, and container diameter. The instrument response for three typical materials is shown in Figure 4; note the density dependence of the AWCC response. Other similar calibration curves were determined for UO_3 and UF_4, but these materials are purer and more uniform so the density variation between batches is negligibly small.

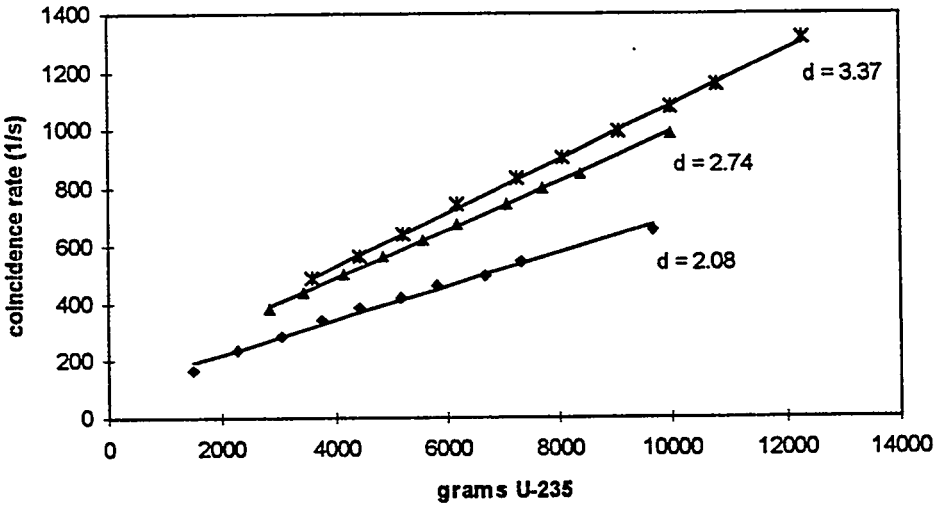

Figure 4: AWCC Calibration curves for U_3O_8 samples of different densities. Calibration range and instrument response depend on the density of the material to be analyzed.

QUALITY ASSURANCE IN THE ENRICHED URANIUM OPERATIONS NDA FACILITY

P.K. May and R.N. Ceo
Analytical Services Organization
Oak Ridge Y-12 Plant[a]
Oak Ridge, TN 37831-8189

ABSTRACT

The Nondestructive Analysis (NDA) Facility at the Oak Ridge Y-12 Plant has characterized process wastes for Enriched Uranium Operations since 1978. Since that time, over 50,000 items have been analyzed. Analysis results are used to determine whether or not recovery of uranium from process wastes is economically feasible.

Our instrument complement includes one large segmented gamma scanner (SGS), two smaller SGS, two solution assay systems (SAS), and an Active Well Coincidence Counter (AWCC). The large SGS is used for analyzing High Efficiency Particulate Air (HEPA) filters and 208-L drums filled with combustible contaminated waste. The smaller SGS are used to analyze 4-L containers of ash and leached residues. The SAS are used to analyze 125 ml bottles of aqueous or organic waste solutions that may contain uranium. The gamma-based NDA techniques are used to identify which process wastes can be discarded, and which must be recycled. The AWCC is used to analyze high-density materials which are not amenable to gamma-ray analysis.

Because of the facility's long history, we have extensive quality assurance data which demonstrate instrument performance. This paper discusses the quality assurance program developed for our facility, including instrument setup parameters and routine control sample results. This paper also presents selected quality assurance charts to illustrate how the data are interpreted. Finally, we will discuss the moving-range-of-two method used to establish our control limits.

INTRODUCTION

The Enriched Uranium Operations NDA Facility has been in continuous operation since its inception in 1978 and some 50,000 analyses have been performed. Over the facility's lifetime, quality assurance measurements have been invaluable aids for process control. Besides the obvious utility of quality assurance measurements, they are also required by the US Department of Energy (DOE) Order 5633.3b for measurement systems used for accountability purposes. The DOE order specifies that "warning" and "action" limits must be observed at ± 2 and ± 3 standard deviations from the process mean, respectively. The DOE order further specifies corrective actions for each quality assurance measurement that exceeds one of these limits. We have developed a quality assurance program for our NDA facility that is useful and complies fully with applicable DOE orders. Our quality assurance program has proven

[a] The Oak Ridge Y-12 Plant is managed by Lockheed Martin Energy Systems, Inc.for the U.S. Department of Energy under Contract DE-AC05-84OR21400

its value by signaling instrument failures, calibration problems, and even variations in processes conducted in nearby areas.

CONTROL PARAMETERS

Gamma-ray Instruments

Our NDA Facility's instrument complement includes one large segmented gamma scanner (SGS), two smaller SGS, and two solution assay systems (SAS). All these transmission-corrected gamma-ray instruments operate on the same basic principles, so their control parameters are similar. These parameters are measured during daily startup to ensure that no significant change has occurred that would require corrective action. After the startup parameters have been evaluated, two control samples are analyzed for each instrument - one at either end of the instrument's calibration curve.

Background Radiation Test

The first control parameter to be measured is the gamma-ray background. A background spectrum is acquired, and the counts over 182 to 190 keV (the U-235 region of interest or ROI) are totaled. The background count is plotted on a control chart and evaluated. Unexpected variations could indicate contamination of the detector or its shield, or the presence of a sample in the detector's field of view. If such a condition is identified, it can be quickly corrected before proceeding with startup. The computer uses the same background count to correct sample results.

Instrument Gain and Offset Stability

Next, the spectrum of the gamma-ray transmission source is used to check amplifier gain and analog-to-digital converter (ADC) zero offset. ^{169}Yb emits gamma rays at 177 keV and 198 keV; spectral positions of these gamma rays are the basis for these checks. The number of channels between the two peak centroids is used to calculate amplifier gain, and the absolute position of the 198 keV peak centroid is used to calculate zero offset. If the peak positions vary beyond preset limits, our procedures require appropriate corrective action.

Pulser Peak Position

The pulser is used to measure deadtime losses due to peak pileup. Its frequency is determined by the power company's line frequency, and its amplitude is controlled by an internal amplifier. Its peak position and count rate are also checked daily to verify instrument stability. If the pulser peak has drifted out of its preset ROI, the pulser must be adjusted or replaced. If the pulser peak has not drifted, but its count rate is outside acceptable limits, adjustment of the amplifier pileup correction or pole/zero circuit is indicated.

Neutron Instruments

The Active Well Coincidence Counter (AWCC) is the only neutron-based instrument currently used in our NDA Facility. As with the gamma-ray instruments, AWCC operation is verified during daily startup to ensure the instrument's good working condition. After AWCC operation is verified, one mid-range control sample is analyzed to test calibration.

Background Totals

The AWCC's internal neutron sources give rise to a large number of uncorrelated counts in the instrument's "Totals" register. If the instrument is in good working order, only random variation is expected in the observed Totals rate. If an instrument malfunction has occurred, or if a sample has been left in the detector well, the Totals rate will change significantly indicating the need for corrective action. During daily startup, a 100-s empty-chamber count is performed to test AWCC operation. The "Totals" count is recorded, plotted, and evaluated before sample analysis can proceed.

CONTROL SAMPLES

In our NDA Facility, control samples, chosen to be physically and chemically similar to the "unknown" items, are periodically analyzed. The gamma-based instruments are evaluated using two control samples each - one at each end of the instrument's calibration range. The AWCC is evaluated using a single mid-range control sample.

Large Segmented Gamma Scanner ("Barrel Scanner")

Two 208-L drums of surrogate combustible waste and two HEPA filters loaded with a known amount of uranium are used as control samples for the large SGS. Repeated analyses of these control samples indicate that the barrel scanner is capable of ± 3.1% precision and 0.8% bias at the upper end of the calibration curve, and ±22% precision (1σ) and -2.4% bias at the low end for 208-L drums.

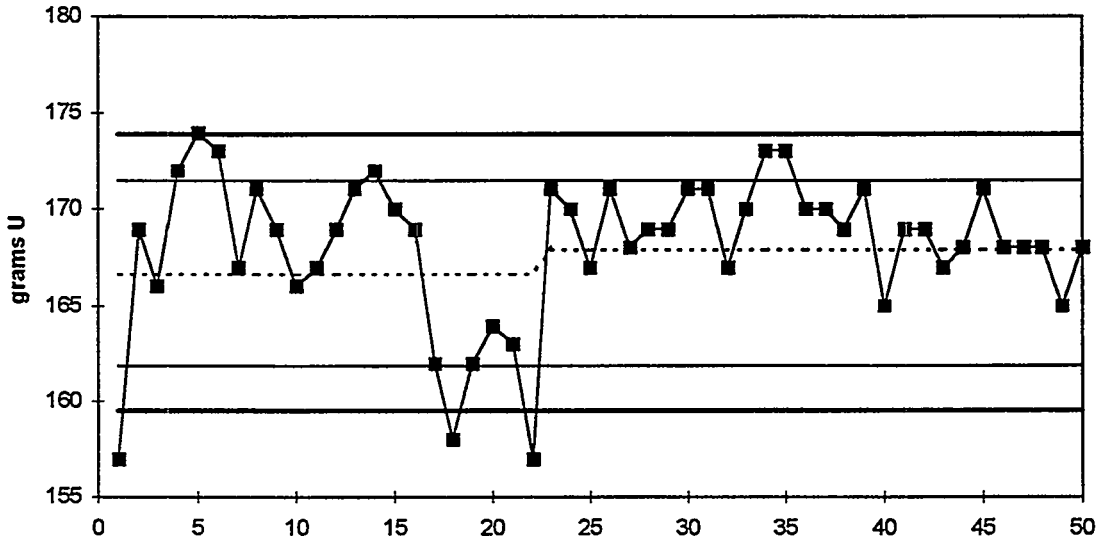

Figure 1: Control chart for 208-L barrel. Data points #17 through #22 show increased dispersion due to a faulty amplifier baseline restorer circuit. Note the mean shift resulting from recalibration after amplifier replacement.

Similar precision and bias have been observed for the filters. Figure 1 shows a typical barrel scanner "individuals" control chart. Dispersion in data points #17 through #22 was attributed to a faulty baseline restorer in the instrument's amplifier. After the amplifier was replaced and the unit recalibrated, the process mean shifted to a value closer to the known value for the control sample.

Small Segmented Gamma Scanner ("Can Scanner")

Two containers of uranium-bearing ash are used as control samples for the small SGS. Repeated control measurements show that this instrument has precision of ±1.2% and -2.1% bias at the upper end of the calibration curve, and ±2.7% precision with bias of 0.1% at the low end. Figure 2 shows a typical can scanner control chart.

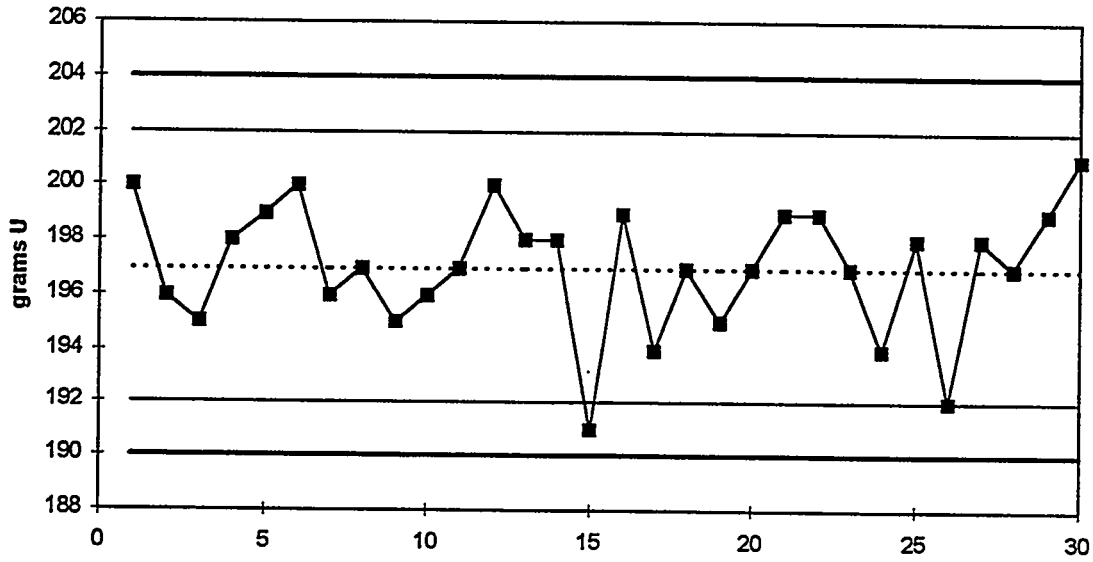

Figure 2: Control chart for can of uranium-bearing ash. The control chart shows that the process is in statistical control. The 2σ-outlier at point #15 is considered a normal occurrence.

Note that this instrument is in statistical control over the measurement period. Note that one 2σ-outlier is considered a normal occurrence since some 5% of measurements can be expected to exceed correctly-established 2σ warning limits.

Solution Assay System

Two 125-ml polyethylene bottles of uranyl nitrate solution are used as control samples for the solution assay system. Routine analyses of these control samples shows instrument precision of ±0.6% and bias of -0.05% at the upper end of the calibration curve, and ±2.3% precision with +2.2% bias at the low end. Figure 3 shows a typical control chart for the Solution Assay System. Two 3σ outliers occurred during the measurement period, and these were attributed to movement of samples in the vicinity of the instrument. The outlier at point #17 occurred when a container of uranium oxide was placed near the instrument during the control sample measurement, but after the background had been counted. The outlier at point #27 was caused when a container of uranium oxide was placed near the instrument during the background count, but removed before the control sample was measured. Additionally, there is an apparent 0.4% mean shift between points #18 and #19 -- this was judged operationally insignificant and no attempt was made to assign a cause.

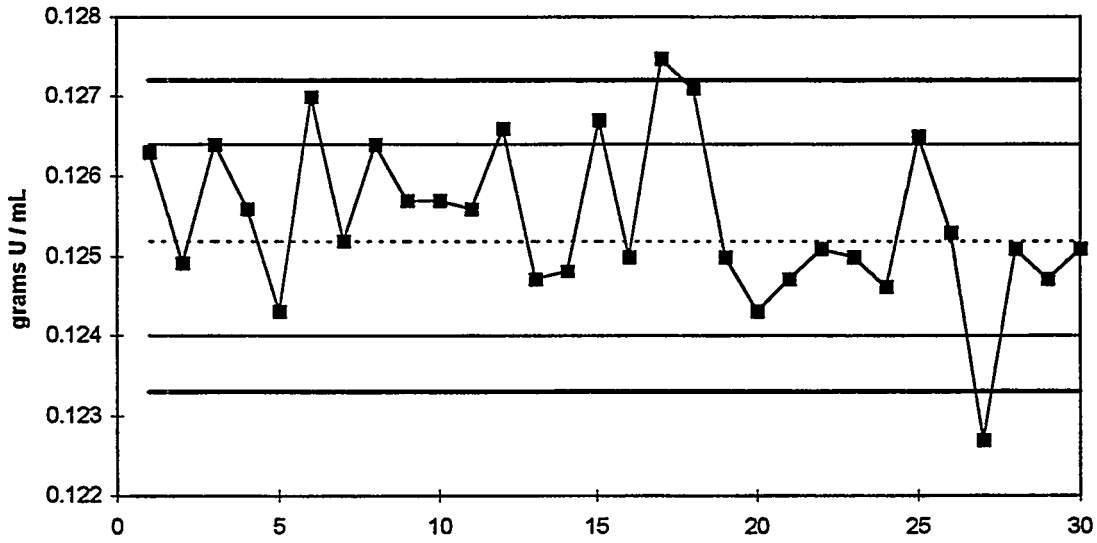

Figure 3: Control chart for bottle of uranyl nitrate solution in SAS. The control chart shows two 3σ outliers caused by variable background. The outlier at point #17 occurred when a container of uranium oxide was placed near the instrument during the control sample measurement, but after the background had been counted. The outlier at point #27 was caused when a container of uranium oxide was placed near the instrument during the background count, but removed before the control sample was measured

Active Well Coincidence Counter (AWCC)

One container of uranium oxide is used as a control sample for the AWCC. Routine analyses of this control sample show instrument precision of ±1.1% and +5.0% bias in the calibration curve midrange. Figure 4 shows a typical control chart for the AWCC. Control data for the AWCC are difficult to interpret, since the results are derived from two independent measurements - container fill height and AWCC analysis. In general, most of the AWCC control problems are caused by poorly-controlled fill height. For example, if a container is dropped after its fill height has been determined, the material inside may be compacted causing AWCC response to be greater than expected. Points #23 and #24 are examples of this type of outlier. When the control results are too low, other problems are indicated. Outliers at points #30 through #33 were caused when the neutron sources were positioned upside-down in the AWCC following a series of experiments.

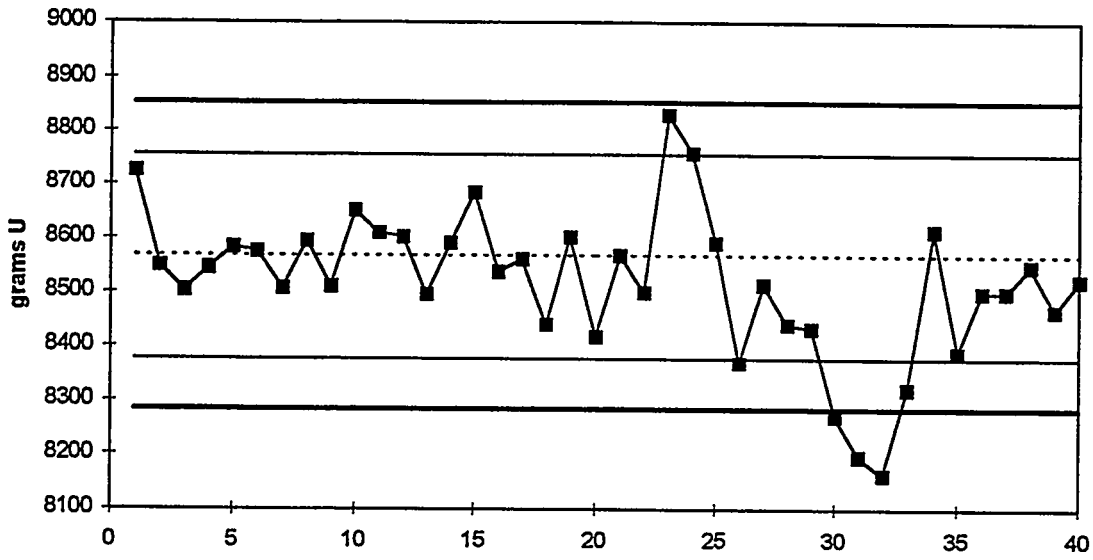

Figure 4: Control chart for container of uranium oxide in AWCC. The control chart shows two out-of-control conditions. Points #23 and #24 show the effects of fill height errors. Points #30 through #33 were caused by improperly-placed neutron sources.

ESTABLISHING CONTROL LIMITS

As mentioned earlier, DOE Order 5633.3B requires "warning" and "action" limits to be set at $\pm 2\sigma$ and $\pm 3\sigma$ from the process mean respectively. There are several statistically justifiable methods of setting these process limits. The Analytical Services Organization at Y-12 uses the moving-range-of-two method[1] for establishing these control limits. In this method, differences between successive values are averaged to calculate the average moving range RBAR, and the data set's standard deviation is calculated as

\

$$\sigma = \text{RBAR}/1.128$$

An out-of-control condition is identified when 1) a single measurement exceeds either 3σ limit; 2) two out of three consecutive measurements exceed either 2σ limit, or 3) eight or more consecutive results fall on one side of the process average. In accordance with the DOE Order, a single control measurement that exceeds either 2σ limit must also be investigated.

REFERENCES

1. L.S. Nelson, "Technical Aids," *Journal of Quality Technology*, Vol. 14, No. 3 (July 1982).

OPERATION AND CONTROL SOFTWARE FOR APNEA

J. H. McClelland, B. H. Storm, Jr.
Lockheed Martin Specialty Components, Largo, Fl.

J. Ahearn, H. W. Hazzard and A. Rubin
Lockheed-Martin Specialty Components, Largo Fl.

K. Fernandez, F. Gulledge, N. Javagal and A. Yadav
University of South Florida, Tampa, Fl.

ABSTRACT

The human interface software for the Lockheed Martin Specialty Components (LMSC) Active/Passive Neutron Examination & Analysis System (APNEA)[a] provides a user friendly operating environment for the movement and analysis of waste drums. It is written in Microsoft Visual C++[b] on a Windows NT platform. Object oriented and multitasking techniques are used extensively to maximize the capability of the system.

A waste drum is placed on a loading platform with a fork lift and then automatically moved into the APNEA chamber in preparation for analysis. A series of measurements is performed, controlled by menu commands to hardware components attached as peripheral devices, in order to create data files for analysis. The analysis routines use the files to identify the pertinent radioactive characteristics of the drum, including the type, location, and quantity of fissionable material.

At the completion of the measurement process, the drum is automatically unloaded and the data are archived in preparation for storage as part of the drum's data signature.

INTRODUCTION

The Graphical User Interface (GUI) based software for the LMSC APNEA is written in a standard windows event driven style, with access to functionality provided by drop down menus. Communication is provided to multiple external hardware devices in order to drive the mechanical components of the system. The software for the interfaces is derived from standard

[a] B. H. Storm, Jr., R. L. Bramblett, Lockheed Martin Specialty Components, Largo, FL, and D. C. Hensley, Oak Ridge National Laboratory, Oak Ridge, TN, "Identification of the Fast and Thermal Neutron Characteristics of TRU Waste Drums"

[b] One Microsoft Way, Redmond, WA, 98052

templates provided by tool kits from both Greenleaf Software, Inc.[c] and NetManage[d]. Interface to the serial devices, i.e., bar code readers, a high voltage supply for the detectors, a MM-165 Zetatron Controller, an alpha contamination wipe test device, and a Programmable Logic Controller (PLC), is accomplished via a Digi International[e] PC/8 card. Interface to radiation monitoring devices at both the inspection station and the APNEA chamber is accomplished via a National Instruments[f] A/D card. Interface to the UNIX based Data Logger[g], which uses Digital Signal Processors (DSP) to accumulate the data collected by the ^{3}He neutron detector tubes surrounding the APNEA chamber, is accomplished using Remote Procedure Calls (RPC) executing over an Ethernet network in a client server fashion. See Figure 1.

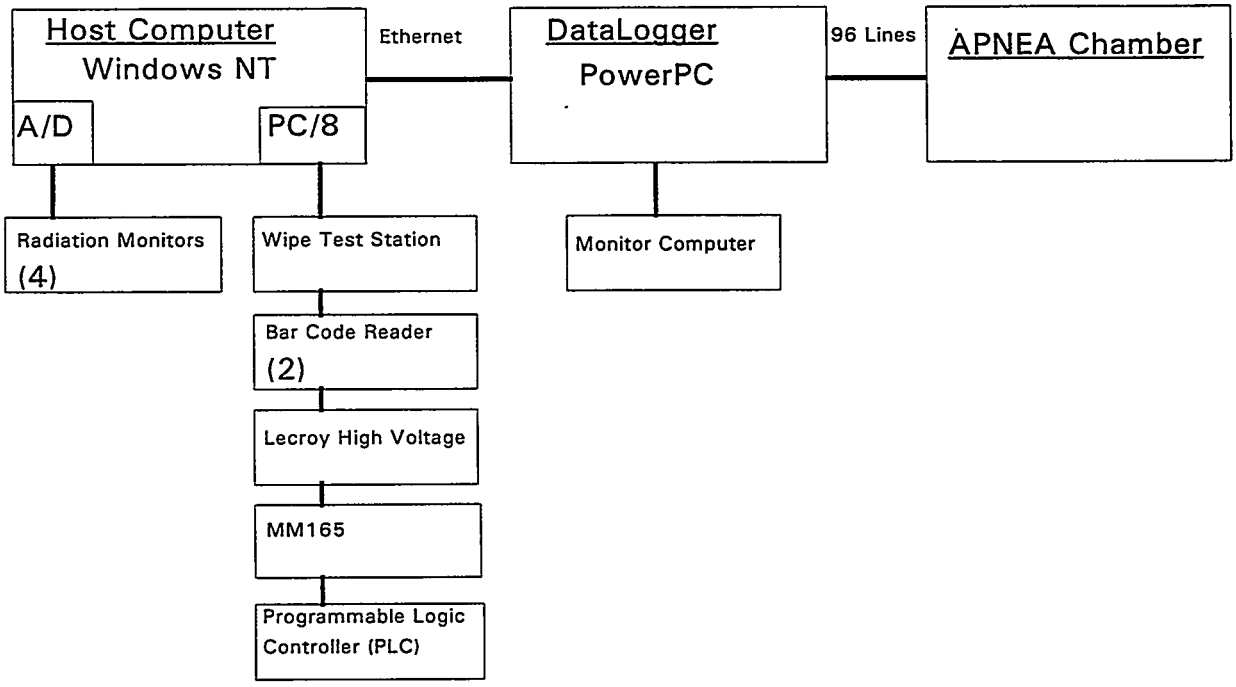

Figure 1. Schematic diagram of the APNEA hardware interfaces.

Upon startup, the Host Software initializes the hardware components and then loads the background processes that initiate the transfer and analysis of data captured by the Data Logger during a measurement cycle. Once initialized, the system is available for operation in either a

[c] 16479 Dallas Parkway, Suite 570, Dallas, TX 75248
[d] 10725 N. De. Anza Blvd., Cupertino, CA 95014
[e] 11011 Bren Rd., Minnetonka, MN, 55343
[f] 6504 Bridge Point Pkwy., Austin, TX, 78730
[g] R. A. Hogle, P. Miller, GE Corporate Research & Development, Schenectady, NY, and R. L. Bramblett, "APNEA List Mode Data Logging and Real-Time Event Accumulation"

Characterization or Production Mode. In Production Mode, a series of menu selections is available to guide the operator through the entire process of drum measurement in an efficient manner. The operator is prompted through the operating sequence in order to reduce human errors and simplify the amount of interaction. In Characterization Mode, the operator may manually select any measurement function and may enter measurement parameters and exert detailed control over the APNEA hardware. This mode is used to acquire data that characterizes system response to drums being assayed. Calibration drums can be loaded and measured in order to provide benchmark readings against which unknown drums can be compared.

Controls are available to monitor system performance. Each program that encounters an error condition, (e.g., attempting to load a drum into the chamber with the chamber door closed), writes a record in a system log that is available for review. At the completion of a measurement, quality control checks are performed to validate the integrity of the data that have been collected. Whenever a condition occurs that necessitates a warning or an error to the operator, a pop up window is presented that displays relevant information about the condition. The operator then chooses a course of action, e.g., retry the activity, ignore the message, or abort the process. Additional reports are available to view measurement configuration parameters, radiation sampling results, control file records, and the hardware interface settings.

MEASUREMENTS

At the heart of the APNEA System is its capability to perform drum measurements in Passive, External Matrix Probe (EMP), and Active Modes. In Passive Mode, data are collected with a drum loaded and turning in the chamber in order to measure fission neutrons using an auto-correlation method. In EMP Mode, a series of from one to six measurements is performed with a drum loaded and turning in the chamber as a ^{252}Cf source is indexed to different heights along the drum. In Active Mode, a neutron generator source, called the Zetatron, is pulsed in order to irradiate the drum and induce fission neutrons as the drum turns in the chamber. In each mode, the emitted neutrons are sensed by the ^{3}He neutron detector tubes surrounding the chamber and recorded by the Data Logger. Any operation that addresses safety concerns, such as starting the Zetatron or moving the ^{252}Cf, requires confirmation by operator input as well as

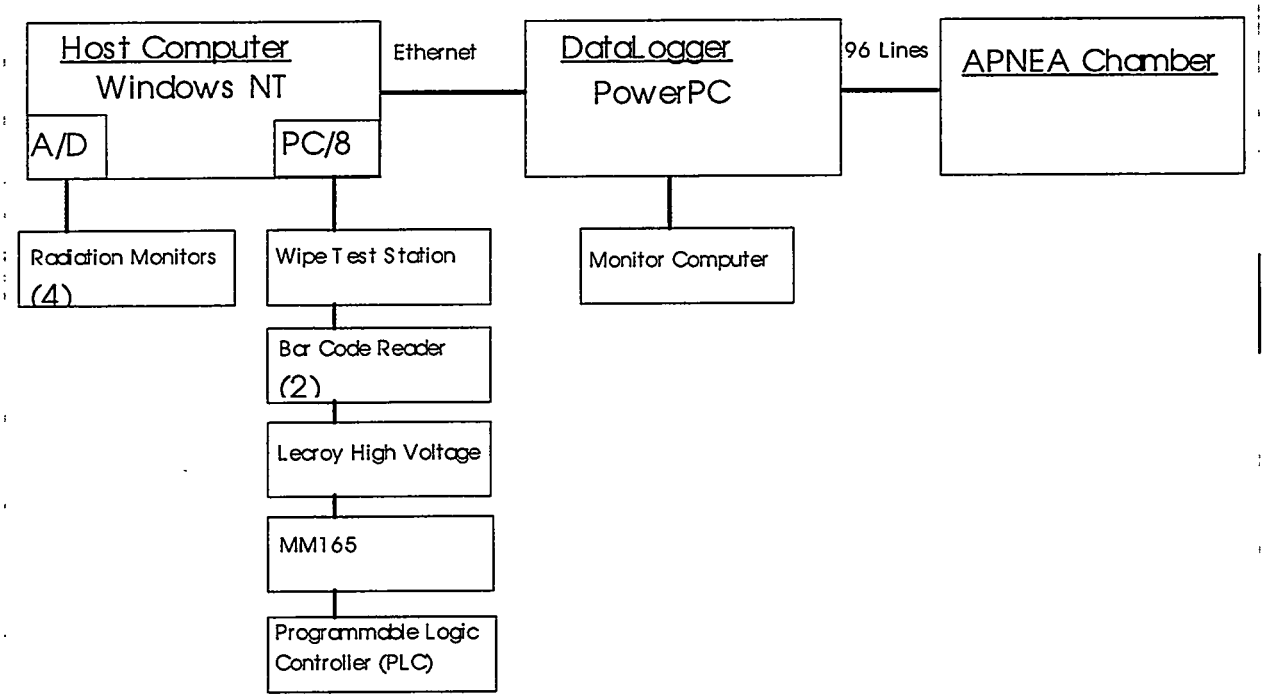

Figure 1. Schematic diagram of the APNEA hardware interfaces.

Upon startup, the Host Software initializes the hardware components and then loads the background processes that initiate the transfer and analysis of data captured by the Data Logger during a measurement cycle. Once initialized, the system is available for operation in either a Characterization or Production Mode. In Production Mode, a series of menu selections is available to guide the operator through the entire process of drum measurement in an efficient manner. The operator is prompted through the operating sequence in order to reduce human errors and simplify the amount of interaction. In Characterization Mode, the operator may manually select any measurement function and may enter measurement parameters and exert detailed control over the APNEA hardware. This mode is used to acquire data that characterizes system response to drums being assayed. Calibration drums can be loaded and measured in order to provide benchmark readings against which unknown drums can be compared.

Controls are available to monitor system performance. Each program that encounters an error condition, (e.g., attempting to load a drum into the chamber with the chamber door closed),

physical controls. A nominal production sequence requires 20 minutes. This is comprised of drum inspection (60 sec), drum loading (180 sec), drum radiation survey (10 sec), ACTIVE (40 sec), EMP (120 sec), PASSIVE (400 sec), drum radiation survey (10 sec), and drum unloading (180 sec). Included in the 20 minutes are about 3 minutes for entry of manual data and notes.

Each of the measurement modes can be selected using a menu command available in either the Characterization or Production Menu. When a measurement is initiated, the host computer transfers a configuration buffer to the Data Logger, so that it can create a session in which to capture data. If configured correctly, the Data Logger will then accept a command to collect data for a specific number of Azimuth Intervals, where an Azimuth Interval is an angular rotation of the drum through 45 degrees. See Figure 2.

When a measurement is complete, the Host Computer writes a record in the Transfer Control File so that the Transfer Program can move the captured data from the Data Logger to the Host Computer. Data transferred to the host computer are stored in a directory structure that is identified by the Drum ID and measurement mode. All data is moved to an archive drive for eventual transfer to CD ROM, while a subset is saved on the production drive for analysis. The Transfer Program completes an individual measurement by issuing a command to the Data Logger to delete the session. Concurrently with the archive and delete processes, the Analysis Initiation Program updates a control file with a record identifying the measurement sub-directory that has been created so that the analysis procedures can find and process the data. Files that must be shared among multiple processes, i.e., transfer and analysis, are synchronized using a kernel level mutual exclusion object (mutex) in order to guarantee that data are not changed simultaneously by two different processes. See Figure 3.

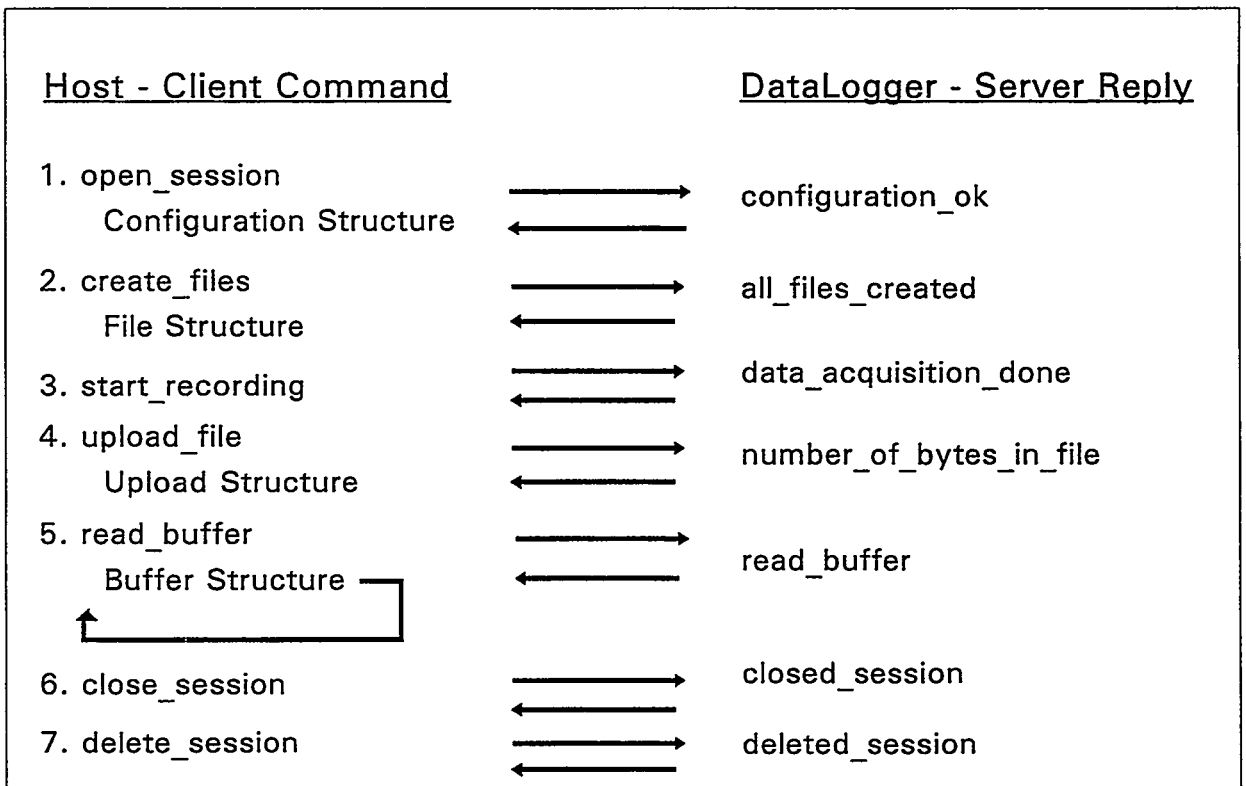

Figure 2. Host - DataLogger Measurement Command Sequence

ANALYSIS CONTROL

Data files are stored in sub directories named with the identification of the drum (read from a bar code), the date and time at which the acquisition began, and the mode of acquisition. This information is included in a header on each of the data files produced, as well as a control file which initializes the 'preprocessing' of the analysis code. The control file provides path information and a status code to the conversion routines. If the status code indicates that the raw data have not been processed, the path information is read and referenced files are opened. In order to assure positive identification of the data set, the path information is compared to the header information contained in each data file. In the event the information does not match, the analysis stops. Agreement allows preprocessing of the data to continue.

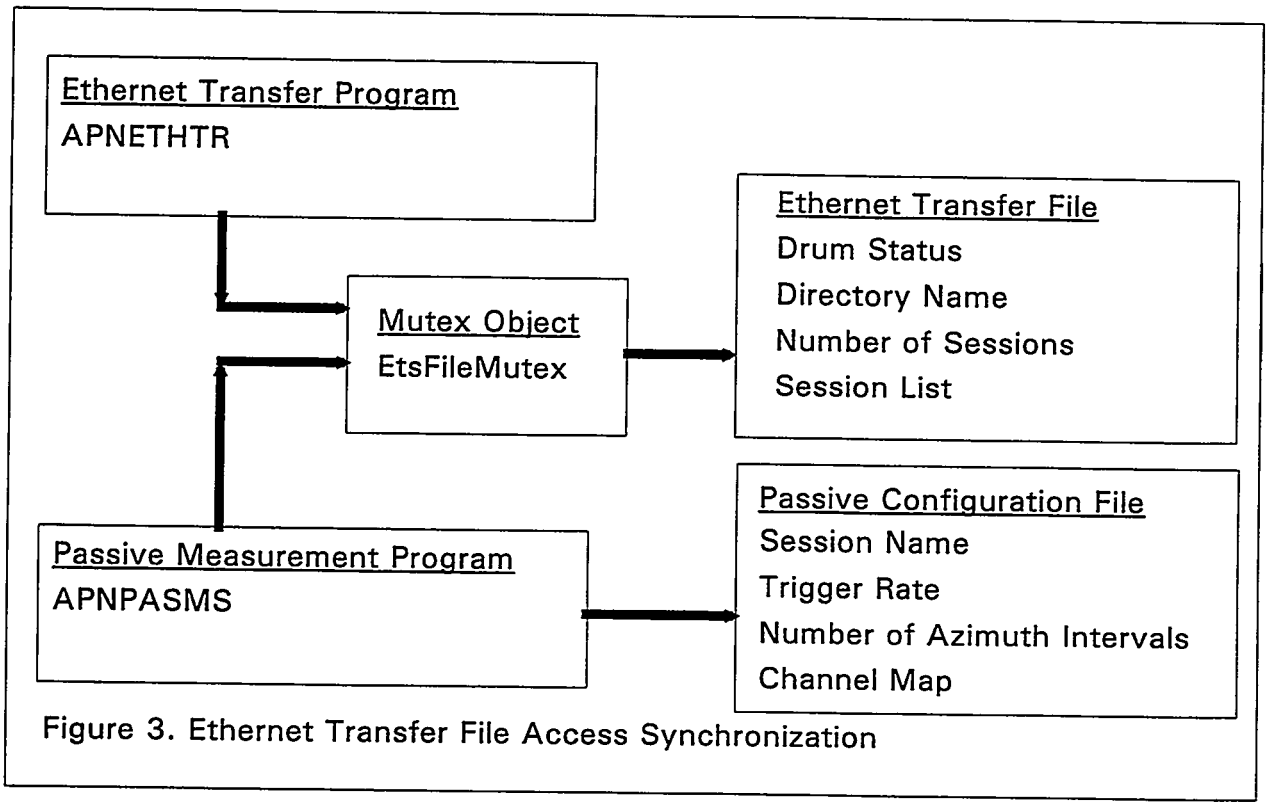

Figure 3. Ethernet Transfer File Access Synchronization

FUTURE WORK

The operation and control software for the APNEA System permits waste drums to be manipulated and analyzed for their fissionable content in an efficient, intuitive, and safe manner. Future enhancements to the system include a remote inspection station, which will prepare drums for inspection separately from their processing, an "Auto-Sequence Mode", which will execute all of the steps in the Production Menu without requiring operator input at each stage, and a CD-ROM jukebox, to automate the task of archiving data.

ACKNOWLEDGMENTS

The authors gratefully acknowledge the work of R. L. Bramblett on requirements definition for the APNEA Operation and Control software and discussions and suggestions by D. K. Steinman of Lockheed-Martin Specialty Components.